**University of Bath**

**PHD**

# Synthesis and reactivity of N-heterocyclic carbine stabilised ruthenium and rhodium hydride complexes

Douglas, Susan Rachel

*Award date:*
2005

*Awarding institution:*
University of Bath

Link to publication

**General rights**
Copyright and moral rights for the publications made accessible in the public portal are retained by the authors and/or other copyright owners and it is a condition of accessing publications that users recognise and abide by the legal requirements associated with these rights.

- Users may download and print one copy of any publication from the public portal for the purpose of private study or research.
- You may not further distribute the material or use it for any profit-making activity or commercial gain
- You may freely distribute the URL identifying the publication in the public portal ?

**Take down policy**
If you believe that this document breaches copyright please contact us providing details, and we will remove access to the work immediately and investigate your claim.

Download date: 13. May. 2019

# Synthesis and reactivity of N-heterocyclic carbene stabilised ruthenium and rhodium hydride complexes

**Susan Rachel Douglas**

A thesis submitted in partial fulfillment of the requirements for the degree of

**Doctor of Philosophy**

UNIVERSITY OF
BATH

University of Bath
Department of Chemistry

November 2005

Attention is drawn to the fact that copyright of this thesis rests with its author. This copy of the thesis has been supplied on condition that anyone who consults it is understood to recognise that its copyright rests with its author and that no quotation from the thesis and no information derived from it may be published without the prior written consent of the author.

This thesis may be made available for consultation within the University library and may be photocopied or lent to other libraries for the purposes of consultation.

UMI Number: U488172

All rights reserved

INFORMATION TO ALL USERS
The quality of this reproduction is dependent upon the quality of the copy submitted.

In the unlikely event that the author did not send a complete manuscript
and there are missing pages, these will be noted. Also, if material had to be removed,
a note will indicate the deletion.


UMI U488172
Published by ProQuest LLC 2013. Copyright in the Dissertation held by the Author.
Microform Edition © ProQuest LLC.
All rights reserved. This work is protected against
unauthorized copying under Title 17, United States Code.


ProQuest LLC
789 East Eisenhower Parkway
P.O. Box 1346
Ann Arbor, MI 48106-1346

30 15 MAR 2006

Ph.D.

**For Maureen**

**An inspiration, now and always.**

# Acknowledgements

Firstly I would like to thank my supervisor Dr. Mike Whittlesey for his constant help and support. Despite the dodgy taste in music he has been continually on hand throughout my PhD and his enthusiasm for the subject is inspirational, motivational and occasionally exasperating!

I would also especially like to thank Dr. Mary Mahon for all of the time she spent solving X-ray crystallography structures for me. I would not have blamed her for giving up on me after the first year but she persevered and thankfully it paid off. Dr. John Lowe not only undertook NMR simulations for me but spent many hours listening to me complain and was constantly encouraging and welcoming. Dr. Andrew Weller has always been there to lend a guiding hand and to reassure me in times of doubt. During my PhD, and my final year project before that, I have always appreciated the time he has taken to listen to me and advise me.

This project has taken me around the UK to Edinburgh, York and Nottingham and I would like to thank everyone who made me feel welcome and facilitated the work I was doing. In particular, Dr. Stuart Macgregor and Richard Diggle at Heriot Watt University, Professor Simon Duckett, Professor Robin Perutz and Kirsten Ampt at the University of York and Professor Mike George and Alex Cowan at the University of Nottingham. Also, thank you to Mrs Whittlesey for putting me up at short notice on an overnight stay in Nottingham.

During the last three years at the University of Bath I have been extremely lucky to share a lab with some wonderful people and I hope to remain friends with many of them. Dr. Rudolph Jazzar spent many hours of his valuable time showing me how to use equipment in the lab and making me feel at home. In addition, Dr. Jose Goicoechea, Dr. Suzanne Burling, Sarah Chatwin, Vicky Brown and Steve Reade have all made my time in and out of the lab extremely enjoyable. In particular I

would like to thank soon-to-be Dr. Belinda Paine for being an amazing friend who has been a continual source of laughter and comfort during the last three years. I could not have chosen anyone better to spend those intense years with. I would also like to thank Purvi Bahtia for being a brilliant office- and house-mate, always understanding and always looking out for me. Dr. Jamie Cotgreave, Dr. Mike Ingleson, Dr. Marie Brown, and Gemma Moxham have become close friends over the last few years and I sincerely hope will continue to be so.

I am not going to risk naming friends who have been there to support me over the last few years for fear of missing someone out but they know who they are and I am forever grateful to them for their love and eternal faith in me. This thesis is a result of their encouragement as much as anything else. In particular, however, I would like to thank Sarah Zohhadi who, despite having far more important things to think about, was still always there in times of need with a smile.

Mum, Dad, Lucy and Holly have been absolutely fantastic and are the best family that anyone could wish for. I am continually grateful for their support in whatever I do. Last but not least, I would like to thank Graham for his unwavering love and friendship and for the music.

# Abbreviations list

| | |
|---|---|
| **BDE** | bond dissociation energy |
| **DFT** | density functional theory |
| **IR** | infrared |
| **TRIR** | time resolved infrared |
| $\nu_L$ | IR shift of L |
| **NMR** | nuclear magnetic resonance |
| $\delta$ | NMR chemical shift |
| $J_{XY}$ | coupling constant of X to Y |
| **EXSY** | exchange spectroscopy |
| **HMBC** | heteronuclear multiple bond correlation |
| **HMQC** | heteronuclear multiple quantum coherence |
| **NOESY** | nuclear overhauser effect spectroscopy |
| $p\mathbf{H_2}$ | *para*hydrogen |
| **UV** | ultraviolet |
| **HOMO** | highest occupied molecular orbital |
| **LUMO** | lowest unoccupied molecular orbital |
| **RCM** | ring closing metathesis |
| **ROMP** | ring opening metathesis polymerisation |
| **TOF** | turn over frequency |
| **TON** | turn over number |
| | |
| **%** | percent |
| **°** | degrees |
| **Å** | angstrom |
| **atm** | atmosphere |
| **°C** | degrees Celsius |
| **$cm^{-1}$** | wavenumber |
| **g** | gram |
| **h** | hour |
| **Hz** | hertz |
| **kcal** | kilocalories |
| **kJ** | kilojoules |
| **M** | molar |
| **min** | minute |
| **mL** | milliLitre |
| **mol** | mole |
| **nm** | nanometre |
| **ppm** | parts per million |
| **s** | second |
| **W** | Watts |
| | |
| **acac** | acetylacetonate |
| **arphos** | $Ph_2PCH_2CH_2AsPH_2$ |

| | |
|---|---|
| **$BAr_F$** | $[B(3,5\text{-}C_6H_3(CF_3)_2)_4]^-$ |
| **Bn** | benzyl |
| **$^t$Bu** | *tert*-butyl |
| **COD** | cyclooctadiene |
| **Cp** | $\eta$-($C_5H_5$) |
| **Cp*** | $\eta$-($C_5Me_5$) |
| **Cy** | cyclohexyl |
| **dmpe** | 1,2-bis(dimethyl)phosphinoethane |
| **dppe** | 1,2-bis(diphenyl)phosphinoethane |
| **dppm** | 1,2-bis(diphenyl)phosphinomethane |
| **dppp** | 1,2-bis(diphenyl)phosphinopropane |
| **Et** | ethyl |
| **L** | generic ligand |
| **$\mu$-L** | bridging ligand |
| **Me** | methyl |
| **OAc** | acetyl |
| **Ph** | phenyl |
| **$^i$Pr** | isopropyl |
| **py** | pyridine |
| **R** | alkyl or aryl |
| **THF** | tetrahydrofuran |
| **X** | halide or O or N donating ligand |
| ***o*** | *ortho* |
| ***m*** | *meta* |
| ***p*** | *para* |

| | |
|---|---|
| **NHC** | N-heterocyclic carbene |
| **$IAdH_2$** | 1,3-diadamantyl-4,5-dihydroimidazol-2-ylidene |
| **$IAdMesH_2$** | 1-adamantyl,3-mesityl-4,5-dihydroimidazol-2-ylidene |
| **I$^n$Bu** | 1,3- dibutylimidazol-2,-ylidene |
| **I$^n$Bu''** | C-H activated I$^n$Bu |
| **I$^t$Bu** | 1,3-di-*tert*-butylimidazol-2-ylidene |
| **IBuMe** | 1-butyl-3-methylimidazol-2-ylidene |
| **(I$^n$Bu(py)I$^n$Bu)** | 1,1'-di(butyl)-3,3'-pyridinediimidazol-2,2'-diylidene |
| **$ICH_2CH_2OMe$** | 1,3-di-2-methoxyethaneimidazolidin-2-ylidene |
| **$ICH_2Ph$** | 1,3-dibenzylimidazolidin-2-ylidene) |
| **ICy** | 1,3-cyclohexyl-imidazol-2-ylidene |
| **$IEt_2Me_2$** | 1,3-diethyl-4,5-dimethylimidazol-2-ylidene |
| **$IEt_2Me_2$''** | C-H activated $IEt_2Me_2$ |
| **IH** | 1,3-imidazol-2-ylidene |
| **IMe** | 1,3-dimethylimidazol-2-ylidene |
| **$IMe_4$** | 1,3-dimethyl-4,5-dimethylimidazol-2-ylidene |
| **$IMe(CH_2)IMe$** | 1,1'-di(methyl)-3,3'-methylenediimidazol-2,2'-diylidene |
| **IMes** | 1,3-bis-(2,4,6-trimethylphenyl)imidazol-2-ylidene |
| **IMes''** | C-H activated IMes |
| **IMes'** | C-C activated IMes |

| | |
|---|---|
| **$IMesH_2$** | 1,3-dimesityl-4,5-dihydroimidazol-2-ylidene |
| **$IMesH_2$''** | C-H activated $IMesH_2$ |
| **IPh** | 1,3-diphenylimidazolidin-2-ylidene |
| **Ipmp** | 1,3-bis-(*p*-methoxyphenyl)imidazol-2-ylidene |
| **IPr** | 1,3-bis(2,6-diisopropylphenyl)imidazol-2-ylidene |
| **$IPrH_2$** | 1,3- bis(2,6-diisopropylphenyl)-4,5-dihydroimidazol-2-ylidene |
| **$I^iPr_2Me_2$** | 1,3-diisopropyl-4,5-dimethylimidazol-2-ylidene |
| **$I^iPr_2Me_2$''** | C-H activated $I^iPr_2Me_2$ |
| **$I^iPr(CH_2)I^iPr$** | 1,1'-di(isoproply)-3,3'-methylenediimidazol-2,2'-diylidene |
| **(IPr(py)IPr)** | 1,1'-di(2,6-diisopropylphenyl)-3,3'-pyridinediimidazol-2,2'-diylidene |

# Table of Contents

# Abstract

This thesis explores the chemistry of both ruthenium and rhodium N-heterocyclic carbene (NHC) complexes, most of which bear hydride ligands. The starting point for the project was the discovery that facile intramolecular C-H and C-C bond activation occurs in the complexes $[Ru(H)_2(IMes)(PPh_3)_2(CO)]$ and $[Ru(H)_2(IMes)_2(PPh_3)(CO)]$. Efforts to understand the reaction mechanisms of these processes *via* attempted isolation of intermediate species, solvent effects and collaborative DFT calculations are described.

The photochemistry of a series of mono and bis alkyl-NHC dihydride ruthenium complexes $[Ru(H)_2(NHC)(PPh_3)_2(CO)]$ and $[Ru(H)_2(NHC)_2(PPh_3)(CO)]$ (NHC = $IEt_2Me_2$, $I^iPr_2Me_2$, ICy), has been investigated by a combination of steady state photolysis, time-resolved spectroscopy and *in situ* photolysis in the presence of *para*hydrogen. The photochemistry is dominated by an isomerisation pathway and concurrent loss of both $H_2$ and $PPh_3$.

The related ruthenium hydride complexes, *cis*- and *trans*-$[RhH(NHC)(PPh_3)_2]$, *cis*- and *trans*-$[RhH(NHC)_2(PPh_3)]$, $[RhH(NHC)_3]$, and *cis*- and *trans*-$[RhH(NHC)_2(CO)]$ (NHC = $IEt_2Me_2$, $I^iPr_2Me_2$, ICy, IMes) have been synthesised from $[RhH(PPh_3)_4]$ and $[RhH(PPh_3)_3(CO)]$. C-H activation of the IMes ligand in *cis*-$[RhH(IMes)(PPh_3)_2]$ has been observed. In addition, the cationic complexes $[Rh(NHC)_3(CO)]^+$ and $[Rh(NHC)_4]^+$ (NHC = $IEt_2Me_2$, $I^iPr_2Me_2$, ICy) have been isolated along with the two dinuclear complexes, $[\{Rh(PPh_3)_2\}_2(\mu\text{-}H)(\mu\text{-}PPh_2)]$ and $[\{Rh(I^iPr_2Me_2)_2(\mu\text{-}CO)\{Rh(PPh_3)_2\}]$. These complexes have been characterised using multinuclear NMR spectroscopy and X-ray crystallography.

# Chapter 1

# Introduction

# 1. Introduction

The two emerging fields of bond activation chemistry and N-heterocyclic carbene (NHC) complexes have become intertwined in recent years with the publication of a significant number of examples of NHC ligands undergoing intramolecular bond activation. This thesis investigates the examples of bond activation that have already been observed in the literature and within the Whittlesey group and discusses some examples of new activation reactions that have been observed. The synthesis of some novel rhodium NHC complexes is reported many of which have been characterised using X-ray diffraction. In addition, the thermal and photolytic chemistry of ruthenium NHC complexes has been investigated.

## 1.1. C-C and C-H bond activation

The large scale cleavage of C-C and C-H bonds is desirable for a number of reasons but particularly for the more effective utilisation of hydrocarbons. For example, breaking a C-H bond in methane and then functionalising it to give methanol has been described as one of the "holy grails" of chemistry.[1] To get two molecules of methanol from one molecule of ethane, however, would be even more desirable (scheme 1.1.).

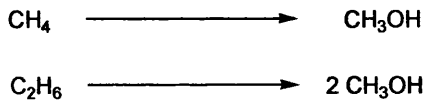


**Scheme 1.1.** Formation of methanol from methane and ethane.

At present, the petroleum industry cleaves large hydrocarbons by passing hydrogen over them at high temperature in the presence of a heterogeneous catalyst. These catalysts are not selective about which hydrocarbon bond they break so a diverse range of products is produced. Therefore, the potential use of transition metal chemistry to selectively and efficiently cleave C-H and C-C bonds is of extreme importance.

Alkane coordination complexes (a possible precursor to bond activation reactions) are also believed to be intermediates in organometallic catalysed reactions such as σ-bond metathesis[2,3] or Zeigler-Natta catalysis.[4,5]

## 1.1.1. Binding of alkanes to metal centres and their C-H activation

The binding of an alkane to a transition metal centre is not as facile as the binding of other substrates such as alkenes, carbon monoxide and dinitrogen, because an alkane does not possess π-electrons or electron lone pairs that can interact directly with the metal centre.[6] However, work by Shilov and co-workers demonstrated that alkanes could be functionalised in the presence of platinum complexes and, although the mechanism of the reaction could not be established, the observation of H/D exchange in the alkane substrates suggested that oxidative addition of the C-H bonds to the platinum centre occurred.[7]

### *1.1.1.1. Intermolecular alkane activation*

The first definitive examples of intermolecular alkane activation, were provided almost simultaneously by Graham[8] and Bergman[9] who demonstrated the activation of a $CH_2$ group in cyclohexane upon photolysis in the presence of $[Ir(CO)_2(Cp^*)]$ and $[Ir(H)_2(PMe_3)(Cp^*)]$ (**1**) ($Cp^* = \eta^5$-$C_5Me_5$) respectively (scheme 1.2. shows the C-H activation of cyclohexane by **1**). Bergman subsequently showed that when the reaction with **1** was carried out at low temperatures in liquid krypton or xenon, other alkane substrates could be activated and stabilised on the metal centre.[10] He concluded that photolysis of **1** leads to loss of $H_2$, leading to the coordinatively unsaturated 16-electron $[Ir(PMe_3)(Cp^*)]$ species. The alkane can then oxidatively add to the metal centre *via* a three-centred transition state (scheme 1.3.). Bergman has since gone on to carry out extensive investigative work into the mechanism of alkane C-H bond activations on various transition metals.[9,11-27]

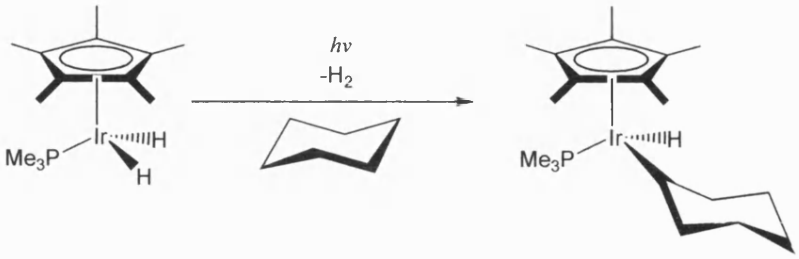


**Scheme 1.2.** The first example of C-H activation of an alkane presented by Bergman.

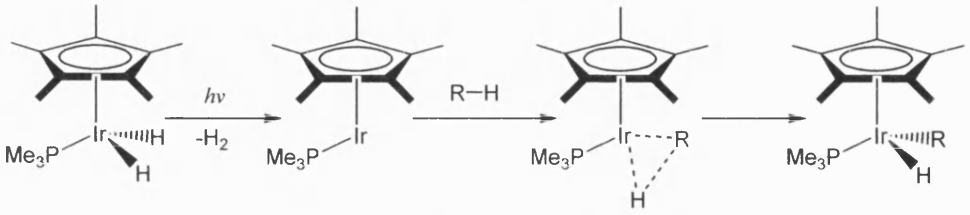


R–H = $C_6H_{12}$, $C_3H_6$, $Me_4C$, $CH_3(CH_2)_3CH_3$, $CH_3CN$, THF, $C_6H_6$

**Scheme 1.3.** Mechanism of intermolecular C-H activation at an Ir(I) centre.

There are four possible transition bonding modes for an alkane to a metal centre (figure 1.1.). Studies carried out by Crabtree and co-workers on a series of structures of C-H-M complexes has suggested that during intermolecular C-H activation, the C-H bond approaches the metal atom end-on (**I**). This results in a strong M-H interaction. The C-H bond then rotates, bringing the carbon atom close to the metal centre to form a three-centred transition state (**II**).[28,29] This transition state agrees well with that calculated by Koga *et al.* for the addition of $CH_4$ to $[RhCl(PH_3)_3]$.[30] Other calculations, however, suggest that alkanes can also bind to metal ions *via* $\eta^2$-$H_2$ coordination (**III**), although this does not necessarily lead to C-H activation.[31,32] Ball has suggested, using dynamic NMR experiments, that the $\eta^2$-$H_2$ mode of binding is a low-energy transition state between two $\eta^2$-CH structures.[33]

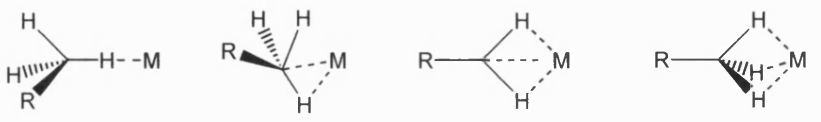


$\eta^1$-CH (**I**) $\eta^2$-CH (**II**) $\eta^2$-$H_2$ (**III**) $\eta^3$-$H_3$ (**IV**)

**Figure 1.1.** Binding modes of alkanes to transition metal centres.

Recently, in 2005, Ball reported the observation of the binding of pentane to a rhenium centre.[34] By $^1$H NMR spectroscopy it could be seen that the pentane binds

to the metal in three different modes, from carbons 1(5), 2(4) and 3 along the alkyl chain (figure 1.2.). These three structures are in a dynamic equilibrium with the $CH_2$ sites being slightly favoured over the $CH_3$ (by 0.5 ± 0.08 kJ $mol^{-1}$). At -100 °C the three isomers are interconverting on a timescale of about 1-10 $s^{-1}$.

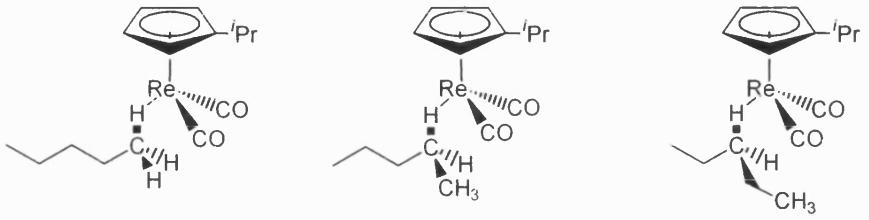


**Figure 1.2.** Three binding modes of pentane to a Re centre.

*1.1.1.2. Intramolecular alkane activation*

Intramolecular C-H activation of ligands already attached to a transition metal centre is a far more commonly reported phenomenon compared to intermolecular activation. This is due to the C-H bond being more kinetically and thermodynamically predisposed to activation. However, many of the factors governing intramolecular C-H activation are poorly understood.[35] For example, it is unclear why species such as $[Re(PMe_3)_2(Cp^*)]$ and $[Fe(PMe_3)_4]$ readily undergo intramolecular C-H activation with one of the phosphine ligands, whereas $[Rh(PMe_3)(Cp^*)]$ and $[Ir(PMe_3)(Cp^*)]$ do not.

van Koten and co-workers have undertaken investigations into the intramolecular C-H activation (or *ortho*-metallation) of various phosphinoarene (PCP) pincer ligands (figure 1.3.) on late transition metals.[36-38] Because the place where the aromatic ring activates is very site specific this *ortho*-metallation reaction lends itself to the possible selective functionalisation of certain C-H bonds. Pincer ligands are particularly useful to study mechanistic aspects of these reactions as they can stabilise reaction intermediates during a reaction, hence allowing further study to be undertaken. In addition, the pincer ligands can slow the rate of the reaction, which can help provide a kinetic insight into the *ortho*-metallation process.

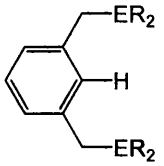


**Figure 1.3.** A generic pincer ligand.

As early as 1968, Cope and Friedrich had proposed that *ortho*-metallation may occur *via* a mechanism analogous to electrophilic aromatic substitutions.[39] This proposal was augmented by van Koten who isolated a number of intermediates on the reaction pathway for C-H bond activation of phosphine pincer ligands on platinum centres.[37]

The cleavage of both intermolecular and intramolecular C-H bonds has been relatively successful with some of the examples from the literature discussed above. C-C bond activation, however, poses more of a challenge. Insertion into a C-C bond is not a thermodynamically forbidden process, although there are few examples that do not involve utilising the relief of ring strain or formation of aromatic products as the driving force.

### 1.1.2. Barriers to C-C activation

C-C activation is particularly difficult on a thermodynamic level.[40] An $sp^3$ C-H bond will favourably break to form a M-H bond and a M-C bond. This is because the bond dissociation energy (BDE) of a single C-H bond) 391-428 kJ $mol^{-1}$) is usually slightly less than that for a M-C bond (124-185 kJ $mol^{-1}$) and M-H bond (approximately 247 kJ $mol^{-1}$) combined. The tendency of a system to undergo C-H activation to give oxidative addition on to a metal centre is actually highly dependent on the M-C bond with metals further down the Periodic Table generally giving stronger M-C bonds and therefore being more favourable sites for C-H activation.[41-43] C-C bonds are very strong (BDE = approximately 356 kJ $mol^{-1}$) and

therefore there is a large thermodynamic barrier going from C-C bonds to C-M-C bonds (scheme 1.4.).

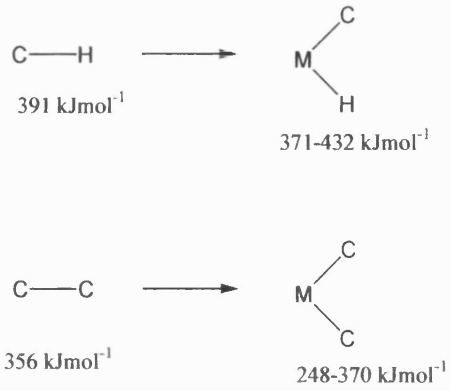


**Scheme 1.4.** Approximate bond dissociation energies of C-H, C-C, C-M-H and C-M-C systems.

This thermodynamic barrier is augmented by various kinetic barriers. Compared to C-H bonds, C-C bonds are very directional in nature. The C-C bond is very symmetrical with the sigma orbitals from the carbon atoms pointing towards each other down the bond. This does not leave an incoming metal with much electron density available to interact with. By comparison, in a C-H bond, the spherical σ orbital of the hydrogen gives a better target for interaction with a metal (figure 1.4.).

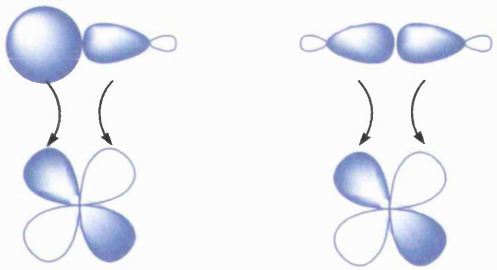

**Figure 1.4.** Influence of orbital directionality on C-H (left) and C-C bond cleavage.

In addition, in the majority of hydrocarbon systems, C-H bonds are statistically more abundant than C-C bonds, making the chances of them coming into contact with an incoming metal greater than that for a C-C bond. C-H bonds also shield the C-C bonds from attack by a metal.[44]

The kinetic barriers for metal insertion into a C-H or C-C bond are independent of the metal. This suggests that the process of insertion is influenced solely by the differences in C-C and C-H bonds and not by the nature of the metals.

One other major difficulty with metal insertion into C-C bonds is that the amount of energy required to overcome the large activation barrier required for C-C bond cleavage often results in thermal decomposition of the metal complex.[45]

1.1.3. Routes to C-C activation

Scheme 1.5. shows how ring strain can be utilised to induce the activation of C-C bonds.[46-50] Strain relief in the product provides the driving force for the reaction. The HOMOs connecting the carbon atoms are bent outwards from the internuclear axis. This makes them kinetically more accessible and more readily available for interaction with a metal (figure 1.5.).[52]

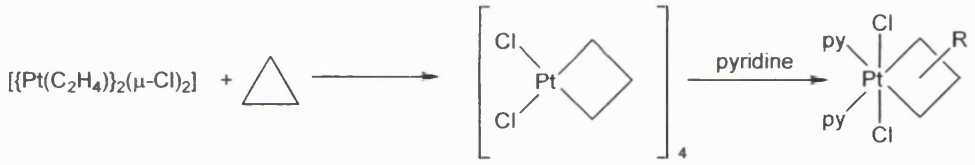


**Scheme 1.5.** Insertion of Pt(II) into C-C bonds of cyclopropane.

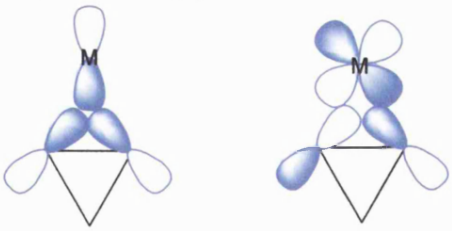


**Figure 1.5.** The $p_y$ orbital of the metal and the cyclopropane σ orbital interact to give a σ bond and the metal $d_{xy}$ and cyclopropane σ* orbitals form a π bond.

The formation of aromatic systems can also induce C-C bonds to break. Scheme 1.6. shows how a molybdenum complex rearranges with the breaking of a Cp-Et bond to give an aromatic group once a vacant site has been generated on the metal.[42] This is a thermodynamically driven process where energy is gained from the generation of aromatic functionalities. The rigidly coordinated cyclopentadiene moiety also forces

the alkyl group towards the metal centre, making the reaction kinetically plausible. When there is a choice, the *endo*-alkyl group that lies closer to the metal centre is always favoured for transferral to the metal.

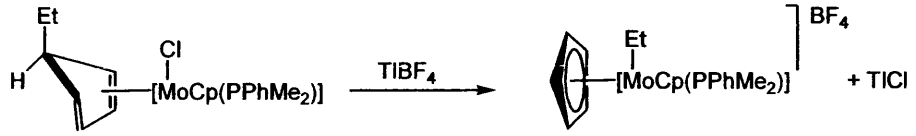


**Scheme 1.6.** Using aromatisation as the driving force to break a C-C bond.

*1.1.3.1. C-C activation using pincer complexes*

Pincer ligands, similar to the ones discussed in section 1.1.1.2., have been developed by Milstein to chelate to a metal centre thus bringing a specific C-C bond close to the metal and promoting its activation. In scheme 1.7., the rhodium metal inserts into the methyl C-H bond at room temperature. Heating at 90 °C converts this to the C-C activated product.[52] This demonstrates the higher thermodynamic stability of the C-C activated complex compared to the C-H activated complex. The reaction is thermodynamically driven by the elimination of methane. The authors postulate that the C-H reaction is reversible and would revert to the original product under an atmosphere of hydrogen.

Computational studies on the formation of PCP pincer rhodium species, suggest that C-H activation is always the kinetically favoured process although C-C activation is actually more stable.[53] It is also suggested that the C-H activated complex can interconvert to the C-C activated complex *via* an intermediate agostic structure (scheme 1.8.). Further calculations suggest that the electronic requirements for C-C and C-H activation are essentially the same (with the key intermediates being 14-electron species) whereas the steric requirements leading to activation differ significantly with chelation appearing to play an important role in C-C activation.[54] When the phosphinoarene ligands have only one phosphine arm to bind to the metal centre, C-H activation generally ensues whilst when the ligands are bidentate, the C-C activated product is more thermodynamically stable.

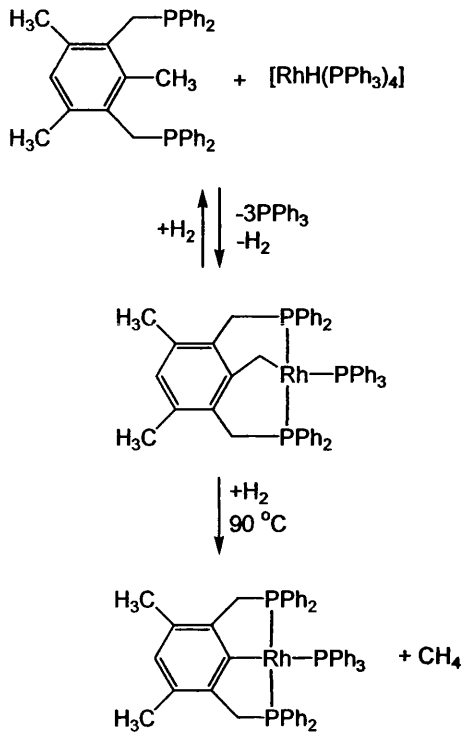


**Scheme 1.7.** Tethered rhodium inserting into a C-C bond.

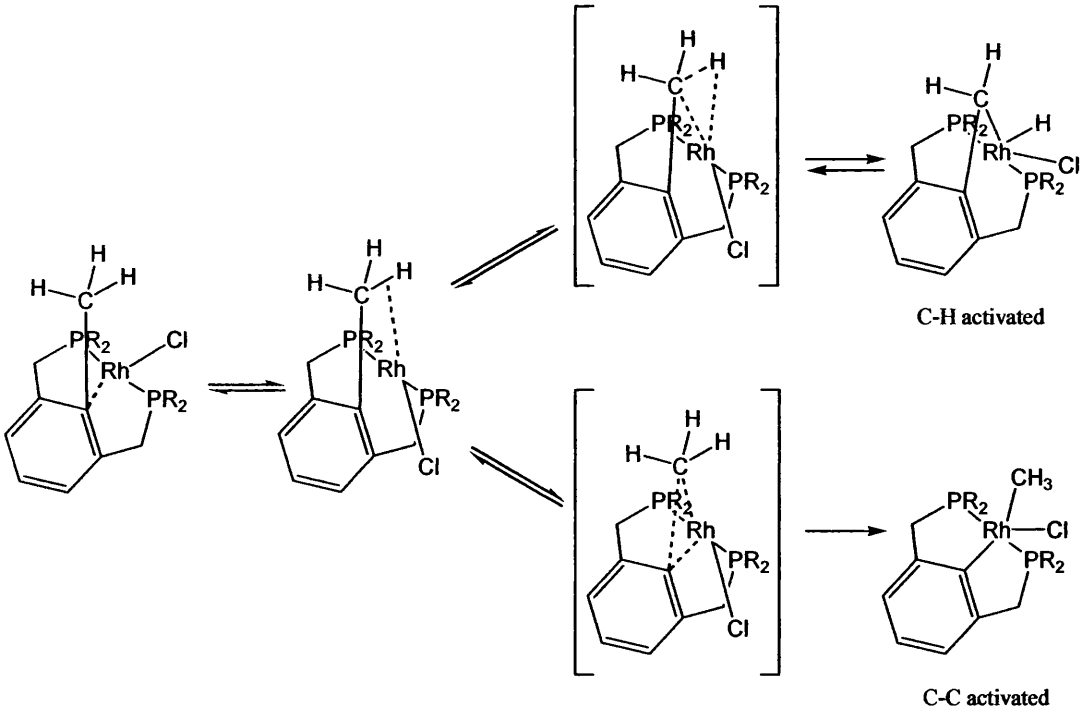


**Scheme 1.8.** Formation of C-H and C-C activation complexes *via* agostic intermediate.

Since the first synthesis of the PCP pincer ligand and its use in a C-C activation reaction, Milstein and his group have created a whole family of similar ligands which also undergo C-C activation. These include PCN[55] and PCO[54] pincer ligands and C-O[56] and C-F[57] bonds have also been observed to undergo intramolecular cleavage in metal pincer complexes whereas N-H bonds are activated intermolecularly.[58] Milstein has also demonstrated that solvents play a crucial part in determining whether the system favours C-H or C-C activation.[54,59] For example, in a system utilising $P^tBu_2$ ligands, he has found that if THF was used as the solvent it led to C-C activation whereas using acetonitrile resulted in C-H activation (scheme 1.9.). Milstein postulates that the reason for this dramatic solvent effect is steric in nature. Acetonitrile is very coordinating and will bind strongly to a metal centre, producing a four coordinate intermediate prior to insertion into the less sterically demanding C-H bond. THF is only loosely bound to the complex, thus the active species in solution is likely to only be three coordinate and more accessible to the C-C bond.

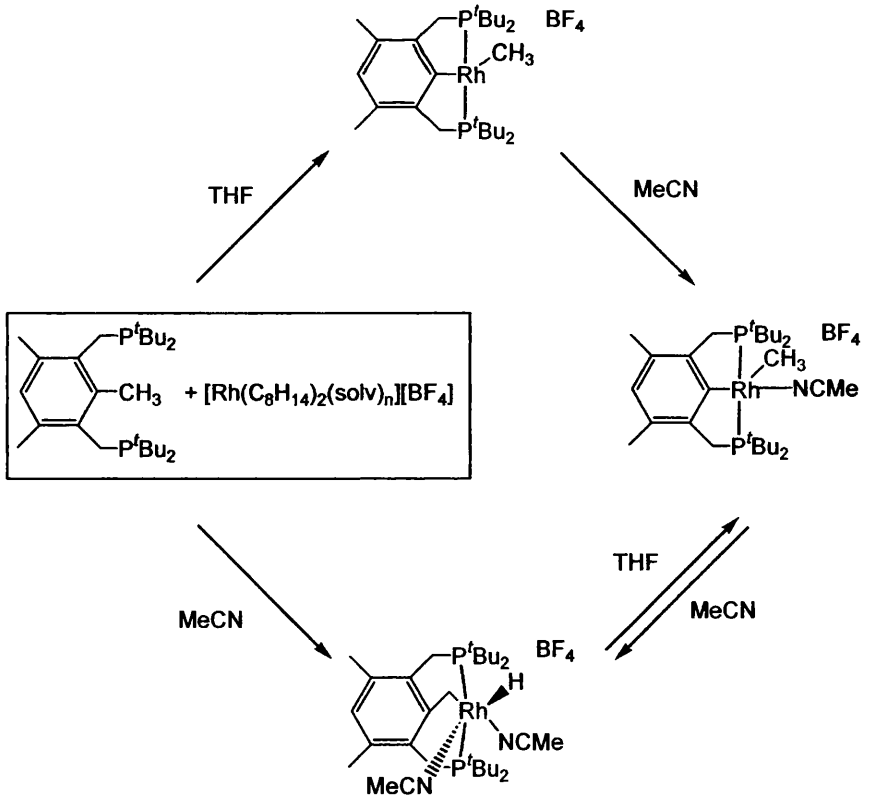


**Scheme 1.9.** Solvent effect on bond activation in PCP system.

Jones has done extensive investigative work on the cleavage of C-C bonds with transition metals.[60-63] He utilises biphenyl ligands and, more recently, aromatic amines to participate in C-C activation. Initially he employed rhodium as the metal centre as this forms strong metal-aryl bonds. This was precoordinated with a substituted cyclopentadienyl ligand, which has been shown to direct the metal to the target C-C bond.[64] Jones believes that this reaction proceeds *via* a C-H activated complex, followed by $\eta^2$ coordination, before the C-C bond is attacked (scheme 1.10.). This work has been extended to include palladium, platinum, cobalt and nickel complexes with chelating PP and PN ligands and aromatic nitriles.[45,62,65-67]

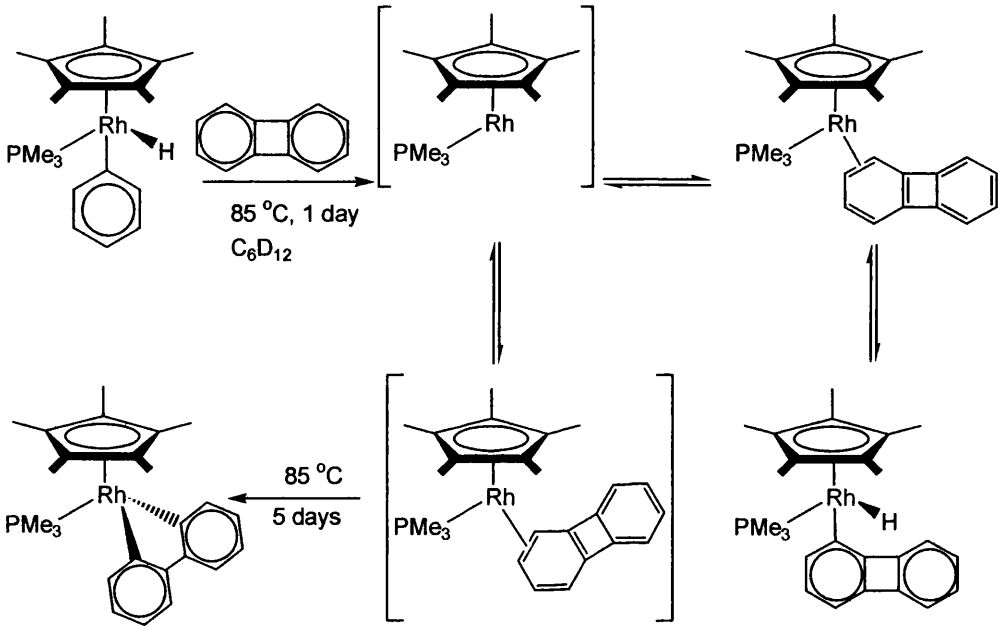


**Scheme 1.10.** C-C activation of biphenyl in rhodium-Cp* complex.

## 1.2. N-heterocyclic carbene complexes

The use of N-heterocyclic carbenes (NHCs) in organometallic chemistry, particularly for applications in homogeneous catalysis, is a rapidly growing area of chemistry. The discovery that NHCs can be used in place of phosphine groups on metal centres, often to give much better catalysts, has prompted a flurry of research

into the area with the best, and most widely employed, examples being synthesised by Grubbs for use in alkene metathesis (figure 1.6.).[68-71]

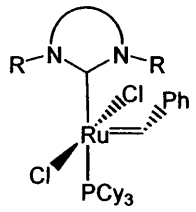


**Figure 1.6.** An example of a generic NHC catalyst developed by Grubbs for alkene metathesis.

This introduction covers the basic chemistry of NHCs and NHC-metal complexes and discusses the bond activation reactions that have been observed in them.

### 1.2.1. N-heterocyclic carbenes

Carbon generally forms compounds where all four of its valence electrons are utilised in bonding to other atoms. In carbenes, however, the carbon atom only forms two bonds thus leaving two spare electrons.

Most carbenes have a bent geometry, with bond angles between 100 ° and 150 °[72] and in these bent molecules, the two non-bonding electrons can exist in two states, known as the triplet and singlet states. The triplet state consists of two unpaired electrons, one in the $sp^2$ hybridised orbital and one in a $p$ orbital. These types of carbenes are generally short lived and difficult to isolate but are detectable as intermediates in reactions using electron spin resonance spectroscopy due to their unpaired electrons. When both electrons reside in a non bonding $sp^2$ hybridised orbital this is known as a singlet state and it results in the presence of an empty $p$ orbital (figure 1.7.).


triplet carbene singlet carbene

**Figure 1.7.** The triplet and singlet states of carbenes.

All carbenes can exist in either a singlet or a triplet state but Bertrand notes that the singlet state is usually favoured over the triplet if there is a larger σ-π separation.[73] Hoffman made the assumption, from investigations into trimethylene ($CH_2CH_2CH_2$), that a triplet ground state arises when the energy levels are separated by less than 1.5 eV and that a singlet states arises when the energy levels are at least 2 eV apart.[74] The importance of the energy gap between the orbitals means that the substituents on the carbenic carbon largely determine the state of the carbene. Carbenes found in the singlet state have electron rich substituents such as Cl, which place π lone pairs next to the carbenic carbon. These can interact with the empty *p* orbital on the carbenic carbon atom, producing a lower energy orbital which the two electrons occupy. Singlet carbenes show both electrophilic and nucleophilic reactivity because they have both an empty *p* orbital and a lone pair of electrons.

As early as 1962, Wanzlick realised that by tuning the vicinal groups on the carbene so that they provide π-donor/σ-acceptor character to fill the empty *p* orbital on the carbene, the electrophilicity of the singlet carbene would be reduced (figure 1.8.). This is because the lone pair on the carbene is stabilised and would reduce the reactivity of the carbene therefore allowing it to be isolated.[75,76]

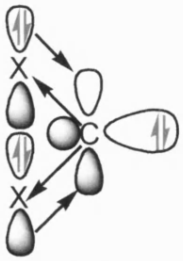


**Figure 1.8.** σ-acceptors and π-donors vicinal to the carbene-carbon atom stabilise singlet carbenes.

It was not until 1991, however, that Arduengo managed to isolate a stable singlet carbene with nitrogens in the vicinal position bearing adamantyl groups (figure 1.9.)[77]. Arduengo attributes Wanzlick's failure to isolate a stable singlet carbene as being due to the inconvenient physical properties of the carbene and possible problems with respect to the purity of the starting material.[78]

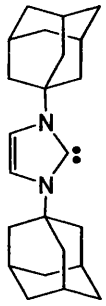

**Figure 1.9.** IAd, first isolated by Arduengo. It is remarkably stable and sealed under a few atmospheres of CO, showed no decomposition for 7 years.

As predicted by Wanzlick, and demonstrated by Arduengo, the electron donating abilities of the vicinal substituents are highly important in stabilising carbenes. Most stable, isolable singlet carbenes have nitrogen donors next to the carbon to donate electron density into the empty π orbitals of the carbon. They also generally form part of a ring and this provides steric stabilisation for the carbene. These types of carbenes are known as N-heterocyclic carbenes (NHCs). Since Arduengo's successful synthesis of the adamantyl substituted NHC (IAd), many other members of the family have been synthesised, including IMe[79], I$^i$Pr$_2$Me$_2$[80], IMesH$_2$[81] and the bidentate NHC IMe(CH$_2$)$_2$IMe[82] (figure 1.10.).

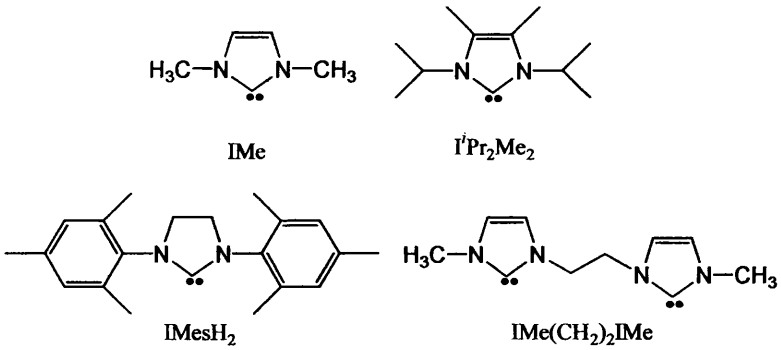


**Figure 1.10.** Series of other NHCs with different functional groups and chelating structures.

The stability of NHCs is greatly affected by the steric parameters of the nitrogen substituents. Although IMe is a moderately stable oil at room temperature (it needs to be kept under an inert atmosphere), generally the larger the R groups, the more stable the carbene.[76] In addition, having substituents on the backbone stabilises the NHC. $IMe_4$ (with methyl groups on the backbone) is a solid at room temperature and can be handled in air (although not for long periods of time).

Certain NHCs, especially those with saturated backbones, have a propensity to dimerise and this has been termed the Wanzlick equilibrium.[83] Herrmann attributes this phenomenon to the shrinking of the singlet-triplet gap when the backbone is saturated.[84] This arises from the loss of π-delocalisation, which adds inherent stabilisation to the free NHC. Recently, Alder *et al.* have carried out an extensive investigation into the kinetics and mechanism of the dimerisation of diaminocarbenes, which are not part of a ring system.[85] They found that the filled $sp^2$ lone pair orbital of one carbene needs to approach the empty *p* orbital of another for dimerisation to proceed (figure 1.11.). However, the bigger the steric bulk of the N-substituents, the more sterically hindered this transition state becomes, hence preventing dimerisation.

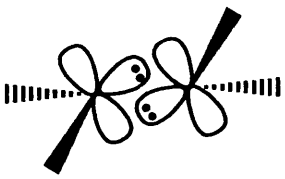

**Figure 1.11.** Transition state geometry for the dimerisation of singlet carbenes.

According to Herrmann, the electronic features of the NCN moiety in NHCs is also crucial to their stability.[84] He attributes this to two effects. Firstly, the difference in electronegativity of nitrogen and carbon accounts for an inductive effect that stabilises the pair of unshared electrons in the in-plane carbene orbital. In addition, the unoccupied *p* orbital yields a π-resonance interaction where the nitrogen atoms donate their lone pairs to the carbon.

1.2.2. A comparison of NHCs to phosphines

Phosphine ligands ($PR_3$) are used to a large degree in organometallic catalysis. This is, in part, due to their relative inertness. Although some examples have been highlighted earlier in this chapter where phosphines have undergone *ortho*-metallation reactions, this is the exception rather than the rule. In general, phosphines act as spectator ligands, stabilising reaction intermediates. In addition, they are labile and can come off the metal centre under the right conditions, leaving a vacant 2-electron site where substrates can bind and undergo transformations. Phosphines provide a rich range of chelate, pincer, tripod and other ligand architectures, which allow tuning and selection of various catalytic pathways.

NHCs are often described as phosphine mimics because they possess many of the same characteristics as phosphines.[76] In particular, the lone pair of electrons which can be donated to a metal. In addition, they are able to be functionalised[86] and to be made chiral.[87] They can also be water soluble,[88-90] like phosphines and have immobilised derivatives, making purification easier.[91]

However, there are important fundamental differences between NHCs and phosphines. NHCs have a two dimensional structure as opposed to the ball shape of phosphines and, when complexed to a metal, the M-C bonds are generally more σ-donating in nature than the more π-accepting M-P bonds. Many NHC based catalysts (for example, those used for the Heck reaction) also exhibit longer life times in catalytic cycles than their phosphine analogues. This has been suggested to be because NHCs are retained on the metal centre better than phosphines.[92] NHC complexes also tend to be more air and moisture stable than the equivalent phosphine complexes.[93]

As the substituents on NHC ligands are an extra bond away from the metal centre compared to phosphines, they provide an umbrella-like influence on the metal, shielding it with the substituents on the nitrogen (figure 1.12.). This allows

coordinatively unsaturated metal centres to be stabilised and also helps small molecules to interact with the metal centre. However, this additional bond also enhances the susceptibility of the substituents to activation. This phenomenon is discussed in more detail later.

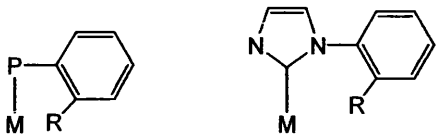


**Figure 1.12.** The R group in a M-NHC complex is one more bond away than in a M-$PR_3$ complex.

Bidentate and tridentate NHC ligands are also known. However, as Crabtree points out,[86] these do not have the same advantages in functionality as their phosphine equivalents because they often do not chelate and will instead bind to two separate metal centres or form other undesirable products.[94] Crabtree attributes this to tendency of NHCs to bind irreversibly to a metal centre. This means that the initial kinetic binding mode is unable to be corrected and thus is retained in the product. Phosphines, however, are more labile and will undergo reversible binding reactions until the thermodynamic, chelated, product is achieved.

Until recently there was no definitive way to compare the steric bulk of various NHC ligands as there is with Tolman's cone angle calculations for phosphines.[95] However, Nolan has now created the concept of percentage buried volume for NHCs. This system is particularly useful as it also allows NHCs to be compared to phosphine ligands.[96] The values have been calculated both experimentally and computationally. The theory takes into account the closest carbon substituent on the NHC (placed at 2 Å in calculated structures) to the metal centre and calculates the volume of a sphere (at 3 Å from the metal centre) that the ligand occupies (% $V_{Bur}$) (figure 1.13.). The values obtained for the % $V_{Bur}$ of various ligands on [Cp*Ru(L)Cl] (L = $PR_3$, NHC) were plotted against experimentally determined bond dissociation energies (BDEs) and clearly show a linear relationship, suggesting that BDEs are essentially controlled by the steric requirements of the ligands (figure 1.14.).

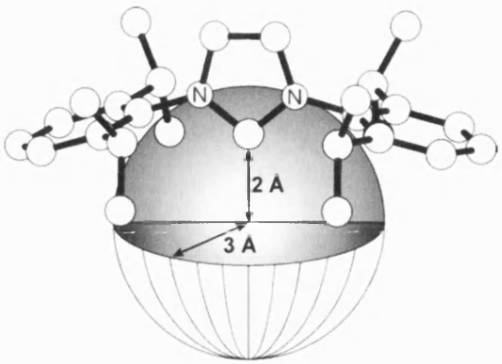


**Figure 1.13.** Sphere dimensions for steric parameter determination (%$V_{Bur}$) of NHC ligands.

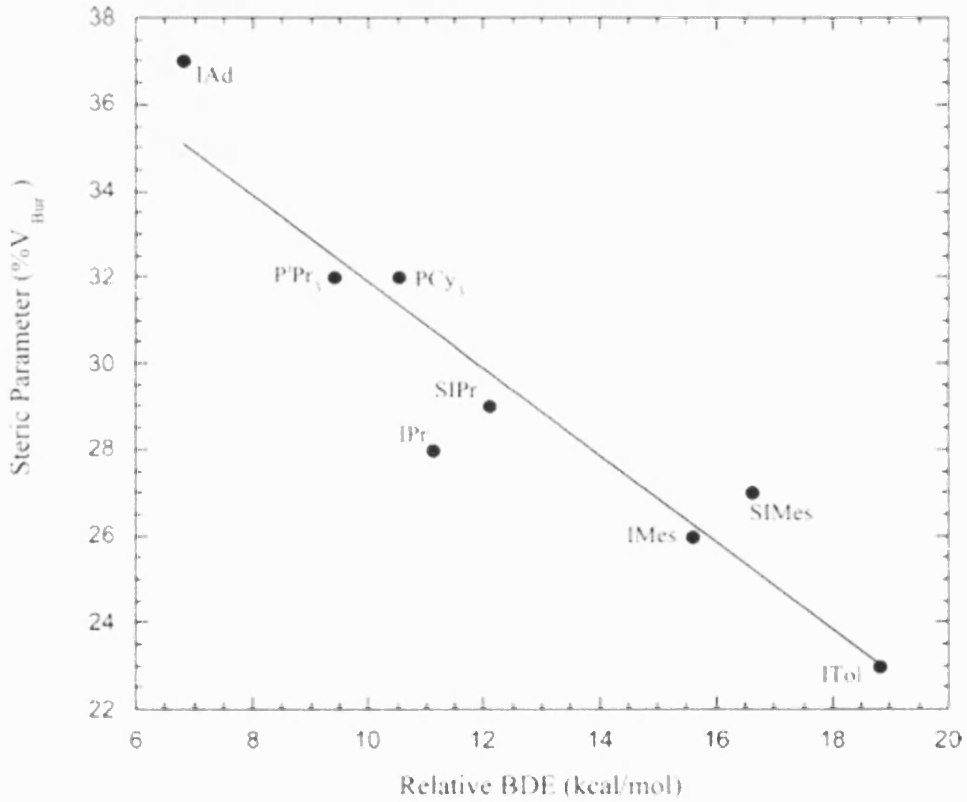


**Figure 1.14.** Relative bond disruption enthalpy (kcal/mol) *vs* steric parameter (%VBur) in the [Cp*Ru(L)Cl] system (slope: -1.01; R: 0.94). SIMes = $IMesH_2$, SIPr = $IPrH_2$.

The steric properties of NHCs are more influential on the ligand sphere than phosphines or the other common spectator ligands, cyclopentadienyls. This is due to their two dimensional structure. Phosphines and cyclopentadienyls are cone shaped so rotation about the M-L bond should not greatly affect either their steric or electronic properties. In monodentate NHC complexes, the NHC ligand will tend to rotate so that any steric clash with the other ligands is minimised.[86]

Having substituents on the backbone of an NHC ligand such as methyl groups or chlorine should, intuitively, affect the reactivity. This has been shown to be the case by Magill and co-workers who determined computationally the relative basicities of a series of NHCs in aqueous solution.[97] I$^i$Pr$_2$Me$_2$ is more basic, and thus more nucleophilic, than the analogous NHC without the methyl groups on the backbone, I$^i$Pr$_2$ (p$K_a$ = 30.4 ± 0.3 for I$^i$Pr$_2$Me$_2$, 28.2 ± 0.3 for I$^i$Pr$_2$). This implies that the methyl groups on the backbone increase the electron donating properties of the NHC ligand.

There have been a few experimental and computational studies into the electronic properties of NHCs as ligands. These have used the IR shifts of $\nu_{CO}$ resonances to compare the influence of N-alkyl and N-aryl groups and also to compare the effect of changing the substituents on the imidazole backbone. In all of these studies very little difference was found between the NHC ligands (in [Ni(L)(CO)$_3$], L = IMes, $\nu_{CO}$ = 2051, 1970 cm$^{-1}$; L = IMesH$_2$, $\nu_{CO}$ = 2052, 1971 cm$^{-1}$; L = ICy, $\nu_{CO}$ = 2050, 1965 cm$^{-1}$)[98] themselves although they were found to be generally better donors than phosphines.[98-100] In contrast, the R group on phosphine ligands significantly changes the $\nu_{CO}$ stretching frequency (in [Ni(L)(CO)$_3$], L = PPh$_3$, $\nu_{CO}$ = 2069, 1990 cm$^{-1}$; L = PCy$_3$, $\nu_{CO}$ = 2056, 1973 cm$^{-1}$)[98]. Crabtree rationalises this phenomenon because of the extra bonds between the donor atom in NHCs and the R group. This means that the donor atom essentially retains the same immediate environment.[86] However, the better donor properties of NHCs compared to phosphines have been shown by comparing $\nu_{CO}$ shifts of analogous complexes both computationally and experimentally. For example, [Rh(Cl)(IMes)$_2$(CO)] has a $\nu_{CO}$ stretching frequency of 1935 cm$^{-1}$ whereas the band for [Rh(Cl)(P$^i$Pr$_3$)$_2$(CO)] comes at 1943 cm$^{-1}$.[101,102]

1.2.3. Metal complexes with NHCs

Although Lappert synthesised metal-NHC complexes in the late 1970s and early 1980s these came from the cleavage of the electron-rich C-C bond in an enetetramine (the dimeric form of the NHC, figure 1.15.) which were neither as versatile or as easy to complex with a metal as Arduengo's free NHCs.[103-128] Lappert's work is still important, however, and his enetetramine method is still used occasionally today.[129] His work is discussed in more detail in chapter 3.

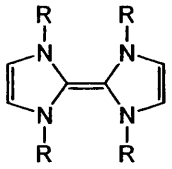

**Figure 1.15.** A generic enetetramine.

Many of the metals of the Periodic Table have now been incorporated into stable metal-NHC complexes. NHCs have an amazing capacity to coordinate to metal centres, whether they are electron rich transition metals ($Pd^0$, $Rh^I$), electron poor main group metal cations ($Be^{2+}$) or high oxidation state metals ($Ti^{IV}$, $Re^{VII}$).[84] The metal-carbon bond is often described as a strong σ-bond and is usually about the length of a typical metal-hydrocarbon single bond (2.1 Å). Compared to phosphines, NHCs have a considerably higher donor capacity to the metal centre, but their π-acceptor capability is only relatively small, more comparable to nitriles and pyridine.

Although NHCs are generally touted as poor π-acceptors, Taube and Clarke noted in 1975, a band at 348 nm in the UV visible spectrum of a ruthenium-NHC complex that suggested that metal-ligand charge transfer, or back-bonding was occurring (figure 1.16.).[130] Since then, calculations have suggested the presence of back-bonding in late transition metal complexes.[131-134] Although these all suggested that σ-bonding accounts for more than 70 % of the stabilising orbital energy, this does suggest that NHC back-bonding is not a negligible effect. Meyer and co-workers suggest that if π-back-bonding in metal-NHC complexes is significant, the length of the N-C bonds in the imidazole ring should increase when the NHC is bound to

more electron-rich metal centres.[135] They compared crystal structures of bis IMes complexes of electron poor $I^+$ that is incapable of back-bonding (N-C = 1.346 Å), Ni(0), which is electron rich and easily back-bonds (N-C = 1.375 Å) and Ag(I), which is somewhere in between (N-C = 1.358 Å). This certainly seems to suggest that back-bonding does play some role in the structure of metal-NHC complexes.

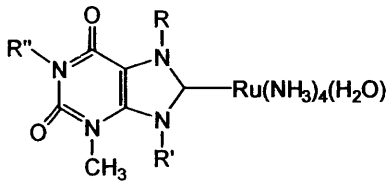


**Figure 1.16.** A ruthenium xanthine complex synthesised by Taube.

Experimental studies have shown that for several metals, NHCs (with the exception of the sterically demanding IAd) can replace phosphine ligands rapidly and without the need for the NHC to be present in excess to drive the equilibrium potential.[76,136,137] However, both Caddick[138] and Baird[139] have noted that phosphine is capable of replacing NHCs in certain systems. Baird has carried out equilibrium studies on the formation of $[Co(Me)_2(IPr)(Cp)]$ from $[Co(Me)_2(PPh_3)(Cp)]$. After approximately four hours an equilibrium had been established, which was then analysed at a range of different temperatures (30, 35, 40, 45 and 50 °C) to obtain equilibrium constants. These show that enthalpically the displacement of $PPh_3$ by IPr is favourable and the exothermicity of this ligand exchange drives the reaction forward. However, in this particular system, the formation of the NHC substituted product is entropically unfavourable and counteracts the forward reaction. This negative entropy is most likely to arise as a result of steric factors. $[Co(Me)_2(IPr)(Cp)]$ is a relatively crowded molecule, causing a significant loss of internal motion compared to the starting materials, which would result in a large negative value for $\Delta S$.

### 1.2.4. Catalytic reactions with NHC complexes

Having a vacant site on the metal is an essential requirement of any homogeneous catalyst. This allows substrates to bind to the metal centre and interact

intramolecularly with other ligands on the metal. Therefore, one or more of the ligands bound to the metal needs to be sufficiently labile to dissociate and allow coordination of substrate molecules.

The most common ligands found in homogeneous catalysis are phosphine groups. This is due to their lability but also the high selectivity that they add to a reaction. For example, the steric bulk of phosphine ligands means that, when attached to a metal catalyst, they will help it hydrogenate terminal alkenes much faster than internal ones.[140]

As already mentioned, Grubbs has demonstrated that replacing a phosphine ligand with an NHC for alkene metathesis leads to higher selectivity and rates of reaction. The many variations of Grubbs catalyst that have now been synthesised and utilised in catalytic cycles are discussed in detail in chapter 2. The replacement of phosphine ligands by NHCs on rhodium catalysts is thoroughly explored in chapter 3.

As well as metathesis reactions, NHC complexes have been found to be efficient in a variety of cross-coupling reactions. Sonogoshira,[141,142] Kumada,[142,143] Buchwald-Hartwig[144], Stille[142,145,146] and Suzuki-Miyaura[146-149] reactions have all been shown to be promising using palladium NHC-based catalysts. There are also many examples of Heck[76,150-155] reactions being successfully catalysed by Pd-NHC complexes. Nolan attributes the excellent ability of NHCs to act as supporting ligands to their thermal stability and their tuneable steric and electronic parameters that stabilise the Pd(0) species prior to oxidative addition of the substrate.[142]

All of these catalysts facilitate coupling reactions, forming a C-C bond between two different substrates. They are all currently receiving much attention and new complexes bearing NHCs are emerging all the time and being tested in catalytic reactions. The Heck reaction, one of the most widely used methods to prepare variously substituted alkenes, dienes and precursors to conjugated polymers, provides an example of how this type of chemistry is proceeding.

*1.2.4.1. Synthesis of Heck catalysts*

Some examples of Heck-type reactions are shown in scheme 1.11. Computational studies on a chelating NHC-phosphine palladium complex [Pd(IH($CH_2$)$PH_3$)] initially suggested that it would be efficient in the Heck reaction[156] and Herrmann *et al* demonstrated this with the synthesis of a diiodo catalyst that was particularly stable and thus gave high catalyst turnover numbers.[153] Cavell and co-workers have now synthesised and trialled a large number of palladium and nickel NHC complexes in the Heck reaction with great success.[157-161] One of the best examples is shown in figure 1.17. and this catalyses the coupling of phenyl iodine and butyl acrylate, going to 90 % completion in 5 hours with a TON of 4,600 (0.02 mol %, 120 °C, $CD_2Cl_2$).[162]

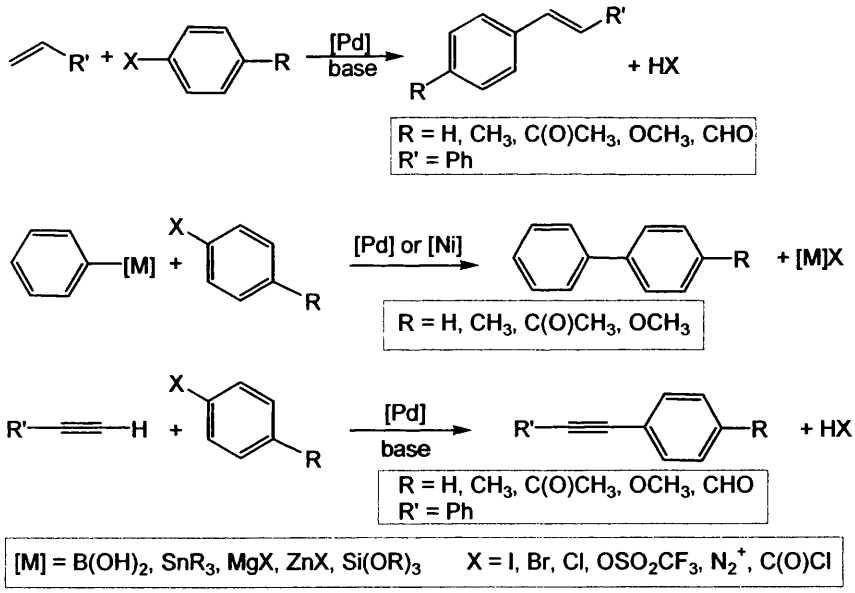


**Scheme 1.11.** Various Heck coupling reactions.

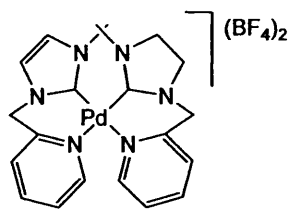


**Figure 1.17.** Structure of one of Cavell's Heck reaction catalysts.

*1.2.4.2. Decomposition of Heck catalysts*

Whilst investigating the Heck reaction with various Pd(NHC) catalysts, Cavell discovered that these types of complexes, particularly cationic ones, can undergo what are probably concerted reductive elimination reactions in solution at room temperature to yield the imidazolium salt and a M(0) species (scheme 1.12.).[157,163] Cavell has shown that as the temperature of the reaction is increased, the rates of migratory insertion and β-elimination, which lead to the Heck coupling product become more competitive with the reductive elimination reaction.[164] Nickel complexes undergo similar reactions to the palladium analogues.[161]

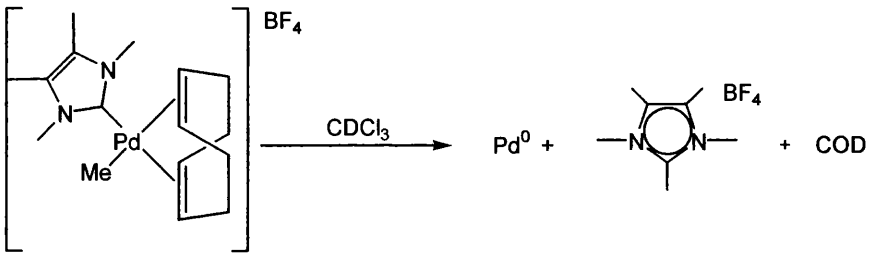


**Scheme 1.12.** The decomposition route of a Pd-NHC complex.

Calculations have shown that this reductive elimination reaction is much more unfavourable, due to the high activation energy barrier, when the ligand used is a chelating NHC.[165] This appears to be because as the reductive elimination reaction proceeds, the bite angle between the other ligands opens up and therefore the angle between the carbene and the methyl group is forced to get smaller. This allows effective orbital overlap and hence rapid reaction. However, if a chelating ligand is present, either as the spectator ligand or one in which the NHC is a part of, this process will be impeded.

Similarly, when these types of complexes are reacted with CO, preliminary addition of CO to the metal centre is rapidly followed by reductive elimination to give both the imidazolium salt and an acylimidazolium salt along with a Pd(0) species. This observation probably accounts for the reason that, to date, there is only one reported successful use of a Pd(NHC) complex in the copolymerisation of CO and ethene.[114]

1.2.5. Oxidative addition of imidazolium salts to metal centres

Previous reports suggested that reactions carried out in imidazolium based ionic liquids led to formation of metal-NHC complexes *via* oxidative addition reactions.[166-168] This is essentially the reverse reaction to the reductive elimination discussed above and leads to the intermolecular breaking of a C-H or C-C bond.

Cavell and Yates used DFT calculations to study Pt(0) complexes, which are generally considered to be more favourable to oxidative addition than Pd(0).[159] From the investigation they concluded that the oxidative addition of the C-C bond of an imidazolium salt to Pt(0) is exothermic ($\Delta H$ = -55.6 kJ $mol^{-1}$), although the activation barrier is quite high (114.5 kJ $mol^{-1}$). Experimental work proved that this reaction was feasible (scheme 1.13.) and this has wide reaching implications for the use of imidazolium salts as ionic liquids, which have been touted as environmentally friendly alternatives to current solvents.[159,169] If the solvent can interact with the catalyst that it is supposed to be solvating then the reaction will be rendered impossible. Recently, Nolan[170] and Crabtree[171] have both reported the oxidative addition of imidazolium salts to Pd(0) centres.

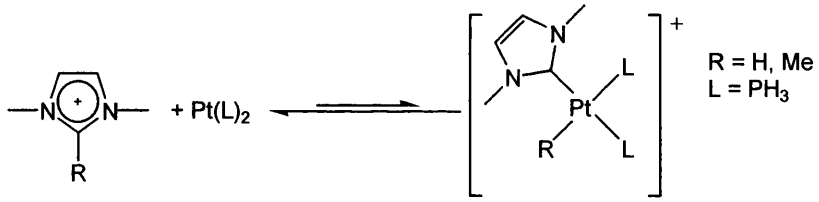


**Scheme 1.13.** Oxidative addition of imidazolium salt to Pd.

Although this oxidative addition process can be problematic when using imidazolium based ionic liquids as a solvent, it can prove useful for generating metal-NHC complexes *in situ*. NHCs are often difficult to handle in the laboratory as they are air and moisture sensitive. This means that large scale preparations of NHC catalysts are very difficult to achieve. Imidazolium salts are generally able to be stored under air at room temperature with no decomposition. Grubbs has been exploring ways to create a catalyst directly from a "protected" form of the free NHC,

adding an alkoxide or trichloromethyl group to the carbene carbon which then eliminates alcohol or chloroform to leave the NHC free to coordinate to the metal centre[172] and this method of synthesis has recently become more widespread.[94,171,173]

## 1.2.6. Abnormal binding of NHCs

Crabtree and Clot have done a lot of investigative work, both synthetically and computationally into the abnormal binding of NHCs onto metal centres. Generally an NHC will bind to a metal *via* the C(2) position. However, Crabtree has found that in certain systems, particularly those with a lot of steric bulk, binding to the metal can occur at the C(5) position (figure 1.18.).[174]


C(2) position C(5) position

**Figure 1.18.** Normal and abnormal binding of NHC ligand to a metal centre.

The imidazolium ligands that Crabtree employed to achieve this abnormal binding have a pyridine moiety on one of the N-arms and an alkyl group ($^{i}$Pr, $^{n}$Bu, Me) on the other side. During reaction with $[Ir(H)_5L_2]$ (L = $PPh_3$), two molecules of $H_2$ were lost to give a bidentate complex, with a Ir-N bond to the pyridine moiety and the NHC group bound to the metal *via* abnormal C(5) binding (scheme 1.14.). Even heating this complex at 100 °C for one hour did not cause the complex to revert to the 2-isomer. When R = Me the abnormal structure was formed in a 55:45 ratio to the C(2) complex. When R = $^{i}$Pr, the C(5) structure is the only isomer formed. These structures have been identified both by X-ray crystallography and heteronuclear NMR studies. In particular, the quaternary carbene resonance is indicative with the C(5) resonance coming at higher field (typically δ 142.0) than the C(2) resonance (δ 169.9).[175]

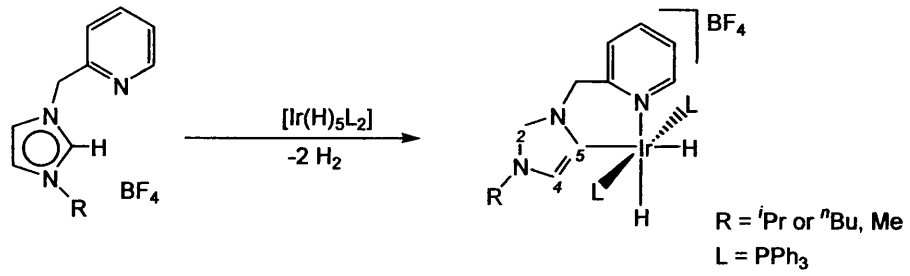


**Scheme 1.14.** Abnormal binding in NHC complex.

Initial DFT calculations on the iridium cation predicted that this abnormal type of binding is, thermodynamically, highly unfavourable in comparison to C(2) bonding (C(5) 41.6 kJ $mol^{-1}$ higher in energy than C(2)).[176] However, further calculations that included the $BF_4^-$ anion reduced the difference in energy between the two isomers to 6.6 kJ $mol^{-1}$ (in favour of the C(2) isomer). In addition, they also suggested that the $BF_4^-$ anion was hydrogen bonded to the C(2) C-H bond when the complex was in the abnormally bound arrangement.[175] From these observations, Crabtree went on to show that when the counterion was $Br^-$, C(2) binding of the NHC was favoured (91:9), whereas when $SbF_6$ was used, C(5) was predominant (89:11) (for the complex where R = Me).

Further studies have also shown that the NHC does not need to be chelating to bind with C(5) geometry, if the C(2) position is blocked with a methyl group, although these complexes are much less stable than those with the pyridine ring.[100]

Similar abnormal binding modes have also recently been observed by Meyer[177] and Danopoulos.[178] Recently, Cavell has extended his investigations into oxidative addition of imidazolium salts onto platinum centres (discussed in section 1.2.5.) and showed that, when the C(2) position is blocked by a methyl group, oxidative addition can occur at the C(5) position.[179] Interestingly, bis NHC complexes could be synthesised with one NHC C(2) bound and one C(5) bound in a one-pot reaction (scheme 1.15.).

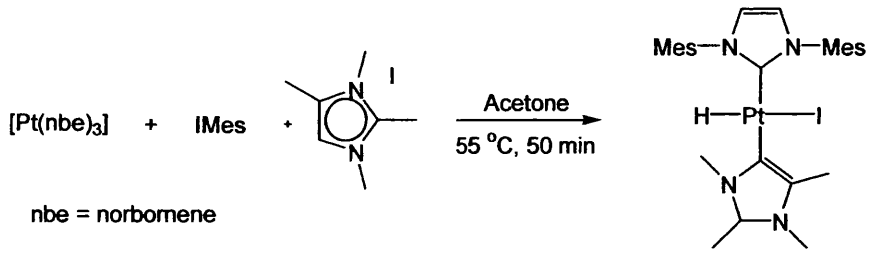


**Scheme 1.15.** Bis NHC complex with one ligand abnormally bound.

Cavell believes that the IMes ligand coordinates first, giving $[Pt(IMes)(nbe)_2]$. The tetramethyl imidazolium salt then undergoes oxidative addition to the metal centre at the C(5)-H position. When neither the C(4) or C(5) carbons have methyl groups on (and one of the N-alkyl groups is an $^n$Bu group), the product of the reaction (in acetone at 55 °C for 50 min), is a mixture of a C(4) and C(5) bound NHC (in a ratio of 1:1.8 with the C(5) isomer predominating (figure 1.19.).

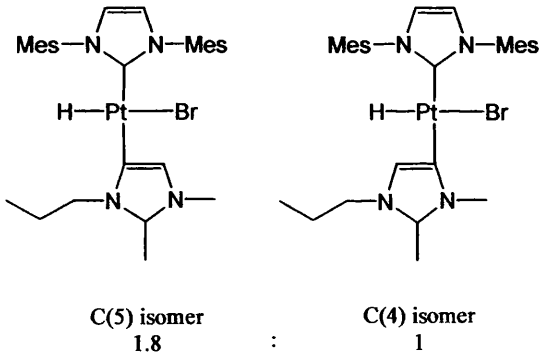


**Figure 1.19.** C(4) and C(5) bound isomers of Cavell's bis NHC complex.

In the presence of alkene these complexes undergo reductive elimination to regenerate the imidazolium salt and bind two equivalents of alkene (scheme 1.16.). The reductive elimination of the normally bound NHC was not observed.

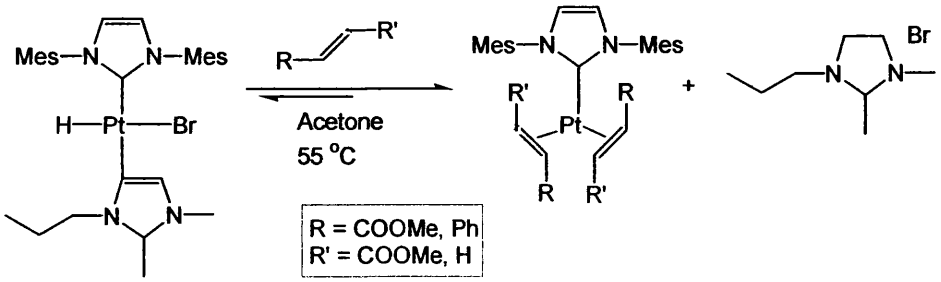


**Scheme 1.16.** Alkene binding to Pt centre after reductive elimination of abnormally bound NHC.

Nolan and Lebel have also found that, in the reaction of the N-mesityl imidazolium salt with $[Pd(OAc)_3]$ in dioxane at 80 °C, a bis NHC complex is formed, with one NHC ligand bound normally, at the C(2) position whilst another, *trans* to it, abnormally bound at the C(5) position.[180] Surprisingly, when the base $Cs_2CO_3$ was added to the reaction, only the C(2) isomer of the bis NHC complex was formed. The C(5) isomer could not be converted directly to the C(2) isomer upon addition of base. The catalytic reactivities of the two isomers proved to be quite different with the abnormally bound isomer proving more efficient in the Heck reaction and the Suzuki-Miyaura reaction (coupling reactions used shown in scheme 1.17) than the normally bound one. This augments Cavell's findings that the abnormally bound isomer is more labile that the normally bound one thus allowing formation of a vacant site to generate a catalytically active species.

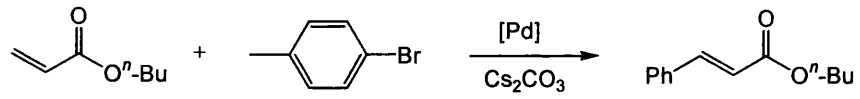


Heck reaction

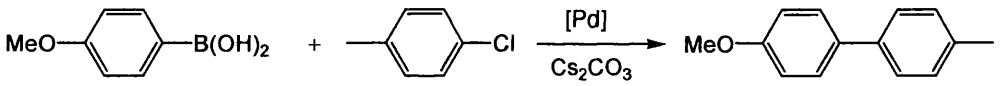


Suzuki-Miyaura reaction

**Scheme 1.17.** The Heck and Suzuki-Miyaura couplings shown above were more efficient when the bis NHC catalyst used had one abnormally bound NHC.

## 1.2.7. C-H bond activation in metal-NHC complexes

As early as 1977, Lappert and co-workers had noted that NHCs can undergo intramolecular C-H activation reactions.[181] Reacting the enetetramines (shown in scheme 1.18.) with $[RuCl_2(PPh_3)_3]$ in xylene at 140 °C led to spontaneous activation of an *ortho* phenyl C-H bond of the coordinated NHC ligand.[122] NMR spectroscopy clearly shows a large shift for the activated aryl proton from above 7 ppm to between 2 and 4 ppm. Lappert suggested that the mechanism involved an ionic species but also mooted the possibility of the involvement of a transient Ru(IV) species *via* oxidative addition of the aryl H and subsequent elimination of $H_2$ or HCl.

However, Lappert notes that in ruthenium complexes, *ortho*-metallation tends to proceed *via* formation of five-membered ring systems as opposed to the four-membered ring systems seen with rhodium and iridium complexes, and therefore initial oxidative addition is probably not sterically viable.

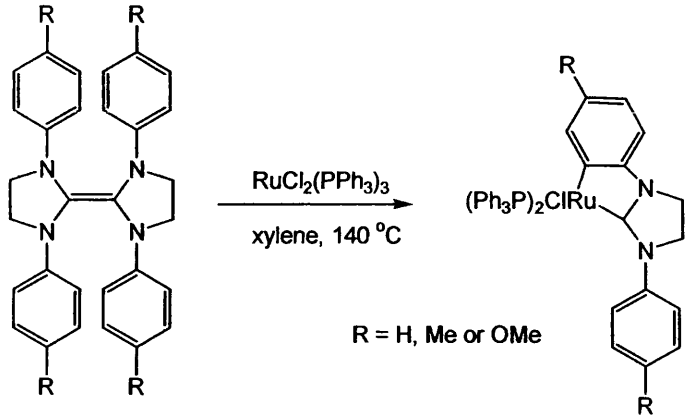


**Scheme 1.18.** C-H activation observed by Lappert in synthesis of a Ru-NHC complex from an enetetramine.

Recently, the observation of C-H activation of NHCs on metal centres has become more frequent, partly of course due to the much more widespread use of these ligands but also because of a better understanding of the nature of NHCs as ligands. Activation is not necessarily a good thing as it can be a potential deactivation route for catalytically important species, but due to the reversible nature of some of the bond activations, the NHC complexes can also be used as hydrogen stores, initially giving substrates $H_2$ but then being able to accept it back at the end of a cycle.

Grubbs found that if the preparation of his second generation metathesis catalyst, $[Ru(Cl)_2(IMesH_2)(PCy_3)(=CHPh)]$ (**2**), was not carried out under rigorously dry conditions, the C-H bond on one of the *ortho* methyl groups on a mesityl ring was activated leading to the product $[Ru(Cl)(IMesH_2)''(PCy_3)(CO)]$ (figure 1.20.).[68]

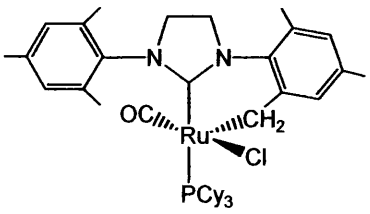


**Figure 1.20.** C-H activation in **2**.

Similar C-H bond activation processes have also been observed by Nolan.[101] At room temperature in THF, the Rh(I) dimer, $[\{Rh(COE)\}_2(\mu\text{-}Cl)_2]$ reacts with 4 equivalents of IMes to give [RhHCl(IMes)(IMes)''] (**3**) in high yield (figure 1.21.). **3** is very reactive, rapidly forming the dihydride complex $[Rh(H)_2Cl(IMes)_2]$ upon addition of $H_2$ at room temperature. Addition of CO to **3** affords $[RhCl(IMes)_2(CO)]$ (scheme 1.19.).

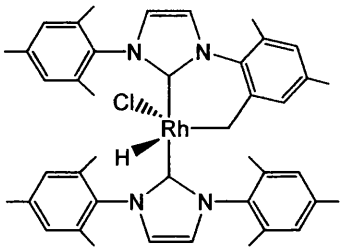

(3)

**Figure 1.21.** C-H activation of IMes on a rhodium centre.

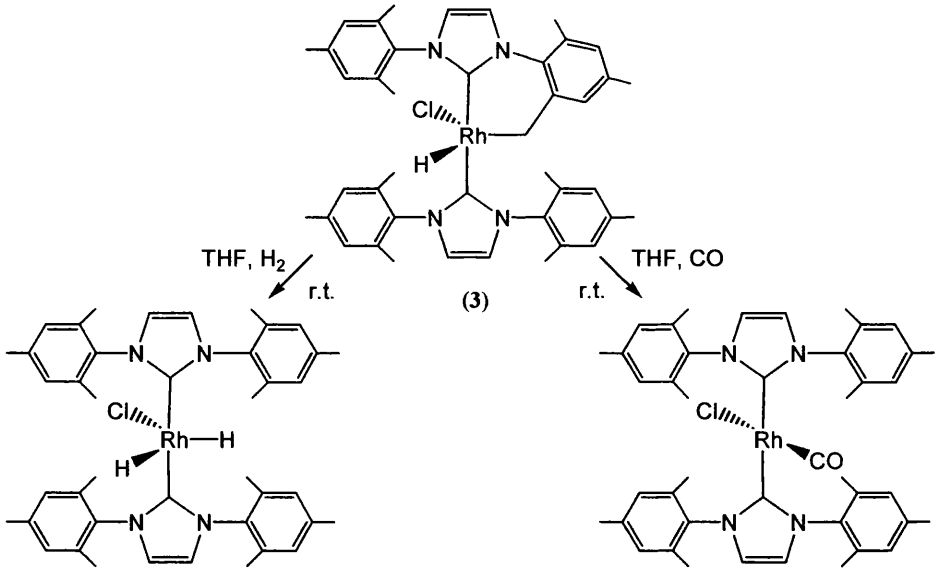


**Scheme 1.19.** Reversal of *ortho*-metallation by addition of $H_2$ or CO.

More recently, Nolan has observed double C-H bond activation of two I$^t$Bu ligands on both rhodium and iridium, giving $[MCl(I^tBu)''_2]$ (M = Rh (**4**) and M = Ir (**5**)) (figure 1.22.).[182,183] This subsequently allowed stabilisation of 14-electron metal centres that are rarely seen. **4** is the major product when the reaction is carried out in benzene. However, when the solvent employed is hexane, the bis NHC product isolated only has one C-H activated ligand, [RhHCl(I$^t$Bu)(I$^t$Bu)''] (**6**).

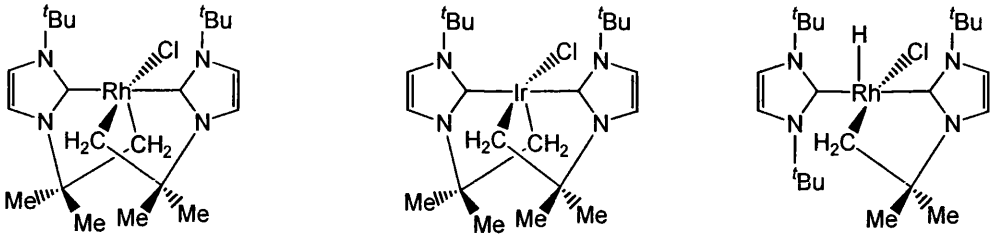

(4) (5) (6)

**Figure 1.22.** Double and single C-H activation in Ir and Rh NHC complexes.

Following the reaction in benzene by NMR spectroscopy showed that **6** forms on the way to **4** with loss of $H_2$ (scheme 1.20.). Although **6** only has one C-H activated NHC, a strong agostic interaction is present in the complex from one of the *tert*-butyl groups from the unmetallated NHC to the rhodium centre. This has been shown both by X-ray diffraction and NMR studies. By $^1$H NMR spectroscopy it can be seen that the hydride ligand and the protons from the agostic *tert*-butyl group are undergoing fluxional exchange in solution at room temperature.

Nolan attributes the influence of solvent on product isolation to differing solubilities of the products and thus, by using pentane as the solvent, was able to isolate the I$^t$Bu dimer, [{Rh(I$^t$Bu)(COE)}$_2$(μ-Cl)$_2$] (**7**) which precipitated out of the solution. Upon dissolution in benzene, **7** reacts with I$^t$Bu to form **4**. Isolated **7**, in a benzene solution free from NHC, is stable.

In the case of the analogous iridium complex, the mono activated complex, [IrHCl(I$^t$Bu)(I$^t$Bu)''], (**8**) (again with a strong agostic interaction to the unactivated I$^t$Bu ligand) was isolated from benzene after stirring at room temperature for 20 h whereas the double activated product, **5**, was isolated from the same solution when it was stirred for 5 days at room temperature. The X-ray structure of **5** is almost analogous to that of **4** but **5** has an additional agostic interaction from one of the unactivated $^t$Bu groups to the metal centre. However, there is no evidence from $^1$H NMR spectroscopy for this agostic interaction being retained in solution. The mixed

dimeric species that precedes the formation of the activated species could not be isolated or observed by $^1$H NMR spectroscopy.

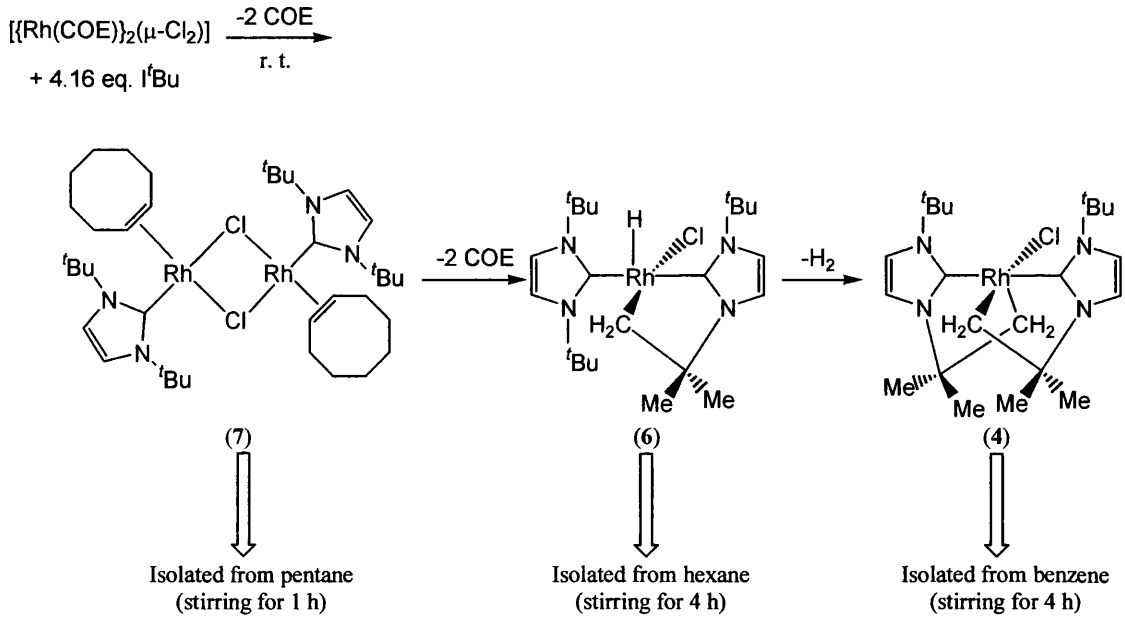


**Scheme 1.20.** Formation of double C-H activated rhodium complex *via* dimer and mono activated complex.

Following the formation of both **4** and **5** by $^1$H NMR spectroscopy gave some insight into the differing rates of reaction. In the reaction of $[\{M(COE)_2\}(\mu\text{-}Cl)_2]$ (M = Rh or Ir) with 2 equivalents of I$^t$Bu, only unreacted starting material and **8** were observed for M = Ir. However, when M = Rh, the reaction was more rapid and gave a mixture of **7**, **6** and **4** as well as starting material.

Addition of $AgPF_6$ to **4** and **5** in $CH_2Cl_2$ led to abstraction of the chloride ligand and formation of the 14-electron complexes $[M(I^tBu)''_2][PF_6]$ (M = Rh (**9**), M = Ir (**10**)) (figure 1.23.). Surprisingly, the iridium cation, **10**, can also be obtained directly from the mono-activated complex, **8**, suggesting that the initially formed cationic complex $[Ir(I^tBu)(I^tBu)''][PF_6]$ must undergo a rapid second cyclometallation (within 2 hours). Bergman has already noted that Ir(III)(Cp*) species such as $[Ir(Me)(PMe_3)(Cp^*)(CH_2Cl_2)][BAr_f]$ are more prone to undergo C-H activation processes than their neutral analogues like $[Ir(Me)(PMe_3)(Cp^*)(OTf)]$.[13] Addition of CO to **4**, **5**, **9** and **10** leads to coordination of CO to the metal centres (scheme 1.21.).

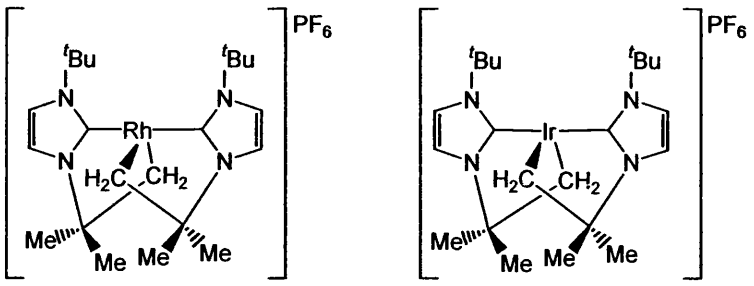


(9) (10)

**Figure 1.23.** Cationic, 14-electron complexes with double C-H activation.

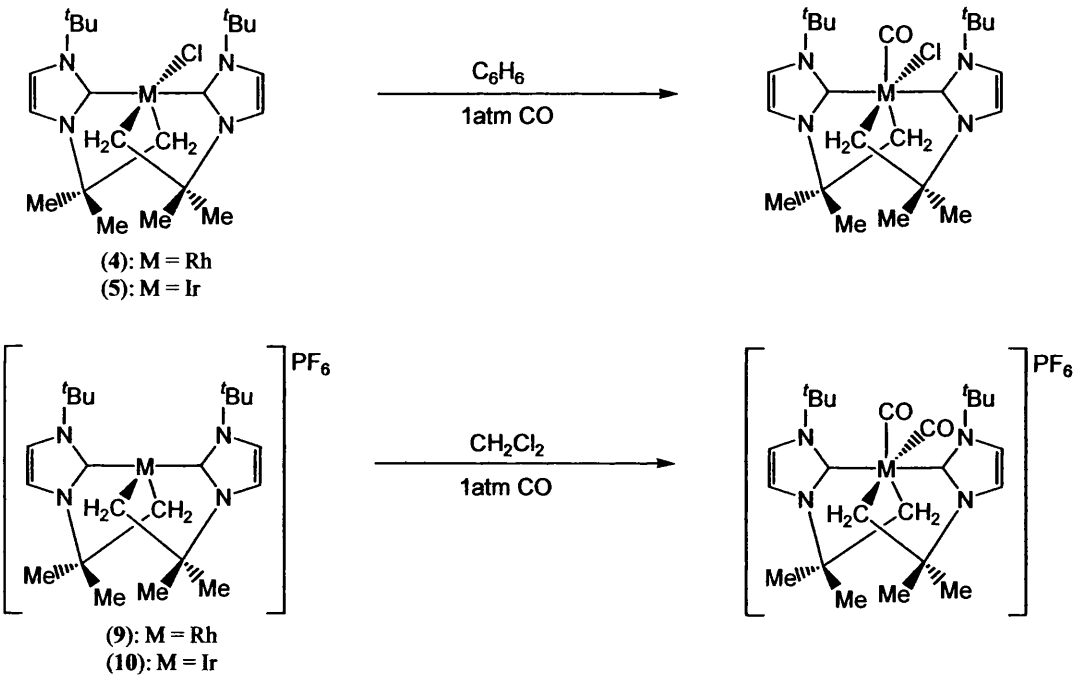


(4): M = Rh
(5): M = Ir

(9): M = Rh
(10): M = Ir

**Scheme 1.21.** Addition of CO to C-H activation products.

Both the π-orbital of the NHC and the σ-orbitals of the C-H bonds from the $^t$Bu groups can donate electron density to alleviate the electron deficiency on the metal of complexes **9** and **10**. By using computational methods, Nolan finds that the π-orbital of the NHC is much preferred over the σ C-H orbitals and this explains the absence of agostic interactions and the remarkable stability of the complexes. This finding augments the growing weight of evidence that NHC ligands are not the simple σ-donating ligands that they were originally assumed to be. In addition to the

back-bonding ability proposed by Meyer[135] and discussed in section 1.2.3., Nolan has now shown that NHCs have the ability to donate electron density from their π-orbitals to the *d* orbitals of electron-poor metal centres. Nolan suggests this finding may explain why NHC-stabilised catalytically active species, which are often highly unsaturated, are often much more stable than their phosphine analogues.

Danopoulos *et al.* have recently synthesised an N-pyridine NHC which, when reacted with $[\{Rh(COD)\}_2(\mu\text{-}Cl)_2]$, initially forms a mono-NHC complex with a close interaction between the metal centre and one of the aryl protons and then, upon addition of $NaBAr_F$, gives a cationic C-H activated cationic species (scheme 1.22.).[184] When $[\{Ir(COD)\}_2(\mu\text{-}Cl)_2]$ was used as the starting material, the neutral mono-NHC activated complex was formed (figure 1.24.).

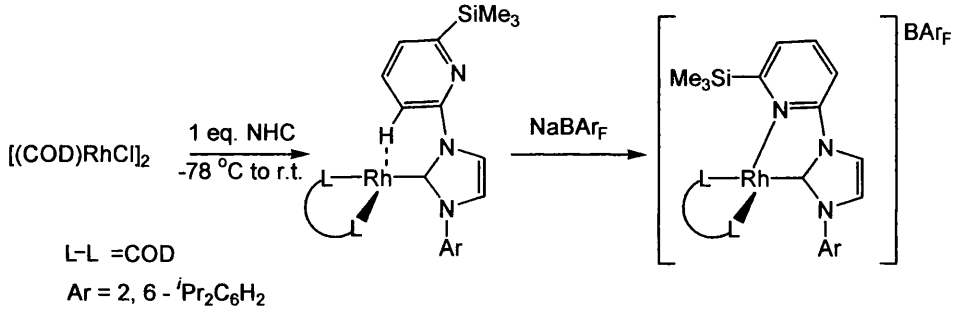


**Scheme 1.22.** C-H activated rhodium NHC complex.

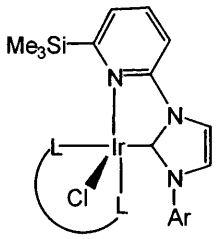


**Figure 1.24.** C-H activation of pyridal NHC on an iridium centre.

Herrmann has investigated the selective functionalisation of an iridium (III)-NHC complex, where the NHC employed is ICy.[185] When $[Ir(CH_3)_2(Cp^*)(ICy)]$ is treated with triflic acid, methane is eliminated to give the cationic species $[Ir(CH_3)(ICy)(Cp^*)][OTf]$. In solution this undergoes further reaction *via* β-hydrogen elimination to give a 1-(2-cyclhexenyl)-3-cyclohexylimidazol-2-ylidene ligand (scheme 1.23.).

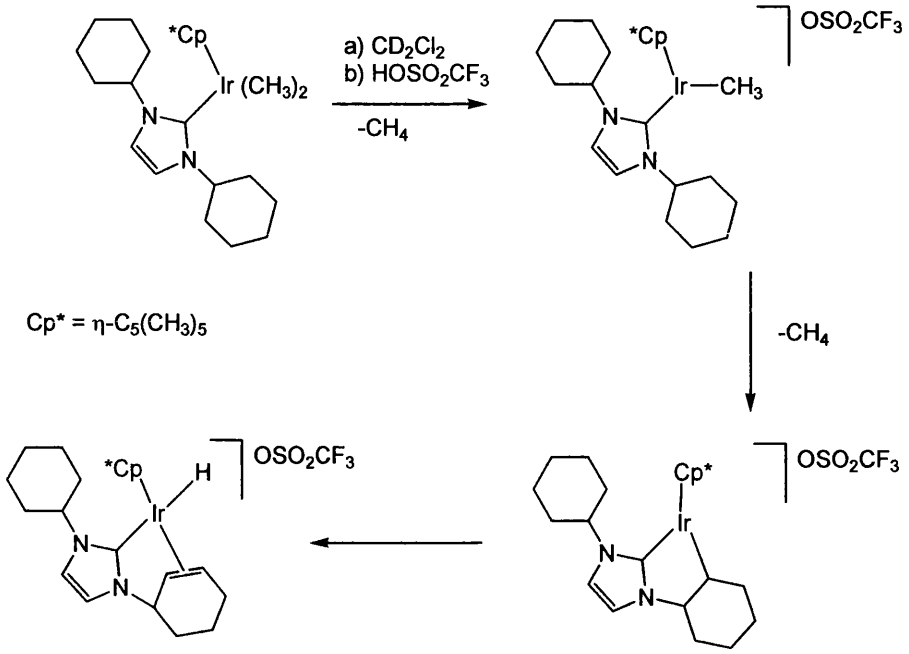


**Scheme 1.23.** C-H activation of a cyclohexyl moiety on an iridium centre.

This reaction results in the formation of a chiral centre at the iridium and at the α-C-H group of the cyclohexyl ligand. Thus, four isomers are theoretically possible, constituting two enantiomers. From Herrmann's investigations on this particular complex it appears that only two isomers are formed: $Ir_SC_R$ and $Ir_RC_S$. This type of reaction could potentially be extremely useful in producing chiral metal complexes for catalysis.

## 1.2.8. Metal-hydride NHC complexes and their bond activation reactions

Metal complexes bearing hydride ligands are well documented for their use in catalysis.[41,186,187] The hydride ligands not only stabilise complexes but are often involved in key insertion steps in catalytic cycles and much of the work in this thesis concentrates on metal-hydride species.

Hydrogenation catalysts are known to involve hydridic intermediates while $[RuHCl(PR_3)_2(=C(X)C_3H_6)]$ (R = $^i$Pr, Cy; X = O, NH) and $[RuHCl(PCy_3)(=C=CH_2)]$ are known to be active metathesis catalysts.[188-190]

However, few hydridometal complexes containing NHCs are known. Morris and co-workers reacted [$RuHCl(PPh_3)_3$] (**11**) with three different NHCs, IMes, $IMesH_2$ and I$^t$Bu.[191] The two mesityl based ligands, when heated with the ruthenium precursor at 66 °C, led to the C-H activated products [$RuH(IMes)''(PPh_3)_2$] (**12**) and [$RuH(IMesH_2)''(PPh_3)_2$] (**13**) (figure 1.25.). Reaction of **12** with CO at 20 °C leads to coordination of CO to the vacant site *trans* to hydride to give [$RuH(IMes)''(PPh_3)_2(CO)$].

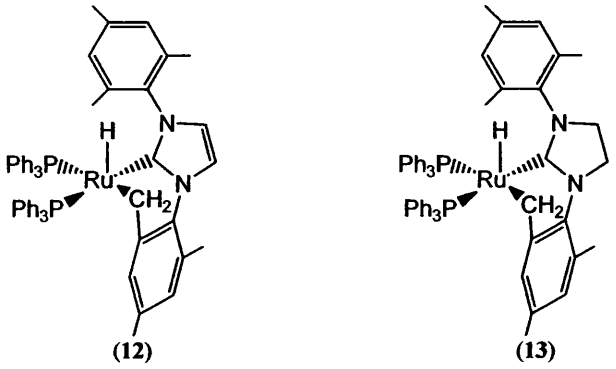


**Figure 1.25.** structures of two C-H activated Ru(NHC) complexes synthesised by Morris.

Attempts to synthesise a bis NHC species were unsuccessful even when a solution of **11** was refluxed with a 10-fold excess of free NHC (IMes or $IMesH_2$) for 7 days. Morris attributes this to the ruthenium centre being too sterically hindered to allow addition of another NHC ligand, although substitution of a phosphine for an NHC ligand would be expected under these conditions.

Reaction of **11** with I$^t$Bu in THF did not lead to an activated complex but instead to a species that the authors assign as "$Ru(I^tBu)(PPh_3)_2$" due its highly reactive nature. When $H_2$ is added to this solution, two isomers of the complex [$RuH_2(I^tBu)(PPh_3)_2$] are isolated in a ratio of 7:3, with the *trans* phosphine arrangement being favoured (figure 1.26.). The crystal structure showed the presence of an agostic interaction between one of the methyl groups on the $^t$Bu ligand and the ruthenium centre.

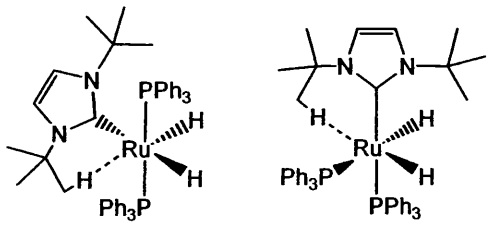


**Figure 1.26.** Two isomers of **14**, showing agostic interactions.

Recent work by Burling *et al.* has shown that a similar reaction occurs when ICy is reacted with **11** in $CH_2Cl_2$ giving [RuHCl(ICy)$(PPh_3)_2$], with an agostic bond from the α-$CH_2$ of the cyclohexyl group.[192] Again, both the *cis* and *trans* phosphine isomers are formed; in this case in a ratio of 1:0.4, with the *trans* isomer again predominating.

The Whittlesey group has synthesised a number of ruthenium hydride complexes bearing a variety of NHC ligands and have investigated them in catalytic reactions.[192-199] Reaction of IMes with [Ru$(H)_2(PPh_3)_3$(CO)] (**15**) at 80 °C leads to formation of the mono and bis NHC species [Ru$(H)_2$(IMes)$(PPh_3)_2$(CO)] (**16**) and [Ru$(H)_2(IMes)_2(PPh_3)$(CO)] (**17**).[198] Addition of trimethylvinylsilane or other alkenes to **16** at room temperature leads to the C-H activated complex [RuH(IMes)''$(PPh_3)_2$(CO)] (**18**) (scheme 1.24.). Most surprisingly, however, heating **15** and IMes at 110 °C leads to formation of a C-C activated product, [RuH(IMes)'$(PPh_3)_2$(CO)] (**19**) (figure 1.27.). This is unexpected as the system is not predisposed to C-C activation like the examples presented in section 1.1.3.

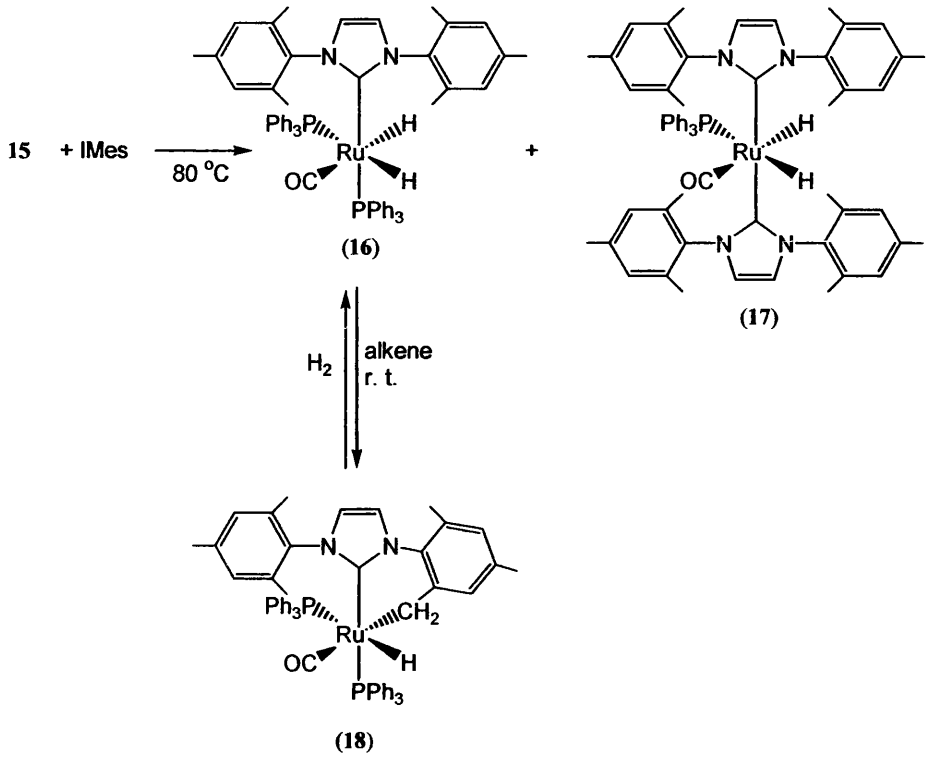


**Scheme 1.24.** Formation of mono, bis and C-H activated Ru-IMes complexes.

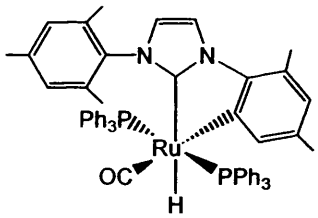


**Figure 1.27.** Structure of **19**.

Changing the precursor to $[Ru(H)_2(AsPh_3)_3(CO)]$ (**20**) leads to an extremely reactive bis NHC complex upon heating with IMes, as reported by Jazzar, Chatwin *et al.*[193,197,200] $[Ru(H)_2(IMes)_2(AsPh_3)(CO)]$ (**21**) is observed by NMR spectroscopy after heating **20** and IMes overnight at 70 °C. However, isolation of **21** proved impossible due to the labile nature of the arsine ligand. Attempts to precipitate the complex from ethanol and hexane led to the five coordinate, 16-electron complexes $[RuH(IMes)_2(OEt)(CO)]$ (**22**) and $[RuH(IMes)_2(OH)(CO)]$ (**23**) respectively. Initially, crystallography and NMR spectroscopy studies suggested that these complexes were the 18-electron *trans* dihydride solvent complexes,

$[Ru(H)_2(IMes)_2(S)(CO)]$ (S = EtOH, $H_2O$).[197] However, further investigation by NMR spectroscopy revealed that the molecules were, in fact, unsaturated. [200,201] Addition of $H_2S$ to **22** leads to the complex $[RuH(IMes)_2(SH)(CO)]$ (**24**), which is completely air stable.[193] Upon addition of more $H_2S$, the bis-hydrosulphido complex, $[Ru(IMes)_2(SH)_2(CO)]$ (**25**) formed. Both **24** and **25** react with CO giving $[RuH(IMes)_2(SH)(CO)_2]$ and $[Ru(IMes)_2(SH)_2(CO)_2]$ (**26**) respectively. Remarkably, reactions of **22, 24** and **26** can all be conducted in the solid state.

Replacing the two phosphine ligands on **16** with the chelating phosphines $Ph_2PCH_2CH_2CH_2PPh_2$ (dppp) or $Ph_2AsCH_2CH_2PPh_2$ (arphos) again lead to C-H activation of IMes upon treatment with $CH_2$=$CHSiMe_3$. However, much higher temperatures were needed to achieve this. [RuH(IMes)''(dppp)(CO)] (**27**) was formed by heating $[RuH_2(IMes)(dppp)(CO)]$ with alkene at 100 °C, whilst three isomers of [RuH(IMes)''(arphos)(CO)] (**28**) were formed by an analogous reaction at 75 °C (figure 1.28.). Both **27** and **28** can be returned to the non activated products upon heating at 80 °C with $H_2$ although the reaction of **27** is very slow (12 hours). Surprisingly, **28** returns to only one isomer of the unactivated complex.

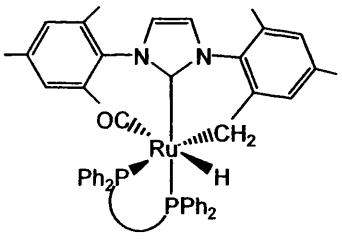


(27)

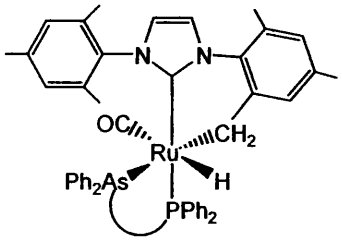


(a)

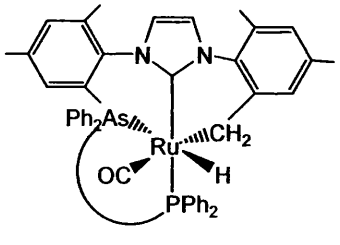


(b)

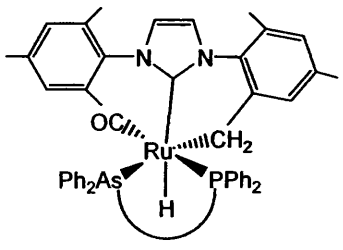


(c)

three isomers of **28**

**Figure 1.28.** Structures of **27** and **28**.

The reversibility of the C-H activation chemistry allows these complexes to be utilised in catalytic chemistry. Paine *et al.* have investigated using $[Ru(H)_2(IMes)(PPh_3)_2(CO)]$ (**16**) as a catalyst for an indirect Wittig reaction on alcohols.[195] The key to the catalytic cycle is being able to take hydrogen from the alcohol (reducing it to the aldehyde) and store it on the metal catalyst whilst the C-C bond formation (taking aldehyde to alkene) is performed by the Wittig reagent. The hydrogen can then be returned to the alkene substrate from the metal in the final step of the reaction, thus giving an alkane from an alcohol in a one pot reaction (scheme 1.25.).

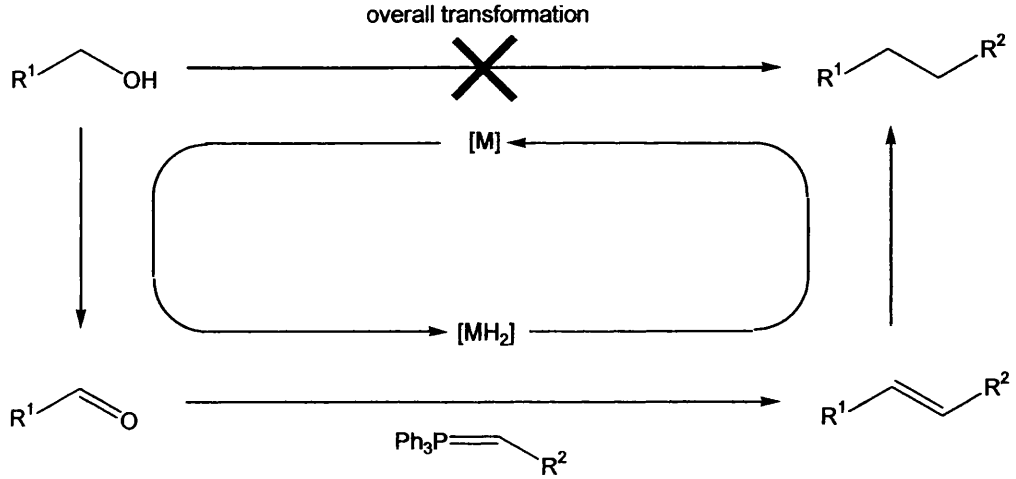


**Scheme 1.25.** The indirect Wittig reaction upon alcohols.

Subsequently the same authors have replaced the IMes ligand of **16** with various alkyl NHCs to give $[Ru(H)_2(IMe_4)(PPh_3)_2(CO)]$, $[RuH_2(IEt_2Me_2)(PPh_3)_2(CO)]$ (**29**) and $[Ru(H)_2(I^iPr_2Me_2)(PPh_3)_2(CO)]$ (**30**).[199,202] As can be seen from figure 1.29., the major differences between these complexes and the IMes analogue, are the methyl groups on the backbones of the NHCs and the position of the NHC ligands around the metal, which lie *trans* to the hydride ligand as opposed to the phosphine (or, as drawn here, in the equatorial position rather than the axial). These new complexes show greatly improved catalytic behaviour in comparison to **16**.

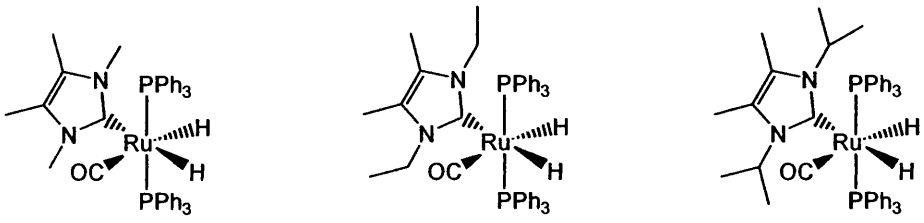

(29) (30)

**Figure 1.29.** Structures of alkyl NHC complexes of ruthenium.

Unusual reactions involving C-H bond activation have been observed in these alkyl NHC complexes.[199] **29** undergoes C-H activation when subjected to $CH_2$=$CHSiMe_3$ to give [RuH(I$Et_2Me_2$)''$(PPh_3)_2$(CO)] (**31**). When this complex is dissolved in ethanol, however, rapid precipitation of the *trans* dihydride complex (**32**) occurs. **32** is unstable in solution, rapidly isomerising to give a mixture of **29** and the axial isomer, **33**. After 40 minutes in solution, **29** was the only hydridic product observable by $^1$H NMR spectroscopy (scheme 1.26.). The rate of isomerisation was unaffected by the nature of the solvent (toluene or pyridine) or by adding excess $PPh_3$ to the solution.

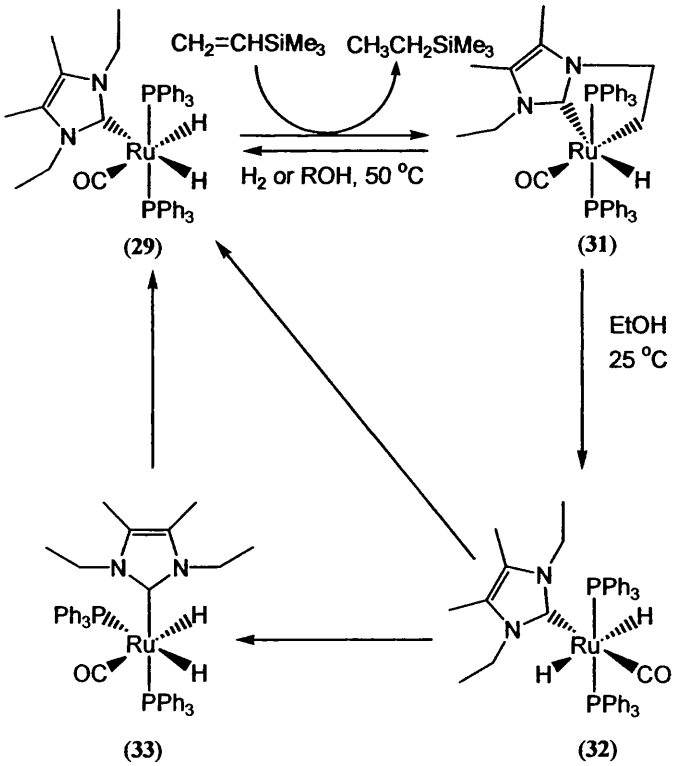


(29) (31) (33) (32)

**Scheme 1.26.** Reactions of **29**, including an unusual *trans* hydride product.

The C-H activated complex of the $I^iPr_2Me_2$ analogue [RuH($I^iPr_2Me_2$)''$(PPh_3)_2(CO)$] (**34**) is, surprisingly, easiest to synthesise by first obtaining the bis NHC complex [$Ru(H)_2(I^iPr_2Me_2)_2(PPh_3)(CO)$] *in situ*, removing the solution under vacuum and redissolving the residue in ethanol. $H_2$ is released and **34** precipitates out of solution. This complex is primarily the isomer with the NHC *trans* to hydride but some with the NHC *trans* to phosphine is also observed (figure 1.30.). The C-H activated complexes are also observed upon heating a benzene solution of [$Ru(H)_2(I^iPr_2Me_2)(PPh_3)_2(CO)$] (**30**). No hydrogen acceptor sources need to be present to obtain **34**.

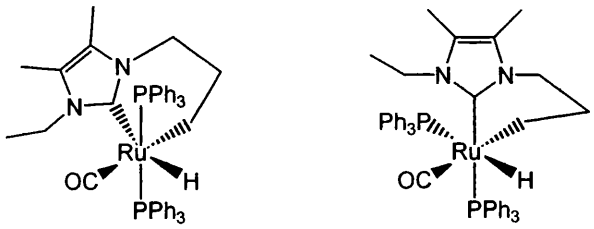


**Figure 1.30.** Two isomers of **34**.

The observation of these facile bond activation reactions provides the starting point for the work reported in this thesis.

## 1.3. Introduction to the structure of the thesis

The initial aim of the project described in this thesis was to investigate the mechanism of the C-C bond activation observed in the ruthenium IMes complex, [RhH(IMes)'$(PPh_3)_2(CO)$] (**19**), described on page 39. In the course of the work, the research was extended to investigate other possible activation reactions of ruthenium and rhodium NHC hydride complexes. Chapter 2 provides an overview of attempts, both computationally and synthetically, to elucidate more about the C-C bond activation reaction to form **19**. As well as the thermal chemistry of the ruthenium hydride complexes, their photolytic properties have also been investigated and some

interesting isomerisation reactions observed. Using a variety of techniques, rate and mechanistic data has been obtained for these reactions.

Chapter 3 describes the synthesis of related rhodium NHC hydride complexes including mono, bis and tris NHC complexes. In addition, novel dimeric and cationic complexes are reported. All of these complexes have been characterised by $^{1}H$ and $^{31}P\{^{1}H\}$ NMR spectroscopy and many have also been analysed by X-ray diffraction. NMR and IR studies have allowed determination of the mechanisms of formation of these complexes.

## 1.4. References


(1) Arndsten, B. A.; Bergman, R. G.; Mobley, T. A.; Peterson, T. H. *A. Chem. Res.* **1995**, *28*, 154.
(2) Ziegler, T.; Foga, E.; Berces, A. *J. Am. Chem. Soc.* **1993**, *115*, 636.
(3) Benson, M. T.; Cundari, T. R.; Moody, E. W. *J. Organomet. Chem.* **1995**, *504*, 1.
(4) Brookhart, M.; Green, M. L. H. *J. Organomet. Chem.* **1983**, *250*, 395.
(5) Krauledat, H.; Brintzinger, H. H. *Angew. Chem.* **1990**, *102*, 1459.
(6) Labinger, J. A.; Bercaw, J. E. *Nature* **2002**, *417*, 507.
(7) Shilov, A. E.; Shteinman, A. A. *Coord. Chem. Rev.* **1977**, *24*, 97.
(8) Hoyano, J. K.; Graham, W. A. G. *J. Am. Chem. Soc.* **1982**, *104*, 3723.
(9) Janowicz, A. H.; Bergman, R. G. *J. Am. Chem. Soc.* **1982**, *104*, 352.
(10) Bengali, A. A.; Arndsten, B. A.; Burger, P. M.; Schultz, R. H.; Weiller, B. H.; Kyle, K. R.; Moore, C. B.; Bergman, R. G. *Pure & Appl. Chem.* **1995**, *67*, 281.
(11) Walsh, P. J.; Hollander, F. J.; Bergman, R. G. *J. Am. Chem. Soc.* **1988**, *110*, 8729.
(12) Tellers, D. M.; Bergman, R. G. *Organometallics* **2001**, *20*, 4819.
(13) Tellers, D. M.; Yung, C. M.; Arndsten, B. A.; Adamson, D. R.; Bergman, R. G. *J. Am. Chem. Soc.* **2002**, *124*, 1400.
(14) Thalji, R. K.; Ahrendt, K. A.; Bergman, R. G.; Ellman, J. A. *J. Am. Chem. Soc.* **2001**, *123*, 9692.
(15) Zuckerman, R. L.; Krska, S. W.; Bergman, R. G. *J. Organomet. Chem.* **1999**, *591*, 2.
(16) Alaimo, P. J.; Arndsten, B. A.; Bergman, R. G. *Organometallics* **2000**, *19*, 2130.
(17) Bergman, R. G.; Gundari, T. R.; Gillespie, A. M.; Gurnoe, T. B.; Harman, W. D.; Klinkman, T. R.; Temple, M. D.; White, D. P. *Organometallics* **2005**, *22*, 2331.
(18) Golden, J. T.; Anderson, R. A.; Bergman, R. G. *J. Am. Chem. Soc.* **2001**, *123*, 5837.
(19) Hartwig, J. F.; Andersen, R. A.; Bergman, R. G. *J. Am. Chem. Soc.* **1991**, *113*, 6492.
(20) Hartwig, J. F.; Bergman, R. G.; Andersen, R. A. *J. Am. Chem. Soc.* **1991**, *113*, 3404.
(21) Ma, Y. N.; Bergman, R. G. *Organometallics* **1994**, *13*, 4648.
(22) Mobley, T. A.; Bergman, R. G. *J. Am. Chem. Soc.* **1998**, *120*, 3253.
(23) Peterson, T. H.; Golden, J. T.; Bergman, R. G. *J. Am. Chem. Soc.* **2001**, *123*, 455.
(24) Schultz, R. H.; Bengali, A. A.; Tauber, M. J.; Weiller, B. H.; Wasserman, E. P.; Kyle, K. R.; Moore, C. B.; Bergman, R. G. *J. Am. Chem. Soc.* **1994**, *116*, 7369.
(25) Skadden, M. B.; Yung, C. M.; Bergman, R. G. *Org. Lett.* **2004**, *6*, 11.
(26) Sun, Y. L.; Bergman, R. G. *J. Am. Chem. Soc.* **1995**, *117*, 5877.
(27) Szewczyk, J. W.; Zuckerman, R. L.; Bergman, R. G.; Ellman, J. A. *Angew. Chem. Int. Ed.* **2001**, *40*, 216.

(28) Crabtree, R. H.; Holt, E. M.; Lavin, M. E.; Morehouse, S. M. *Inorg. Chem.* **1985**, *24*, 1986.
(29) Crabtree, R. H. *Angew. Chem. Int. Ed.* **2003**, *32*, 789.
(30) Koga, N.; Morokuma, K. *Chem. Rev.* **1991**, *91*, 823.
(31) Blomberg, M. R. A.; Siegbahn, P. E. M.; Svensson, M. *J. Phys. Chem.* **1994**, *98*, 2062.
(32) Hall, C.; Perutz, R. N. *Chem. Rev.* **1996**, *96*, 3125.
(33) Geftakis, S.; Ball, G. E. *J. Am. Chem. Soc.* **1998**, *120*, 9953.
(34) Lawes, D. J.; Geftakis, S.; Ball, G. E. *J. Am. Chem. Soc.* **2005**, *127*, 4134.
(35) Jones, W. D.; Feher, F. J. *Acc. Chem. Res.* **1989**, *22*, 91.
(36) Dani, P.; Toorneman, M. A. M.; van Klink, G. P. M.; van Koten, G. *Organometallics* **2000**, *19*, 5287.
(37) Albrecht, M.; Dani, P.; Lutz, M.; Spek, A. L.; van Koten, G. *J. Am. Chem. Soc.* **2000**, *122*, 11822.
(38) van Koten, G. *Pure & Appl. Chem.* **1989**, *61*, 1681.
(39) Cope, A. C.; Friedrich, E. C. *J. Am. Chem. Soc.* **1968**, *90*, 909.
(40) Jones, W. D.; Feher, F. J. *Acc. Chem. Res.* **1989**, *22*, 91.
(41) Crabtree, R. H. *The Organometallic Chemistry of the Transition Metals*; 3rd ed.; Wiley-Interscience: New York, 2001.
(42) Murakami, M.; Ito, Y. *Topics in Organometallic Chemistry: Activation of Unreactive Bonds and Organic Synthesis*: Heidelberg, 1999.
(43) Simoes, J. A. M.; Beauchamp, J. L. *Chem. Rev.* **1990**, *90*, 629.
(44) Rybtchinski, B.; Milstein, D. *Angew. Chem. Int. Ed.* **1999**, *38*, 870.
(45) Edelbach, B. L.; Lachicotte, R. J.; Jones, W. D. *J. Am. Chem. Soc.* **1998**, *120*, 2843.
(46) Tipper, C. H. F. *J. Chem. Soc.* **1955**, 2045.
(47) Irwin, W. J.; McQuillin, F. J. *Tetrahedron Lett.* **1968**, *16*, 1937.
(48) Adams, D. M.; Chatt, J.; Guy, R.; Sheppard, N. *J. Chem. Soc.* **1961**, 738.
(49) Gillard, R. D.; Keeton, M.; Mason, R.; Pilbrow, M. F.; Russell, D. R. *J. Organomet. Chem.* **1971**, *33*, 247.
(50) McQuillin, F. J.; Powell, K. G. *J. Chem. Soc. Dalton Trans.* **1972**, 2123.
(51) Milstein, D.; Rybtchinski, B. *Angew. Chem. Int. Ed.* **1999**, *38*, 870.
(52) Gozin, M.; Weisman, A.; Ben-David, Y.; Milstein, D. *Nature* **1993**, *364*, 699.
(53) Sundermann, A.; Uzan, O.; Milstein, D.; Martin, J. M. L. *J. Am. Chem. Soc.* **2000**, *122*, 7095.
(54) Rybtchinski, B.; Oevers, S.; Montag, M.; Vigalok, A.; Rozenberg, H.; Martin, J. M. L.; Milstein, D. *J. Am. Chem. Soc.* **2001**, *123*, 9064.
(55) Gandelman, M.; Vigalok, A.; Shimon, L. J. W.; Milstein, D. *Organometallics* **1997**, *16*, 3981.
(56) van der Boom, M. E.; Liou, S. Y.; Ben-David, Y.; Vigalok, A.; Milstein, D. *Angew. Chem. Int. Ed. Engl.* **1997**, *36*, 625.
(57) van der Boom, M. E.; Ben-David, Y.; Milstein, D. *J. Am. Chem. Soc.* **1999**, *121*, 6652.
(58) Kanzelberger, M.; Zhang, X.; Emge, T. J.; Goldman, A. S.; Zhao, J.; Incarvito, C.; Hartwig, J. F. *J. Am. Chem. Soc.* **2003**, *125*, 13644.

(59) van der Boom, M. E.; Milstein, D. *Chem. Rev.* **2003**, *103*, 1759.
(60) Perthuisot, C.; Edelbach, B. L.; Zubris, D. L.; Jones, W. D. *Organometallics* **1997**, *16*, 2016.
(61) Perthuisot, C.; Jones, W. D. *J. Am. Chem. Soc.* **1994**, *116*, 3647.
(62) Müller, C.; Iverson, C. N.; Lachicotte, R. J.; Jones, W. D. *J. Am. Chem. Soc.* **2001**, *123*, 9718.
(63) Garcia, J. J.; Brunkan, N. M.; Jones, W. D. *J. Am. Chem. Soc.* **2002**, *124*, 9547.
(64) Green, M.; Wong, L. *Chem. Commun.* **1984**, 1442.
(65) Edelbach, B. L.; Vicic, D. A.; Lachicotte, R. J.; Jones, W. D. *Organometallics* **1998**, *17*, 4784.
(66) Edelbach, B. L.; Lachicotte, R. J.; Jones, W. D. *Organometallics* **1999**, *18*, 4040.
(67) Müller, C.; Lachicotte, R. J.; Jones, W. D. *Organometallics* **2002**, *21*, 1975.
(68) Trnka, T. M.; Morgan, J. P.; Sanford, M. S.; Wilhelm, T. E.; Scholl, M.; Choi, T. L.; Ding, S.; Day, M. W.; Grubbs, R. H. *J. Am. Chem. Soc.* **2003**, *125*, 2546.
(69) Bielawski, C. W.; Grubbs, R. H. *Angew. Chem. Int. Ed.* **2000**, *39*, 2903.
(70) Hajela, S.; Lee, C. W.; Love, J. A.; Morgan, J. P.; Grubbs, R. H. *Abs. Pap. Am. Chem. Soc.* **2002**, *224*, 246.
(71) Louie, J.; Grubbs, R. H. *Organometallics* **2002**, *21*, 2153.
(72) Claydon, J.; Greeves, N.; Warren, S.; Wothers, P. *Organic Chemistry*; Oxford University Press Inc: Oxford, 2001.
(73) Bertrand, G. In *Reactive Intermediate Chemistry*; Moss, R. A., Platz, M. S., Jones, M., Eds.; John Wiley and Sons: New York, 2004.
(74) Hoffman, R. *J. Am. Chem. Soc.* **1968**, *90*, 1475.
(75) Wanzlick, H. W. *Angew. Chem. Int. Ed.* **1962**, *1*, 75.
(76) Herrmann, W. A.; Weskamp, T.; Böhm, V. P. W. In *Advances in Organometallic Chemistry*, 2001; Vol. 48.
(77) Arduengo, A. J.; Harlow, R. L.; Kline, M. *J. Am. Chem. Soc.* **1991**, *113*, 361.
(78) Arduengo, A. J.; Goerlich, J. R.; Krafczyk, R.; Marshall, W. J. *Angew. Chem. Int. Ed.* **1998**, *37*, 1963.
(79) Arduengo, A. J.; Dias, H. V. R.; Harlow, R. L.; Kline, M. *J. Am. Chem. Soc.* **1992**, *114*, 5530.
(80) Kuhn, N.; Kratz, T. *Synthesis-Stuttgart* **1993**, 561.
(81) Arduengo, A. J.; Goerlich, J. R.; Marshall, W. J. *J. Am. Chem. Soc.* **1995**, *117*, 11027.
(82) Lee, H. M.; Lu, C. Y.; Chen, C. Y.; Chen, W. L.; Lin, H. C.; Chiu, P. L.; Cheng, P. Y. *Tetrahedron* **2004**, *60*, 5807.
(83) Böhm, V. P. W.; Herrmann, W. A. *Angew. Chem. Int. Ed.* **2000**, *39*, 4036.
(84) Herrmann, W. A.; Köcher, C. *Angew. Chem. Int. Ed. Engl.* **1997**, *36*, 2163.
(85) Alder, R. W.; Blake, M. E.; Chaker, L.; Harvey, J. N.; Paolini, F.; Schutz, J. *Angew. Chem. Int. Ed.* **2004**, *43*, 5896.
(86) Crabtree, R. H. *J. Organomet. Chem.* **2005**, *in press*.
(87) Seiders, T. J.; Ward, D. W.; Grubbs, R. H. *Org. Lett.* **2001**, *3*, 3225.
(88) Csabai, P.; Joó, F. *Organometallics* **2004**, *23*, 5640.

(89) Ozdemir, I.; Yigit, B.; Çetinkaya, B.; Ulku, D.; Tahir, M. N.; Arici, C. *J. Organomet. Chem.* **2001**, *633*, 27.
(90) Sini, G.; Eisenstein, O.; Crabtree, R. H. *Inorg. Chem.* **2002**, *41*, 602.
(91) Varray, S.; Lazaro, R.; Martinez, J.; Lamaty, F. *Organometallics* **2003**, *22*, 2426.
(92) Garrou, P. E. *Chem. Rev.* **1981**, *81*, 229.
(93) Arduengo, A. J.; Bannenberg, T. *The Strem Chemiker* **2002**, *19*.
(94) Mata, J. A.; Chianese, A. R.; Miecznikowski, J. R.; Poyatos, M.; Peris, E.; Faller, J. W.; Crabtree, R. H. *Organometallics* **2004**, *23*, 1253.
(95) Tolman, C. A. *Chem. Rev.* **1977**, *77*, 313.
(96) Hillier, A. C.; Sommer, W. J.; Yong, B. S.; Petersen, J. L.; Cavallo, L.; Nolan, S. P. *Organometallics* **2003**, *22*, 4322.
(97) Magill, A. M.; Cavell, K. J.; Yates, B. F. *J. Am. Chem. Soc.* **2004**, *126*, 8717.
(98) Dorta, R.; Stevens, E. D.; Scott, N. M.; Costabile, C.; Cavallo, L.; Hoff, C. D.; Nolan, S. P. *J. Am. Chem. Soc.* **2005**, *127*, 2485.
(99) Perrin, L.; Clot, E.; Eisenstein, O.; Loch, J. A.; Crabtree, R. H. *Inorg. Chem.* **2001**, *40*, 5806.
(100) Chianese, A. R.; Kovacevic, A.; Zeglis, B. M.; Faller, J. W.; Crabtree, R. H. *Organometallics* **2004**, *23*, 2461.
(101) Huang, J. K.; Stevens, E. D.; Nolan, S. P. *Organometallics* **2000**, *19*, 1194.
(102) Hun, K.; Rosini, G. P.; Goldman, A. S.; Nolan, S. P. *J. Am. Chem. Soc.* **1995**, *117*, 5082.
(103) Cardin, D. J.; Çetinkaya, B.; Çetinkaya, E.; Lappert, M. F. *J. Chem. Soc. Dalton Trans.* **1973**, 514.
(104) Çetinkaya, B.; Çetinkaya, E.; Lappert, M. F. *J. Chem. Soc. Dalton Trans.* **1973**, 906.
(105) Cardin, D. J.; Çetinkaya, B.; Çetinkaya, E.; Lappert, M. F.; Randall, E. W.; Rosenber.E *J. Chem. Soc. Dalton Trans.* **1973**, 1982.
(106) Cardin, D. J.; Çetinkaya, B.; Lappert, M. F. *J. Organomet. Chem.* **1974**, *72*, 139.
(107) Çetinkaya, B.; Lappert, M. F.; McLaughl.Gm; Turner, K. *J. Chem. Soc. Dalton Trans.* **1974**, 1591.
(108) Lappert, M. F.; Oliver, A. J. *J. Chem. Soc. Dalton Trans.* **1974**, 65.
(109) Çetinkaya, B.; Hitchcock, P. B.; Lappert, M. F.; Shaw, D. B.; Spyropoulos, K.; Warhurst, N. J. W. *J. Organomet. Chem.* **1993**, *459*, 311.
(110) Anderson, D. M.; Bristow, G. S.; Hitchcock, P. B.; Jasim, H. A.; Lappert, M. F.; Skelton, B. W. *J. Chem. Soc. Dalton Trans.* **1987**, 2843.
(111) Böhm, V. P. W.; Gstöttmayr, C. W. K.; Weskamp, T.; Herrmann, W. A. *J. Organomet. Chem.* **2000**, *595*, 186.
(112) Çetinkaya, B.; Dixneuf, P.; Lappert, M. F. *J. Chem. Soc. Dalton Trans.* **1974**, 1827.
(113) Çetinkaya, E.; Hitchcock, P. B.; Küçükbay, H.; Lappert, M. F.; Aljuaid, S. *J. Organomet. Chem.* **1995**, *491*, C7.
(114) Gardiner, M. G.; Herrmann, W. A.; Reisinger, C. P.; Schwarz, J.; Spiegler, M. *J. Organomet. Chem.* **1999**, *572*, 239.

(115) Chamizo, J. A.; Hitchcock, P. B.; Jasim, H. A.; Lappert, M. F. *J. Organomet. Chem.* **1993**, *451*, 89.
(116) Doyle, M. J.; Lappert, M. F.; Pye, P. L.; Terreros, P. *J. Chem. Soc. Dalton Trans.* **1984**, 2355.
(117) Coleman, A. W.; Hitchcock, P. B.; Lappert, M. F.; Maskell, R. K.; Müller, J. H. *J. Organomet. Chem.* **1985**, *296*, 173.
(118) Hartshorn, A. J.; Lappert, M. F.; Turner, K. *J. Chem. Soc. Dalton Trans.* **1978**, 348.
(119) Hitchcock, P. B.; Lappert, M. F.; McLaughlin, G. M.; Oliver, A. J. *J. Chem. Soc. Dalton Trans.* **1974**, 68.
(120) Hitchcock, P. B.; Lappert, M. F.; Pye, P. L. *J. Chem. Soc. Dalton Trans.* **1977**, 2160.
(121) Hitchcock, P. B.; Lappert, M. F.; Pye, P. L. *J. Chem. Soc. Dalton Trans.* **1978**, 826.
(122) Hitchcock, P. B.; Lappert, M. F.; Pye, P. L.; Thomas, S. *J. Chem. Soc. Dalton Trans.* **1979**, 1929.
(123) Hitchcock, P. B.; Lappert, M. F.; Thomas, S. A.; Thorne, A. J.; Carty, A. J.; Taylor, N. J. *J. Organomet. Chem.* **1986**, *315*, 27.
(124) Lappert, M. F.; Pye, P. L. *J. Chem. Soc. Dalton Trans.* **1977**, 2172.
(125) Lappert, M. F.; Pye, P. L. *J. Chem. Soc. Dalton Trans.* **1977**, 1283.
(126) Lappert, M. F.; Pye, P. L. *J. Chem. Soc. Dalton Trans.* **1978**, 837.
(127) Lappert, M. F.; Pye, P. L.; McLaughlin, G. M. *J. Chem. Soc. Dalton Trans.* **1977**, 1272.
(128) Lappert, M. F.; Pye, P. L.; Rogers, A. J.; McLaughlin, G. M. *J. Chem. Soc. Dalton Trans.* **1981**, 701.
(129) Ozdemir, I.; Demir, S.; Çetinkaya, B. *J. Mol. Catal. A. Chem.* **2004**, *215*, 45.
(130) Clarke, M. J.; Taube H.; *Bioinorg. Chem.* **1975**, *4*, 143.
(131) Abernethy, C. D.; Codd, G. M.; Spicer, M. D.; Taylor, M. K. *J. Am. Chem. Soc.* **2003**, *125*, 1128.
(132) Boehme, C.; Frenking, G. *Organometallics* **1998**, *17*, 5801.
(133) Deubel, D. V. *Organometallics* **2002**, *21*, 4303.
(134) Termaten, A. T.; Schakel, M.; Ehlers, A. W.; Lutz, M.; Spek, A. L.; Lammertsma, K. *Chem. Eur. J.* **2003**, *9*, 3577.
(135) Hu, X. L.; Castro-Rodriguez, I.; Olsen, K.; Meyer, K. *Organometallics* **2004**, *23*, 755.
(136) Huang, J.; Stevens, E. D.; Nolan, S. P.; Peterson, J. L. *J. Am. Chem. Soc.* **1999**, *121*, 2674.
(137) Huang, J.; Schanz, H.-J.; Stevens, E. D.; Nolan, S. P. *Organometallics* **1999**, *18*, 2370.
(138) Titcomb, L. R.; Caddick, S.; Cloke, F. G. N.; Wilson, D. J.; McKerrecher, D. *Chem. Commun.* **2001**, 1388.
(139) Simms, R. W.; Drewitt, M. J.; Baird, M. C. *Organometallics* **2002**, *21*, 2958.
(140) Chatt, J. In *Homogeneous Catalysis with Metal Phosphine Complexes*; Pignolet, L. H., Ed.; Plenum Press: New York, 1983.
(141) Kuhl, S.; Schneider, R.; Fort, Y. *Organometallics* **2003**, *22*, 4184.

(142) Hillier, A. C.; Grasa, G. A.; Viciu, H. M. L.; Yang, C.; Nolan, S. P. *J. Organomet. Chem.* **2002**, *653*, 69.
(143) Ozdemir, I.; Demir, S.; Çetinkaya, B. *Tetrahedron* **2005**, *61*.
(144) Novarro, O.; Marion, N.; Scott, N. M.; González, J.; Amoroso, D.; Bell, A.; Nolan, S. P. *Tetrahedron* **2005**, *61*, 9716.
(145) Herrmann, W. A.; Böhm, V. P. W.; Gstöttmayr, C. W. K.; Grosche, M.; Reisinger, C. P.; Weskamp, T. *J. Organomet. Chem.* **2001**, *617-618*, 616.
(146) Weskamp, T.; Böhm, V. P. W.; Herrmann, W. A. *J. Organomet. Chem.* **1999**, *585*, 348.
(147) Shi, M.; Qian, H.-X. *Tetrahedron* **2005**, *61*, 4949.
(148) Arentsen, K.; Caddick, S.; Cloke, F. G. N. *Tetrahedron* **2005**, *61*, 9710.
(149) Bedford, R. B.; Betham, M.; Coles, S. J.; Frost, R. M.; Hursthouse, M. B. *Tetrahedron* **2005**, *61*, 9663.
(150) Frey, G. D.; Schutz, J.; Herdtweck, E.; Herrmann, W. A. *Organometallics* **2005**, *24*, 4416.
(151) Mayr, M.; Wurst, K.; Chen, A. C. *Chem. Eur. J.* **2004**, *10*, 1256.
(152) Lee, H. M.; Zeng, J. Y.; Hu, C. H.; Lee, M. T. *Inorg. Chem.* **2004**, *43*, 6822.
(153) Herrmann, W. A.; Elison, M.; Fischer, J.; Köcher, C.; Artus, G. R. J. *Angew. Chem. Int. Ed.* **1995**, *34*, 2371.
(154) Schwarz, J.; Böhm, V. P. W.; Gardiner, M. G.; Grosche, M.; Herrmann, W. A.; Hieringer, W.; Raudaschl-Sieber, G. *Chem. Eur. J.* **2000**, *6*, 1773.
(155) Tulloch, A. A. D.; Danopoulos, A. A.; Tooze, R. P.; Cafferkey, S. M.; Kleinhenz, S.; Hursthouse, M. B. *Chem. Commun.* **2000**, 1247.
(156) Albert, K.; Gisdakis, P.; Rösch, N. *Organometallics* **1998**, *17*, 1608.
(157) McGuinness, D. S.; Green, M. J.; Cavell, K. J.; Skelton, B. W.; White, A. H. *J. Organomet. Chem.* **1998**, *565*, 165.
(158) Magill, A. M.; McGuinness, D. S.; Cavell, K. J.; Britovsek, G. S. P.; Gibson, V. C.; White, A. J. P.; White, A. H.; Skelton, B. W. *J. Organomet. Chem.* **2001**, *617*, 546.
(159) McGuinness, D. S.; Cavell, K.; Yates, B. F. *Chem. Commun.* **2001**, 355.
(160) Done, M. C.; Ruther, T.; Cavell, K. J.; Kliner, M.; Peacock, E. J.; Braussand, N.; Skelton, B. W.; White, A. H. *J. Organomet. Chem.* **2000**, *607*, 78.
(161) McGuinness, D. S.; Mueller, W.; Wasserscheid, P.; Cavell, K. J.; Skelton, B. W.; White, A. H.; Englert, U. *Organometallics* **2002**, *21*, 175.
(162) McGuinness, D. S.; Cavell, K. J. *Organometallics* **2000**, *19*, 741.
(163) Cavell, K. J.; McGuinness, D. S. *Coord. Chem. Rev.* **2004**, *248*, 671.
(164) McGuinness, D. S.; Cavell, K. J.; Skelton, B. W.; White, A. H. *Organometallics* **1999**, *18*, 1596.
(165) McGuinness, D. S.; Saendig, N.; Yates, B. F.; Cavell, K. J. *J. Am. Chem. Soc.* **2001**, *123*, 4029.
(166) Carmichael, A. J.; Earle, M. J.; Holbrey, J. D.; McCormac, P. B.; Seddon, K. R. *Org. Letts.* **1999**, *1*, 997.
(167) Xu, L.; Chen, W.; Xiao, J. *Organometallics* **2000**, *19*, 1123.
(168) Mathews, C. J.; Smith, P. J.; Welton, T. *Chem. Commun.* **2000**, 1249.
(169) Nielsen, D. J.; Magill, A. M.; Yates, B. F.; Cavell, K.; Skelton, B. W.; White, A. H. *Chem. Commun.* **2002**, 2500.

(170) Viciu, M. S.; Grasa, G. A.; Nolan, S. P. *Organometallics* **2001**, *20*, 3607.
(171) Gründemann, S.; Albrecht, M.; Kovacevic, A.; Faller, J. W.; Crabtree, R. H. *J. Chem. Soc. Dalton Trans.* **2002**, 2163.
(172) Morgan, J. P.; Grubbs, R. H. *Org. Lett.* **2000**, *2*, 3153.
(173) Viciano, M.; Mas-Marzá, E.; Poyatos, M.; Sanaú, M.; Crabtree, R. H.; Peris, E. *Angew. Chem. Int. Ed.* **2005**, *44*, 444.
(174) Gründemann, S.; Kovacevic, A.; Albrecht, M.; Faller, J. W.; Crabtree, R. H. *Chem. Commun.* **2001**, 2274.
(175) Kovacevic, A.; Gründemann, S.; Miecznikowski, J. R.; Clot, E.; Eisenstein, O.; Crabtree, R. H. *Chem. Commun.* **2002**, 2580.
(176) Gründemann, S.; Kovacevic, A.; Albrecht, M.; Faller, J. W.; Crabtree, R. H. *J. Am. Chem. Soc.* **2002**, *124*, 10473.
(177) Hu, X.; Castro-Rodriguez, I.; Meyer, K. *Organometallics* **2003**, *22*, 3016.
(178) Danopoulos, A. A.; Tsoureas, N.; Wright, J. A.; Light, M. E. *Organometallics* **2004**, *23*, 166.
(179) Bacciu, D.; Cavell, K. J.; Fallis, I. A.; Ooi, L. *Angew. Chem. Int. Ed.* **2005**, *44*, 5282.
(180) Lebel, H.; Janes, M. K.; Charette, A. B.; Nolan, S. P. *J. Am. Chem. Soc.* **2004**, *126*, 5046.
(181) Hitchcock, P. B.; Lappert, M. F.; Pye, P. L. *J. Chem. Soc.-Chem. Commun.* **1977**, 196.
(182) Scott, N. M.; Dorta, R.; Stevens, E. D.; Correa, A.; Cavallo, L.; Nolan, S. P. *J. Am. Chem. Soc.* **2005**, *127*, 3516.
(183) Dorta, R.; Stevens, E. D.; Nolan, S. P. *J. Am. Chem. Soc.* **2004**, *126*, 5054.
(184) Danopoulos, A. A.; Winston, S.; Hursthouse, M. B. *J. Chem. Soc. Dalton Trans.* **2002**, 3090.
(185) Prinz, M.; Grosche, M.; Herdtweck, E.; Herrmann, W. A. *Organometallics* **2000**, *19*, 1692.
(186) Dedieu, A. *Transition Metal Hydrides*; VCH: New York, 1992.
(187) Song, J.-S.; Szalda, R.; Bullock, R. M.; Lawrie, C. J. C.; Rodkin, M. A.; Norton, J. R. *Angew. Chem. Int. Ed.* **1992**, *31*, 1233.
(188) Coalter, J. N.; Caulton, K. G. *New J. Chem.* **2001**, *25*, 697.
(189) Ferrando-Miguel, G.; Coalter, J. N.; Gerard, H.; Huffman, J. C.; Eisenstein, O.; Caulton, K. G. *New J. Chem.* **2002**, *26*, 687.
(190) Jung, S.; Ilg, K.; Wolf, J.; Werner, H. *Organometallics* **2001**, *20*, 2121.
(191) Abdur-Rashid, K.; Fedorkiw, T.; Lough, A. J.; Morris, R. H. *Organometallics* **2004**, *23*, 86.
(192) Burling, S.; Kociok-Kohn, G.; Mahon, M. F.; Whittlesey, M. K.; Williams, J. M. J. *Organometallics* **2005**, *24*, 5868
(193) Chatwin, S. L.; Diggle, R. A.; Jazzar, R. F. R.; Macgregor, S. A.; Mahon, M. F.; Whittlesey, M. K. *Inorg. Chem.* **2003**, *42*, 7695.
(194) Chilvers, M. J.; Jazzar, R. F. R.; Mahon, M. F.; Whittlesey, M. K. *Adv. Synth. Catal.* **2003**, *345*, 1111.
(195) Edwards, M. G.; Jazzar, R. F. R.; Paine, B. M.; Shermer, D. J.; Whittlesey, M. K.; Williams, J. M. J.; Edney, D. D. *Chem. Commun.* **2004**, 90.
(196) Jazzar, R. F. R. PhD thesis, University of Bath, 2003.

(197) Jazzar, R. F. R.; Bhatia, P. H.; Mahon, M. F.; Whittlesey, M. K. *Organometallics* **2003**, *22*, 670.
(198) Jazzar, R. F. R.; Macgregor, S. A.; Mahon, M. F.; Richards, S. P.; Whittlesey, M. K. *J. Am. Chem. Soc.* **2002**, *124*, 4944.
(199) Burling, S.; Mahon, M. F.; Paine, B. M.; Whittlesey, M. K.; Williams, J. M. J. *Organometallics* **2004**, *23*, 4537.
(200) Chatwin, S. L.; Davidson, M. G.; Doherty, C. L.; Donald, S.; Jazzar, R. F. R.; Macgregor, S. A.; Mahon, M. F.; MacIntyre, G. M.; Whittlesey, M. K. *Organometallics*, **2005**, *in press*.
(201) Using proton coupled $^{13}C$ NMR experiments gave doublets for the carbenic carbons and the carbonyl carbon, which is consistent with there only being one hydride present. If there were two hydrides in the same environment, the quaternary carbons would be triplets.
(202) Paine, B. M. *personal communication*

# Chapter 2

# Ruthenium NHC complexes

# 2. Ruthenium N-heterocyclic carbene complexes

## 2.1. Introduction

Of all the metals studied bearing NHCs, ruthenium has proved one of the most successful in catalytic reactions.[1,2] Because of this, it has played a pivotal role in the development of many other transition metal NHC complexes that can now be used in catalytic applications.

Apart from being successful catalytic systems, ruthenium NHC complexes have also been shown to undergo a variety of unusual bond activation reactions, as already discussed in chapter 1.

This chapter gives a brief overview of the extensive ruthenium NHC chemistry that has been undertaken in recent years, focussing on structural rather than catalytic properties. The investigations carried out into the formation of the C-C activated complex [RuH(IMes)'$(PPh_3)_2$(CO)] (**19**) are presented and compared to the results from DFT calculations carried out by the Macgregor group at Heriot Watt University in Edinburgh.

Examination of the photochemistry of new alkyl-NHC ruthenium complexes is presented and investigation into the rates and mechanisms of product formation is discussed. Much of this work was carried out in collaboration with Professor Simon Duckett at the University of York. Further rate data has been obtained from preliminary TRIR experiments at the University of Nottingham in collaboration with Professor Mike George. In addition the Macgregor group have again undertaken DFT calculations to add a further dimension to the results.

## 2.2. Ruthenium NHC complexes

### 2.2.1. Structure and reactivity of Grubbs' metathesis catalyst

Alkene metathesis provides a way of breaking and remaking C=C bonds and is used every day in the chemical and pharmaceutical industries. Depending on the conditions employed, metathesis reactions can lead to ring closing metathesis (RCM) or ring opening metathesis polymerisation (ROMP). The importance of this reaction has led to the recent award of the Nobel Prize for chemistry to three of the scientists who have developed it.[3] The general mechanism for the metathesis reaction was first proposed by Chauvin and it is now accepted that the reaction proceeds through a metallocyclobutane intermediate (scheme 2.1.).[4,5]

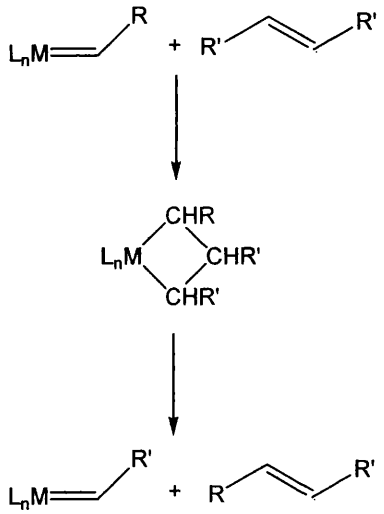


**Scheme 2.1.** Mechanism of metathesis reactions through a metallocyclobutane.

The bis phosphine catalyst $[Ru(Cl)_2(PCy_3)_2(=CHPh)]$ (**35**),[6-8] synthesised by Grubbs has been used extensively for metathesis reactions in organic and polymer chemistry as it is highly reactive to alkene moieties even in the presence of other common functional groups.[9] However, the lifetime of this catalyst was too short to give high product yields in some of the more difficult ring-closing reactions. Therefore, Grubbs substituted one of the phosphine ligands for an NHC group to give $[Ru(Cl)_2(NHC)(PCy_3)(=CHPh)]$ (NHC = $IMesH_2$ (**2**), IMes (**36**)) (figure 2.1.). This

led to a dramatic increase in reactivity.[10-17] For example, the ring closing metathesis of the methyl malonate ester (scheme 2.2.) only goes to 82 % completion with **35**, whereas with **2** 100 % conversion is obtained. In addition, the more sterically bulky $^t$Bu analogue that does not react at all in the presence of **35** also goes to 100 % completion with **2** present.[10] In addition, Nolan found that the thermal stability of **36** is far better than that of **35**, showing no decomposition after 14 days of continuous heating at 60 °C.[15] **35** shows decomposition after 1 hour at 60 °C.

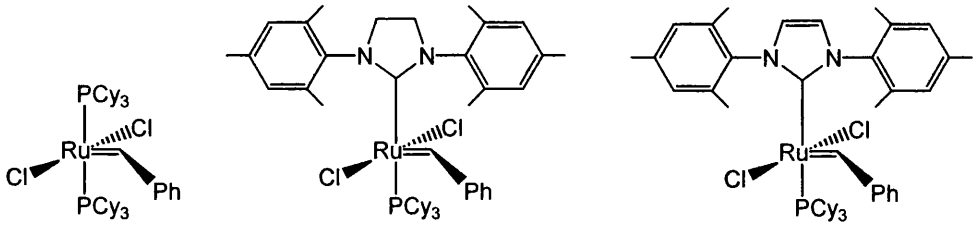


(35) (2) (36)

**Figure 2.1.** Structures of **35**, **2** and **36**.

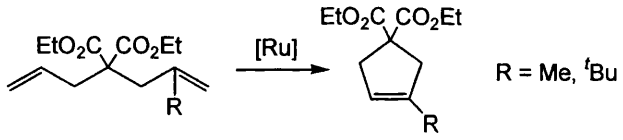


**Scheme 2.2.** RCM of malonate ester catalysed by **35** and **2**.

The higher reactivities of **2** and **36** were initially attributed to the increased labilisation of the phosphine group due to a large *trans* effect from the NHC ligands. Nolan showed that the bond dissociation energies of NHCs from ruthenium metal centres are generally higher than phosphines (table 2.1.).[18] This stronger bonding should enhance the rate of phosphine dissociation as well as leading to more stable intermediates than those bearing simply a phosphine ligand during catalytic cycles. This should lead to higher activity in catalysis.

| L | Relative BDE (kJ mol$^{-1}$) |
|---|---|
| IMes | 65.5 |
| ICy | 89.0 |
| ITol | 79.0 |
| IPCl | 78.1 |
| IAd | 28.6 |
| IMesCl | 50.8 |
| IPr | 46.6 |
| $PCy_3$ | 44.1 |
| $P^iPr_3$ | 39.5 |

**Table 2.1.** Relative BDE of various ligands from [RuCl(Cp*)L]

However, Grubbs found that phosphine dissociation in the $IMesH_2$ bearing catalyst, **2**, was extremely slow relative to that in the bis phosphine complex, **35**.[19] This was an unexpected finding and so Grubbs carried out an in depth investigation, subtly changing the ligands on the ruthenium centre and investigating rates of phosphine exchange.[20] This threw up some interesting results.

$PCy_3$ and $PCp_3$ (Cp = cyclopentyl) are believed to have very similar steric and electronic parameters but replacing $PCy_3$ with $PCp_3$ in **35** led to a four fold increase in the rate of phosphine dissociation. Similarly, the rate of phosphine dissociation in **36**, which has an IMes ligand, is an order of magnitude slower than in **2**, which has an $IMesH_2$ ligand. Work by Nolan *et al.* has suggested that IMes and $IMesH_2$ have very similar steric and electronic properties.[21] Substitution of the $PCy_3$ ligand in **2** for $PPh_3$ leads to a 50 fold increase in rate of phosphine dissociation. Nolan and Fogg have noted that changing the phosphine ligand from $PCy_3$ to $PPh_3$ in the similar complex, [RuHCl(IMes)($PR_3$)(CO)] also greatly enhances the lability of the phosphine.[22] Thus it appears that the rate of phosphine dissociation is extremely sensitive to the type of phosphine and NHC on the complex and is more than a simple electronic effect. For all of the complexes examined, the rate of phosphine exchange was independent of phosphine concentration, implying that a dissociative mechanism is taking place.

*2.2.1.1. Phosphine dissociation from metathesis catalysts*

From the calculations carried out on phosphine dissociation, Grubbs has proposed a general mechanism for ruthenium catalysed alkene metathesis reactions, which involves phosphine being lost in a dissociative fashion, before being replaced by the alkene substrate (scheme 2.3.). This mechanism has since been endorsed both experimentally and computationally.[23-25] The recoordination of phosphine competes with the alkene, making the catalyst relatively inefficient as it can only complete a few turnovers before phosphine rejoins, forming the original complex. When NHC complexes are used, although the initial loss of phosphine is slow, once it is off, the coordination of alkene into the vacant site is much more favoured than the rebinding of phosphine. Thus, NHC complexes can complete many turnovers of the reaction before recoordinating with phosphine. In fact, Grubbs has shown that $[Ru(Cl)_2(IMesH_2)(PCy_3)(=CHPh)]$ (**2**) selectively binds alkenes over free phosphine by over four orders of magnitude, compared to $[Ru(Cl)_2(PCy_3)_2(=CHPh)]$ (**35**), and attributes this to the higher σ-donor properties of NHCs relative to alkyl phosphines.

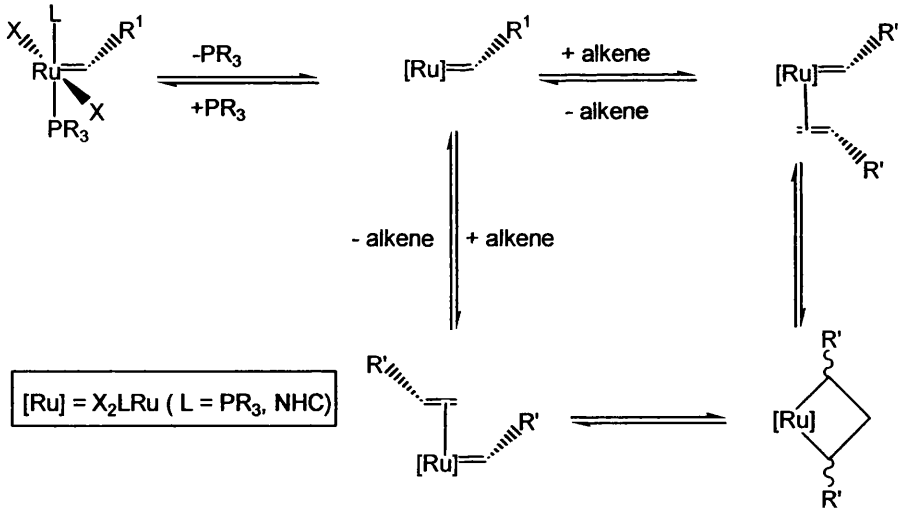


**Scheme 2.3.** Alkene metathesis mechanism as proposed by Grubbs.

The observation that NHCs are excellent σ-donors is supported by experimental work carried out by Cavell and co-workers, which suggest that in Pd(0)-alkene complexes, those bearing NHC ligands as opposed to phosphine ligands, promote and stabilise metal-alkene backbonding (NHC in this instance = $IMe_4$).[26] The two

extremes of metal-alkene bonding can theoretically be represented as pure donor or pure acceptor (figure 2.2.). Comparison of the $^{1}H$ and $^{13}C$ NMR shifts of the free alkene to that bound to a Pd-NHC complex, shows a strong upfield shift when it is bound to the metal centre ($^{1}H$ NMR, free alkene **H**RC=C**H**R (R = COOH): δ 7.05, bound alkene **H**RC=C**H**R: δ 3.34; $^{13}C\{^{1}H\}$ NMR, free alkene HR**C**=**C**HR: δ 136.6; bound alkene HR**C**=**C**HR: δ 38.2). This implies that the alkene is well shielded by the π-backbonding from the metal centre, which is made more electron rich by the presence of the NHC. This lessens the double bond character of the alkene and pushes the NMR shifts upfield.

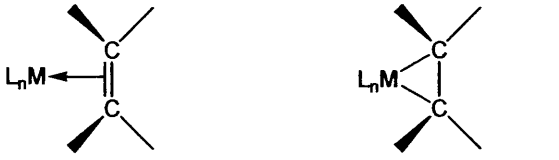


pure donor bonding pure acceptor bonding

**Figure 2.2.** Comparison of two bonding extremes of alkenes.

Recently, Piers has synthesised a 14-electron NHC complex (**37**), which can immediately bind alkene in the catalytic cycle, without having to undergo phosphine loss first (figure 2.3.).[27]

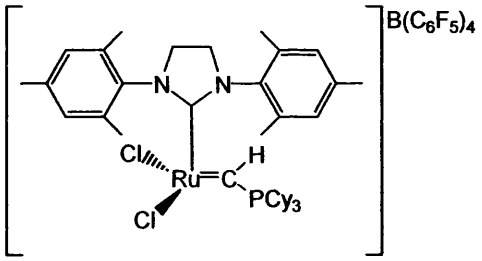


(37)

**Figure 2.3.** 14-electron variation on Grubbs' catalyst.

Initially, it was hoped that this species would be even more catalytically active than [$Ru(Cl)_2(IMesH_2)(PCy_3)$(=CHPh)] (**2**) as the complex would not have to undergo initial phosphine loss before binding alkene. In addition, there would be no free ligand in solution to compete with alkene binding. Indeed Piers found that in the

RCM of diallyldiethylmallonate, **37** led to higher conversion (90 % in 4 hours) than **2** (25 %) over the same amount of time.

More interestingly from a mechanistic point of view, however, Piers has used **37** to observe, for the first time, the predicted metallocyclobutane intermediate that Chauvin predicted was an integral part of the mechanism of the metathesis reaction (page 57).[28] Addition of 2.2 equivalents of ethene to **37** at -50 °C led to quantitative generation of the metallocyclobutane intermediate after 2-3 hours (figure 2.4.) along with the phosphonium salt $[CH_2{=}CHPCy_3][B(C_6F_5)_4]$. Piers used $^1H$-$^1H$ NMR correlations and selective decoupling experiments to show that the multiplets observed in the $^1H$ NMR spectrum at δ 6.6 ($H_B$) and -2.6 ($H_A$) (in a 4:2 ratio) were coupled to each other. Using $^{13}C$ labelled ethene led to further splitting of these resonances whilst the rest of the spectra remained unperturbed. The formation of the ruthenacyclobutane was demonstrated to be reversible by addition of an excess of $^{13}C$ labelled ethene to a previously unlabelled complex. Over time, the metallocyclobutane was converted to the labelled analogue.

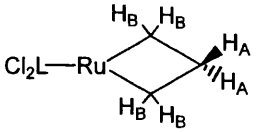


**Figure 2.4.** Metallocyclobutane intermediate showing protons observed by $^1H$ NMR spectroscopy.

*2.2.1.2. Solvent effects on second generation metathesis catalysts*

It has been noted that **36** and other Grubbs' metathesis catalysts bearing N-aryl substituents on the NHCs are more active in toluene whereas those with N-alkyl substituents are more active in chlorinated solvents.[29-31] From NMR studies, Fürstner observed that in $CD_2Cl_2$ not only was rotation around the C-Ru bond in **36** restricted, which has already been reported,[32] but that rotation of the mesityl substituents around the C-N bond was also hindered.[33] This is shown by the presence of two lines for the mesityl protons in $CD_2Cl_2$, which coalesce to just one when the complex is dissolved in $C_6D_6$, showing that the mesityl rings are moving around more rapidly.

The authors suggest that this is due to π-π stacking interactions between complex molecules, which have been seen in the crystal structures, between the benzylidene unit and the N-aryl substituents. Aromatic solvents could compete for interactions with the aryl substituents, reducing the stabilising effect of the π-π stacking, and giving the NHC ligands more rotational freedom. This rotational freedom allows the NHCs to move more freely once phosphine has dissociated from the complex, thus allowing the unsaturated complex to be stabilised and hence more active than in non-aromatic solvents.

*2.2.1.3. Decomposition of Grubbs' catalysts*

Dinger and Mol have noted degradation of both first and second generation Grubbs' metathesis catalysts with aliphatic alcohols and benzyl alcohol. Along with others,[34-36] they found that when $[Ru(Cl)_2(PCy_3)_2(=CHPh)]$ (**35**) was subjected to aliphatic primary alcohols, especially in the presence of additional base, $[RuHCl(PCy_3)_2(CO)]$ (**38**) was produced (figure 2.5.).[37] If benzyl alcohol is used in place of the aliphatic alcohol, $[RuClPh(PCy_3)_2(CO)]$ (**39**) is formed. They determined that these reactions occurred *via* an alcohol dehydrogenation pathway, producing toluene and alkane as byproducts. Both these degradation complexes are active alkene isomerisation catalysts, external alkenes reorganising to the internal alkene with 95 % selectivity.

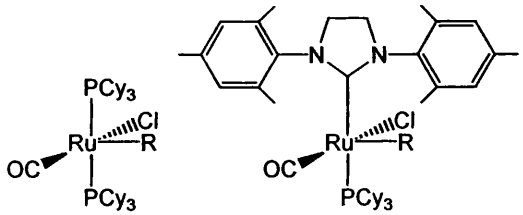


(**38**) R=H (**39**) R=Ph (**40**) R=H (**41**) R=Ph

**Figure 2.5.** Structures of decomposition products of Grubbs' catalysts.

When $[Ru(Cl)_2(IMesH_2)(PCy_3)(=CHPh)]$ (**2**) was reacted with methanol in the presence of triethylamine, the analogous decomposition product to that seen with **35**, $[RuHCl(IMesH_2)(PCy_3)(CO)]$ (**40**) was formed as the major product.[38] This could not be isolated as it is extremely soluble in all common organic solvents and the

authors postulate this may be because it is not a solid at room temperature. The complex could be precipitated from pentane at -78 °C but upon warming to room temperature gave only an oily residue that was highly air sensitive. **38**, the degradation product from **35**, was also observed, which is surprising as this would necessitate the exchange of $IMesH_2$ for $PCy_3$, which does not fit with the BDEs calculated by Nolan (page 59, L = IMes, BDE = 65.5 kJ $mol^{-1}$; L = $PCy_3$, BDE = 44.1 kcal $mol^{-1}$ on [RuCl(Cp*)(L)]).[18] Two other unidentified products were also observed by $^1H$ and $^{31}P$ NMR spectroscopy.

In contrast to the reaction of **35** with benzyl alcohol, which led cleanly to **39**, **2** gave a number of products. Again, this seems attributable to the relative lability of the $IMesH_2$ ligand under the conditions used (60 °C). Only 30 % of the desired phenylruthenium complex, [RuClPh($IMesH_2$)($PCy_3$)(CO)] (**41**) was formed and **38**, **39** and **40** were also observed (25 %, 5 % and 10 % respectively of the total by $^{31}P$ NMR spectroscopy). The other products could not be identified. **41** was found to be far more active for alkene isomerisation than **38** or **39**.

Grubbs has also shown that this carbonylation reaction also occurs with [$Ru(Cl)_2$(IMes)($PCy_3$)(=CHPh)] (**36**).[39] It was found that heating **35** and **2** in the presence of oxygen-containing substrates such as ethyl vinyl ether for prolonged periods of time also led to the carbonylation products.

More recently, Hong *et al.* have monitored the decomposition route of [$Ru(Cl)_2$($IMesH_2$)($PCy_3$)(=$CH_2$)], an intermediate in the metathesis reaction of **2**.[40] When this complex was heated in $C_6D_6$ at 55 °C, the major decomposition product was found to be a dinuclear compound with a bridging carbide and an $\eta^6$ bond between one of the ruthenium centres and one of the mesityl groups (figure 2.6.). [$CH_3PCy_3$][Cl] is produced concurrently to the bis metal species and this leads the authors to conclude that decomposition occurs by the proposed mechanism shown in scheme 2.4. Initially, $PCy_3$ dissociates and the resulting 14-electron metal fragment (**II**) is attacked by the free phosphine on the methylidene group (**III**). $H_2C$=$PCy_3$

then dissociates, leaving a 12-electron fragment (**IV**) that then reacts with **II** to give a chloride bridged dimer (**V**). $H_2C{=}PCy_3$, that is free in solution, can abstract HCl from this complex and the terminal alkylidyne that is then formed on one of the ruthenium centres (**VI**) undergoes oxidative addition to the other metal centre with migration of the two chlorides to give the product (**VII**).

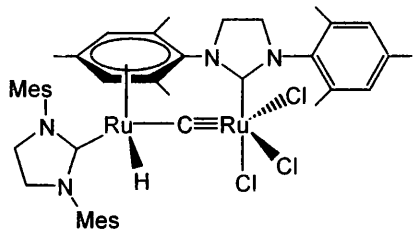


**Figure 2.6.** Decomposition product from $[Ru(Cl)_2(IMesH_2)(PCy_3)(=CH_2)]$.

*2.2.1.4. Alkene isomerisation by [Ru(Cl)$_2$(IMes)(PCy$_3$)(=CHPh)] (36)*

Bourgeois *et al.* found that using $[Ru(Cl)_2(IMes)(PCy_3)(=CHPh)]$ (**36**) in the ring closing metathesis of various dienes that required elevated temperatures and extended reaction times led to formation of an isomerised product of the initial diene in 5-10 % yield as well as the expected metathesis product.[31] Alkene isomerisation has been observed before when decomposition of the ruthenium catalyst occurs,[41-43] however, in this case the authors believe that it is **36** itself that is catalysing the reaction. This phenomenon has also been observed by Fürstner *et al.*[30] who noted formation of a 20-membered-macrolactone ring as well as the desired 21-membered product in the RCM of the diene shown in scheme 2.5. This is attributed to an isomerisation of the double bond in the starting diene, followed by elimination of propene instead of ethene during ring closure.

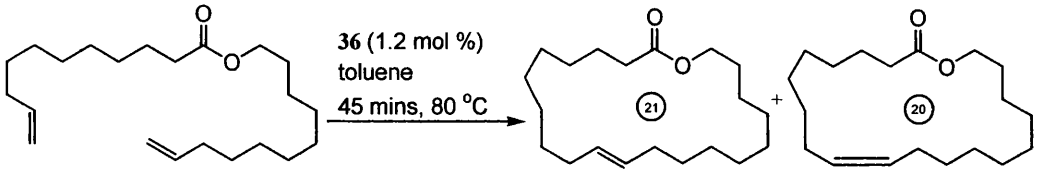


**Scheme 2.4.** Formation of two macrolactone rings from RCM of the diene, catalysed by **36**.

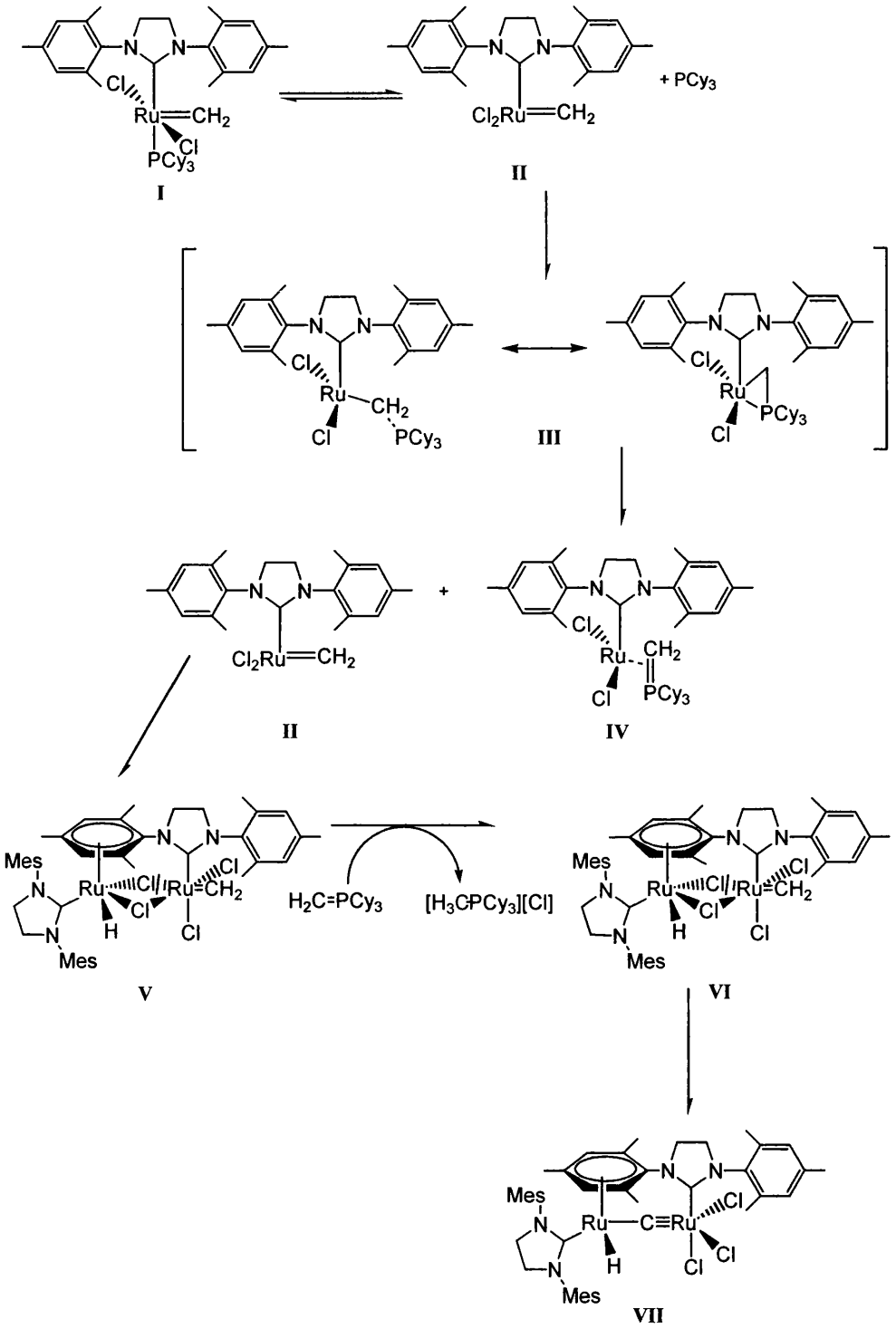


**Scheme 2.5.** Proposed mechanism of degradation of $[Ru(Cl)_2(IMesH_2)(PCy_3)(=CH_2)]$.

Bourgeois *et al.* have proposed a mechanism for this isomerisation (scheme 2.6.). Once **36** has coordinated to the less sterically crowded alkene moiety in the diene, the reaction can proceed along two routes. Firstly, the conventional metathesis reaction occurs, *via* a metallocyclobutane intermediate. However, along the second pathway, deprotonation at the allylic position leads to a π-allyl complex, responsible for the double bond migration. This complex is stabilised by the benzylidene carbon as the high oxidation state of the ruthenium will not favour the formation of a hydride complex. The IMes ligand, with its high σ-donating ability, increases the basicity of the benzylidene and adds to this stabilising effect. There is also the potential for an agostic interaction to occur between the unsaturated metal centre and the allylic hydrogen.

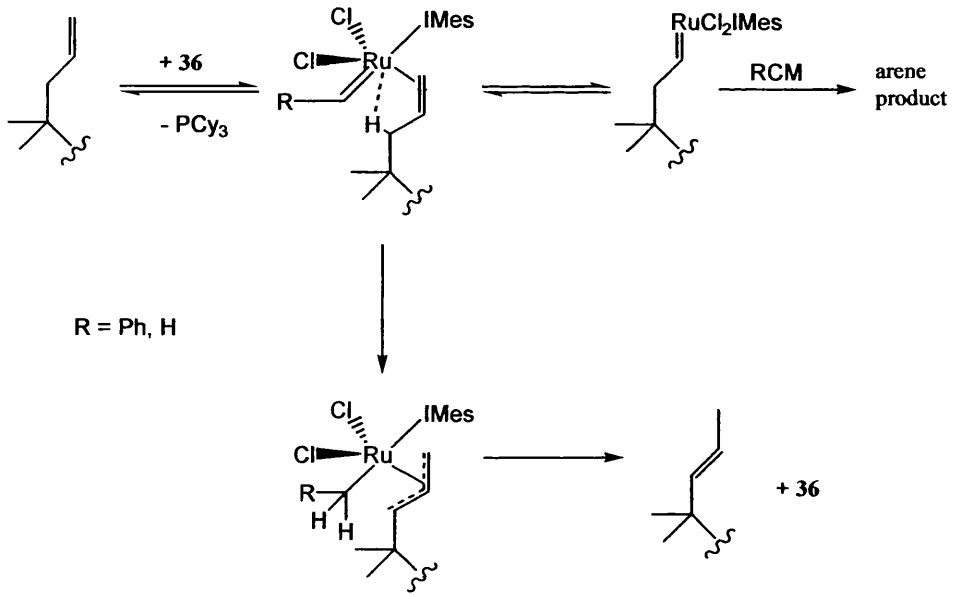


**Scheme 2.6.** Postulated mechanism of isomerisation observed in reactions with **36**.

The overall distribution between the metathesis product and the isomerisation product is highly dependent on the solvent used (scheme 2.7. and table 2.2.). The authors rationalise this in terms of coordination ability. The more coordinating solvents will prevent the second double bond from coordinating to the metal centre, thus preventing the process of ring closing metathesis and favouring the route to isomerisation.

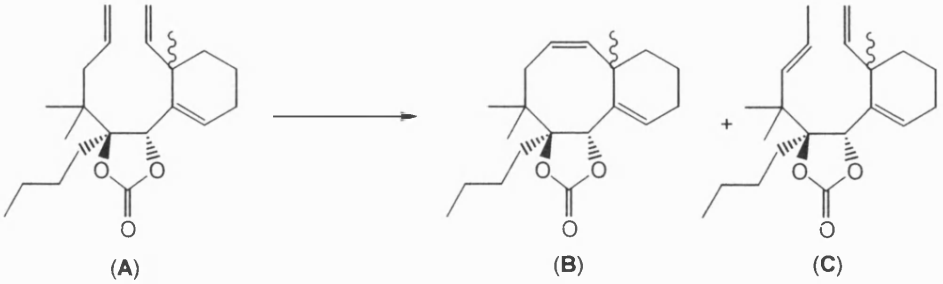


**Scheme 2.7.** Metathesis and isomerisation observed using **36**.

| Solvent | Boiling point (° C) | Metathesis product (B) (%) | Isomerisation product (C) (%) |
|---|---|---|---|
| Benzene | 80 | 50-70 | 30-50 |
| Toluene | 110 | 20 | 80 |
| DCE | 83 | 90 | 10 |
| DME | 85 | 0 | 100 |

**Table 2.2.** Ratio of (B) to (C) in catalysis of (A) by **36**.

In systems where ring closing metathesis occurs rapidly, isomerisation of the substrates is not observed as the coordination of the second double bond occurs before isomerisation has a chance to take place. Addition of additives, such as $PCy_3$, which goes on to form $O{=}PCy_3$, to the reaction mixture also inhibited isomerisation by binding to the metal centre strongly enough to prevent π-allyl or agostic bond formation but not so strongly as to prevent metallocyclobutane formation.

*2.2.1.5. Bis NHC catalysts*

Grubbs has gone on to synthesise bis NHC analogues of his metathesis catalysts, $[Ru(Cl)_2(IMesH_2)(IMes)(=CHPh)]$ (**42**) and $[Ru(Cl)_2(IMesH_2)_2(=CHPh)]$ (**43**) (figure 2.7.).[39] The crystal structure of **42** has been obtained although it possesses significant disorder between the two NHC ligands. Both **42** and **43** are extremely stable products and the NHCs should be hard to dissociate from the complex, which according to the mechanistic model proposed by Grubbs, should hinder the catalytic cycle.[12,19] At 80 °C, **43** shows activity in both RCM and ROMP reactions, suggesting that some initiation can occur. To test for this, **43** was heated in the presence of excess $PCy_3$ to trap out any of the 14-electron complex,

$[Ru(Cl)_2(IMesH_2)(=CHPh)]$ as $[Ru(Cl)_2(IMesH_2)(PCy_3)(=CHPh)]$ (**2**). After 16 hours at 80 °C the ratio of **43** to **2** was 1:1.4. After 36 hours it was 1:6.3. This shows that the 14-electron, active complex is forming and that it is probably extremely active even in small quantities. It also demonstrates that under certain conditions phosphine can replace NHC, as discussed in section 1.2.3.

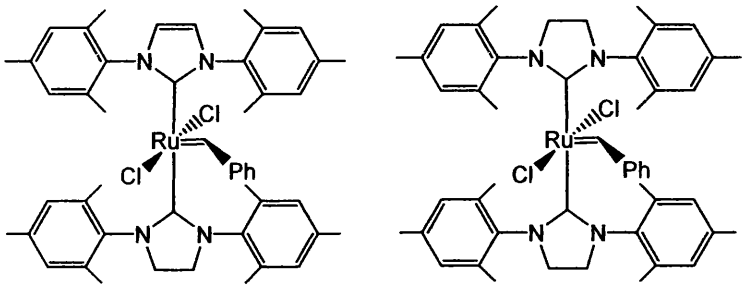


(42) (43)

**Figure 2.7.** Structures of Grubbs bis NHC complexes.

Herrmann and co-workers had already noted the phenomenon of loss of NHC from bis NHC complexes a few years earlier in the two bis NHC complexes they synthesised, $[Ru(Cl)_2(IPr)_2(=CHR)]$ and $[Ru(Cl)_2(ICy)_2(=CHR)]$, which were both extremely active in ROMP and RCM reactions.[32] Herrmann has also carried out DFT calculations for the ligand dissociation energies for various model complexes of the formula $[Ru(Cl)_2(L^1)(L^2)(=CH_2)(CH=CH)]$ ($L^1$, $L^2$ = $PH_3$, $PMe_3$, NHC).[2] These are presented in table 2.3. and show that bis NHC species should undergo ligand dissociation less readily than bis phosphine or mixed phosphine/NHC complexes. Experimentally, it was found that adding a large excess of $PCy_3$ to a bis NHC complex (NHC = ICy, IPr) did not lead to any formation of the mixed complex.

| Model compound | $\Delta E$ for $PH_3$ | $\Delta E$ for $PMe_3$ | $\Delta E$ for IH |
|---|---|---|---|
| $L^1 = L^2 = PH_3$ | 76.4 (81.5) | | |
| $L^1 = L^2 = PMe_3$ | | 113.4 (108.4) | |
| $L^1 = L^2 = IH$ | | | 189.0 (177.2) |
| $L^1 = PH_3$, $L^2 = IH$ | 78.5 (66.4) | | 197.0 (208.7) |
| $L^1 = PMe_3$, $L^2 = IH$ | | 109.2 (104.6) | 176.4 (182.3) |

**Table 2.3.** BDEs (in kJ $mol^{-1}$) for model complexes of the general formula $[RuCl_2(L^1)(L^2)(=CH_2)(CH=CH)]$, with (and without) ethene coordination.

Fogg's group have synthesised two bis IMes analogues of Grubbs' catalyst, $[Ru(Cl)_2(IMes)_2(=CH_2=CMe_2)]$ (**44**) and $[Ru(Cl)_2(IMes)_2(=CHPh)]$ (**45**).[44] **44** was not isolable due to its high solubility in all solvents but **45** precipitated as a crystalline air-stable solid that was good enough for X-ray diffraction studies. Fogg's complexes have not been investigated in catalytic reactions.

*2.2.1.6. Modifying the NHC on the second generation Grubbs' catalyst*

Jafarpour[18,45] Buchmeiser[46-48], Dinger[49], Fürstner[33] ,Herrmann[32], Harrison[50], Piers[27] and Grubbs himself[8,13,36,39,43,51,52] have all undertaken modifications to the second generation Grubbs' metathesis catalyst. Some of the complexes synthesised are shown in figure 2.8. No definitive trends have been found with these catalysts. Different metathesis reactions show different trends for the effectiveness of the catalysts and no one complex outperforms all the others in a majority of reactions.

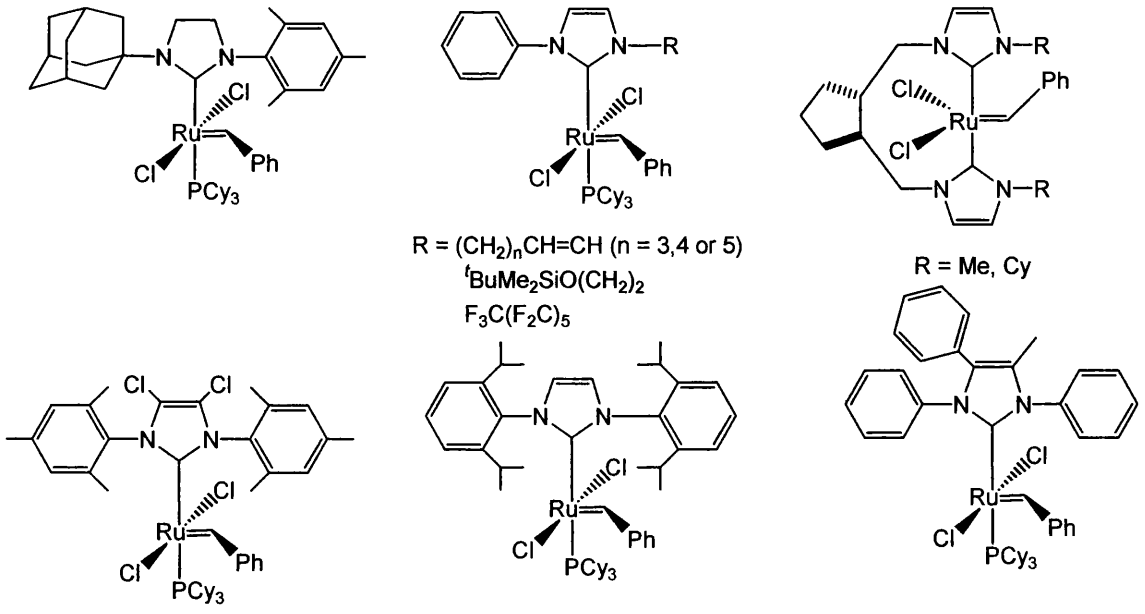


**Figure 2.8.** A series of variations of the Grubbs' second generation metathesis catalyst.

## 2.2.2. New ruthenium NHC complexes

The success of Grubbs' second generation catalyst led to similar substitutions being carried out on phosphine-bearing ruthenium catalysts, including by Nolan[22,53-55], Baratta[56], Joó[57], Çetinkaya[58], Crabtree[59,60] and Danopoulos.[61] Some of these are shown in figure 2.9. They have been used to catalyse both the direct hydrogenation of alkenes and cycloalkenes and the transfer hydrogenation of aldehydes as well as the dimerisation of alkynes and the transformation of alkenes to aldehydes. However, some Ru-NHC complexes have been found to be catalytically inactive.

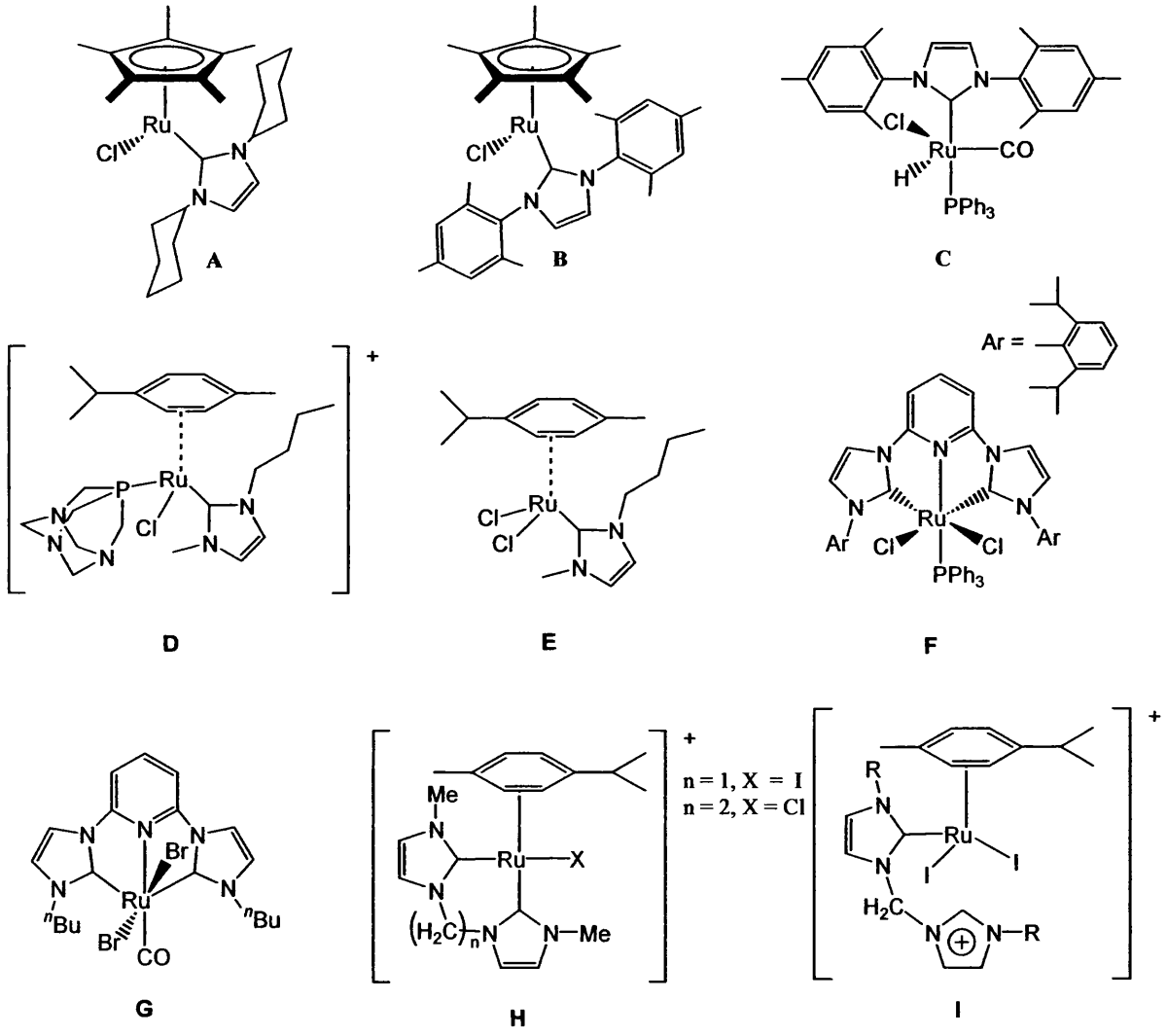


**Figure 2.9.** A range of Ru-NHC complexes with applications in alkyne coupling (**A, B**), hydrogenation of alkenes (**C-F**) and transfer of alkenes to aldehydes (**G**). **H** and **I** have no reported activity in catalytic reactions.

## 2.3. Aim of this work

The formation of the C-C activated complex [Ru(H)(IMes)'$(PPh_3)_2$(CO)] (**19**) in a relative facile reaction from the heating of [$Ru(H)_2(PPh_3)_3$(CO)] (**15**) and 3 equivalents of IMes at 100 °C for 21 days (section 1.2.8.) is intriguing because the system is not predisposed to undergo C-C activation, unlike the other complexes reported in the literature, which have been presented in section 1.1.3. The use of DFT calculations have been employed to try and gain an insight into the reasons that C-C bond activation is observed in this complex. These have been carried out by the Macgregor group at the University of Heriot Watt in Edinburgh. Initial calculations involved simplifying the models drastically using $PH_3$ ligands instead of $PPh_3$ and IH or IMe as the NHC. However, recently these models have been improved to include more steric bulk.

Experimental work in the laboratory has been carried out to try and directly prove the results obtained from the computational work. In addition, the effect of solvent on the activation reaction has been investigated.

## 2.4. Preliminary computational studies on bond activations in Ru-NHC complexes

Computational studies on CO stretching frequencies of [Ru(L)$(PH_3)_2$(CO)] and [$Ru(H)_2$(L)$(PH_3)_2$(CO)] (L = $PH_3$, IH, IMe)[62] suggest that replacing phosphine with an NHC ligand leads to a lowering of the $\nu_{CO}$ stretching frequency by 30-50 $cm^{-1}$ (table 2.4.). This is consistent with the ruthenium centre becoming more electron rich when NHC ligands are present. These complexes were examined in a variety of intermolecular bond reactions.

| Metal species | L | $\nu_{CO}$ ($cm^{-1}$) |
|---|---|---|
| $Ru(L)(PH_3)_2(CO)$ | $PH_3$ | 1934.6 |
| | IH | 1885.2 |
| | IMe | 1903.5 |
| $Ru(H)_2(L)(PH_3)_2(CO)$ | $PH_3$ | 1976.5 |
| | IH | 1940.3 |
| | IMe | 1944.3 |

**Table 2.4.** Calculated IR stretching frequencies for various ruthenium complexes.

Initial investigations by Diggle *et al.* centred on the ability of unsaturated ruthenium centres to promote intermolecular bond activations in the small molecules $H_2$, $CH_4$ and $C_2H_6$. Surprisingly, despite the increased electron rich nature of the NHC species, implied from the IR data, the difference in reactivity between $[Ru(PH_3)_3(CO)]$, $[Ru(IH)(PH_3)_2(CO)]$ and $[Ru(IH)_2(PH_3)(CO)]$ was negligible. When the NHC ligand was replaced by IMe and the calculations repeated, the activation energies for all the reactions were increased, suggesting that the activation barrier arises from a predominately steric effect rather than an electronic one. Models show that the IMe ligand has to move from the staggered position that it occupies, to accommodate the incoming substrate, costing more energy. Presumably this effect can only get greater as the steric bulk of the ligands increases.

The similarity in reactivity of the $PH_3$ and IH complexes can be rationalised if the models are broken down and consideration given to the orbitals around the metal. This shows that replacing a phosphine with an NHC does not lead to a significantly better Lewis base, although this does occur to some extent. However, the change in ligand does lead to a significant decrease in the Lewis acid properties of the fragment. These effects destabilise both orbitals leading to no change in the HOMO-LUMO gap overall (figure 2.10.).

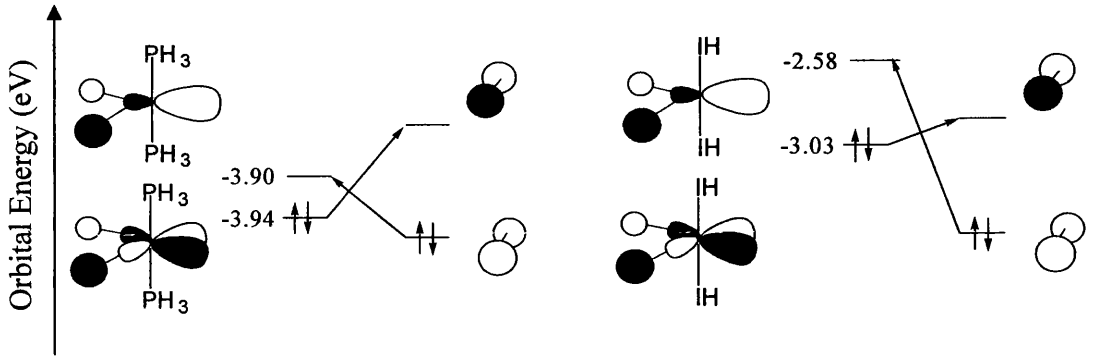


**Figure 2.10.** Computer generated difference in frontier orbitals between bis phosphine and bis NHC complexes of ruthenium.

The authors found that oxidative addition was a favourable process for $H_2$, both kinetically and thermodynamically. The latter effect was attributed to the formation of two strong Ru-H bonds in preference to the one or two relatively weak Ru-C bonds that would form from the oxidative addition of $CH_4$ or $C_2H_6$. This trend has been noted previously by Martinho-Simões and Beauchamp.[63] The favoured kinetics of the addition of $H_2$ lie with the spherical nature of the hydrogen atom, which allows for the formation of an efficient Ru-H interaction.[64,65] The electrons from the metal can be stabilised in the σ* orbital of the hydrogen atom whereas the $sp^3$ orbital from the $CH_3$ is less accessible and necessitates the $CH_4$ to distort as it approaches the metal fragment. This effect is exacerbated for the C-C bond activation in $C_2H_6$.

The initial calculations performed on intermolecular activation of small molecules were extended to intramolecular activation of substituents on the NHCs themselves.[66] The models used were still significantly simplified with $PH_3$ being used as the phosphine ligands. However, one of the H substituents on IH was replaced with a phenyl ring bearing H or Me at the *ortho*-position (figure 2.11.).

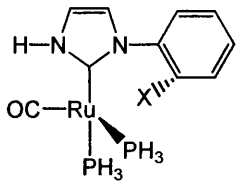


**Figure 2.11.** Molecule used in computer modelling approach to C-X bond activation.

The mechanism of C-H activation can lead to *cis* and *trans* products (where the Ru-H bond is *cis* or *trans* to the CO) (scheme 2.8.) and the viability of both pathways have been calculated.

Computing energy profiles for the *cis* and *trans* routes to C-H activation (numbers in scheme 2.8.) show that the flipping of the phenyl ring that would need to occur to produce the *trans* isomer is extremely unfavourable.[67] Calculations on the length of the *ortho*-C-H bond of the phenyl ring show that it is longer (1.25 Å (*trans*), 1.24 Å (*cis*)) than in the free NHC ligand (1.1 Å). This suggests that an agostic interaction is occurring between the C-H bond and the ruthenium centre. This agostic interaction is lost during flipping of the phenyl ring, as evidenced by the reduction in C-H bond length to 1.11 Å. This suggests that in mono NHC activated complexes the activated phenyl ring would sit *trans* to the CO, with the Ru-H bond *trans* to a phosphine. This is the case in the IMes activated product, [Ru(H)(IMes)''$(PPh_3)_2$(CO)] (**18**), seen by the Whittlesey group and discussed in chapter 1 (section 1.2.8.)[68] but not in the activated alkyl NHC complexes [Ru(H)($IEt_2Me_2$)''$(PPh_3)_2$(CO)] (**31**) or [Ru(H)($I^iPr_2Me_2$)''$(PPh_3)_2$(CO)] (**34**) seen by the same group.[69,70] However, the NHC is in a different geometry in the unactivated alkyl NHC complexes which probably leads to the different geometry of the activated species. Also, the ethyl and isopropyl substituents probably have less of a barrier to rotation or 'flipping' compared to a phenyl ring.

Similar calculations for C-C activation, carried out with a methyl group at the *ortho* position on the phenyl ring, show that the reaction goes through one transition state where lengthening of the Ar-Me bond is noted (from 1.51 to 1.82 Å) (scheme 2.9.). The phenyl ring and the imidazol ring become more planar to each other as the insertion of the metal centre into the Ar-Me bond takes place. Compared to the C-H activation described previously, the activation energy barrier for C-C activation is much larger (95.3 kJ $mol^{-1}$ compared to 0.55 and 0.59 kJ $mol^{-1}$ for *cis* and *trans* C-H activation). This highlights the steric effects of the methyl group, which inhibit the formation of an agostic complex and restrict the interaction of the ruthenium metal

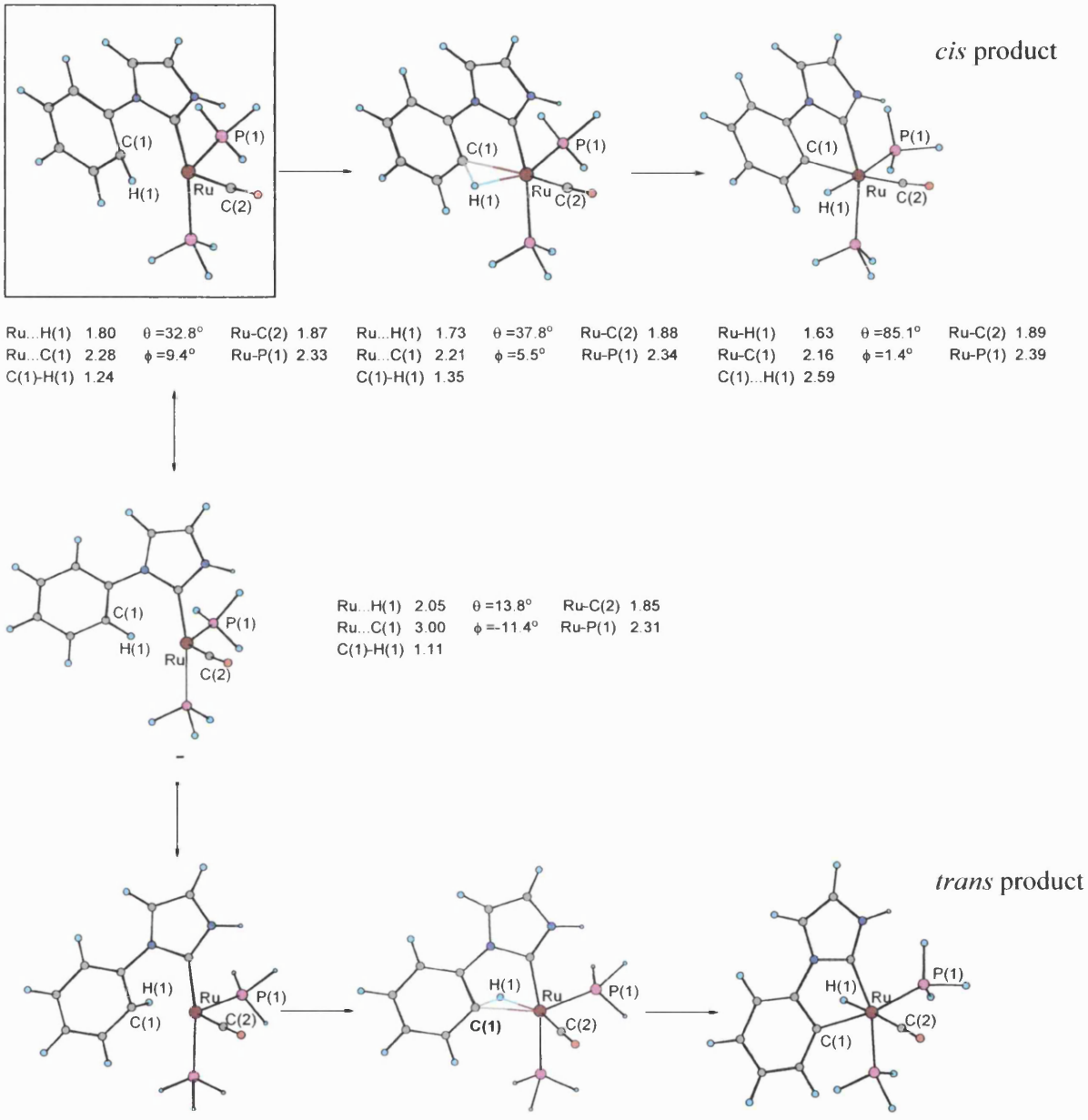


**Scheme 2.8.** C-H activation mechanism, from calculations, showing both *cis* and *trans* pathways for C-H activation, including intermediates, transition states and products. All bond lengths and distances are in Angstroms (Å).

centre with the Ar-Me bond. The *trans* influence of the CO has again affected the geometry, so that the CO lies *trans* to the phenyl group rather than the methyl ligand. The CO ligand does indeed lie *trans* to the phenyl group in [RuH(IMes)'$(PPh_3)_2$(CO)] (**19**), although this is a stage further on from what has been calculated, after methane has been lost.

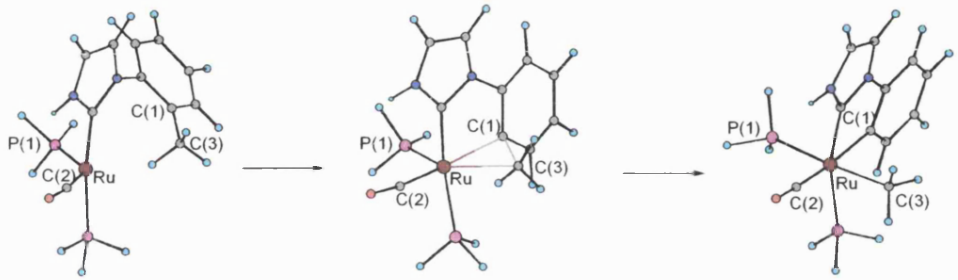


Ru...C(3) 3.17 θ =24.7° Ru-C(2) 1.84
Ru...C(1) 3.59 ϕ =-56.5° Ru-P(1) 2.33
C(1)-C(3) 1.51

Ru...C(3) 2.42 θ =46.2° Ru-C(2) 1.89
Ru...C(1) 2.19 ϕ =-14.0° Ru-P(1) 2.31
C(1)-C(3) 1.82

Ru-C(3) 2.45 θ =87.8° Ru-C(2) 1.89
Ru-C(1) 2.26 ϕ =-1.2° Ru-P(1) 2.36
C(1)...C(3) 3.10

**Scheme 2.9.** C-C activation mechanism, from computational calculations, showing the *cis* pathway, including the intermediate, transition state and product. All bond lengths and distances are in Angstroms (Å).

## 2.5. Characterisation of ruthenium hydride complexes by NMR spectroscopy

The hydride ligands on the activated complexes, [RuH(IMes)''$(PPh_3)_2$(CO)] (**18**) and [RuH(IMes)'$(PPh_3)_2$(CO)] (**19**), and the starting materials, [$Ru(H)_2(PPh_3)_3$(CO)] (**15**) and [$Ru(H)_2$(IMes)$(PPh_3)_2$(CO)] (**16**), make the reactions easy to follow by $^1$H NMR spectroscopy. In addition, the number and geometry of the phosphine ligands give distinctive coupling patterns in the hydride resonances as well as defined resonances in the $^{31}P\{^1H\}$ NMR spectra. The hydride resonances for **15**, **16**, **18** and **19** are shown in figures 2.12. to 2.15. Both **15** and **16** exhibit two hydride resonances due to the two inequivalent hydrides on the ruthenium centre. Each hydride in **15** couples to three phosphines, and to the other hydride. This gives two doublets of doublets of triplets (δ -6.53 ($^2J_{HP}$ = 15.3 Hz, $^2J_{HP}$ = 30.5 Hz, $^2J_{HH}$ = 6.1 Hz), -8.29, ($^2J_{HP}$ = 74.5 Hz, $^2J_{HP}$ = 28.1 Hz, $^2J_{HH}$ = 6.1 Hz)). The $^{31}P\{^1H\}$ NMR exhibits a

doublet and a triplet (δ 58.2 (d); 46.1 (t), $^2J_{PP}$ = 16.8 Hz). When one of the phosphines is replaced by an IMes ligand in **16** there are still two phosphine environments but now only one phosphine ligand in each. This leads to a doublet of doublets of doublets for each hydride (δ -6.36 ($^2J_{HP}$ = 26.8, $^2J_{HP}$ = 23.6, $^2J_{HH}$ = 6.0 Hz), -8.08 ($^2J_{HPt}$ = 81.2, $^2J_{HPc}$ = 33.6, $^2J_{HH}$ = 6.0 Hz)). Again, there are two resonances in the phosphorus spectrum, this time both are doublets (δ 59.0, 47.8, $^2J_{PP}$ = 14.8 Hz).

The C-H and C-C activated complexes only have one hydride resonance and hence have simpler splitting patterns. The proton on **18** exhibits a broad doublet of doublets due to coupling to two different phosphine environments (δ -7.97 ($^2J_{HP}$ = 102.4, $^2J_{HP}$ = 30.8 Hz)). The $^{31}P\{^1H\}$ NMR spectrum again consists of two doublets (δ 53.7; 28.4, $^2J_{PP}$ = 18.1 Hz). The NMR spectra of **19** are simpler still as the phosphines on the metal centre are equivalent leading to one triplet in the hydride region (δ -6.99, $^2J_{HP}$ = 28.4 Hz) and a singlet in the $^{31}P\{^1H\}$ NMR spectrum (δ 55.1).

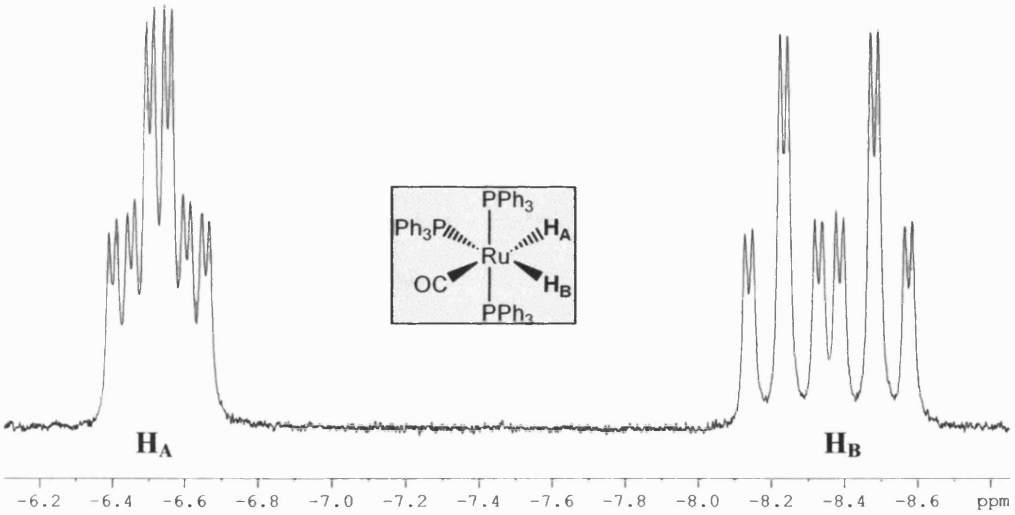


**Figure 2.12.** Hydride region in $^1H$ NMR spectrum of **15** ($C_6D_6$, 400 MHz, 25 °C).

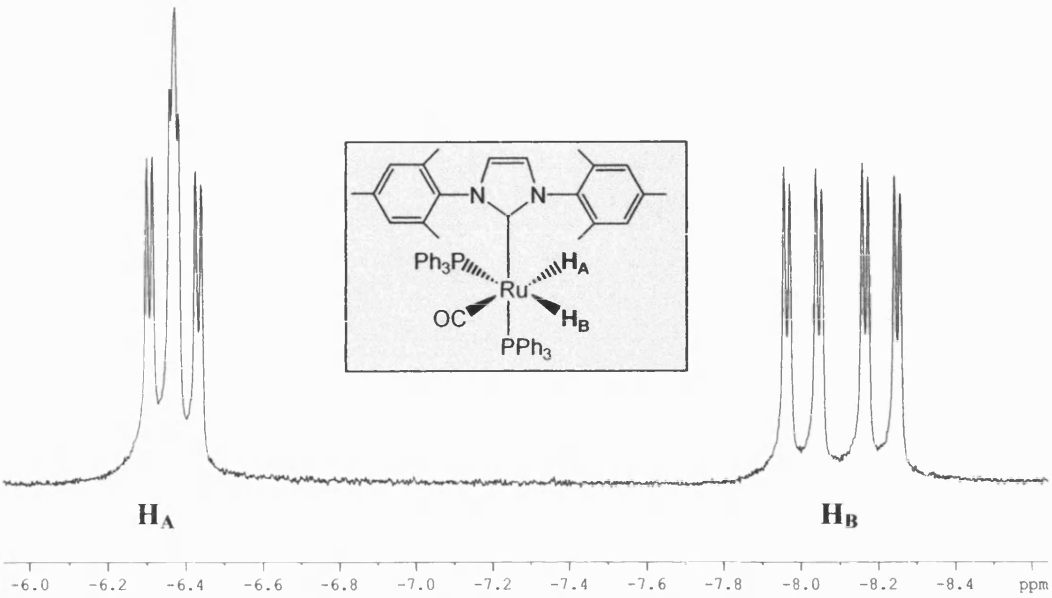


**Figure 2.13.** Hydride region in $^1$H NMR spectrum of **16** ($C_6D_6$, 400 MHz, 25 °C).

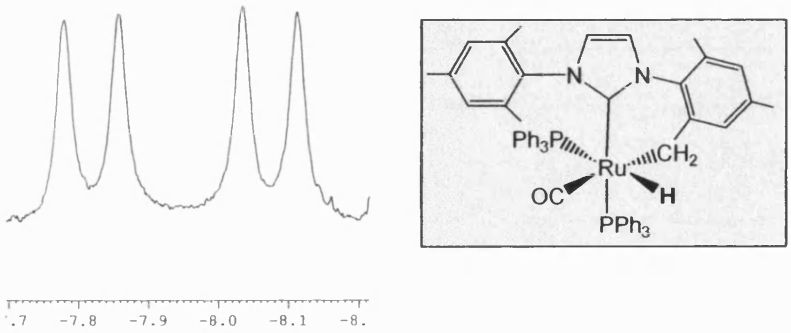


**Figure 2.14.** Hydride region in $^1$H NMR spectrum of **18** ($C_6D_6$, 400 MHz, 25 °C).

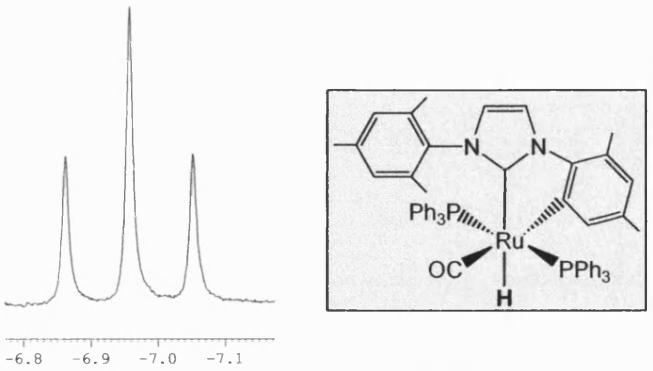


**Figure 2.15.** Hydride region in $^1$H NMR spectrum of **19** ($C_6D_6$, 400 MHz, 25 °C).

## 2.6. C-C activation *via* a bis NHC species

From the geometry of **19** it is clear that the auxiliary ligands must be involved in formation of the complex. The hydride ligand is *trans* to the IMes ligand, whereas on **16** and **17** the hydrides are *trans* to a phosphine and the CO group. The hydride on the C-H activated complex, **18**, is also *trans* to a phosphine. This suggests that once C-C activation of the mesityl ring has occurred, the subsequent loss of methane from the reaction sphere is not straightforward.

### 2.6.1. Further computational studies using full ligand models

Work in the laboratory suggests that **19** forms *via* **17**.[68,71] Using simplistic models of the complexes bearing IH and $PH_3$ substituents, did not provide any insight into why **17** may be more favourable to undergo C-C activation than **16**, as the differences between energy profiles were negligible (activation barrier for C-C activation of 95.3 kJ $mol^{-1}$ for mono NHC and 91.9 kJ $mol^{-1}$ for bis NHC). When the model complexes were modified to include the steric bulk of the phenyl groups on the phosphine and the mesityl groups on the NHC, the differences in activation energies for C-C activation between the mono and bis systems was greater (118.8 kJ $mol^{-1}$ for mono NHC and 88.8 kJ $mol^{-1}$ for bis NHC).[72] This suggests that C-C bond activation is easier when the *trans* ligand is an NHC and the fact that this difference was only noted upon inclusion of steric bulk implies that the effect is steric rather than electronic. However, by increasing the complexity of the computational models so much, a large degree of accuracy is lost and so these figures cannot be taken as definitive evidence that the bis NHC species is more prone to C-C activation than the mono NHC species. In addition, if **19** forms from **17**, IMes must be lost at some point and replaced by phosphine. Though this has been observed and discussed in chapter 1 (page 23) it is not energetically favourable.

There are three routes along which the C-C activation reaction could proceed from **17** to give **19** in the observed geometry (scheme 2.10.). Pathways A and B both

involve loss of $PPh_3$ and formation of either a dihydrogen complex (A) or oxidative addition of $H_2$ to give a seven coordinate Ru(IV) intermediate (B). $CH_4$ is then lost *via* either a σ-bond metathesis process (A) or reductive elimination (B). Alternatively, reaction may proceed *via* a 6-coordinate Ru(IV) dihydride intermediate (C). These options were established using DFT calculations by the Macgregor group. To try and determine experimentally which pathway occurs, isolation of **17** was of the utmost importance.

### 2.6.2. Attempted isolation of $[RuH_2(IMes)_2(PPh_3)(CO)]$ (17)

The characteristic $^1H$ and $^{31}P\{^1H\}$ NMR shifts allowed the formation of this complex to be easily monitored by NMR spectroscopy. The $^1H$ NMR spectrum shows two doublets of doublets in the hydride region. One is at δ –5.89, which is attributed to the hydride *cis* to the $PPh_3$ group due to its relatively small HP coupling constant (18.8 Hz). The other comes at δ –7.39 and from the larger coupling constant (93.5 Hz) is clearly *trans* to the phosphine. The $^1J_{HH}$ value is 7.1 Hz which is consistent with *cis* hydride coupling (figure 2.16.). The $^{31}P\{^1H\}$ NMR spectrum shows just one peak. This is a singlet at δ 47.3.

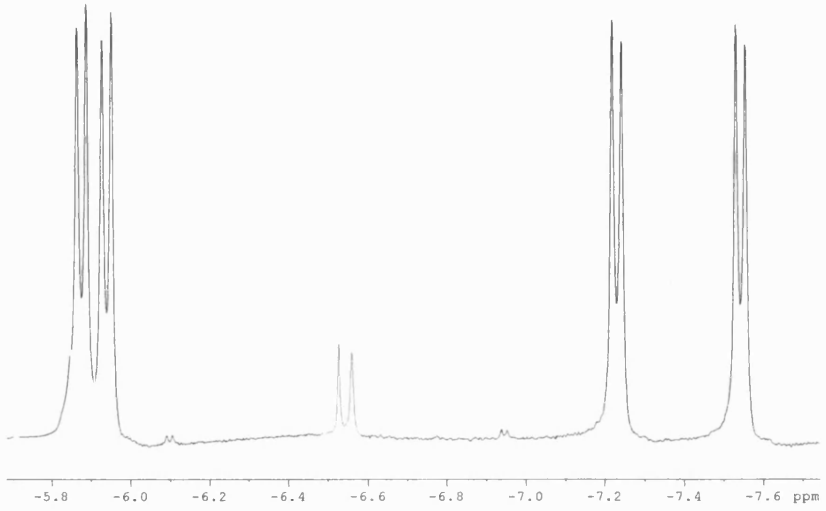


**Figure 2.16.** Hydride region in $^1H$ NMR spectrum of **17** ($d_8$-THF, 400 MHz, 25 °C) with some unidentified side products.

Two main methods were employed to try and isolate this complex.

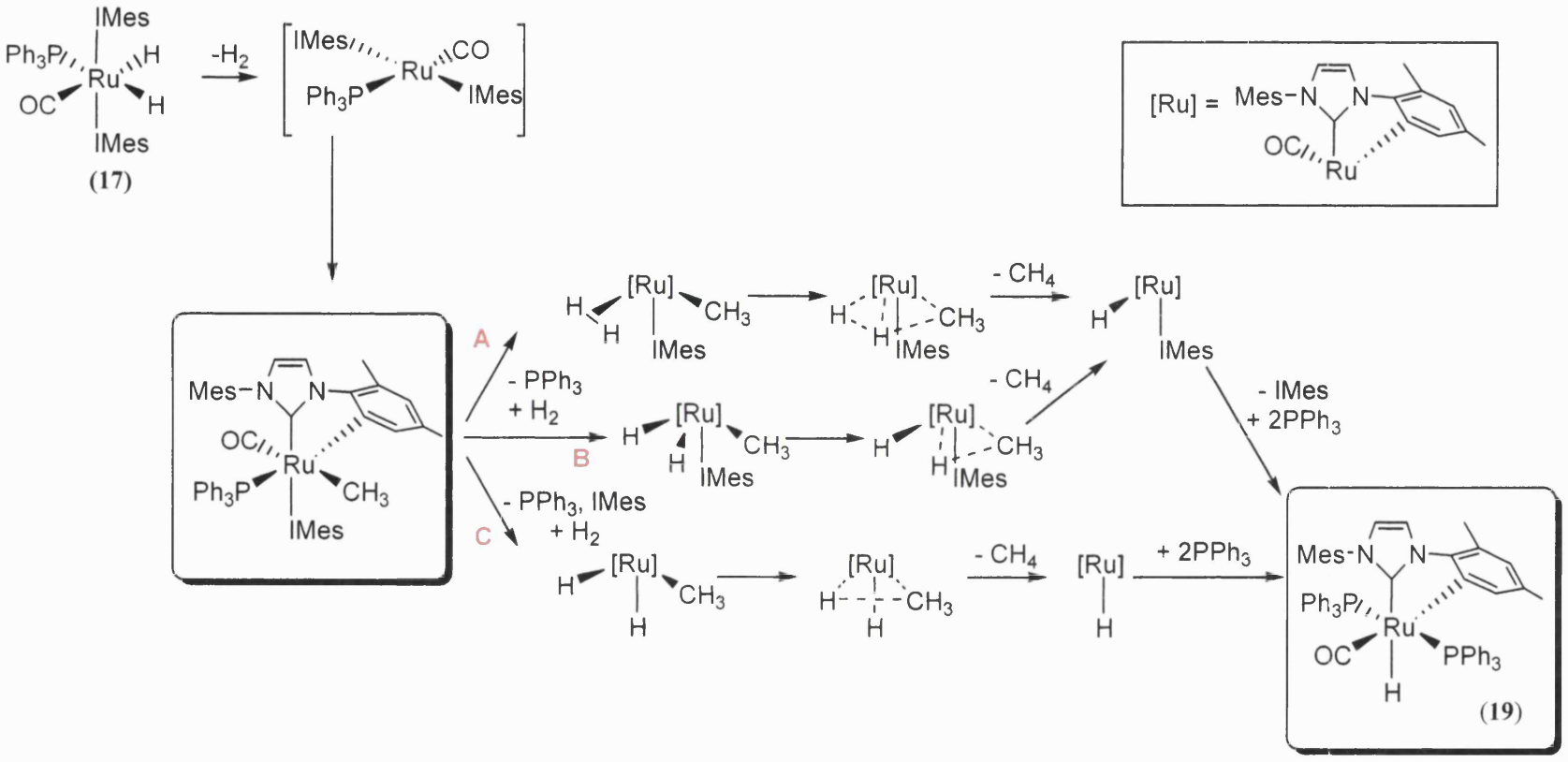


**Scheme 2.10.** Proposed reaction mechanisms for formation of **19**.

*2.6.2.1. Controlled reaction of [$RuH_2(PPh_3)_3(CO)$] (15) with IMes*

This experiment had to be carefully planned due to the many unknown factors in the C-C activation reaction pathway. It was known that heating the reaction past 80 °C pushes the reaction to the C-C activated product and that free IMes has to be present in large excess to drive the reaction. It is not known whether this is due to decomposition processes that are ongoing or to promote phosphine exchange reactions. The type of solvent employed is also thought to have a significant bearing on whether C-C activation occurs and this is discussed in more detail in section 2.6.3.

Unfortunately it was found that even when 50 equivalents of IMes were used in THF at 80 °C an equilibrium was formed between $[Ru(H)_2(PPh_3)_3(CO)]$ (**15**), $[Ru(H)_2(IMes)(PPh_3)_2(CO)]$ (**16**) and $[RuH(IMes)'(PPh_3)_2(CO)]$ (**19**). The reaction was also attempted by starting from **16** and adding 20 equivalents of IMes. This reaction proceeded until the ratio of bis:mono NHC complex was approximately 5:1 but then proceeded no further.

Attempts were made to separate the complexes from each other by columning the solution through silica using hexane/THF (1:1) in a glove box. Very little separation was observed, however, and free $PPh_3$ was also not found to be removed using this method.

*2.6.2.2. Reaction of [$RuH_2(AsPh_3)_3(CO)$] (20) with IMes and $PPh_3$.*

Heating $[Ru(H)_2(AsPh_3)_3(CO)]$ (**20**) (0.05 g) with three equivalents of IMes (0.05 g) in benzene (0.6 mL) at 80 °C leads to formation of the bis NHC arsine complex, $[RuH_2(IMes)_2(AsPh_3)(CO)]$ (**21**) already discussed in section 1.2.8. (page 43). As noted previously isolation of this complex is not possible due to the highly reactive nature of the arsine ligand. Adding $PPh_3$ (0.01 g) directly to a solution of **21** led to

complete conversion of **21** to $[Ru(H)_2(IMes)_2(PPh_3)(CO)]$ (**17**) by NMR spectroscopy.

However, there are still many difficulties with this chemistry. Firstly, the highly sensitive nature of both bis NHC species (**17** and **21**) means that all experimental conditions had to be kept exceptionally dry and air free to prevent formation of the hydroxy hydride complex, $[RuH(IMes)_2(OH)(CO)]$ (**23**). All glassware was flame dried and solvents were condensed into the reaction under vacuum. The free phosphine, which is easily detectable by NMR, and the free arsine, which is not, both need to be removed. The easiest way to eliminate the free phosphine is to make sure that no excess is added to the reaction in the first place and hence remove the need to try and separate it out. Unfortunately, phosphine does appear to have to be present in a slight excess to lead to complete conversion of **21** to **17**.

The removal of free phosphine and arsine proved extremely difficult. Columning the solution was unsuccessful, as detailed above. Adding $CuCl_2$, a technique used by Grubbs and co-workers,[7] effectively removed the $PPh_3$ but the chloride ions also interacted with **17**, leading to decomposition. The most effective method was to pump off the solvent, redissolve the residue in pentane (ca. 1.0 mL) and filter the solution at -78 °C by immersing the solution in dry ice/acetone. The free ligands are soluble in pentane whereas the product is not but multiple purifications are still necessary to completely separate them. Unfortunately, as the filtration has to be carried out using a filter cannula this leads to contamination with the hydroxy complex, **23**, as the labile phosphine group reacts with even the smallest amount of residual moisture in the cannula. After multiple purifications, the amount of **23** in solution becomes significant. Attempts were made to recrystallise the bis NHC complex, **17**, directly from solution. However, this was unsuccessful, again due to the extremely reactive nature of **17**. Attempts to prepare analogues of **17** with the potentially less labile phosphine ligands $PCy_3$ and $PMe_3$ were unsuccessful and led to a mixture of products.

Conrad *et al.* have also noted the difficulty in isolating bis IMes species although they attributed this to the high solubility of the complexes rather than problems with reactivity.[44] Work in the Whittlesey group has also found that the more NHCs there are round the metal, the harder they are to isolate due to their higher solubility in a large number of common solvents.[73] Although bis NHC complexes have been isolated, tris NHC complexes that have been observed by NMR are extremely soluble and were unable to be isolated. Grubbs has noted the difficulty in removing free phosphine during the synthesis of $[Ru(Cl)_2(IMesH_2)(PCy_3)(=CHPh)]$ (**2**), which is also extremely sensitive to air and moisture.[11]

Despite the failure to isolate clean $[Ru(H)_2(IMes)_2(PPh_3)(CO)]$ (**17**), there is evidence that it is on the pathway to the C-C activated species, **19**. Heating a solution that primarily contained **17** overnight at 100 °C led to loss of **17** and formation of **19**. However, in addition to the presence of the complex, IMes, $PPh_3$ and $AsPh_3$ were present in solution so it is unclear whether these free ligands had a part to play.

An IR spectrum of **17** was run after a sample in THF had been placed into a solution cell whilst in the glove box. A spectrum run immediately upon removal from the glove box gave a strong $\nu_{CO}$ peak at 1869 $cm^{-1}$, along with a smaller $\nu_{CO}$ peak at 1888 $cm^{-1}$. After leaving the sample on the bench for half an hour, the peak at 1869 $cm^{-1}$ had disappeared and the one at 1888 $cm^{-1}$ was much stronger. A $^1H$ NMR spectrum run on the sample showed very little **17** left in solution and the growth of a singlet at -6.45 ppm. This implies that the 1869 $cm^{-1}$ peak is attributable to the $\nu_{CO}$ stretching frequency of **17**. The $\nu_{CO}$ stretching frequency of **16**, in THF, is 1940 $cm^{-1}$, 70 wavenumbers higher. The values calculated by the Macgregor group for IH complexes suggested that for each NHC added, $\nu_{CO}$ decreases by 30-50 wavenumbers.[62] The significant difference between the substituents on the nitrogen between IMes and IH may well explain why the gap is slightly bigger than predicted even though, as has already been discussed (section 1.2.2., page 22), the type of NHC ligand generally does not seem to have an effect on $\nu_{CO}$ stretching frequencies.

2.6.3. Solvent effects on the formation of $[Ru(H)_2(IMes)_2(PPh_3)(CO)]$ (17) and $[Ru(H)_2(IMes)'(PPh_3)_2(CO)]$ (19)

As has already been discussed in sections 1.1.3.1., 1.2.7. and 2.2.1.2. the type of solvent that complexes are dissolved in can affect the type of bond activation they undergo and their catalytic reactivity. Investigation by NMR spectroscopy showed that when the formation of $[Ru(H)_2(IMes)'(PPh_3)_2(CO)]$ (**19**) is carried out in $C_6D_6$, H/D exchange into the phenyl rings of the free triphenylphosphine and the hydride occurs.[68] The *ortho* positions of free $PPh_3$ in solution also exhibit H/D exchange. No H/D exchange is observed upon heating $[Ru(H)_2(IMes)(PPh_3)_2(CO)]$ (**16**) with IMes to form $[Ru(H)_2(IMes)_2(PPh_3)(CO)]$ (**17**). There is also no H/D exchange observed when THF is employed as the solvent in the formation of **19** at 110 °C. This implies that the solvent is intimately involved in the C-C activation step. For this reason the effect of four different solvents on the formation of **17** and **19** were compared.

Four samples of $[Ru(H)_2(PPh_3)_3(CO)]$ (**15**) (0.50 g) and free IMes (0.50 g) were prepared and each was dissolved in a J. Young's resealable NMR tube, in a different solvent: $C_6D_6$, $d_8$-THF, $d_{12}$-cyclohexane and fluorobenzene (approximately 0.6 mL, with a $C_6D_6$ capillary in the tube in the case of fluorobenzene for ease of study by NMR spectroscopy). The samples were heated at 80 °C for 154 hours and then at 110 °C for 128 hours. They were monitored regularly by $^1H$ and $^{31}P\{^1H\}$ NMR spectroscopy.

The reactions in $C_6D_6$ and $d_8$-THF progressed at different rates at 80 °C, forming ratios of $[Ru(H)_2(IMes)(PPh_3)_2(CO)]$ (**16**) to $[Ru(H)_2(IMes)_2(PPh_3)(CO)]$ (**17**) to $[RuH(IMes)'(PPh_3)_2(CO)]$ (**19**) of 5.9:1:0.8 and 1.6:1:0.4 respectively after 154 hours at 80 °C (figure 2.17.). Upon increasing the temperature to 110 °C, the formation of **19** was greatly increased and after 21 hours at 110 °C the ratio of **17** to **19** was 0.3:1 in $C_6D_6$ and 0.1:4 in $d_8$-THF (figure 2.18.). A significant amount of **16** was left in the reaction in $C_6D_6$ (it is still just about the predominant product) whereas there was no **16** left in $d_8$-THF. As already noted,[68] H/D exchange is

observed by $^{31}P\{^{1}H\}$ NMR spectroscopy in the reaction in $C_6D_6$ but not the one in $d_8$-THF.

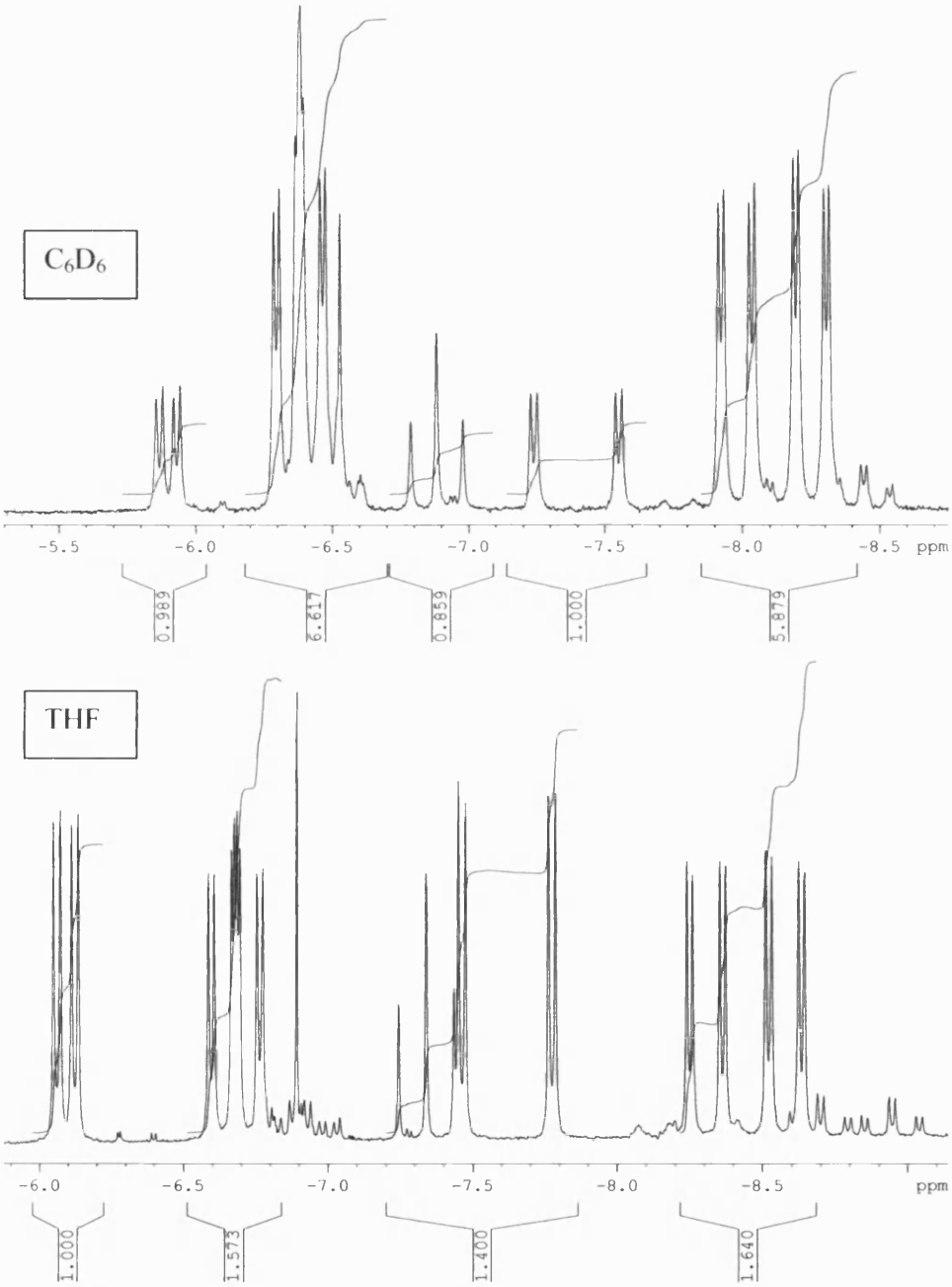


**Figure 2.17.** Hydride region of $^{1}H$ NMR spectrum showing ratio of **16**:**17**:**19** formed from **15** and IMes in $C_6D_6$ (5.9:1:0.8) and $d_8$-THF (1.6:1:0.4) after 154 hours at 80 °C (300 MHz, 25 °C).The value for **19** in $d_8$-THF is calculated from subtraction of the **17** peak at δ -6.1 from the combined resonance at δ -7.5.

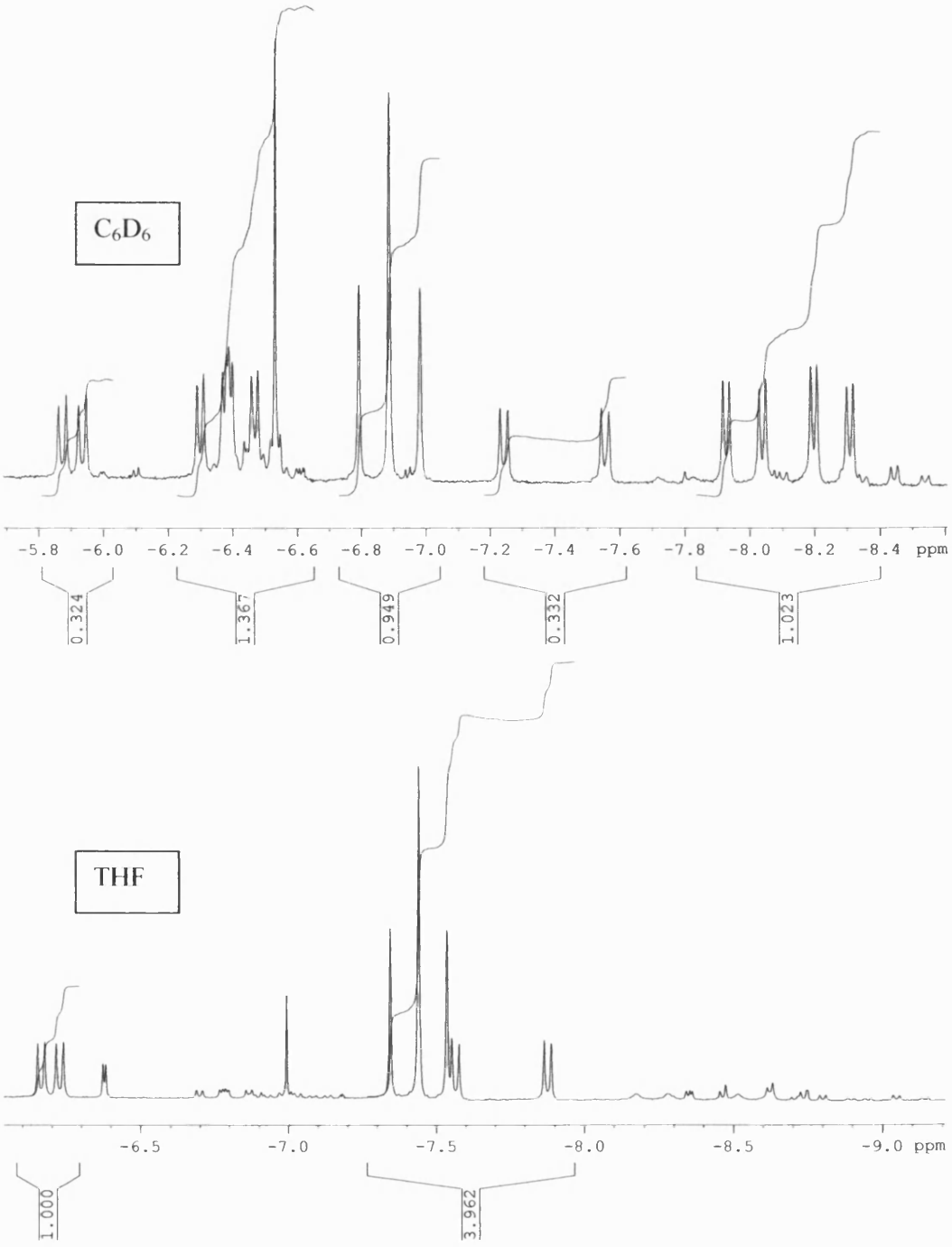


**Figure 2.18.** Hydride region of $^1$H NMR spectrum showing ratio of **16**:**17**:**19** formed from **15** and IMes in $C_6D_6$ (1:0.3:1) and $d_8$-THF (0:1:4) after 154 hours at 80 °C plus 21 hours at 110 °C (300 MHz, 25 °C).

In fluorobenzene a spurious singlet peak at δ -6.45 was the most prominent product, although this does not form until the sample was heated at 110 °C. This appears to be the same decomposition product formed when **17** was left exposed to the air (page 85) but the exact structure is unknown. After 154 hours at 80 °C very little **17** and no **19** had formed although a significant amount of **16** was present and there was also unreacted **15** left. Once the sample was heated to 110 °C, both **17** and **19** are seen (in approximately a 1:1 ratio to each other) along with a small amount of **16**. However, the major complex in solution was still unreacted **15** (figure 2.20.).

Using $d_{12}$-cyclohexane as the solvent both **16** and **17** were formed although not in particularly high yields (after 154 hours at 80 °C, **15**:**16**:**17**:**19** = 9:6:1:0). The unidentified singlet was again present in significant amounts. A small amount of **19** was observed when the sample was heated at 110 °C for 98 hours as was a large doublet at δ -6.50. This implies that there is only one hydride and one phosphine ligand left on the metal centre suggesting that the solvent may have bound to the metal centre as well as either the IMes or phosphine ligand undergoing bond activation (figure 2.19.). What is extremely interesting in this reaction, however, was the formation, upon heating at 110 °C, of the C-H activated product, **18** (previously only seen upon addition of alkene to **16**[68]) with the concurrent loss of **16** (figure 2.21.).

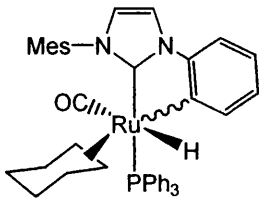


**Figure 2.19.** Plausible structure of product belonging to doublet at δ -6.50 in reaction of **15** and IMes in cyclohexane at 100 °C.

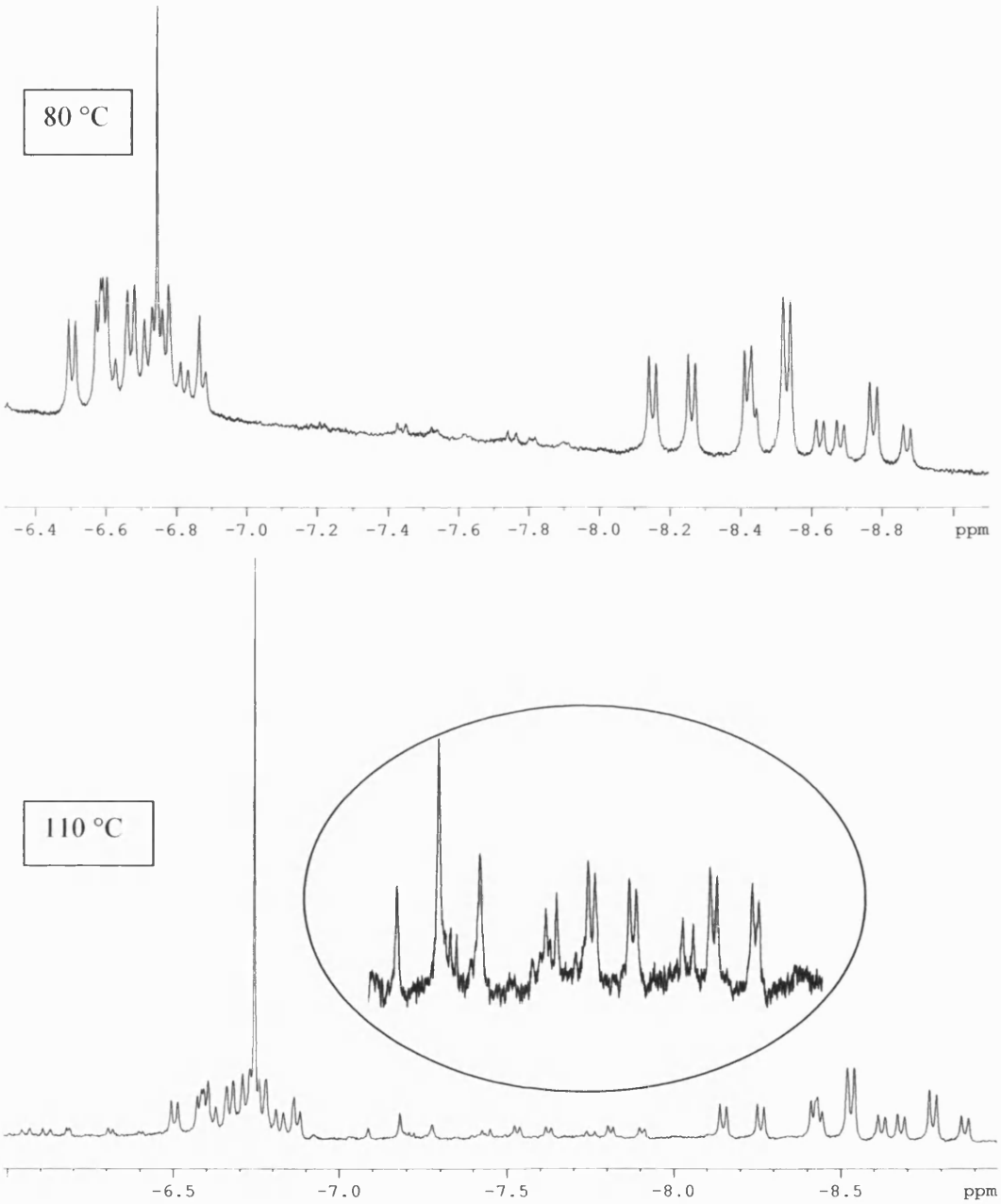


**Figure 2.20.** Hydride region of $^{1}H$ NMR spectrum showing reaction of **15** and IMes in fluorobenzene at 80 °C for 154 hours and then a further 21 hours at 110 °C ($C_6D_6$, 300 MHz, 25 °C).

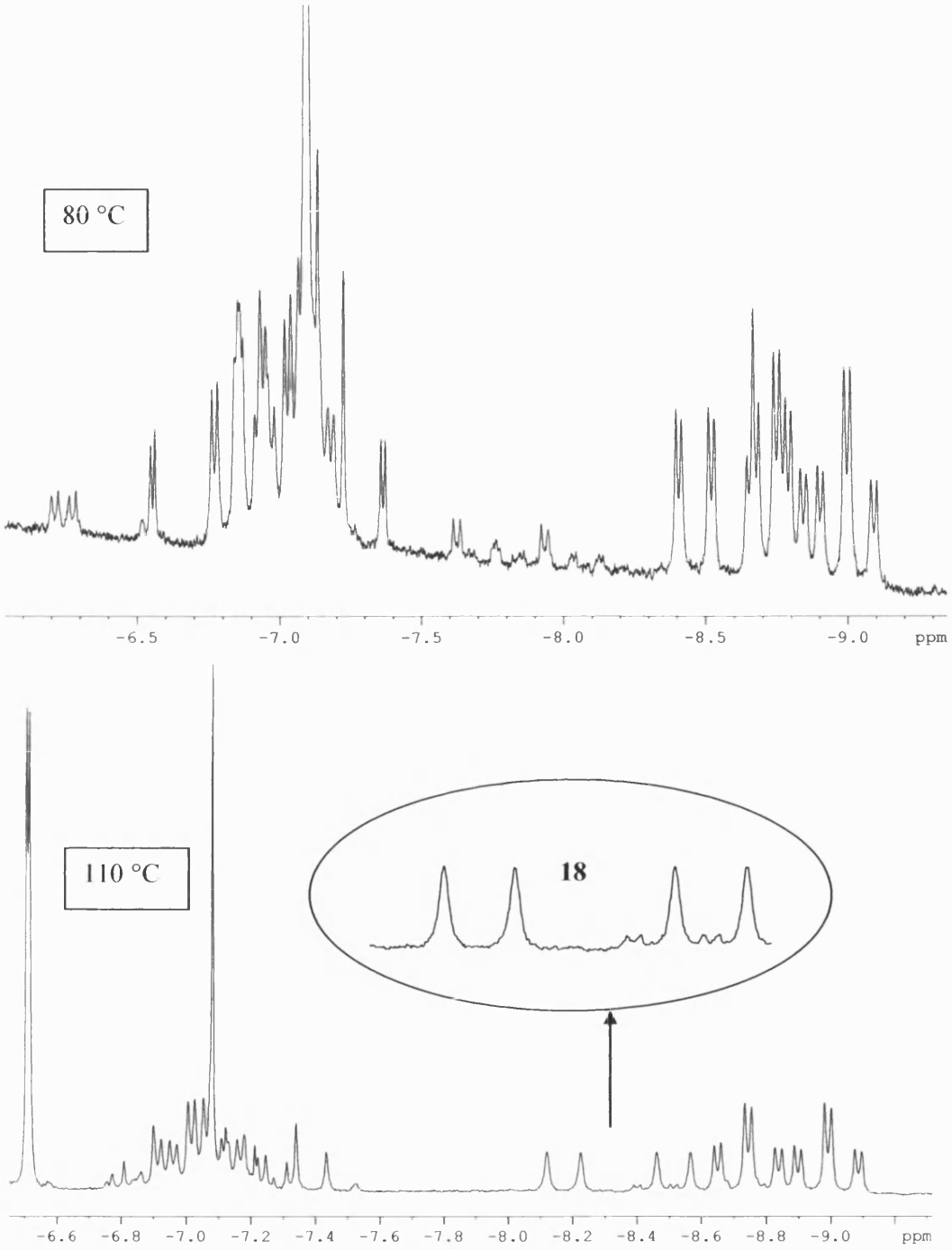


**Figure 2.21.** Hydride region of $^1$H NMR spectrum showing reaction of **15** and IMes in $d_{12}$-cyclohexane at 80 °C for 154 hours and then a further 98 hours at 110 °C ($d_{12}$-cyclohexane, 300 MHz, 25 °C).

## 2.7. Formation of [RuH(IMes)'(PPh$_3$)$_2$(CO)] (19) from [RuH(IMes)''(PPh$_3$)$_2$(CO)] (18)

A plausible theory, suggested by the computational studies, proposed that C-H activation could be on the pathway to C-C activation.[74] This is because the energy of C-H activation for [Ru(IMes)(L)(PPh$_3$)] is much lower than the energy of C-C activation (L = PPh$_3$, C-H activation = 57.1 kJ mol$^{-1}$, C-C activation = 118.8 kJ mol$^{-1}$; L= IMes, C-H activation = 29.0 kJmol$^{-1}$, C-C activation = 88.8 kJ mol$^{-1}$). The observed formation of [RhH(IMes)''(PPh$_3$)$_2$(CO)] (**18**) in cyclohexane discussed above suggested that it may be possible that at high temperature in other solvents **18** initially forms and then rapidly continues on to [RuH(IMes)'(PPh$_3$)$_2$(CO)] (**19**) (scheme 2.11.).

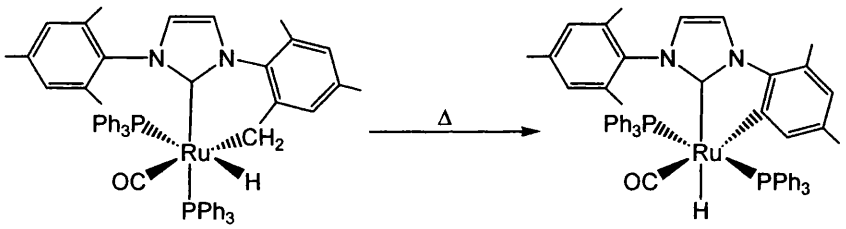


(18) (19)

**Scheme 2.11.** Possible formation of **19** from heating **18**.

To investigate whether **18** could lead on to **19** a clean sample of **18** was formed in a J. Young's resealable NMR tube from [Ru(H)$_2$(IMes)(PPh$_3$)$_2$(CO)] (**16**) (0.02 g) and 1 atmosphere of ethene in $C_6D_6$ (0.6 mL). After 1 hour at room temperature **18** was the sole product and the solution was pumped to dryness to ensure complete removal of ethene and ethane. The residue was then redissolved in $C_6D_6$ and the solution was heated at 100 °C for three hours. After this time a small amount of **19** was seen by $^1$H NMR spectroscopy, along with a lot of residual **18**. However, there was also a significant amount of the tris phosphine starting material, [Ru(H)$_2$(PPh$_3$)$_3$(CO)] (**15**) (figure 2.22.). This shows that heating **18** at elevated temperatures leads to loss of the IMes ligand. Unfortunately this means that it is impossible to say whether **19** is forming directly from **18** or whether **19** is forming from the bis NHC species.

Although $[Ru(H)_2(IMes)_2(PPh_3)(CO)]$ (**17**) cannot be distinguished in the hydride region, some of the decomposition product, $[RuH(IMes)_2(OH)(CO)]$ (**23**), is present, suggesting that **17** may have formed but has reacted with residual moisture in solution. There is an unexplained doublet present at δ -7.37 ($^2J_{HP}$ = 28.0 Hz). After **48** hours at 100 °C, no **18** remains in the reaction mixture, **19** and **17** are both present but **15** is by far the major product. Free IMes is also visible by $^1$H NMR spectroscopy. When this reaction is repeated with addition of free IMes to the solution of **18**, the major product is **23**, with a small amount of **19** present and no evidence for **15**. A summary of the products formed upon heating of **18** is shown in scheme 2.12.

These findings suggest that **19** does form by going through **17** and not through **18**.

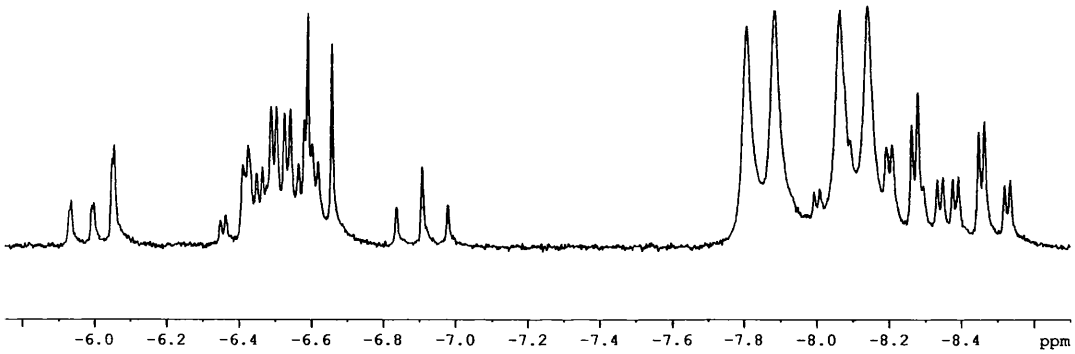


**Figure 2.22.** Hydride region of $^1$H NMR after heating solution of **16** at 100°C overnight ($C_6D_6$, 400 MHz, 25 °C).

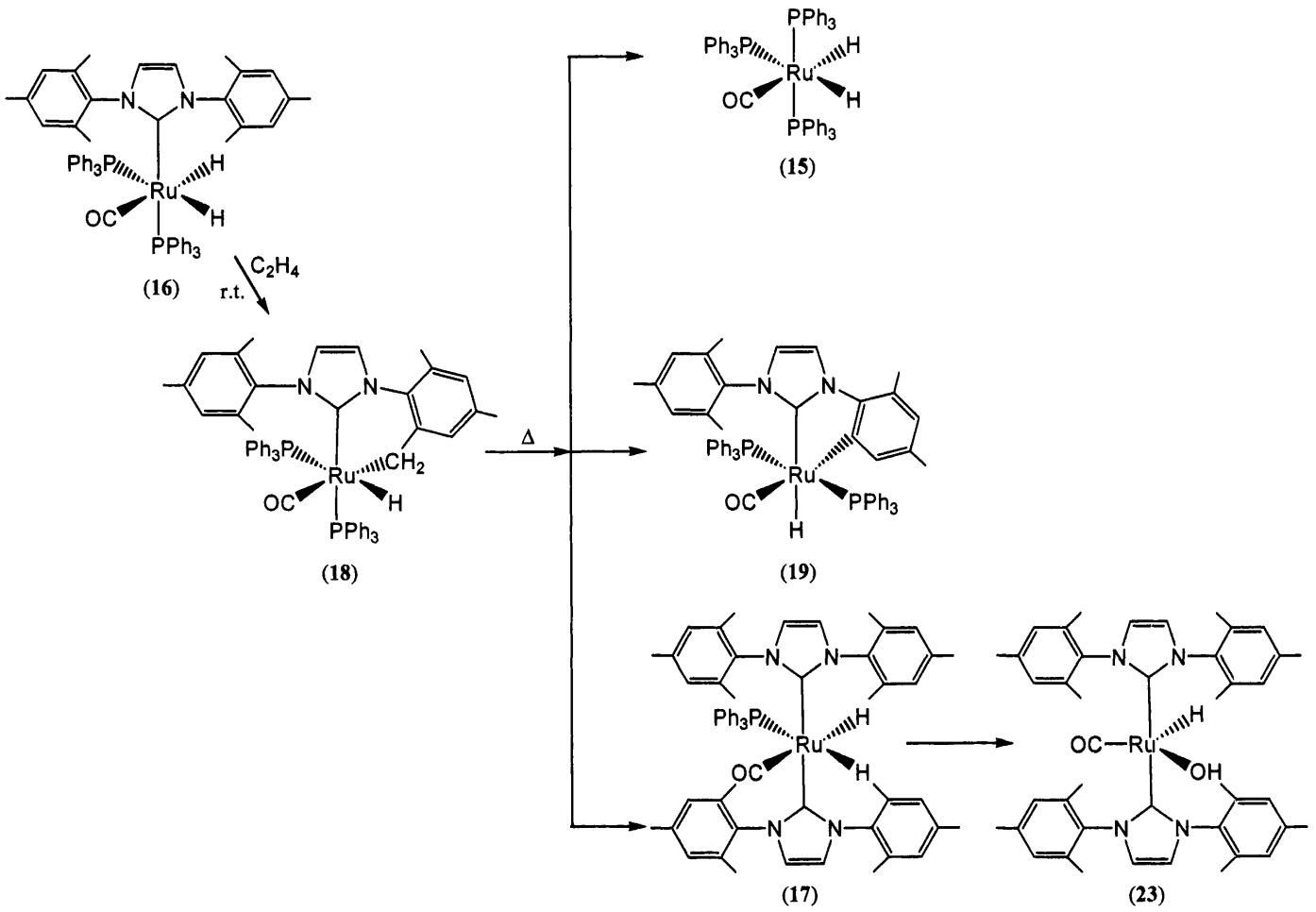


**Scheme 2.12.** Compounds formed from heating **18** at 100 °C.

## 2.8. Photolysis of ruthenium NHC complexes

Failure to access $[Ru(H)_2(IMes)_2(PPh_3)(CO)]$ (**17**) cleanly by simple substitution for studies of C-C activation, led to a change in approach and the attempt to access possible C-H and/or C-C activation pathways photochemically.

Precedent in the literature suggested that exposing *cis* dihydride complexes to UV light should lead to loss of $H_2$,[75-78] leaving a vacant site on the metal. Without the presence of free ligands in solution, it was hoped that on exposure to UV light, complexes such as $[Ru(H)_2(IMes)(PPh_3)_2(CO)]$ (**16**) would undergo bond activation from the NHC ligands in a cleaner reaction than that which could be achieved in thermal reactions.

### 2.8.1. Reactions of $[M(H)_2(dmpe)_2]$ under photolysis

The reactions of $[Fe(H)_2(dmpe)_2]$ (**46**) and $[Ru(H)_2(dmpe)_2]$ (**47**) (dmpe = $Me_2PCH_2CH_2PMe_2$) in the presence of UV light have been extensively investigated and are typical of many complexes that undergo $H_2$ loss when irradiated.[79-82] Both complexes have been shown to be reactive to small molecules when irradiation is carried out in their presence. These reactions for **46** are summed up in scheme 2.13.[83-86]

The recombination of $H_2$ to **46** is far slower than that to **47** and this means reactivity of hydrocarbons with **46** is a lot faster than with **47**.[80,87] As the back reaction is slower, it allows the reaction with other substrates to proceed more rapidly. This suggests that the two complexes exist in a different geometry. **47** is proposed to exist in a square planar geometry whereas **46** has a butterfly shape, allowing it to be weakly solvated and thus stabilised for back-side attack by substrates.[77,87]

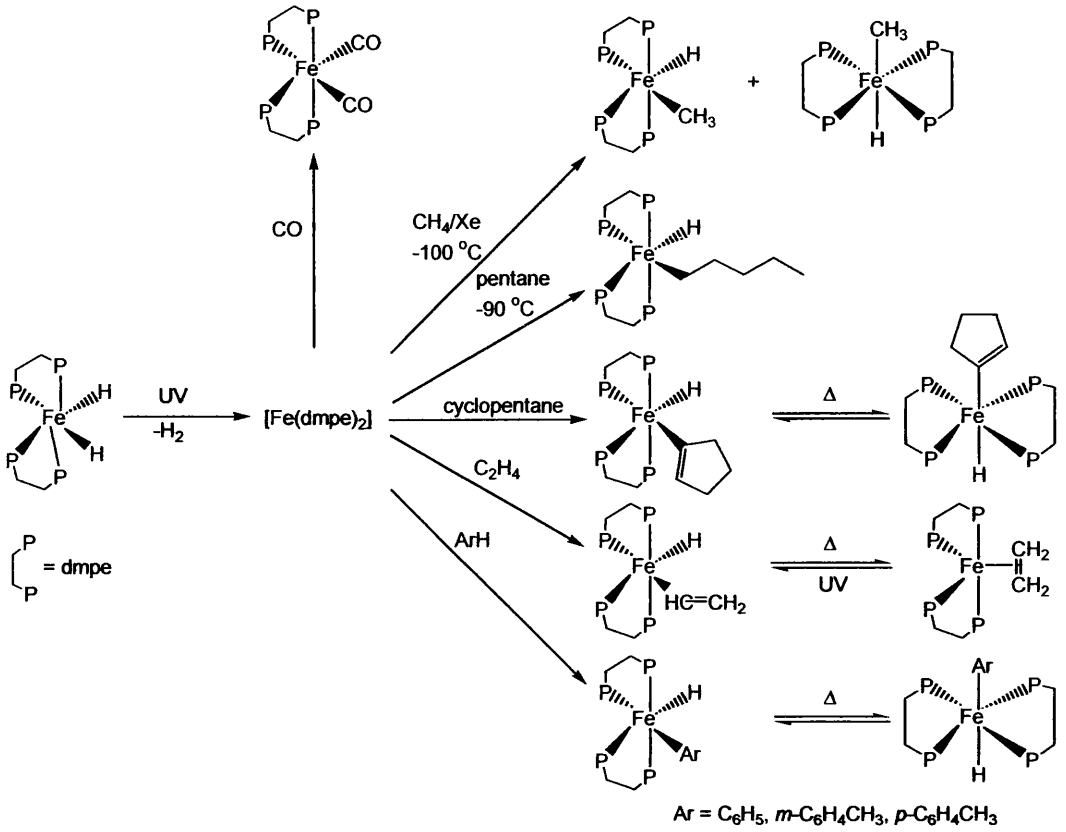


**Scheme 2.13.** Reactions of **46**, under UV in the presence of various hydrocarbons and CO.

2.8.2. Photolysis of $[Ru(H)_2(NHC)_x(PPh_3)_y(CO)]$ complexes (NHC = $IEt_2Me_2$, $I^iPr_2Me_2$, ICy, IMes, x = 1, 2, y = 1, 2)

A sample of $[Ru(H)_2(IMes)(PPh_3)_2(CO)]$ (**16**) was dissolved in deuterated toluene in a J. Young's resealable NMR tube (concentration = 0.02 mol $dm^{-3}$) and was subjected to UV light (Hg arc, $\lambda > 285$ nm, 125 W) at room temperature. Even after 13 hours under these conditions, no change to the complex was observed. Prolonged irradiation (100 hours) led to decomposition of **16** and concurrent formation of a doublet in the hydride region ($\delta$ -6.54 ($^2J_{HP}$ = 26.5 Hz)), which has not been assigned but suggests loss of both one hydride and a phosphine ligand. No evidence for C-H or C-C activation was found.

The new ruthenium alkyl-NHC complex, $[Ru(H)_2(IEt_2Me_2)(PPh_3)_2(CO)]$ (**29**) (figure 2.23.) has recently been synthesised in the Whittlesey group and has already been discussed in chapter 1, pages 43 and 44.[71]

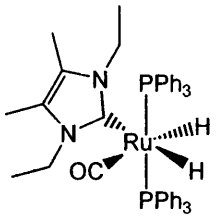


(**29**)

**Figure 2.23.** Structure of the alkyl NHC complex **29**.

When a sample of **29** was irradiated at room temperature in $d_8$-toluene (concentration = 0.02 mol $dm^{-3}$), NMR spectroscopy showed that isomerisation of the complex occurred so that the NHC ligand moved from a position *trans* to hydride to a position *trans* to phosphine (**33**), which is the same geometry as found in **16**. The geometries of the complexes are readily assigned from the appearance of their hydride resonances in the $^1H$ NMR spectra. The starting material, **29**, exhibits a doublet of triplets for each hydride resonance (δ -5.96 ($^2J_{HP}$ = 26.3 Hz, $^2J_{HH}$ = 5.5 Hz), -9.41 ($^2J_{HP}$ = 24.7 Hz, $^2J_{HH}$ = 5.5 Hz)) from coupling to two equivalent phosphines and each other. Isomerisation to **33** leads to a change in the coupling pattern as the phosphines now become inequivalent (δ -5.62 ($^2J_{HP}$ = 30.7 Hz, $^2J_{HP}$ = 21.4 Hz, $^2J_{HH}$ = 2.7 Hz), -7.60 ($^2J_{HP}$ = 85.6 Hz, $^2J_{HP}$ = 28.5 Hz, $^2J_{HH}$ = 2.7 Hz)) (figure 2.24.).

The formation of **33** is seen within minutes. After five hours, the ratio of **29**:**33** was approximately 1:1.8. After this time the complexes begin to degrade upon further exposure to UV light, evidenced by the appearance of free $PPh_3$ in the $^{31}P\{^1H\}$ NMR spectrum.

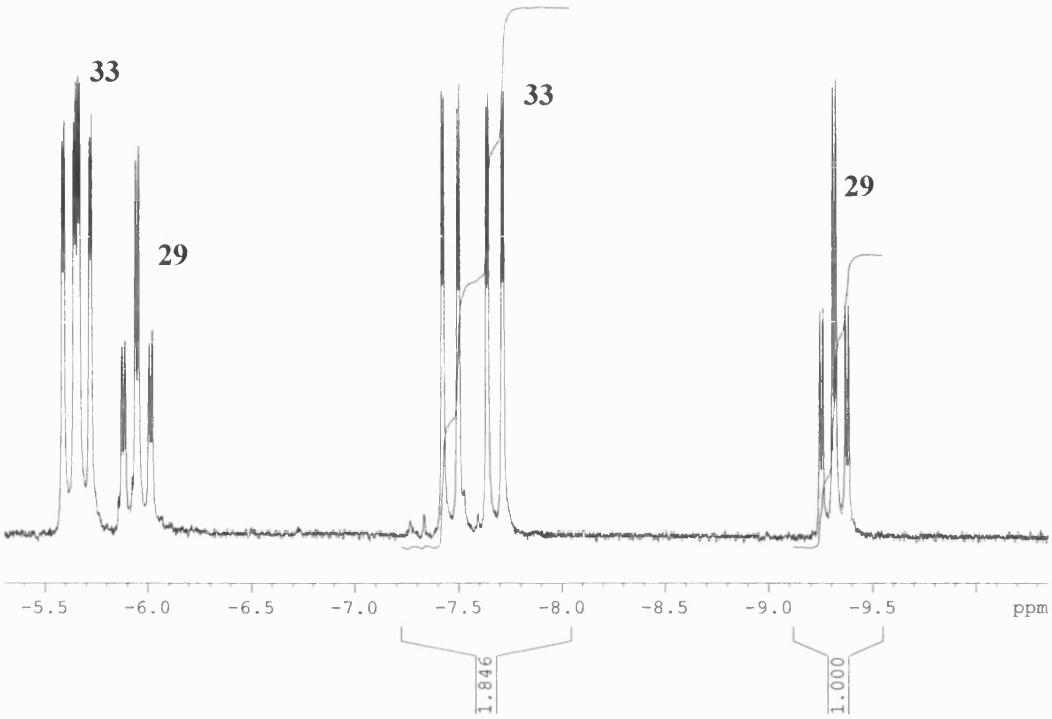


**Figure 2.24.** Hydride region of $^{1}H$ NMR spectrum of photolysis of **29** to give **33** at 25 °C for 5 hours ($d_8$-toluene, 400 MHz, 25 °C).

When photolysis of **29** was performed at low temperature (< -50 °C) and placed directly into the NMR spectrometer probe at -50 °C, the presence of a second isomerisation product with *cis* phosphines as well as *cis* hydrides (**48**) was observed (scheme 2.14.). Again, this appears after a matter of minutes and becomes more predominate with further irradiation. Decomposition begins to occur after it is exposed to more than five hours of UV light. **48** displays a second order resonance due to the AA'XX' (A=A' = $^{1}H$, X = X' = $^{31}P$) spin system in the complex. Therefore, although there is only one chemical shift for the hydride ligands, they do actually couple to each other, as well as the phosphorus ligands, giving a second order doublet (figure 2.25.).

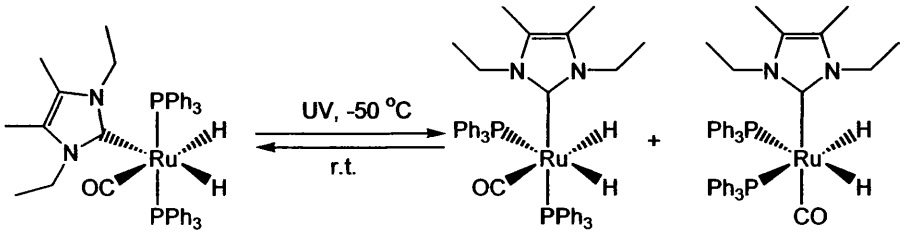


**Scheme 2.14.** Isomerisation of **29** to **33** and **48** under UV light.

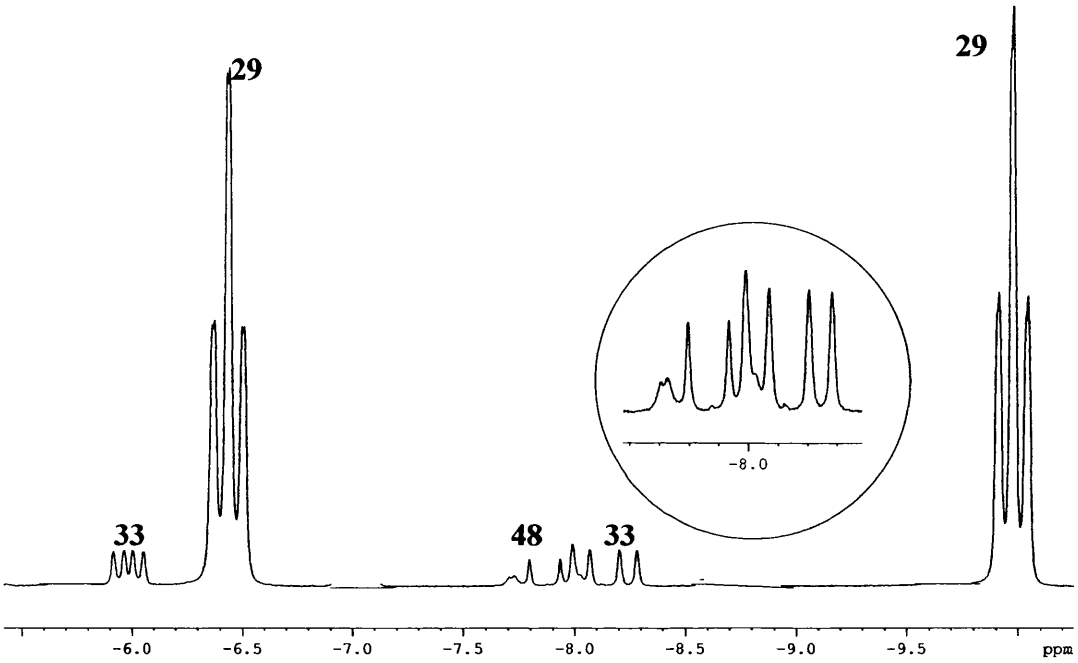


**Figure 2.25.** $^1$H NMR hydride shifts of **29**, **33** and **48** after 2.5 hours of photolysis at -50 °C with one of the resonances for **33** and that for **48** enlarged for clarity ($d_8$-THF, 400 MHz, -50 °C).

Removal of the solvent after 5 hours of photolysis gave a sticky, brown solid containing a mixture of **29** and **33**. This was used to record an IR spectrum which displayed $\nu_{CO}$ resonances for **29** and **33** at 1913 cm$^{-1}$ and 1877 cm$^{-1}$ respectively. It is somewhat difficult to explain this dramatic shift in frequency of the carbonyl bands as in both cases CO is *trans* to hydride and only the relative orientation of the two phosphine ligands changes. However, as discussed in section 2.8.2.5., this is a consistent observation.

The isomerisation reaction readily reverses at room temperature (when the reaction has been taken to a ratio of 3:1 **29**:**33**, the complete reformation of **29** from **33** in solution occurs over 12 hours with the sample being kept in the dark).

The Eyring plot for the reisomerisation of **33** to **29** was created by monitoring the reaction at a series of temperatures from 10 °C to 60 °C by $^{1}$H NMR spectroscopy (figure 2.26.). This generates values for $\Delta H^{\#}$ of 90.25 (± 50.85) kJ mol$^{-1}$ and $\Delta S^{\#}$ of -33.62 (± 184.84) JK$^{-1}$mol$^{-1}$. The large error on the value of $\Delta S^{\#}$ occurs because it is calculated by extrapolation to infinite temperature. Lente *et al.* have recently published a new way of calculating $\Delta S^{\#}$, by rearranging the linear equation and basing $\Delta S^{\#}$ on the slope rather than the intercept.[88] When this new calculation is used the value for $\Delta S^{\#}$ is -29.50(± 65.57) kJ mol$^{-1}$. $\Delta H^{\#}$ is recalculated as 90.25 (± 19.97) JK$^{-1}$mol$^{-1}$ although obviously, by the same logic, this value is unreliable as it is calculated by extrapolation to infinite temperature. These values suggest an intramolecular reaction. Intramolecular ligand exchange has been demonstrated to occur in the tris phosphine complex, $[Ru(H)_2(PPh_3)_3(CO)]$ (**15**)[89] and the authors believe that the exchange occurs *via* a trigonal twist mechanism.[90]

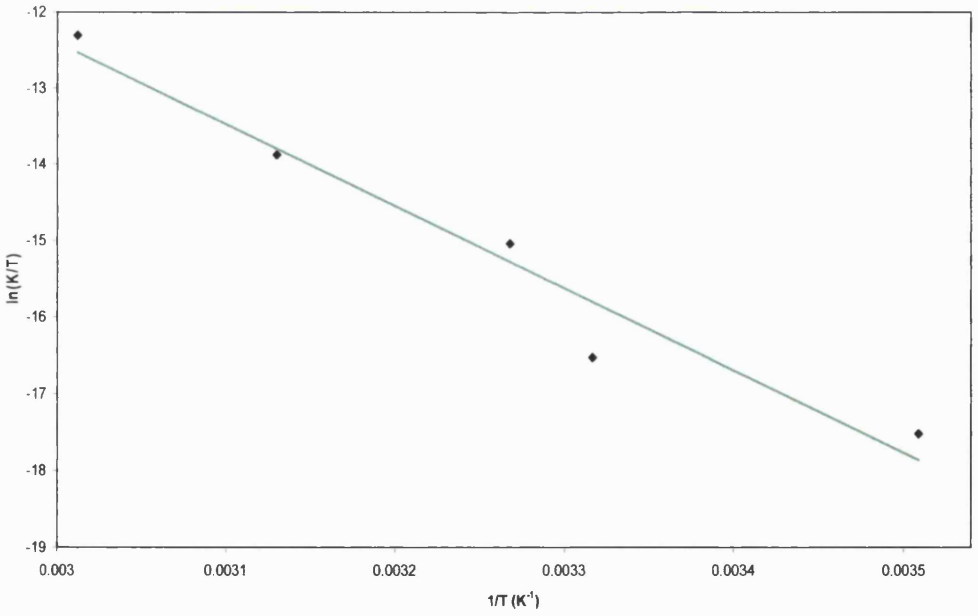


**Figure 2.26.** Eyring plot for the reisomerisation of **33** to **29**.

The isomerisation reaction was an unexpected result and suggested that photolysis of the alkyl-NHC complexes led to a much more complicated reaction than $H_2$ loss or that two or more pathways were involved. Investigation into what the mechanism of isomerisation may involve was carried out at the University of York in collaboration with the Duckett group where there is the facility to follow reactions by NMR spectroscopy *in situ* through the use of a HeCd laser ($\lambda$ = 325 nm) piped into the probe of a 400 MHz NMR spectrometer.

The reaction was carried out at -50 °C to maximise the chance of observing intermediate species. What emerged from these experiments was that the isomerisation reaction occurs extremely rapidly, with a substantial amount of product (in a 1:1 ratio of **33** to **48**) observed after only 30 seconds of photolysis (figure 2.28.(a)). Photolysis of **29** in $d_8$-toluene at -50 °C did lead to formation of some C-H activated product [Ru(H)($IEt_2Me_2$)''$(PPh_3)_2$(CO)] (**31**) after two minutes of irradiation. This is assigned from the single hydride resonance in the $^1$H NMR spectrum ($\delta$ -7.00) that couples to two inequivalent phosphorus signals at 56.9 ($^2J_{HP}$ = 102.0 Hz, $^2J_{PP}$ = 18 Hz) and 36.6 ($^2J_{HP}$ = 28.0 Hz, $^2J_{PP}$ = 18 Hz). The size of these couplings suggests that the complex has the structure shown in figure 2.27., with the activated NHC ligand *trans* to phosphine, and not the geometry obtained in the thermal reaction of **29** with $CH_2$=$CHSiMe_3$ where the NHC lies *trans* to a hydride ligand and the two phosphine ligands are equivalent (shown in scheme 1.25, page 44).[69,70] **31** is stable indefinitely at room temperature but upon addition of hydrogen to the solution at room temperature, reverts to **33** and then on to **29** overnight.

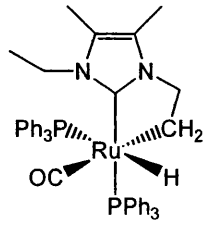


**Figure 2.27.** Structure of **31** obtained from the photolysis of **29**.

Experiments at York showed that after 240 seconds of irradiation, conversion of **29** to a mixture of *ax*-($IEt_2Me_2$)-[Ru(H)$_2$($IEt_2Me_2$)$(PPh_3)_2$(CO)] (**33**),

$[RuH(IEt_2Me_2)''(PPh_3)_2(CO)]$ (**31**) and *cis*-H-*cis*-$PPh_3$-$[Ru(H)_2(IEt_2Me_2)(PPh_3)_2(CO)]$ (**48**) from **29** was almost 20 % (figure 2.28.(b)) and after an hour in the NMR spectrometer in York, the reaction had gone to completion (figure 2.28.(c)). The higher conversion obtained compared to that seen in the set-up at Bath is probably due to the much more intense and rigorous photolysis conditions focussed on the sample in the spectrometer in York. The solutions used in York are also less concentrated (0.004 mol $dm^{-3}$). From observations of reactions in Bath it does appear that the concentration of the solution has some effect on rate of isomerisation. However, no quantitative results have been obtained to substantiate this.

Figure 2.29. shows how the ratio of products, **33**, **48** and **31** to **29** changes over time under photolysis. Over time, the ratio of **48** lessens in comparison to the other two products, suggesting that it is not particularly stable.

*2.8.2.1. Using parahydrogen in photolysis*

*Para*hydrogen is a relatively new technique that has been effectively utilised in monitoring the loss of $H_2$ from *cis* dihydride complexes, particularly by Duckett and Bargon.[91,92]

Hydrogen, like any diatomic molecule which is magnetically active, exists in different, isomeric spin states. These are the αβ-βα, antisymmetric spin state, known as the *para*-isomer and the three symmetric, degenerate spin states, αα, ββ and αβ+βα, known as the *ortho*-isomers. These spin configurations have different energies and therefore are temperature dependent. Lower temperatures favour *p*-$H_2$ so that at -273 °C, $H_2$ is 100 % *p*-$H_2$. At -196 °C (the temperature of liquid nitrogen), the ratio is closer to 1:1 (51.86 % *p*-$H_2$) and at room temperature *o*-$H_2$ is favoured (74.87 %).

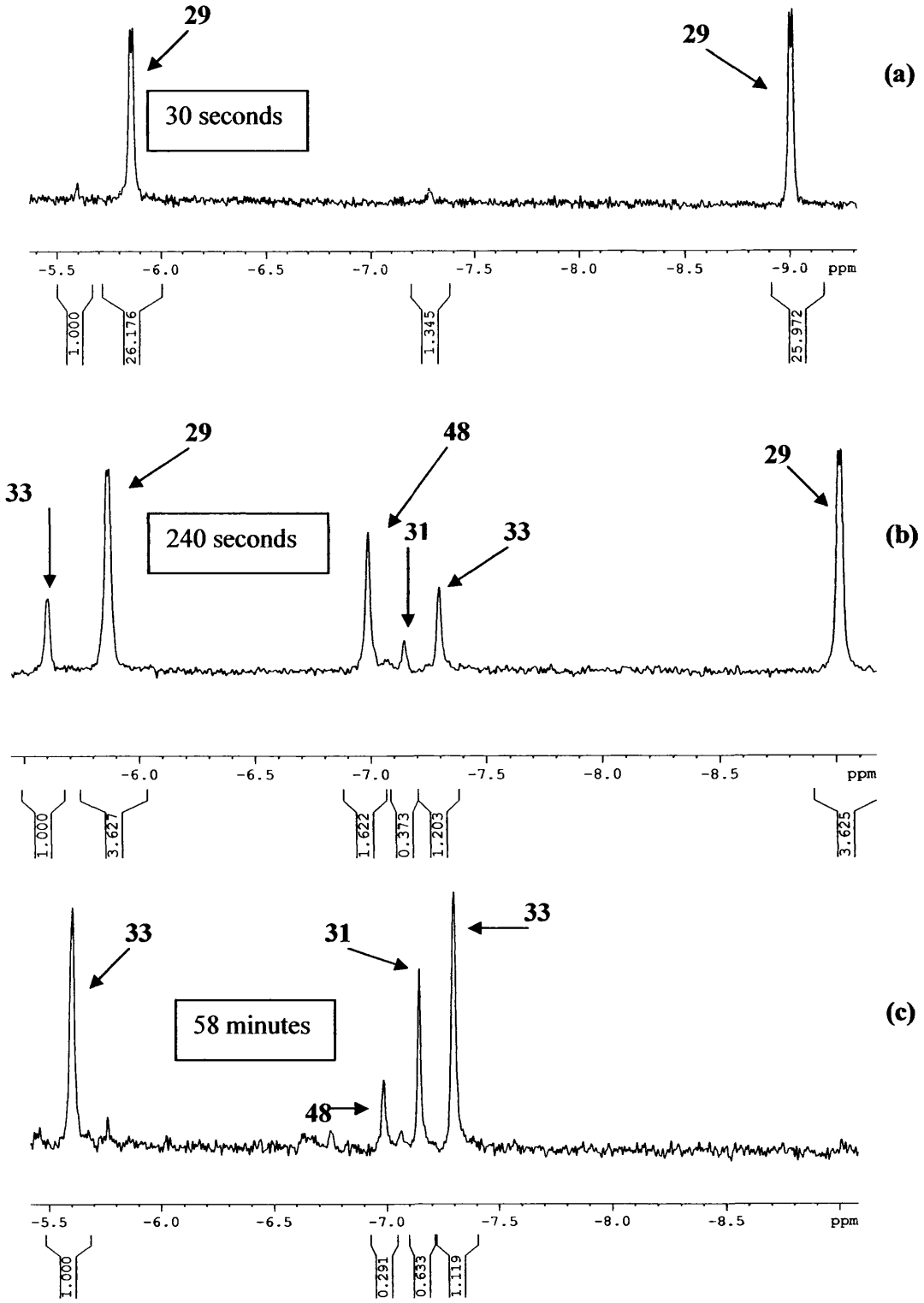


**Figure 2.28.** Hydride region of $^{1}H\{^{31}P\}$ NMR recorded following *in situ* photolysis of *eq*-$IEt_2Me_2$-$[Rh(H)_2(IEt_2Me_2)(PPh_3)_2(CO)]$ (**29**) in $d_8$-toluene at -50 °C for (a) 30 seconds, (b) 240 seconds and (c) 58 minutes ($d_8$-toluene, 400 MHz, -50 °C).

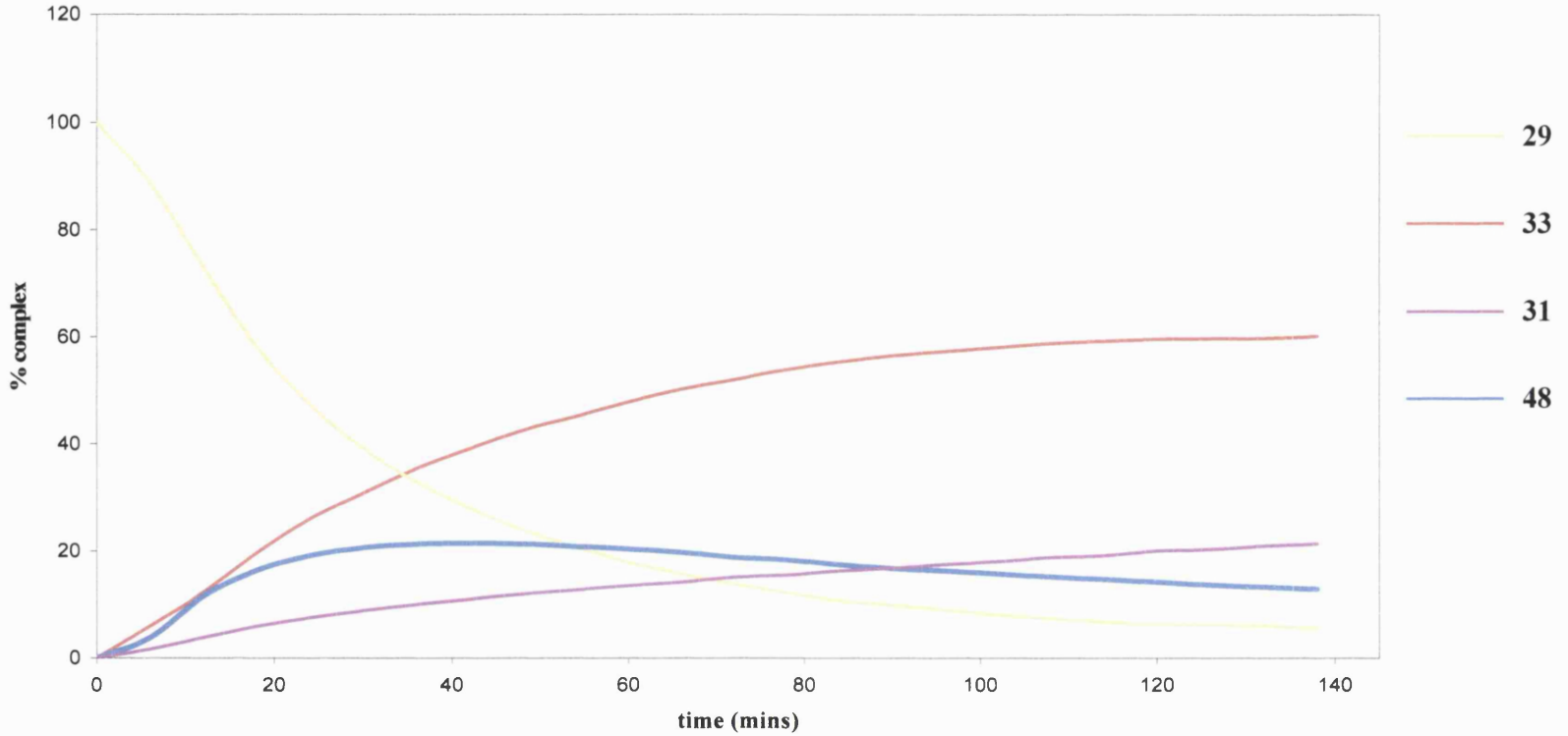


**Figure 2.29.** Graph of rate of product formation from **29** when irradiated with UV light at -50 °C in $d_8$-toluene (concentration 0.004 mol $dm^{-3}$). % complex based on integral of hydride resonances to the aromatic region.

Interconversion between the *ortho* and *para* spin states is symmetry forbidden. However, addition of a *para*magnetic catalyst readily circumvents this selection rule, allowing *p*-$H_2$ to be synthesised in a laboratory. Upon removal of the catalyst even warming the sample does not lead to rapid reconversion of the sample to primarily *o*-$H_2$.

2.8.2.1.1. Use of *para*hydrogen in NMR experiments[93]

In an AX system populated by atmospheric hydrogen, the four energy levels, αα, αβ, βα and ββ are almost equally populated. This means than when placed into a magnetic field, four transitions are possible giving rise to two doublets in a $^1$H NMR spectrum. When *p*-$H_2$ is present in the molecule only αβ and βα are populated (figure 2.30.). Four transitions are still possible but the doublets in this instance are antiphase. In addition, because of the vast population differences, signals are enhanced by a few orders of magnitude compared with a standard NMR spectrum.

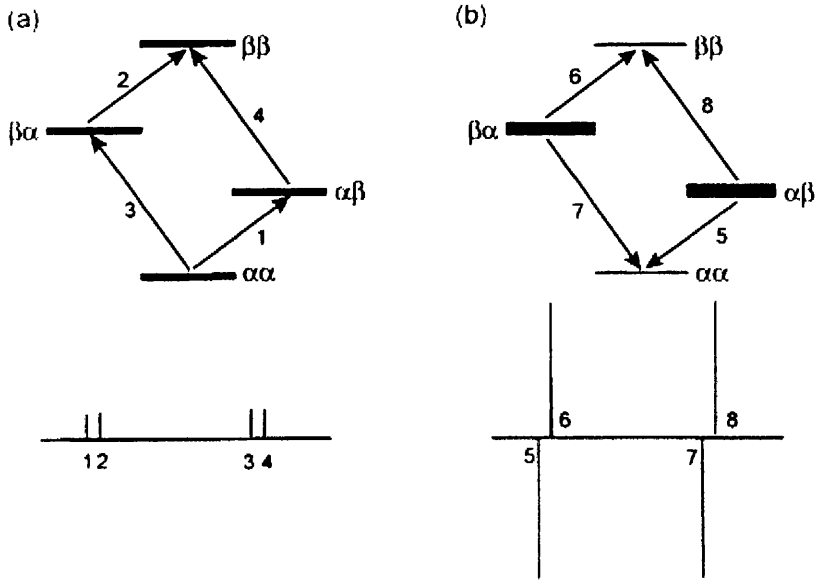


**Figure 2.30.** Energy level diagram for an AX system and the corresponding NMR patterns, (a) Boltzmann distribution, (b) *p*-$H_2$ derived distribution.

Because the addition of *p*-$H_2$ to a metal centre corresponds to the synthesis of an extreme spin state, release of the enhanced hydride ligands from the metal will result in them reverting to *o*-$H_2$ and thus, depending on the rate of exchange between the hydride ligands and hydrogen in solution, the *p*-$H_2$ enhancement will eventually be lost.

*Para*hydrogen itself is NMR inactive as it has a nuclear spin of 0. This is a useful phenomenon as free *p*-$H_2$ does not contaminate NMR spectra. In addition, the growth of the *o*-$H_2$ peak can be directly compared to the rate of $H_2$ exchange, as *p*-$H_2$ converts to *o*-$H_2$ when it leaves the metal centre.

Duckett has investigated the photolysis of a series of ruthenium dihydride complexes in the presence of *para*hydrogen.[76,93-98] *Para*hydrogen is useful in studies such as these as, by $^1$H NMR spectroscopy, it can show whether and at what rate hydrogen comes on and off the metal centre. Its ability to enhance NMR signals is also extremely useful as it can highlight transient intermediates that may not be present in high enough concentration to observe using conventional NMR experiments. For example, in the case of $[Ru(H)_2(PMe_3)_2(CO)_2]$, which exists in solution as the *cis*-, *trans*-, *cis*- isomer (*ctc*), the *ccc*-isomer is only detectable upon *p*-$H_2$ labelling.

2.8.2.1.2. Using *p*-$H_2$ in the photolysis of $[Ru(H)_2(IEt_2Me_2)(PPh_3)_2(CO)]$ (**29**)

When the reaction described on pages 101 and 102 was repeated (0.004 mol dm$^{-3}$, $d_8$-toluene, HeCd, 325 nm, 0.038 W, -50 °C) in the presence of 3 atm of *p*-$H_2$, immediate enhancement into **29**, **33** and **48** was observed (figure 2.31.). This shows that, under UV light, $H_2$ is indeed coming on and off all of the complexes. The resonances for **29** showed only a slight enhancement, as there was still a substantial amount of unenhanced product in solution. The out of phase signals from **29** were lost after about 30 seconds but were retained in **48** for closer to 90 seconds and in **33** for 210 seconds. The ratio of the *p*-$H_2$ enhanced hydride signals for **33** to **29** in this NMR spectrum proved to be 7.1:1.[99] This ratio should match the selectivity of $H_2$

addition to the 16-electron intermediate generated by $H_2$ loss from **29** if it is assumed that these species are formed with an equal retention of the *p*-$H_2$ derived spin state.

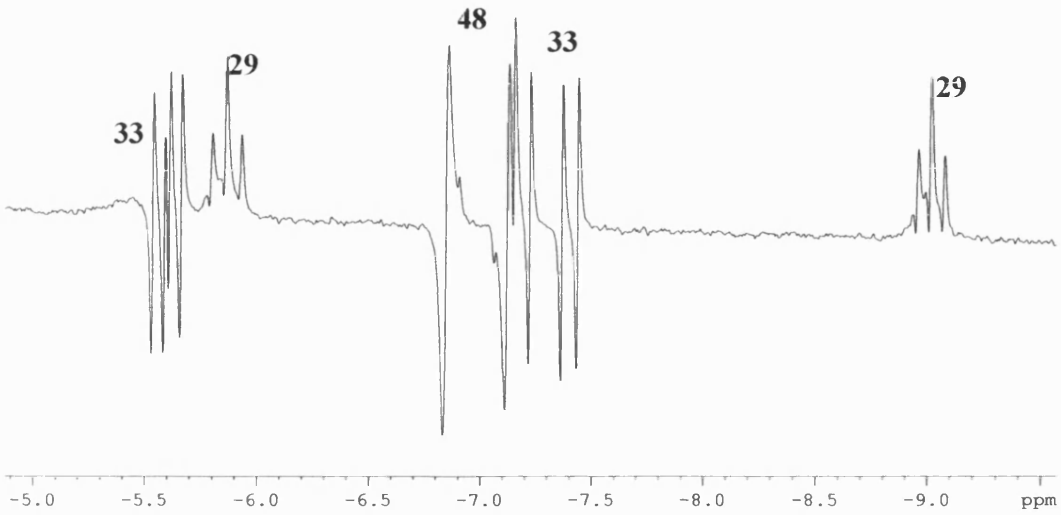


**Figure 2.31.** Hydride region of $^1$H NMR spectrum showing photolysis of **29** with *p*-$H_2$ at -50 °C after 30 seconds ($d_8$-toluene, 400 MHz, -50 °C).

Addition of *p*-$H_2$ to an initial solution of **29** and subsequent photolysis at -50 °C completely halted formation of the C-H activated complex **31**. However, after approximately 2 minutes of irradiation, two broad lumps appeared in the $^1$H NMR spectrum (δ –5.42 and δ –4.92), which are assigned to an $\eta^2$-$H_2$ complex (figure 2.32.). The signals began to coalesce upon warming from -70 °C to -50 °C and rapidly disappeared when taken to -40 °C. $T_1$ measurements were performed and gave values of approximately 15 ms and 22 ms. $T_1$ is the measurement of spin-lattice relaxation time or the time the excess energy of the nuclei takes to equilibrate with the surroundings.[100] The measurement of $T_1$ for $\eta^2$-$H_2$ ligands assumes that the relaxation of the resonances from the coordinated protons is solely due to dipole-dipole interactions with other coordinated hydride ligands. The short H-H separation of $\eta^2$-$H_2$ ligands will lead to distinctively short $T_1$ relaxation times.[101] The $T_1$ measurements for this system are of a similar magnitude to those of other Ru dihydrogen complexes such as $[Ru(H_2)(CNH)(dppe)][OTf]_2$ (13.6 ms at 27 °C on a 300 MHz spectrometer, 5.9 ms at -50 °C on a 200 MHz spectrometer) and $[Ru(H_2)(CN)(dppe)_2][OTf]$ (12.4 ms at -33 °C on a 300 MHz spectrometer).[102]

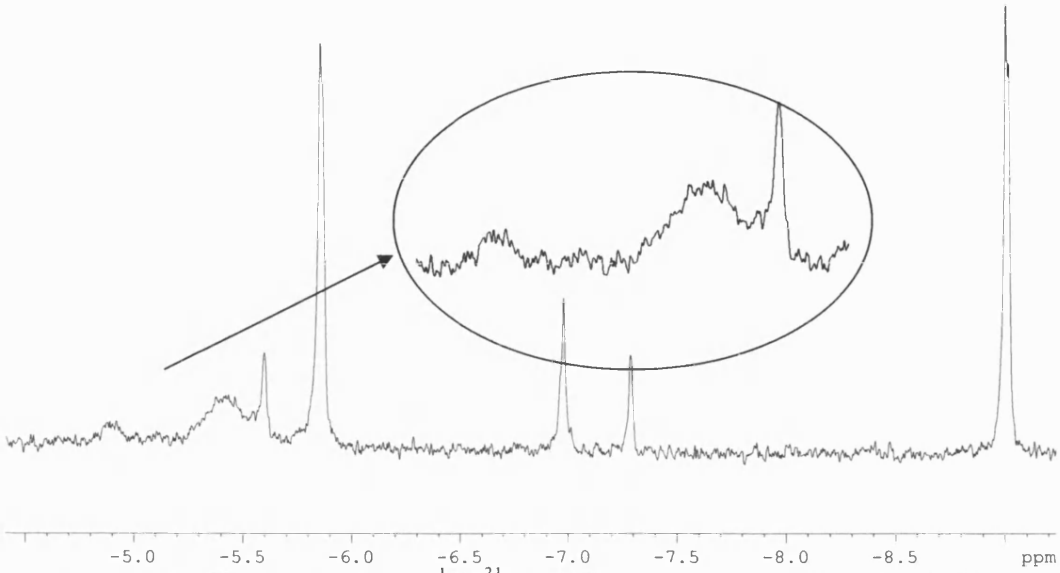


**Figure 2.32.** Hydride region of $^{1}H\{^{31}P\}$ NMR showing formation of probable dihydrogen species (highlighted) after 120 seconds of photolysis in $d_8$-toluene at -50 °C ($d_8$-toluene, 400 MHz, -50 °C).

When the photolysis of **29** was carried out in the presence of $PPh_3$ (15 equivalents) or $H_2$ (1 atm), formation of the $\eta^2$-$H_2$ species is suppressed, therefore suggesting that it is $[Ru(H)_2(\eta^2\text{-}H_2)(IEt_2Me_2)(PPh_3)(CO)]$ (**49**), in which the $Ru(H)_2/\eta^2$-$H_2$ ligands exchange on the NMR timescale. Interestingly, observation of **49** corresponds to the point where the *p*-$H_2$ enhancement in the hydride resonances of **33** is no longer visible. This suggests that rapid exchange of the $\eta^2$-$H_2$ ligand with free $H_2$ leads to the destruction of the *para* spin state which is necessary to see the out of phase effect.

Giunta *et al.* have prepared examples of NHC complexes bearing a dihydrogen ligand, $[Ru(H)_2(\eta^2\text{-}H_2)_2(IMes)(PCy_3)]$ and $[Ru(H)_2(\eta^2\text{-}H_2)_2(IMes)_2]$.[103,104] These complexes are active in the intermolecular activation of C-H bonds in aromatic substrates at room temperature. This same reactivity is not seen in the bis phosphine analogue $[Ru(H)_2(\eta^2\text{-}H_2)_2(PCy_3)_2]$, showing that the presence of an NHC ligand makes a substantial difference to reactivity in these types of complexes. Heinekey and co-workers have also reported a dihydrogen NHC complex using a chelating

NHC ligand on an iridium centre, $[Ir(\eta^2\text{-}H_2)(Cp^*)][X]_2$ (X = $PF_6$, Cl).[105] The $T_1$ value for this complex is 37 ms at -33 °C on a 750 MHz spectrometer.

Although *p*-$H_2$ experiments showed that **29** is losing $H_2$, isomerisation could still result from loss of a two-electron donor ligand ($PPh_3$, CO, $IEt_2Me_2$). Competing phosphine and hydrogen loss pathways upon photolysis have been observed in $[Ru(H)_2(PMe_3)_4]$[106,107] and $[OsH_4(PMe_2Ph)_3]$ .[108]

Addition of excess phosphine or pyridine to the starting solution of **29** (0.004 mol $dm^{-3}$) was found to slow the rate of isomerisation, as did changing the solvent from $d_8$-toluene to $d_8$-THF. This suggests a pathway involving loss of a two electron donor from the metal centre. Addition of hydrogen sped up the rate of reaction. A graph showing the rates of formation of **33** under various reaction conditions is shown in figure 2.33.

Photolysis of **29** in $d_8$-toluene in the presence of an 8.6 fold excess of pyridine and no $H_2$ led to the immediate formation of a new species, which displayed doublet of doublet hydride resonances at δ –3.30 ($^2J_{HH}$ = -9.0 Hz, $^2J_{HP}$ = 31.5 Hz) and δ –14.20 ($^2J_{HH}$ = -9.0 Hz,$^2J_{HP}$ = 21.0 Hz), identifying it as a mono-phosphine containing complex (figure 2.34.). This is probably the pyridine coordinated complex $[Ru(H)_2(IEt_2Me_2)(PPh_3)(C_5H_5N)(CO)]$ (**50**) and is comparable to $[Ru(H)_2(CO)(dppe)(C_5H_5N)]$ which has hydride signals at δ –3.27 ($^2J_{HP}$ = 26 Hz) and δ –14.17 ($^2J_{HP}$ = 27 Hz).[96] Both formation of **33** and **48** were significantly reduced in the presence of pyridine. This suggests that **29** undergoes photochemically induced phosphine dissociation as the dominant reaction pathway and leads to **50** *via* trapping of the same 16-electron intermediate that leads to **33**. When the reaction of **29** and pyridine is carried out in the presence of *p*-$H_2$, the formation of **49** is quenched and enhancement of all the hydride containing species in solution lasts for many minutes.

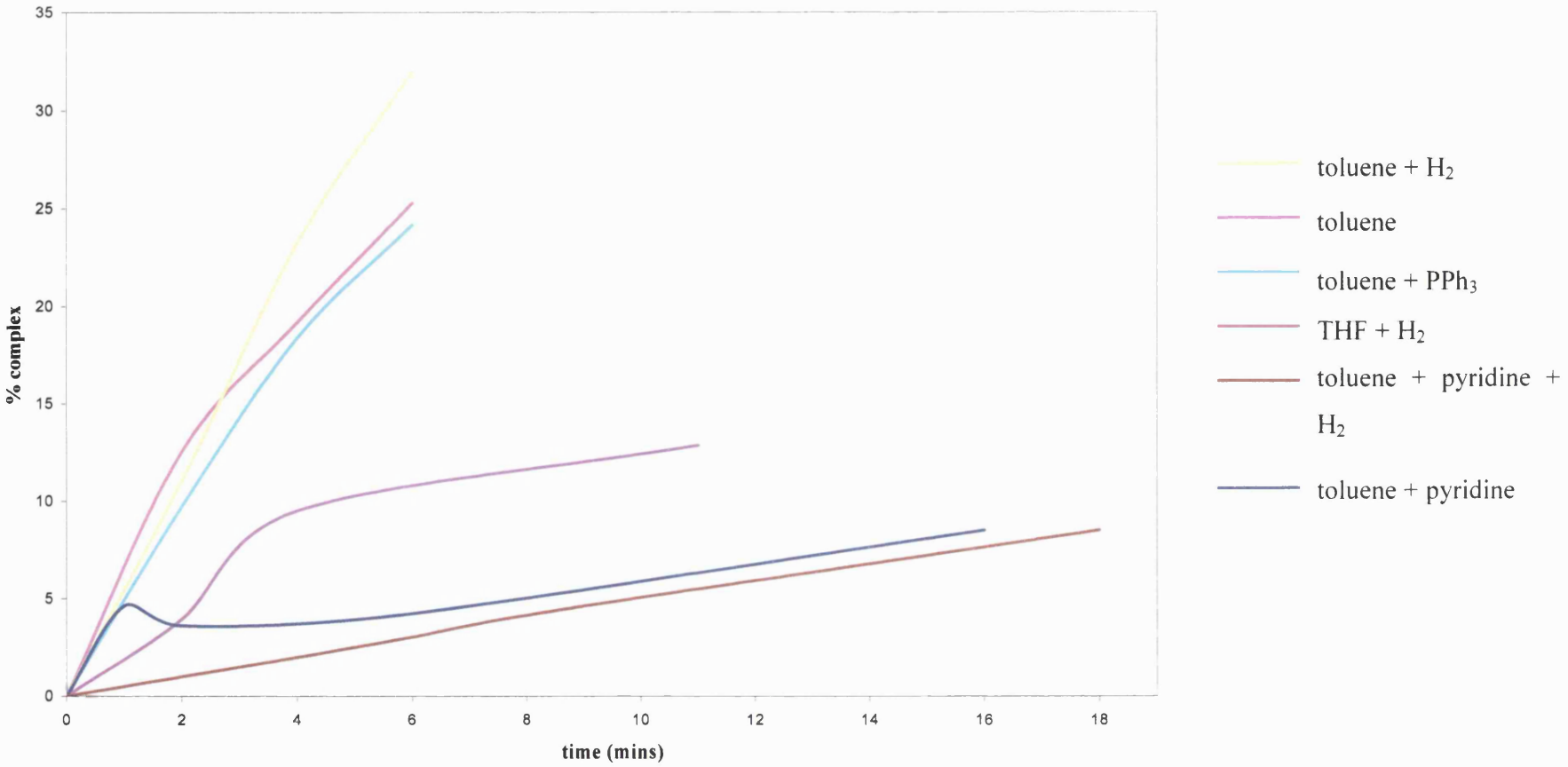


**Figure 2.33.** Formation of **33** under various reaction conditions when irradiated with UV light at -50 °C (concentration 0.004 mol $dm^{-3}$). % complex based on integral of hydride resonances to the aromatic region.

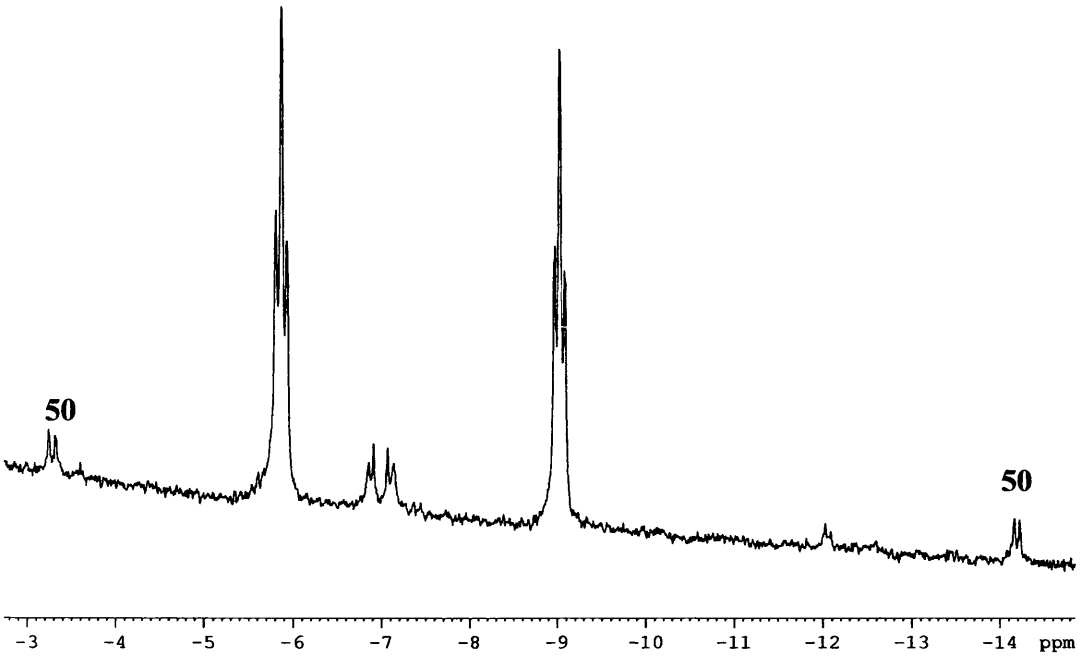


**Figure 2.34.** Hydride region of $^1$H NMR spectrum showing formation of $[Ru(H)_2(IEt_2Me_2)(PPh_3)(C_5H_5N)(CO)]$ (**50**) upon photolysis of **29** with pyridine in $d_8$-toluene at -50 °C ($d_8$-toluene, 400 MHz, -50 °C).

Addition of free $IEt_2Me_2$ to **29** and subsequent photolysis at -50 °C led to formation of $[Ru(H)_2(IEt_2Me_2)_2(PPh_3)(CO)]$ (**51**), which exhibits two doublets of doublets in the hydride region of the proton spectrum (δ -5.51 ($^2J_{HH}$ = 4.8 Hz, $^2J_{HP}$ = 39.7 Hz), -8.91 ($^2J_{HH}$ = 4.8 Hz, $^2J_{HP}$ = 26.8 Hz)). The $^2J_{HP}$ values show that the phosphine is *cis* to both of the hydrides, showing that the two NHC ligands are *cis* to each other, as found in the thermal isomer.[109] Addition of IMes to the reaction led to the mixed NHC complex $[Ru(H)_2(IEt_2Me_2)(IMes)(PPh_3)(CO)]$ but this could not be isolated.

The reactions discussed above are summarised in the reaction scheme in scheme 2.15.

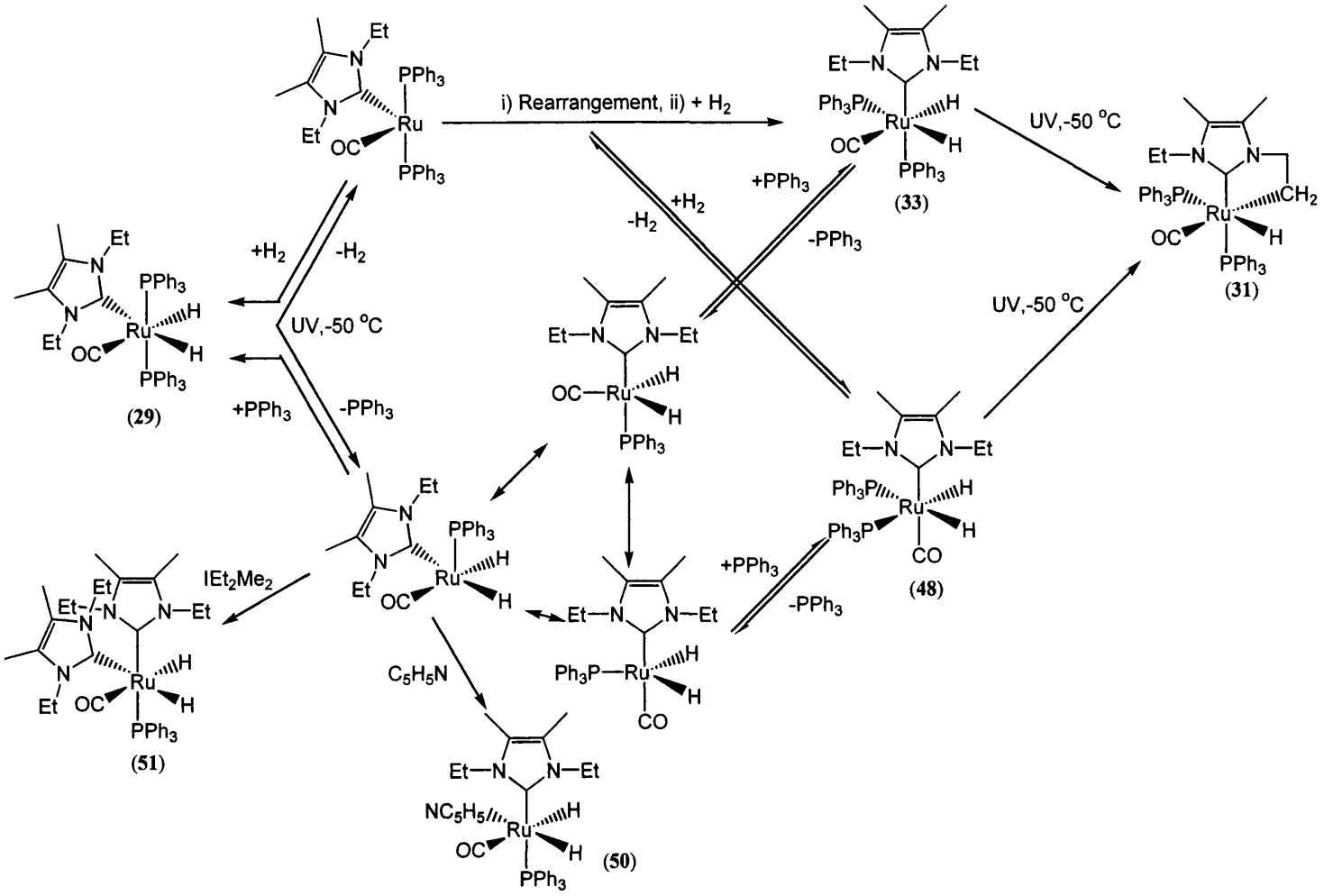


**Scheme 2.15.** Reactions of **29** upon photolysis.

*2.8.2.2. TRIR studies on $[Ru(H)_2(IEt_2Me_2)(PPh_3)_2(CO)]$ (29)*

The extensive steady state photochemistry displayed by **29** prompted a preliminary investigation of the time-resolved reactivity of **29** on a microsecond timescale by time resolved infrared (TRIR) spectroscopy in collaboration with Professor Mike George at the University of Nottingham. The presence of the CO groups on **29** and the intermediates formed when it is irradiated allows TRIR spectroscopy to be employed as CO ligands have distinctive $\nu_{CO}$ stretching frequencies that are highly dependant on the ancillary ligands at the metal centre as well as the oxidation state of the metal complex. TRIR spectroscopy measures changes in intensity of the $\nu_{CO}$ bands. The starting material exhibits a negative peak or "bleach", as it is photolysed away, whereas any new intermediates will display positive absorption peaks.

The TRIR spectrum recorded 16 μs after flash photolysis (355 nm, power = 5 mJ per pulse) of a sample of **29** in $C_6D_6$ (0.013 mol $dm^{-3}$) is shown in figure 2.35. and shows loss of **29** and formation of five new carbonyl absorption bands. Two main bands were observed at 1911 $cm^{-1}$ and 1856 $cm^{-1}$ with weaker features at 1955 $cm^{-1}$, 1878 $cm^{-1}$ and 1820 $cm^{-1}$. The spectrum was recorded in a point by point fashion with 2 $cm^{-1}$ separations between 2004 $cm^{-1}$ and 1778 $cm^{-1}$ and the solution was drawn through the IR cell after every shot, ensuring it was fresh each time. The TRIR spectrum measured at 150 μs (figure 2.35.) after the laser flash shows that the bands at 1955 $cm^{-1}$ and 1878 $cm^{-1}$ arise from longer lived photoproducts in the reaction compared to those at 1911 $cm^{-1}$ and 1856 $cm^{-1}$.

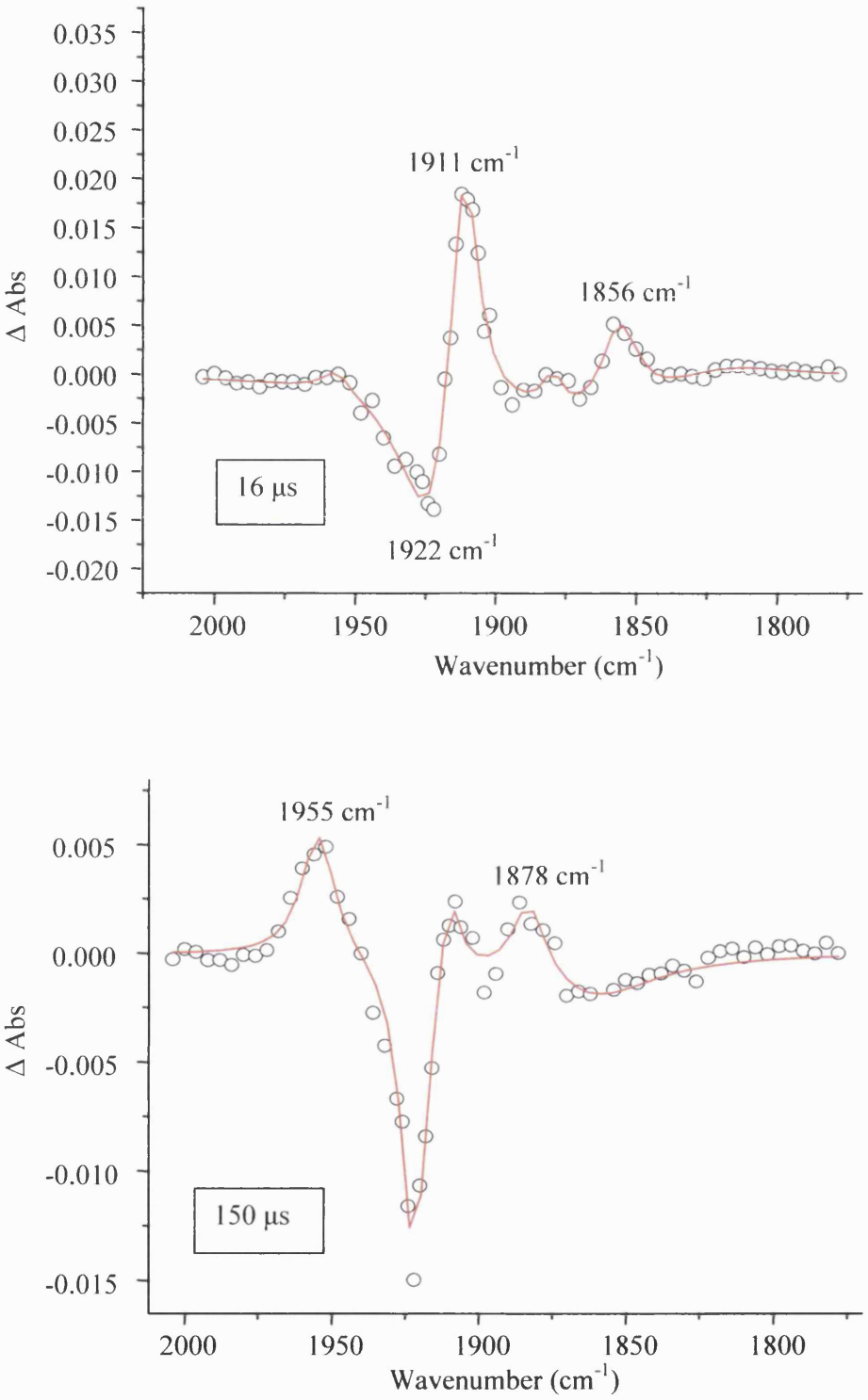


**Figure 2.35.** TRIR spectra recorded 16 µs and 150 µs after flash of irradiation of **29** in $C_6D_6$ under Ar ($1.3 \times 10^{-2}$ mol $dm^{-3}$, 355 nm, 5 mJ/pulse).

The bleach of the CO band for the parent complex **29** under an atmosphere of argon is extremely wide and was visible in the TRIR measurements from 1928 to 1862 $cm^{-1}$. This added an element of difficulty in fitting the data as the presence of the bleach overlapped with some of the photoproduct peaks. The bleach for **29** is presented in figure 2.36. From this it can be seen that the loss of **29** under UV is extremely rapid (> 1 x $10^{-6}$ s) but that it slowly reforms over approximately 1 ms. However, it should be noted that the roll off of the IR detector occurs in this time frame making a linear fit on this data impossible. Upon replacement of argon by 1 atm of $H_2$, the extent of the parent bleach is reduced but the rate of the parent reforming is unaffected ($k_{obs}$ = 5.2 x $10^4$ $s^{-1}$).

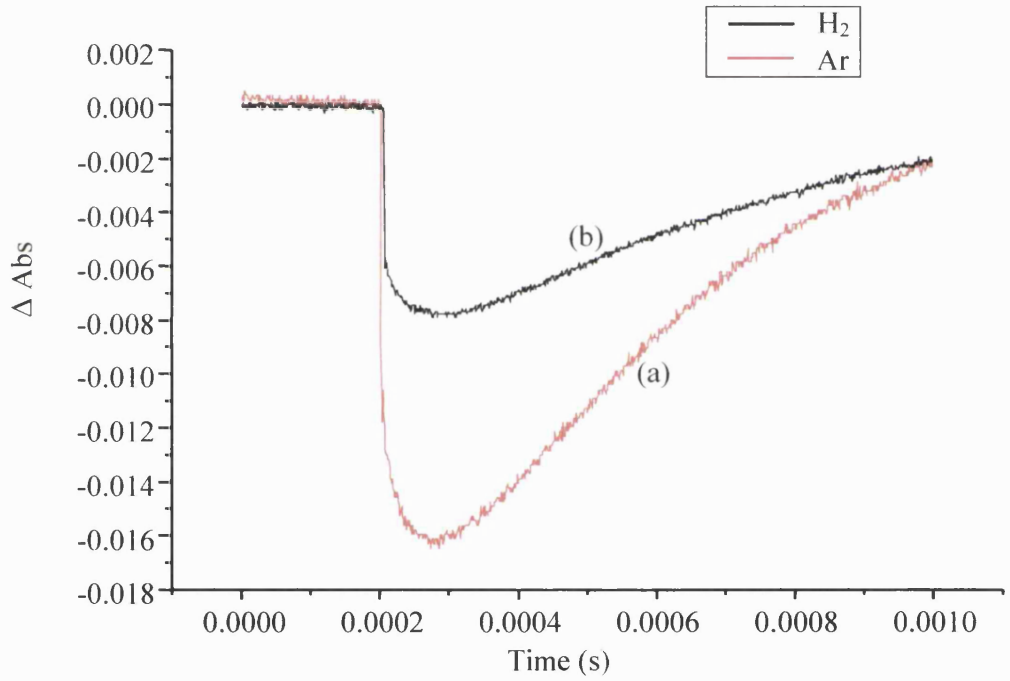


**Figure 2.36.** TRIR spectrum measured at 1922 $cm^{-1}$ under (a) 1 atm Ar and (b) 1 atm $H_2$.

The kinetic behaviour of the transient species formed at 1856 $cm^{-1}$ is shown in figure 2.37. Under 1 atm of Ar, this species displays a first order decay over approximately 200 μs ($k_{obs}$ = 1.5 x $10^4$ $s^{-1}$). Intriguingly, under 1 atm of $H_2$, the transient becomes longer lived, decaying again with first order kinetics over approximately 800 μs (kobs = 2.6 x $10^3$ $s^{-1}$).

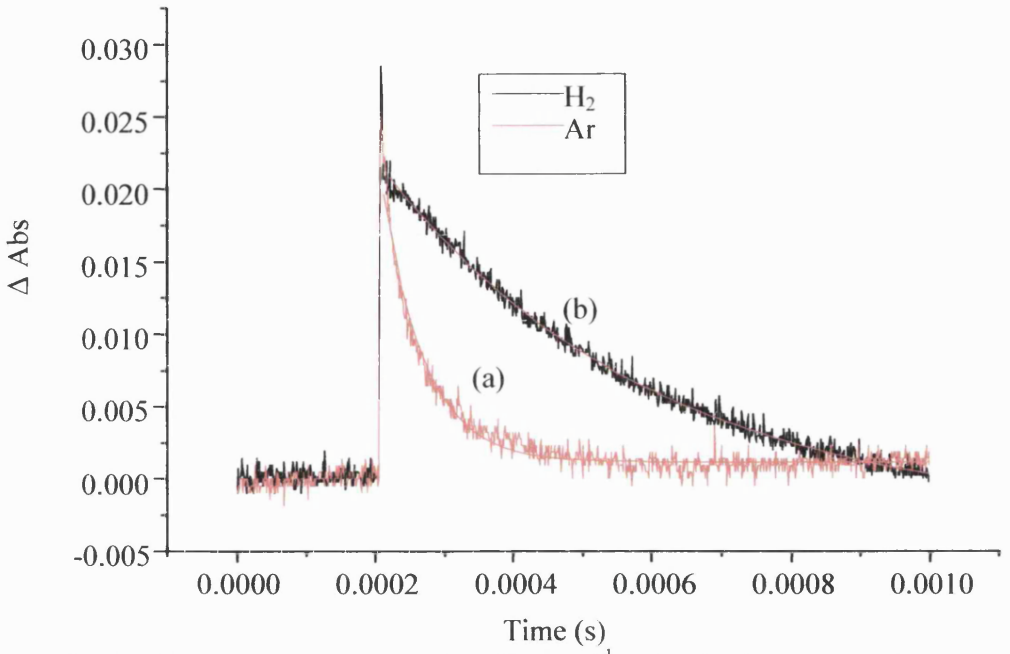


**Figure 2.37.** TRIR spectrum measured at 1856 $cm^{-1}$ under (a) 1 atm Ar and (b) 1 atm $H_2$.

In contrast, monitoring the decay of the transient at 1911 $cm^{-1}$ shows kinetic behaviour that is essentially the same in the presence of Ar or $H_2$ ($k_{obs}$ (Ar) = 1.4 x $10^4$ $s^{-1}$, $k_{obs}$ ($H_2$) = 1.9 x $10^4$ $s^{-1}$) (figure 2.38.). Given that $H_2$ affects the transient at 1956 $cm^{-1}$ but not that at 1911 $cm^{-1}$, it can be concluded that the two transient species are not the same.

Time resolved traces showing the kinetic behaviour of the weaker transient signals at 1820 $cm^{-1}$, 1878 $cm^{-1}$ and 1955 $cm^{-1}$ are shown in figures 2.39. to 2.41. Little can be said about the species at 1820 $cm^{-1}$ without further experiments due to the fast nature of the signal decay. The transient signals at 1878 $cm^{-1}$ and 1955 $cm^{-1}$ are not formed within the rise time of the instrument but grow in over approximately 100 μs in the presence of Ar ($k_{obs}$ (1878 $cm^{-1}$) = 3.0 x $10^4$ $s^{-1}$, $k_{obs}$ (1955 $cm^{-1}$) = 3.7 x $10^4$ $s^{-1}$). These similar $k_{obs}$ values imply that both bands arise from the same species. The similar rates of decay also suggest that the $\nu_{CO}$ peaks arise from the same species (although as these occur over the time associated with detector roll off, further experiments with other detectors that function over longer lifetimes are required to establish accurate kinetic data). However, $H_2$ appears to have an affect on the band

at 1878 $cm^{-1}$ but not the one at 1955 $cm^{-1}$, which somewhat contradicts the supposition that they belong to the same photoproduct. Further experiments are clearly necessary.

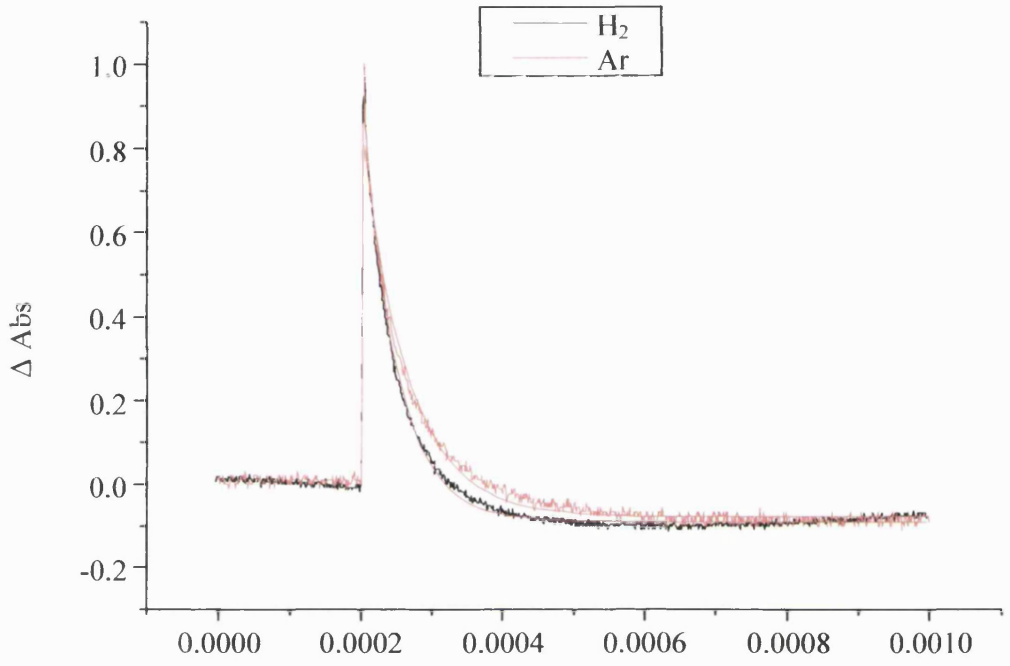


**Figure 2.38.** TRIR spectrum measured at 1911 $cm^{-1}$ under 1 atm Ar and 1 atm $H_2$.

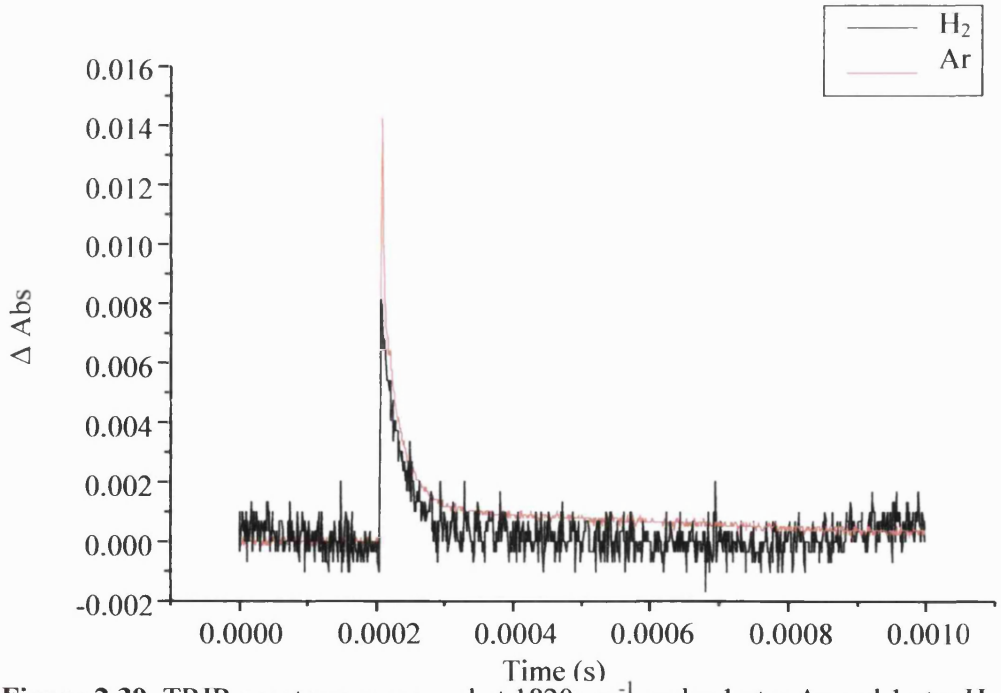


**Figure 2.39.** TRIR spectrum measured at 1820 $cm^{-1}$ under 1 atm Ar and 1 atm $H_2$.

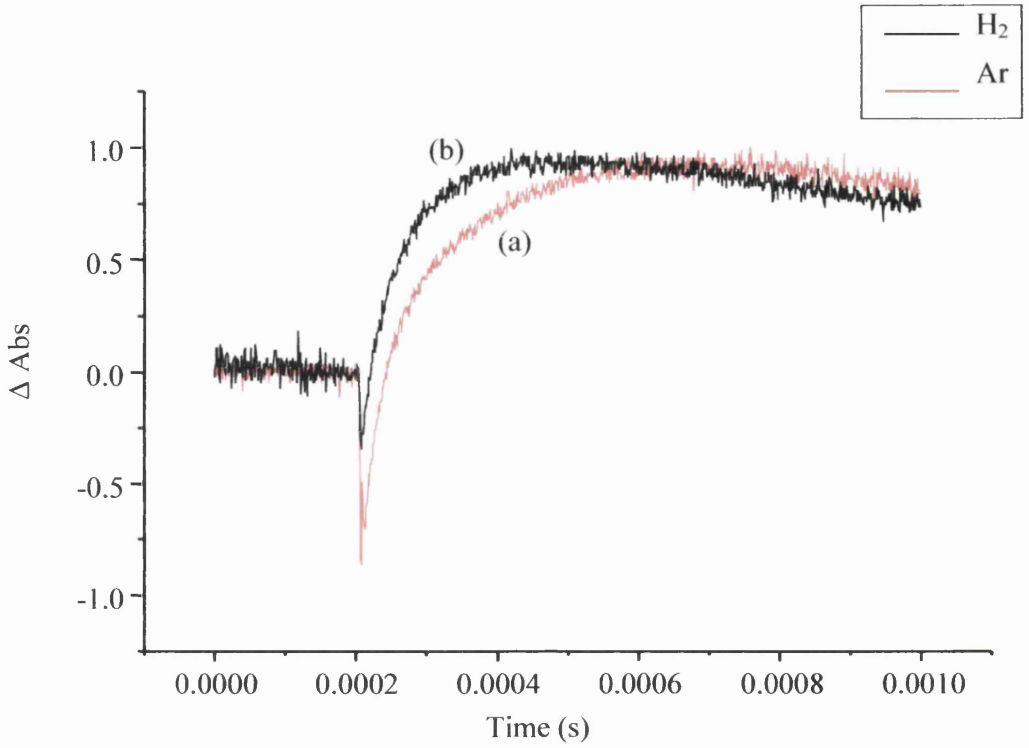


**Figure 2.40.** TRIR spectrum measured at 1878 $cm^{-1}$ under (a) 1 atm Ar and (b) 1 atm $H_2$.

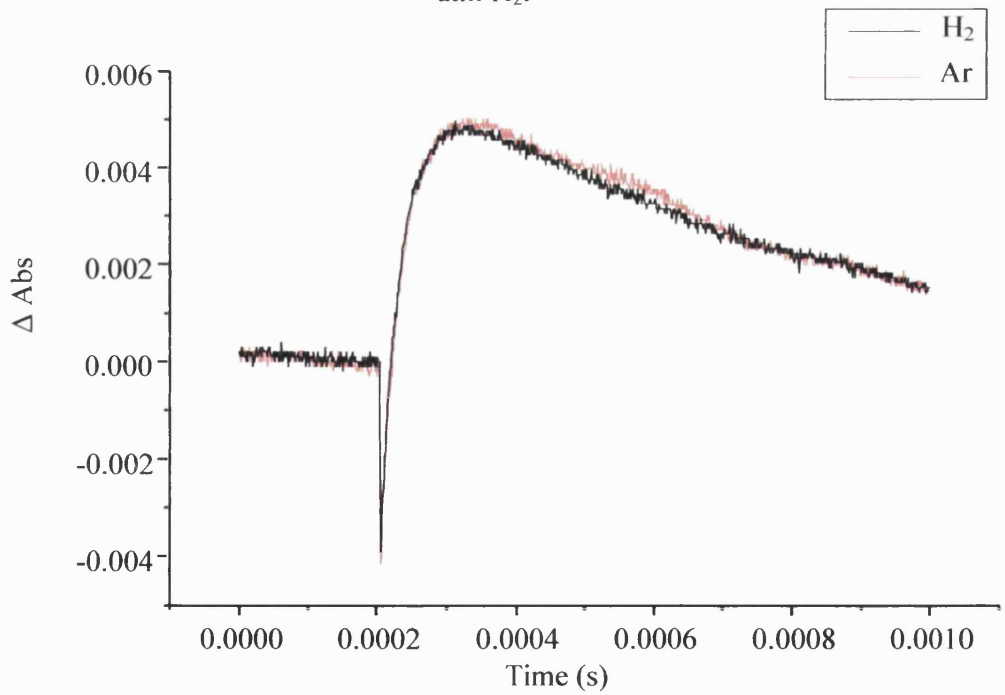


**Figure 2.41.** TRIR spectrum measured at 1955 $cm^{-1}$ under 1 atm Ar and 1 atm $H_2$.

A summary of what was observed by TRIR is presented is scheme 2.16. and discussed below.

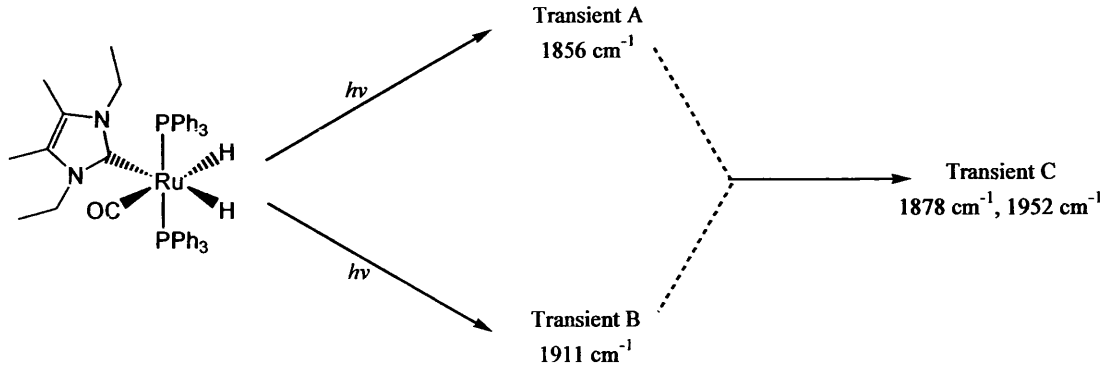


**Scheme 2.16.** Summary of the transients observed by TRIR spectroscopy.

Photolysis of **29** in $C_6D_6$ under Ar affords two new CO bands 16 μs after the flash at 1911 $cm^{-1}$ and 1856 $cm^{-1}$. These must arise from two different species as the effect of replacing Ar for $H_2$ is not the same on the kinetics of each absorption.

Transient B is attributed to the phosphine loss species $[Ru(H)_2(IEt_2Me_2)(PPh_3)(CO)]$ as its kinetics are unaffected by being under an atmosphere of $H_2$ and the position of the band, at 1911 $cm^{-1}$, is consistent with a coordinatively unsaturated Ru(II) species. Adding excess $PPh_3$ to the solution and establishing how the rate of decay of transient B changes would provide further evidence for whether or not this species is indeed the $PPh_3$ loss product.

The value of $k_{obs}$ for decay of B (1.4 x $10_4$ $s^{-1}$) is somewhat smaller than the values of $k_{obs}$ for formation of C (3.0 x $10^4$ $s^{-1}$ and 3.7 x$10^4$ $s^{-1}$) suggesting that B may not be a precursor for C.

The nature of transient A remains to be established. The low carbonyl stretching frequency (1856 $cm^{-1}$) suggests a Ru(0) species, such as the $H_2$ loss photoproduct, $[Ru(IEt_2Me_2)(PPh_3)_2(CO)]$. Comparison to the TRIR spectroscopy studies carried out by George and Perutz on $[Ru(H)_2(PPh_3)_3(CO)]$ (**15**)[110,111] shows a $\nu_{CO}$ band at 1845 $cm^{-1}$. This decayed with first order kinetics ($k_{obs}$ = 3 x $10^3$ $s^{-1}$) under an argon

atmosphere. The rate of of $k_{obs}$ increases linearly addition of $H_2$. This species is assigned unequivocally as $[Rh(PPh_3)_3(CO)]$ on the basis of its $\nu_{CO}$ band[112,113] and its kinetics with $H_2$. However, transient A decays more slowly in the presence of $H_2$ suggesting it is not a simply $H_2$ loss species and that $H_2$ actually aids in the stabilisation of the intermediate. Therefore, A could be the dihydrogen complex $[Ru(\eta^2\text{-}H_2)(IEt_2Me_2)(PPh_3)_2(CO)]$.

The same studies by TRIR carried out by Perutz and co-workers on the photolysis of (**15**) show a similar reaction profile to that seen in the TRIR of **29** (figure 2.42.).[110,111] Two longer lived $\nu_{CO}$ bands were observed at 1843 and 1974 $cm^{-1}$. These are not dissimilar to the peaks at 1952 $cm^{-1}$ and 1878 $cm^{-1}$ observed during the photolysis of **29** and assigned to transient C. Perutz assigns the bands obtained from photolysis of **15** to a long-lived dinuclear species. It is therefore likely that a similar species is being formed during photolysis of **29**. However, more detailed kinetic studies need to be carried out before it is clear what it is forming from.

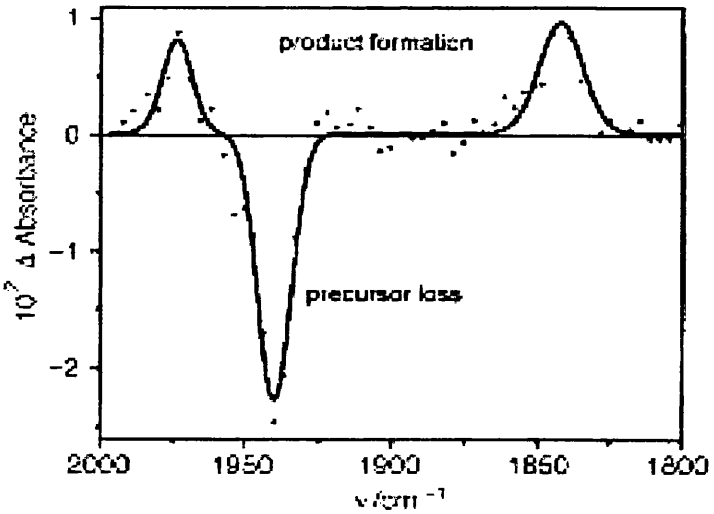


**Figure 2.42.** TRIR plot of **15** recorded 1 μs after laser flash photolysis (λ = 355 nm) in $C_6D_6$. The negative peak is due to loss of **15**, the positive peaks are due to photoproducts.

DFT calculations on a simplified model of **15**, $[Ru(H)_2(PH_3)_3(CO)]$, by Moreno and co-workers, suggest that $H_2$ elimination could occur as rapidly as 37 fs.[106,114] In addition, it appears that the lengthening of the Ru-H distance and the shortening of the H-H bond are taking place almost simultaneously. The authors conclude that the mechanism of $H_2$ loss is almost purely dissociative and arises due to a decrease in electron density on the metal centre when the molecule is moved to an excited state upon irradiation. Initially, the loss of electron density is mostly distributed amongst the donor ligands on the metal while the Ru-H bonds remain unchanged. This phenomenon induces weakening of the metal-hydride bonds and favours formation of $H_2$. The influence of a more donating NHC on this type of system remains to be elucidated.

### *2.8.2.3. Preliminary calculations on isomerisation of $[Ru(H_2)(IEt_2Me_2)(PPh_3)_2(CO)]$ (29)*

Preliminary calculations have been carried out by Richard Diggle and Steven Donald of the University of Heriot Watt into the energetics of hydrogen addition to the four-coordinate species $[Ru(IEt_2Me_2)(PPh_3)_2(CO)]$.[115] Using the simplified ligands IH and $PH_3$ in place of $IEt_2Me_2$ and $PPh_3$, to ease modelling and therefore to investigate the complexes from a purely electronic stand point, it was found that the four ligands can form two arrangements around the metal centre (figure 2.43.). When the two phosphine ligands are *trans* to each other (A), the ligands adopt a virtually square planar arrangement whereas when IH is in the axial position (B), the species exists in a butterfly conformation. B is thermodynamically more stable than A by 9.6 kJ $mol^{-1}$.

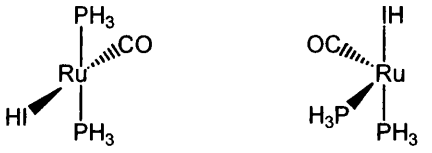


A B

**Figure 2.43.** Two arrangements of ligands on four-coordinate hydrogen-loss species.

Addition of $H_2$ to A can lead directly back to the analogue of *eq*-($IEt_2Me_2$)-[$Ru(H)_2(IEt_2Me_2)(PPh_3)_2(CO)$] (**29**) and is energetically downhill by 13.8 kJ $mol^{-1}$. The formation of this isomer comes from bending of the IH-Ru-C bond (scheme 2.17.). Bending of P-Ru-P bonds (scheme 2.18.) leads to an isomer, which is the analogue of *ax*-($IEt_2Me_2$)-[$Ru(H)_2(IEt_2Me_2)(PPh_3)_2(CO)$] (**33**). Computationally, it was found that it is easiest to bend a P-Ru-P bond in these systems, than an IH-Ru-P bond with the hardest being an IH-Ru-IH bond. The isomer analogous to *cis*-H-*cis*-$PPh_3$-[$Ru(H)_2(IEt_2Me_2)(PPh_3)_2(CO)$] (**48**) is computed to be 8.9 kJ $mol^{-1}$ more stable than the *trans* phosphine analogue of **29**. The axial IH isomer (analogue of **33**) is 16.5 kJ $mol^{-1}$ more stable than the *trans* phosphine. This suggests that **33** and **48** are thermodynamically more stable than **29**, explaining why they form when $H_2$ is removed from **29** under UV. The instability of **48** above -50 °C and the reisomerisation of **33** back to **29** at room temperature must be due to kinetic factors and may not involve $H_2$ loss.

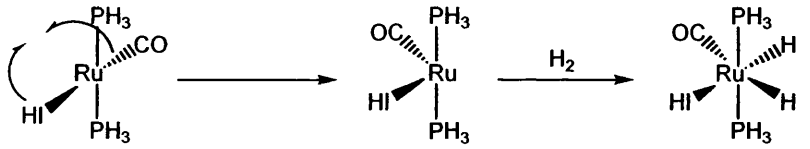


A

**Scheme 2.17.** Addition of $H_2$ to four coordinate species to form an analogue of **29**.

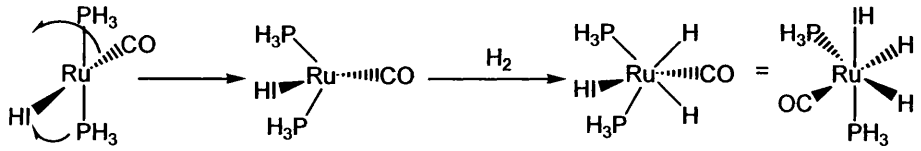


A

**Scheme 2.18.** Addition of $H_2$ to four coordinate species to form an analogue of **33**.

*2.8.2.4. Other mono Ru(NHC) complexes under photolysis*

A sample of the analogous alkyl NHC complex, *eq*-(ICy)-[$Ru(H)_2(ICy)(PPh_3)_2(CO)$] (**52**) (0.02 mol $dm^{-3}$),[116] undergoes a similar isomerisation upon irradiation with UV light (Hg arc, $\lambda > 285$ nm, 125 W), isomerising from the equatorial ($\delta$ -6.43 ($^2J_{HP}$ = 26.3 Hz, $^2J_{HH}$ = 4.4 Hz), -9.97 ($^2J_{HP}$ = 25.8 Hz, $^2J_{HH}$ = 4.4 Hz)) isomer to *ax*-(ICy)-

$[Ru(H)_2(ICy)(PPh_3)_2(CO)]$ (**53**) (δ -5.58 ($^2J_{HP}$ = 35.9 Hz, $^2J_{HP}$ = 19.8 Hz), -8.14 ($^2J_{HP}$ = 84.5 Hz, $^2J_{HP}$ = 31.3 Hz)), with evidence for the *cis* phosphine isomer (**54**) as well (δ -7.87 ($^2J_{HP}$ = 54.9 Hz)) (figure 2.44).

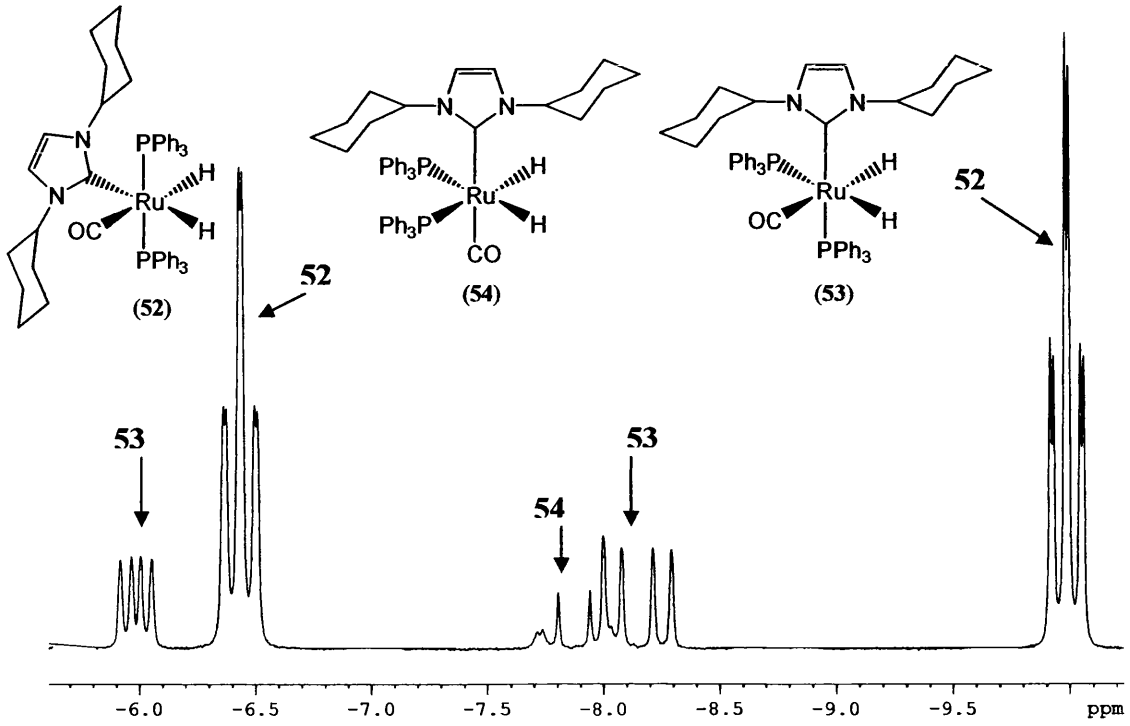


**Figure 2.44.** $^1$H NMR hydride shifts of **52**, **53** and **54** after 2.5 hours of photolysis at -50 °C ($d_8$-THF, 400 MHz, -50 °C).

After five hours, the ratio of **52**:**53** was approximately 1:3. This suggests that the isomerisation of **52** to **53** is occurring faster than in the ethyl analogue $[Ru(H)_2(IEt_2Me_2)(PPh_3)_2(CO)]$ which only went to a ratio of 1:18 in the same time (page 102). However, quantitative data has not been obtained to back this up.

$[Ru(H)_2(I^iPr_2Me_2)(PPh_3)_2(CO)]$ (**30**) (δ -5.87 ($^2J_{HP}$ = 24.8 Hz, $^2J_{HH}$ = 4.8 Hz), -9.98 ($^2J_{HP}$ = 23.3 Hz, $^2J_{HH}$ = 4.8 Hz)) also isomerises (δ -5.48 ($^2J_{HP}$ = 39.6 Hz, $^2J_{HP}$ = 20.2 Hz, $^2J_{HH}$ = 3.6 Hz), δ -7.70 ($^2J_{HP}$ = 88.0 Hz, $^2J_{HP}$ = 32.4 Hz, $^2J_{HH}$ = 3.6 Hz)) but then rapidly forms the axial C-H activated isomer (**34**), which is again a different geometry to that observed upon heating of **30** (page 47) (δ -7.73 ($^2J_{PP}$ = 106.0 Hz, $^2J_{HP}$ = 30.0 Hz)), which is the predominate product (figure 2.45).

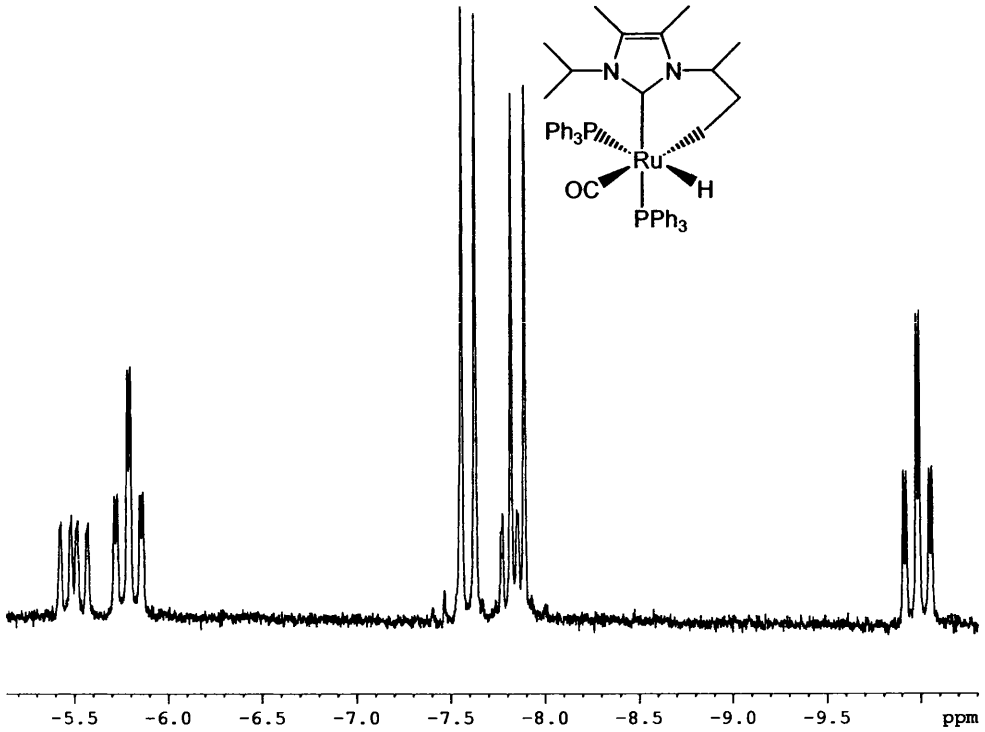


**Figure 2.45.** Hydride region of $^1$H NMR showing isomerisation of **30** followed by C-H activation to give **34** after 3 hours under photolysis at room temperature in $C_6D_6$ ($C_6D_6$, 400 MHz, 25 °C).

*2.8.2.5. Photolysis of [Ru(H)$_2$(NHC)$_2$(PPh$_3$)(CO)]*

A similar isomerisation is observed upon irradiation of the bis ICy complex, *eq,ax*-(ICy)$_2$-[Ru(H)$_2$(ICy)$_2$(PPh$_3$)(CO)] (**55**).[116] Upon irradiation (0.02 mol dm$^{-3}$ in $d_8$ toluene) with UV light (Hg arc, $\lambda > 285$ nm, 125 W, 25 °C), the hydride region of the $^1$H NMR showed loss of the doublets of doublets arising from **55** (δ -5.39 ($^2J_{HP}$ = 40.1 Hz, $^2J_{HH}$ = 4.4 Hz), -9.10 ($^2J_{HP}$ = 30.2, $^2J_{HH}$ = 4.4 Hz)) and appearance of two new doublets at δ -5.00 ($^2J_{HP}$ = 37.9 Hz) and -7.48 ($^2J_{HP}$ = 99.3 Hz) (figure 2.46.). This new product is attributed to the isomerisation product in which the two NHC ligands are *trans* to each other *ax,ax*-(ICy)$_2$-[Ru(H)$_2$(ICy)$_2$(PPh$_3$)(CO)] (**56**) (scheme 2.19.). The hydride coupling in **56** is too small to detect. After 14 hours irradiation at room temperature the ratio of **56**:**55** is about 0.8:1 but product is seen immediately upon isomerisation. After 4 days of photolysis at room temperature, **56** is by far the predominant product (**56**:**55** 9:1) but some decomposition is observed by the

production of free phosphine and some new, although weak, unidentifiable peaks in the hydride region of the $^1$H NMR spectrum. Intriguingly, in contrast to the mono NHC species, the thermal reisomerisation of **56** to reform **55** requires heating at 60 °C for 8 hours to return the sample to solely **55**.

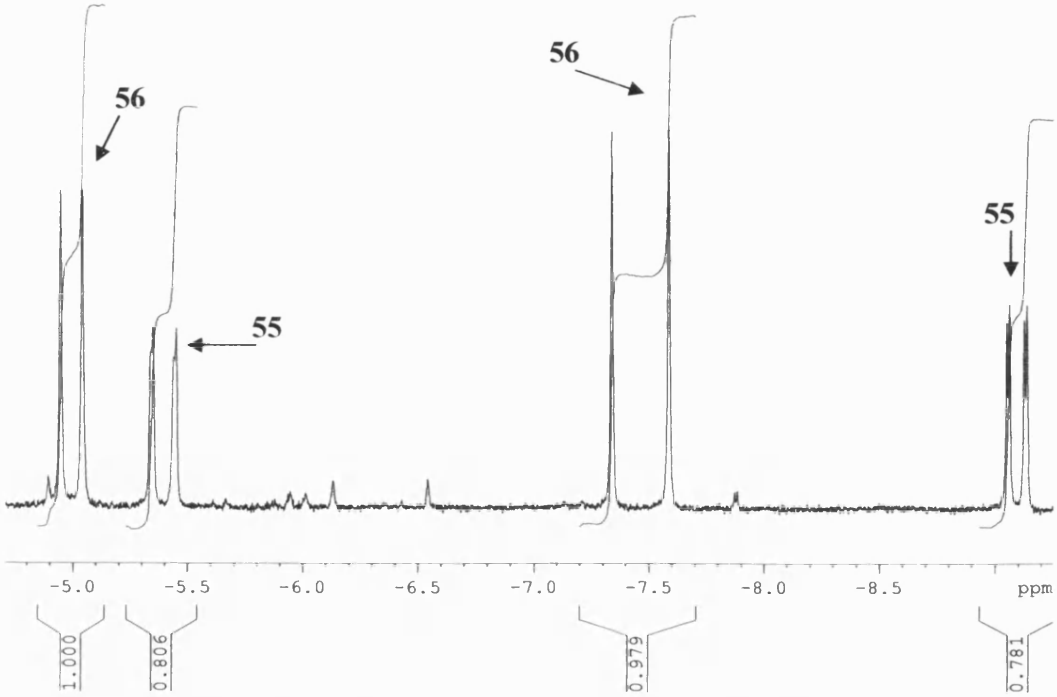


**Figure 2.46.** Hydride region of $^1$H NMR spectrum showing isomerisation of *eq*,*ax*-(ICy)$_2$-[Ru(H)$_2$(ICy)$_2$(PPh$_3$)(CO)] (**55**) to *ax*,*ax*-(ICy)$_2$-[Ru(H)$_2$(ICy)$_2$(PPh$_3$)(CO)] (**56**) after 14 hours photolysis at room temperature in $C_6D_6$ (400 MHz, 25 °C).

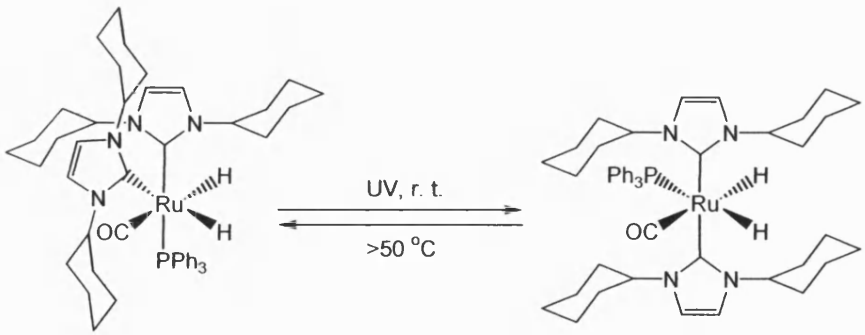


**Scheme 2.19.** Isomerisation of **55** to **56** under UV light.

The Eyring plot for the reisomerisation of **56** to **55**, run over a range of temperatures from 65 °C to 120 °C, gave values for $\Delta H^{\#}$ of 116.16 (± 16.56) kJ $mol^{-1}$ and $\Delta S^{\#}$ of 14.16 (± 45.80) $JK^{-1}mol^{-1}$ (figure 2.47.). Recalculation using Lente's method[88] (described on page 100) gave extremely similar values and margins of error for both $\Delta H^{\#}$ and $\Delta S^{\#}$. Although the values for $\Delta H^{\#}$ and $\Delta S^{\#}$ are slightly higher than those for the reisomerisation of **33** to **29**, within experimental error they are the same, suggesting that the mechanism of isomerisation is similar in both bis and mono NHC complexes. The analogous bis NHC complex $[Ru(H)_2(IMe_4)_2(PPh_3)(CO)]$ has been irradiated and found to undergo the same isomerisation from a *cis* arrangement of NHC ligands (δ -5.58 ($^2J_{HP}$ = 35.6 Hz, $^2J_{HH}$ = 2.8 Hz), -8.71 ($^2J_{HP}$ = 14.8 Hz, $^2J_{HH}$ = 2.8 Hz)) to a *trans* one (δ -5.31 ($^2J_{HP}$ = 35.2 Hz), δ -7.12 ($^2J_{HP}$ = 104.0 Hz)). The bis $IEt_2Me_2$ complex, **51**, and the mixed $IEt_2Me_2$/IMes complex, synthesised by addition of the free NHC ligands to **29** followed by irradiation (page 111) also begin to isomerise to a *trans* arrangement of NHCs once they have formed as the original *cis* complex.

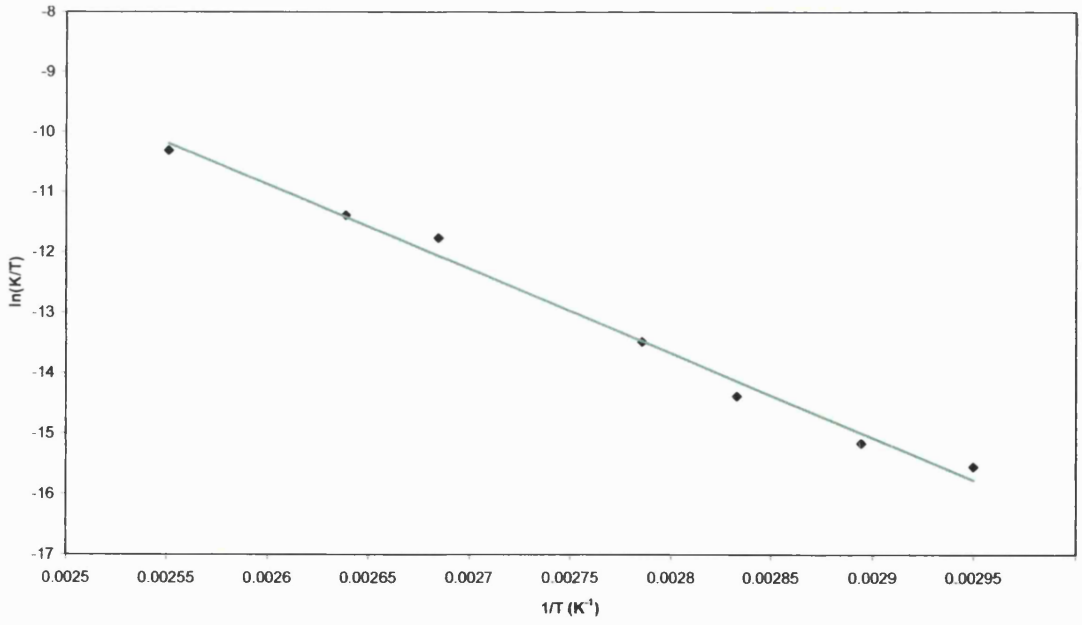


**Figure 2.47.** Eyring plot for the reisomerisation of **56** to **55**.

The IR spectrum of **56** shows a much lower frequency $\nu_{CO}$ band (1864 $cm^{-1}$) compared to that for **55** (1889 $cm^{-1}$). Again, this must be due to the *cis* arrangement of the ligands around the CO rather than what is *trans* to it as this is a hydride in both cases.

The photolysis of **55** (0.004 mol $dm^{-3}$) was also measured using the *in situ* laser system at the University of York (HeCd, 325 nm, 0.038 W). In this, more controlled system, the isomerisation of **55** was shown to be extremely rapid, going to 50 % within 15 minutes and to completion within an hour. When 3 atm of *p*-$H_2$ was added to a sample of **55** and irradiated at -50 °C, immediate enhancement was observed into the hydride signals of both the starting material and product (figure 2.48.). After two minutes all enhancement had been lost and this coincides with formation of a broad resonance at δ -5.54, which is probably an $\eta^2$-$H_2$ complex, similar to that observed in photolysis of *eq*-$IEt_2Me_2$-$[Ru(H)_2(IEt_2Me_2)(PPh_3)_2(CO)]$ (**29**). This species is apparent at -50 °C and -40 °C but is lost upon cooling to -70 °C or warming to above -40 °C. Warming the sample from -70 °C to -50 °C led to reappearance of the peak but cooling it down from higher than -40 °C did not. Photolysing the same sample again at -50 °C led to reformation of the broad signal.

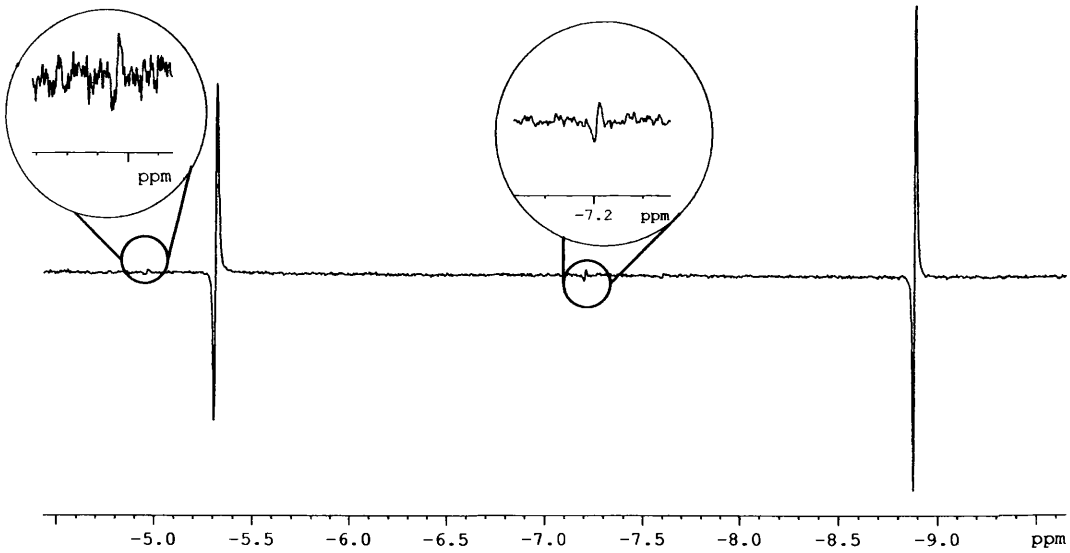


**Figure 2.48.** Hydride region of $^1H\{^{31}P\}$ NMR spectrum following 30 seconds of photolysis of **55** with *p*-$H_2$ at -50 °C ($d_8$-toluene, 400 MHz, -50 °C).

During the *in situ* photolysis of **55** at -50 °C, two other unidentified products were observed after approximately 2 minutes (figure 2.49.). One resonates as a singlet in the hydride region of the $^{1}H$ NMR (with $^{31}P$ coupling) at δ -3.65 and has no phosphorus present. This is likely to be a solvent complex, such as $[Ru(H)_2(ICy)_2(toluene)(CO)]$. There is also a doublet present in the hydride region (δ -6.87 ($^{2}J_{HP}$ = 142.0 Hz)) and this correlates to a singlet in the $^{31}P\{^{1}H\}$ NMR spectrum at δ 25.0. The fact that these peaks belong together was established using a $^{1}H$-$^{31}P\{^{1}H\}$ HMQC experiment. This suggests the loss of one of the NHC ligands or the CO to give a complex such as $[Ru(H)_2(ICy)(PPh_3)(toluene)(CO)]$ or $[Ru(H)_2(ICy)_2(PPh_3)(toluene)]$.

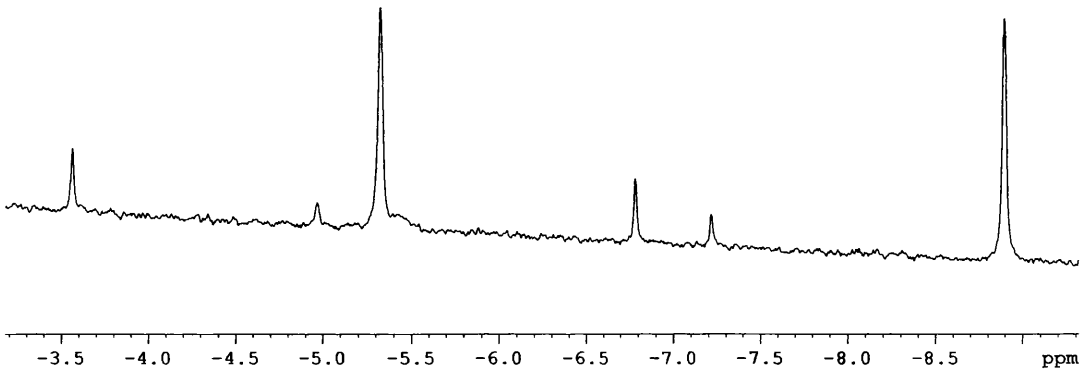


**Figure 2.49.** Hydride region of $^{1}H\{^{31}P\}$ NMR after 8 minutes of *in situ* photolysis of **55** at the University of York. Run without phosphine coupling for clarity ($d_8$-toluene, 400 MHz, -50 °C).

As for **29**, photolysis of **55** in the presence of pyridine slowed isomerisation to **53** and led to formation of two new resonances in the hydride region (δ -2.25, -14.41, $^{2}J_{HH}$ = 3.7 Hz). This is assigned to the complex $[Ru(H)_2(ICy)_2(C_5H_5N)(CO)]$. The experiments carried out with *p*-$H_2$ and pyridine on the isomerisation reaction of *eq,ax*-$(ICy)_2$-$[Ru(H)_2(ICy)_2(PPh_3)(CO)]$ (**55**) to *ax,ax*-$(ICy)_2$-$[Ru(H)_2(ICy)_2(PPh_3)(CO)]$ (**56**) suggest that $H_2$ loss and phosphine loss are occurring under photolysis. This is similar to what has been observed for the mono-NHC complex *eq*-$IEt_2Me_2$-$[Ru(H)_2(IEt_2Me_2)(PPh_3)_2(CO)]$ (**29**). The bis NHC complex, **55**, also appears to lose CO or NHC due to the formation of complexes that contain hydrides but no phosphines.

Preliminary calculations on simplified analogues of these bis NHC complexes (using IH for ICy and $PH_3$ for $PPh_3$) put the *trans* NHC complex (analogue of **56**) as 14.4 kJ $mol^{-1}$ more stable than the *cis* NHC complex (analogue of **55**).

## 2.9. Conclusions

Although evidence points towards the formation of the C-C activated complex, $[RuH(IMes)'(PPh_3)_2(CO)]$ (**19**) from the bis IMes species, $[Ru(H)_2(IMes)_2(PPh_3)(CO)]$ (**17**), the lack of success in isolating **17** has hindered mechanistic studies on this reaction. Theoretical studies suggest that C-H activation of IMes may be on the pathway to C-C activation. However, this has not been established experimentally and in fact seems unlikely.

The solvent employed appears to have an important bearing on whether the mono IMes species, $[Ru(H)_2(IMes)(PPh_3)_2(CO)]$ (**16**), goes on to C-C or C-H activate. The reactions in THF and benzene both lead to formation of a substantial amount of **19** but the reaction in THF was faster and cleaner, leading to predominantly **19** after 21 hours at 110 °C. After the same amount of time in benzene, the predominant product was still **16**. It is likely that some stabilisation of an intermediate complex in the mechanism of formation of **19** is necessary and the better coordinating properties of THF compared to benzene help to do this. It has been shown that $C_6D_6$ undergoes H/D exchange with the hydride and phosphine ligands on **17** and **19** in solution which is further evidence for intimate involvement of solvent. Benzene may need to undergo activation before it can stabilise an intermediate whereas THF does not. This would explain why **19** forms faster in THF as there is one less process to undergo during the reaction.

In fluorobenzene, formation of **16**, **17** and **19** is much slower than in benzene, which supports the theory that coordinating solvents are necessary for progression of the reaction. THF is a more coordinating solvent than benzene, which in turn is more coordinating than fluorobenzene.[117]

The most surprising reaction, however, comes when using cyclohexane as the solvent. This leads to formation of some of the C-H activated complex, [RuH(IMes)''$(PPh_3)_2(CO)$] (**18**), albeit in small yields. Previously, this complex has only been observed upon addition of alkene to **16**. The presence of a doublet in the hydride region of the $^1H$ NMR spectrum suggests possible formation of a solvated complex due to loss of a phosphine ligand. If this is so and the complex could be isolated, this may well provide an insight into the mechanism of both the C-H and C-C activation of the IMes ligand.

Irradiation of the mono IMes complex, **16**, with UV light led to formation of an unidentified product after prolonged exposure. In contrast, photolysing dihydride alkyl NHC ruthenium complexes has led to observation of some highly unusual chemistry. Both mono and bis alkyl-NHC complexes underwent isomerisation when photolysed with NHCs *trans* to hydride moving to a position *trans* to $PPh_3$ or NHC. The complexes have been shown to undergo both hydrogen and phosphine loss and, in collaboration with the Universities of York and Nottingham, the reaction has been studied on a microsecond to second timescale (scheme 2.20.). Photolysis of the mono $IEt_2Me_2$ complex, *eq*-($IEt_2Me_2$)-[$Ru(H)_2(IEt_2Me_2)(PPh_3)_2(CO)$] (**29**), in the absence of hydrogen does eventually lead to a C-H activation product, [RuH($IEt_2Me_2$)''$(PPh_3)_2(CO)$] (**31**), which is stable at room temperature. The $I^iPr_2Me_2$ analogue of this complex, *eq*-($I^iPr_2Me_2$)-[$Ru(H)_2(I^iPr_2Me_2)(PPh_3)_2(CO)$] (**30**) undergoes activation much more rapidly and the activated complex, [RuH($I^iPr_2Me_2$)''$(PPh_3)_2(CO)$] (**34**), is the major product after 2 hours of photolysis. Addition of various substrates has led to further understanding of the mechanism of these reactions although there is a substantial amount of scope for further investigations.

The bis NHC complex, *eq,ax*-$(ICy)_2$-[$Ru(H)_2(ICy)_2(PPh_3)(CO)$] (**55**), also isomerises and as well as losing phosphine and $H_2$ appears to lose either CO or ICy in a minor pathway. A full investigation of what is occurring to the bis NHC complexes under UV light, both on the NMR and TRIR timescales, still needs to be carried out.

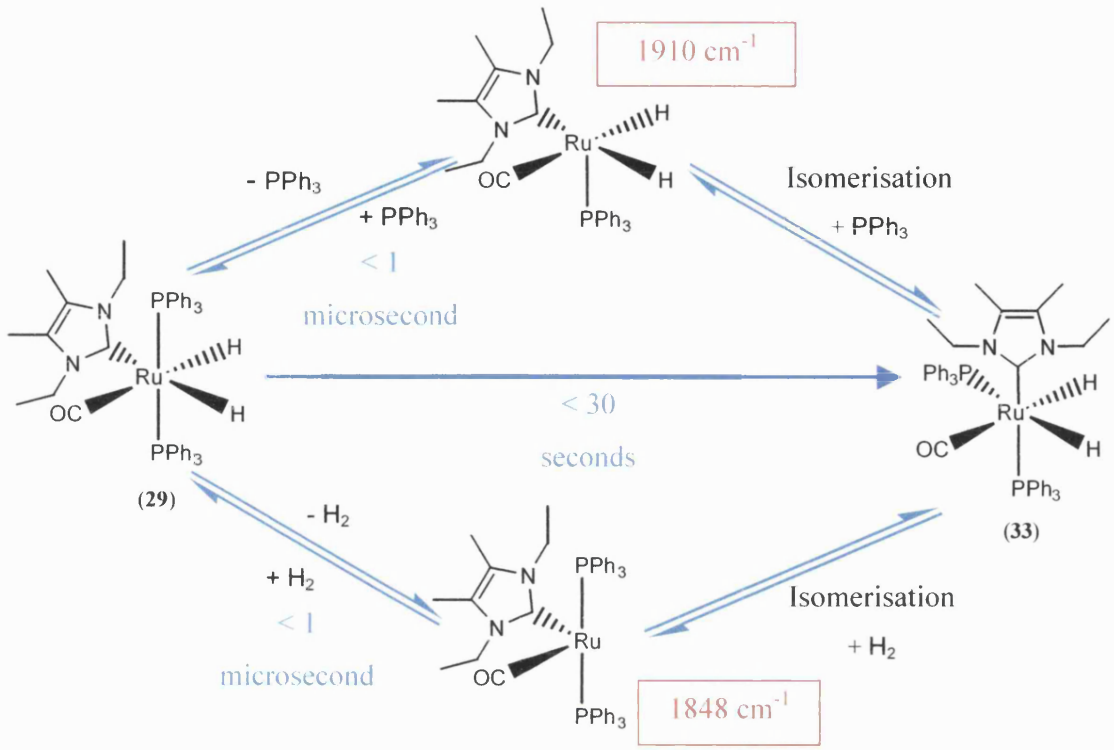


**Scheme 2.20.** Overview of isomerisation reaction of **29**.

The thermal reisomerisation of both the mono and bis NHC complexes is potentially even more interesting than the initial isomerisation under UV light. UV light stimulates $H_2$ and $PPh_3$ loss from the complexes to induce isomerisation of the NHC ligand from *trans* to the hydride to *trans* to the phosphine or the NHC. Loss of $H_2$ and $PPh_3$ from the complexes does not occur upon heating and so the fact that the NHCs return from *trans* to phosphine or NHC to *trans* to hydride at elevated temperature but without the presence of UV light implies that the reisomerisation is not necessarily occurring *via* a route involving $H_2$ or $PPh_3$ loss. The value of $\Delta S^{\#}$ (-29.50 (± 64.57) $JK^{-1}mol^{-1}$) obtained from the Eyring plot of the thermal back reaction of the mono $IEt_2Me_2$ complex suggests that the process is intramolecular and reported studies on the tris phosphine complex, $[Ru(H)_2(PPh_3)_3(CO)]$ (**15**), suggest that this could occur *via* a trigonal twist mechanism.

## 2.10 References


(1) Huang, J.; Schanz, H.-J.; Stevens, E. D.; Nolan, S. P. *Organometallics* **1999**, *18*, 2370.
(2) Weskamp, T.; Kohl, F. J.; Hieringer, W.; Gleich, D.; Herrmann, W. A. *Angew. Chem. Int. Ed.* **1999**, *38*, 2416.
(3) Harries-Rees, K. *Chemistry World* **2005**, *2*, 42.
(4) Herisson, J. L.; Chauvin, Y. *Makromol. Chem.* **1970**, *141*, 161.
(5) Crabtree, R. H. *The Organometallic Chemistry of the Transition Metals*; 3rd ed.; Wiley-Interscience: New York, 2001.
(6) Schwab, P.; Grubbs, R. H.; Ziller, J. W. *J. Am. Chem. Soc.* **1996**, *118*, 100.
(7) Dias, E. L.; Nguyen, S. T.; Grubbs, R. H. *J. Am. Chem. Soc.* **1997**, *119*, 3887.
(8) Dias, E. L.; Grubbs, R. H. *Organometallics* **1998**, *17*.
(9) Trnka, T. M.; Grubbs, R. H. *Acc. Chem. Res.* **2001**, *34*, 18.
(10) Scholl, M.; Trnka, T. M.; Morgan, J. P.; Grubbs, R. H. *Tet. Lett.* **1999**, *40*, 2247.
(11) Morgan, J. P.; Grubbs, R. H. *Org. Lett.* **2000**, *2*, 3153.
(12) Sanford, M. S.; Love, J. A.; Grubbs, R. H. *J. Am. Chem. Soc.* **2001**, *123*, 6543.
(13) Ung, T.; Hejl, A.; Grubbs, R. H.; Schrodi, Y. *Organometallics* **2004**, *23*, 5399.
(14) Dinger, M. B.; Mol, J. C. *Adv. Synth. Catal.* **2002**, *344*, 671.
(15) Huang, J.; Stevens, E. D.; Nolan, S. P.; Peterson, J. L. *J. Am. Chem. Soc.* **1999**, *121*, 2674.
(16) Huang, J.; Schanz, H.-J.; Stevens, E. D.; Nolan, S. P. *Organometallics* **1999**, *18*, 5375.
(17) Schmidt, B. *Eur. J. Org. Chem.* **2004**, 1865.
(18) Jafarpour, L.; Nolan, S. P. *J. Organomet. Chem.* **2001**, *617-618*, 17.
(19) Sanford, M. S.; Ulman, M.; Grubbs, R. H. *J. Am. Chem. Soc.* **2001**, *123*, 749.
(20) The rate of exchange of bound with free phosphine and is calculated using the computer program CIFIT (Bain, A.D.; Kramer, J. A., *J. Magn. Res.*, **1978**, *29*, 433). It is independent of [$PCy_3$] over a wide range of concentrations.
(21) Dorta, R.; Stevens, E. D.; Scott, N. M.; Costabile, C.; Cavallo, L.; Hoff, C. D.; Nolan, S. P. *J. Am. Chem. Soc.* **2005**, *127*, 2485.
(22) Dharmasena, U. L.; Foucault, H. M.; dos Santos, E. N.; Fogg, D. E.; Nolan, S. P. *Organometallics* **2005**, *24*, 1056.
(23) Adlhart, C.; Hinderling, C.; Baumann, H.; Chen, P. *J. Am. Chem. Soc.* **2000**, *122*, 8204.
(24) Adlhart, C.; Chen, P. *J. Am. Chem. Soc.* **2004**, *126*, 3496.
(25) Cavallo, L. *J. Am. Chem. Soc.* **2002**, *124*, 8965.
(26) McGuinness, D. S.; Cavell, K. J.; Skelton, B. W.; White, A. H. *Organometallics* **1999**, *18*, 1596.

(27) Romero, P. E.; Piers, W. E.; McDonald, R. *Angew. Chem. Int. Ed.* **2004**, *43*, 6161.
(28) Romero, P. E.; Piers, W. E. *J. Am. Chem. Soc.* **2005**, *127*, 5032.
(29) Ackermann, L.; Fürstner, A.; Weskamp, T.; Kohl, F. J.; Herrmann, W. A. *Tet. Lett.* **1999**, *40*, 4787.
(30) Fürstner, A.; Thiel, O. R.; Ackermann, L.; Schanz, H.-J.; Nolan, S. P. *J. Org. Chem.* **2000**, *65*.
(31) Bourgeois, D.; Pancrazi, A.; Nolan, S. P.; Prunet, J. *J. Organomet. Chem.* **2002**, *643-644*, 247.
(32) Weskamp, T.; Schattenman, W. C.; Spiegler, M.; Herrmann, W. A. *Angew. Chem. Int. Ed.* **1998**, *37*, 2490.
(33) Fürstner, A.; Ackermann, L.; Gabor, B.; Goddard, R.; Lehmann, C. W.; Mynott, R.; Stelzer, F.; Thiel, O. R. *Chem. Eur. J.* **2001**, *7*, 3236.
(34) Drouin, S. D.; Zamanian, F.; Fogg, D. E. *Organometallics* **2001**, *20*, 5495.
(35) Fogg, D. E.; Amoroso, D.; Drouin, S. D.; Snelgrove, J.; Conrad, J. C.; Zamanian, F. *J. Mol. Catal. A-Chem.* **2002**, *190*, 177.
(36) Louie, J.; Bielawski, C. W.; Grubbs, R. H. *J. Am. Chem. Soc.* **2001**, *123*, 11312.
(37) Dinger, M. B.; Mol, J. C. *Organometallics* **2003**, *22*, 1089.
(38) Dinger, M. B.; Mol, J. C. *Eur. J. Inorg. Chem.* **2003**, 2827.
(39) Trnka, T. M.; Morgan, J. P.; Sanford, M. S.; Wilhelm, T. E.; Scholl, M.; Choi, T. L.; Ding, S.; Day, M. W.; Grubbs, R. H. *J. Am. Chem. Soc.* **2003**, *125*, 2546.
(40) Hong, S. H.; Day, M. W.; Grubbs, R. H. *J. Am. Chem. Soc.* **2004**, *126*, 7414.
(41) Ulman, M.; Grubbs, R. H. *J. Org. Chem.* **1999**, *64*, 7202.
(42) Bourgeois, D.; Pancrazi, A.; Ricard, L.; Prunet, J. *Angew. Chem. Int. Ed.* **2000**, *39*, 725.
(43) Maynard, H. D.; Grubbs, R. H. *Tet. Lett.* **1999**, *40*, 4137.
(44) Conrad, J. C.; Yap, G. P. A.; Fogg, D. E. *Organometallics* **2003**, *22*, 1986.
(45) Jafarpour, L.; Stevens, E. D.; Nolan, S. P. *J. Organomet. Chem.* **2000**, *606*, 49.
(46) Mayr, M.; Mayr, B.; Buchmeiser, M. R. *Angew. Chem. Int. Ed.* **2001**, *40*, 3839.
(47) Buchmeiser, M. R. *Bioorg. Med. Chem. Lett.* **2002**, *12*, 1837.
(48) Dinger, M. B.; Nieczypor, P.; Mol, J. C. *Organometallics* **2003**, *22*, 5291.
(49) Dinger, M. B.; Mol, J. C. *Adv. Synth. Catal.* **2002**, *344*, 671.
(50) Marshall, C.; Ward, M. F.; Harrison, W. T. A. *J. Organomet. Chem.* **2005**, *690*, 3970.
(51) Seiders, T. J.; Ward, D. W.; Grubbs, R. H. *Org. Lett.* **2001**, *3*, 3225.
(52) Louie, J.; Grubbs, R. H. *Organometallics* **2002**, *21*, 2153.
(53) Lee, H. M.; Smith, D. C.; He, Z.; Stevens, E. D.; Yi, C. S.; Nolan, S. P. *Organometallics* **2001**, *20*, 794.
(54) Yi, C. S.; Lee, D. W.; He, Z. *Organometallics* **2000**, *19*, 2909.
(55) Yi, C. S.; Lee, D. W. *Organometallics* **1999**, *18*, 5152.
(56) Baratta, W.; Del Zotto, A.; Rigo, P. *Chem. Commun.* **1997**, 2163.
(57) Csabai, P.; Joó, F. *Organometallics* **2004**, *23*, 5640.

(58) Ozdemir, I.; Yigit, B.; Çetinkaya, B.; Ulku, D.; Tahir, M. N.; Arici, C. *J. Organomet. Chem.* **2001**, *633*, 27.
(59) Sini, G.; Eisenstein, O.; Crabtree, R. H. *Inorg. Chem.* **2002**, *41*, 602.
(60) Poyatos, M.; Mata, J. A.; Falomir, E.; Crabtree, R. H.; Peris, E. *Organometallics* **2003**, *22*, 1110.
(61) Danopoulos, A. A.; Winston, S.; Motherwell, W. B. *Chem. Commun.* **2002**, 1376.
(62) Diggle, R. A.; Macgregor, S. A.; Whittlesey, M. K. *Organometallics* **2004**, *23*, 1857.
(63) Martinho-Simoes, J. A.; Beauchamp, J. L. *Chem. Rev.* **1990**, *90*, 629.
(64) Blomberg, M. R. A.; Brandemark, U.; Siegbahn, P. E. M. *J. Am. Chem. Soc.* **1983**, *105*, 5557.
(65) Saillard, J.-Y.; Hoffmann, R. *J. Am. Chem. Soc.* **1984**, *106*, 2006.
(66) Diggle, R. A.; Kennedy, A. A.; Macgregor, S. A.; Whittlesey, M. K. *In press* **2005**.
(67) Kennedy, A. A.; Diggle, R. A.; Macgregor, S. A. MChem report, Heriot Watt University, Edinburgh, 2004.
(68) Jazzar, R. F. R.; Macgregor, S. A.; Mahon, M. F.; Richards, S. P.; Whittlesey, M. K. *J. Am. Chem. Soc.* **2002**, *124*, 4944.
(69) Burling, S.; Mahon, M. F.; Paine, B. M.; Whittlesey, M. K.; Williams, J. M. J. *Organometallics* **2004**, *23*, 4537.
(70) Paine, B. M., *personal communication.*
(71) Jazzar, R. F. R. PhD thesis, University of Bath, 2003.
(72) Diggle *et al.*, unpublished results.
(73) Burling, Paine *et al.*, unpublished results.
(74) Macgregor *et al.*, unpublished results.
(75) Montiel-Palma, V.; Pattison, D. I.; Perutz, R. N.; Turner, C. *Organometallics* **2004**, *23*, 4034.
(76) Schott, D.; Sleigh, C. J.; Lowe, J. P.; Duckett, S. B.; Mawby, R. J.; Partridge, M. G. *Inorg. Chem.* **2002**, *41*, 2960.
(77) Perutz, R. N. *Chem. Soc. Rev.* **1993**, *22*, 361.
(78) Perutz, R. N. *Pure Appl. Chem.* **1998**, *70*, 2211.
(79) Cronin, L.; Nicasio, M. C.; Perutz, R. N.; Peters, R. G.; Roddick, D. M.; Whittlesey, M. K. *J. Am. Chem. Soc.* **1995**, *117*, 10047.
(80) Hall, C.; Jones, W. D.; Mawby, R. J.; Osman, R.; Perutz, R. N.; Whittlesey, M. K. *J. Am. Chem. Soc.* **1992**, *114*, 7425.
(81) Bergamini, P.; Sostero, S.; Traverso, O. *J. Organomet. Chem.* **1986**, *299*, C11.
(82) Osman, R.; Perutz, R. N.; Rooney, A. D.; Langley, A. J. *J. Phys. Chem.* **1994**, *98*, 3562.
(83) Baker, M. V.; Field, L. D. *J. Am. Chem. Soc.* **1986**, *108*, 7433.
(84) Baker, M. V.; Field, L. D. *J. Am. Chem. Soc.* **1987**, *109*, 2825.
(85) Field, L. D.; George, A. V.; Messerle, B. A. *J. Chem. Soc., Chem. Commun.* **1991**, 1339.
(86) Schaad, D. R.; Landis, C. R. *J. Am. Chem. Soc.* **1990**, *112*, 1628.

(87) Whittlesey, M. K.; Mawby, R. J.; Osman, R.; Perutz, R. N.; Field, L. D.; Wilkinson, M. P.; George, M. W. *J. Am. Chem. Soc.* **1993**, *115*, 8627.
(88) Lente, G.; Fábián, I.; Poë, A. *New J. Chem.* **2005**, *29*, 759.
(89) Ball, G. E.; Mann, B. E. *J. Chem. Soc., Chem. Commun.* **1992**, 561.
(90) Ray, P. C.; Dutt, N. K. *Journal of the Indian Chemical Society* **1943**, *20*, 81.
(91) Duckett, S. B.; Sleigh, C. J. *Prog. Nucl. Magn. Reson. Spectrosc.* **1999**, *34*, 71.
(92) Natterer, J.; Bargon, J. *Prog. Nucl. Magn. Reson. Spectrosc.* **1997**, *31*, 293.
(93) Duckett, S. B.; Blazina, D. *Eur. J. Inorg. Chem.* **2003**, 2901.
(94) Blazina, D.; Duckett, S. B.; Dyson, P. J.; Johnson, B. F. G.; Lohman, J. A. B.; Sleigh, C. J. *J. Am. Chem. Soc.* **2001**, *123*, 9760.
(95) Duckett, S. B.; Mawby, R. J.; Partridge, M. G. *Chem. Commun.* **1996**, 383.
(96) Dunne, J. P.; Blazina, D.; Aiken, S.; Carteret, H. A.; Duckett, S. B.; Jones, J. A.; Poli, R.; Whitwood, A. C. *Dalton Trans.* **2004**, 3616.
(97) Schott, D.; Callaghan, P.; Dunne, J.; Duckett, S. B.; Godard, C.; Goicoechea, J. M.; Harvey, J. N.; Lowe, J. P.; Mawby, R. J.; Muller, G.; Perutz, R. N.; Poli, R.; Whittlesey, M. K. *Dalton Trans.* **2004**, 3218.
(98) Sleigh, C. J.; Duckett, S. B.; Mawby, R. J.; Lowe, J. P. *Chem. Commun.* **1999**, 1223.
(99) The conversion to **48** cannot be estimated since enhancement of the hydride signals in this species is the result of their origin in a second order spin system.
(100) Banwell, C. N.; McCash, E. M. *Fundamentals of Molecular Spectroscopy*; 4th ed.; McGraw-Hill: London, 1994.
(101) Desrosiers, P. J.; Cai, L. H.; Lin, Z. R.; Richards, R.; Halpern, J. *J. Am. Chem. Soc.* **1991**, *113*, 4173.
(102) Fong, T. P.; Lough, A. J.; Morris, R. H.; Mezzetti, A.; Rocchini, E.; Rigo, P. *J. Chem. Soc., Dalton Trans.* **1998**, 2111.
(103) Giunta, D.; Hölscher, M.; Lehmann, C. W.; Mynott, R.; Wirtz, C.; Leitner, W. *Adv. Synth. Catal.* **2003**, *345*, 1139.
(104) Buskens, P.; Giunta, D.; Leitner, W. *Inorg. Chim. Acta* **2004**, *357*, 1969.
(105) Vogt, M.; Pons, V.; Heinekey, D. M. *Organometallics* **2005**, *24*, 1832.
(106) Vendrell, O.; Moreno, M.; Lluch, J. M. *J. Chem. Phys.* **2004**, *121*, 6258.
(107) Montiel-Palma, V.; Perutz, R. N.; George, M. W.; Jina, O. S.; Sabo-Etienne, S. *Chem. Commun.* **2000**, 1175.
(108) Bruno, J. W.; Huffman, J. C.; Green, M. A.; Zubkowski, J. D.; Hatfield, W. E.; Caulton, K. G. *Organometallics* **1990**, *9*, 2556.
(109) Paine, B. M. *et al.*, unpublished results.
(110) Colombo, M.; George, M. W.; Moore, J. N.; Pattison, D. I.; Perutz, R. N.; Virrels, I. G.; Ye, T. Q. *J. Chem. Soc., Dalton Trans.* **1997**, 2857.
(111) Colombo, M. G.; George, M. W.; Moore, J. N.; Pattison, D. I.; Perutz, R. N.; Virrels, I. G.; Ye, T. Q. *Laser Chem.* **1999**, *19*, 283.
(112) Mawby, R. J.; Perutz, R. N.; Whittlesey, M. K. *Organometallics* **1995**, *14*, 3268.
(113) Whittlesey, M. K.; Perutz, R. N.; Virrels, I. G.; George, M. W. *Organometallics* **1997**, *16*, 268.

(114) Torres, L.; Gelabert, R.; Moreno, M.; Lluch, J. M. *Chem. Phys.* **2003**, *286*, 149.
(115) Diggle *et al.*, unpublished results.
(116) Burling, S.; Kociok-Kohn, G.; Mahon, M. F.; Whittlesey, M. K.; Williams, J. M. J. *Organometallics* **2005**, *24*, 5868.
(117) Butts, M. D.; Scott, B. L.; Kubas, G. J. *J. Am. Chem. Soc.*, **1996**, *118*, 11831.

# Chapter 3

# Rhodium NHC complexes

# 3. Rhodium N-heterocyclic carbene complexes

## 3.1. Introduction

Rhodium phosphine complexes have played a pivotal role in the development of organometallic catalysis,[1] with Wilkinson's catalyst, $[RhCl(PPh_3)_4]$, being one of the best known and widely employed examples. Despite the extensive use of complexes such as Wilkinson's complex in catalysis, only a limited number of rhodium-NHC analogues have been synthesised, and investigated in catalysis. This chapter begins with a review of the chemistry and mechanisms of some of the more popular phosphine based rhodium catalysts as well as the structures of the NHC analogues that have been synthesised.

The synthesis of a host of new Rh(I) complexes bearing one, two, three and four NHC ligands is presented. These structures have been characterised using multinuclear NMR spectroscopy, IR spectroscopy, elemental analysis and X-ray diffraction. As discussed in section 1.2.7., Nolan and Danopoulos have showed that NHC ligands on rhodium centres can undergo C-H bond activation and it was hoped that bond activation of NHCs at rhodium centres could be established to compare with those already found at ruthenium centres and presented in chapter 2. While no activations of alkyl substituted NHCs have been observed, an example of spontaneous C-H bond activation with an IMes ligand at room temperature has been observed and is reported here.

## 3.2. Rhodium complexes in catalysis

### 3.2.1. Wilkinson's catalyst

Wilkinson's catalyst[2] $[RhCl(PPh_3)_3]$ (**57**) is the best known of the catalytically active Rh(I) complexes and is widely used for alkene hydrogenation (turnover rates of typically 0.05-0.25 $s^{-1}$)[3] as well as hydrosilylation[4] and hydroboration.[5]

During alkene hydrogenation, **57** first forms a dihydride species which then binds to alkene in what is the rate determining step. This alkene dihydride complex undergoes a migratory insertion prior to elimination of alkane in the final reductive elimination step. This regenerates the active catalytic species to reinitiate the cycle (scheme 3.1.).

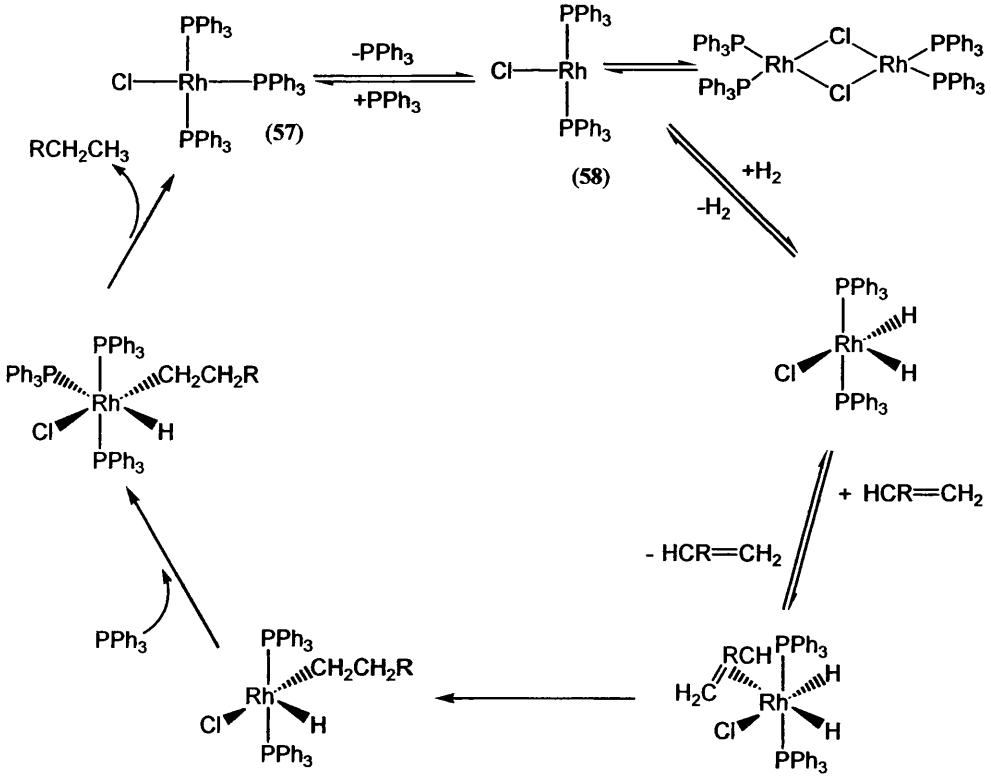


**Scheme 3.1.** Mechanism of alkene hydrogenation by **57**.

The mechanism of hydrogen association to the rhodium centre has received much study. Wilkinson proposed in his initial publication that the addition of $H_2$ occurred after loss of one of the phosphine ligands.[2] Subsequent work by Meakin *et al.*[6] and Halpern *et al.*[7] suggests that this bisphosphine species $[RhCl(PPh_3)_2]$ (**58**) has only a transient existence in solution.

Tolman and Halpern both independently came to the conclusion that **58** exists in a dimeric form $[\{Rh(PPh_3)_2\}_2(\mu\text{-}Cl)_2]$ in solution, where the two $Cl^-$ ligands bridge the rhodium centres (scheme 3.1.).[6,8] The equilibrium lies far to the right, so that the dimeric species is the principle dissociation product in solution. From Halpern's work, however, it appears that when $H_2$ is present, the reaction of **58** with $H_2$ to give $[Rh(H)_2Cl(PPh_3)_2]$ is sufficiently fast to inhibit formation of the dimer, meaning that it does not interfere significantly with the overall reaction of $[RhCl(PPh_3)_2]$ with $H_2$. After carrying out thorough investigations into the rate of hydrogen addition to **58** (both as a three coordinate species and as a dimer) and to **57**, Halpern concluded that Wilkinson was correct in his original assumption that the monomeric **58** is highly reactive and thus likely to be extremely important in **57**-catalysed hydrogenation and related reactions.[9,10]

Brown *et al.* used dynamic NMR experiments to study intra- and intermolecular $PPh_3$ exchange in **57** and its hydrogen addition product $[Rh(H)_2Cl(PPh_3)_3]$ **($H_2$)-57**.[3] This showed that phosphine loss from **57** was as quick as $H_2$ loss. In addition, they postulated, from computer modelling and NMR studies, that the loss of phosphine from **($H_2$)-57** could result in a complex with a *cis* arrangement of phosphine ligands (scheme 3.2.). Phosphine loss can occur from *trans* to the hydride (**I** or **II**) or from *trans* to another phosphine (**II** or **III**). These five-coordinate intermediates can all interconvert with each other and with **IV** and **V**. Although the relative energies of these isomers is unknown, the $P^iPr_3$ analogue, which has been observed, has the same structure as **I**. Brown showed, using dynamic NMR experiments, that both $P_a$ and $P_b$ were exchanging with free phosphine in solution and that it was occurring within the timescale of turnover rates in catalytic hydrogenation.

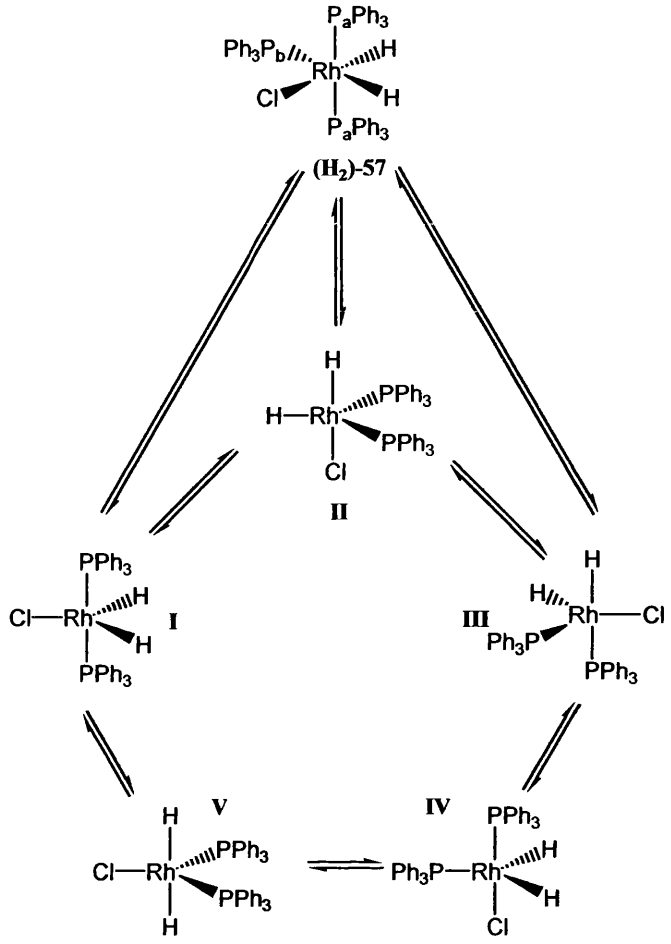


**Scheme 3.2.** The possible geometries of the five-coordinate phosphine loss complex.

Molecular modelling of alkene-bound intermediates, by the same authors,[3] suggests that a structure bearing *trans*-phosphine ligands would be impossibly strained due to van der Waals forces between the coordinated alkene and one of the phosphine ligands (figure 3.1.). The previous observation that *cis*-phosphine intermediates are formed upon phosphine loss from **(H2)-57**, adds further credibility to the theory that a *cis*-phosphine species plays an important role in the mechanism of alkene hydrogenation by **57**.


**Figure 3.1.** The two isomers of alkene bound intermediates, bearing *trans* and *cis* arrangements of phosphine ligands, in alkene hydrogenation by **57**.

More recently, the use of *para*hydrogen has allowed new intermediates in the hydrogenation reactions catalysed by **57** to be observed due to the enhancement of proton signals in NMR spectra.[11-14] When alkene was added to the reaction, an alkene bound product was observed that contained *cis* phosphines. This suggests, like Brown postulated, that a *cis*-phosphine intermediate is important in alkene hydrogenation and that its lifetime is so short (as evidenced by the inability to observe it using conventional NMR methods) that it must be a very reactive intermediate in the reaction.

In addition, *para*hydrogen studies found evidence that dimeric species are important in the reactions, as suggested by Halpern and Tolman, and that the presence of free phosphine inhibits their formation, thus enhancing the catalytic ability of **57**.

### 3.2.2. Catalysis using [RhH(PPh$_3$)$_2$(CO)]

[RhH(PPh$_3$)$_2$(CO)] (**59**) is an active hydrogenation and hydroformylation catalyst.[15,16] The hydroformylation reaction adds CO and $H_2$ across a double bond (which is normally in the terminal position).[17] Addition of $H_2$ and CO can proceed through either Markovnikov or anti-Markovnikov addition. Markovnikov addition leads to an internal aldehyde and these products are less desirable. Therefore anti-Markovnikov addition is preferred, giving linear aldehydes (scheme 3.3.).

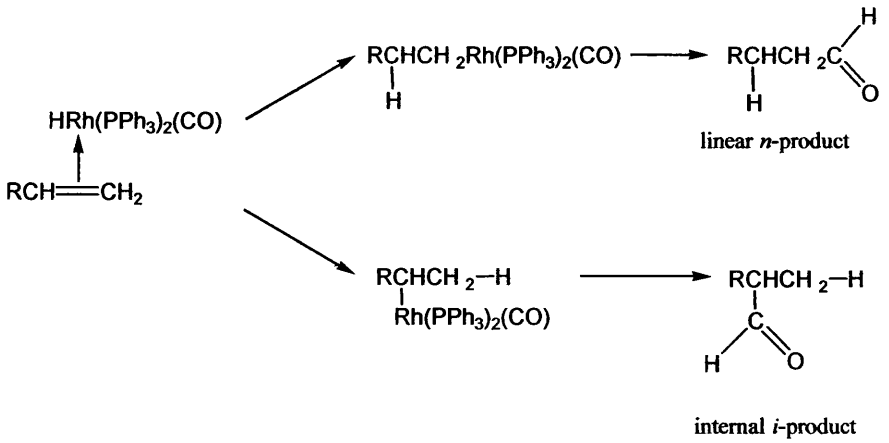


**Scheme 3.3.** Formation of *n* and *i* isomers of aldehydes in the hydroformylation reaction.

The proposed mechanism consists of migratory insertion of the CO to the metal alkyl group which has already been formed from migratory insertion of the alkene into the Rh-H bond (scheme 3.4.).[16]

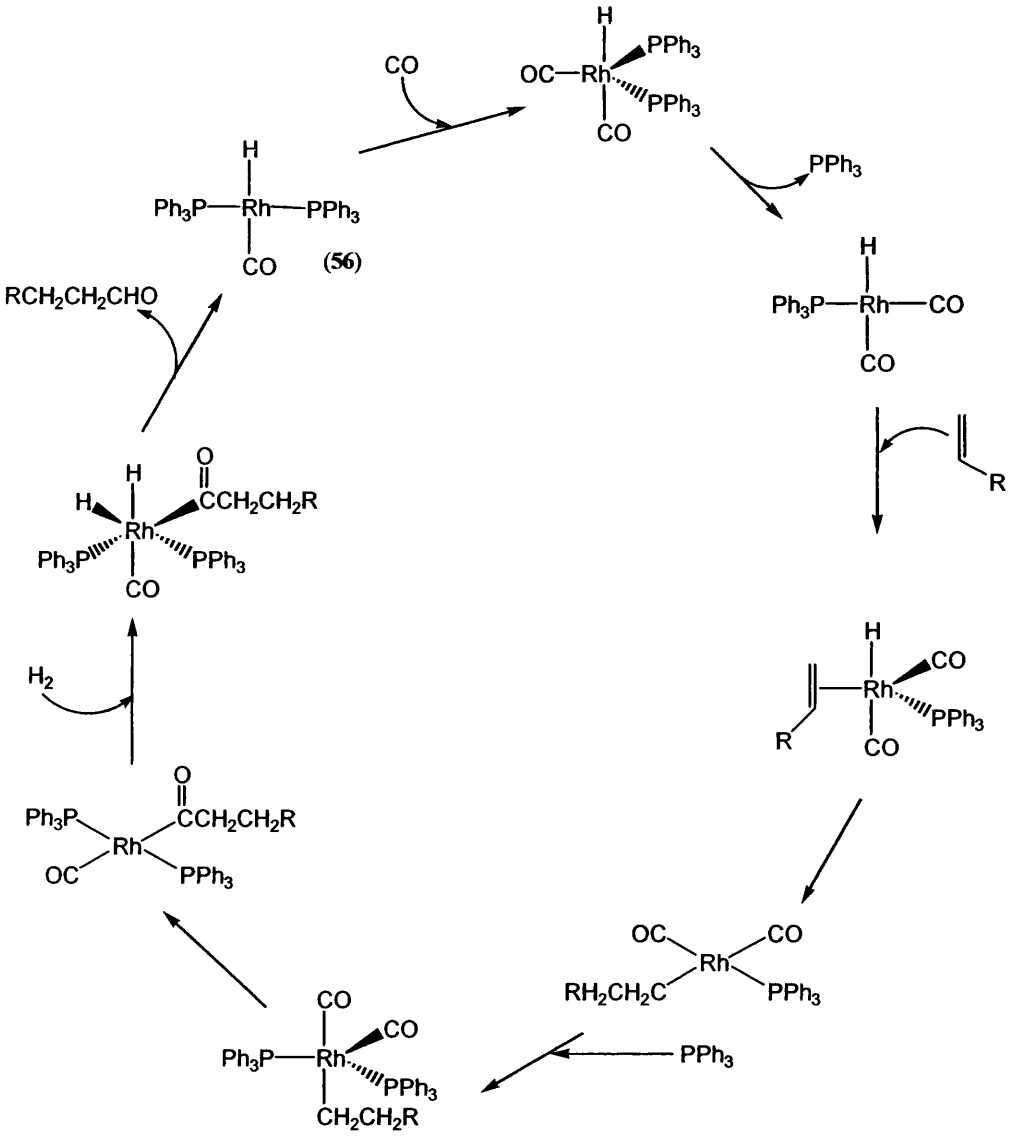


**Scheme 3.4.** Mechanism of hydroformylation, catalysed by **59**.

Large excesses of phosphine (usually greater than 0.3 M) need to be added to the reaction mixture if a high selectivity for the linear isomer is desired. This is because, under the added CO pressure, **59** is in equilibrium with di- and tri-carbonyl species which are less selective for the linear isomer (scheme 3.5.).[18] Pruett and Smith found that the pressures of CO and $H_2$ also greatly affected the selectivity of **59**.[19] They

found that lowering the pressure of a 1:1 ratio $CO:H_2$ atmosphere led to a much higher ratio of linear product (*n*) to branched (*i*). For example, in the hydroformylation of methyl methacrylate ($CH_2C(CH_3)COOCH_3$), a pressure of 170 atm led to an *n:i* ratio of 0.3:1 whilst a pressure of 7.5-14.5 atm gave a 24:1 ratio (5 mol % catalyst, 100-110 °C).

$$HRh(CO)_3(PPh_3) \underset{CO}{\overset{PPh_3}{\rightleftharpoons}} HRh(CO)_2(PPh_3)_2 \underset{CO}{\overset{PPh_3}{\rightleftharpoons}} HRh(CO)(PPh_3)_3$$

**Scheme 3.5.** Equilibrium of **59** with $PPh_3$ and CO.

Pruett and Smith found that changing the phosphine group had pronounced effects on the reaction. By varying the electronegativity and bulkiness of the ligand, the percentage of *n* aldehyde produced was significantly altered (table 3.1.). If the $PPh_3$ ligand on **59** is changed for an alkyl phosphine, less *n*-aldehyde is produced. This is attributed to those phosphines with more back-bonding capability being able to prevent a large charge build up on the rhodium centre and hence reducing the likelihood of the catalyst reacting with CO. Those catalysts bearing bulkier $PR_3$ groups are also more likely to lose phosphine and react with CO thus leading to less linear product.

| Nature of R in $PR_3$ | Temperature (°C) | Reaction time (min) | % *n* octanol |
|---|---|---|---|
| *n*-Butyl | 90 | 225 | 71 |
| Phenyl | 90 | 35 | 82 |
| *n*-Butoxy | 110 | 60 | 81 |
| Phenoxy | 90 | 50 | 86 |
| *o*-Methylphenoxy | 90 | 52 | 78 |
| *o,o*-Dimethylphenoxy | 90 | 80 | 47 |
| *o*-Phenylphenoxy | 90 | 95 | 52 |
| *p*-Phenylphenoxy | 90 | 70 | 85 |
| *p*-Chlorophenoxy | 90 | 55 | 93 |
| *p*-Methoxyphenoxy | 90 | 270 | 83 |

*5 % Rh/C[20] (10 g), 112 g octene, 200 mL toluene, 0.05 mol $PR_3$, 5-7 atm of 1:1 $CO:H_2$*

**Table 3.1.** Effect of changing $PR_3$ group on hydroformylation reaction.

Abatjoglou *et al.* have studied the degradation pathways of phosphine in rhodium catalysed hydroformylation and hydrogenation reactions.[21] During propene hydroformylation catalysed by **59**, triphenylphosphine is slowly converted to

propyldiphenylphosphine. The rate of this conversion is decreased when additional $PPh_3$ is added to the reaction, implying that coordinatively unsaturated complexes are required for the propyldiphenylphosphine to form. The mechanism proposed is shown in scheme 3.6. It involves a carbon-phosphorus bond of one of the coordinated $PPh_3$ groups oxidatively adding to a coordinatively unsaturated rhodium(I) complex (**I**) to form a rhodium(III) intermediate (**II**). When higher concentrations of propene are present, formation of a propene insertion product is favoured (**III**) and reductive elimination of the $C_3H_7$ ligand and the $PPh_2$ ligand from the rhodium leads to formation of propyldiphenylphosphine (**IV**). Lower concentrations of propene lead to formation of phosphido-bridged rhodium complexes. The formation of propyldiphenylphosphine reduces the selectivity of the catalyst but the dimeric species slow the activity. For example, the hydrogenation of propene (and the formation of propyldiphenylphosphine) diminishes after 3-4 hours reaction time. This is accompanied by a change in colour of the catalyst from yellow to dark brown.

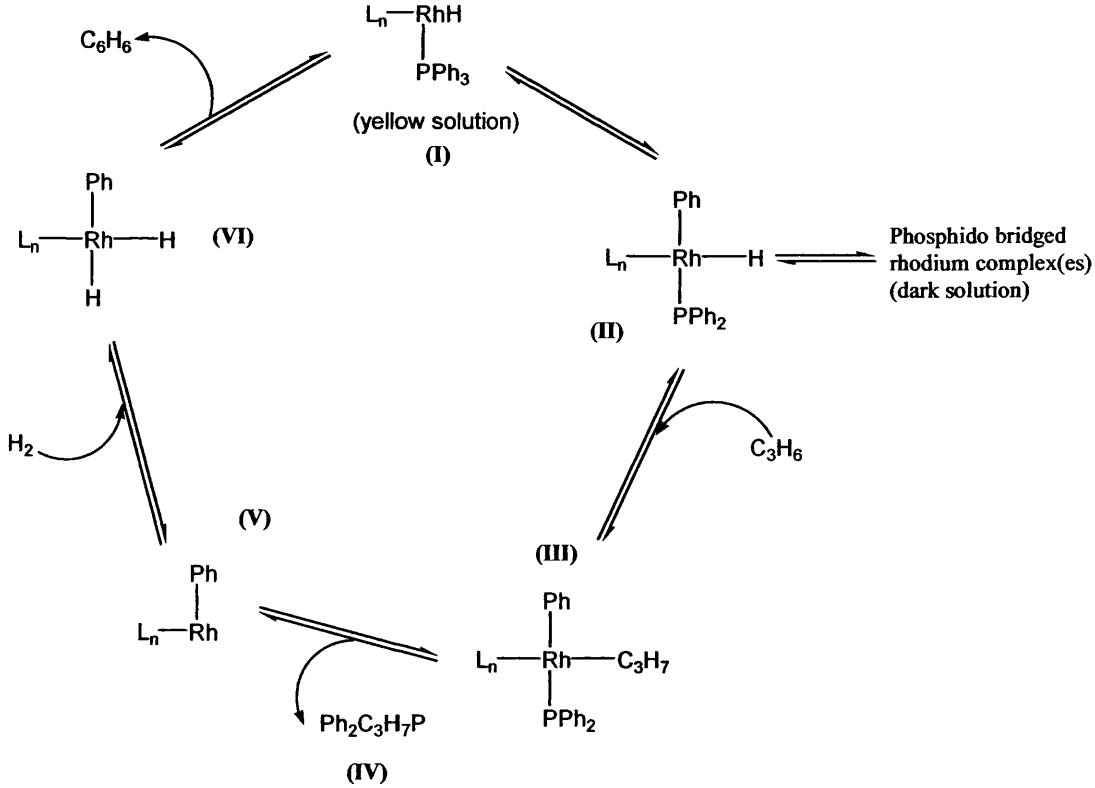


**Scheme 3.6.** Mechanism of $PPh_3$ activation in the hydroformylation reaction.

## 3.3. Swapping $PR_3$ for NHC

### 3.3.1. Synthesis of rhodium NHC complexes from enetetramines

Lappert had synthesised a significant number of Rh-NHC complexes from enetetramine starting materials before free NHCs became readily available.[22-28] Enetetramines, which are dimers of NHCs, can be synthesised by distillation of a 1,2-bis(dialkylamino)-ethane with *N,N*-dimethylformamide dimethyl acetal[29] or $CH(OEt)_3$[30] or by thermolysis of 1,3-diarylimidazolium trichloride[31] (scheme 3.7.). Lappert utilised the electron rich alkene bond in these species to encourage coordination to a number of transition metal centres in high yield. The rhodium complexes synthesised were prepared from one of three starting materials, *trans*-$[RhCl(PPh_3)_2(CO)]$, $[\{Rh(COD)\}(\mu\text{-}Cl)]_2$ and $[RhCl(PPh_3)_3]$ (**57**). Reaction with an enetetramine resulted in $PPh_3$ displacement or $(\mu\text{-}Cl)_2$ bridge splitting. Lappert has synthesised at least 45 rhodium mono NHC complexes. Many of these, including $[RhCl(IPh)(PPh_3)_2]$ (**60**) are direct analogues of Wilkinson's catalyst and were prepared by heating **57** and enetetramine for 1 hour at 140 °C in xylene. The two $PPh_3$ groups in **60** are *trans* to each other as are the phosphines in all the other $[RhCl(NHC)(PPh_3)_2]$ complexes that Lappert has synthesised. This can be seen from the appearance of a single doublet in the $^{31}P\{^1H\}$ NMR spectra (typically, δ 110-120 ($J_{PRh}$ = 156 Hz)).

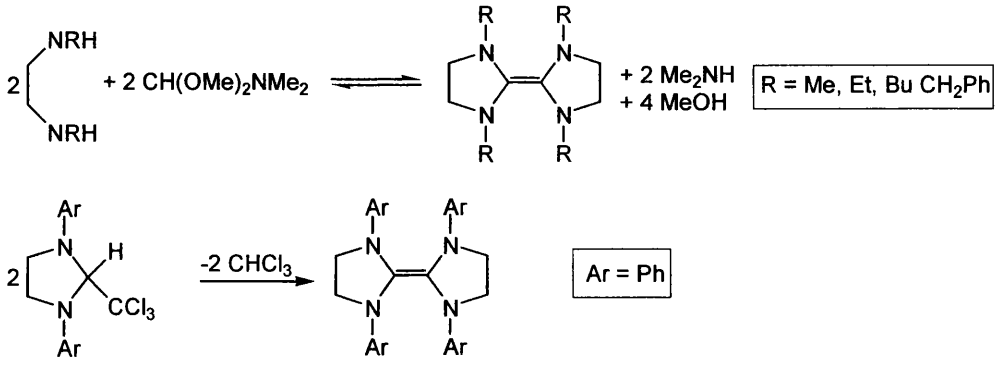


**Scheme 3.7.** Synthesis of enetetramines.

3.3.1.1. $[RhCl(NHC)(PPh_3)_2]$ complexes in catalysis

Lappert and Maskell studied two NHC analogues of **57**, $[RhCl(IMe)(PPh_3)_2]$ (**61**) and $[RhCl(ICH_2Ph)(PPh_3)_2]$ (**62**), as catalysts for the hydrosilylation of ketones and alkynes.[32] They found that after 4 hours at 100 °C, **61** converted 98 % of acetophenone to the silyl ether using triethylsilane, whilst **62** only went to 23 % in the same time at 120 °C. The bis NHC species $[RhCl(IMe)_2(CO)]$ gave no conversion at all. Interestingly, the hydrosilylation of butan-2-one, again using triethylsilane and catalysed by **61**, worked significantly better in $CH_2Cl_2$ than in toluene (50 % conversion at 40 °C cf. 18 % at 100 °C).

In the hydrosilylation of PhC≡CH with triethylsilane, three products are possible, as shown in scheme 3.8. **61** gave a 99 % conversion to silylated products over one hour at 100 °C. This consisted of 74 % *trans*-isomer, 4 % *cis*-isomer and 22 % α-product. In contrast, **57** gives 77 % *trans*-product and 23 % *cis* product.

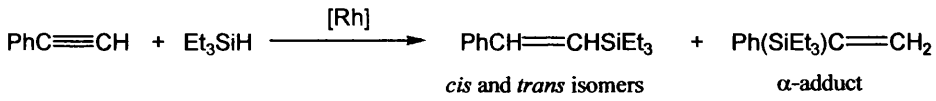


**Scheme 3.8.** Products of hydrosilylation of phenylacetylene by $Et_3Si$.

Çetinkaya *et al.* have prepared analogues of Lappert's complexes,[33] again using enetetramines, this time bearing 2-methoxyethyl substituents on the N groups of the NHC (scheme 3.9.). $[RhCl(ICH_2CH_2OMe)(PPh_3)_2]$ (**63**) has a *trans* phosphine arrangement as evidenced by the $^{31}P\{^1H\}$ NMR spectrum (δ 30.8 ($J_{PRh}$ = 158 Hz)) and was found to be an active cyclopropanation catalyst (69 % (*cis*:*trans* = 25:75)) in converting styrene with functional diazomethane derivatives of the general formula, $N_2CHCO_2Me$ to the cyclic product (80 °C, 4 hours) (scheme 3.10.). The authors moot the possibility that the $CH_2CH_2OMe$ arms on the NHC may act as hemilabile ligands once $PPh_3$ has been lost from the rhodium complex. However, they could not find any evidence for this during a study of the mechanism.

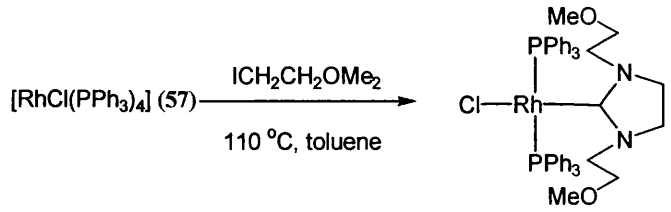


(63)

**Scheme 3.9.** Synthesis of **63** by Çetinkaya et al.

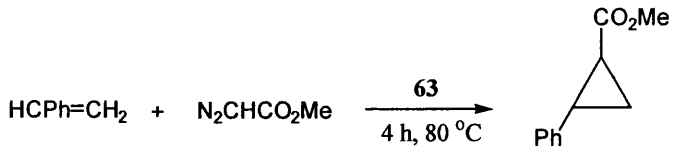


**Scheme 3.10.** Cyclopropanation of styrene and $N_2CHCO_2Me$ by **63**.

3.3.2. Structure and activity of [RhCl(IMes)($PPh_3$)$_2$] (**64**)

Recently, Crudden's group have synthesised [RhCl(IMes)($PPh_3$)$_2$] (**64**), another analogue of Wilkinson's catalyst, by addition of free IMes to **57** in toluene at room temperature.[17] Unlike Lappert's complexes and **63**, the two $PPh_3$ ligands are *cis* to each other, presumably due to the larger steric bulk of IMes.

Investigation by Nolan[34] suggested that the *trans*-influence of IMes in **64** is similar to that of $PPh_3$ in **57**. This is shown by the very small difference in Rh-Cl and Rh-P bond lengths between **64** and **57** (**64**: Rh-Cl = 2.3941(4) Å, Rh-P (*cis* to NHC) = 2.2158(4) Å, Rh-P (*trans* to NHC) = 2.3053(4) Å; **57**: Rh-Cl = 2.376(4) Å, Rh-P (*cis* to Cl) = 2.332(4), 2.334(3) Å, Rh-P (*trans* to Cl) = 2.214(4) Å)[35] and from the very similar coupling constants in the $^{31}P\{^1H\}$ NMR spectrum (**64**: $^2J_{PP}$ = 39 Hz; **57**: $^2J_{PP}$ = 38 Hz). This in contrast to the findings of Lappert when comparing complexes of the type [RhCl(L)($PPh_3$)(CO)] (L = $PPh_3$ or NHC) where the NHC ligands led to lowering of the $^{31}P$-$^{103}Rh$ coupling constant, which is indicative of a higher *trans* influence ligand.[26] [RhCl($PPh_3$)$_2$(CO)] (*trans* $PPh_3$ groups) has a coupling constant of 129 Hz compared to [RhCl(IPh)($PPh_3$)(CO)] (*trans* $PPh_3$ and NHC) with a coupling constant of 117 Hz.

Nolan also discovered that the thermal stability of **64** was greater than that of **57**. Upon heating, **57** loses a phosphine ligand to give **58** in its dimeric form. **64**, on the other hand, shows no decomposition or formation of the corresponding $[\{Rh(IMes)(PPh_3)\}_2(\mu\text{-}Cl)_2]$ dimer after heating at 65 °C for 24 hours.

*3.3.2.1. Use of [RhCl(IMes)(PPh$_3$)$_2$] (64) in catalytic reactions*

Nolan's group investigated the activity of **64** in alkene hydroboration and aldehyde methylenation[34] and found little difference between the activity of **57** and **64** in either reaction. As a catalyst in hydroformylation reactions, **64** was found to be extremely selective, giving between 94 and 98 % branched product over linear on a variety of alkenes.[17] However, the turnover rate was extremely slow, giving only approximately 7 turnovers/hour (1 mol % **64**, 34 atm of $H_2$ and 34 atm CO at 60 °C for 20-22 h).

Further investigation by Crudden and co-workers into the mechanism of catalysis by **64** and an analogue bearing P(*p*-tolyl)$_3$ groups, led to some surprising results.[36] The unusual *cis* orientation of the phosphine ligands should enhance catalytic activity. This is because the assumed strong σ-donating abilities of the IMes ligand should facilitate the dissociation of the phosphine *trans* to it. However, dissociation of the *trans* phosphine in **64** is at least ten times slower than in **57**. At room temperature no exchange between bound phosphine on **64** and free phosphine was observed (**57** exchanges at a rate of 0.3 $s^{-1}$ at 25 °C) [3] but **64** began to show slow exchange above 50 °C. Exchange was only observed into the *trans* phosphine with the one in the *cis* position being firmly bound.

In the P(*p*-tolyl)$_3$ analogue of **64**, exchange was found to occur at 0.91 $s^{-1}$ at 60 °C when 5 equivalents of free phosphine were added. When the amount of free phosphine was increased to 50 equivalents the rate of exchange did not change significantly. This implies a dissociative mechanism for the exchange. This slow dissociation has been attributed to the poor performance of **64** in catalysis in

comparison to **57**. The hydrogenation of isosafrole (scheme 3.11.) proceeded at only two turnovers per hour when employing **64**, whilst with **57** the turnover rate was 40 $h^{-1}$.

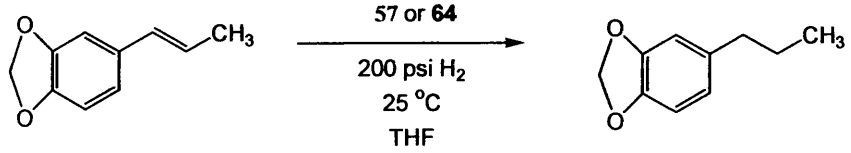


**Scheme 3.11.** Hydrogenation of isosafrole.

The slowing of phosphine dissociation on substitution of a phosphine ligand for an NHC ligand has also been observed by Grubbs for his alkene metathesis catalysts (as discussed in section 2.2.1.1.).[37,38] As has been well documented, the second generation Grubbs' alkene metathesis catalysts are extremely effective compared to their phosphine analogues unlike **64** in comparison to **57**.

By passing CO across **64**, Crudden also synthesised [RhCl(IMes)($PPh_3$)(CO)] (**65**).[17] This is also a very selective hydroformylation catalyst, producing primarily branched products, but it has half the activity of **64**. However, in this instance, free $PPh_3$ can be added into the reaction, which increases the catalytic activity to approximately twice that of [RhCl($PPh_3$)$_2$(CO)] (**59**) by converting the active species back to **64**.

Crudden's group have also recently reported the synthesis of a series of analogues of **64**, bearing a variety of phosphine ligands (figure 3.2.).[39] These are all effective alkene hydrogenation catalysts and it was also found that upon addition of CuCl, the rate of reaction was enhanced by two orders of magnitude (table 3.2.). This is due to CuCl being a phosphine sponge[40] and illustrates how important the loss of phosphine is in the catalytic effectiveness of these type of complexes.

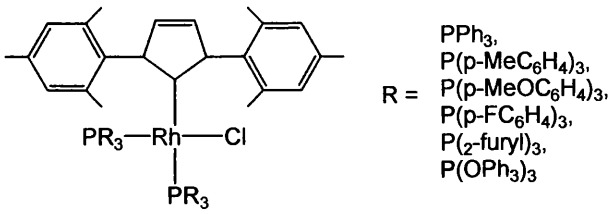


**Figure 3.2.** Series of Rh-IMes complexes synthesised by Crudden *et al.*

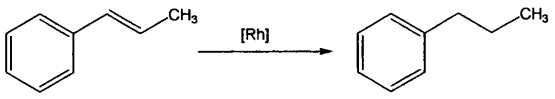


| Phosphine | TOF ($h^{-1}$) with and without CuCl | |
|---|---|---|
| | None | CuCl |
| $PPh_3$ | 24 | 331 |
| P(*p*-$MeOC_6H_4)_3$ | 5 | 417 |
| P(*p*-$FC_6H_4)_3$ | 43 | 161 |
| P(2-furyl)$_3$ | 9 | 24 |
| P($OPh_3$) | 0.25 | 0.4 |
| **57** | 297 | 243 |

*0.75 % cat, 0.1 M substrate, 100 psi H2, 60 °C, THF, 15 minutes, 1 eq. of CuCl.*

**Table 3.2.** A comparison of the alkene hydrogenation abilities of various Rh(IMes) catalysts to **57**.

The solvent employed to undertake these catalytic reactions was found to affect the rate of activity, with toluene significantly less effective than THF (table 3.3.). Although the authors give no explanation for this, presumably it could be postulated that the THF solvates and stabilises a phosphine loss complex more easily than toluene.

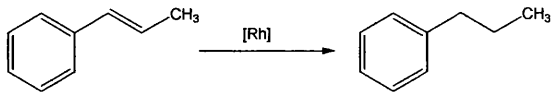


| Phosphine | TOF ($h^{-1}$) | | | |
|---|---|---|---|---|
| | In THF | | In toluene | |
| | None | CuCl | None | CuCl |
| $PPh_3$ | 24 | 331 | 3.5 | 188 |
| P(*p*-$MeOC_6H_4)_3$ | 5 | 417 | 2.3 | 190 |
| P(*p*-$FC_6H_4)_3$ | 43 | 161 | 24 | 123 |

*0.75 % cat, 0.1 M substrate, 7atm $H_2$, 60 °C, 15 minutes (THF), 30 minutes (toluene), 1 eq. of CuCl.*

**Table 3.3.** Comparison of TOFs for various Rh-IMes complexes in THF and toluene.

## 3.3.3. Decomposition of rhodium-NHC complexes

### *3.3.3.1. Decomposition of [RhCl(IMes)($PPh_3$)$_2$] (64) in dichloroethane*

Whilst the Crudden group were investigating the catalytic potential of **64** they discovered that dissolving it in dichloroethane and heating it to 60 °C led to the formation of **57** in addition to a dimeric NHC species with an ethyl bridge formed by interaction with the solvent (scheme 3.12.). This decomposition pathway could well account for why Lebel and co-workers found that **64** was active for the methenylation of aldehydes in THF but not in $CD_2Cl_2$.[34] However, it should be noted that although Lebel found that **57** retained activity for methylenation of 6-(*tert*-butyldimethylsilyloxy)-1-pentenal in $CD_2Cl_2$, it was inactive in dichloroethane.[41] This suggests that solvent may play a larger part in these catalytic reactions than simply leading to decomposition of the complex. The carbonylated complex **65** did not show the same decomposition in dichloroethane as **64**.

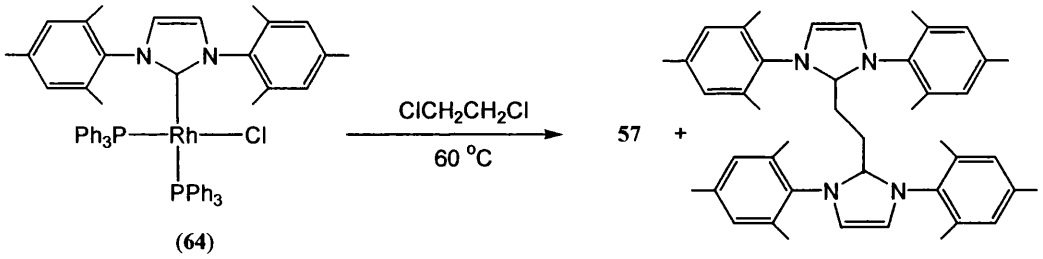


**Scheme 3.12.** Decomposition of **64** in dichloroethane.

### *3.3.3.2. Decomposition of other rhodium-NHC complexes*

Datt *et al.* investigated the catalytic ability of [Rh(NHC)(acac)(CO)] (NHC = IPr, IMes) for the hydroformylation reaction of hex-1-ene.[42] In the absence of additional free ligands such as $PPh_3$ and P(O-2,4-$^t$Bu$_2$-Ph)$_3$ no catalytic activity was observed. When auxiliary ligands were added, hydroformylation activity was comparable to [Rh(acac)(CO)$_2$] with the same added ligand. Thus it appears that no additional benefit is derived from having NHC in the catalyst precursor. This is due to decomposition of the NHC complexes under the hydroformylation conditions that

## 3.3.3. Decomposition of rhodium-NHC complexes

### *3.3.3.1. Decomposition of [RhCl(IMes)($PPh_3$)$_2$] (64) in dichloroethane*

Whilst the Crudden group were investigating the catalytic potential of **64** they discovered that dissolving it in dichloroethane and heating it to 60 °C led to the formation of **57** in addition to a dimeric NHC species with an ethyl bridge formed by interaction with the solvent (scheme 3.12.). This decomposition pathway could well account for why Lebel and co-workers found that **64** was active for the methenylation of aldehydes in THF but not in $CD_2Cl_2$.[34] However, it should be noted that although Lebel found that **57** retained activity for methylenation of 6-(*tert*-butyldimethylsilyloxy)-1-pentenal in $CD_2Cl_2$, it was inactive in dichloroethane.[41] This suggests that solvent may play a larger part in these catalytic reactions than simply leading to decomposition of the complex. The carbonylated complex **65** did not show the same decomposition in dichloroethane as **64**.

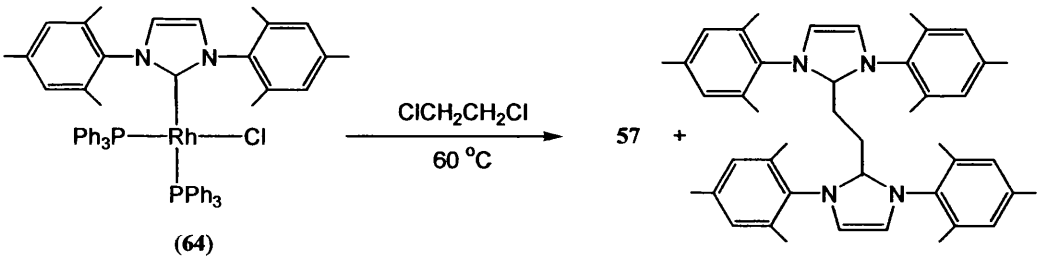


**Scheme 3.12.** Decomposition of **64** in dichloroethane.

### *3.3.3.2. Decomposition of other rhodium-NHC complexes*

Datt *et al.* investigated the catalytic ability of [Rh(NHC)(acac)(CO)] (NHC = IPr, IMes) for the hydroformylation reaction of hex-1-ene.[42] In the absence of additional free ligands such as $PPh_3$ and P(O-2,4-$^t$Bu$_2$-Ph)$_3$ no catalytic activity was observed. When auxiliary ligands were added, hydroformylation activity was comparable to [Rh(acac)(CO)$_2$] with the same added ligand. Thus it appears that no additional benefit is derived from having NHC in the catalyst precursor. This is due to decomposition of the NHC complexes under the hydroformylation conditions that

were employed (85 °C and 60 bar 1:1 $H_2$:CO). Reaction of [Rh(IMes)(acac)(CO)] with an excess of phosphine results in the formation of [Rh(IMes)(acac)($PR_3$)], as seen by $^{31}P\{^1H\}$ NMR. Upon lowering the pressure to 20 bar, and with addition of $PPh_3$, the formation of [$RhH(PPh_3)_2(CO)_2$] was observed by phosphorus NMR.

### 3.3.4. Oxidative addition of MeI to a rhodium-NHC complex

Martin *et al.* have investigated the oxidative addition of MeI to [$RhI(IMe)_2(CO)$] (**66**) and [$RhI(IMes)_2(CO)$] (**67**) and compared the reaction to that using phosphine analogues.[43] MeI undergoes oxidative addition to **66** but the reaction is slow and reversible. The product then undergoes a migratory insertion step to yield an acetyl complex. The product was tentatively assigned as [$RhI_2(IMe)_2(COCH_3)$], with both the iodine and NHC ligands adopting mutually *trans* geometries. However, the authors postulate that the complex could also exist as an iodide bridged dimer. **67** showed no reaction with MeI even when dissolved in neat MeI.

When MeI is reacted with analogous complexes bearing alkyl phosphines rather than NHCs, the reaction stops once the MeI has added across the metal, without forming the acetyl complex. In addition, the rate of reaction for these complexes is much faster (ca. 3.5 times when $PR_3$ = $PEt_3$) suggesting that the nucleophilicity of the Rh centre towards MeI in **66** is less than its phosphine counterpart. This is an unexpected result and one that Martin *et al.* explain as being due to sterics. However, although they comment that the vacant sites at the rhodium centre are blocked by the substituents from the NHCs, which lie above and below the rhodium coordination plane, this supposition is based upon crystallography data, which does not necessarily lead to correct interpretation of how the complexes behave in solution.

Using Nolan's concept of buried volume (chapter 1, section 1.2.2.), $PH_3$ has a $\%V_{Bur}$ of 17 and $PCy_3$ of 26 on $Ni(CO)_x(L)$ (x = 2 or 3, L = NHC or $PR_3$). The value for $PEt_3$ would probably lie within this range. The $\%V_{Bur}$ value for IMes is 26. There is

no value for IMe but ICy is 23.[44] Thus, using Nolan's calculations, the sterics of the NHCs do not seem to be enough to cause such a discrepancy in the rates of oxidative addition.

Crabtree also notes that the planar geometry of NHCs compared to the cone shaped phosphine ligands means that whenever possible NHCs will rotate around the M-C bond, presenting its slim axis to the bulky plane of the complex, thus minimising steric interference from the NHC.[45]

### 3.3.5. Rhodium complexes bearing chelating NHC ligands

Peris, Crabtree and others have synthesised rhodium(III) NHC complexes where the NHC ligands consist of two imidazole moieties linked by various organic groups. The two carbenic carbons can both join to the metal, forming bidentate groups as in figure 3.3.[46] The chelating bonding mode has been demonstrated by NMR spectroscopy and X-ray crystallography. The high *trans* effect of the NHC is shown from the crystal structure of $[RhI_2(I^iPr(CH_2)I^iPr)(OAc)]$ (**68**) where the Rh-OAc bonds are longer (2.166(6), 2.181(6) Å) than in the parent carboxylate complexes, $[Rh(OAc)_2(L)]_2$ (L = Py, CO, $PF_3$, $P(OPh)_3$, $PPh_3$) (2.01-2.06 Å). Bidentate ligands should provide more stable catalysts as they are less likely to degrade[47] and Peris and Crabtree showed that **68** catalyses the hydrogenation of ketones and imines *via* hydrogen transfer with $^i$PrOH/KOH at 82 °C.

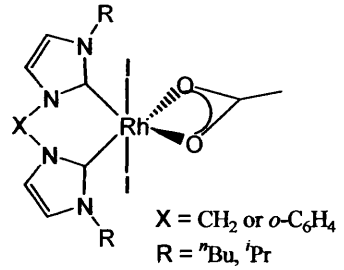


**Figure 3.3.** Chelating NHC ligand.

Peris and Crabtree have investigated the effect that changing the length of the linker, $(CH_2)_n$, between the imidazole rings has on complex formation and found that by

using longer linkers (where $n$ = 3 or 4), Rh(I) chelating NHC complexes are produced.[45] If $n$ = 1 or 2, Rh(III) complexes such as those described above are formed or binuclear Rh(I) species where the bis-NHC now bridges the two rhodium centres (scheme 3.13.). All these complexes are extremely stable, the Rh(I) cations particularly so when the counterion is changed from the initial $Cl^-$ group to $[PF_6]^-$.

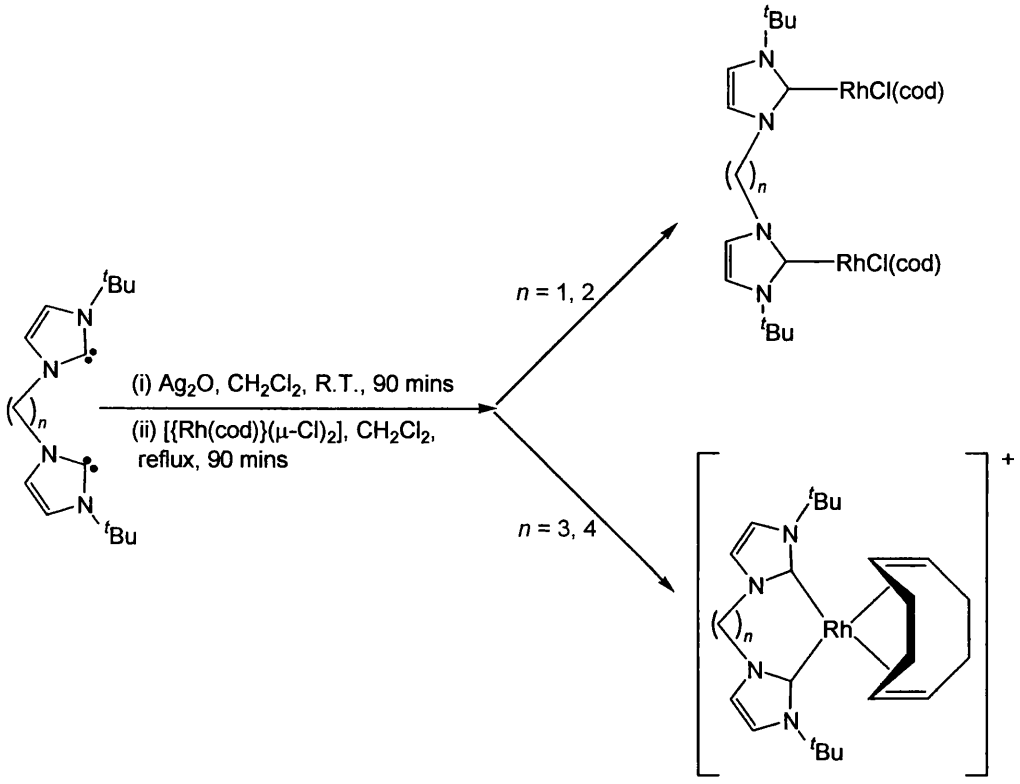


**Scheme 3.13.** Formation of Rh(I) products using bis NHCs.

Burling *et al.* found that in the reaction of $[\{Rh(COD)\}_2(\mu\text{-}OEt)_2]$ with the bidentate imidazolium salt $[IMe(CH_2)IMe][X]_2$ (X = $BPh_4$, $PF_6$), keeping the reaction rigorously halide free, led to formation of a mononuclear rhodium complex with a chelating NHC as opposed to a binuclear complex with a bridging ligand.[48] The reasons for this are unclear. Using this method they synthesised $[Rh(IMe(CH_2)IMe)(COD)][PF_6]$, which was then reacted with CO to give $[Rh(IMe(CH_2)IMe)(CO)_2][PF_6]$. This has been found to effectively catalyse the cyclisation of 4-pentyn-1-amine to 2-methyl-1-pyrroline (scheme 3.14.), giving an 85 % conversion in 16 hours at 60 °C at a catalyst loading of 1.5 mol %. This is

significantly faster than the analogous complex bearing an N-donating chelating ligand (figure 3.4.).[49]

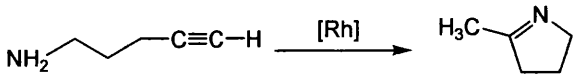


**Scheme 3.14.** Cyclisation of 4-pentyn-1-amine to 2-methyl-1-pyrroline.

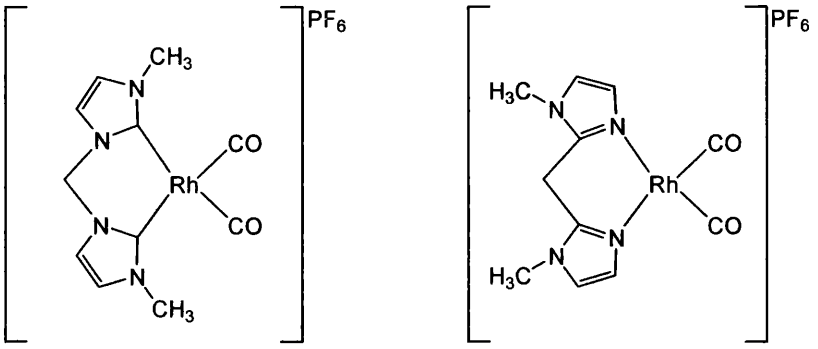


85 % conversion
Turn over rate = 10 $h^{-1}$

49 % conversion
Turn over rate = 2 $h^{-1}$

**Figure 3.4.** Comparison of chelating NHC and N-donor ligand in cyclisation of 4-pentyn-1-amine to 2-methyl-1-pyrroline in $d_8$-THF at 60 °C with 1.5 % catalyst loading.

Similar complexes have also been synthesised by Baker *et al.* with bulkier chelating NHC ligands (figure 3.5.).[50] These have not been trialled in catalytic reactions but have been shown to be sensitive to electrochemical reactions, with [Rh(NHC)(COD)][$PF_6$] going from Rh(I) to Rh(II) in cyclovoltammetry studies.

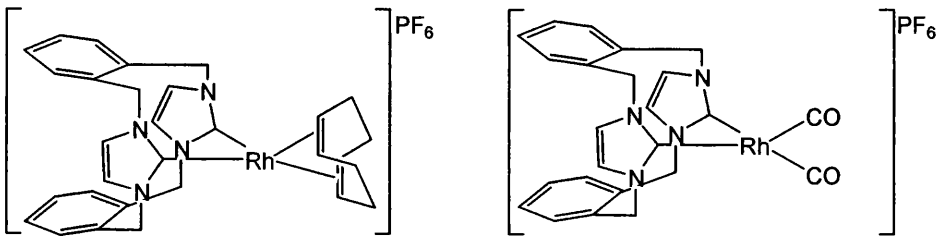


**Figure 3.5.** Chelating NHC rhodium complexes synthesised by Baker *et al.*

### 3.3.6. Use of rhodium-NHC complexes as radiopharmaceuticals

Youngs' group have investigated the use of rhodium NHC complexes as radiopharmaceuticals.[51] $^{105}Rh$ is an extremely useful tool in cancer therapy because it emits beta particles that are suitable for radiation therapy as well as a gamma particle that can be used for imaging. The $t_{1/2}$ of $^{105}Rh$ is 36.4 hours, which is ideal as it has sufficient time to kill tumour cells but does not remain radioactive in the body for long periods. It is feasible that NHCs could be synthesised bearing targeting substituents such as peptides, allowing them to interact with the body and deliver $^{105}Rh$ to specific areas.

$^{105}Rh$ is only available from [$RhCl_3 \cdot xH_2O$], thus it is important to synthesise potential complexes from this starting material well within the 36.4 hour half life. Youngs reports two approaches to achieve this: synthesising NHC complexes directly from the [$RhCl_3 \cdot xH_2O$] starting material and converting [$RhCl_3 \cdot xH_2O$] to a different rhodium precursor before reaction with NHCs. The latter method, although successful in synthesising Rh(NHC) complexes, is impractical as the synthesis is undertaken in acetonitrile, which is toxic and therefore not suitable for medicinal use. It also involves several synthetic steps, which is undesirable when working with radioactive starting materials.

Wanniarachchi *et al.* have reported the synthesis of Rh(NHC) complexes *via* transmetallation from silver NHC complexes (scheme 3.15.)[52] and Youngs used this approach to synthesise rhodium NHC complexes from [$RhCl_3 \cdot xH_2O$] (scheme 3.16.). This led to the synthesis of two extremely stable rhodium complexes each bearing two bidentate NHCs in few enough steps to preserve the $^{105}Rh$. The synthesis is carried out in DMSO, which has been approved for use in humans, although synthesis in water would be ideal.

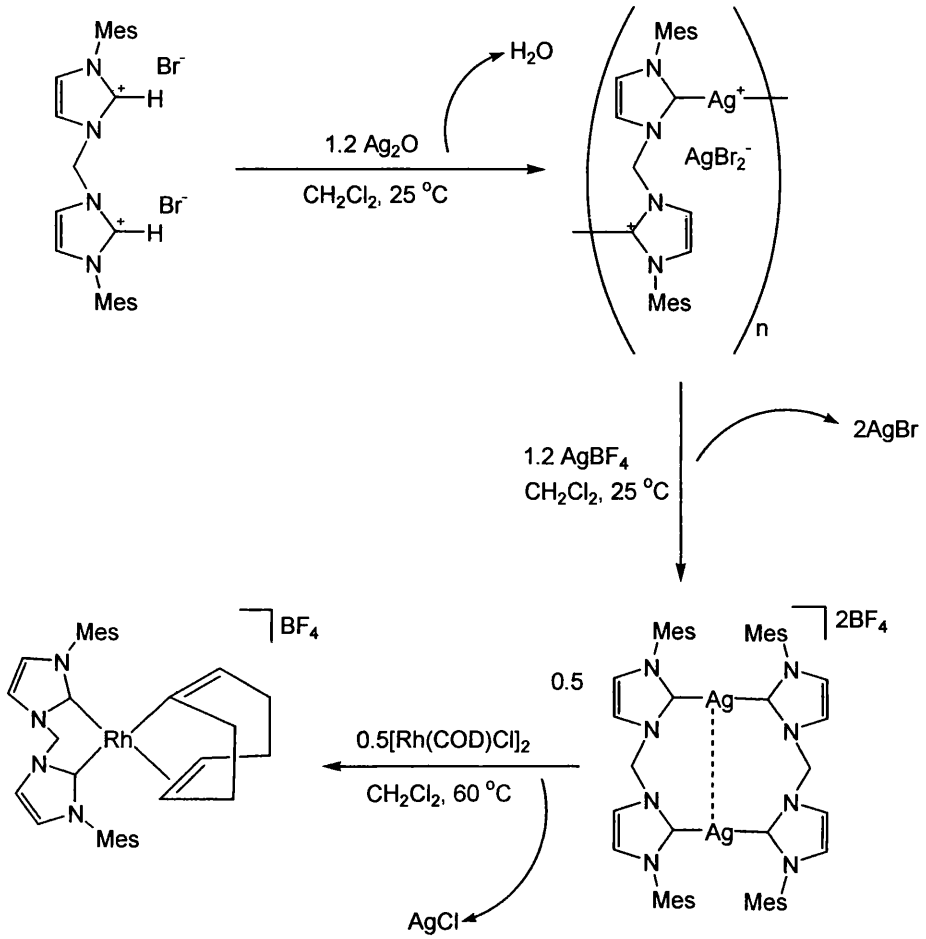


**Scheme 3.15.** Synthesis of [Rh(NHC)(COD)][$BF_4$] *via* transmetallation from Ag.

3.3.7. Rhodium-NHC complexes bearing hydride ligands

Nolan has prepared two Rh(NHC) complexes bearing a hydride ligand. Both arise from C-H activation of the NHC and have already been discussed in detail in chapter 1 (section 1.2.7.). These are the only two reported rhodium hydride complexes bearing NHC ligands and they have not been investigated in any catalytic cycles.

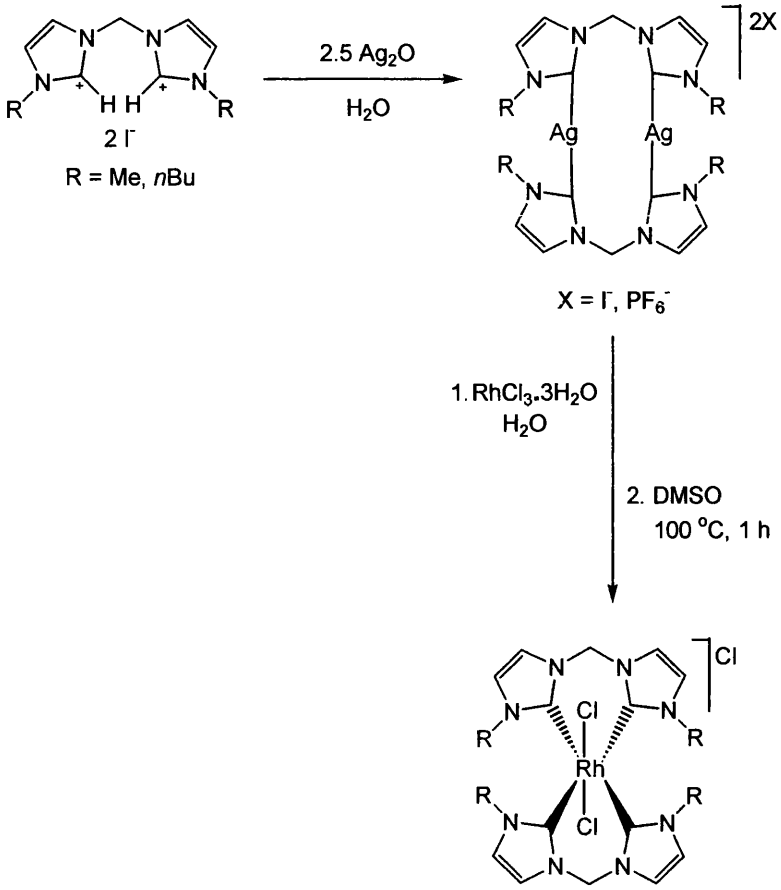


**Scheme 3.16.** Synthesis of Rh(NHC) complexes from [$RhCl_3 \cdot H_2O$] using transmetallation

## 3.4. Aim of this work

The aim of this project was to synthesise new hydride-bearing rhodium NHC complexes, to investigate their structural characteristics and to look at their potential to undergo bond activation so allowing direct comparison to the ruthenium systems discussed in chapter 2. The addition of free NHC to two rhodium precursors led to an enormous array of Rh(NHC) products being formed simultaneously. These ranged from monomeric, hydride bearing species, to dimeric and cationic complexes. For any one reaction of rhodium precursor and ligand, a large and varied number of complexes were produced in tandem. The reactions are summarised in schemes 3.17. and 3.18.

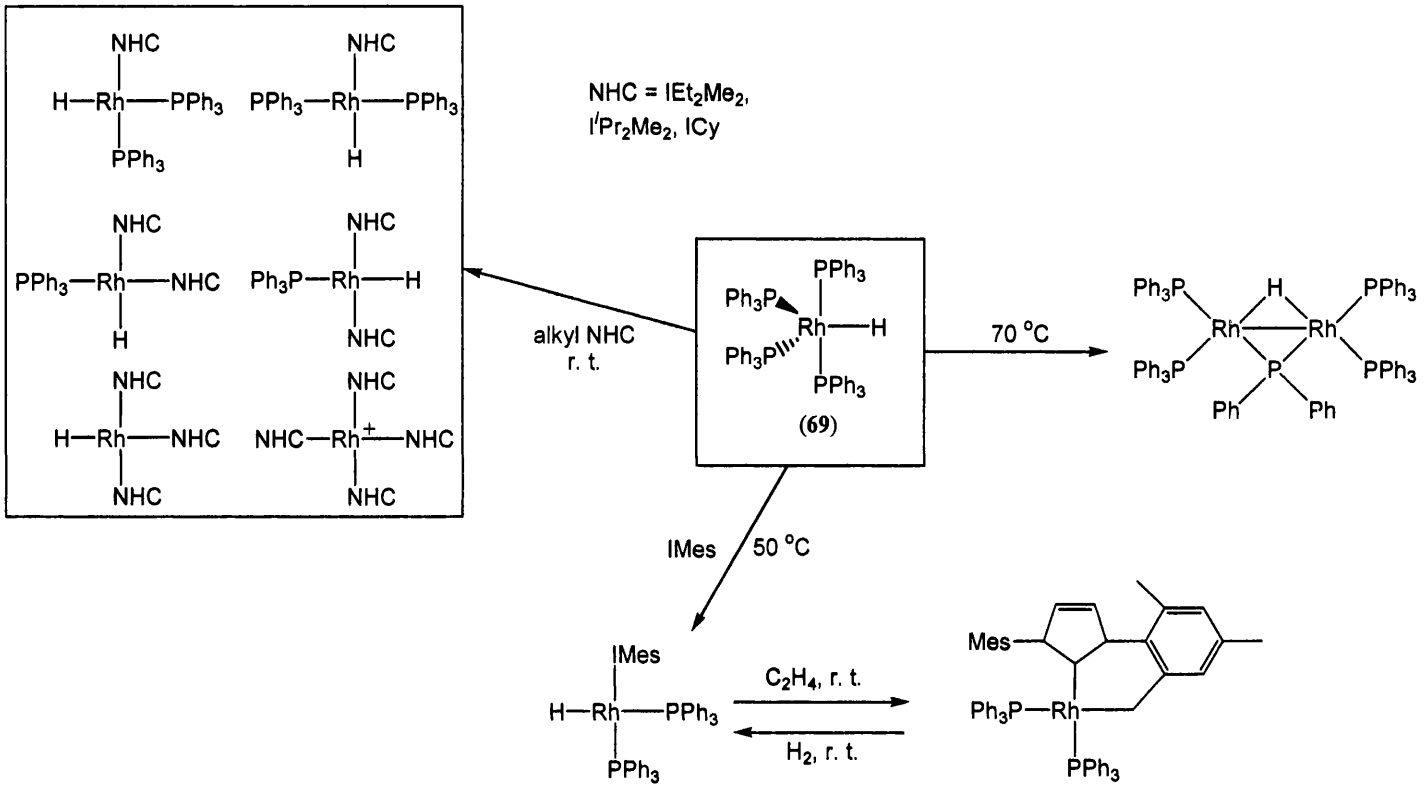


**Scheme 3.17.** Formation of a variety of Rh-NHC complexes from **69**.

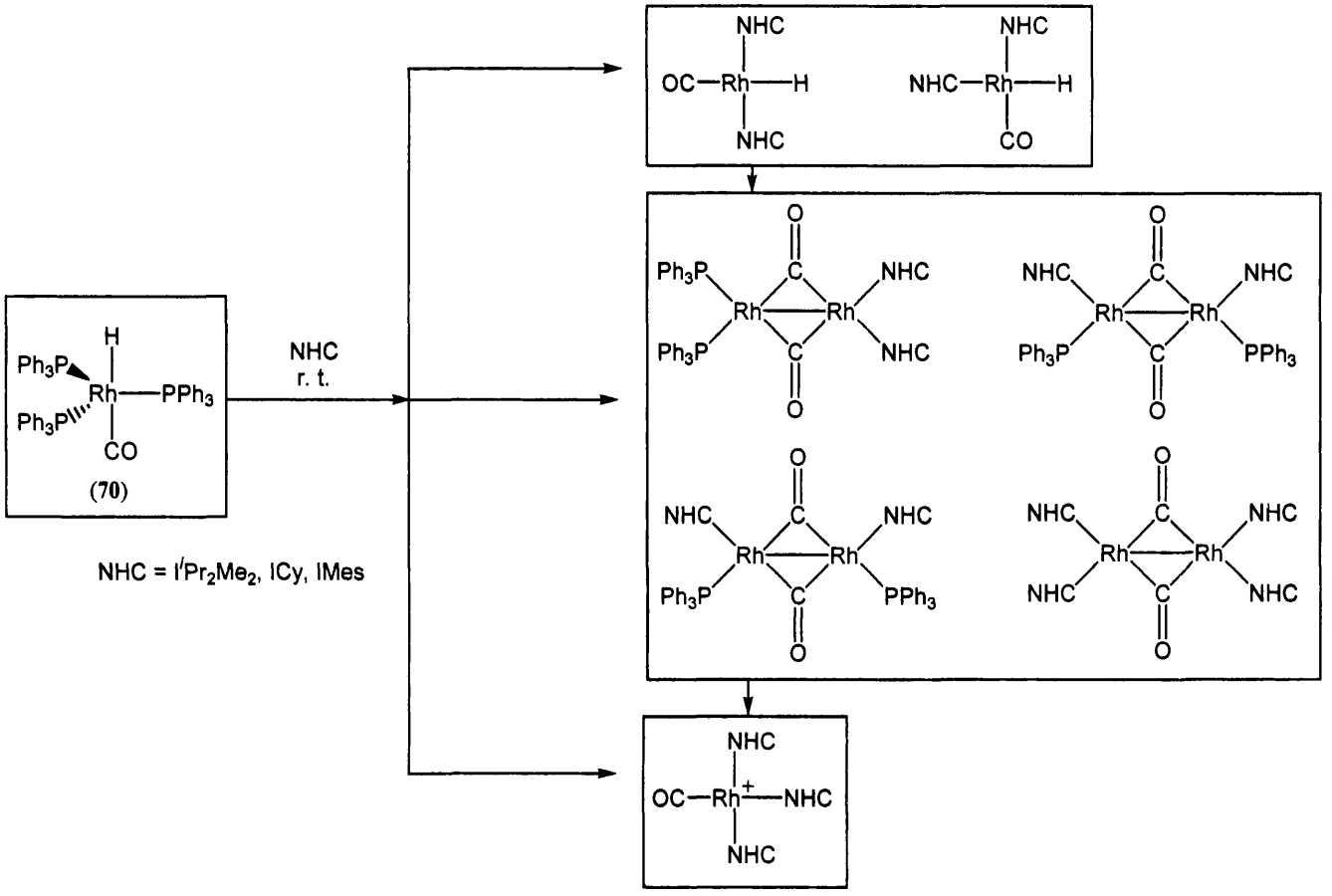


**Scheme 3.18.** Complexes formed in a one-pot reaction of **70** plus free NHC at room temperature.

## 3.5. Synthesis of new rhodium complexes

Addition of excess free NHC to the rhodium complexes $[RhH(PPh_3)_4]$ (**69**) and $[RhH(PPh_3)_3(CO)]$ (**70**) led to formation of *cis*- and *trans*-$[RhH(NHC)(PPh_3)_2]$, *cis*- and *trans*-$[RhH(NHC)_2(PPh_3)]$ and *cis*- and *trans*-$[RhH(NHC)_2(CO)]$. These products were characterised by multinuclear NMR and IR spectroscopy and, in cases where they could be isolated, X-ray diffraction and elemental analysis. In addition, two dimeric species and a significant number of cationic species have been isolated from the reaction mixtures and fully characterised.

### 3.5.1. Reactivity of $[RhH(PPh_3)_4]$ with alkyl N-heterocyclic carbenes

When excess (2-6 equivalents) of the N-alkyl substituted NHCs $IEt_2Me_2$, $I^iPr_2Me_2$ or ICy were added to $[RhH(PPh_3)_4]$ (**69**) in THF or benzene, reaction proceeded rapidly at room temperature to give a mixture of mono- and bis-NHC complexes with both *cis* and *trans* orientations (scheme 3.19.). The four complexes, *cis*- and *trans*-$[RhH(NHC)(PPh_3)_2]$ (NHC = $IEt_2Me_2$ (**71**), $I^iPr_2Me_2$ (**72**), ICy (**73**)) and *cis*- and *trans*-$[RhH(NHC)_2(PPh_3)]$ (NHC = $IEt_2Me_2$ (**74**), $I^iPr_2Me_2$ (**75**), ICy (**76**)) were all identified by $^1H$ and $^{31}P\{^1H\}$ NMR spectroscopy.

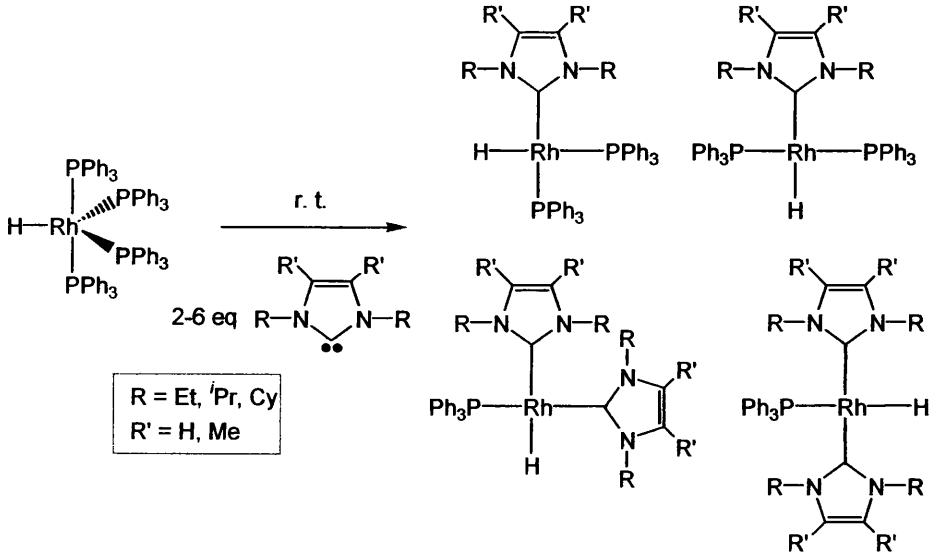


**Scheme 3.19.** Reaction of **69** with free NHC.

By monitoring the reaction by $^{1}H$ and $^{31}P\{^{1}H\}$ NMR spectroscopy it can be seen that all the complexes are formed immediately with the mono NHC species predominating. However, over a longer period at room temperature, the bis NHC products increased, with the eventual ratio of all four products dependant on the nature and number of equivalents of NHC employed. For example, reaction between **69** and four equivalents of $I^{i}Pr_2Me_2$ gave a 1:4.9:1.4:1.2 ratio of *cis*-**72**:*trans*-**72**:*cis*-**75**:*trans*-**75** after 48 hours at room temperature, whilst, in the same time, reaction of **69** with four equivalents of ICy gave *trans*-**73**:*cis*-**76**:*trans*-**76** in a ratio of 1:2.9:33.8 with no evidence for *cis*-**73**. This is only seen as a product when less than 2 equivalents of ICy are used. Although *cis*-**73** can been seen by $^{1}H$ NMR spectroscopy forming early on in the reaction of **69** and excess ICy, it quickly reacts with more free NHC to give *cis* and *trans*-**76**.

Assignment of the products and their relative stereochemistries was readily achieved by $^{1}H$ and $^{31}P\{^{1}H\}$ NMR spectroscopy. The hydride signals were particularly characteristic of the number and orientation of the phosphine ligands due to the $^{1}H$-$^{31}P$ coupling constants. For example *cis*- and *trans*-**72** (figure 3.6.) have hydride resonances at δ -6.10 and δ -10.13 ppm respectively. The former is a doublet of doublets of doublets, with coupling to a *trans* phosphine ligand ($^{2}J_{HP}$ = 111.9 Hz), a *cis* phosphine group ($^{2}J_{HP}$ = 24.7 Hz) and to the rhodium centre ($J_{HRh}$ = 30.2 Hz). The latter appears as a doublet of triplets, with coupling to the rhodium centre ($J_{HRh}$ = 10.4 Hz) and coupling to two equivalent phosphine groups ($^{2}J_{HP}$ = 25.4 Hz). Similarly, *cis*- and *trans*-**75** give two doublets of doublets at -9.54 and -5.34 respectively, both have coupling to rhodium ($J_{HRh}$ = 15.4 Hz and 34.6 Hz) and one triphenylphosphine ligand ($J_{HP}$ = 32.2 and 121.0 Hz). The difference in the values of the coupling constants arises from the nature of the ligand *trans* to the hydride.

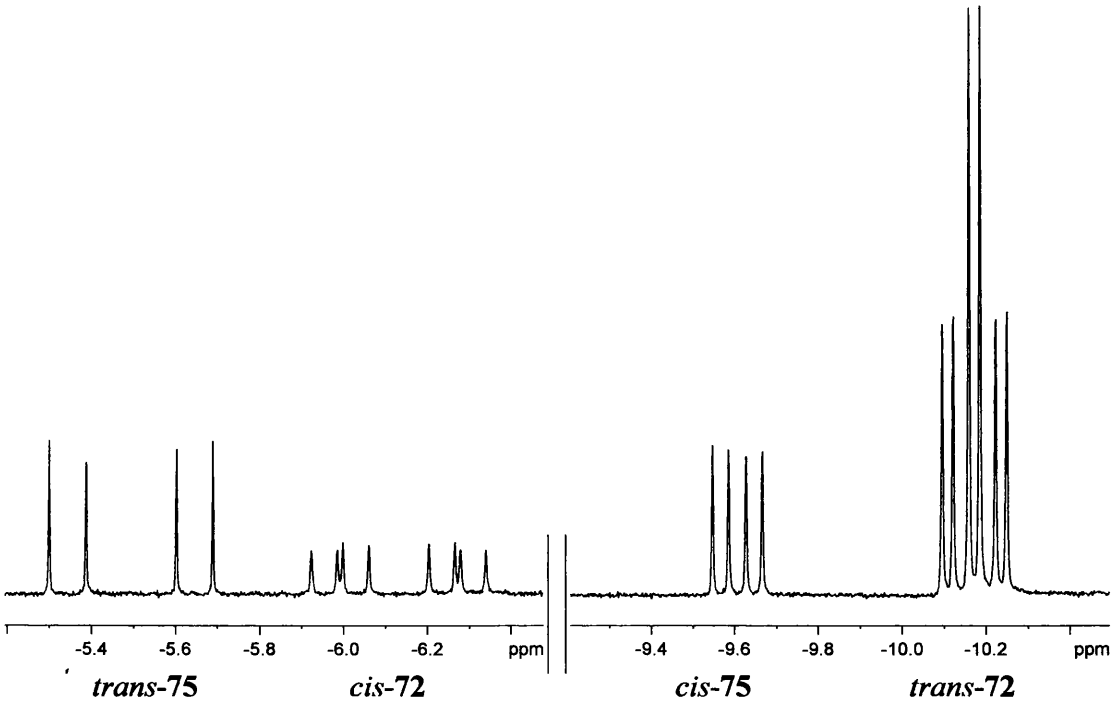


**Figure 3.6.** Hydride region of $^{1}H$ NMR for *cis*- and *trans*-**72** and *cis*- and *trans*-**75** in $C_6D_6$ (400 MHz, 25 °C).

The splittings on the $^{31}P\{^{1}H\}$ resonances are also affected by the ligands *trans* to them. In the reaction of **69** with $I^{i}Pr_2Me_2$, for example, five $^{31}P$ resonances are observed: δ 41.6 (dd, $J_{PRh}$ = 138.9 Hz, $^{2}J_{PP}$ = 23.0 Hz), 49.7 (dd, $J_{PRh}$ = 148.5 Hz, $^{2}J_{PP}$ = 23.0 Hz) (*cis*-**72**), 42.7 (d, $J_{PRh}$ = 176.4 Hz) (*trans*-**72**), 37.9 (d, $J_{PRh}$ = 138.1) (*cis*-**75**) and 52.1 (d, $J_{PRh}$ = 161.1 Hz) (*trans*-**75**). The much larger coupling constant between rhodium and phosphine when the complex changes from a *trans*-P-Rh-P to a *trans*-P-Rh-NHC arrangement has been noted previously by Lappert.[26] Lappert's observations about the *cis* influence of the NHC ligand may explain the increase in $^{1}J_{PRh}$ on the *trans*-H-Rh-P bond when going from *cis*-**72** (with one *cis*-NHC) to *trans*-**75** (with two *cis*-NHCs). 2D HMQC experiments on mixtures of these solutions clearly showed the four separate hydride and phosphorus resonances and how they correlate (figure 3.7.).

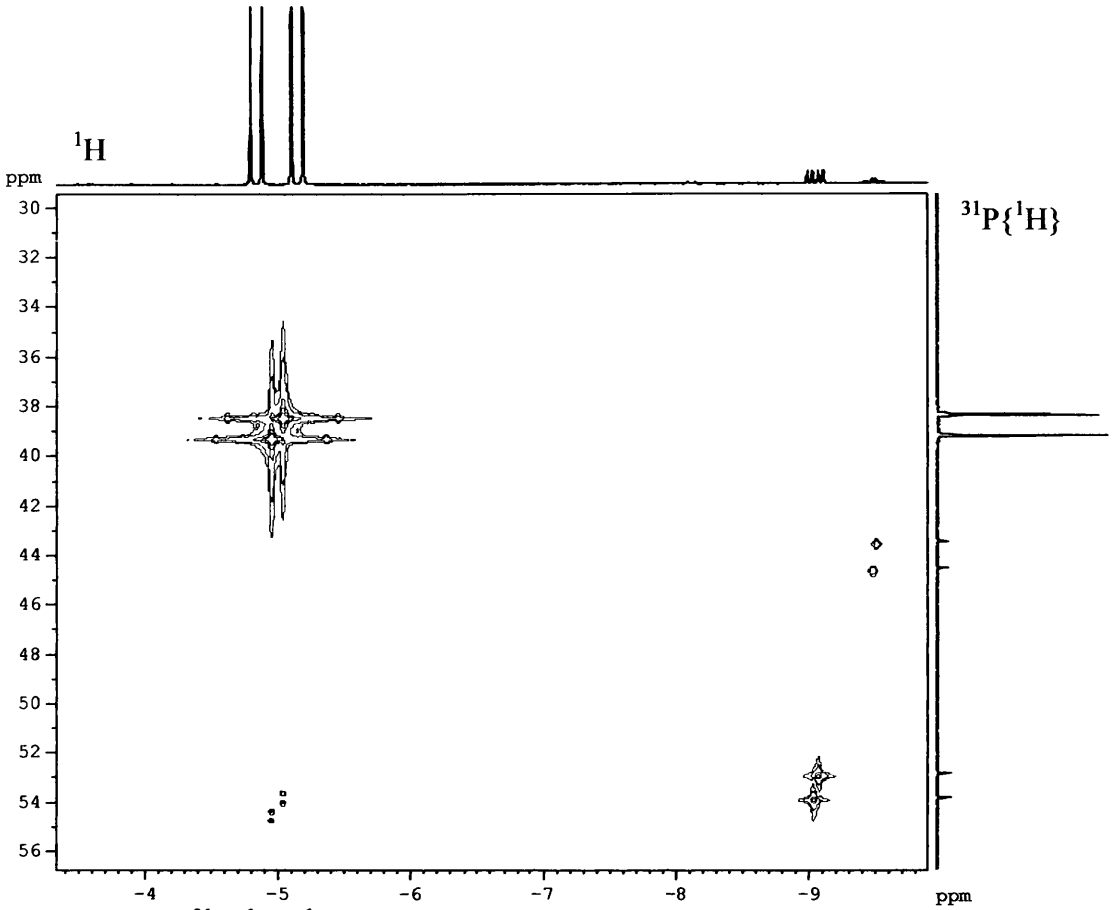


**Figure 3.7.** $^{31}P\{^1H\}$-$^1H$ HMQC of *trans*-**72** and *cis*- and *trans*-**75** ($d_8$-THF, 162 MHz for $^{31}P$, 25 °C).

Crystals of *trans*-**72** were grown from a concentrated ethanol solution at -5 °C and analysed by X-ray diffraction. The subsequent structure (figure 3.8.) revealed that the complex in the solid state has a highly distorted square planar geometry with P-Rh-P and NHC-Rh-P angles of 160.39(3) ° and 99.804(13) ° respectively (table 3.4.). This is significantly different to $[RhH(PPh_3)_3]$ (**77**), which has a distorted geometry and lies somewhere between square planar and tetrahedral (P(1)-Rh-P(2) = 151.7(2) °, P(1)-Rh-P(2) = 104.0(2) °, P(2)-Rh-P(3) = 102.4(2) °).[53] Presumably the more 3D nature of the phosphine groups adds a significant amount of steric hindrance to the complex, pushing it away from a square planar geometry. All four substituents around the rhodium centre in **72** are in the same plane with the two phosphorus atoms bent towards the hydride ligand. The imidazole ring of the NHC is planar and almost perpendicular to the central plane (approximately 83.7 ° out of

the plane). This phenomenon has been noted before and is common amongst $d^8$ square-planar metal-NHC complexes.[45,54]

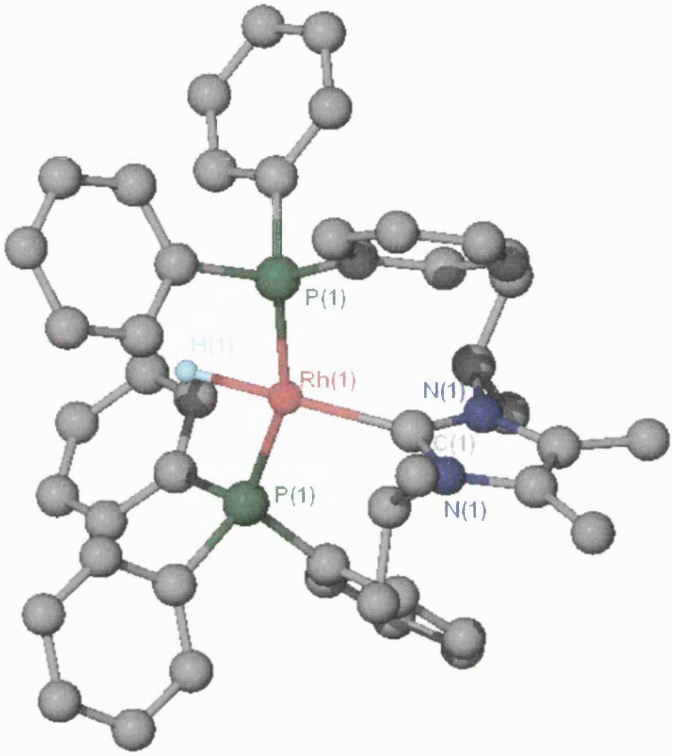


**Figure 3.8.** Molecular structure of **72** determined by X-ray crystallography.

| **Bond lengths (Å)** | | | |
|---|---|---|---|
| Rh(1)-C(1) | 2.068(2) | Rh(1)-P(1)' | 2.2368(4) |
| Rh(1)-P(1) | 2.2368(4) | | |
| **Bond angles (°)** | | | |
| P(1)-Rh(1)-P(1)' | 160.39(3) | C(1)-Rh(1)-P(1)' | 99.804(13) |
| C(1)-Rh(1)-P(1) | 99.804(13) | | |

**Table 3.4.** Selected bond lengths and angles for **72**.

As would be expected, the Rh-C bond in **72** is much shorter (2.068(2) Å) compared to the $PPh_3$ group *trans* to the hydride in **77** (2.316(6) Å) but the two *trans* phosphines in **72** have only slightly shorter Rh-P bonds in comparison to **77** (**72**: 2.2368(4) Å, **77**: 2.274(6), 2.262(5) in **77**).

When a significant excess of $IEt_2Me_2$ and ICy (more than 6 equivalents) are added to $[RhH(PPh_3)_4]$ (**69**) it is possible to push the reaction through to form complexes of the general formula $[RhH(NHC)_3]$ (NHC = $IEt_2Me_2$ (**78**), ICy (**79**)). Both complexes exhibited a simple doublet in the hydride region of the $^1H$ NMR spectrum (**78**: δ -7.35 (d, $J_{HRh}$ = 22.0 Hz), **79**: δ -8.12 (d, $J_{HRh}$ = 21.4 Hz)) and two doublet resonances at low field in the $^{31}C\{^1H\}$ NMR spectrum, attributable to the two different carbenic carbon environments (**78**: δ 205.2 (d, $J_{CRh}$ = 58 Hz) 202.0 (d, $J_{CRh}$ = 40 Hz), **79**: δ 205.2 (d, $J_{CRh}$ = 47.0 Hz), 200.8 (d, $J_{CRh}$ = 46.0 Hz)). Unfortunately these complexes proved to be extremely soluble and could not be isolated.

NMR data for all of the alkyl NHC complexes synthesised from **69** are summarised in table 3.5.. From this it can be seen that, although all the shifts and coupling constants are very similar for each type of complex, there are trends within the data. In those complexes where a phosphine ligand lies *trans* to the hydride, namely in *cis*-$[RhH(NHC)(PPh_3)_2]$ and *trans*-$[RhH(NHC)_2(PPh_3)]$, the signal for the hydride ligand in the $^1H$ NMR spectrum comes at a higher field than when the ligand *trans* to the hydride is an NHC. For example, in **71** the *cis* isomer (with $PPh_3$ *trans* to H) has a hydride resonance at δ -5.70 compared to the *trans* isomer (with NHC *trans* to H) at δ -9.59. It is also clear that resonances for the hydride ligand on complexes bearing $I^iPr_2Me_2$ ligands are at higher field than those with ICy and $IEt_2Me_2$ ligands, which come at similar shifts to each other (although ICy complexes are generally slightly higher). This trend is not repeated in the $^{31}P\{^1H\}$ or $^{13}C\{^1H\}$ NMR spectra with analogous complexes showing similar shifts.

| Complex | $^1$H NMR for hydride | | | | $^{31}$P{$^1$H} NMR for $PPh_3$ groups | | | $^{13}$C{$^1$H} NMR for carbenic carbon | | |
|---|---|---|---|---|---|---|---|---|---|---|
| | δ | $J_{HRh}$ | $^2J_{HPtrans}$ | $^2J_{HPcis}$ | δ | $J_{PRh}$ | $^2J_{PP}$ | δ | $J_{CRh}$ | $^2J_{CP}$ |
| *cis*-**71** | -5.70 | 24.7 | 113.0 | 25.2 | 49.2 (*t* to C)<br>41.4 (*t* to P) | 148.1<br>136.5 | 24.5<br>24.5 | n/o | | |
| *cis*-**72** | -6.10 | 30.2 | 111.9 | 24.7 | 49.7 (*t* to C)<br>41.6 (*t* to P) | 148.5<br>139.0 | 23.0<br>23.0 | n/o | | |
| *cis*-**73** | -5.88 | 30.2 | 112.0 | 25.2 | 49.2 (*t* to C)<br>42.6 (*t* to P) | 148.1<br>142.9 | 24.5<br>24.5 | n/o | | |
| *trans*-**71** | -9.59 | 11.0 | n/a | 23.6 | 45.4 | 170.0 | n/a | n/o | | |
| *trans*-**72** | -10.13 | 10.5 | n/a | 25.5 | 42.7 | 176.2 | n/a | 198.6 | 47.5 | 10.5 |
| *trans*-**73** | -9.49 | 11.0 | n/a | 24.7 | 44.1 | 175.1 | n/a | 199.8 | 46.9 | 11.0 |
| *cis*-**74** | -8.82 | 15.9 | n/a | 29.1 | 38.5 | 135.2 | n/a | 197.2<br>185.3 | 57.0<br>42.2 | 13.8<br>15.6 |
| *cis*-**75** | -9.54 | 15.3 | n/a | 32.2 | 37.9 | 138.1 | n/a | n/o | | |
| *cis*-**76** | -9.05 | 15.4 | n/a | 32.4 | 38.8 | 136.6 | n/a | n/o | | |
| *trans*-**74** | -4.67 | 35.1 | 121.3 | n/a | 54.7 | 159.7 | n/a | 199.9 | 46.0 | 10.1 |
| *trans*-**75** | -5.43 | 34.6 | 121.0 | n/a | 52.1 | 161.1 | n/a | 200.5 | 45.3 | 11.0 |
| *trans*-**76** | -4.99 | 34.6 | 122.4 | n/a | 53.3 | 160.9 | n/a | 199.3 | 44.7 | 11.0 |
| **78** | -7.35 | 22.0 | n/a | n/a | n/a | n/a | n/a | 205.2<br>202.0 | 58.0<br>40.0 | n/a<br>n/a |
| **79** | -8.12 | 21.4 | n/a | n/a | n/a | n/a | n/a | 205.2<br>200.8 | 47.0<br>46.0 | n/a<br>n/a |

**Table 3.5.** Selected NMR data for complexes of the general formula $[RhH(NHC)_x(PPh_3)_y]$ (x = 1,2 or 3, y = 1 or 2, NHC = $IEt_2Me_2$, $I^iPr_2Me_2$, ICy) recorded in $d_8$-THF (n/a = not applicable, n/o = not obtainable due to low intensity of signal. $^1$H NMR recorded at 400 MHz, $^{31}$P{$^1$H} NMR at 121 MHz and $^{13}$C{$^1$H} NMR at 100 MHz).

The trends in coupling constants are also interesting to note. The $^{31}P$-$^{103}Rh$ coupling constants are strongly influenced by the ligands *trans* to them. By far the biggest values (in excess of 170 Hz) come when the phosphine is *trans* to another $PPh_3$ group and *cis* to an NHC and a hydride, as in *trans*-**71**, **72** and **73**. Those *trans* to hydride and *cis* to two NHCs, such as *trans*-**74**, **75** and **76**, are the next largest (approximately 160 Hz) and those *trans* to NHC (*cis*-**74**, **75** and **76**) are the smallest at about 136 Hz. The two phosphine resonances in *cis*-**71**, **72** and **73**, however, do not fit in with this trend, and despite one being *trans* to NHC and one *trans* to hydride they have almost the same values at around 150 Hz. This shows that the *cis* ligands on the complexes must also have a significant effect on the *J* values.

### 3.5.2. Reactivity of $[RhH(PPh_3)_4]$ with IMes

The reaction of **69** with IMes at room temperature took far longer than with the alkyl NHCs. Although product was seen instantly at room temperature, the reaction took almost three weeks to go to completion. At 50 °C this rate was greatly enhanced and, by NMR, all the starting material had disappeared after 16 hours to afford a single hydride-containing product. This had appeared as an unusual peak, consisting of a doublet of doublets with broad lumps on the outer edges (figure 3.9.). When the sample was cooled to -30 °C, the signal separated out into a simple doublet of doublet of doublets ($\delta$ -6.98, $^2J_{HPtrans}$ = 109.2 Hz, $^2J_{HPcis}$ = 33.2 Hz, $J_{HRh}$ = 22.8 Hz)), analogous to those seen for *cis*-**71**, *cis*-**72** and *cis*-**73** (figure 3.10.). This suggested the complex was *cis*-$[RhH(IMes)(PPh_3)_2]$ (**80**).

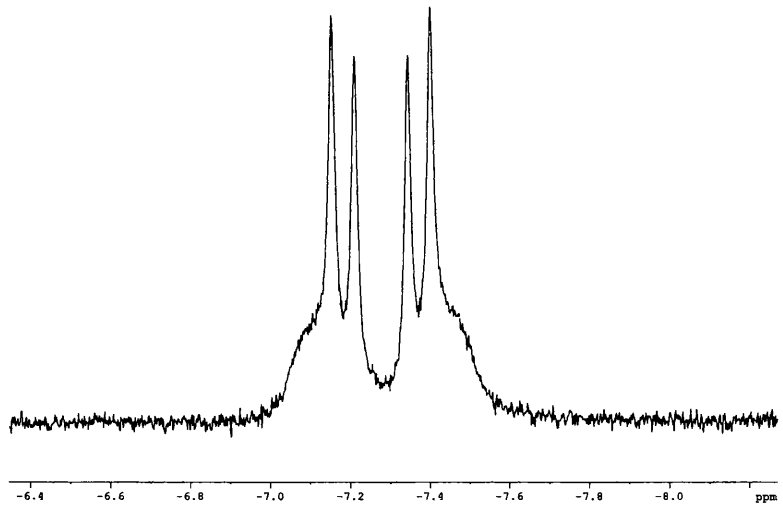


**Figure 3.9.** Hydride resonance of **80** (400 MHz, 25 °C) in $d_8$-THF.

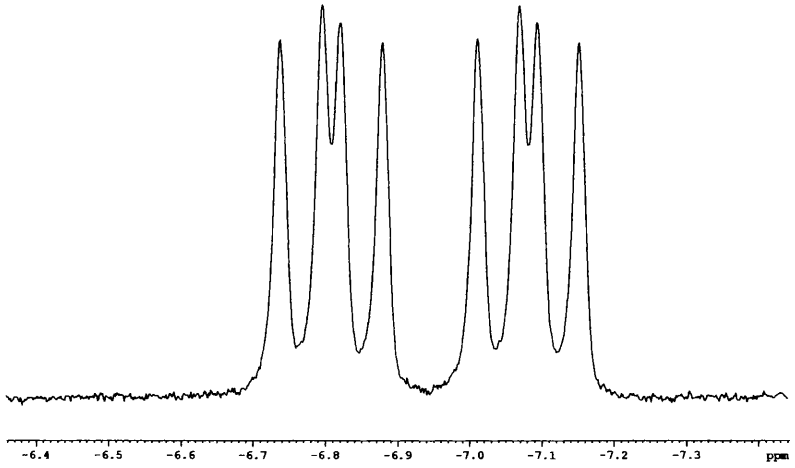


**Figure 3.10.** Hydride resonance of **80** (400 MHz, -30 °C) in $d_8$-THF.

The $^{31}P\{^1H\}$ NMR spectrum of **80** is also convoluted at room temperature (figure 3.13.). It consists of two broad doublet of doublets centred at δ 39.5 ($J_{PRh}$ = 171.0 Hz, $^2J_{PP}$ = 57.0 Hz) and δ 36.7 ($J_{PRh}$ = 146.0 Hz, $^2J_{PP}$ = 57.0 Hz) which, from a $^{31}P\{^1H\}$-$^1H$ NMR correlation, couple to the hydride resonance. These phosphorus resonances sharpen at -30 °C.

The X-ray crystal structure of **80** is shown in figure 3.11. with selected bond lengths and angles in table 3.6. As would be expected the Rh-C bond length (2.024(2) Å) is marginally longer than that found in *cis*-[RhCl(IMes)($PPh_3$)$_2$] (**64**) (2.0527(14) Å)[34]

due to the stronger *trans* influence of the hydride compared to the chloride. As in *trans*-**72** the five central atoms are all in the same plane, with the two ligands *cis* to the hydride bending towards it, away from the bulkier phosphine group (C(1)-Rh(1)-P(2) = 155.43(8) Å). Like in *trans*-**72**, the imidazole ring of the NHC is close to perpendicular to the central plane, although **80** is slightly more distorted than **72** (approximately 75.7 ° out of the central plane). This is probably due to the steric bulk of this particular complex.

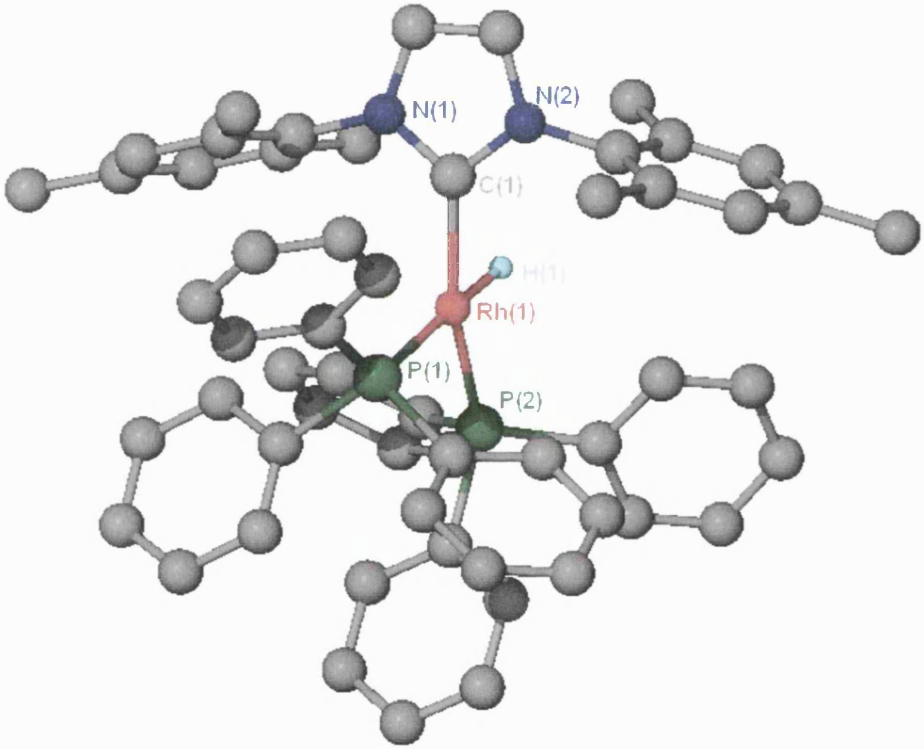


**Figure 3.11.** Molecular structure of **80** determined by X-ray crystallography.

| **Bond lengths (Å)** | | | |
|---|---|---|---|
| Rh(1)-C(1) | 2.024(3) | Rh(1)-P(2) | 2.2527(8) |
| Rh(1)-P(1) | 2.2894(8) | | |
| **Bond angles (°)** | | | |
| C(1)-Rh(1)-P(2) | 155.43(8) | P(2)-Rh(1)-P(1) | 99.38(3) |
| C(1)-Rh(1)-P(1) | 105.14(8) | | |

**Table 3.6.** Selected bond lengths and angles for **80**.

A crystalline sample of **80**, isolated and dissolved in THF, appeared to slowly lose phosphine and form another hydride containing complex, with a $^1$H NMR signal centred at δ -22.54. This resonance was a doublet of doublets, suggesting that it was coupling to only one phosphorus ligand, as well as the rhodium centre ($^2J_{HP}$ = 28.0 Hz, $J_{HRh}$ = 20.0 Hz). This could be a THF substitution product [RhH(IMes)($PPh_3$)(THF)] (**81**). Upon heating at 50 °C the ratio of **81** relative to **80** increases. This suggests that **80** undergoes loss of a $PPh_3$ ligand due to the steric crowding around the rhodium centre. Without excess free phosphine present to rejoin the molecule, the solvent THF can replace a $PPh_3$ ligand giving the solvato complex. The THF molecule must lie *trans* to the hydride, therefore pushing it upfield (figure 3.12.). EXSY experiments, carried out to see whether **80** and **81** are in equilibrium with each other, were inconclusive. **81** exhibits a doublet by $^{31}P\{^1H\}$ NMR spectroscopy at δ 42.0 ($^1J_{PRh}$ = 116.0 Hz). The facile loss of a $PPh_3$ ligand from the coordination sphere of **80** may explain the broadness of its hydride resonance.

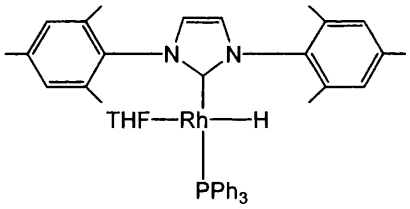


**Figure 3.12.** Proposed structure for **81**.

Upon the addition of IMes to a solution of **69**, a second, minor product is formed along with **80**, and can be seen by $^{31}P\{^1H\}$ NMR spectroscopy.. This consists of two doublet of doublets, which are sharp at room temperature (δ 44.9, $J_{PRh}$ = 155.0 Hz, $^2J_{PP}$ = 60.2 Hz; 36.0, $J_{PRh}$ = 142.1 Hz, $^2J_{PP}$ = 60.2 Hz), and are not part of a hydride containing species (figure 3.13.).

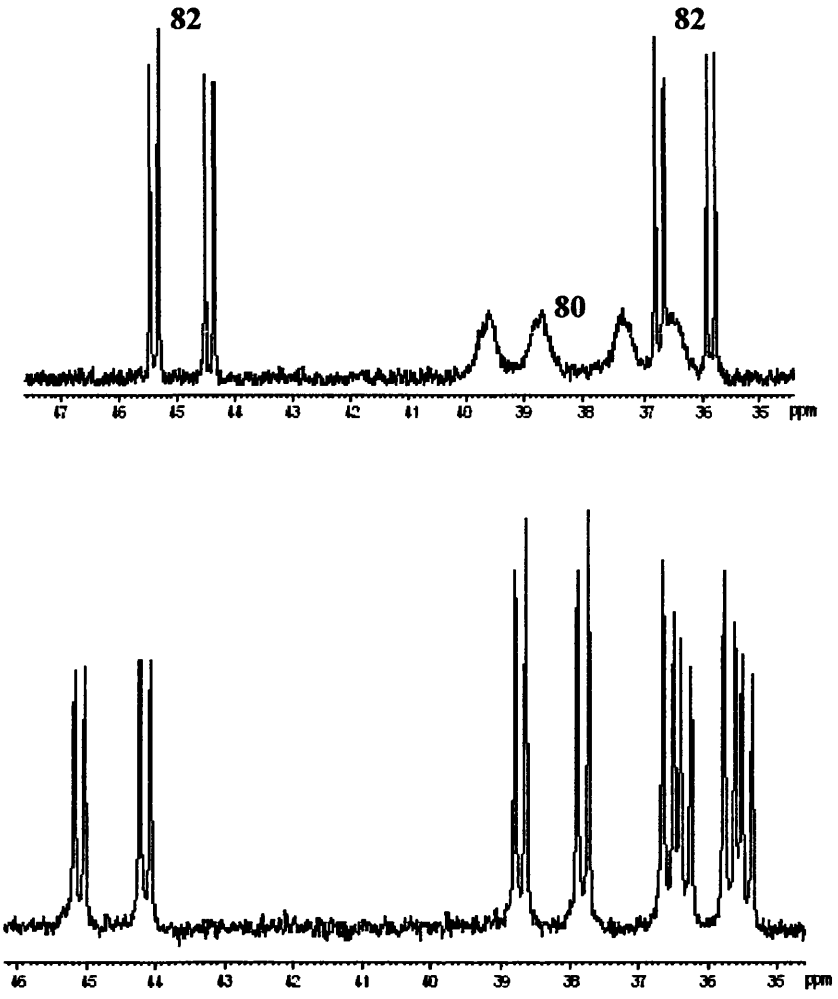


**Figure 3.13.** $^{31}P\{^{1}H\}$ NMR of **80** and **82** at 25 °C (top) and -30 °C (bottom) ($d_8$-THF, 400 MHz).

This second product has been identified as the C-H activated product (**82**), arising from *ortho* $CH_3$ cleavage (scheme 3.20.). When 1 atm of ethene is added to a THF solution of **80** and heated at 50 °C for two hours, **80** is fully converted to **82**. Addition of an atmosphere of $H_2$ to **82** at room temperature overnight reconverts the sample primarily back to **80**. However, some **82** remains, even under an $H_2$ atmosphere. Heating of **80** at 50 °C under an inert atmosphere also leads to formation of more **82**, although this is much slower than when a hydrogen acceptor source is present.

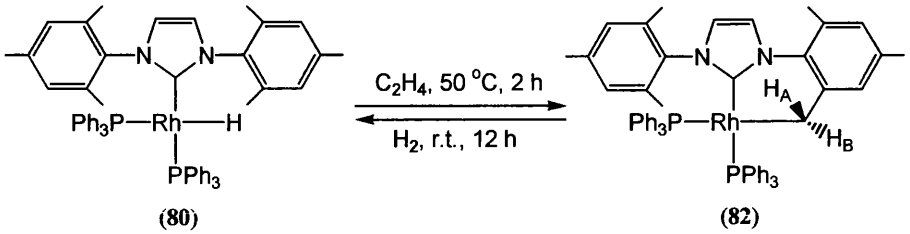


(80) (82)

**Scheme 3.20.** Formation of **82** from **80**.

**82** has been characterised using both 1D and 2D NMR experiments. From $^{31}P\{^{1}H\}$-$^{1}H$ HMQC, the sharp peaks in the phosphorus spectrum couple to two separate methylene protons (δ 2.54 and 1.33). These are attributed to the two diastereotopic protons on the activated arm (A and B). These should both be doublets of doublets of doublets of doublets although the signals are broad due to the coupling constants being very similar in size. $^{13}C\{^{1}H\}$-$^{1}H$ HMQC experiments reveal that the methylene carbon appears at δ 26.2 in the $^{13}C\{^{1}H\}$ NMR spectrum as a doublet of doublet of doublets ($J_{CRh}$ = 58.2 Hz, $^{2}J_{CPtrans}$ = 18.8 Hz, $^{2}J_{CPcis}$ = 11.0 Hz) (figure 3.14.).

[RhHCl(IMes)''(IMes)] (**3**), synthesised by Nolan and already discussed within section 1.2.7., only exhibits one proton resonance for the Rh-$CH_2$ group (δ 2.41) and this does not show any coupling to rhodium. The reasons for this are unclear.

### 3.5.3. Thermolysis reactions of [$RhH(PPh_3)_4$] (69)

#### *3.5.3.1. Formation of [{$Rh(PPh_3)_2$}$_2$($\mu$-$PPh_2$)($\mu$-H)] (83)*

When **69** is heated at 70 °C for 4 days, the starting material dimerises to give a binuclear rhodium complex in which each Rh centre has two terminal $PPh_3$ groups and are bridged by $PPh_2$ and a hydride ligand (**83**) (figure 3.15.). This compound was first noted when trying to react **69** with $IMesH_2$. The higher activation energy

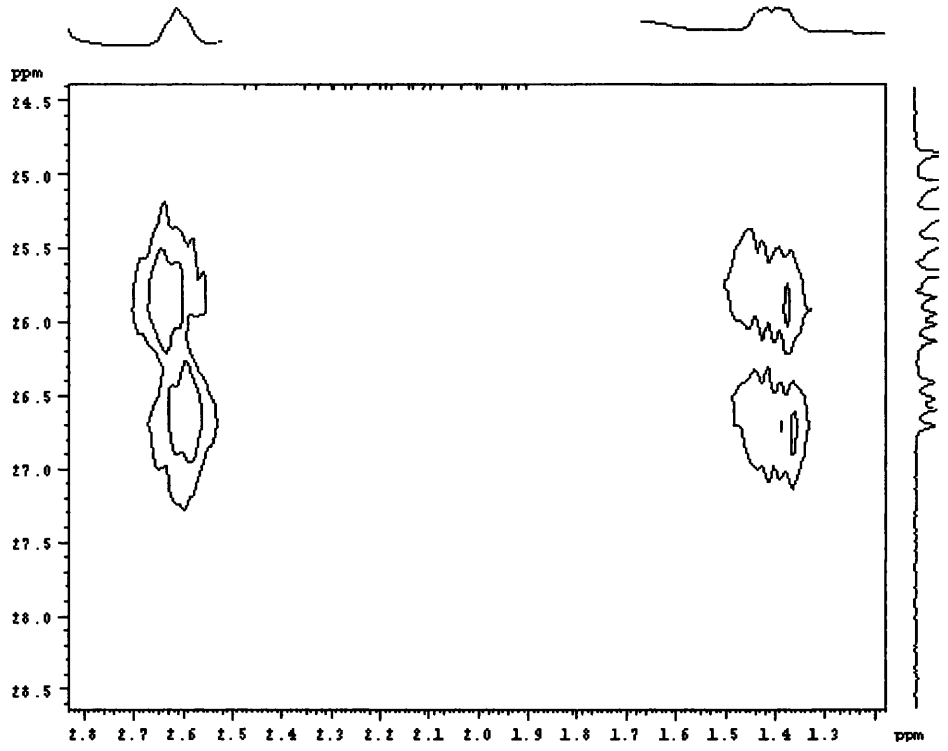


**Figure 3.14.** $^{13}C\{^1H\}$-$^1H$ HMQC of **82** showing activated $CH_2$ resonance. ($d_8$-THF, 100 MHz for $^{13}C$, 25 °C).

that is obviously needed for coordination of this particular NHC ligand necessitated the sample being heated at higher temperatures, which led to observation of **83**. At no point was any reaction between $IMesH_2$ and **69** or **83** detected.[55] **83** displays one complex multiplet in the hydride region of the $^1H$ NMR spectrum (figure 3.16.). The extensive splitting of this signal arises from coupling to both rhodium nuclei and the terminal phosphine as well as the bridging phosphide, giving a doublet of triplet of triplet of triplets. The splitting of this peak is actually much simpler than this because $J_{HRh}$ and $J_{HPcis}$ are quite similar in size.

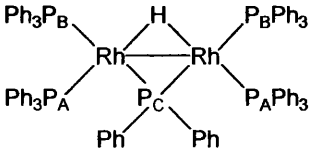


**Figure 3.15.** Structure of **83**.

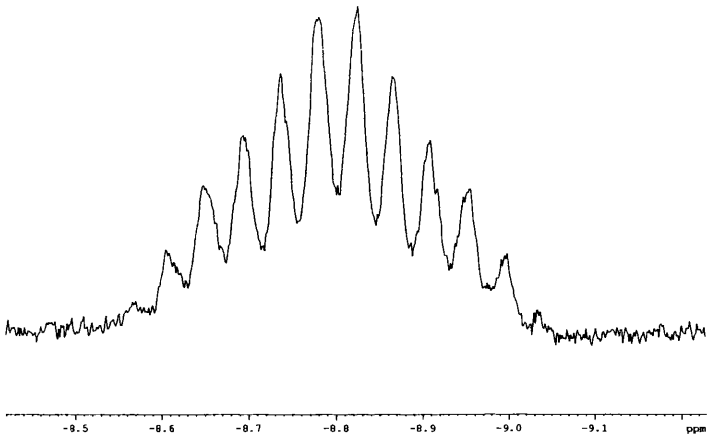


**Figure 3.16.** Bridging hydride resonance of **83** (400 MHz, 25 °C) in $d_8$-THF.

The $^{31}P\{^1H\}$ NMR spectrum for **83** consists of two complex multiplets at δ 41.9 and 31.4 and a strongly downfield shifted triplet of triplets for the bridging phosphido ligand (δ 174.1, $^1J_{PRh}$ = 136.5 Hz, $^2J_{PcPB}$= 221.0 Hz, $^2J_{PcPA}$ = 15.5 Hz,). This very low field resonance is consistent with there being a strong Rh-Rh interaction in the complex,[56,57] as reported by Arif *et al.* for the similar structure [{Rh($^t$Bu$_2$PH)(CO)}$_2$(μ-H)(μ-$^t$Bu$_2$P)][58] and Meek *et al.* for [{(PEt$_3$)$_2$Rh}(μ-PPh$_2$)$_2${Rh(COD)}].[59] Garrou has shown that a Pd complex with a bridging phosphide, and no Pd-Pd bond has a bridging PPh$_2$ shift at -127 ppm, whilst a similar complex with a Pd-Pd bond has a shift at 204 ppm.[56]

The $^{31}P\{^1H\}$ NMR of **83** was simulated using *g-NMR*.[60] This gave an incredibly close match and allowed the shifts for the terminal $^{31}P$ peaks *trans* to hydride and those *trans* to PPh$_2$ to be assigned as well as elucidating the coupling constants for all of the interactions. Figure 3.17. shows the $^{31}P\{^1H\}$ NMR experimentally determined spectrum alongside that simulated by *g-NMR*.

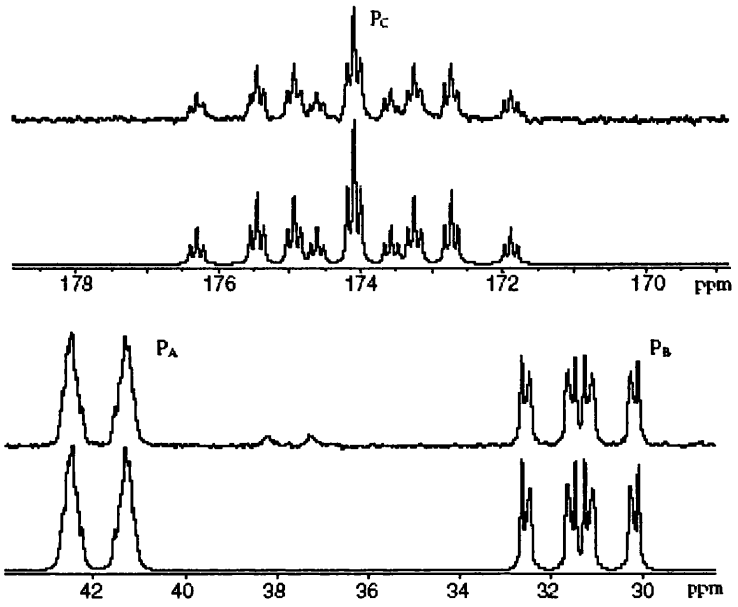


**Figure 3.17.** Experimental (top) and simulated (bottom) $^{31}P\{^{1}H\}$ NMR spectra ($d_8$-THF, 162 MHz, 25 °C) for **83**.

The structure of **83**, including the presence of a Rh-Rh bond was determined unequivocally by X-ray crystallography, as shown in figure 3.18. The Rh-Rh distance is slightly longer than that reported by Arif *et al.* for the μ-P$^t$Bu$_2$ complex (2.9226(2) cf. 2.906(2) Å) but still well within the upper limit for a Rh-Rh bond (3.2 Å).[61] The complex is also slightly asymmetrical, with the two Rh-P bonds from the bridging phosphido moiety being unequal in length (2.2378(5) and 2.2488(5) Å). All four terminal Rh-P bonds are also of different lengths (2.3266(5), 2.2599(5), 2.3320(5) and 2.2454(5) Å). The dimer is slightly asymmetrical in terms of angles. The bridging phosphide is placed almost centrally along the Rh-Rh bond (P(1)-Rh(1)-Rh(2) = 49.515(13) Å, P(1)-Rh(2)-Rh(1) = 49.188(13) Å) but the geometries of the terminal phosphines around each rhodium are noticeably different (P(3)-Rh(1)-P(2) = 98.619(19) Å, P(5)-Rh(2)-P(4) = 102.269(18) Å). Selected bond lengths and angles for **83** are shown in table 3.7.

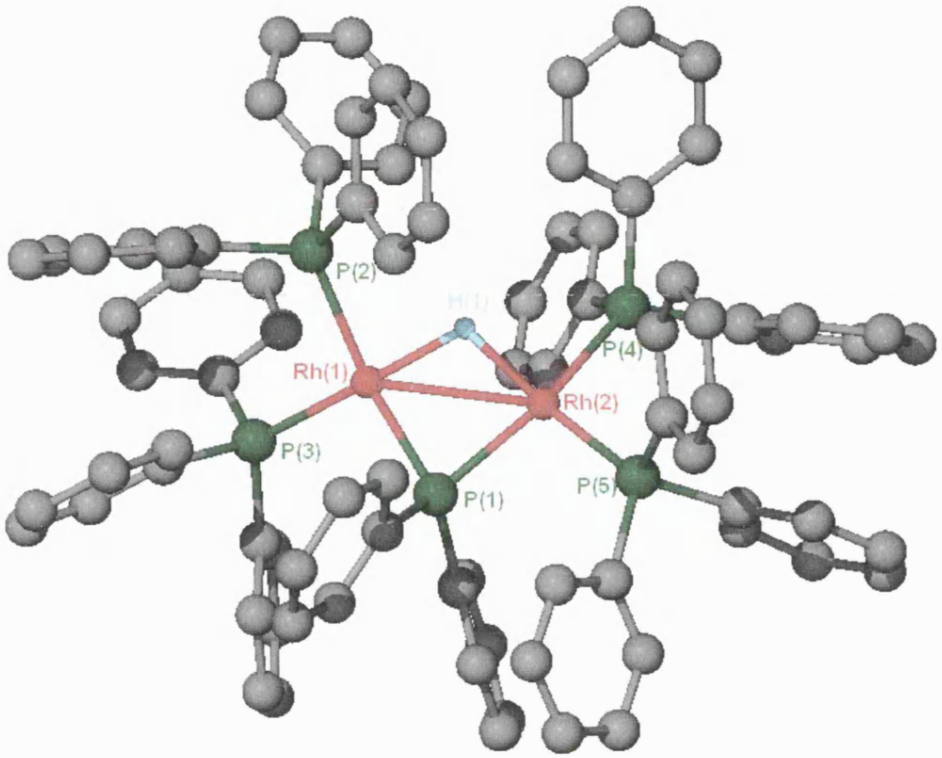


**Figure 3.18.** Molecular structure of **83** determined by X-ray crystallography.

| **Bond lengths (Å)** | | | |
|---|---|---|---|
| Rh(1)-Rh(2) | 2.9226(2) | Rh(1)-P(3) | 2.2599(5) |
| Rh(1)-P(1) | 2.2378(5) | Rh(2)-P(4) | 2.3320(5) |
| Rh(2)-P(1) | 2.2488(5) | Rh(2)-P(5) | 2.2454(5) |
| Rh(1)-P(2) | 2.3266(5) | | |
| **Bond angles (°)** | | | |
| Rh(1)-P(1)-Rh(2) | 81.297(16) | P(1)-Rh(2)-Rh(1) | 49.188(13) |
| P(1)-Rh(1)-P(2) | 148.80(2) | P(3)-Rh(1)-P(2) | 98.619(19) |
| P(1)-Rh(1)-P(3) | 101.097(19) | P(5)-Rh(2)-P(1) | 99.809(18) |
| P(1)-Rh(2)-P(4) | 150.255(19) | P(5)-Rh(2)-P(4) | 102.269(18) |
| P(1)-Rh(1)-Rh(2) | 49.515(13) | P(5)-Rh(2)-Rh(1) | 147.224(14) |

**Table 3.7.** Selected bond lengths and angles for **83**.

The two rhodium atoms, the bridging phosphide and the bridging hydride all lie in one plane with the terminal phosphines protruding out. The two phosphines *cis* to the hydride (P(2) and P(4)) come out from the plane in opposing directions as do P(3) and P(5), which are *cis* to the bridging phosphide. This is presumably solely a steric effect.

The growth of a peak at 7.10 ppm in the $^1$H NMR spectrum during the formation of **83** suggests that benzene is being eliminated from the reaction. This could occur after intramolecular oxidative addition of one of the P-C bonds to the rhodium centre, leading to a fragment such as "$(PPh_3)_2Rh^{n+}(PPh_2)$", which can then react with **69** (still present in solution) and lose phosphine leading to the formation of the observed dimeric species **83** (scheme 3.21.).

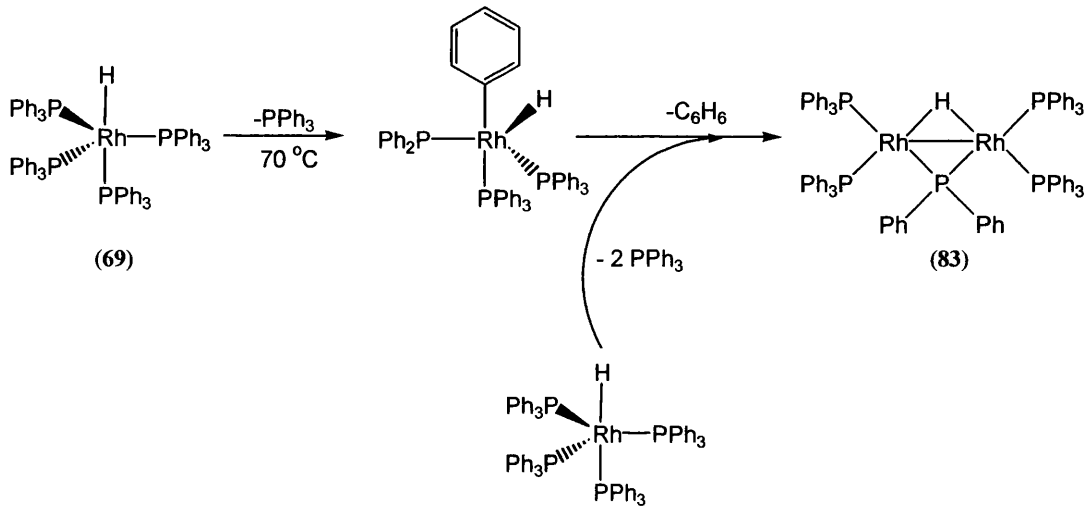


**Scheme 3.21.** Proposed mechanism of formation of **83** from **69**.

*3.5.3.2. Formation of $[Rh(PPh_3)'(PPh_3)_2]$*

Circumstantial evidence that C-H activation of $PPh_3$ in **69** occurs comes from heating a solution of **69** at lower temperature (50 °C). This leads to C-H activation from a phenyl group on one of the phosphine ligands (figure 3.19.). This complex has been observed previously by Keim as a product when heating $[RhMe(PPh_3)_3]$.[62] Heating a solution containing solely **69** at 50 °C for 16 hours leads to this same product, which is clearly shown by $^{31}P\{^1H\}$ NMR, comprising of three phosphine resonances, all doublets of doublets of doublets (δ 43.1 ($^2J_{PPcis}$ = 28.3 Hz, $^2J_{PPtrans}$ = 311.6 Hz, $J_{PRh}$ = 179.0 Hz), 37.9 ($^2J_{PPcis}$ = 28.3 Hz, $^2J_{PPcis}$ = 33.5 Hz, $J_{PRh}$ = 122.2 Hz), -56.4 ($^2J_{PPcis}$ = 33.5 Hz, $^2J_{PPtrans}$ 311.6 Hz, $J_{PRh}$ = 119.8 Hz). The highfield resonance at -56.4 is indicative of an *ortho*-metallated phosphine.

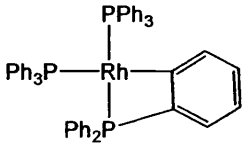


**Figure 3.19.** C-H activated phosphine.

3.5.4. Reactivity of $[RhH(PPh_3)_3(CO)]$ with N-heterocyclic carbenes

While reaction of **69** with NHCs afforded products in which at least some of the initial phosphine ligands were retained, $[RhH(PPh_3)_3(CO)]$ (**70**) reacted with $I^iPr_2Me_2$, ICy and IMes rapidly at room temperature to give the four coordinate bis NHC species $[RhH(NHC)_2(CO)]$ (NHC = $I^iPr_2Me_2$ (**84**), ICy (**85**), IMes (**86**)).

With IMes and ICy only the *trans*- arrangement of NHC ligands was observed but $I^iPr_2Me_2$ showed formation of *cis*- and *trans*-**84** in a 1:8 ratio by $^1H$ NMR spectroscopy. The presence of the *cis* isomer cannot be a steric effect. Using the concept of buried volume, introduced in section 1.2.2., it can be seen that $I^iPr_2Me_2$ is much bulkier than ICy.[63] Calculations carried out on nickel centres have determined that complexes with ICy ligands have an extremely small % $V_{Bur}$ (23, close to the analogous $PPh_3$ complexes) in comparison to complexes containing $I^tBu$ ligands (37). $I^tBu$ can be assumed to be comparable in size to $I^iPr_2Me_2$ despite $I^tBu$ having an additional methyl group on the arm as $I^iPr_2Me_2$ has methyl groups on the backbone, which would add to its bulk.

This suggests that the observation of a *cis* arrangement of NHCs on **84** must be due to electronic effects. As discussed in chapter 1 (page 21) Magill *et al.* have shown that the presence of methyl groups on the backbone of $I^iPr_2Me_2$ makes it more basic, and thus more nucleophilic, than the analogous NHC without the methyl groups on the backbone.[64] This implies that the methyl groups on the backbone increase the electron donating properties of the NHC ligand. This means that an $I^iPr_2Me_2$ ligand may well be more stable *trans* to a hydride ligand than ICy or IMes. Therefore, although **85** and **86** may well form both isomers, the high *trans* effect of

the hydride ligand means the *cis*-arrangement is far less stable and immediately rearranges to give the *trans*-product. Having the CO ligand, which is a good π-acceptor *trans* to the hydride, which is a good σ-donor, also stabilises the complexes.

Herrmann has noted the formation of both *cis*- and *trans*-isomers of $[RhCl(IMe)_2(CO)]$[65] although they were prepared from different routes and the reaction of $[\{Rh(CO)\}_2(\mu\text{-}Cl)_2]$ and IMe had to be kinetically controlled to obtain the *cis*-isomer.

The lack of phosphine ligands on these complexes led to less complicated hydride resonances in the $^1H$ NMR spectra. All appeared as simple doublet resonances (*cis*-**84**: δ -6.44 ($J_{HRh}$ = 19.2 Hz), *trans*-**84**: δ -4.84 ($J_{HRh}$ = 25.8 Hz), **85**:δ -4.55 ($J_{HRh}$ = 25.8 Hz,), **86**: δ -4.71 ($J_{HRh}$ = 26.3 Hz). The $^{13}C\{^1H\}$ NMR spectra of **85** and **86** both showed single low field doublets for the carbene resonance at δ 197.7 ($J_{CRh}$ = 44.1 Hz) and 192.5 ($J_{CRh}$ = 46.0 Hz) respectively confirming that the carbenes are *trans* to each other. A strong $\nu_{CO}$ IR absorption band was also recorded for each complex (**85**: 1919 $cm^{-1}$, **86**: 1914 $cm^{-1}$). The analogous complex, *trans*-$[RhCl(IMe)_2(CO)]$ has an IR band at 1924 $cm^{-1}$.[65] The CO stretching frequencies in NHC-transition metal complexes have been the subject of much investigation both experimentally and theoretically in an effort to determine the relative σ-donating properties of different NHCs.[26,44,66,67] N-aryl carbenes would be expected to be more electron donating than N-alkyl carbenes, hence weakening the C≡O bond and causing the absorption to shift to lower frequency. However, despite the potential differences in the donating abilities of N-alkyl and N-aryl NHCs, very little difference is observed in $\nu_{CO}$. This trend is also reflected with **85** and **86** where the two absorptions are very similar and is also illustrated in the two iodo complexes, $[RhI(NHC)_2(CO)]$ (NHC = IMe (**66**), IMes (**67**)), discussed earlier where **67**, bearing two IMes ligands has a $\nu_{CO}$ absorption at 1937 $cm^{-1}$ and the analogous complex, **66**, with two IMe ligands has a $\nu_{CO}$ absorption at 1943 $cm^{-1}$.[43] This phenomenon has also been discussed on page 21.

The crystal structure of **86** (figure 3.20.) reveals, like *trans*- [RhH(I$^i$Pr$_2$Me$_2$)(PPh$_3$)$_2$] (**72**), a distorted square planar geometry, although to a much lesser degree, with a C(2)-Rh-C(23) bond angle of 172.91(7) °. All four substituents around the rhodium centre again lie in the same plane with the distortion in the C(2)-Rh-C(23) plane coming from the NHC ligands bending slightly away from the CO group. Neither of the two imidazole rings lies exactly perpendicular to the plane (62.507 ° and 70.341 ° out of plane). The Rh-carbene bond lengths (2.0165(16), 2.0191(17) Å) are shorter than in the similar complex *trans*-[RhCl(IMe)$_2$(CO)].[65] Significant bond lengths and angles are presented in table 3.8.

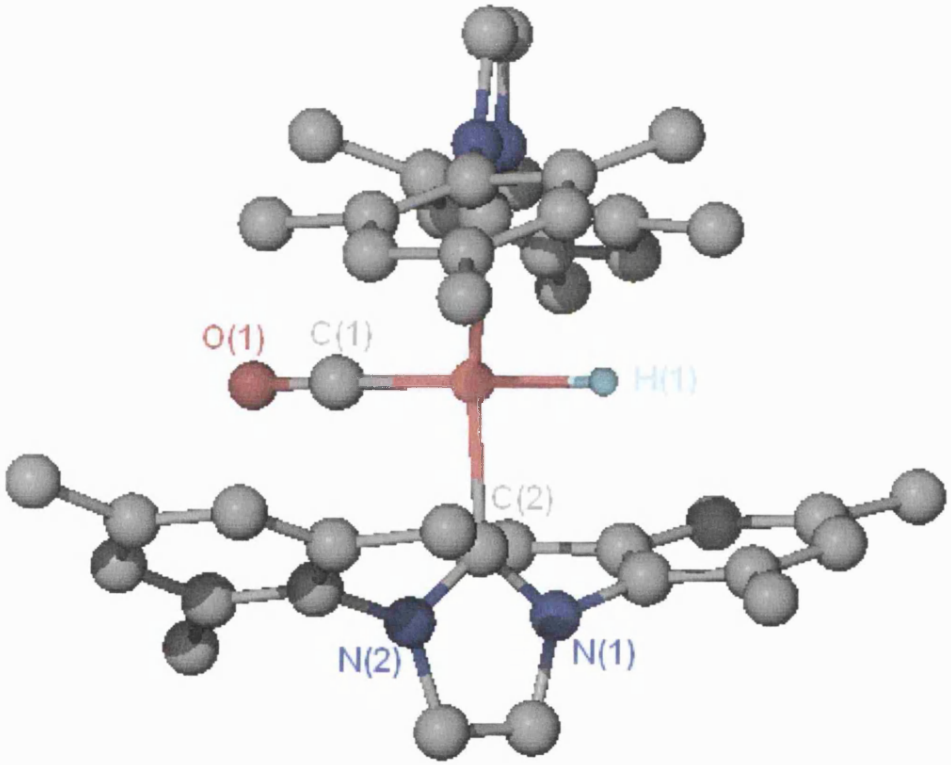


**Figure 3.20.** Molecular structure of **86** determined by X-ray crystallography.

| **Bond lengths (Å)** | | | |
|---|---|---|---|
| Rh(1)-C(1) | 1.843(2) | Rh(1)-C(23) | 2.0165(16) |
| Rh(1)-C(2) | 2.0191(17) | O(1)-C(1) | 1.144(3) |
| **Bond angles (°)** | | | |
| C(23)-Rh(1)-C(2) | 172.91(7) | C(1)-Rh(1)-C(2) | 92.41(8) |
| C(1)-Rh(1)-C(23) | 94.61(8) | | |

**Table 3.8.** Selected bond lengths and angles for **86**.

### *3.5.4.1. Formation of [{(PPh$_3$)$_2$Rh}(μ-CO)$_2${Rh(I$^i$Pr$_2$Me$_2$)$_2$}] (87)*

As has already been discussed on page 180, when I$^i$Pr$_2$Me$_2$ is reacted with **70**, both *cis*- and *trans*-**84** form. This is likely to be due to the higher electron donating ability of the I$^i$Pr$_2$Me$_2$ stabilising the *cis* orientation of NHCs. By $^{31}P\{^1H\}$ NMR spectroscopy, it was apparent that there was a third, stable complex forming. This consisted of a lone doublet of doublets at δ 37.6 ($J_{PRh}$ = 236.5 Hz, $^2J_{PRh}$ = 7.7 Hz) (figure 3.21.) and has been confirmed as arising from the unsymmetrical carbonyl bridged dimer [{(PPh$_3$)$_2$Rh}(μ-CO)$_2${Rh(I$^i$Pr$_2$Me$_2$)$_2$}] (**87**).

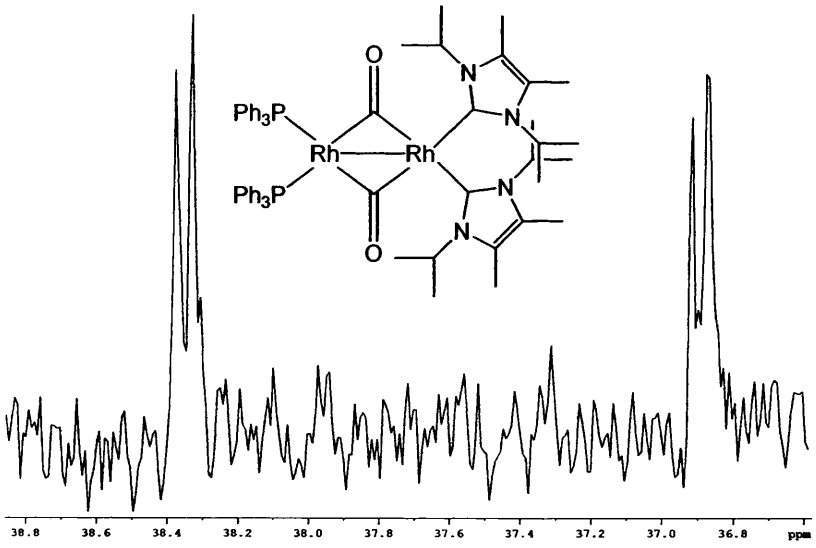


**Figure 3.21.** $^{31}P\{^1H\}$ NMR spectrum of **87** in $d_8$-THF (162 MHz, 25 °C).

The structure of this product has been established unambiguously by X-ray crystallographic studies (figure 3.22.), which show a distorted square planar Rh bis NHC fragment (C(6)-Rh(2)-C(2) = 94.87(12) °) connected to a distorted tetrahedral Rh(PPh$_3$)$_2$ unit (P(1)-Rh(1)-P(2) = 122.91(3) °) *via* two bridging CO ligands and a Rh-Rh bond (table 3.9.). This is significantly different from the analogous complex bearing four terminal phosphine groups, synthesised by Singh *et al.*, where the P(1)-Rh(1)-P(2) angle is 103 °.[68]

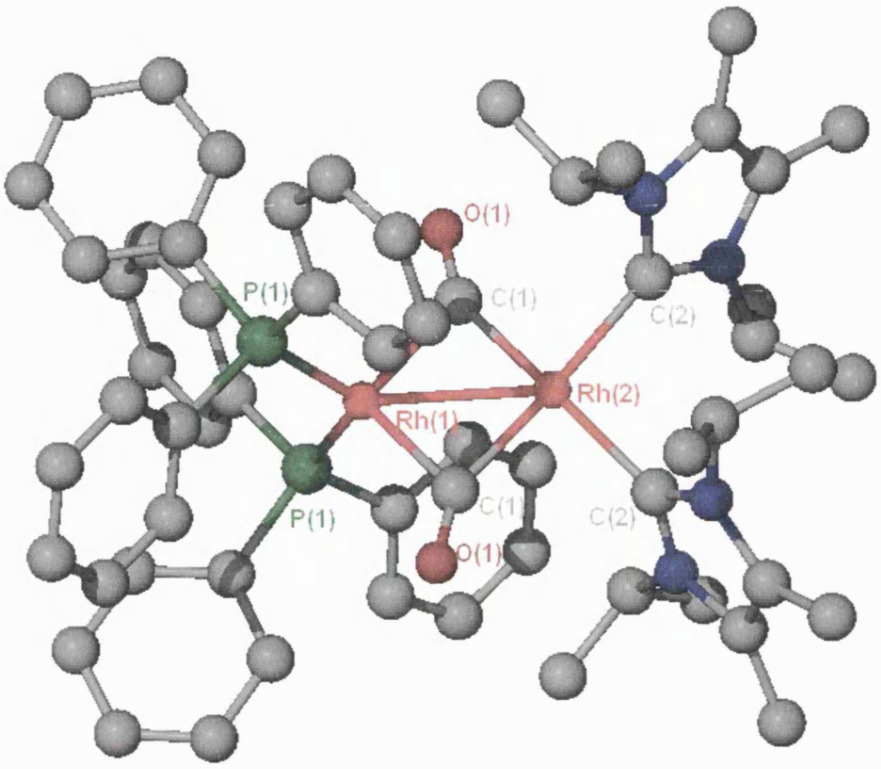


**Figure 3.22.** Molecular structure of **87** determined by X-ray crystallography.

| **Bond lengths (Å)** | | | |
|---|---|---|---|
| Rh(1)-Rh(2) | 2.6939(3) | Rh(2)-C(1) | 2.005(3) |
| Rh(1)-C(1) | 1.995(3) | Rh(2)-C(2) | 2.073(2) |
| Rh(1)-P(1) | 2.3019(6) | | |
| **Bond angles (°)** | | | |
| C(1)-Rh(1)-Rh(2) | 47.82(8) | C(2)'-Rh(2)-C(2) | 94.87(12) |
| C(1)-Rh(2)-Rh(1) | 132.57(6) | C(1)-Rh(2)-C(1)' | 95.03(16) |
| C(2)-Rh(2)-Rh(1) | 118.543(16) | C(1)-Rh(1)-P(1)' | 109.60(3) |
| C(2)'-Rh(2)-Rh(1) | 132.57(6) | C(1)-Rh(1)-P(1) | 107.83(3) |
| P(1)-Rh(1)-Rh(2) | 47.52(8) | P(1)'-Rh(1)-P(1) | 122.91(3) |
| C(1)'-Rh(1)-C(1) | 95.64(16) | O(1)-C(1)-Rh(1) | 125.7(3) |
| C(1)-Rh(2)-C(2)' | 168.07(7) | O(1)-C(1)-Rh(2) | 149.6(3) |
| C(1)-Rh(2)-C(2) | 86.29(9) | | |

**Table 3.9.** Selected bond lengths and angles for **87**.

The rhodium atoms and bridging CO ligands lie in the same plane, with the NHCs lying slightly off and the phosphine groups protruding a significant amount as can be

seen in figure 3.23. The CO groups are angled towards the $PPh_3$ ligands although one is significantly more acute than the other (O(1)-C(1)-Rh(1) = 125.7(3) O(1)-C(1)-Rh(2) = 149.6(3) Å). $[((PCy_3)_2Rh)(\mu\text{-}CO)_2(Rh(PCy)_3(CO))]$ (**88**), synthesised by Freeman and Young,[69] also has the central atoms in the same plane and in addition the terminal phosphorus and carbon atoms are also in that central plane. The larger steric bulk of $PPh_3$ in **87** obviously pushes the terminal phosphorus atoms well out of the plane whilst the carbons from the smaller NHC ligands are only slightly removed.

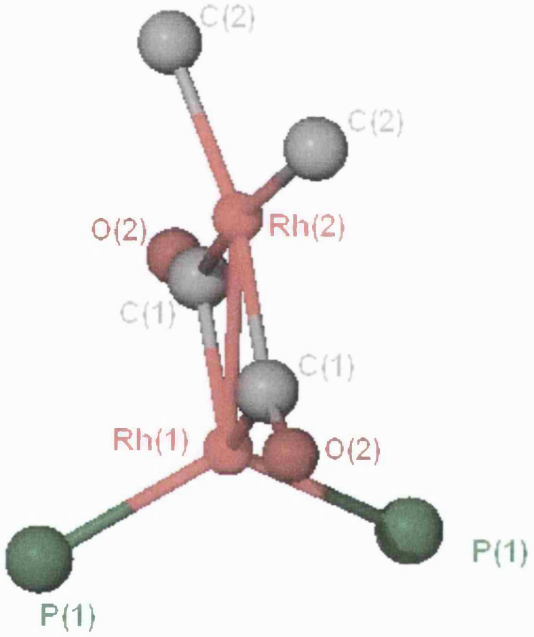


**Figure 3.23.** Central fragment of X-ray crystallographic structure of **87**.

The Rh-Rh bond distance (2.6939(3) Å) in **87** is comparable to other, similar, complexes in the literature.[68-70] The bridging carbonyls are almost equidistant from each rhodium (1.995(3) and 2.005(3) Å) in contrast to the structure of **88** where they are closer to Rh(2) (bearing two $PCy_3$ ligands) by 0.117 and 0.171 Å. Albright and co-workers have attributed this type of asymmetry to electronic differences between the two rhodium atoms.[71] That this distortion does not exist in **87** may be evidence for the similar electronic properties of phosphines and NHCs in the complex. When

all four terminal ligands are $PPh_3$ the CO groups are centred exactly between the two rhodium atoms (Rh(1/2)-C(1) = 2.051 (6) Å, Rh(1/2)-C(2) = 1.956(7) Å).[68]

The IR spectrum of **87** shows a single $\nu_{CO}$ stretching frequency at 1708 $cm^{-1}$. In contrast, **88** exhibits two bands, at 1773 and 1728 $cm^{-1}$ as does $[\{(PPh_3)_2(CO)Rh\}(\mu\text{-}CO)_2\{Rh(PPh_3)(CO)_2\}]$ (1799 and 1774 $cm^{-1}$).[72] The presence of terminal CO groups as well as the poorer σ-donating $PR_3$ ligands on these latter two complexes contribute to their higher frequencies relative to **87**.

*3.5.4.2. Evidence for dimeric species bearing ICy NHCs*

Upon addition of only one equivalent of ICy to **70**, a doublet of doublets can be seen by $^{31}P\{^1H\}$ NMR (δ 38.5, $J_{PRh}$ = 231.6 Hz, $^2J_{PRh}$ = 8.1 Hz) analogous to that observed for **87** and thus attributable to $[\{(PPh_3)_2Rh\}(\mu\text{-}CO)_2\{Rh(ICy)_2\}]$. In addition there are two further doublets present in the $^{31}P\{^1H\}$ NMR spectrum, both appearing at δ 35.9 with slightly different rhodium-phosphine coupling constants ($J_{PRh}$ = 181.4 and 199.3 Hz). These are most likely due to the *cis* and *trans* isomers of $[\{(ICy)(PPh_3)Rh\}_2(\mu\text{-}CO)_2]$.

When a THF solution of $[RhH(PPh_3)_3(CO)]$ (**70**) and 4 equivalents of ICy was agitated for a few minutes at room temperature then pumped to dryness and a nujol mull IR run of some of the residue, a $\nu_{CO}$ band at 1666 $cm^{-1}$ was noted, suggesting a complex with bridging carbonyls was present. Redissolving the rest of the residue in $d_8$-THF showed that there were no product phosphorus peaks by $^{31}P\{^1H\}$ NMR. This suggests that, by adding more equivalents of ICy, the dimeric species formed is $[\{Rh(ICy)_2\}_2(\mu\text{-}CO)_2]$.

The rapid formation of dimeric species from hydride containing species can be seen visually from the significant amount of hydrogen gas given off upon initial addition of solvent to samples of **70** and free NHC.

### 3.5.5. Formation of $[Rh(NHC)_3(CO)]^+$

When THF or benzene solutions of the reaction mixtures of **70** and free NHC were left to stand at room temperature for more than a day, cationic, monomeric, tris NHC carbonyl complexes, $[Rh(NHC)_3(CO)]^+$ (NHC = $I^iPr_2Me_2$ (**89**) and ICy (**90**)) precipitated out of solution as crystalline solids. These complexes were isolated in better yields (approximately 30 %) from layering reaction solutions with hexane or pentane.

The crystals were regularly good enough to analyse using X-ray diffraction. However, the associated anions were generally unidentifiable by X-ray diffraction or NMR spectroscopy. Those anions that were identified were surprising as they were fragments of ligands from those present in the initial solution. An example of this is $[Rh(I^iPr_2Me_2)_3(CO)][(PMe_2)_3(O)_4)H]$, (**91**) which was identified by X-ray studies. As the starting phosphines have phenyl groups, the appearance of an anion with a phosphorus centre bearing methyl groups was inexplicable.

It was found that by dissolving the cationic product isolated from the original solution in $CH_2Cl_2$ (0.6 mL) and stirring in a saturated aqueous solution of $KPF_6$ (0.02 g in 1.0 mL), the anions were universally substituted to yield the $[PF_6]^-$ salts.

Crystal structures have been obtained for both **89** and **90**. These are shown in figures 3.24 and 3.25 respectively. Both are pseudo-square planar in geometry (bond lengths and angles are presented in tables 3.10 and 3.11). The Rh-carbene bond lengths for the NHC ligands *trans* to the CO group are longer than those *trans* to NHC due to the high *trans* influence of CO (2.1490(13) Å cf. 2.0775(13) Å and 2.0738(14) Å for **89**). The chelating NHC, 4 coordinate Rh(I) cations, $[Rh(I^iBu(CH_2)_nI^iBu)(COD)][PF_6]$ (n = 2, 3) synthesised by Peris *et al.* and discussed in section 3.3.5., have slightly shorter Rh-carbene bond lengths (n = 2: Rh-C = 2.034(4), 2.048(4) Å, n = 3: Rh-C = 2.038(3), 2.029(3) Å). This is probably due to the small *trans* effect of the COD ligand compared to NHC and CO.

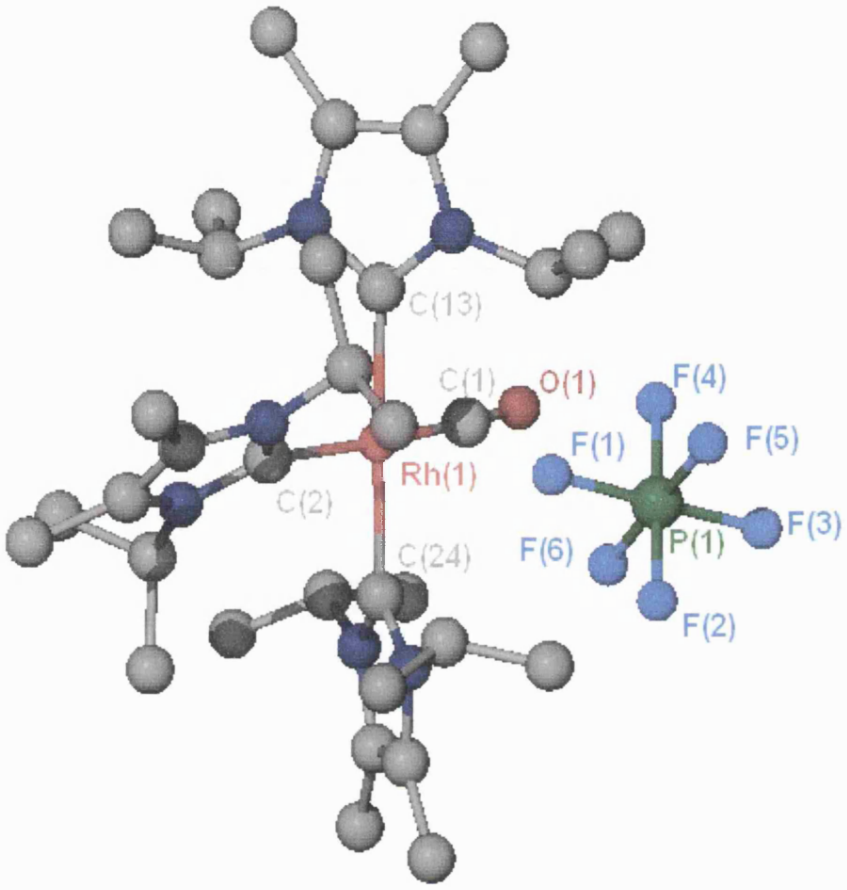


**Figure 3.24.** Molecular structure of **89** determined by X-ray crystallography.

| **Bond lengths (Å)** | | | |
|---|---|---|---|
| Rh(1)-C(1) | 1.8367(15) | Rh(1)-C(2) | 2.0738(14) |
| Rh(1)-C(24) | 2.1490(13) | O(1)-C(1) | 1.1415(19) |
| Rh(1)-C(13) | 2.0775(13) | | |
| **Bond angles (°)** | | | |
| C(13)-Rh(1)-C(24) | 177.56(5) | C(1)-Rh(1)-C(24) | 90.23(6) |
| C(1)-Rh(1)-C(2) | 176.38(6) | C(13)-Rh(1)-C(2) | 90.01(5) |
| C(24)-Rh(1)-C(2) | 91.90(5) | C(1)-Rh(1)-C(13) | 87.95(6) |

**Table 3.10.** Selected bond lengths and angles for **89**.

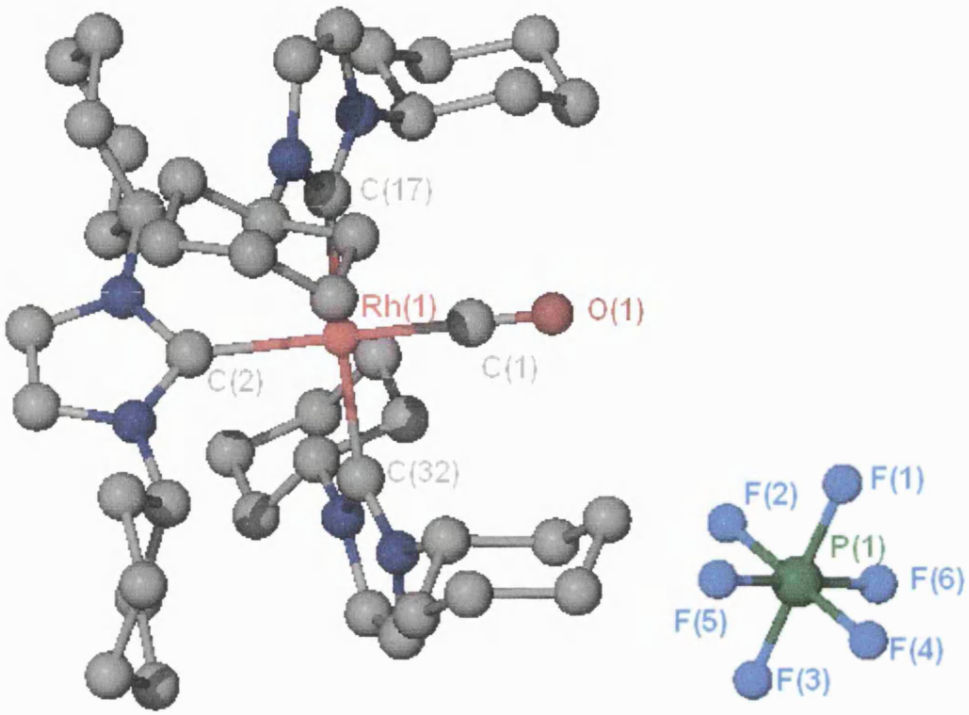


**Figure 3.25.** Molecular structure of **90** determined by X-ray crystallography.

| **Bond lengths (Å)** | | | |
|---|---|---|---|
| Rh(1)-C(1) | 1.8322(15) | Rh(1)-C(2) | 2.0638(11) |
| Rh(1)-C(32) | 2.1321(12) | O(1)-C(1) | 1.143(2) |
| Rh(1)-C(17) | 2.0642(11) | | |
| **Bond angles (°)** | | | |
| C(1)-Rh(1)-C(2) | 177.86(7) | C(17)-Rh(1)-C(2) | 90.93(5) |
| C(17)-Rh(1)-C(32) | 177.39(5) | C(1)-Rh(1)-C(32) | 89.05(6) |
| C(32)-Rh(1)-C(2) | 91.60(5) | C(1)-Rh(1)-C(17) | 88.44(6) |

**Table 3.11.** Selected bond lengths and angles for **90**.

The Rh-CO distances (1.8367(15) Å (**89**) and 1.8322(15) Å (**90**)) are comparable to those in $[Rh(PPh_3)_3(CO)][BF_4]$ (**92**)(1.865(4) Å), synthesised by Hope's group upon addition of $HBF_4 \cdot Et_2O$ to a saturated solution of **70** (figure 3.26.).[73] **92** has a significantly distorted square planar geometry (P(1)-Rh(1)-P(2) = 171.39°) (table 3.12.) presumably due to the much bulkier $PPh_3$ ligands. In addition, the two *trans* $PPh_3$ ligands are not equidistant from the rhodium centre (2.3280(10), 2.3799(9) Å) as observed for the NHC ligands in **89** (2.0775(13), 2.0738(14) Å) and **90** (2.0642(11), 2.0638(11) Å).

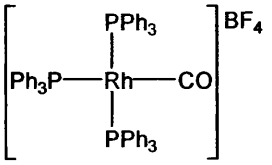


**Figure 3.26.** Structure of **92**, synthesised by Hope *et al.*

| **Bond lengths (Å)** | | | |
|---|---|---|---|
| Rh(1)-C(1) | 1.865(4) | Rh(1)-P(3) | 2.3968(9) |
| Rh(1)-P(1) | 2.3280(10) | C(1)-O(1) | 1.135(5) |
| Rh(1)-P(2) | 2.3799(9) | | |
| **Bond angles (°)** | | | |
| C(1)-Rh(1)-P(1) | 86.91(12) | C(1)-Rh(1)-P(3) | 175.86(12) |
| C(1)-Rh(1)-P(2) | 84.96(12) | P(1)-Rh(1)-P(3) | 95.90(3) |
| P(1)-Rh(1)-P(2) | 171.39(3) | P(2)-Rh(1)-P(3) | 92.37(3) |

**Table 3.12.** Selected bond lengths and angles for **92**.

The three imidazole rings of the NHC ligands in **89** are all twisted out of the central plane. The imidazole ring of the NHC ligand *trans* to the CO group lies at a 52.887 ° angle out of the plane with the other two imidazole rings of the NHC ligands *trans* to each other, lying at 67.042 ° and 63.597 ° out of the plane. In **90** the imidazole ring of the NHC ligand *trans* to the CO lies at 52.297 ° out of the plane and the two imidazole rings of the *trans* NHC ligands lie at the same angle (64.046 °). The slight difference in the geometries of the ligands around the rhodium centre in **89** and **90** may simply arise from packing differences of the anion and cation in the crystal lattice.

The bond lengths of **91** (the complex analogous to **89** but with a different counterion) are very close to **89**, but the angles are significantly different (table 3.13.). This implies that changing the anion makes a difference to the shape of the cation.

| **Bond lengths (Å)** | | | |
|---|---|---|---|
| Rh(1)-C(1) | 1.833(2) | Rh(1)-C(2) | 2.0762(18) |
| Rh(1)-C(24) | 2.1362(19) | O(1)-C(1) | 1.147(3) |
| Rh(1)-C(13) | 2.0770(18) | | |
| **Bond angles (°)** | | | |
| C(1)-Rh(1)-C(2) | 178.14(9) | C(24)-Rh(1)-C(2) | 90.39(7) |
| C(13)-Rh(1)-C(24) | 175.89(7) | C(1)-Rh(1)-C(13) | 88.58(8) |
| C(13)-Rh(1)-C(2) | 92.67(7) | C(1)-Rh(1)-C(24) | 88.44(8) |

**Table 3.13.** Selected bond lengths and angles for **91**.

In the process of growing crystals of $[Rh(ICy)_3(CO)]$ (**90**) the formation of clear crystals were observed as well as the yellow ones of **90**. From X-ray diffraction analysis these were identified as $ICyHPF_6$ (**93**), a species with a hydrogen bond between a $PF_6$ anion and the imidazolium proton of an imidazolium salt. **93** was also formed when a $CH_2Cl_2$ solution of free ICy was stirred into a saturated $[PF_6]^-$ solution of water suggesting that protonation of free NHC occurs from the solvent. The crystal structure of **93** is shown in figure 3.27., with bond lengths and angles in table 3.14. $^1$H NMR spectroscopy for **93** showed characteristic shifts at δ 8.53 (t, $^4J_{HH}$ = 1.70 Hz) for the imidazolium proton and at 7.31 (d, $J^4_{HH}$ = 1.70 Hz) for the backbone protons. $I^iPr_2Me_2HPF_6$ (**94**) was also observed by $^1$H and $^{31}P\{^1H\}$ NMR spectroscopy.

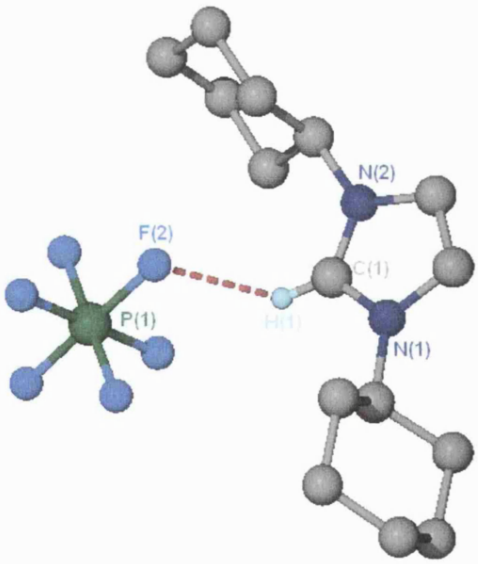


**Figure 3.27.** Molecular structure of **93** determined by X-ray crystallography.

| Bond lengths (Å) | | | |
|---|---|---|---|
| F(1)-H(1) | 2.236(16) | N(2)-C(1) | 1.3240(17) |
| N(1)-C(1) | 1.3263(17) | | |
| **Bond angles (°)** | | | |
| P(1)-F(1)-H(1) | 123.4(4) | C(1)-N(1)-C(2) | 108.02(11) |

**Table 3.14.** Selected bond lengths and angles for **93**.

Datt noted the formation of what appeared to be the cationic rhodium species $[Rh(IMes)(PPh_3)(CO)_3]^+$ and $[Rh(Mes)(P(O\text{-}2,4\text{-}^tBu_2\text{-}Ph)_3)(CO)_3]^+$ from [Rh(IMes)(acac)(CO)], with addition of $PPh_3$ and $P(O\text{-}2,4\text{-}^tBu_2\text{-}Ph)_3$ respectively, in the hydroformylation reaction described earlier (section 3.3.3.2.).[42] The conditions of this reaction are much harsher (85 °C and 20 bar $H_2$:$CO_2$) than needed to form **89** and **90** but nonetheless show that cationic rhodium species forming from neutral Rh(I) precursors is not without precedent.

Very recently, Haynes and co-workers have synthesised rhodium cations bearing chelating ligands, with two NHC moieties and a pyrimidine group all bound to the rhodium centre, as well as a CO ligand (figure 3.28.).[74] This complex is formed by reacting the free tridentate NHC with the dimeric species, $[\{Rh(OAc)\}_2(\mu\text{-}CO)_2]$ at 50 °C for 24 hours. The $\nu_{CO}$ stretching frequencies of these complexes (R = Me (1982 $cm^{-1}$), R = Et (1983 $cm^{-1}$), R = $CH_2Ph$ (1982 $cm^{-1}$)) are higher than observed in **89** and **90**, suggesting that the tridentate ligand is not as good a donor as the three monodentate NHC ligands.

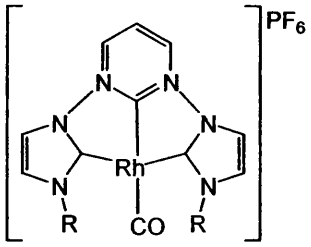


R = Me, Et, $CH_2Ph$

**Figure 3.28.** Chelating ligand on rhodium centre to give cationic species.

*3.5.5.1. Mechanism of formation of $[Rh(NHC)_3(CO)]^+$*

The fact the cations form from the dimeric species discussed earlier (sections 3.5.4.1. and 3.5.4.2.) has been confirmed by the synthesis of a mixed NHC species. Starting from an isolated solution of the mixed dimer $[\{Rh(I^iPr_2Me_2)\}_2(\mu\text{-}CO)_2\{Rh(PPh_3)_2\}]$ (**87**), approximately one equivalent of ICy was added and led immediately to $[Rh(I^iPr_2Me_2)_2(ICy)(CO)]^+$ (**95**) (scheme 3.22.).

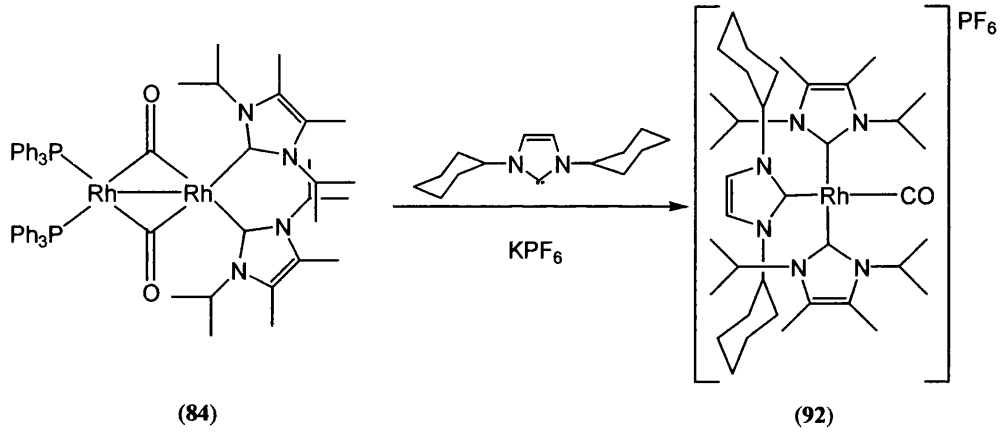


(84) (92)

**Scheme 3.22.** Formation of **93** from **87**.

**93** was isolated and crystallised as the $[PF_6]^-$ salt. The crystal structure is shown in figure 3.29. along with the table of bond lengths and angles (table 3.14.). The ICy NHC has joined the rhodium centre *trans* to the CO group. As in **89** and **90**, the Rh-carbene bond length (2.1341(13) Å) *trans* to CO is longer than the Rh-C bonds to the two $I^iPr_2Me_2$ ligands (2.0818(13) and 2.0677(13) Å), which are *trans* to each other.

The mechanism of formation of cationic species from the dimeric species, presumably results from decomposition of the dimer into two three-coordinate Rh(I) species. These then react with a molecule of free NHC in solution to give the cations (scheme 3.23.). The presence of a bis phosphine intermediate resulting from the breakdown of **87** is supported by the appearance of a doublet in the $^{31}P\{^1H\}$ NMR spectrum at δ 34.5 ($J_{PRh}$ = 205.9 Hz) upon addition of one equivalent of $I^iPr_2Me_2$ to **87** at room temperature. This species disappears upon further addition of $I^iPr_2Me_2$.

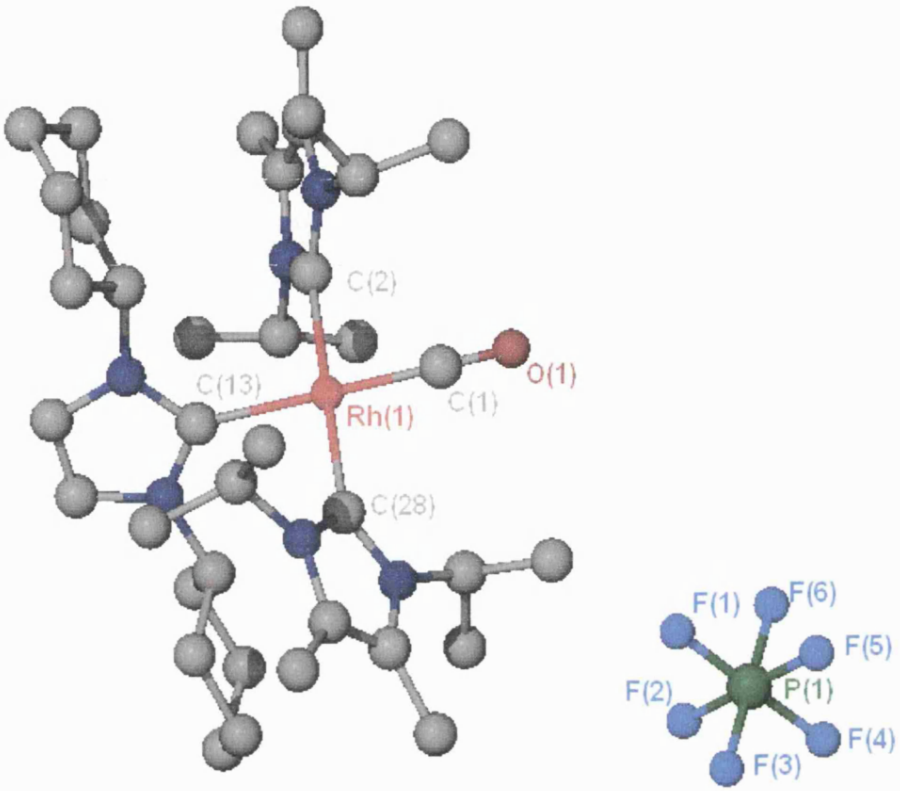


**Figure 3.29.** Molecular structure of **95** determined by X-ray crystallography.

| **Bond lengths (Å)** | | | |
|---|---|---|---|
| Rh(1)-C(1) | 1.8392(14) | Rh(1)-C(2) | 2.0677(13) |
| Rh(1)-C(28) | 2.0818(13) | Rh(1)-C(13) | 2.1341(13) |
| **Bond angles (°)** | | | |
| C(1)-Rh(1)-C(2) | 87.26(6) | C(1)-Rh(1)-C(28) | 92.26(6) |
| C(2)-Rh(1)-C(28) | 178.34(5) | C(1)-Rh(1)-C(13) | 173.92(6) |
| C(2)-Rh(1)-C(13) | 89.93(5) | C(28)-Rh(1)-C(13) | 90.70(5) |

**Table 3.15.** Selected bond lengths and angles for **95**.

Although free phosphine is present in solution, NHC must react more favourably with the three-coordinate species, or substitute any phosphine ligand that binds there. It also appears that using ICy as the NHC causes the reaction from dimer through to cation to proceed more rapidly that with $I^iPr_2Me_2$ as ICy dimeric species were only observed when the amount of ICy added was substantially reduced. The higher instability of ICy dimers may result from the poorer electron donating ability of ICy compared to $I^iPr_2Me_2$ or from the larger steric bulk of $I^iPr_2Me_2$ compared to

ICy stabilising the dimeric species. This fact has already been discussed as the possible cause of the lack of observed formation of mononuclear complexes bearing *cis* ICy ligands (page 180).

Following the reaction between $[RhH(PPh_3)_3(CO)]$ **70** and free $I^iPr_2Me_2$ supports the observation that the cationic species form after the hydridic and dimeric species in solution. **67** (0.05 g) and $I^iPr_2Me_2$ (4 equivalents) were placed into a J. Young's resealable ampoule in the glove box. Upon removal from the glove box, THF (approximately 1 mL) was added to the solids. The mixture was briefly agitated to encourage dissolution of the solids and the solution was rapidly transferred to an IR solution cell. An IR spectrum of the solution was recorded approximately every two minutes. Initially (within three minutes of dissolving starting materials) the CO stretching frequency of the bis NHC hydride complex $[RhH(I^iPr_2Me_2)_2(CO)]$ (**84**) was the most intense peak (1924 $cm^{-1}$), with a small amount of two or more dimeric species present (1602 $cm^{-1}$ and 1577 $cm^{-1}$). These lower wavenumber peaks grew over the next 130 minutes and the peak at 1924 $cm^{-1}$ began to lose intensity. The appearance of a new terminal CO peak at 1973 $cm^{-1}$ attributed to $[Rh(I^iPr_2Me_2)_3(CO)]^+$ (**89**) also appeared (figure 3.30.). This suggests that the hydridic complex forms almost instantaneously, followed very rapidly by the dimeric compounds. The cationic species begin to appear after approximately 6 minutes and become more prevalent over a further two hours. The loss of **89** and the dimeric species during this time without the formation of any other CO-containing species suggests that the cationic species do form as a result of a breakdown of the dimeric complexes.

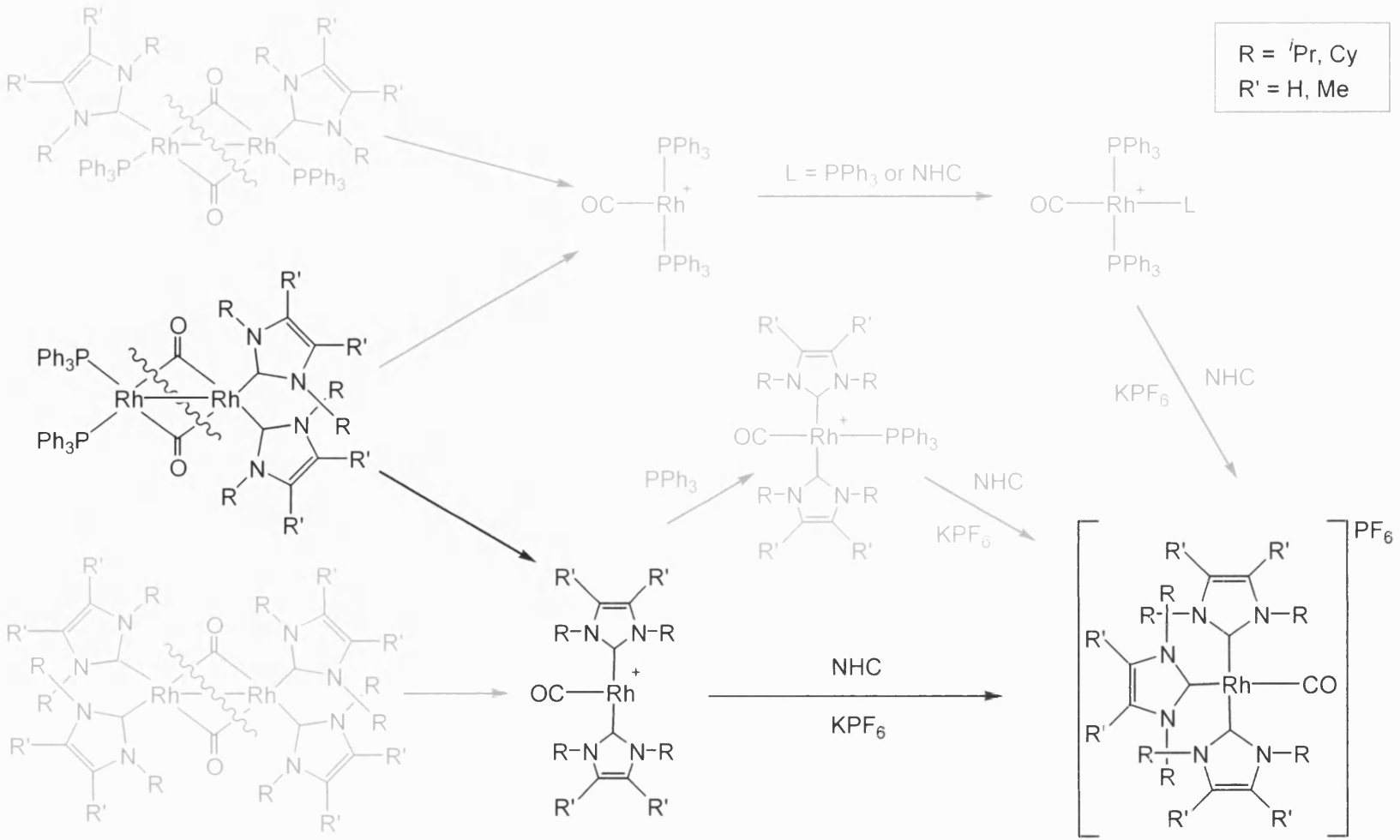


**Scheme 3.23.** Possible mechanism to show formation of cationic rhodium complexes $[Rh(NHC)_3(CO)][X]$.

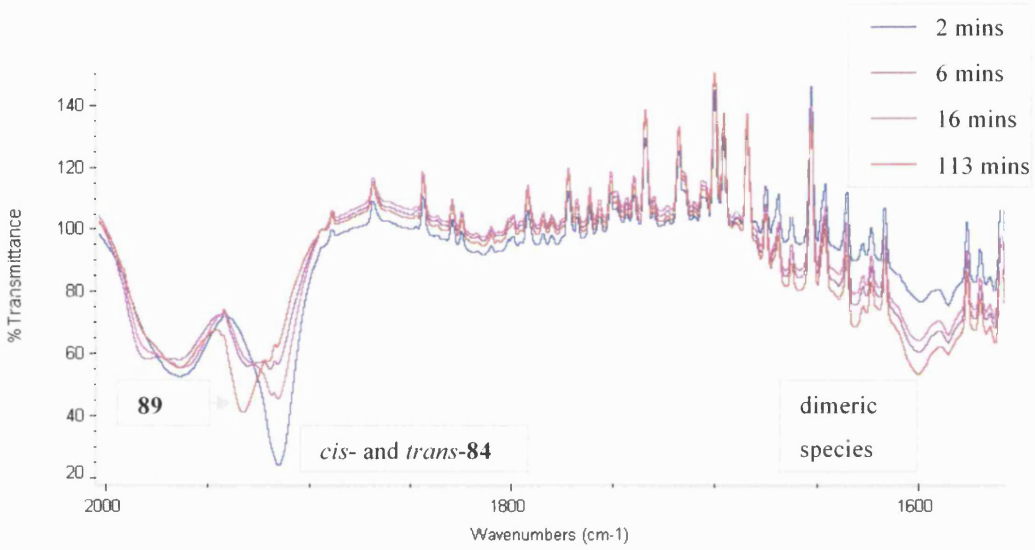


**Figure 3.30.** Monitoring formation of products from reaction of **70** and $I^iPr_2Me_2$ run in a solution cell in THF.

*3.5.5.2. NMR studies of $[Rh(NHC)_3(CO)]^+$*

$^{13}C\{^1H\}$ NMR studies of **89** and **90** show two distinct low field doublet resonances assigned to the Rh-carbene carbon (**89**: δ 179.5 ($J_{CRh}$ = 39.5 Hz), 179.0 ($J_{CRh}$ = 43.2 Hz); **90** δ 180.6 ($J_{CRh}$ = 42.3 Hz), 178.7 ($J_{CRh}$ = 46.0 Hz)). Those with the smaller *J* values are likely to be *trans* to the carbonyl group as it is a good π-acceptor and hence leads to a decrease in the coupling constant.[75] The $^1H$ NMR spectrum also shows resonances, in a 2:1 ratio, for the backbone protons and the N-substituents, as would be expected. **89** exhibits broadening of all the peaks in the $^1H$ NMR spectrum at room temperature. Cooling a sample of **89** in $CD_2Cl_2$ to -70 °C in the NMR spectrometer led to the appearance of three resonances for the CH protons on the $^i$Pr arms (δ 5.88, 5.16, 5.00 compared to the two signals at δ 5.50 and 5.00 seen at room temperature). The significant splitting of the two components of the peak at 5.50 ppm to two distinct peaks at 5.88 and 5.16 ppm suggests that when the ligands are static, the CO group has a big impact on the shift of the protons. Its high electron density causes the protons closer to it to be shielded and pushes their NMR resonances upfield. Cooling of a sample of **89** leads to a initial broadening of the methyl resonances between δ 2.5 and δ 0.5. These then sharpen and separate at -70

°C. The change in $^1$H NMR spectrum for **89** over a series of temperatures is shown in figure 3.31.

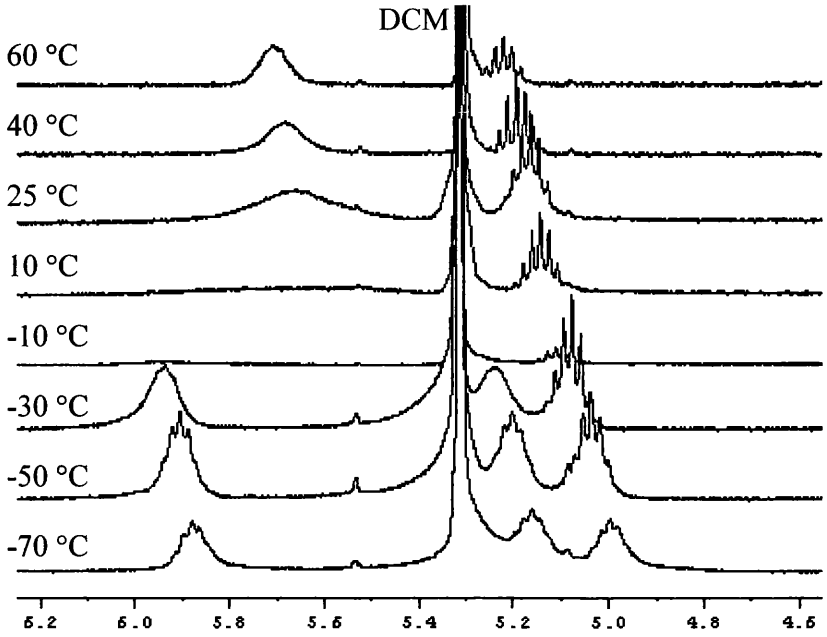


**Figure 3.31.** VT spectroscopy studies of the NCH protons in **89** in $CD_2Cl_2$ (400 MHz).

3.5.6. Formation of $[Rh(NHC)_4]^+$

Similar cationic species to those formed from reaction of $[RhH(PPh_3)_3(CO)]$ (**70**) with NHCs have been observed from the reaction of $[RhH(PPh_3)_4]$ (**69**) with alkyl NHCs to give complexes of the general formula $[Rh(NHC)_4]^+$ (NHC = $IEt_2Me_2$ (**96**), $I^iPr_2Me_2$ (**97**), ICy (**98**)). These only form in very small yield (approximately 5-10 %) and although all the cations have been fully characterised by heteronuclear NMR, the only crystal structure that has been obtained with a solvable anion is $[Rh(IEt_2Me_2)_4][PPh_2O_2]$ (**96**) (figure 3.32.). This complex is almost exactly square planar (table 3.16.) and the Rh-C bonds are all the same length (2.04 Å), within experimental error.

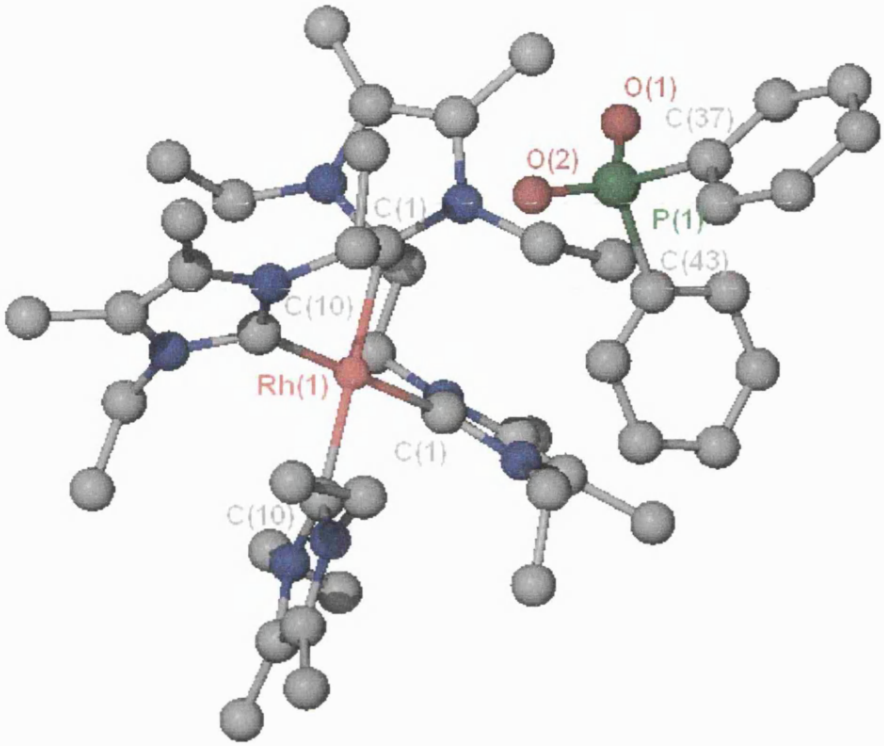


**Figure 3.32.** Molecular structure of **96** determined by X-ray crystallography (two molecules of $C_6H_6$ removed for clarity).

| **Bond lengths (Å)** | | | |
|---|---|---|---|
| Rh(1)-C(1) | 2.042(4) | Rh(1)-C(1)' | 2.042(4) |
| Rh(1)-C(10)' | 2.047(4) | Rh(1)-C(10) | 2.047(4) |
| **Bond angles (°)** | | | |
| C(1)-Rh(1)-C(10)' | 179.86(18) | C(19)-Rh(2)-C(19)' | 90.1(2) |
| C(28)'-Rh(2)-C(19) | 178.97(17) | C(10)'-Rh(1)-C(10) | 89.7(2) |
| C(1)'-Rh(1)-C(10)' | 90.37(14) | C(28)-Rh(2)-C(28)' | 89.6(2) |
| C(28)'-Rh(2)-C(19)' | 90.18(13) | C(1)-Rh(1)-C(1)' | 89.5(2) |

**Table 3.16.** Selected bond lengths and angles for **96**.

The only similar structures in the literature are two tetrakis silylene complexes recently synthesised by Pfaltz and co-workers (**99** and **100**) (scheme 3.24.).[76]

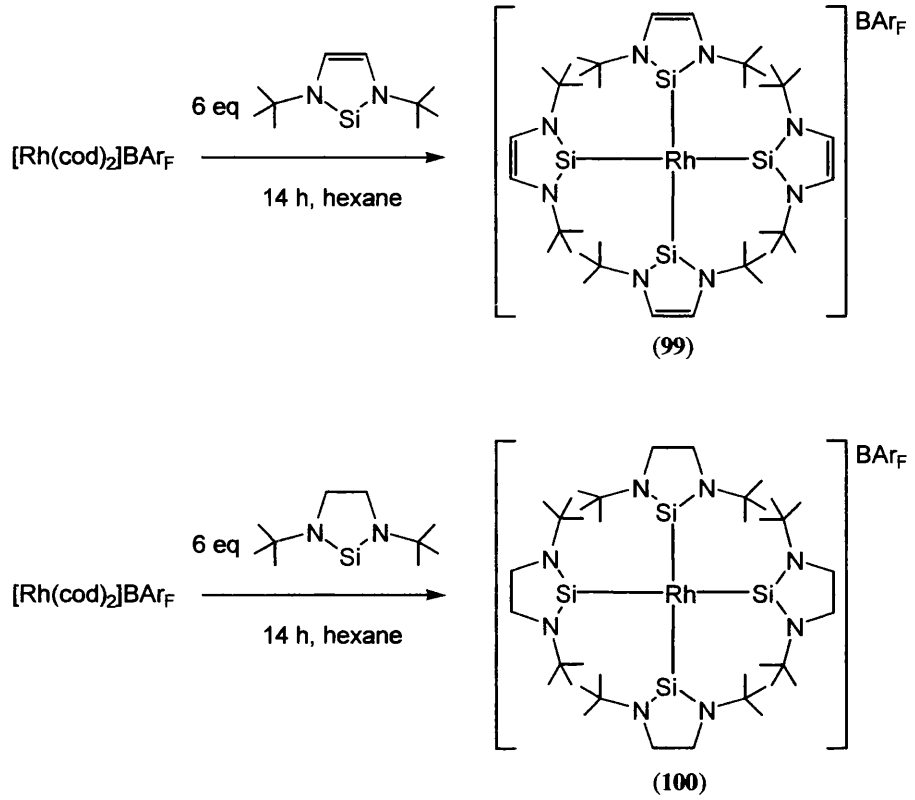


**Scheme 3.24.** Synthesis of **99** and **100** by Pfaltz and co-workers.

Pfaltz obtained crystal structures of both complexes. As would be expected, the Rh-Si bonds (all close to 2.3 Å) are somewhat longer than the Rh-carbene bonds in **96**. **99** and **100** are also square planar, although slightly more distorted than **96** (**99**: Si(1)-Rh(1)-Si(1)' = 94.63(4) °, Si(1)-Rh(1)-Si(2) = 173.86(2) °, Si(1)-Rh(1)-Si(2)' = 86.72(2) °, **96**: C(1)-Rh(1)-C(1)' = 89.5 °, C(1)'-Rh(1)-C(10) = 179.86 °, C(1)'-Rh(1)-C(10)' = 90.31 °). Again, this is probably a steric effect. The rhodium atom and the four carbenic carbons of **96** all lie in the same plane. The imidazole rings of the NHC ligands sit out of the plane by 63.048 ° and 60.920 ° with the ligands lying *trans* to each other being exactly perpendicular. (figure 3.33.).

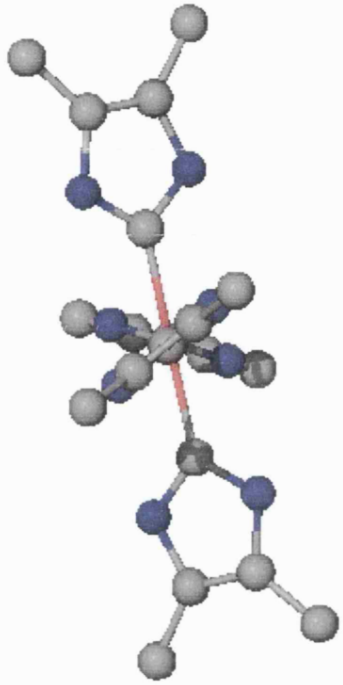

**Figure 3.33.** Position of four $IEt_2Me_2$ groups in X-ray crystallographic structure of **96** (ethyl groups removed for clarity).

This complex is extremely symmetrical and, for this reason, interpretation of the $^1H$ and $^{31}C\{^1H\}$ NMR spectra is straightforward. There is one low field resonance in the $^{13}C\{^1H\}$ NMR spectrum at δ 192.3 (d, $J_{CRh}$ = 45.0 Hz), from the carbenic carbon while the methyl protons on the imidazole backbone and on the ethyl arms each give only one resonance in the $^1H$ NMR spectrum at δ 2.04 and 0.44 respectively. There are, however, two resonances observed for the methylene protons from the ethyl groups (δ 5.41 and 3.78). This is due to restricted rotation of the N-substituents causing the two methylene protons to become diastereotopic (figure 3.34.). This inequivalence is also apparent from the splitting patterns of these peaks, which are doublets of quartets, coupling not only to the methyl group but also to each other ($^2J_{HH}$ = 6.6 Hz, $^3J_{HMe}$ = 7.1 Hz). The more deshielded protons, which would be those pointing away from the metal centre, can be attributed to the shift at 5.41 ppm.

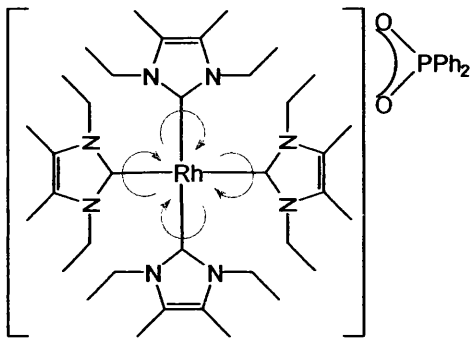


**Figure 3.34.** NHCs rotate around the Rh-C bonds in **96** but the ethyl arms are static leading to different environments for the methylene protons by NMR.

A crystal structure of $[Rh(ICy)_4]^+$ (**98**) has also been obtained but in this instance it was impossible to solve the anion crystallographically (figure 3.35.). The cation, however, shows similar characteristics to **96**. The *trans* NHCs are perpendicular to each other, although their angle out of the plane is much less than in **96** (51.226 ° for all four imidazole rings) presumably reflecting the larger steric bulk of the cyclohexyl rings compared to the ethyl groups. **98** is more symmetrical than **96**, with the geometry being exactly square planar. The Rh-carbene bonds in **98** (table 3.17, all 2.070 (5) Å) are also longer than in **96**. This suggests that $IEt_2Me_2$ is a better σ donor than ICy, probably due to the methyl groups on the backbone.

The $^1H$ NMR spectrum of **98** is straightforward, like that of **96**, exhibiting only three resonances: a singlet at δ 7.41 for the NHC backbone protons, a broad multiplet at δ 6.30-4.42 for the *ipso* protons on the cyclohexyl arms and another broad multiplet at δ 2.81-0.73 for the $CH_2$ protons on the cyclohexyl groups. This shows that the four NHC ligands around the rhodium centre are all in the same environment.

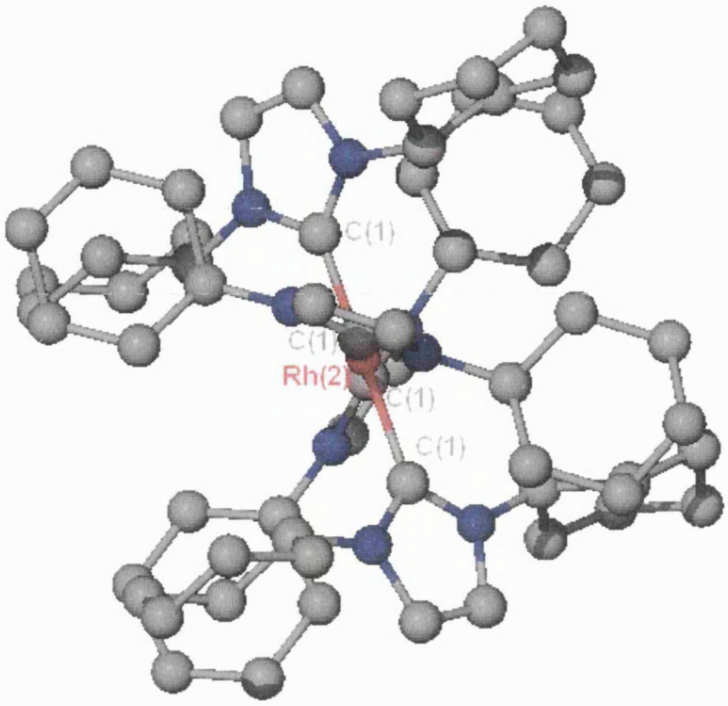


**Figure 3.35.** Molecular structure of **98** determined by X-ray crystallography.

| **Bond lengths (Å)** | | | |
|---|---|---|---|
| Rh(1)-C(1) | 2.070(5) | Rh(1)-C(1)' | 2.070(5) |
| Rh(1)-C(10)' | 2.070(5) | Rh(1)-C(10) | 2.070(5) |
| **Bond angles (°)** | | | |
| C(1)'-Rh(2)-C(1) | 179.8(3) | C(1)-Rh(2)-C(1)''' | 90.000(1) |
| C(1)''-Rh(2)-C(1)''' | 179.8(3) | C(1)'-Rh(2)-C(1)'' | 90.000(1) |
| C(1)-Rh(2)-C(1)'' | 90.000(1) | C(1)'-Rh(2)-C(1)''' | 90.000(1) |

**Table 3.17.** Bond lengths and angles for **98**.

*3.5.6.1. Substitution of unknown anion in $[Rh(I^iPr_2Me_2)_4]^+$ (97) with $[PF_6]^-$*

Unfortunately, substitution of the anions that formed in solution with the tetrakis NHC species was not as facile as in the $[Rh(NHC)_3(CO)]^+$ species. Only the anion in **97** was successfully substituted with $[PF_6]^-$ to give the complex $[Rh(I^iPr_3Me_2)_4][PF_6]$ (**101**). This was isolated as a crystalline solid but unfortunately the crystal structure had significant internal disorder meaning that it was impossible to refine to a high standard. This was attributed to the high symmetry of the complex. Interestingly,

however, the substitution of the anions in **97** by $[PF_6]^-$ caused the crystalline solid to change from yellow to purple.

3.5.6.1.1. UV visible studies on $[Rh(I^iPr_2Me_2)_4]^+$ with $[PF_6]^-$ and the unknown anion

UV-visible spectra of both **97** and **101** were recorded (figure 3.36.). Ideally, the UV-visible spectrum of a square planar $d_8$ complex, such as **101**, should show three charge transfer bands from the three possible movements of electrons shown in figure 3.37.

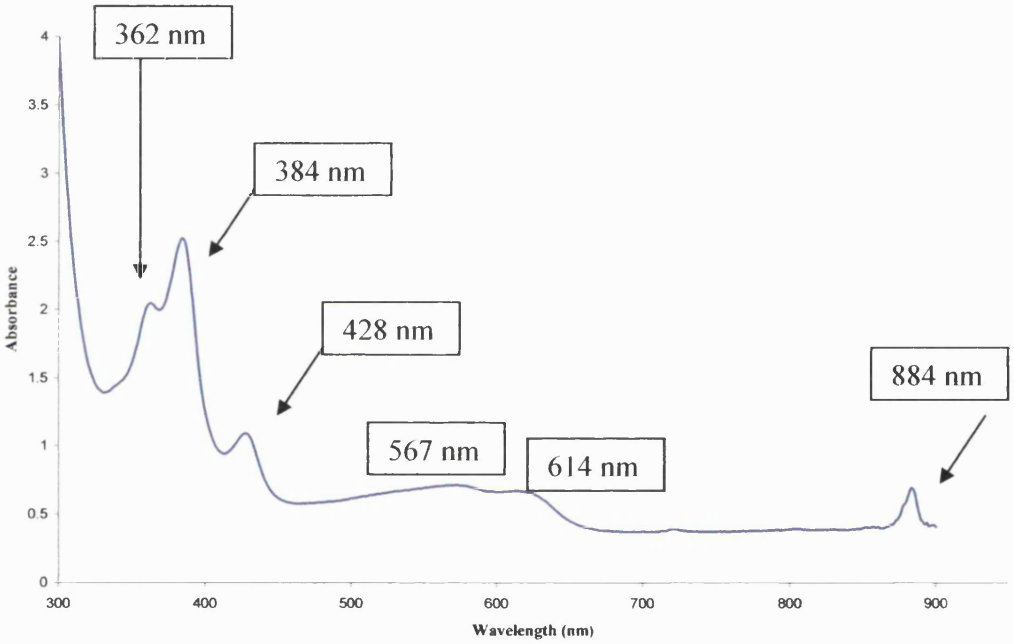


**Figure 3.36.** UV-visible spectrum of **101** run in $CH_2Cl_2$ at room temperature.

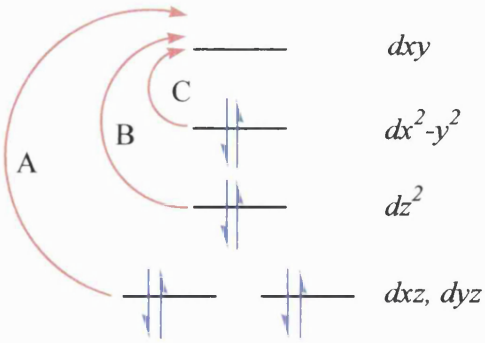


**Figure 3.37.** *d-d* transitions possible upon irradiation with UV light.

The UV-visible spectrum of **101** is more complicated than the expected three transitions. This could be due to charge transfers taking place between the metal and the ligands. These are likely to be metal to ligand charge transfers (MLCT). Aromatic ligands often show MLCT transitions as they have low-lying $\pi^*$ orbitals.[77] The imidazolium moiety of an NHC is strictly aromatic by application of Hückel's rule, which states that an aromatic ring must be planar with a *p* orbital on each atom and that the *p* orbital system must contain $(4n + 2)$ $\pi$ electrons overall (where n is any integer).[78] As the imidazole ring has 6 $\pi$ electrons it, it fits this rule and can be considered aromatic. In addition, the low oxidation state of the rhodium (I) centre means that its *d* orbitals will be relatively high in energy and the transitions will be able to occur at low energy.[77]

$[Rh(CNEt)_4]^+$, another Rh(I) square planar complex, shows five bands in the UV-visible spectrum (435 nm, 380 nm, 333 nm, 308 nm, 282 nm).[79] These are all assigned to MLCT and these are likely to obscure any *d-d* transitions that are occurring. The same phenomenon is seen in $[Rh(diphos)_2]^+$ complexes (diphos = 1,2-bis(diphenylphosphino)ethane or 1,2-bis(diphenylphosphino)ethene).[80,81]

A UV-visible spectrum was run of **97** to compare the spectrum of the complex before substitution of the unknown anions by $[PF_6]^-$. This showed substantial differences in the lower end of the spectrum (figure 3.38.).

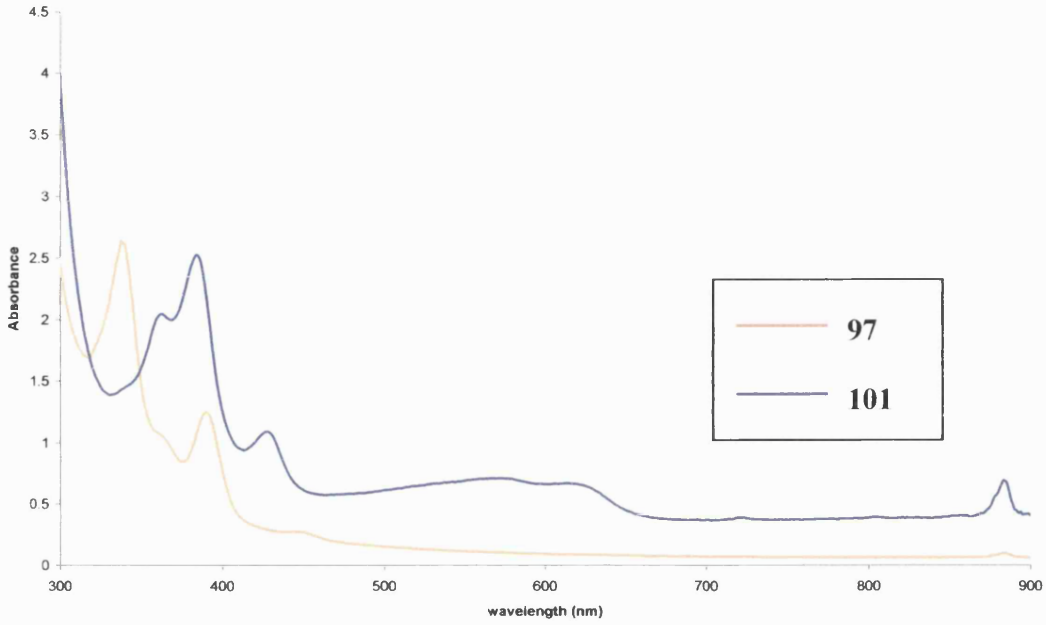


**Figure 3.38.** Comparison of UV spectra of **97** and **101** (run in $CH_2Cl_2$) at room temperature.

3.5.6.1.2. NMR studies on $[Rh(I^iPr_2Me_2)_4]^+$ with $[PF_6]^-$ and the unknown anion

The $^1H$ NMR spectrum of **101** is extremely broad and does not sharpen even at -70 °C. There is also no change to the spectrum at higher temperatures (up to 50 °C). This suggests that the complex has a much more convoluted structure in solution than is expected. Conversely, the $^1H$ NMR of **97** is simple and straightforward like that observed in **96** and **98** (and discussed on pages 201 and 202), showing just four resonances, a septet at δ 6.07 ($^3J_{HH}$ = 7.2 Hz) due to the CH protons on the $^i$Pr arms, a singlet at δ 2.16 from the backbone methyl groups and two doublets at δ 1.46 ($^3J_{HH}$ = 7.2 Hz) and 0.58 ($^3J_{HH}$ = 7.2 Hz) due to the methyl groups on the $^i$Pr arms (figure 3.39.).

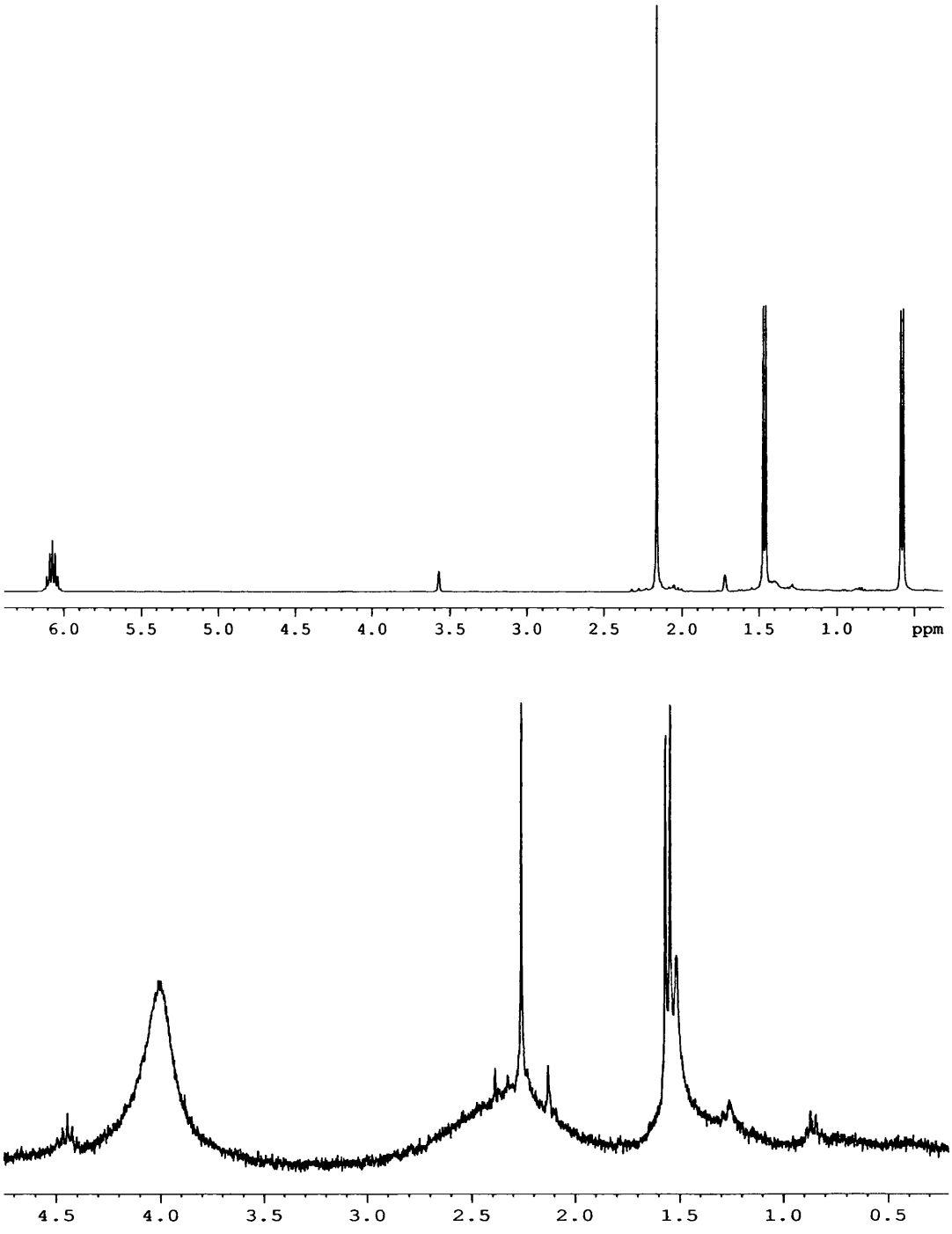


**Figure 3.39.** $^{1}H$ NMR of **97** (top, in $d_8$-THF) and **101** (bottom in $CD_2Cl_2$) (400MHz, 25 °C).

The difference between the UV-visible and $^1$H NMR spectra for **97** and **101** indicates the importance of the anion in these complexes. Unfortunately attempts to replace the anion in **97** with $BPh_4^-$ or $OTf^-$ led to decomposition of the complex to give the hydrogen bonded imidazolium species $I^iPr_2Me_2HBPh_4$ and $I^iPr_2Me_2HOTf$, which are similar to $[PF_6]^-$ complexes which have been isolated and discussed on page 191.

### *3.5.6.2. Mechanism of formation of $[Rh(NHC)_4]^+$*

The probability that these tetrakis NHC complexes form from the initial hydride containing species, **71**, **72**, **73**, **74**, **75** and **76**, analysed in section 3.5.1. is supported by plotting the ratio of the hydride peaks in the $^1$H NMR spectrum to the aromatic region at a series of times during the first 14 hours of the reaction. The number of aromatic protons will be the same at any point in the reaction and so the whole region can be set as one integral and given an arbitrary value. The hydride integrals can then be directly compared to each other and the total reaction mixture. As can be seen in figure 3.40., when 2 equivalents of ICy are added to $[RhH(PPh_3)_4]$ (**69**) at room temperature, *trans*-**73** forms extremely rapidly and some *cis*-**73** is also present. These rapidly decrease in intensity over time and although there is growth of the bis NHC products, *cis*- and *trans*-**76**, the major product is obviously something non-hydridic. The formation of any dimeric products analogous to $[\{Rh(PPh_2)_2\}(\mu\text{-}H)(\mu\text{-}PPh_2)]$ (**83**) have not been observed and it is feasible that these type of complexes do not form or that if they do are extremely unstable and break apart too rapidly to be seen on a NMR timescale. Certainly, even in low temperature $^1$H and $^{31}P\{^1H\}$ NMR experiments, no evidence for bridging hydride or phosphide ligands has been observed.

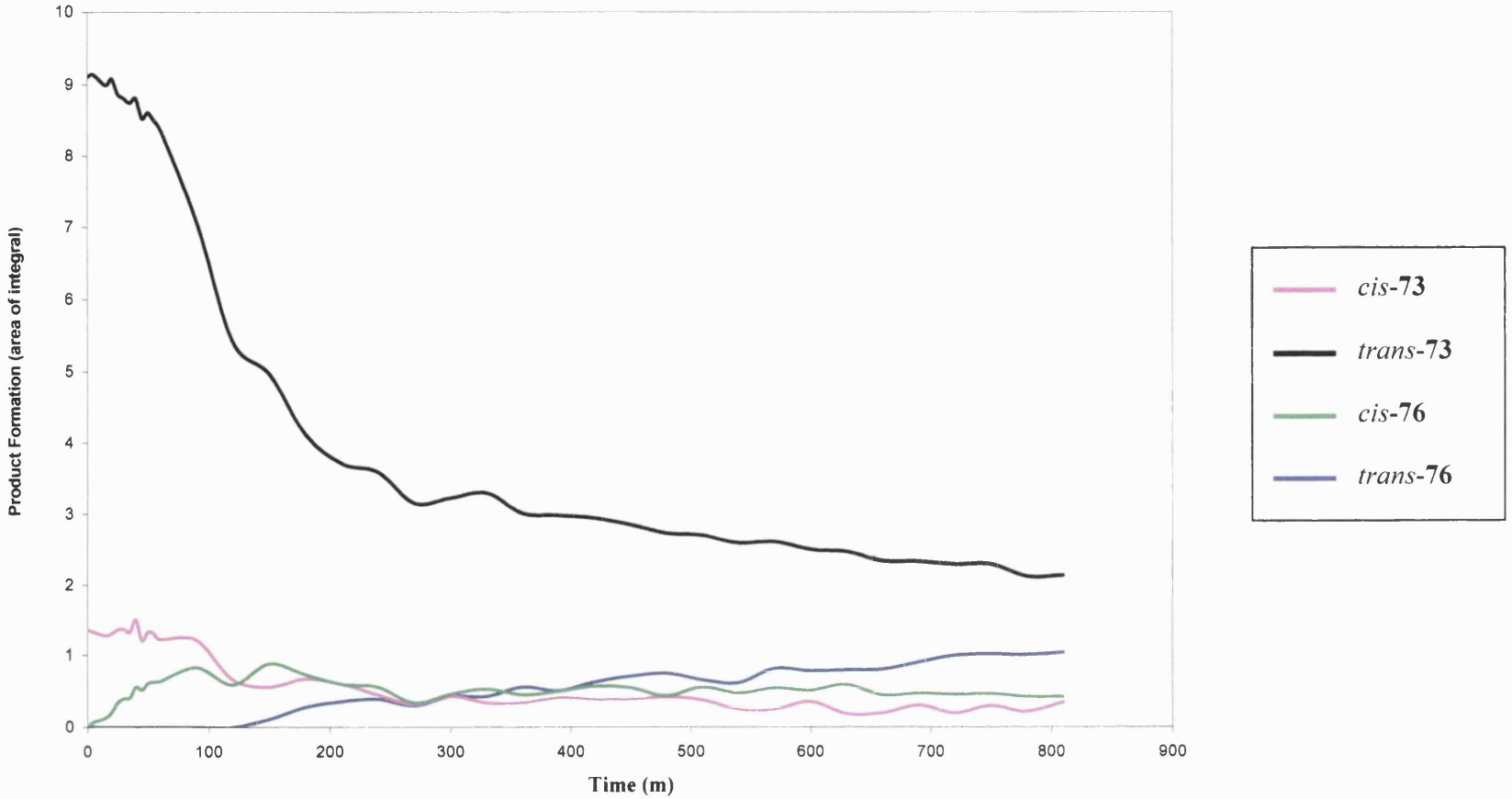


**Figure 3.40.** Formation of hydride containing products in the reaction of **69** and 2 eq. ICy.

### 3.5.7. Thermolysis of [RhH(PPh$_3$)$_3$(CO)] (70)

Like [RhH(PPh$_3$)$_4$] (**69**), when the carbonyl complex [RhH(PPh$_3$)$_3$(CO)] (**70**) is heated at 70 °C overnight it appears to form a dimeric species with a bridging PPh$_2$ ligand. This is attributed to [{Rh(CO)}$_2$(μ-H)(μ-PPh$_2$)] (**102**) (figure 3.41.).

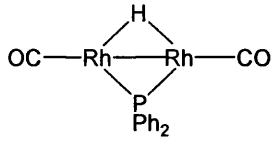


**Figure 3.41.** Proposed structure of **102**.

The coupling patterns for the hydride ligand and the bridging phosphide are much simpler than in **83**, showing that there are no terminal phosphines. The $^1$H NMR has one hydride peak at δ -11.65 (dt, $^2J_{HP}$ = 16 Hz $^1J_{HRh}$ = 20 Hz). The peak is distorted due to the similarity of the coupling constants causing the triplet signals to overlap (figure 3.42.). The $^{31}$P{$^1$H} NMR spectrum exhibits a shift at δ 186.2 (t, $^1J_{PRh}$ = 117.3 Hz), characteristic of a bridging PPh$_2$ over a Rh-Rh bond (see section 3.5.4.1.). The hydride and bridging phosphine peaks are clearly shown to couple to each other from a $^{31}$P{$^1$H} HMQC experiment. To add further credibility to this structure, the $^{13}$C{$^1$H} NMR has a doublet of triplets at δ 208.9 ($^2J_{CP}$ = 10.1 Hz $^1J_{CRh}$ = 60.4 Hz).

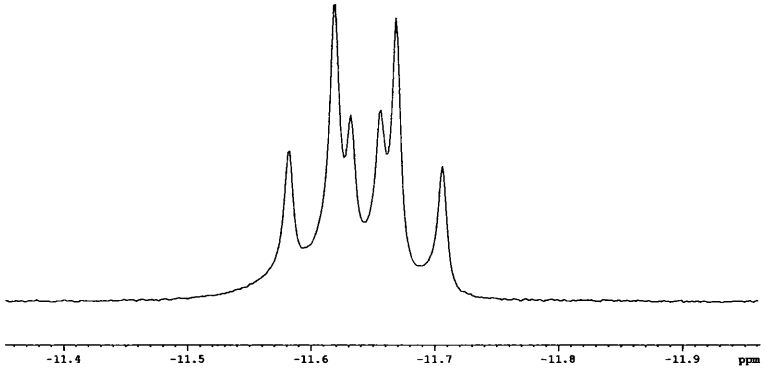


**Figure 3.42.** Hydride resonance of **102** in $d_8$-THF (400 MHz, 25 °C).

Upon further heating, a trimeric complex can also be seen by multinuclear NMR. This was identified by X-ray crystallography as [{Rh(CO)}$_3$(PPh$_3$)$_2$(μ-PPh$_2$)$_3$] (**103**)

(figure 3.43.) and has already been synthesised by Billig *et al.*[82] The $^{31}P\{^{1}H\}$ NMR shows a multiplet at δ 135.0 for the bridging phosphines and another multiplet at δ 41.5 for the terminal phosphines. The unique Rh atom in **103** is coordinatively unsaturated, being only 14-electron. However, as a cluster, the complex is 46-electron, which is known amongst these sort of structures.[83] The electrons are likely to be delocalised over the three rhodium centres, adding stability to the complex.

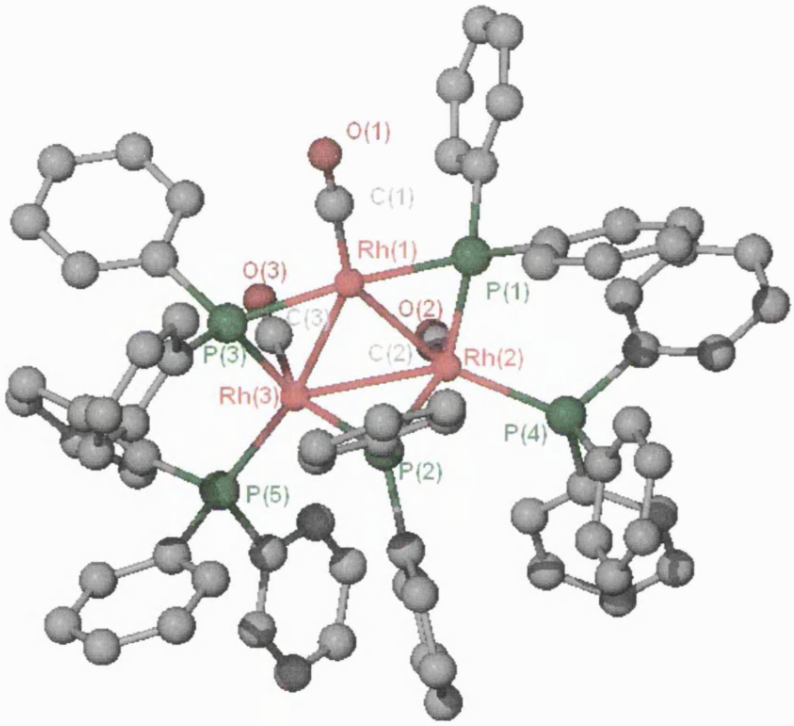


**Figure 3.43.** Molecular structure of **103** determined by X-ray crystallography.

**103** could well form from **102** and residual **70** in solution with the loss of two $PPh_3$ ligands and two molecules of benzene.

### 3.5.8. Reactivity of rhodium-NHC complexes

Preliminary studies have been carried out to probe the reactivity of the Rh-NHC complexes reported in this chapter. Addition of $CO_2$ to solutions containing the

hydridic species *cis*- and *trans*-[RhH(I$^i$Pr$_2$Me$_2$)(PPh$_3$)$_2$] (**72**), *cis*- and *trans*-[RhH(I$^i$Pr$_2$Me$_2$)$_2$(PPh$_3$)] (**75**), *cis*- and *trans*-[RhH(ICy)(PPh$_3$)$_2$] (**73**) and *cis*- and *trans*-[RhH(ICy)$_2$(PPh$_3$)] (**76**) led to insertion of $CO_2$ in all cases into the Rh-H bonds. However, reactivity of the mono and bis NHC complexes was generally very different. The mono NHC species, **72** and **73**, only reacted when subjected to more than one atmosphere of $CO_2$ and immediately underwent loss of $CO_2$ to reform the hydride complexes when the $CO_2$ atmosphere was removed. In contrast, the *cis*- and *trans*-isomers of the bis NHC species **75** and **76** reacted readily with 1 atmosphere of $CO_2$ and did not decompose when the solution was degassed and placed under argon, giving *cis* and *trans*-[Rh(I$^i$Pr$_2$Me$_2$)$_2$(PPh$_3$)(OC(O)H)] (**104**) and *cis* and *trans*-[Rh(ICy)$_2$(PPh$_3$)(OC(O)H)] (**105**) respectively. As the *trans* isomers of the bis NHC hydride complexes are predominant in solution the *trans* isomers of the formate complexes (figure 3.44.) were easier characterise by NMR spectroscopy and so all data presented here refers to the *trans* isomers. *Trans*-**105** gave a characteristic peak in the $^1$H NMR spectrum at δ 8.60 (dd, $J_{HRh}$ = 1.6 Hz, $^2J_{HP}$ = 7.1 Hz) for the formate proton.

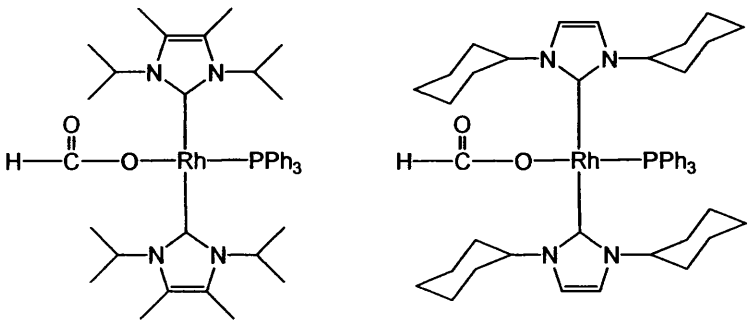


(104) (105)

**Figure 3.44.** Structures of **104** and **105**.

The bis NHC carbonyl species, **85** and **86** reacted with $CO_2$ in a similar manner to give [Rh(ICy)$_2$(CO)(OC(O)H)] (**106**) and [Rh(IMes)$_2$(CO)(OC(O)H)] (**107**) (figure 3.45.). Again, they exhibit the characteristic formate proton peak by NMR at δ 8.60 ($J_{HC}$ (with $^{13}CO_2$) = 188.8 Hz, $^3J_{HRh}$ = 1.6 Hz) (**106**) and 8.00 (**107**). $^{13}C\{^1H\}$ NMR spectroscopy also gives characteristic resonances for the formate carbon at δ 167.0

for **106** and δ 167.3 (which is split to a doublet ($J_{CH}$ = 188.3 Hz) upon use of $^{13}CO_2$) for **107**.

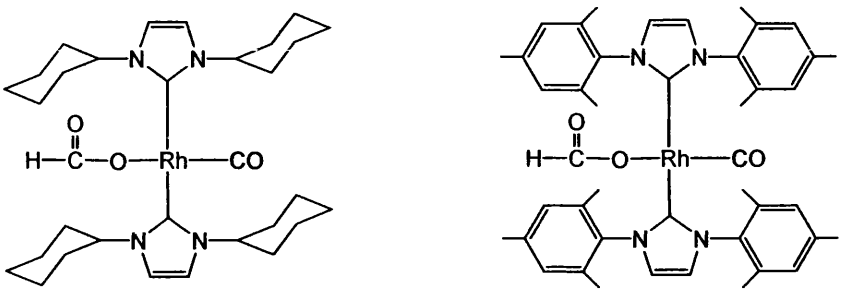

(106) (107)

**Figure 3.45.** Structures of **106** and **107**.

The fact that $CO_2$ is indeed inserting into **86** was confirmed by IR spectroscopy. In **107**, made from $^{12}CO_2$, IR bands appear at 1932 ($\nu_{CO}$), 1633 ($\nu_{OCOasym}$) and 1320 ($\nu_{OCOsym}$) $cm^{-1}$. When $^{13}CO_2$ was added to **86** to give $^{(13)}$**107**, the formate bands shifted to 1594 ($\nu_{OCOasym}$) and 1263 ($\nu_{OCOsym}$) $cm^{-1}$. Reduced mass calculations place the $^{13}C$ formate bands at 1561 and 1262 $cm^{-1}$.

CHN studies showed that the empirical formula was correct ({found (calculated)} for **107**: C {67.12 (67.34)} H {5.88 (6.29)} N {7.15 (7.14)}) but attempts to study crystals of **107** by X-ray diffraction proved difficult as there was extensive disorder across the formate and CO groups. This meant that it was impossible to see whether the OC(O)H group was bound to the rhodium in a $\kappa^1$ or $\kappa^2$ manner (figure 3.46.).

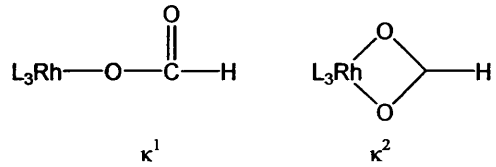

$\kappa^1$ $\kappa^2$

**Figure 3.46.** The two possible bonding modes of a formate group to a metal centre.

The frequency of the asymmetric $\nu_{OCO}$ IR band of **107** (1633 $cm^{-1}$) is indicative of a $\kappa^1$ formate species. As discussed in the literature,[84,85] monodentate formate

complexes have asymmetric bands that appear above 1600 $cm^{-1}$, whilst bidentate shifts appear under 1600 $cm^{-1}$.

### 3.5.9. Formation of zwitterionic NHC:$CO_2$ adducts

When $CO_2$ was added to solutions of Rh-NHC complexes that could not be isolated and therefore contained free NHC, large amounts of white solid crashed out of the THF solution upon addition of $CO_2$. The solid obtained from a reaction mixture containing free ICy was isolated, dissolved in $CH_2Cl_2$ and layered with hexane. This produced crystals suitable for X-ray diffraction and allowed the complex to be identified as the zwitterionic NHC:$CO_2$ adduct, ICy:$CO_2$ (**108**). Further studies showed that addition of $CO_2$ to a THF solution containing free NHC ($I^iPr_2Me_2$, ICy, IMes) led to immediate formation of NHC:$CO_2$ adducts. Analogues of these have already been isolated including $I^iPr_2Me_2$:$CO_2$ (**109**)[86], IMe:$CO_2$[87] and IPr:$CO_2$[88] (figure 3.47.).

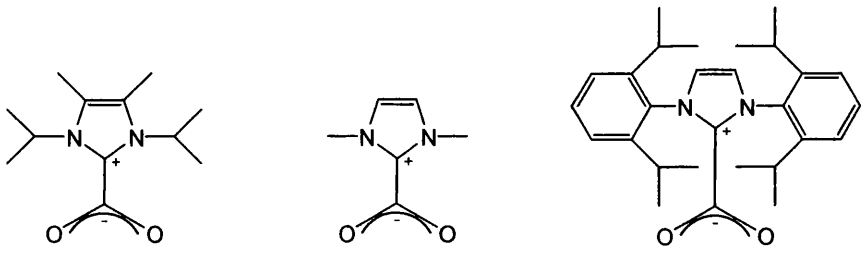

(**109**)

**Figure 3.47.** Structures of reported NHC:$CO_2$ zwitterions.

The crystal structure of **108** is shown in figure 3.48. The significant bond lengths and angles for all four NHC:$CO_2$ adduct structures are compared in table 3.18.. The most significant thing to note is that of all the structures, **108** is the only one that has perceptibly different C-O bond lengths (1.2432(16) and 1.2396(16) Å). This implies that the charge on the OCO moiety is not centralised. In addition, the C-N bond distances of the imidazole ring are quite different (1.3511(16) and 1.3783(17) Å), suggesting the positive charge is also slightly delocalised between one of the

nitrogens and the imidazole ring. This phenomenon has also been noted in IPr:$CO_2$ (C-N distances are 1.334(4) and 1.376(4) Å).[88]

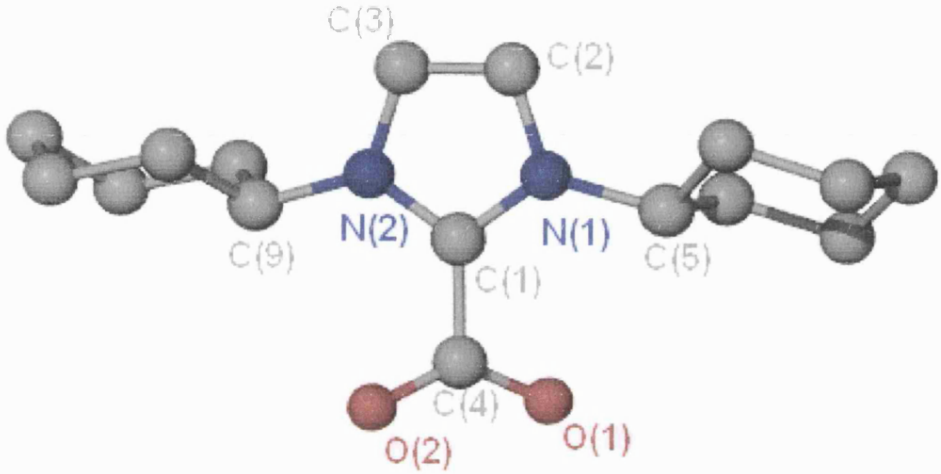


**Figure 3.48.** Molecular structure of **108** determined by X-ray crystallography.

| Bond lengths (Å) | C(4)-O(1) | C(4) - O(2) | C(1)-C(4) | C(1)-N(1) | C(1)-N(2) |
|---|---|---|---|---|---|
| ICy:$CO_2$ (**108**) | 1.2432(16) | 1.2396(16) | 1.5342(18) | 1.3511(16) | 1.3783(17) |
| I$^i$Pr$_2$Me$_2$:$CO_2$ (**109**) | 1.231(3) | 1.231(3) | 1.536(5) | 1.336(3) | 1.336(3) |
| IMe:$CO_2$ | 1.2398(15) | 1.2398(15) | 1.523(3) | 1.3452(16) | 1.3452(16) |
| IPr:$CO_2$ | 1.225(4) | 1.221(4) | 1.511(4) | 1.334(4) | 1.376(4) |

| Bond angles (°) | O(1)-C(4)-O(2) | N(1)-C(1)-N(2) |
|---|---|---|
| ICy:$CO_2$ (**108**) | 130.00(13) | 109.08(11) |
| I$^i$Pr$_2$Me$_2$:$CO_2$ (**109**) | 131.2(4) | 108.0(3) |
| IMe:$CO_2$ | 129.8(2) | 107.15(16) |
| IPr:$CO_2$ | 129.9(3) | 107.1(2) |

**Table 3.18.** Selected bond lengths (Å) and angles (°) for **108** and other NHC:$CO_2$ zwitterions. Numbering system is that used in **108** and is not comparable with published data.

The imidazole ring, the backbone methyl groups and the $CO_2$ carbon all sit in the same plane with the two oxygen atoms 180 ° to each other and 45 ° out of the central plane. The two cyclohexyl rings lie in the same plane as each other and perpendicular to the imidazole ring.

**108** shows two IR bands at 1656 and 1461 $cm^{-1}$ compared with the positions reported for IPr:$CO_2$ at 1687 $cm^{-1}$ [88] and **109** at 1666 and 1437 $cm^{-1}$.[86] Louie *et al.*

report that **109** decarboxylates between 136 and 164 °C.[88] It is also suggested that **109** equilibrates with free $CO_2$, as addition of $^{13}CO_2$ to a solution of **109** leads to enhancement of the carbonyl peak of the complex. This could explain the spurious elemental analysis results obtained for **108**. Although percentage hydrogen and nitrogen measurements were extremely close to values calculated, percentage carbon measured was consistently around 5 % lower than the calculated values. However, no detailed investigation has been carried out into the possibility that decarboxylation of **108** is occurring.

## 3.6. Conclusions

A series of mono, bis, tris and tetrakis rhodium NHC complexes, some neutral, hydridic species and some cationic complexes, have been synthesised. These have been extensively characterised by spectroscopic and crystallographic techniques. This has allowed comparison of the structures over a whole range of rhodium-NHC complexes, giving an insight into how addition of more NHC ligands affects the structure, and hence the chemical properties of complexes.

From table 3.19., it can be seen that the angle that the imidazole ring is set away from the central plane of the complex decreases as more NHC ligands are complexed to the metal centre, although the effect is less pronounced between three and four NHCs. From these angles it can also be surmised that IMes has the greatest steric effect around a metal centre, followed by $I^iPr_2Me_2$ then $IEt_2Me_2$ and ICy. This assumption is based solely on the amount that the ligands are pushed out of the metal centre but agree well with Nolan's buried volume model (discussed in section 1.2.2.). From the Rh-carbene bond lengths also presented in table 3.19., it appears that $IEt_2Me_2$ is the best σ donor, due to the shorter bond lengths in $[Rh(IEt_2Me_2)_4]^+$ (**96**) compared to $[Rh(ICy)_4]^+$ (**98**). It is likely that this is due to the methyl groups on the backbone. However, by the same token, comparison of the Rh-carbene bond lengths in $[Rh(I^iPr_2Me_2)_3(CO)]^+$ (**89**) and $[Rh(ICy)_3(CO)]^+$ (**90**), suggest that ICy is a

better σ donor than $I^iPr_2Me_2$. However, as $I^iPr_2Me_2$ is more sterically bulky than ICy, these elongated Rh-C bonds are probably likely to be due to steric effects.

| | NHC | Angle out of plane (°) | Rh-carbene bond lengths (Å) | | | |
|---|---|---|---|---|---|---|
| **72** | $I^iPr_2Me_2$ | 83.662 | 2.068(2) | | | |
| **80** | IMes | 75.732 | 2.024(3) | | | |
| **86** | IMes | 70.341<br>62.507 | 2.0165(16) | 2.0191(17) | | |
| **89** | $I^iPr_2Me_2$ | 67.042<br>63.597<br>52.887 | 2.1490(13) | 2.0775(13) | 2.0738(14) | |
| **90** | ICy | 64.046<br>52.295 | 2.1321(12) | 2.0642(11) | 2.0638(11) | |
| **95** | $I^iPr_2Me_2$/<br>ICy | 64.318<br>57.139<br>54.320 | 2.1341(13) | 2.0818(13) | 2.0677(13) | |
| **96** | $IEt_2Me_2$ | 63.048<br>60.920 | 2.047(4) | 2.047(4) | 2.042(4) | 2.042(4) |
| **98** | ICy | 51.226 | 2.070(5) | 2.070(5) | 2.070(5) | 2.070(5) |

**Table 3.19.** Comparison of angles of imidazole rings out of plane and Rh-carbene bond lengths across a series of mono, bis, tris and tetrakis NHC Rh complexes.

As discussed early on in the introduction of this chapter, Rh-NHC complexes bearing chloride ligands have been synthesised by Lappert, Çetinkaya and Crudden and have been found to be active in various catalytic cycles, including silylation,[32] cyclopropanation[33] and hydroformylation[34]. However, nothing has been reported on the effectiveness of hydride bearing Rh-NHC complexes in catalysis and the new complexes reported in this thesis have yet to be investigated in detail in catalysis. Weberskirch has recently proposed that in the hydroformylation of 1-octene by Rh-NHC COD complexes, the active catalyst is actually a hydrido-carbonyl species (scheme 3.25).[89]

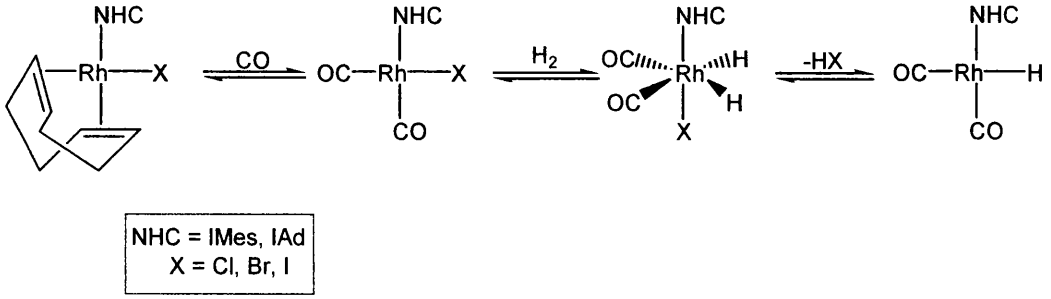


**Scheme 3.25.** Mechanism proposed by Weberskirch for the formation of catalytically active $[RhH(NHC)(CO)_2]$ in hydroformylation of 1-octene.

This suggests that the hydrido-carbonyl complexes synthesised and reported here may well be active catalysts in hydroformylation reactions.

Spontaneous C-H activation of an IMes ligand has been observed at room temperature to give $[Rh(IMes)''(PPh_3)_2]$ (**82**). Similar C-H activations have not been seen on the alkyl NHC complexes synthesised, even upon heating. This may simply be due to sterics as the bulky IMes ligand is forced to twist in such a way on the metal centre that the complex becomes predisposed to C-H activation. That this C-H activation is reversible on addition of $H_2$ may enable this complex to be used as a catalyst in indirect Wittig reactions like the ruthenium complex, $[RuH(IMes)(PPh_3)_2(CO)]$ (**16**), which also undergoes reversible C-H activation of the IMes ligand and has been described in chapter 2.

The cationic complexes, $[Rh(NHC)_4]^+$ (NHC = $IEt_2Me_2$, $I^iPr_2Me_2$, ICy), that have been isolated from reaction of rhodium hydride precursors with free NHC at room temperature, are highly unusual and without precedent in the literature. Indeed, it had been suggested that it was not possible to attach four NHCs around a rhodium centre.[76] A rare mixed NHC species, $[Rh(I^iPr_2Me_2)(ICy)(CO)][PF_6]$ (**95**), has also been synthesised. The rapid ease of synthesis of these complexes from $[RhCl_3 \cdot xH_2O]$, their high stability and the probability of being able to make them in biologically inert solvents, suggests that they could be used in applications such as radiation delivery to tumour cells, which was discussed in section 3.3.6.

## 3.7. References


(1) Collman, J. P.; Hegedus, L. S. *Principles and Applications of Organotransition Metal Chemistry*; University Science Books: California, 1980.

(2) Young, J. F.; Osbourn, J. A.; Jardine, F. H.; Wilkinson, G. *J. Chem. Soc. D. Chem. Commun.* **1965**, 131.

(3) Brown, J. M.; Evans, P. L.; Lucy, A. R. *J. Chem. Soc., Perkin Trans. 2* **1987**, 1589.

(4) Haszeldine, R. N.; Parish, R. V.; Parry, D. J. *J. Organomet. Chem.* **1968**, *9*, 13.

(5) Mannig, D.; Noth, H. *Angew. Chem. Int. Ed.* **1985**, *24*, 878.

(6) Meakin, P.; Tolman, C. A.; Jesson, J. P. *J. Am. Chem. Soc.* **1972**, *94*, 3240.

(7) Halpern, J.; Wong, C. S. *J. Chem. Soc., Chem. Commun.* **1973**, 629.

(8) Arai, H.; Halpern, J. *Chem. Commun.* **1971**, 1571.

(9) Halpern, J.; Okamoto, T.; Zakhariev, A. *J. Mol. Catal.* **1976**, *2*, 65.

(10) Halpern, J. *Inorg. Chim. Acta* **1981**, *50*, 11.

(11) Bargon, J.; Kandels, J.; Kating, P. *J. Chem. Phys.* **1993**, *98*, 6153.

(12) Kating, P.; Wandelt, A.; Selke, R.; Bargon, J. *J. Phys. Chem.* **1993**, *97*, 13313.

(13) Duckett, S. B.; Newell, C. L.; Eisenberg, R. *J. Am. Chem. Soc.* **1994**, *116*, 10548.

(14) Duckett, S. B.; Newell, C. L.; Eisenberg, R. *J. Am. Chem. Soc.* **1997**, *119*, 2068.

(15) Brown, C. K.; Wilkinson, G. *J. Chem. Soc. A* **1970**, 327.

(16) Jones, N. L.; Ibers, J. A. *Homogeneous Catalysis with Metal Phosphine Complexes*; Plenum Press: New York, 1983.

(17) Chen, A. C.; Ren, L.; Decken, A.; Crudden, C. M. *Organometallics* **2000**, *19*, 3459.

(18) Pruett, R. L.; Smith, J. A. *J. Org. Chem.* **1969**, *34*, 327.

(19) Baker, M. V.; Brown, D. H.; Haque, R. A.; Skelton, B. W.; White, A. H. *Dalton Trans.* **2004**, 3756.

(20) Although Pruett and Smith utilised rhodium on carbon as the metal catalyst source, the comparative studies that they make are still valid. They note that preformed $[RhH(PPh_3)_3(CO)]$ (**59**) acted in an identical manner.

(21) Abatjoglou, A. G.; Billig, E.; Bryant, D. R. *Organometallics* **1984**, *3*, 923.

(22) Çetinkaya, B.; Dixneuf, P.; Lappert, M. F. *J. Chem. Soc. Dalton Trans.* **1974**, 1827.

(23) Lappert, M. F. *J. Organomet. Chem.* **1988**, *358*, 185.

(24) Chamizo, J. A.; Hitchcock, P. B.; Jasim, H. A.; Lappert, M. F. *J. Organomet. Chem.* **1993**, *451*, 89.

(25) Çetinkaya, E.; Hitchcock, P. B.; Jasim, H. A.; Lappert, M. F.; Spyropoulos, K. *J. Chem. Soc., Perkin Trans. 1* **1992**, 561.

(26) Doyle, M. J.; Lappert, M. F.; Pye, P. L.; Terreros, P. *J. Chem. Soc., Dalton Trans.* **1984**, 2355.

(27) Hitchcock, P. B.; Lappert, M. F.; Pye, P. L. *J. Chem. Soc., Dalton Trans.* **1977**, 2160.
(28) Çetinkaya, B.; Hitchcock, P. B.; Lappert, M. F.; Shaw, D. B.; Spyropoulos, K.; Warhurst, N. J. W. *J. Organomet. Chem.* **1993**, *459*, 311.
(29) Winberg, H. W.; Carnaham, J. E.; Coffmann, D. D.; Brown, M. *J. Am. Chem. Soc.* **1965**, *87*, 2055.
(30) Wanzlick, H. W.; Esser, F.; Kleiner, H.-J. *Chem. Ber.* **1963**, 1208.
(31) Wanzlick, H. W.; Schikora, E. *Angew. Chem.* **1960**, *72*, 494.
(32) Lappert, M. F.; Maskell, R. K. *J. Organomet. Chem.* **1984**, *264*, 217.
(33) Çetinkaya, B.; Ozdemir, I.; Dixneuf, P. H. *J. Organomet. Chem.* **1997**, *534*, 153.
(34) Grasa, G. A.; Moore, Z.; Martin, K. L.; Stevens, E. D.; Nolan, S. P.; Paquet, V.; Lebel, H. *J. Organomet. Chem.* **2002**, *658*, 126.
(35) Bennet, M. J. *Inorg. Chem.* **1977**, *16*, 655.
(36) Allen, D. P.; Crudden, C. M.; Calhoun, L. A.; Wang, R. Y. *J. Organomet. Chem.* **2004**, *689*, 3203.
(37) Sanford, M. S.; Ulman, M.; Grubbs, R. H. *J. Am. Chem. Soc.* **2001**, *123*, 749.
(38) Sanford, M. S.; Love, J. A.; Grubbs, R. H. *J. Am. Chem. Soc.* **2001**, *123*, 6543.
(39) Allen, D. P.; Crudden, C. M.; Calhoun, L. A.; Wang, R.; Decken, A. *J. Organomet. Chem.* **2005**, *In press*.
(40) Lipshutz, B. H.; Frieman, B.; Birkedal, H. *Org. Lett.* **2004**, *6*, 2305.
(41) Lebel, H.; Paquet, V. *J. Am. Chem. Soc.* **2004**, *126*, 320.
(42) Datt, M. S.; Nair, J. J.; Otto, S. *J. Organomet. Chem.* **2005**, *690*, 3422.
(43) Martin, H. C.; James, N. H.; Aitken, J.; Gaunt, J. A.; Adams, H.; Haynes, A. *Organometallics* **2003**, *22*, 4451.
(44) Dorta, R.; Stevens, E. D.; Scott, N. M.; Costabile, C.; Cavallo, L.; Hoff, C. D.; Nolan, S. P. *J. Am. Chem. Soc.* **2005**, *127*, 2485.
(45) Mata, J. A.; Chianese, A. R.; Miecznikowski, J. R.; Poyatos, M.; Peris, E.; Faller, J. W.; Crabtree, R. H. *Organometallics* **2004**, *23*, 1253.
(46) Albrecht, M.; Crabtree, R. H.; Mata, J. A.; Peris, E. *Chem. Commun.* **2002**, 32.
(47) Tongi, A.; Venanzi, L. M. *Angew. Chem. Int. Ed.* **1994**, *33*, 497.
(48) Burling, S.; Field, L. D.; Li, H. L.; Messerle, B. A.; Turner, P. *Eur. J. Inorg. Chem.* **2003**, 3179.
(49) Burling, S.; Field, L. D.; Messerle, B. A.; *Organometallics*, **2002**, *19*, 87.
(50) Baker, M. V.; Brayshaw, S. K.; Skelton, B. W.; White, A. H.; Williams, C. C. *J. Organomet. Chem.* **2005**, *690*, 2312.
(51) Quezada, C. A.; Garrison, J. C.; Panzner, M. J.; Tessier, C. A.; Youngs, W. J. *Organometallics* **2004**, *23*, 4846.
(52) Wanniarachchi, Y. A.; Khan, M. A.; Slaughter, L. M. *Organometallics* **2004**, *23*, 5881.
(53) Strauss, S. H.; Diamond, S. E.; Mares, F.; Shriver, D. F. *Inorg. Chem.* **1978**, *17*, 3064.
(54) Huang, J.; Schanz, H.-J.; Stevens, E. D.; Nolan, S. P. *Organometallics* **1999**, *18*, 2370.

(55) Reaction between $[RuH_2(PPh_3)_3(CO)]$ and $IMesH_2$ also does not occur whereas the reaction between this precursor and IMes is relatively facile as reported in chapter 2.
(56) Garrou, P. E. *Chem. Rev.* **1981**, *81*, 229.
(57) Stradiotto, M.; Fujdala, K. L.; Tilley, T. D. *Helv. Chim. Acta* **2001**, *84*, 2958.
(58) Arif, A. M.; Jones, R. A.; Seeberger, M. H.; Whittlesey, B. R.; Wright, T. C. *Inorg. Chem.* **1986**, *25*, 3943.
(59) Meek, D. W.; Kreter, P. E.; Christoph, G. G. *J. Organomet. Chem.* **1982**, *231*, C53.
(60) Budzelaar, P. H. M. *g-NMR, Version4*; Cherwell Scientific Publishing Ltd, Oxford, UK, 1995-1997.
(61) Cowie, M.; Dwight, S. K. *Inorg. Chem.* **1980**, *19*, 209.
(62) Keim, W. *J. Organomet. Chem.* **1968**, *14*, 179.
(63) Scott, N. M.; Nolan, S. P. *Eur. J. Inorg. Chem.* **2005**, *10*, 1815.
(64 Magill, A. M.; Cavell, K. J.; Yates, B. F. *J. Am. Chem. Soc.* **2004**, *126*, 8717.
(65) Herrmann, W. A.; Fischer, J.; Öfele, K.; Artus, G. R. J. *J. Organomet. Chem.* **1997**, *530*, 259.
(66) Lee, M. T.; Hu, C. H. *Organometallics* **2004**, *23*, 976.
(67) Simms, R. W.; Drewitt, M. J.; Baird, M. C. *Organometallics* **2002**, *21*, 2958.
(68) Singh, P.; Dammann, C. B.; Hodgson, D. J. *Inorg. Chem.* **1973**, *12*, 1335.
(69) Freeman, M. A.; Young, D. A. *Inorg. Chem.* **1986**, *25*, 1556.
(70) Burch, R. R.; Muetterties, E. L.; Schultz, A. J.; Gebert, E. G.; Williams, J. M. *J. Am. Chem. Soc.* **1981**, *103*, 5517.
(71) Kang, S.; Albright, T. A.; Wright, T. A.; Jones, R. A. *Organometallics* **1985**, *4*, 666.
(72) Chan, A. S. C.; Shieh, H.-S.; Hill, J. R. *J. Chem. Soc. - Chem. Commun.* **1983**, 688.
(73) Clark, H. C. S.; Coleman, K. S.; Fawcett, J.; Holloway, J. H.; Hope, E. G.; Langer, J.; Smith, I. M. *J. Fluor. Chem.* **1998**, *91*, 207.
(74) Wilson, J. M.; Sunley, G. J.; Adams, H.; Haynes, A. *J. Organomet. Chem.* **2005**, *In press*.
(75) Iggo, J. A. *NMR Spectroscopy in Inorg. Chem.*; Oxford University Press, 1999.
(76) Neumann, E.; Pfaltz, A. *Organometallics* **2005**, *24*, 2008.
(77) Shriver, D. F.; Atkins, P. W. *Inorg. Chem.*; 3rd ed.; Oxford University Press: Oxford, 1999.
(78) McMurry, J. *Organic Chemistry*; 4th ed.; Brooks/Cole Publishing Company: Pacific Grove, California, 1996.
(79) Lever, A. B. P. *Inorganic Electronic Spectroscopy*; Elsevier Science: Amsterdam, 1986.
(80) Geoffroy, G. L.; Wrighton, M. S.; Hammond, G. S.; Gray, H. B. *J. Am. Chem. Soc.* **1974**, *96*, 3105.
(81) Geoffroy, G. L.; Isci, H.; Litrenti, J.; Mason, W. R. *Inorg. Chem.* **1977**, *16*, 1950.
(82) Billig, E.; Jamerson, J. D.; Pruett, R. L. *J. Organomet. Chem.* **1980**, *192*, C49.

(83) Burch, R. R.; Muetterties, E. L.; Thompson, M. R.; Day, V. W. *Organometallics* **1983**, *2*, 474.
(84) Whittlesey, M. K.; Perutz, R. N.; Moore, M. H. *Organometallics* **1996**, *15*, 5166.
(85) Bradley, M. G.; Roberts, D. A.; Geoffroy, G. L. *J. Am. Chem. Soc.* **1981**, *103*, 379.
(86) Kuhn, N.; Steimann, M.; Weyers, G. *Z.Naturforsch.(B)* **1999**, *54*, 427.
(87) Holbrey, J. D.; Reichert, M.; Tkatchenko, I.; Bouajila, E.; Walter, O.; Tommasi, I.; Rogers, R. D. *Chem. Commun.* **2003**, 28.
(88) Duong, H. A.; Tekavec, T. N.; Arif, A. M.; Louie, J. *Chem. Commun.* **2004**, 112.
(89) Bortenschlager, M.; Schütz, J.; von Preysing, D.; Nuyken, O.; Herrmann, W. A.; Weberskirch, R. *J. Organomet. Chem.*, **2005**, *in press*.

# Chapter 4

# Experimental

# 4. Experimental

## 4.1. General procedures

All manipulations were carried out using standard Schlenk line, high vacuum and dry glove box techniques under argon or nitrogen.

Solvents were purchased from Fisher, were distilled under nitrogen and stored under argon. Ethanol and 1-hexanol were distilled over magnesium turnings and iodine. Hexane, THF and benzene were collected from purple solutions of sodium dispersion and benzophenone with a few additional drops of ethylene glycol in the case of hexane. Toluene and pyridine were dried over sodium. Pentane was distilled over $CaH_2$ and stored over a potassium mirror. All solvents were used dried and degassed unless otherwise stated.

Deuterated NMR solvents (purchased from Sigma-Aldrich) were dried over potassium, transferred *via* vacuum and stored over potassium mirrors except for $CDCl_3$ and $CD_2Cl_2$ which were dried over $CaH_2$.

NMR data was recorded on Varian Mercury 400 MHz or Bruker Avance 400 MHz and 300 MHz spectrometers. The reference compound in $^{31}P\{^1H\}$ NMR experiments was $H_3PO_4$ and $CFCl_3$ in $^{19}F$, both referenced externally to 0 ppm. For the $^1H$ NMR experiments, the protio solvent present in the NMR tube was taken as the reference. ($CHCl_3$: δ 7.26, $CDHCl_2$: δ 5.31, $C_6D_5H$: δ 7.15, $d_7$-THF: δ 3.57, $CD_2HC_6D_5$ (toluene): δ 2.09, $d_4$-pyridine: δ 8.72). $^{13}C$ NMR experiments were also referenced internally ($CDCl_3$: δ 77.4, $CD_2Cl_2$: δ 53.1, $C_6D_6$: δ 128.7, $d_8$-THF: δ 25.3, $CD_3C_6D_5$: δ 21.3, $d_5$-pyridine: δ 123.5). Values throughout this section are quoted in ppm.

IR spectra were obtained on a Nicolet Nexus FTIR spectrometer and recorded as nujol mulls unless otherwise stated.

Absorption spectra were measured using a Perkin Elmer Lambda 20 UV-visible spectrometer. Samples were analysed in a 10.0 mm path length quartz cell, fitted with a PTFE tap and borosilicate degassing bulb.

UV photolysis studies at the University of Bath were carried out using an Oriel 125 W mercury arc lamp. Samples, typically of a concentration of 0.02 mol $dm^{-3}$ in deuterated solvent in a J. Young's resealable NMR tube, were immersed in either deionised water (for room temperature conditions) or a dry ice/acetone mix (< -50 °C) in a partially silvered dewer.

The set-up for *in situ* photolysis at the University of York has been described in detail elsewhere.[1,2] It consisted of a HeCd laser beam ($\lambda$ = 325 nm, 55mW) guided towards the sample through a modified probe of a Bruker Avance 400 MHz NMR spectrometer, which irradiated the sample (typically 0.004 mol $dm^{-3}$ concentration) from the side. *Para*hydrogen was prepared by cooling $H_2$ to -253 °C over a paramagnetic catalyst (activated charcoal) as has been described previously.[3]

TRIR measurements were carried out at the University of Nottingham and details of the diode laser based TRIR apparatus have been described in more detail previously.[4] The IR source is a continuous wave IR diode laser (Mütek MDS 1100). In these experiments, the change in IR transmission at one IR frequency was measured by an appropriate fast MCT detector, following UV excitation of the sample by a pulsed Nd:YAG laser (Spectra Physics Quanta-Ray GCR-12; 355 or 266 nm) which initiates the photochemical reactions. A spectrum was built up on a 'point-by-point' basis by repeating this measurement at different infrared frequencies.

X-ray crystallography studies were performed on a Nonius KappaCCD machine typically at 150 K. Structure calculations and drawings were carried out using the SHELX suite of programmes.[5,6]

All chemicals were purchased from Sigma-Aldrich, except for [$RhCl_3 \cdot xH_2O$] and [$RuCl_3 \cdot H_2O$], which were kindly donated by Johnson Matthey plc., and used as received unless otherwise stated. Trimethylvinylsilane was stored over molecular sieves. Ethene (Aldrich, 99.9%), $D_2$ (Aldrich, 99.8%), $^{13}CO$ (Cambridge Isotopes, 99%), and $^{13}CO_2$ (Cambridge Isotopes, 99%) were used as received.

Elemental analyses were performed at the University of Bath and Elemental Microanalysis Ltd, Okehampton, Devon.

## 4.2. Methods of synthesis

### 4.2.1. N-heterocyclic carbenes

**1,3-diethyl-4,5-dimethylimidazol-2-ylidene ($IEt_2Me_2$):** The NHC was prepared from the thiol salt using a method adapted from the literature.[7] 13.8 g (100 mmol) diethyl thiourea and 8.8 g (100 mmol) 3-hydroxy-2-butanone were refluxed in 250 mL of 1-hexanol for 12 hours in a 3-necked round bottomed flask. The solvent was removed on the rotary evaporator and the residue washed with water (100 mL) and undried ether (100 mL). The white solid obtained (1,3-diethyl-4,5-dimethylimidazolium thione) was dried under vacuum. 1.8 g of this product was dissolved in THF (30 mL) in a 3-necked round bottomed flask and cooled in an ice bath. 1.0 g potassium (finely chopped) was added and the mixture refluxed under a slow flow of argon for 4 hours during which time a sticky blue solid (KS) formed. The solution was filtered using a cannula filter and the filtrate pumped down to dryness under vacuum. A pale yellow oil was obtained. Yield: 1.3 g (83 %). $^1H$ NMR ($C_6D_6$, 400 MHz, 25 °C): δ 3.79 (q, $^3J_{HMe}$ = 7.1 Hz, 4H, $CH_2CH_3$), 1.69 (s, 6H, $H_3CC{=}CCH_3$ backbone), 0.44 (t, $^3J_{HH}$ = 7.1 Hz, 6H, $CH_2CH_3$).

**1,3-diisopropyl-4,5-dimethylimidazol-2-ylidene ($I^iPr_2Me_2$):** The NHC was prepared from the thiol salt using a method adapted from the literature.[7] 16.0 g (100 mmol) di-isopropyl thiourea and 8.8 g (100 mmol) 3-hydroxy-2-butanone were refluxed in 250 mL of dry 1-hexanol for 12 hours in a 3-necked round bottomed flask. The solvent was removed on the rotary evaporator, washed with water (100 mL) and undried ether (100 mL) and the residue recrystallised from ethanol/water (1:1, 50 mL) overnight at -20 °C. The colourless needles that precipitated (1,3-diisopropyl-4,5-dimethylimidazolium thione) were filtered and dried under vacuum. 1.1 g of this product was dissolved in dry THF (30 mL) in a 3-necked round bottomed flask and cooled in an ice bath. 0.5 g potassium (finely chopped) was added and the mixture was refluxed for 4 hours during which time a sticky blue solid formed. This was filtered using a cannula filter and the filtrate was pumped down to dryness under vacuum to give a pale yellow solid in quantitative yield. $^1$H NMR (THF, 300 MHz, 25 °C): δ 4.18 (sept, $^3J_{HH}$ = 6.6 Hz, 2H, C**H**$(CH_3)_2$), 2.05 (s, 6H, $\mathbf{H_3}$CC=CC$\mathbf{H_3}$ backbone), 1.40 (d, $^3J_{HH}$ = 6.6 Hz, 12H, CH(C$\mathbf{H_3}$)$_2$).

**1,3-cyclohexyl-imidazol-2-ylidene (ICy):** A suspension of paraformaldehyde (3.0 g) in toluene (15 mL) was cooled in an ice bath. Cyclohexylamine (23.0 mL, 200 mmol) was added dropwise over 1 hour. HCl (4M in dioxane, 25.0 mL) was then added dropwise over 30 mins, maintaining the temperature below 25 °C. The white cloudy mixture was allowed to warm to room temperature before addition of glyoxal (11.5 mL). The mixture was stirred for 1 hour before toluene (30 mL) was added. Water (10.8 mL) was removed from the reaction mixture using a Dean-Stark trap. The volatiles were removed from the remaining mixture *in vacuo* affording ICy•HCl as a brown sticky solid. This was dissolved in water (75 mL) and tetrafluoroboric acid (13 mL) was added, immediately precipitating ICy•$HBF_4$ as a pale brown solid. Yield 26.0 g (41 %). $^1$H NMR ($CDCl_3$, 400 MHz, 25 °C): δ 8.91 (t, $^4J_{HH}$ = 1.7 Hz, 1H C-**H**), 7.41 (d, $^4J_{HH}$ = 1.7 Hz, 2H, **HC=CH** backbone), 4.29 (tt, $^3J_{HH}$ = 11.9, $^4J_{HH}$ = 3.9 Hz, 2H, *ipso*-**CH** Cy), 2.17-2.13 (m, 4H, Cy C$\mathbf{H_2}$), 1.90-1.87 (m, 4H, Cy C$\mathbf{H_2}$), 1.73-1.62 (m, 6H, Cy C$\mathbf{H_2}$), 1.50-1.39 (m, 4H, Cy C$\mathbf{H_2}$), 1.30-1.18 (m, 2H, Cy C$\mathbf{H_2}$).

NaH (0.3 g, 12.5 mmol) and NaO$^t$Bu (0.03 g, 0.3 mmol) were added to ICy•$HBF_4$ (2.0 g, 5.2 mmol) in a Schlenk flask and dried under vacuum for several hours. THF (20 mL) was added at room temperature and the mixture stirred for 4 hours. The volatiles were removed *in vacuo* producing a solid brown residue. Sublimation at 100 °C for 1 hour afforded ICy as an air-sensitive white solid, which was retrieved in a glove box. Yield: 0.8 g (66 %). $^1$H NMR ($C_6D_6$, 400 MHz, 25 °C): δ 6.61 (s, 2H, **HC=CH** backbone), 4.10 (tt, $^3J_{HH}$ = 11.8, $^4J_{HH}$ = 3.7 Hz, 2H, *ipso*-**CH** Cy), 2.06 (m, 4H, Cy $CH_2$), 1.69-1.62 (m, 8H, Cy $CH_2$), 1.49-1.46 (m, 2H, Cy $CH_2$), 1.30-1.01 (m, 6H, Cy $CH_2$).

**1,3-bis-(2,4,6-trimethylphenyl)imidazol-2-ylidene (IMes):** This procedure was adapted from the method reported in literature.[8,9]

Bis-(2,4,6-trimethylphenyl)imine: 67.6 g (500.0 mmol) of 2,4,6-trimethylphenylamine and 36.3 g of a 40 % aqueous glyoxal solution (250.0 mmol) were added to a 500 mL round bottomed flask and dissolved in 250 mL of undried ethanol. The mixture was stirred for 3 days at room temperature during which time a thick yellow solid precipitated out. The precipitate was isolated by filtration through a Buchner filter and washed with cold, undried ethanol (100 mL). By reducing the filtrate to about 50 % and leaving the solution in the fridge over night, a second crop of solid was obtained. The product was dried initially in air and then under vacuum. Yield: 68.5 g (94 %).$^1$H NMR ($CDCl_3$, 300 MHz, 25 °C): δ 8.13 (s, 2H, **HC=CH** backbone), 6.93 (s, 4H, *m*-**CH**), 2.32 (s, 6H, *p*-$CH_3$), 2.19 (s, 12H, *o*-$CH_3$).

Synthesis of 1,3-dimesitylimidazolium chloride: 19.3 g (66.0 mmol) of bis-(2,4,6-trimethylphenyl)imine and 2.0 g (66.0 mmol) of paraformaldehyde were dissolved in undried toluene in a 1 L round bottomed flask. The reaction mixture was heated to 100 °C then immediately allowed to cool to 40 °C at which point 16.5 mL (66.0 mmol) of 4M HCl in dioxane was added *via* pipette. The solution turned dark orange and was stirred at 70 °C for 5 hours after which time a light brown solid precipitated out of the now dark brown solution. The reaction was stirred at room temperature for

a further 36 hours and the solid product was collected by Buchner filtration, washed with cold THF (100 mL) and air dried. Yield: 14.3 g (63 %).$^1$H NMR (undried $CDCl_3$, 300 MHz, 25 °C): δ 10.31 (s, 1H, **CH**), 7.65 (s, 2H, **HC=CH**), 6.88 (s, 4H, *m*-**CH**), 2.22 (s, 6H, *p*-$\mathbf{CH_3}$), 2.04 (s, 12H, *o*-$\mathbf{CH_3}$).

1,3-bis-(2,4,6-trimethylphenyl)imidazol-2-ylidene (IMes): 4.0 g (0.028 mol) of 1,3-dimesitylimidazolium chloride and 1.4 g (0.036 mol) of KO$^t$Bu were placed in a flame dried Schlenk tube and dried under vacuum overnight. The solids were then cooled using dry ice/acetone whilst 50 mL of THF was added. The reaction was left stirring in the dry ice/acetone bath for 20 mins and then gradually warmed to room temperature and stirred for another 15 mins. After this time, the solution was reduced to dryness under vacuum and the solid pumped on for 2 hours to make sure no residual solvent was present. The solid was redissolved in toluene, filtered through a glass filter cannula, under argon to remove all traces of KCl and pumped to dryness. Hexane was added and the mixture stirred until a precipitate began to appear. This was left at -30 °C overnight to enforce precipitation of the NHC. The fine cream solid was collected by cannula filtration. Yield: 2.2 g (62 %). $^1$H NMR ($C_6D_6$, 300 MHz, 25 °C): δ 6.80 (s, 4H, *m*-**CH**), 6.51 (s, 2H, **HC=CH**), 2.16 (s, 6H, *p*-$\mathbf{CH_3}$), 2.14 (s, 12H, *o*-$\mathbf{CH_3}$).

### 4.2.2. Ruthenium precursors

**[Ru(Cl)$_2$(AsPh$_3$)$_3$(CO)]:** This method was based on a literature route.[10] Triphenylarsine (7.4 g, 2.4 mmol) was dried under vacuum for 30 mins in a 500 mL 3-necked round bottomed flask. This was then dissolved in approximately 200 mL of undried, degassed 2-methoxyethanol. [$RuCl_3$•x$H_2O$] (1.2 g, 4.5 mmol) dissolved in approximately 60 mL of undried, degassed 2-methoxyethanol and aqueous formaldehyde (88 mL, 40% w/v solution, degassed by argon bubbling) were added rapidly and successively to the boiling methoxyethanol solution of $AsPh_3$. The mixture was heated to reflux for 2 hours under a slow flow of argon, during which time the solution became pale orange. After cooling, the solution was reduced in

volume to 80 mL before addition of 80 mL of cold, undried methanol. The yellow precipitate formed was separated by filtration on a Buchner funnel and washed with cold, undried ethanol (2 x 50 mL) and undried hexane (50 mL). The resultant product was dried under vacuum to give 4.1 g (81 %, based on $[RuCl_3 \cdot 3H_2O]$) of yellow microcrystalline powder. IR ($cm^{-1}$): 1949 ($\nu_{CO}$)

**$[Ru(H)_2(AsPh_3)_3(CO)]$ (20):** This method was based on a literature route .[10] $[Ru(Cl)_2(AsPh_3)_3(CO)]$ (2.1 g, 1.7 mmol) and $NaBH_4$ (4.0 g, 1.1 mmol) were placed in a 500 mL 3-necked round bottomed flask. They were dissolved in EtOH (200 mL), brought to reflux and stirred for 1.5 hours. After cooling, the resulting tan slurry was filtered on a Buchner filter and washed with 3 x 100 mL of undried ethanol. The solid was dissolved in undried toluene (100 mL) and this solution was filtered using a Buchner filter. Removal of the solvent *in vacuo* afforded a brown residue which was dissolved in 100 mL of undried ethanol. The solution was stirred overnight, during which time a white powder precipitated out. The powder was filtered, washed twice with 2 x 100 mL of dry ethanol, followed by 100 mL of dry hexane. The final product was then dried under vacuum to give 1.8 g (89 %) of white powder. $^1H$ NMR ($C_6D_6$, 300 MHz, 25 °C): $\delta$ -9.44 (d, $^2J_{HH}$ = 6.6 Hz, 1H, Ru-H), -9.92 (d, $^2J_{HH}$ = 6.6 Hz, 1H, Ru-H); IR ($cm^{-1}$): 1930 ($\nu_{CO}$).

**$[Ru(H)_2(PPh_3)_3(CO)]$ (15):** This method has been adapted from the literature.[9,11] Three Schlenk tubes, (1) (2) and (3), were charged with $[RuCl_3 \cdot xH_2O]$ (2.1 g, 8 mmol) in 80 mL of ethanol; aqueous formaldehyde (80 mL, 40 % w/v solution, degassed by argon bubbling) and potassium hydroxide (2.40 g, 40 mmol) in 80 mL of ethanol respectively. Solutions (1), (2) and (3) were added rapidly and successively to a boiling solution of $PPh_3$ (12.6 g, 48 mmol) in EtOH (280 mL). The solution was heated at reflux under a slow flow of argon for 25 mins and then cooled in an ice bath. The resulting grey precipitate was filtered on a Buchner filter and washed with 2 x 50 mL of undried ethanol, 50 mL of deionised water and 50 mL of undried hexane. The crude powder was dissolved in undried benzene (100 mL) and passed through neutral alumina (ca. 2 g). The solution was reduced *in vacuo* until

solid had just begun to precipitate at which point undried methanol (50 mL) was stirred in to enforce precipitation. This was filtered to yield a white solid. Yield: 5.0 g (68 %, based on [$RuCl_3 \cdot H_2O$]). $^1H$ NMR ($C_6D_6$ 300 MHz, 25 °C): δ -6.53 (ddt, $^2J_{HP}$ = 15.3 Hz, $^2J_{HP}$ = 30.5 Hz, $^2J_{HH}$ = 6.1 Hz, 1H, Ru-**H**), -8.29 (ddt, $^2J_{HP}$ = 74.5 Hz, $^2J_{HP}$ = 28.1 Hz, $^2J_{HH}$ = 6.1 Hz, 1H, Ru-**H**); $^{31}P\{^1H\}$ NMR ($C_6D_6$, 121 MHz, 25 °C): δ 58.2 (d, $^2J_{PP}$ = 16.8 Hz, $PPh_3$), 46.1 (t, $^2J_{PP}$ = 16.8 Hz, $PPh_3$); IR ($cm^{-1}$): 1960 ($\nu_{CO}$).

4.2.3. Ruthenium-NHC complexes

***trans*-(IMes)-[$Ru(H)_2(IMes)_2(AsPh_3)(CO)$] (21):**

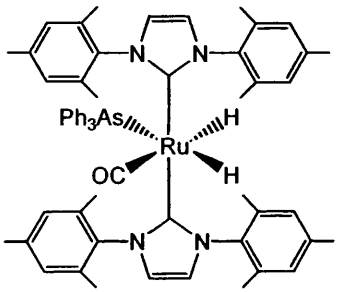


Into a flame-dried Young's ampoule was placed [$Ru(H)_2(AsPh_3)_3(CO)$] (**20**) (0.05 g, 0.048 mmol) and IMes (0.05g, 0.16 mmol). Benzene (20 mL) was vacuum condensed in and the solution heated at 75 °C for four days. The solution turned a deep red and NMR spectroscopy of a sample extracted and redissolved in $C_6D_6$ showed the major product to be **21**. Isolation of the complex proved impossible due to the highly reactive nature of the $AsPh_3$ group. $^1H$ NMR ($C_6D_6$, 400 MHz, 25 °C): δ -5.71 (d, $^2J_{HH}$ = 5.9 Hz , Ru-**H**), -8.93 (d, $^2J_{HH}$ = 5.9 Hz, Ru-**H**).

***trans*-[Ru(H)$_2$(IMes)$_2$(PPh$_3$)(CO)] (17):**

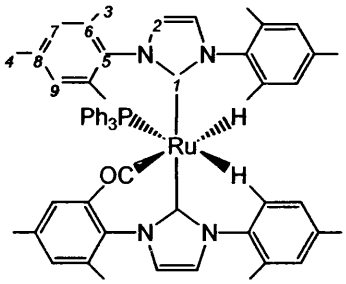

$PPh_3$ (0.013 g, recystallised twice from ethanol) was added to a solution of *trans*-[Ru(H)$_2$(IMes)$_2$(AsPh$_3$)(CO)] (**21**) (synthesised from 0.05 g **20**) in the glove box. NMR studies showed complete conversion to **17** immediately at room temperature. The product could not be isolated due to the highly reactive nature of the $PPh_3$ group. $^1$H NMR ($C_6D_6$, 300 MHz, 25 °C): δ 7.33–7.25 (m, 15H, $PPh_3$), 6.94, 6.79 (both br s, 4H, **H***9*, **H***7*), 6.09 (s, 4H, **HC=CH**), 2.35 (s, 12H, **H***4*), 2.15 (s, 24H, **H***3*), -5.89 (dd, $^2J_{HP}$ = 18.8 Hz, $^2J_{HH}$ = 7.1 Hz, 1H, Ru-**H**), -7.39 (dd, $^2J_{HP}$ = 93.5 Hz, $^2J_{HH}$ = 7.1 Hz, 1H, Ru-**H**); $^{31}$P{$^1$H} NMR ($C_6D_6$, 162 MHz, 25 °C): δ 47.3 (s, Ru-**P**Ph$_3$); selected $^{13}$C{$^1$H} NMR ($C_6D_6$, 100 MHz, 25 °C): δ 205.9 (d, $^2J_{CP}$ = 8.5 Hz, Ru-**C**O), 187.2 (d, $^2J_{CP}$ = 6.8 Hz, Ru-**C**:); IR (cm$^{-1}$) ( $C_6D_6$): 1869 ($\nu_{CO}$).

**[Ru(H)$_2$(IMes)(PPh$_3$)$_2$(CO)] (16):**

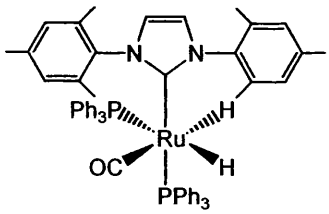

The preparation for this complex is adapted from that reported in the literature.[12] [Rh(H)$_2$(PPh$_3$)$_3$(CO)] (**15**) (0.5 g, 0.55 mmol) and IMes (0.5 g, 1.65 mmol) were dissolved in 30 mL toluene and the mixture heated at 80 °C for 3 days. Removal of solvent gave a dark oily residue to which was added 30 mL ethanol. After stirring the solution for 2 hours at room temperature a white solid precipitated. This was filtered under argon using a cannula filter and washed with ethanol (3 x 10 mL) and hexane (1 x 10 mL) to give [Ru(H)$_2$(IMes)(PPh$_3$)$_2$(CO)] (**16**). Yield: 0.24 g (45 %). $^1$H NMR ($C_6D_6$, 400 MHz, 25 °C): δ -6.36 (ddd, $^2J_{HPc}$ = 26.8, $^2J_{HPc}$ = 23.6, $^2J_{HH}$ =

6.0 Hz, 1H, Ru-**H**), -8.08 (ddd, $^2J_{HPt}$ = 81.2, $^2J_{HPc}$ = 33.6, $^2J_{HH}$ = 6.0 Hz, 1H, Ru-**H**); $^{31}P\{^1H\}$ NMR ($C_6D_6$, 162 MHz, 25 °C): δ 59.0 (d, $^2J_{PP}$ = 14.8 Hz, Ru-**P**$Ph_3$), 47.8 (d, $^2J_{PP}$ = 14.8 Hz, Ru-**P**$Ph_3$).

**[RuH(IMes)"($PPh_3$)$_2$(CO)] (18):**

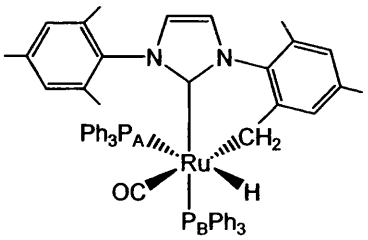


0.02 g (0.21 mmol) of [Ru(H)$_2$IMes($PPh_3$)$_2$(CO)] (**16**) was put in a resealable Young's NMR tube and dissolved in $C_6D_6$, which was vacuum condensed in to the tube. 1 atm of ethene was added and this led to complete conversion of the complex to the C-H activated product, **18**, at room temperature within 15 minutes. $^1H$ NMR ($C_6D_6$, 400 MHz, 25 °C): δ -7.97 (dd, $^2J_{HPA}$ = 102.4, $^2J_{HPB}$ = 30.8 Hz, 1H, Ru-**H**); $^{31}P\{^1H\}$ NMR ($C_6D_6$, 162 MHz, 25 °C): δ 53.7 (d, $^2J_{PP}$ = 18.1 Hz, Ru-**P**$Ph_3$), 28.4 (d, $^2J_{PP}$ = 18.1 Hz, **P**$Ph_3$).

**[Ru(H)$_2$(IMes)'($PPh_3$)$_2$(CO)] (19):**

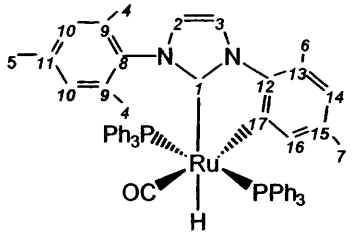


The preparation has been reported in the literature.[12] [Ru(H)$_2$($PPh_3$)$_3$(CO)] (**15**) (0.70 g, 0. 76 mmol) was heated with IMes (0.80 g, 2.6 mmol) in 20 mL toluene for 12 days at 110 °C. Removal of the solvent gave a dark oil, which was stirred in ethanol for 24 hours to afford a white precipitate. This was washed with ethanol (3 x 10 mL) and hexane (1 x 10 mL) to give **18**. Yield: 0.1 g (46 %). $^1H$ NMR ($C_6D_5CD_3$, 400 MHz, 25 °C): δ 7.51 (d, $^3J_{HH}$ = 1.6 Hz, 1H, **H***3*), 7.38-7.30 (12H, m, $PPh_3$), 6.95-6.90 (18H, m, $PPh_3$), 6.83 (2H, s, **H***10*), 6.35 (1H, br s, **H***14*), 6.19 (d, $^3J_{HH}$ = 1.6 Hz,

1H, **H***2*), 6.14 (1H, br s, **H***16*), 2.29 (3H, s, $CH_3$*6*), 2.17 (3H, s, $CH_3$*5*), 1.73 (3H, s, $CH_3$*7*), 1.56 (6H, s, $CH_3$*4*), -6.99 (1H, t, $^2J_{HP}$ = 28.4 Hz, Ru-**H**); $^{31}P\{^1H\}$ NMR ($C_6D_5CD_3$, 162 MHz, 25 °C): δ 55.1 (s, $PPh_3$); IR ($cm^{-1}$): 1914 ($\nu_{CO}$).

***eq*-($IEt_2Me_2$)-[$Ru(H)_2(IEt_2Me_2)(PPh_3)_2(CO)$] (29):**

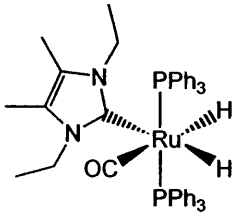


The complex was prepared according to literature procedures.[13] $[Ru(H)_2(PPh_3)_3(CO)]$ (**15**) (1.4 g, 1.53 mmol) and $IEt_2Me_2$ (700 mg, 4.60 mmol) were heated at 70 °C in toluene (20 mL) for 20 hours. The volatiles were then removed *in vacuo* and the red/brown oily residue stirred in ethanol (30 mL) overnight. The resulting beige solution was filtered to yield a green solid, which was subsequently dissolved in benzene and heated for 1 hour at 70 °C. The solution turned pink and a white solid precipitated out. The volatiles were removed *in vacuo* and the solid dissolved in THF (10 mL) and layered with hexane (30 mL) affording **29** as a white, crystalline solid. Yield 0.48 g (39 %). $^1H$ NMR ($d_8$-THF, 400 MHz, 25 °C): δ 7.62-7.48 (m, 12H, $PPh_3$), 7.25-7.07 (m, 18H, $PPh_3$), 3.69 (q, $^3J_{HH}$ = 6.6 Hz, 2H, $CH_2CH_3$), 3.28 (q, $^3J_{HH}$ = 6.6 Hz, 2H, $CH_2CH_3$), 2.00 (s, 3H, $H_3CC{=}CCH_3$ backbone), 1.72 (s, 3H, $H_3CC{=}CCH_3$), 1.01 (t, $^3J_{HH}$ = 6.6 Hz, 3H, $CH_2CH_3$), 0.34 (t, $^3J_{HH}$ = 6.6 Hz, 3H, $CH_2CH_3$), -6.38 (dt, $^2J_{HP}$ = 26.3 Hz, $^2J_{HH}$ = 5.5 Hz, 1H, Ru-**H**), -9.99 (dt, $^2J_{HP}$ = 24.7 Hz, $^2J_{HH}$ = 5.5 Hz, 1H, Ru-**H**); $^{31}P\{^1H\}$ NMR ($d_8$-THF, 162 MHz, 25 °C) δ 63.7 (s, Ru-$PPh_3$); IR ($cm^{-1}$): 1913 ($\nu_{CO}$).

***ax*-($IEt_2Me_2$)-[$Ru(H)_2(IEt_2Me_2)(PPh_3)_2(CO)$] (33):**

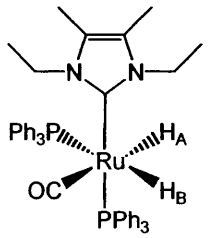


*eq*-($IEt_2Me_2$)-[$Ru(H)_2(IEt_2Me_2)(PPh_3)_2(CO)$] (**29**) (0.010 g, 0.012 mmol) was put into a J. Young's resealable NMR tube, dissolved in approximately 0.6 mL of $d_8$-THF or $d_8$-toluene and subjected to UV light ($\lambda > 285$ nm) for 5 hours at -50 °C. After this amount of time 45 % had converted to the axial isomer by $^1H$ NMR spectroscopy. $^1H$ NMR ($d_8$-THF, 400 MHz, -30 °C): δ 7.78-6.81 (m, 30H, $PPh_3$), 4.64 (dq, $^3J_{HMe}$ = 7.1 Hz, $^2J_{HH}$ = 20.9 Hz, 1H C**Ha**$HCH_3$), 4.51 (dq, $^3J_{HMe}$ = 7.1 Hz, $^2J_{HH}$ = 20.9 Hz, 1H, C**Hb**$HCH_3$), 4.30 (dq, $^3J_{HMe}$ = 7.1 Hz, $^2J_{HH}$ = 20.9 Hz, 1H, C**Hc**$HCH_3$), 2.90 (dq, $^3J_{HMe}$ = 7.1 Hz, $^2J_{HH}$ = 20.9 Hz, 1H, C**Hd**$HCH_3$), 2.04 (s, 3H, $\mathbf{H_3}CC{=}CCH_3$ backbone), 1.84 (s, 3H, $H_3CC{=}CC\mathbf{H_3}$ backbone), 1.23 (t, $^3J_{HH}$ = 7.1 Hz, 3H, $CH_2C\mathbf{H_3}$), 1.15 (t, $^3J_{HH}$ = 7.1 Hz, 3H, $CH_2C\mathbf{H_3}$), -6.03 (ddd, $^2J_{HP}$ = 30.7 Hz, $^2J_{HP}$ = 21.4 Hz, $^2J_{HH}$ = 2.7 Hz, 1H, Ru-$\mathbf{H_A}$), -8.10 (ddd, $^2J_{HP}$ = 85.6 Hz, $^2J_{HP}$ = 28.5 Hz, $^2J_{HH}$ = 2.7 Hz, 1H, Ru-**H**); $^{31}P\{^1H\}$ NMR ($d_8$-THF, 162 MHz, -30 °C): δ 64.45 (d, $^2J_{PP}$ = 15.45 Hz, Ru-$\mathbf{PPh_3}$), 51.1 (d, $^2J_{PP}$ = 15.5 Hz, Ru-**P**); $^{13}C$ NMR ($d_8$-THF, 100 MHz, -30 °C) δ 208.1 (m, Ru-**C**O), 186.3 (dd, $^2J_{CP}$ = 78.1 Hz, $^2J_{CP}$ = 8.3 Hz, Ru-**C**:); IR ($cm^{-1}$): 1877 ($\nu_{CO}$).

***eq, ax*-($ICy)_2$-[$Ru(H)_2(ICy)_2(PPh_3)(CO)$] (55):[14]**

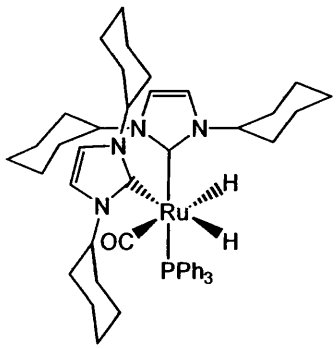

$[Ru(H)_2(PPh_3)_3(CO)]$ (**15**) (0.275 g, 0.3 mmol) and ICy (0.23 g, 1.0 mmol) were dissolved in toluene (30 mL) and heated at 70 °C in a Schlenk flask under argon for 16 hours. The volatiles were removed *in vacuo* and the residue washed with hexane (2 x 10 mL) and filtered. The resulting cream solid was dissolved in THF (10 mL) and layered with hexane to yield cream coloured crystals of **55**. Yield 0.14 g (53 %). $^1H$ NMR ($C_6D_6$, 400 MHz, 25 °C): δ 7.88 (m, 6H, $PPh_3$), 7.12 (m, 6H, $PPh_3$), 7.04 (m, 3H, $PPh_3$), 6.63 (br s, 2H, **HC**=CH backbone), 6.59 (d, $^3J_{HH}$ = 2.2 Hz, 1H, HC=**CH** backbone), 6.56 (d, $J_{HH}$ = 2.2 Hz, 1H, **HC**=**CH** backbone), 5.93 (br s, 2H, *ipso*-**CH** Cy), 5.48 (m, 1H, *ipso*-**CH** Cy), 5.28 (m, 1H, *ipso*-**CH** Cy), 2.91 (m, 1H, *ipso*-**CH** Cy), 2.37 (m, 2H, Cy $CH_2$), 1.87-0.77 (m, 38H, Cy $CH_2$), -5.39 (dd, $^2J_{HP}$ = 40.1 Hz, $^2J_{HH}$ = 4.4 Hz, 1H, Ru-**H**), -9.10 (dd, $^2J_{HP}$ = 30.2, $^2J_{HH}$ = 4.4 Hz, 1H, Ru-**H**); $^{31}P\{^1H\}$ ($C_6D_6$, 162 MHz, 25 °C): δ 60.8 (s, Ru-**P**$Ph_3$); IR ($cm^{-1}$): 1864 ($\nu_{CO}$).

***ax,ax*-(ICy)$_2$-[Ru(H)$_2$(ICy)$_2$(PPh$_3$)(CO)] (56):**

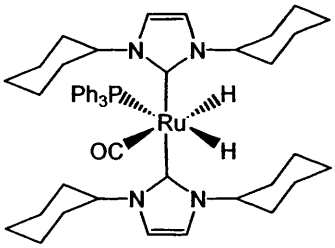


*eq*-ICy-$[Ru(H)_2(ICy)_2(PPh_3)(CO)]$ (**55**) (0.010 g, 0.012 mmol) was put into a J. Young's resealable NMR tube and dissolved in $C_6D_6$. The sample was subjected to UV light (λ > 285nm) for three days at room temperature. This resulted in the isomerisation of the compound to give the *trans* NHC product in 92 % yield, by $^1H$ NMR spectroscopy. $^1H$ NMR ($C_6D_6$, 400 MHz, 25 °C): δ 8.32–6.42 (m, 19H, $PPh_3$ and **HC**=**CH** backbone), 6.15-5.16 (m, 4H, *ipso*-**CH** Cy), 3.23-0.43 (m, 40H, Cy $CH_2$), -5.00 (d, $^2J_{HP}$ = 37.9 Hz, 1H, Ru-$H_A$), -7.48 (d, $^2J_{HP}$ = 99.3 Hz, 1H, Ru-**63**); $^{31}P\{^1H\}$ NMR ($C_6D_6$, 162 MHz, 25 °C): δ 50.0 (s, Ru-**P**$Ph_3$); $^{13}C\{^1H\}$ NMR ($C_6D_6$, 100 MHz, 25 °C): δ 210.6 (d, $^2J_{CP}$ = 4.6 Hz, Ru-**C**O), 192.6 (d, $^2J_{CP}$ = 8.3 Hz, Ru-**C**:), 143.2 (d, $J_{CP}$ = 23.9 Hz, P(*i*-$C_6H_5)_3$), 134.9 (d, $^2J_{CP}$ = 11.9 Hz, P(*o*-$C_6H_5)_3$), 128.8 (s, P(*p*-$C_6H_5)_3$), 128.2 (d, $^3J_{CP}$ = 7.4 Hz, P(*m*-$C_6H_5)_3$), 117.1 (s, **HC**=**CH**

backbone) 59.0 (s, *ipso*-CH Cy), 34.0, 27.0, 26.8 (all s, Cy $CH_2$); IR ($cm^{-1}$): 1889 ($\nu_{CO}$).

4.2.4. Rhodium precursors

**[RhH(PPh$_3$)$_4$] (69):** The method was adapted from the literature.[15] Hot solutions of [$RhCl_3$•x$H_2O$] (0.26 g, 1.0 mmol) and potassium hydroxide (0.4 g) in ethanol (20 mL each) were added rapidly and successively to a vigorously stirred, boiling solution of triphenylphosphine (recrystallised twice from ethanol, 2.62 g, 10 mmol) in ethanol (100 mL) in a 3-necked round bottomed flask. The mixture was brought to reflux for 25 mins and then allowed to cool to room temperature. The precipitated product was filtered through a cannula filter and then washed with ethanol (50 mL), water (degassed, 50 mL), ethanol (50 mL) and hexane (50 mL). The yellow solid was then dried under vacuum overnight to remove all traces of solvent. Yield: 1.0 g, (75 %, based on [$RhCl_3$•3$H_2O$]). $^1$H NMR ($C_6D_6$, 400 MHz, 25 °C): δ 8.00-6.50 (m, 60H, $PPh_3$), -8.06 (d, $^1J_{HRh}$ = 13.2 Hz, 1H, Rh-**H**); $^{31}P\{^1H\}$ NMR ($C_6D_6$, 162 MHz, 25 °C): δ 37.8 (br s, Rh-**P**$Ph_3$); IR ($cm^{-1}$): 2035 ($\nu_{HRh}$).

**[RhH(PPh$_3$)$_3$(CO)] (70):** Adapted from literature.[15] [$RhCl_3$•x$H_2O$] (0.26 g, 1.0 mmol) in 20 mL hot ethanol was added to a vigorously stirred, boiling solution of recrystallised triphenylphosphine (twice from ethanol, 2.64 g, 10 mmol) in 100 mL of ethanol in a 3-necked round bottomed flask. After a 15 second delay, aqueous formaldehyde (10 mL, 40 % w/v solution) and potassium hydroxide (0.4 g) in ethanol were added rapidly and successively to the reaction mixture. The mixture was brought to reflux for 15 mins and then allowed to cool to room temperature. The precipitated product was filtered through a cannula filter and then washed with ethanol (50 mL), water (degassed, 50 mL), ethanol (50 mL) and hexane (50 mL). The bright yellow, crystalline solid was then dried under vacuum overnight to remove all traces of solvent. Yield 0.63 g (60 %, based on [$RhCl_3$•3$H_2O$]). $^1$H NMR ($C_6D_6$, 400 MHz, 25 °C): δ 8.32-6.58 (m, 45H, Rh-$PPh_3$), -9.26 (br s, 1H, Rh-**H**);

$^{31}P\{^{1}H\}$ NMR ($C_6D_6$, 162 MHz, 25 °C): δ 40.8 (d, $^{1}J_{PRh}$ = 153.2 Hz, Rh-**P**$Ph_3$), 29.6 (br s, Rh-**P**$Ph_3$); IR ($cm^{-1}$): 2041 ($\nu_{HRh}$), 1921 ($\nu_{CO}$).

### 4.2.5. Rhodium-NHC complexes

#### *4.2.5.1. [RhH(NHC)$_x$(PPh$_3$)$_y$] (NHC = IEt$_2$Me$_2$, I$^i$Pr$_2$Me$_2$, ICy, x = 1, 2 or 3 y = 0, 1 or 2)*

In a typical procedure, [$RhH(PPh_3)_4$] (**69**) (0.05 g, 0.043 mmol) and free NHC ($IEt_2Me_2$, $I^iPr_2Me_2$, ICy 2-6 equivalents) were put into a J. Young's resealable NMR tube in the glove box. Approximately 0.6 mL of $C_6D_6$ or $d_8$-THF was added *via* vacuum transfer. Immediate reaction occurred at room temperature to give a mixture of products bearing one, two, three or four NHCs (scheme 4.1.). The ratio of products that formed was dependent on the amount of NHC added and the length of time the reaction was left for. In many cases, mixtures could not be separated. In these instances, resonances associated with the NHC groups could not be assigned to specific products due to overlapping signals. Thus, the NMR data for analogues of **I-V** presented below reports definitive resonances only. When an isomer for a particular complex is not reported it is because it was not observed. The data for the cationic species (analogues of **VI**) are reported later in section 4.2.8.

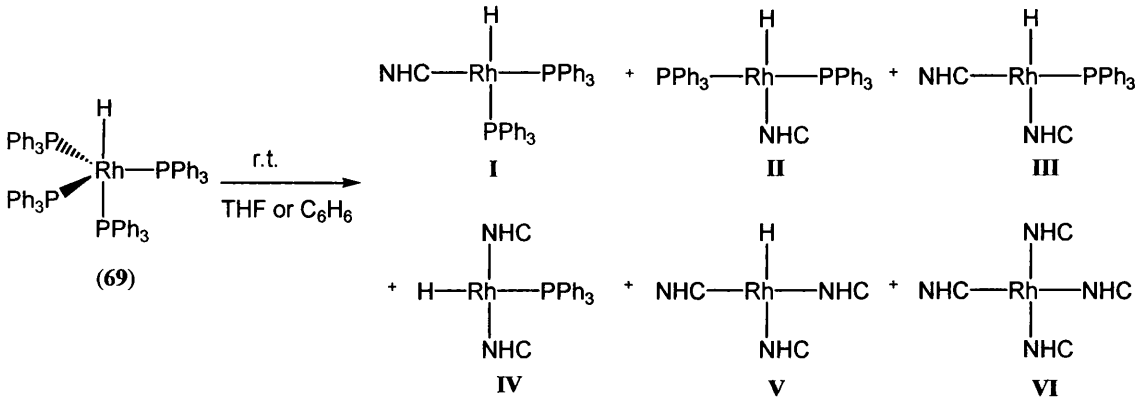


**Scheme 4.1.** Formation of 6 NHC containing products from reaction of **69** and free NHC at room temperature.

***cis-[RhH(IEt$_2$Me$_2$)(PPh$_3$)$_2$] (cis-71):***

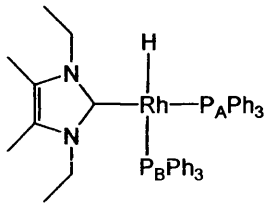


Selected NMR data: $^1$H NMR ($d_8$-THF, 400 MHz, 25 °C): δ -5.70 (ddd, $^2J_{HP_B}$ = 113.0 Hz, $^2J_{HP_A}$ = 25.2 Hz, $^1J_{HRh}$ = 24.7 Hz, 1H, Rh-**H**); $^{31}$P{$^1$H} NMR ($d_8$-THF, 162 MHz, 25 °C): δ 49.2 (dd, $^1J_{PRh}$ = 148.1 Hz, $^2J_{PP}$ = 24.5 Hz, Rh-**P$_A$**Ph$_3$), 41.4 (dd, $^1J_{PRh}$ = 136.5 Hz, $^2J_{PP}$ = 24.5 Hz, Rh-**P$_B$**Ph$_3$).

***trans-[RhH(IEt$_2$Me$_2$)(PPh$_3$)$_2$] (trans-71):***

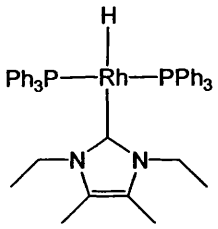


Selected NMR data: $^1$H NMR ($d_8$-THF, 400 MHz, 25 °C): δ -9.59 (dt, $^2J_{HP}$ = 23.6 Hz, $^1J_{HRh}$ = 11.0 Hz, 1H, Rh-**H**); $^{31}$P{$^1$H} NMR ($d_8$-THF, 162 MHz, 25 °C): δ 45.4 (d, $^1J_{PRh}$ = 175.0 Hz, Rh-**P**Ph$_3$).

***cis-[RhH(IEt$_2$Me$_2$)$_2$(PPh$_3$)] (cis-74):***

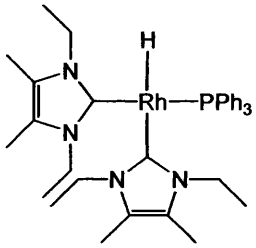


Selected NMR data: $^1$H NMR ($d_8$-THF, 400 MHz, 25 °C): δ -8.82 (dd, $^2J_{HP}$ = 29.1 Hz, $^1J_{HRh}$ = 15.9 Hz, 1H, Rh-**H**); $^{31}$P{$^1$H} NMR ($d_8$-THF, 162 MHz, 25 °C): δ 38.5 (d, $^1J_{PRh}$ = 135.2 Hz, Rh-**P**Ph$_3$); $^{13}$C{$^1$H} NMR ($d_8$-THF, 100 MHz, 25 °C): δ 197.2 (dd, $^1J_{CRh}$ = 57.0 Hz, $^2J_{CP}$ = 13.8 Hz, Rh-**C**:), 185.3 (dd, $^1J_{CRh}$ = 42.2 Hz, $^2J_{CP}$ = 15.6 Hz, Rh-**C**:).

***trans-[RhH(IEt$_2$Me$_2$)$_2$(PPh$_3$)] (trans-74):***

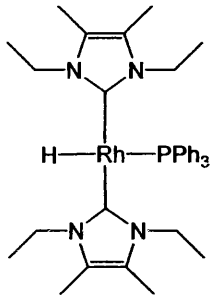

Selected NMR data: $^1$H NMR ($d_8$-THF, 400 MHz, 25 °C): δ -4.67 (dd, $^2J_{HP}$ = 121.3 Hz, $^1J_{HRh}$ = 35.1 Hz, 1H, Rh-**H**); $^{31}$P{$^1$H} NMR ($d_8$-THF, 162 MHz, 25 °C): 54.7 (d, $^1J_{PRh}$ = 159.7, Rh-**P**Ph$_3$); $^{13}$C{$^1$H} NMR ($d_8$-THF, 100 MHz, 25 °C): δ 199.9 (dd, $^1J_{CRh}$ = 46.1 Hz, $^2J_{CP}$ = 10.1 Hz, Rh-**C**:).

***[RhH(IEt$_2$Me$_2$)$_3$] (78):***

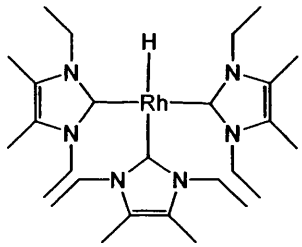

Selected NMR data: $^1$H NMR ($d_8$-THF, 400 MHz, 25 °C): δ -7.35 (d, $^1J_{HRh}$ = 22.0 Hz, 1H, Rh-**H**); $^{13}$C{$^1$H} NMR ($d_8$-THF, 100 MHz, 25 °C): δ 205.2 (d, $^1J_{CRh}$ = 58.0 Hz, Rh-**C**:), 202.0 (d, $^1J_{CRh}$ = 40.0 Hz, Rh-**C**:).

***cis-[RhH(I$^i$Pr$_2$Me$_2$)(PPh$_3$)$_2$] (cis-72):***

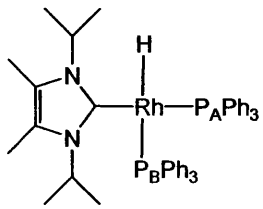

Selected NMR data: $^1$H NMR ($d_8$-THF, 400 MHz, 25 °C): δ 6.12 (sept, $^3J_{HH}$ = 7.2 Hz, 2H, NC**H**(CH$_3$)$_2$), -6.10 (ddd, $^2J_{HP_B}$ = 111.9 Hz, $^1J_{HRh}$ = 30.2 Hz, $^2J_{HP_A}$ = 24.7 Hz, 1H, Rh-**H**); $^{31}$P{$^1$H} NMR ($d_8$-THF, 162 MHz, 25 °C): δ 49.7 (dd, $^1J_{PRh}$ = 148.5

Hz, $^2J_{PP}$ = 23.0 Hz, Rh-$\mathbf{P_A}Ph_3$), 41.6 (dd, $^1J_{PRh}$ = 138.9 Hz, $^2J_{PP}$ = 23.0 Hz, Rh-$\mathbf{P_B}Ph_3$).

***trans-[RhH(I$^i$Pr$_2$Me$_2$)(PPh$_3$)$_2$] (trans-72):***

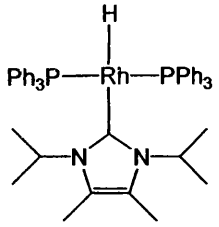


Removal of solvent from the initial reaction mixture gave a dark coloured residue. This was dissolved in the minimum amount of ethanol (ca. 0.5 mL) and cooled at -5 °C overnight to afford small orange crystals. These were fully characterised by X-ray crystallography. $^1$H NMR ($d_8$-THF, 400 MHz, 25 °C): δ 7.80-6.80 (m, 30H, $PPh_3$), 5.93 (sept, $^3J_{HH}$ = 6.7 Hz, 2H, NC**H**$(CH_3)_2$), 2.13 (s, 6H, $\mathbf{H_3}CC{=}C\mathbf{CH_3}$ backbone), 0.71 (d, $^3J_{HH}$ = 6.9 Hz, 12H, NCH(C**H**$_3)_2$), -10.13 (dt, $^1J_{HRh}$ = 10.5 Hz, $^2J_{HP}$ = 25.5 Hz, 1H, Rh-**H**); $^{31}$P{$^1$H} NMR ($d_8$-THF, 162 MHz, 25 °C): δ 42.7 (d, $^1J_{PRh}$ = 176.2 Hz, Rh-**P**); $^{13}$C{$^1$H} NMR ($d_8$-THF, 100 MHz, 25 °C): δ 198.6 (dt, $^1J_{CRh}$ = 47.5 Hz, $^2J_{CP}$ = 10.5 Hz, Rh-**C**:), 142.7 (virtual t, $|^1J_{CP} + {}^3J_{CP}|$ = 16.1 Hz, P(*i*-$\mathbf{C}_6H_6$)), 134.8 (virtual t, $|^2J_{CP} + {}^4J_{CP}|$ = 6.1 Hz, P(*o*-$\mathbf{C}_6H_6$)), 128.4 (s, P(*p*-$\mathbf{C}_6H_6$)), 127.8 (virtual t, $|^3J_{CP} + {}^5J_{CP}|$ = 3.7 Hz, P(*m*-$\mathbf{C}_6H_6$)), 124.7 (s, $H_3\mathbf{C}C{=}\mathbf{C}CH_3$ backbone), 53.8 (s, N**C**H$(CH_3)_2$), 21.5 (s, NCH(**C**H$_3)_2$), 10.3 (s, $H_3\mathbf{C}C{=}\mathbf{C}CH_3$ backbone); CHN % {found (calculated)}: C {69.90 (69.80)} H {6.49 (6.39)} N {3.53 (3.46)}.

***cis-[RhH(I$^i$Pr$_2$Me$_2$)$_2$(PPh$_3$)] (cis-75):***

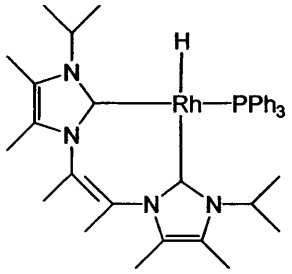

Selected NMR data: $^1$H NMR ($d_8$-THF, 400 MHz, 25 °C): δ 6.09 (sept, $^3J_{HH}$ = 7.5 Hz, 2H, NC**H**(CH$_3$)$_2$), 5.71 (sept, $^3J_{HH}$ = 7.5 Hz, 2H, NC**H**(CH$_3$)$_2$), -9.54 (dd, $^2J_{HP}$ = 32.2 Hz, $^1J_{HRh}$ = 15.4 Hz, 1H, Rh-**H**); $^{31}$P{$^1$H} NMR ($d_8$-THF, 162 MHz, 25 °C): δ 37.9 (d, $^1J_{PRh}$ = 138.1, Rh-**P**Ph$_3$).

***trans-[RhH(I$^i$Pr$_2$Me$_2$)$_2$(PPh$_3$)] (trans-75):***

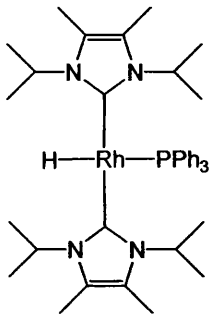


Selected NMR data: $^1$H NMR ($d_8$-THF, 400 MHz, 25 °C): δ 6.50 (sept, $^3J_{HH}$ = 7.1 Hz, 4H, NC**H**(CH$_3$)$_2$), -5.43 (dd, $^2J_{HP}$ = 121.0 Hz, $^1J_{HRh}$ = 34.6 Hz, 1H, Rh-**H**); $^{31}$P{$^1$H} NMR ($d_8$-THF, 162 MHz, 25 °C): δ 52.1 (d, $^1J_{PRh}$ = 161.1 Hz, Rh-**P**Ph$_3$); $^{13}$C{$^1$H} NMR ($d_8$-THF, 100 MHz, 25 °C): δ 200.5 (dd, $^1J_{CRh}$ = 45.3 Hz, $^2J_{CP}$ = 11.0 Hz, Rh-**C**:).

***cis-[RhH(ICy)(PPh$_3$)$_2$] (cis-73):***

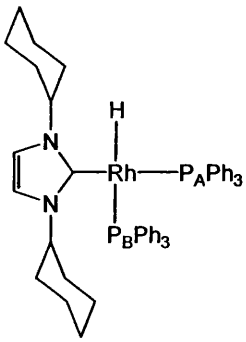


Selected NMR data: $^1$H NMR ($d_8$-THF, 400 MHz, 25 °C): δ -5.88 (ddd, $^2J_{HP_B}$ = 112.0 Hz, $^1J_{HRh}$ = 30.2 Hz, $^2J_{HP_A}$ = 25.2 Hz, 1H, Rh-**H**); $^{31}$P{$^1$H} NMR ($d_8$-THF, 162 MHz, 25 °C): δ 49.2 (dd, $^1J_{PRh}$ = 148.1 Hz, $^2J_{PP}$ = 24.5 Hz, Rh-**P$_A$**Ph$_3$), 42.6 (dd, $^1J_{PRh}$ = 142.9 Hz, $^2J_{PP}$ = 24.5 Hz, Rh-**P$_B$**Ph$_3$).

***trans-[RhH(ICy)(PPh$_3$)$_2$] (trans-73):***

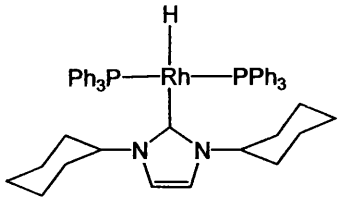


$^1$H NMR ($d_8$-THF, 400 MHz, 25 °C): δ 7.78-6.89 (m, 30H, Rh-PPh$_3$), 6.83 (s, 2H, **HC=CH** backbone), 4.75 (m, 2H, *ipso*-**CH** Cy), 2.90-0.26 (m, 20H, Cy **CH$_2$**), -9.49 (dt, $^2J_{HP}$ = 24.7 Hz, $^1J_{HRh}$ = 11.0 Hz, 1H, Rh-**H**); $^{31}$P{$^1$H} NMR ($d_8$-THF, 162 MHz, 25 °C): δ 44.0 (d, $^1J_{PRh}$ = 175.1 Hz, Rh-**P**); $^{13}$C{$^1$H} NMR ($d_8$-THF, 100 MHz, 25 °C): δ 199.8 (dt, $^1J_{CRh}$ = 46.9 Hz, $^2J_{CP}$ = 11.0 Hz, Rh-**C**:), 142.4 (virtual t, $|^1J_{CP} + {}^3J_{CP}|$ = 17.5 Hz, P(*i*-**C**$_6$H$_6$)), 134.8 (virtual t, $|^2J_{CP} + {}^4J_{CP}|$ = 8.3 Hz, P(*o*-**C**$_6$H$_6$)), 128.5 (s, P(*p*-**C**$_6$H$_6$)), 127.8 (virtual t, $|^3J_{CP} + {}^5J_{CP}|$ = 3.7 Hz, P(*m*-**C**$_6$H$_6$)), 116.4 (s, **HC=CH** backbone), 60.6 (s, N**C**(C$_5$H$_{10}$)), 33.8, 26.6, 26.4 (all s, Cy **CH$_2$**).

***cis-[RhH(ICy)$_2$(PPh$_3$)] (cis-76):***

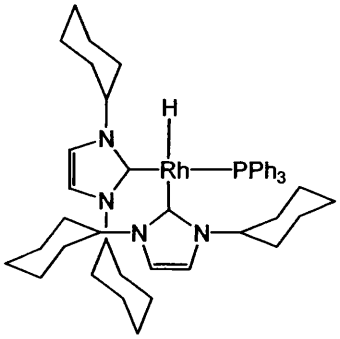


Selected NMR data: $^1$H NMR ($d_8$-THF, 400 MHz, 25 °C): δ -9.05 (dd, $^2J_{HP}$ = 32.4 Hz, $^1J_{HRh}$ = 15.4 Hz, 1H, Rh-**H**); $^{31}$P{$^1$H} NMR ($d_8$-THF, 162 MHz, 25 °C): δ 38.8 (d, $^1J_{PRh}$ = 136.6 Hz, Rh-**P**Ph$_3$).

***trans-[RhH(ICy)$_2$(PPh$_3$)] (trans-76):***

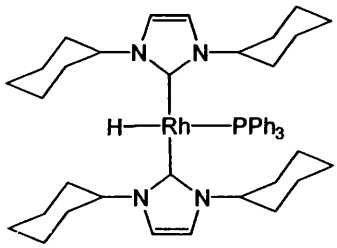


$^1$H NMR ($d_8$-THF, 400 MHz, 25 °C): δ 7.45-7.00 (m, 15H, PPh$_3$), 6.75 (s, 4H, **HC=CH** backbone), 5.31 (m, 4H, *ipso*-**CH** Cy), 2.26-0.60 (m, 40H, Cy **CH$_2$**), -4.99 (dd, $^2J_{HP}$ = 122.4 Hz, $^1J_{HRh}$ = 34.6 Hz, 1H, Rh-**H**); $^{31}$P{$^1$H} NMR ($d_8$-THF, 162 MHz, 25 °C): δ 53.3 (d, $^1J_{PRh}$ = 160.9, Rh-**PPh$_3$**); $^{13}$C{$^1$H} NMR ($d_8$-THF, 100 MHz, 25 °C): δ 199.3 (dd, $^1J_{CRh}$ = 44.7 Hz, $^2J_{CP}$ = 11.0 Hz), 143.7 (d, $J_{CP}$ = 19.0 Hz, P(*i*-**C$_6$H$_6$**)), 133.9 (d, $^2J_{CP}$ = 12.4 Hz, P(*m*-**C$_6$H$_6$**)), 127.5 (d, $^3J_{CP}$ = 7.3 Hz, P(*o*-**C$_6$H$_6$**)), 127.4 (s, P(*p*-**C$_6$H$_6$**)), 115.4 (s, **HC=CH** backbone), 59.1 (s, *ipso*-**CH** Cy), 36.4, 26.8, 26.7 (all s, Cy **CH$_2$**).

***[RhH(ICy)$_3$] (79):***

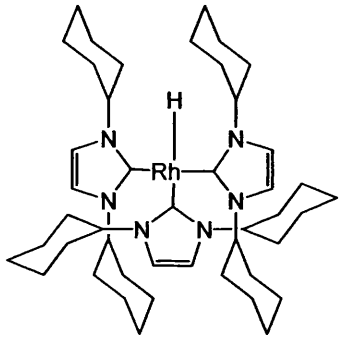


Selected NMR data: $^1$H NMR ($d_8$-THF, 400 MHz, 25 °C): δ -8.12 (d, $^1J_{HRh}$ = 21.4 Hz, 1H, Rh-**H**); $^{13}$C{$^1$H} NMR ($d_8$-THF, 100 MHz, 25 °C): δ 205.2 (d, $^1J_{HRh}$ = 47.0 Hz, Rh-**C**:), 200.8 (d, $^1J_{CRh}$ = 46.0 Hz, Rh-**C**:).

*4.2.5.2. Reaction of IMes with [RhH(PPh$_3$)$_4$] (69)*

***cis-[RhH(IMes)(PPh$_3$)$_2$] (80):***

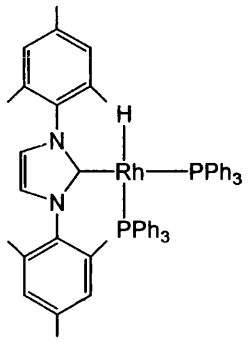


[RhH(PPh$_3$)$_4$] (**69**) (0.05 g, 0.043 mmol) and free IMes (0.05 g, 0.25 mmol) were put into a J. Young's resealable NMR tube in the glove box. Approximately 0.6 mL of $C_6D_6$ or $d_8$-THF was added *via* vacuum transfer. The solution was heated at 50 °C for 48 hours at which point there was no **69** left and **80** could be seen by $^1$H and $^{31}$P{$^1$H} NMR spectroscopy. Layering the initial THF solution with EtOH led to growth of crystals suitable for X-ray diffraction. However, the complex could not be obtained in large enough quantities to assign $^{13}$C{$^1$H} NMR data. CHN analysis could not be performed as some C-H activated product was always present. $^1$H NMR ($d_8$-THF, 400 MHz, -50 °C): δ 8.10-6.60 (m, 34H, PPh$_3$ and *m*-C**H**), 6.24 (d, $^3J_{HH}$ = 20 Hz, 1H, **HC**=C**H** backbone), 6.10 (d, $^3J_{HH}$ = 20 Hz, 1H, **HC**=C**H** backbone), 2.29 (s, 6H, *p*-C**H**$_3$), 1.89 (s, 6H, *o*-C**H**$_3$), 1.78 (s, 6H, *o*-C**H**$_3$), -6.98 (d, $^2J_{HP}$ = 109.2 Hz, $^2J_{HPc}$ = 33.2 Hz, $^1J_{HRh}$ = 22.8 Hz, 1H, Rh-**H**); $^{31}$P{$^1$H} NMR ($d_8$-THF, 162 MHz, 25 °C): δ 39.5 (br, dd, $^1J_{PRh}$ = 171.0 Hz, $^2J_{PP}$ = 57.0 Hz), 36.7 (br, dd, $^1J_{PRh}$ = 146.0 Hz, $^2J_{PP}$ = 57.0 Hz); $^{13}$C{$^1$H} NMR ($d_8$-THF, 100 MHz, 25 °C): δ 209.8 (m, Rh-**C**:).

***[Rh(IMes)''(PPh$_3$)$_2$] (82):***

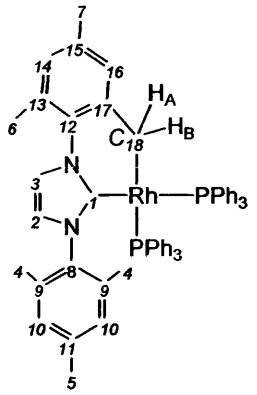


A solution of [RhH(IMes)(PPh$_3$)$_2$] (**80**) formed *in situ* in THF was degassed and 1 atmosphere of ethene was added at room temperature. The solution was then heated at 50 °C for 1.5 hours at which point the sole product was **82**. Attempted isolation of the complex was unsuccessful. Assignment was primarily performed using $^{13}C\{^1H\}$-$^1H$ HMBC and $^{13}C\{^1H\}$-$^1H$ HMQC spectra. $^1H$ NMR (*d*$_8$-THF, 400 MHz, 25 °C): δ 7.17-6.76 (m, 30H, Rh-PPh$_3$), 6.44 (s, 1H, **H***14*), 6.41 (s, 1H, **HC=CH** backbone), 5.11 (s, 1H, **H***16*), 2.54 (m, 1H, **H***18$_A$*), 1.78 (s, 3H, **H***7*), 1.33 (m, 1H, **H***18$_B$*), 0.70 (br s, 3H, **H***6*); $^{31}P\{^1H\}$ NMR (*d*$_8$-THF, 162 MHz, 25 °C):δ 44.9 (dd, $^1J_{PRh}$ = 155.0 Hz, $^2J_{PP}$ = 60.2 Hz, Rh-**P**Ph$_3$), 36.0 (dd, $^1J_{PRh}$ = 142.1 Hz, $^2J_{PP}$ = 60.2 Hz, Rh-**P**Ph$_3$); $^{13}C\{^1H\}$ NMR (*d*$_8$-THF, 100 MHz, 25 °C): δ 201.0 (ddd, $^2J_{CP}$ = 105.7 Hz, $^1J_{CRh}$ = 57.9 Hz, $^2J_{CP}$ = 15.6 Hz, Rh-**C***1*), 146.1 (dd, $^2J_{CRh}$ = 6.4 Hz, $^3J_{CP}$ = 1.8 Hz, **C***17*), 138.2 (s, **C***15*), 135.8 (s, **C***12*), 129.1 (s, **C***13*), 124.2 (s, **C***16*), 123.0 (s, **C***14*), 26.2 (ddd, $^1J_{CRh}$ = 58.2 Hz, $^2J_{CP}$ = 18.8 Hz, $^2J_{CP}$ = 11 Hz, **C***18*), 21.3 (s, **C***7*), 16.4 (s, **C***6*).

*4.2.5.3. [RhH(NHC)$_2$(CO)] (NHC = I$^i$Pr$_2$Me$_2$, ICy, IMes)*

[RhH(PPh$_3$)$_3$(CO)] (**70**) (0.05 g, 0.043 mmol) and free NHC (I$^i$Pr$_2$Me$_2$, ICy, IMes, 2-6 equivalents) were put into a J. Young's resealable NMR tube in the glove box. Approximately 0.6 mL of $C_6D_6$ or *d*$_8$-THF was added *via* vacuum transfer. Immediate reaction occurred at room temperature to afford complexes of the general formula [RhH(NHC)$_2$(CO)] and [Rh(NHC)$_3$(CO)]$^+$ (scheme 4.2.). In many cases,

mixtures could not be separated. In these instances, resonances associated with the NHC groups could not be assigned to specific products due to overlapping signals. Thus, the NMR data for analogues of **I** and **II** presented below reports definitive resonances only. When an isomer for a particular complex is not reported it is because it was not observed. The data for the cationic species (analogues of **III**) are reported later in section 4.2.8.

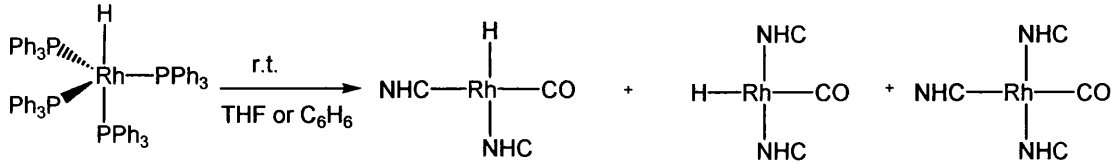


**Scheme 4.2.** Formation of 3 NHC containing products from reaction of **70** and free NHC at room temperature.

***cis-[RhH(I$^i$Pr$_2$Me$_2$)$_2$(CO)] (cis-84):***

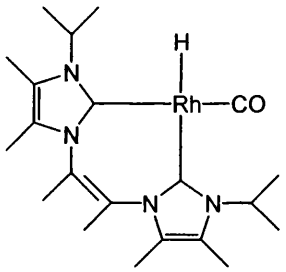


Selected NMR data: $^1$H NMR ($d_8$-THF, 400 MHz, 25 °C): δ 6.12 (sept, $^3J_{HH}$ = 6.6 Hz, 2H, C**H**(CH$_3$)), 5.66 (sept, $^3J_{HH}$ = 6.6 Hz, 2H, C**H**(CH$_3$)), -6.44 (d, $^1J_{HRh}$ = 19.2 Hz, 1H, Rh-**H**).

***trans-[RhH(I$^i$Pr$_2$Me$_2$)$_2$(CO)] (trans-84):***

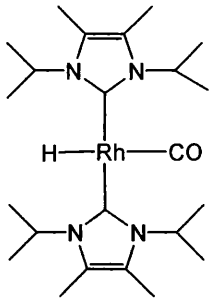

Selected NMR data: $^1$H NMR ($d_8$-THF, 400 MHz, 25 °C): δ 6.00 (sept, $^3J_{HH}$ = 6.6 Hz, 4H, *ipso*-C**H** Cy), -4.84 (d, $^1J_{HRh}$ = 25.8 Hz, 1H, Rh-**H**).

***trans-[RhH(ICy)$_2$(CO)] (85):***

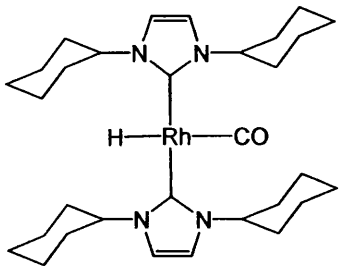


Selected NMR data: $^1$H NMR ($d_8$-THF, 400 MHz, 25 °C): δ 7.04 (s, 4H, **HC=CH** backbone), 5.30 (m, 4H, *ipso*-C**H** Cy), 2.53-0.77 (m, 40H, Cy C**H**$_2$), -4.55 (d, $^1J_{HRh}$ = 25.8 Hz, 1H, Rh-**H**); $^{13}$C{$^1$H} NMR ($d_8$-THF, 100 MHz, 25 °C): δ 196.0 (d, $^1J_{CRh}$ = 59.7 Hz, Rh-**C**O), 192.5 (d, $^1J_{CRh}$ = 46.0 Hz, Rh-**C**:), 116.2 (s, H**C=C**H backbone), 60.3 (s, *ipso*-**C**H Cy), 34.0, 26.8, 26.4 (all s, Cy **C**H$_2$); IR (cm$^{-1}$): 1919 ($\nu_{CO}$).

***trans-[RhH(IMes)$_2$(CO)] (86):***

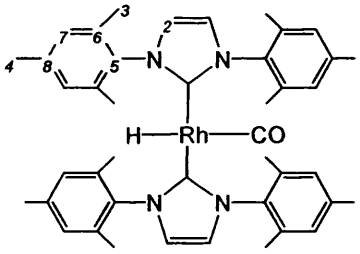


Removal of solvent from the original solution gave a light brown sticky solid. Dissolving this in ethanol (1 mL) gave immediate precipitation of a bright yellow microcrystalline solid identified as **86**. Crystals were not able to be obtained directly from this solid. However, crystals of excellent quality were grown from a crude benzene solution of the compound (with free NHC and free phosphine present), layered with hexane. $^1$H NMR ($d_8$-THF, 400 MHz, 25 °C): δ 6.91 (s, 4H, **HC=CH** backbone), 6.74 (s, 8H, *m*-C**H**), 2.37 (s, 12H, *p*-C**H**$_3$), 1.78 (s, 24H, *o*-C**H**$_3$), -4.71 (d, $^1J_{HRh}$ = 26.3 Hz, 1H, Rh-**H**); $^{13}$C{$^1$H} NMR ($d_8$-THF, 100 MHz, 25 °C): δ 197.7 (d, $^1J_{CRh}$ = 44.1 Hz, Rh-:**C**), 194.5 (d, $^1J_{CRh}$ = 60.7 Hz, Rh-**CO**), 138.7 (s, **C***5*), 136.8

(s, C*8*), 136.4 (s, C*6*), 128.9 (s, C*7*), 121.1 (s, HC=CH backbone), 21.1 (s, *p*-$CH_3$), 18.4 (s, *o*-$CH_3$); IR ($cm^{-1}$): 2036 ($\nu_{HRh}$), 1914 ($\nu_{CO}$); CHN % {found (calculated)}: C {69.80 (69.72)} H {6.65 (6.67)} N {7.56 (7.36)}.

4.2.6. Rhodium formate products

**[Rh(ICy)$_2$(PPh$_3$)(OC(O)H)] (105):**

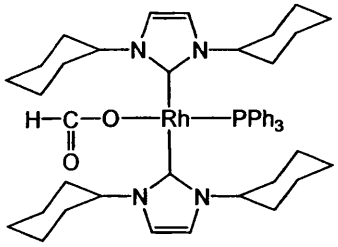


*trans*-[RhH(ICy)$_2$(PPh$_3$)] (**76**) was formed in $C_6D_6$ in a J. Young's resealable NMR tube. 1 atm $CO_2$ was then added at room temperature. Volatiles were removed *in vacuo* and the residue was washed with hexane affording a yellow/orange, oily solid. $^1$H NMR ($C_6D_6$, 400 MHz, 25 °C): δ 8.60 (dd, $^3J_{HRh}$ = 1.6 Hz, $^4J_{HP}$ = 7.1 Hz, 1H, OC(O)**H**), 6.48 (s, 4H, **HC=CH** backbone), 5.65 (m, 4H, *ipso*-**CH** Cy), 2.18–0.37 (m, 40H, Cy $CH_2$); $^{31}P\{^1H\}$ NMR ($C_6D_6$, 162 MHz, 25 °C): δ 56.6 (d, $^1J_{PRh}$ = 217.0 Hz, Rh-**P**Ph$_3$).

**[Rh(ICy)$_2$(CO)(O$^{13}$C(O)H)] (106):**

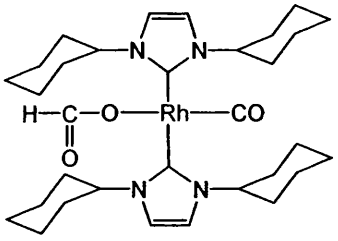


A solution of [RhH(ICy)$_2$(CO)] (**85**) in $C_6D_6$ formed in a J. Young's resealable NMR tube was degassed. 1 atm of $^{13}CO_2$ was added at room temperature and the solution immediately changed from dark red to a bright yellow. A bright yellow precipitate also formed immediately. This was removed by cannula filtration and the volatiles removed *in vacuo*. The residue was washed with hexane affording a

sticky yellow solid. $^1$H NMR ($C_6D_6$, 400 MHz, 25 °C): δ 8.60 (dd, $^1J_{HC}$ = 188.8 Hz, $^3J_{HRh}$ = 1.6 Hz , 1H, OC(O)**H**), 6.56 (s, 4H, **HC=CH** backbone), 5.88 (tt, $^3J_{HH}$ = 12.1 Hz, $^4J_{HH}$ = 3.8 Hz, 4H, *ipso*-**CH** Cy), 1.95–0.73 (m, 40H, Cy **CH$_2$**); $^{13}$C{$^1$H} NMR ($C_6D_6$, 100 MHz, 25 °C): δ 193.2 (d, $^1J_{CRh}$ = 77.2 Hz, Rh-**C**O), 185.4 (d, $^1J_{CRh}$ = 42.3 Hz, Rh-**C**:), 167.0 (s, **O**C(O)H) 117.2 (s, **HC=CH** backbone), 60.81 (s, *ipso*-**CH** Cy), 34.9, 27.1, 26.6 (all s, Cy **CH$_2$**); IR (cm$^{-1}$): 1930 ($\nu_{CO}$), 1619 ($\nu_{OCOasym}$), 1237 ($\nu_{OCOsym}$).

**[Rh(IMes)$_2$(CO)(OC(O)H)] (107):**

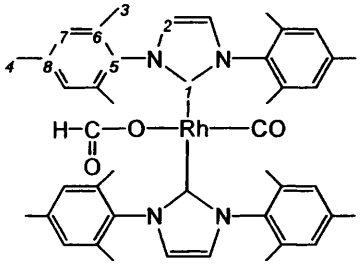


A sample of [RhH(IMes)$_2$(CO)] (**86**) (0.02 g) was dissolved in $C_6D_6$ in a J. Young's resealable NMR tube and degassed. 1 atm $CO_2$ was added at room temperature and this immediately resulted in the solution changing from bright yellow to almost colourless. IR spectra of both $^{12}CO_2$ and $^{13}CO_2$ material was recorded. $^1$H NMR ($C_6D_6$, 400 MHz, 25 °C): δ 8.00 (s, 1H, OC(O)**H**), 6.86 (s, 8H, *m*-**CH**), 6.13 (s, 4H, **HC=CH** backbone), 2.29 (s, 12H, *p*-**CH$_3$**), 2.03 (s, 24H, *o*-**CH$_3$**); $^{13}$C{$^1$H} NMR ($C_6D_6$, 100 MHz, 25 °C): δ 191.9 (d, $^1J_{CRh}$ = 77.2 Hz, Rh-**C**O), 188.67 (d, $^1J_{CRh}$ = 44.1 Hz, **C***1*), 167.3 (s, **O**C(O)H (from $^{13}$C{$^1$H}-$^1$H HMBC $^1J_{CH}$ = 188.3 Hz)), 138.0, 137.6, 136.7 (all s, **C***5* **C***6*, **C***8*), 129.9 (s, **C***7*), 122.6 (s, **C***2*), 21.9 (s, *p*-**CH$_3$**), 19.5 (s, *o*-**CH$_3$**); IR (cm$^{-1}$): 1932 ($\nu_{CO}$), 1633 ($\nu_{OCOasym}$), 1320 ($\nu_{OCOsym}$), 1594 ($\nu_{O^{13}COasym}$), 1263 ($\nu_{O^{13}COsym}$); CHN % {found (calculated)}: C {67.12 (67.34)} H {5.88 (6.29)} N {7.15 (7.14)}.

**ICy:$CO_2$ (108):**

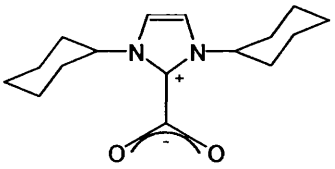

A solution of ICy (0.02 g) in degassed THF (0.6 mL) was cooled using liquid $N_2$. $CO_2$ was condensed across using a vacuum. As the solution was warmed, a pale yellow solid immediately precipitated out. Crystals were grown from $CD_2Cl_2$ layered with hexane and the compound was identified by X-ray diffraction techniques as a zwitterionic species consisting of a carbene:$CO_2$ adduct, which is formed in quantitative yield. $^1$H NMR ($CD_2Cl_2$, 400 MHz, 25 °C): δ 7.01 (s, 2H, **HC=CH** backbone), 5.05 (tt, $^3J_{HH}$ = 11.5 Hz, $^4J_{HH}$ = 3.8 Hz, 2H, *ipso*-**CH** Cy), 2.14 (m, 4H Cy **$CH_2$**), 1.86 (m, 4H, Cy **$CH_2$**), 1.61-1.37 (m, 12H, Cy **$CH_2$**); $^{13}$C {$^1$H} NMR ($CD_2Cl_2$, 100 MHz, 25 °C): δ 155.4 (s, C:-$CO_2$), 144.4 (s, **C**:-$CO_2$), 116.5 (s, **HC=CH** backbone), 58.3 (s, *ipso*-**CH**), 33.8, 25.6 (both s, Cy **$CH_2$**), 25.3 (s, *p*- Cy **$CH_2$**); IR ($cm^{-1}$): 1658 ($\nu_{OCOasym}$), 1461 ($\nu_{OCOsym}$).

4.2.7. Dimeric and trimeric species

**[{Rh(PPh$_3$)$_2$}$_2$(μ-H)(μ-PPh$_2$)] (83):**

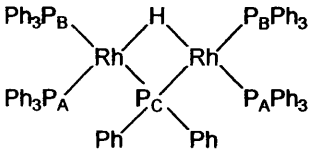


A solution of [RhH(PPh$_3$)$_4$] (**69**) (0.05 g, 0.043 mmol) heated in THF (0.75 mL) at 70 °C for 4 days (or 100 °C overnight) dimerises to the complex **83**. Small red crystals were grown from THF/ethanol. Yield: 0.02 g (38 %). $^1$H NMR ($d_8$-THF, 400 MHz, 25 °C): δ 7.81-6.15 (m, 70H, aromatic protons), -8.81 (m, 1H, Rh-**H**-Rh); $^{31}$P NMR ($d_8$-THF, 162 Hz, 25 °C): δ 174.1 (ttt, measured from spectra: $^1J_{PRh}$ = 136.5 Hz, $^2J_{PcPB}$= 221.0 Hz, $^2J_{PcPA}$ = 15.5 Hz, **$P_C$**), 41.9 (m, values from simulation: $^1J_{PARh}$ = 195.3 Hz, $^1J_{PA'Rh}$ = 7.8 Hz, $^4J_{PAPA'}$= 34.7 Hz, $^2J_{PAPB}$ = 28.6 Hz, $^4J_{PAPB'}$ = 4.0 Hz, $^2J_{PAPc}$ = 15.0 Hz, **$P_A$**), 31.4 (m, values from simulation: $^1J_{PBRh}$ = 158.2 Hz, $^1J_{PB'Rh}$ =

2.9 Hz, $^4J_{P_BP_{B'}}$ = 2.3 Hz, $^2J_{P_BP_A}$ = 28.6 Hz, $^4J_{P_{B'}P_A}$ = 4.03 Hz, $^2J_{P_BP_C}$ = 221.3, $\mathbf{P_B}$); CHN % {found (calculated)}: C {67.88 (70.01)} H {5.05 (4.97)}.

**[{Rh(CO)}$_2$(μ-H)(μ-PPh$_2$)] (102):**

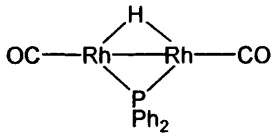


A THF solution of [RhH(PPh$_3$)$_3$(CO)] (**70**) (0.10 g (0.086 mmol) in 0.6 mL) was heated at 70 °C for 1 day. After this time about 50 % had dimerised to give **102**. $^1$H NMR ($d_8$-THF, 400 MHz, 25 °C): δ 7.19-6.81 (m, 10H, Rh-PPh$_2$-Rh), -11.65 (dt, $^2J_{HP}$ = 16 Hz $^1J_{HRh}$ = 20 Hz, 1H, Rh-**H**-Rh); $^{31}$P NMR ($d_8$-THF, 162 Hz, 25 °C): δ 186.2 (t, $^1J_{PRh}$ = 113.4 Hz, Rh-**P**Ph$_2$-Rh); $^{13}$C{$^1$H} NMR ($d_8$-THF, 100 MHz, 25 °C): δ 208.9 ($^1J_{CRh}$ = 60.4 Hz, $^2J_{CP}$ = 10.1 Hz, Rh-**C**O).

**[{Rh(CO)}$_3$(PPh$_3$)$_2$(μ-PPh$_2$)$_3$] (103):**

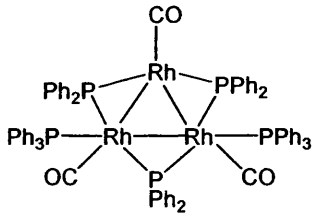


This complex has been reported in the literature.[16] A THF solution of [RhH(PPh$_3$)$_3$(CO)] (**70**) (0.10 g (0.086 mmol) in 0.6 mL) was heated at 70 °C for 4 days. After this time the solution was pumped to dryness under vacuum, redissolved in 2 mL of toluene and layered with 10 mL of ethanol. This yielded dark green crystals suitable for X-ray diffraction analysis. Yield 0.06 g (47 %). $^1$H NMR ($d_8$-THF, 400 MHz, 25 °C): δ 8.50-5.87 (m, aromatic protons); $^{31}$P{$^1$H} NMR ($d_8$-THF, 162 Hz, 25 °C): δ 135.0 (m, Rh-**P**Ph$_2$-Rh), 41.5 (m, Rh-**P**Ph$_3$).

**[{Rh(I$^i$Pr$_2$Me$_2$)$_2$)}(μ-CO)$_2${Rh(PPh$_3$)$_2$}] (87):**

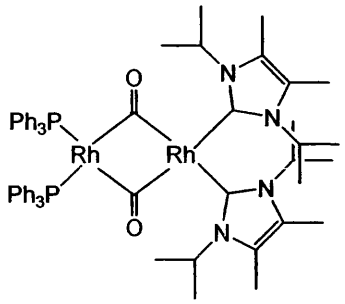


[RhH(PPh$_3$)$_3$(CO)] (**70**) (0.025 g, 0.027 mmol) and I$^i$Pr$_2$Me$_2$ (0.014 g, 0.08 mmol) were dissolved in $C_6D_6$ in a J. Young's resealable NMR tube. From the $^1$H NMR spectrum this appeared to form a mixture of *cis*- and *trans*-[RhH(IPr$_2$Me$_2$)$_2$(CO)]. However, a small amount of **87** was seen by phosphorus NMR and when the solution was layered with hexane large, dark red crystals of **87** were isolated. Yield: 0.01 g (32 %). $^1$H NMR ($C_6D_6$, 400 MHz, 25 °C): δ 7.89-7.69 (m, 12H, PPh$_3$), 7.11-6.92 (m, 18H, PPh$_3$), 6.02 (sept, $^3J_{HH}$ = 7.1 Hz, 4H, NH(CH$_3$)$_2$), 1.75 (s, 12H, H$_3$CC=CCH$_3$ backbone), 1.26 (d, $^3J_{HH}$ = 7.1 Hz, 12H, NH(CH$_3$)$_2$), 0.98 (d, $^3J_{HH}$ = 7.13 Hz, 12H, NH(CH$_3$)$_2$); $^{31}$P{$^1$H} NMR ($C_6D_6$, 162 MHz, 25 °C): δ 37.6 (dd, $^1J_{PRh}$ = 236.5 Hz, $^2J_{PRh}$ = 7.7 Hz, Rh-PPh$_3$); $^{13}$C{$^1$H} NMR ($C_6D_6$, 100 MHz, 25 °C)[17]: δ 191.2 (d, $^1J_{CRh}$ = 57.0 Hz, Rh-C:), 141.5 (virtual t, $|^1J_{CP} + {}^3J_{CP}|$= 12.9 Hz, P(*i*-C$_6$H$_6$)), 135.2 (virtual t, $|^2J_{CP} + {}^4J_{CP}|$= 8.3 Hz, P(*m*-C$_6$H$_6$)), 124.6 (s, CH$_3$C=CCH$_3$ backbone), 54.1 (s, C(CH$_3$)$_2$), 22.3, 21.7 (both s, C(CH$_3$)$_2$), 11.0 (s, CH$_3$C=CCH$_3$); IR (cm$^{-1}$): 1708 ($\nu_{CO}$); CHN % {found (calculated)}: C {62.33 (62.83)} H {6.27 (6.15)} N {4.93 (4.88)}.

4.2.8. Cationic species

**[Rh(IEt$_2$Me$_2$)$_4$][P(Ph$_2$)(O)$_2$] (96):**

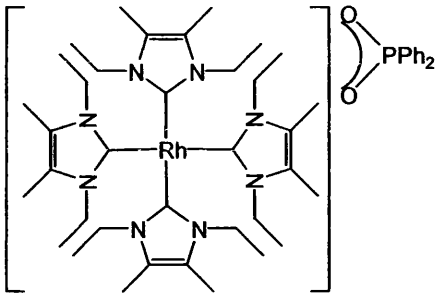


[RhH(PPh$_3$)$_4$] (**69**) (0.05 g, 0.043 mmol) and IEt$_2$Me$_2$ (0.014 g, 0.092 mmol) were dissolved in dry $d_8$-THF in a J. Young's resealable NMR tube. When the solution was pumped dry, redissolved in benzene and layered with hexane, pale yellow crystals of **96** precipitated out. $^1$H NMR ($d_8$-THF, 400 MHz, 25 °C): δ 5.41 (dq, $^3J_{HMe}$ = 7.1 Hz, $^2J_{HH}$ = 6.6 Hz, 8H, C**Ha**HCH$_3$), 3.78 (dq, $^3J_{HMe}$ = 7.1 Hz, $^2J_{HH}$ = 6.6 Hz, 8H, C**Hb**HCH$_3$), 2.04 (s, 24H, **H**$_3$CC=CC**H**$_3$ backbone), 0.44 (t, $^3J_{HH}$ = 7.1 Hz, 24H, CH$_2$C**H**$_3$); $^{13}$C{$^1$H} NMR ($d_8$-THF, 100 MHz, 25 °C): δ 192.3 (d, $^1J_{CRh}$ = 45.0 Hz, Rh-**C**:), 124.3 (s, CH$_3$**C**=**C**CH$_3$ backbone), 43.9 (s, **C**H$_2$CH$_3$), 14.5 (s, CH$_2$**C**H$_3$), 9.4 (s, **C**H$_3$C=**C**CH$_3$ backbone).

**[Rh(IPr$_2$Me$_2$)$_4$]$^+$ (97):** [RhH(PPh$_3$)$_4$] (**69**) (0.05 g, 0.043 mmol) and I$^i$Pr$_2$Me$_2$ (0.048 g, 0.26 mmol) were dissolved in dry $d_8$-THF. When this solution was pumped to dryness, dissolved in benzene and layered with hexane, pale yellow crystals precipitated out. These were identified by NMR as **97** but the anion could not be identified. $^1$H NMR ($d_8$-THF, 400 MHz, 25 °C): δ 6.07 (sept, $^3J_{HH}$ = 7.2 Hz, 8H, NC**H**(CH$_3$)$_2$), 2.16 (s, 24H, **H**$_3$CC=CC**H**$_3$ backbone), 1.46 (d, $^3J_{HH}$ = 7.2 Hz, 24H, NCH(C**H**$_3$)$_2$), 0.58 (d, $^3J_{HH}$ = 7.2 Hz, 24H, NCH(C**H**$_3$)$_2$); $^{13}$C{$^1$H} NMR ($d_8$-THF, 100 MHz, 25 °C): δ 192.5 (d, $^1J_{CRh}$ = 46.9 Hz, Rh-**C**:), 125.4 (s, H$_3$**C**C=**C**CH$_3$ backbone), 53.2 (s, N**C**H(CH$_3$)$_2$), 20.9 (s, NCH(**C**H$_3$)$_2$), 10.5 (s, **H**$_3$CC=CC**H**$_3$ backbone).

**[Rh(I$^i$Pr$_2$Me$_2$)$_4$][PF$_6$] (101):**

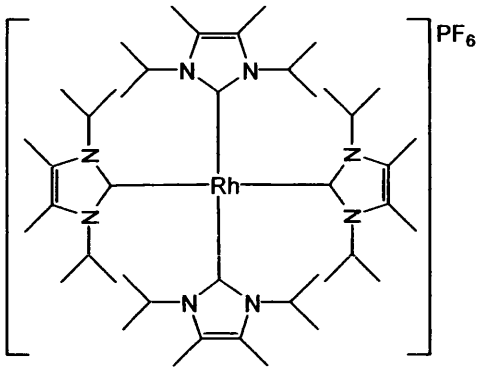


A sample of **97** (ca. 0.02 mg) was dissolved in $CD_2Cl_2$ (0.6 mL) and a saturated water solution of $KPF_6$ (0.01 g in 2 mL) was stirred in and agitated for 15 mins. This led to substitution of the unknown anion to give **101**. Although the solution did not change colour, cuboid crystals that grew from a $CD_2Cl_2$ solution layered with pentane were a lilac colour when viewed through one face and red wine coloured when viewed through a different face. Unfortunately the X-ray diffraction data was unable to be solved to within a low enough $R^2$ value due to the high symmetry of the complex. $^1$H NMR ($CD_2Cl_2$, 400 MHz, 25 °C): δ 4.00 (br, 8H, NC**H**(CH$_3$)$_2$), 2.16 (br s, 24H, **H**$_3$CC=CC**H**$_3$ backbone), 1.55 (br d, $^3J_{HH}$ = 6.9 Hz, 48H, NCH(C**H**$_3$)$_2$); $^{31}$P{$^1$H} NMR ($CD_2Cl_2$, 162 MHz, 25 °C): δ -145.0 (sept, $J_{PF}$ = 711.0 Hz, $PF_6^-$); IR (cm$^{-1}$): 722 ($\nu_{PF}$).

**[Rh(ICy)$_4$]$^+$ (98):**

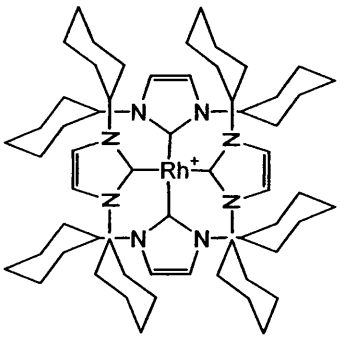


ICy (0.15 g, 0.65 mmol) and [RhH(PPh$_3$)$_4$] (**69**) (0.13 g, 0.11 mmol) were dissolved in $d_8$-THF in a J. Young's resealable ampoule. The solution was stirred at room

temperature for 24 hours. After this time the THF was removed *in vacuo* and the remaining sticky red solid redissolved in benzene (0.3 mL). This was layered with hexane. Pale yellow crystals precipitated out and from X-ray analysis were identified as $[Rh(ICy)_4]^+$. The crystal data was unfortunately not good enough to identify the anion conclusively. $^1H$ NMR ($d_8$-THF, 400 MHz, 25 °C): δ 7.81-6.80 (m, 10H, anion), 7.41 (s, 8H, **HC=CH** backbone), 6.30-4.42 (br m, 8H, *ipso*-**CH** Cy), 2.81-0.73 (br m, 80H, Cy $CH_2$).

**$[Rh(I^iPr_2Me_2)_3(CO)][(P((CH_3)_2)_3(O)_4)H]$ (91):**

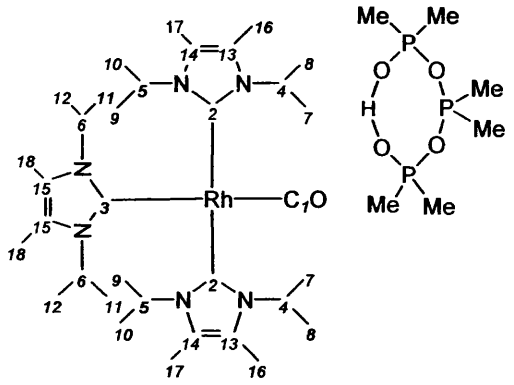

$[RhH(PPh_3)_3(CO)]$ (**70**) (0.025 g, 0.027 mmol) and $I^iPr_2Me_2$ (0.027 g, 0.16 mmol) were dissolved in $d_8$-THF in a J. Young's resealable NMR tube. Upon layering the solution with hexane, crystals of **91** grew, which were analysed using X-ray diffraction. It is likely that the anion associated with each molecule of $[Rh(^iIPr_2Me_2)_3(CO)]^+$ is different $^1H$ NMR ($d_8$-THF, 400 MHz, -70 °C): δ 6.03 (sept, $^3J_{HH}$ = 6.9 Hz, 2H, **H***4/5*), 5.34 (sept, $^3J_{HH}$ = 6.9 Hz, 2H, **H***4/5*), 5.16 (sept, $^3J_{HH}$ = 6.85 Hz, 2H, **H***6*), 2.35 (s, 6H, **H***16/17*), 2.25 (s, 12H, **H***18*), 1.48 (broad, 12H, **H***11/12*), 0.74 (d, $^3J_{HH}$ = 6.9 Hz, 12H, **H***8/7/9/10*), 0.67 (d, $^3J_{HH}$ = 6.9 Hz, 12H, **H***8/7/9/10*); $^{13}C\{^1H\}$ NMR ($d_5$-pyridine, 100 MHz, 25 °C): δ 192.2 (d, $^1J_{CRh}$ = 62.5 Hz, Rh-**C***1*), 180.1 (d, $^1J_{CRh}$ = 46.9 Hz, Rh-**C***3*), 179.2 (d, $^1J_{CRh}$ = 42.3 Hz, Rh-**C***2*) 126.2 (s, **C***15*), 126.2 (s, **C***13/14*), 51.7 (s, **C***6*), 51.0 (s, **C***4/5*), 23.5, 23.3 (both s, **C***11/12*), 22.6, 21.9 (both s, **C***7/8/9/10*), 10.4 (s, **C***18*), 10.3 (s, **C***16/17*); IR ($cm^{-1}$): 1955 ($\nu_{CO}$); CHN % {found (calculated)}: C {57.20 (52.23)} H {7.92 (8.66)} N {8.47 (9.14)}.

**[Rh(I$^i$Pr$_2$Me$_2$)$_3$(CO)][PF$_6$] (89):**

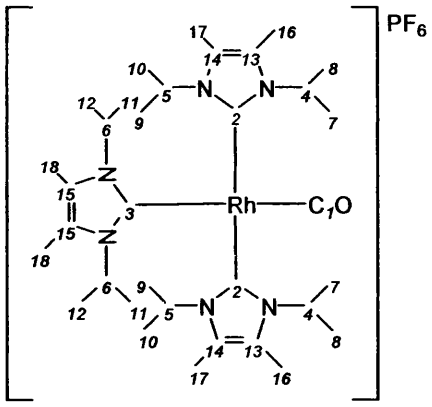


[RhH(PPh$_3$)$_3$(CO)] (**70**) (0.025 g, 0.027 mmol) and I$^i$Pr$_2$Me$_2$ (0.027 g, 0.16 mmol) were dissolved in $d_8$-THF in a J. Young's resealable NMR tube. Upon layering the solution with hexane, yellow crystals grew, which were identified as [Rh(I$^i$Pr$_2$Me$_2$)$_3$(CO)]$^+$ by NMR spectroscopy. A saturated, degassed solution of $KPF_6$ (0.01 g) in deionised water (2 mL) was stirred into a $CD_2Cl_2$ solution of [Rh(I$^i$Pr$_2$Me$_2$)$_3$(CO)]$^+$ (0.6 mL) and agitated for 15 mins. The water layer was then removed *via* cannula. The counterions were replaced to give **89**. Yellow crystals of excellent quality were grown from a $CD_2Cl_2$ solution layered with pentane. $^1$H NMR ($CD_2Cl_2$, 400 MHz, -70 °C): δ 5.88 (br sept, $^3J_{HH}$ = 6.6 Hz, 2H, **H***5/6*), 5.16 (br sept, $^3J_{HH}$ = 6.6 Hz, 2H, **H***4*), 5.00 (br sept, $^3J_{HH}$ = 6.6 Hz, 2H, **H***5/6*), 2.18 (s, 6H, **H***16*), 2.09 (s, 6H, **H***14/15*), 2.05 (s, 6H, **H***14/15*), 1.45 (d, $^3J_{HH}$ = 6.6 Hz, 6H, **H***7/8*), 1.38 (br t (actually two d overlapping), 12H, **H***7/8* and **H***9/10/11/12*), 1.30 (d, $^3J_{HH}$ = 6.55Hz, 6H, **H***9/10/11/12*), 0.57 (d, $^3J_{HH}$ = 6.55Hz, 6H, **H***9/10/11/12*), 0.48 (d, $^3J_{HH}$ = 6.55Hz, 6H, **H***9/10/11/12*); $^{19}$F NMR ($CD_2Cl_2$, 376.5 MHz, 25 °C): δ 73.6 (d, $^1J_{FP}$ = 709.2 Hz, $PF_6^-$); $^{31}$P{$^1$H} NMR ($CD_2Cl_2$, 162 MHz, 25 °C): δ -144.47 (sept, $^1J_{PF}$ = 709.2 Hz, $PF_6^-$); $^{13}$C{$^1$H} NMR ($CD_2Cl_2$, 100 MHz, 25 °C): δ 191.2 (d, $^1J_{CRh}$ = 64.3 Hz, Rh-**C**O), 179.47 (d, $^1J_{CRh}$ = 39.5 Hz, Rh-**C***3*), 179.0 (d, $^1J_{CRh}$ = 43.2 Hz, Rh-**C***2*) 126.7 (s, **C***15*), 125.5 (d, 6.4 Hz, **C***13/14*), 53.3 (s, **C***6*), 50.6 (s, **C***4/5*), 21.8, 21.5 (both s, **C***16/17*), 20.18 (s, **C***18*), 10.0 (s, **C***7/8/9/10*), 8.0 (s, **C***11/12*); IR (cm$^{-1}$): 1953 ($\nu_{CO}$), 722 ($\nu_{PF}$); CHN % {found (calculated)}: C {50.00 (49.94)} H {7.40 (7.33)} N {10.29 (10.18)}.

**[Rh(ICy)$_3$(CO)][PF$_6$] (90):**

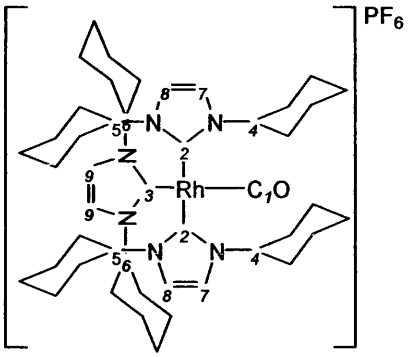


[RhH(PPh$_3$)$_3$(CO)] (**70**) (0.025 g, 0.027 mmol) and ICy (0.037 g, 0.16 mmol) were combined in a J. Young's resealable NMR tube and dissolved in $C_6D_6$ or $d_8$-THF and left at room temperature. After 48 hours a yellow crystalline solid precipitated out of solution. This was identified by NMR spectroscopy as being [Rh(ICy)$_3$(CO)]$^+$. $^1$H NMR ($d_5$-pyridine, 400 MHz, 25 °C): δ 7.67 (s, 2H, **H*9***), 7.48 (s, 4H, **H*7/8***), 4.68 (br m, 4H, **H*4/5***), 4.34 (br m, 2H, **H*6***), 2.55-0.60 (m, 60H, Cy **CH$_2$**); $^{13}$C NMR ($d_5$-pyridine, 100 MHz, 25 °C): δ 192.1 (d, $^1J_{CRh}$ = 61.6 Hz, Rh-**C*1***), 180.79 (d, $^1J_{CRh}$ = 41.4 Hz, **C*2***), 178.55 (d, $^1J_{CRh}$ = 46.0 Hz, **C*3***), 120.1 (s, **C*9***), 119.2 (s, **C*7/8***), 60.5 (s, **C*6***), 58.8 (s, **C*4/5***), 35.7 (s), 34.1 (s), 25.8 (m), 25.2 (s), 24.8 (s) (all Cy **CH$_2$**); IR (cm$^{-1}$): 1952 ($\nu_{CO}$).

A saturated, degassed solution of $KPF_6$ (0.01 g) in deionised water (2 mL) was stirred into a $CD_2Cl_2$ solution of [Rh(ICy)$_3$(CO)]$^+$ (0.6 mL) and agitated for 15 mins. The water layer was then removed *via* cannula. This resulted in the substitution of the unknown anions for [PF$_6$]$^-$ giving **90** in complete conversion. Large yellow crystals were grown from a $CD_2Cl_2$ solution, layered with pentane. $^1$H NMR ($CD_2Cl_2$, 400 MHz, 25 °C): δ 7.09 (s, 4H, **H*8/9***), 7.03 (s, 2H, **H*9***), 4.6 (br m, 2H, **H*6***), 4.34 (br m, 4H, **H*4/5***), 2.41-0.17 (m, 60H, Cy **CH$_2$**); $^{19}$F NMR ($CD_2Cl_2$, 376.5 MHz, 25 °C): δ 73.6 (d, $^1J_{FP}$ = 711.3 Hz, **PF$_6$**); $^{31}$P{$^1$H} NMR ($CD_2Cl_2$, 162 MHz, 25 °C): δ -144.5 (sept, $^1J_{PF}$ = 711.3 Hz, **PF$_6$**); $^{13}$C{$^1$H} NMR ($CD_2Cl_2$, 100 MHz, 25 °C): δ 190.9 (d, $^1J_{CRh}$ = 62.5 Hz, Rh-**C*1***), 180.6 (d, $^1J_{CRh}$ = 42.3, Rh-**C*2***), 178.7 (d, $^1J_{CRh}$ = 46.0, Rh-**C*3***), 118.3 (s, **C*9***), 117.7 (s, **C*7/8***), 59.5 (s, **C*6***), 58.1 (s, **C*4/5***),

34.4, 33.8, 25.1, 24.7, 24.2, 24.0 (all s, ICy); IR ($cm^{-1}$): 1956 ($\nu_{CO}$), 723 ($\nu_{PF}$); CHN % {found (calculated)}: C {56.2 (56.78)} H {7.32 (7.46)} N {8.46 (8.64)}.

**[Rh(I$^i$Pr$_2$Me$_2$)$_2$(ICy)(CO)][PF$_6$] (95):**

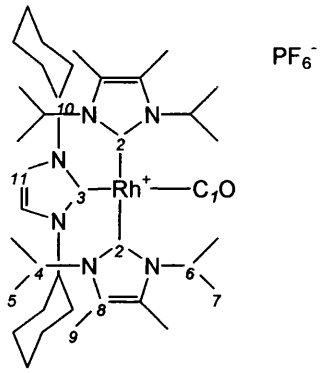


[{Rh(PPh$_3$)$_2$}(μ-CO)$_2${Rh(I$^i$Pr$_2$Me$_2$)$_2$}] (**87**) (0.10 g, 0.0875 mmol) and ICy (0.02 g, 0.086 mmol) were dissolved in $d_8$-THF (0.6 mL) in a J. Young's resealable NMR tube. Reaction was observed immediately at room temperature by $^{31}$P NMR and after a few days at room temperature a yellow solid precipitated out. This was dissolved in $CD_2Cl_2$ (0.6 mL) and a degassed solution of $KPF_6$ (0.01 g) in deionised water (2 mL) was stirred in. The water was taken off by cannula and the remaining $CD_2Cl_2$ solution layered with pentane (2 mL). Small, bright yellow crystals grew which were suitable for analysis by X-ray diffraction and were identified as **95**. $^1$H NMR ($CD_2Cl_2$, 400 MHz, 25 °C): δ 7.00 (s, 1H, **HC=CH** backbone), 5.57 (sept, $^3J_{HH}$ = 7.1 Hz, 4H, NC**H**(CH$_3$)$_2$), 4.45 (tt, $^3J_{HH}$ = 6.9 Hz, $^4J_{HH}$ = 4.05 Hz, 2H, *ipso*-C**H** Cy), 2.21 (s, 12H, **H$_3$**CC=CC**H$_3$** backbone), 1.45 (d, $^3J_{HH}$ = 7.1 Hz, 24H, NCH(C**H$_3$**)), 1.82-0.74 (m, 20H, Cy C**H$_2$**); $^{31}$P{$^1$H} NMR ($CD_2Cl_2$, 162 MHz, 25 °C): δ -144.5 (sept, $^1J_{PF}$ = 711.0 Hz, **PF$_6^-$**); IR (cm-1): 1956 ($\nu_{CO}$), 721 ($\nu_{PF}$); $^{13}$C{$^1$H} NMR ($CD_2Cl_2$, 100 MHz, 25 °C): δ 194.7 (d, $^1J_{CRh}$ = 74.5 Hz, Rh-C*1*), 185.1 (d, $^1J_{CRh}$ = 42.3 Hz, C*2*), 178.0 (d, $^1J_{CRh}$ = 40.4 Hz, Rh-C*3*), 128.2 (d, $^3J_{CRh}$ = 11.9 Hz, C*8*), 118.0 (s, C*11*), 58.1 (d, $^3J_{CRh}$ = 13 Hz, C*10*), 51.4, 50.7 (both s, C*4/6*), 22.0 (s, C*9*), 21.8, 20.6, 20.1 (all s, Cy **CH$_2$**), 10.1, 7.8 (both s, C*5/7*); CHN % {found (calculated)}: C {52.53 (50.53)} H {7.42 (7.05)} N {9.67 (8.58)}.

**ICyHPF$_6$ (93):**

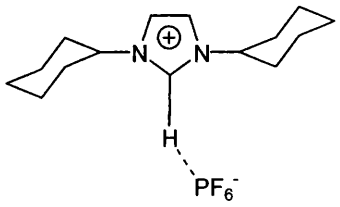

$KPF_6$ (0.01 g) in degassed deionised water (2 mL) was added to a $CH_2Cl_2$ (0.6 mL) solution containing free ICy. When the solution was layered with diethylether, very pale yellow crystals grew that were suitable for X-ray diffraction and were identified as **94**. $^1$H NMR ($CD_2Cl_2$, 300 MHz, 25 °C): δ 8.53 (t, $^4J_{HH}$ = 1.70 Hz, 1H, **CH**), 7.31 (d, $^4J_{HH}$ = 1.7 Hz, 2H, **HC=CH** backbone), 4.23 (tt, $^3J_{HH}$ = 12.0 Hz, $^4J_{HH}$ = 4.0 Hz, 2H, *ipso*-**CH** Cy), 2.27-1.17 (m, 20H, ICy **CH$_2$**); $^{19}$F NMR ($CD_2Cl_2$, 376.5 MHz, 25 °C): δ 73.1 (d, $^1J_{FP}$ = 711.0 Hz, **PF$_6^-$**); $^{31}$P NMR ($CD_2Cl_2$, 162 MHz, 25 °C): δ -144.4 (sept, $^1J_{PF}$ = 711.0 Hz, **PF$_6^-$**); IR (cm$^{-1}$): 723 ($\nu_{PF}$); CHN % {found (calculated)}: C {47.20 (47.62)} H {6.30 (6.66)} N {7.31 (7.40)}.

**I$^i$Pr$_2$Me$_2$HPF$_6$ (94):**

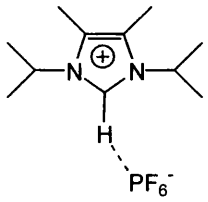

$KPF_6$ (0.01 g in 2 mL of degassed, deionised water) was added to a $CH_2Cl_2$ solution (0.6 mL) containing free I$^i$Pr$_2$Me$_2$, from NMR the presence of **95** could be seen. $^1$H NMR ($CD_2Cl_2$, 300 MHz, 25 °C): δ 8.26 (br s, 1H, **CH** imidazolium proton), 4.45 (sept, $^3J$ = 6.6 Hz, 2H, **CH**(CH$_3$)$_2$), 2.27 (s, 6H, **CH$_3$**C=CC**H$_3$** backbone), 1.57 (d, $^3J$ = 6.6 Hz, 12H, CH(**CH$_3$**)$_2$); $^{31}$P NMR ($CD_2Cl_2$, 162 MHz, 25 °C): δ -144.4 (sept, $^1J_{PF}$ = 711.0 Hz, **PF$_6^-$**); 723 ($\nu_{PF}$).

## 4.3. References


(1) Messerle, B. A.; Sleigh, C. J.; Partridge, M. G.; Duckett, S. B. *J. Chem. Soc., Dalton Trans.* **1999**, 1429.

(2) Dunne, J. P.; Blazina, D.; Aiken, S.; Carteret, H. A.; Duckett, S. B.; Jones, J. A.; Poli, R.; Whitwood, A. C. *Dalton Trans.* **2004**, 3616.

(3) Anwar, M. S.; Blazina, D.; Carteret, H. A.; Duckett, S. B.; Halstead, T. K.; Jones, J. A.; Taylor, R. J. K. *Magn. Reson. Chem.* **2005**, *43*, 200.

(4) George, M. W.; Poliakoff, M.; Turner, J. J. *Analyst* **1994**, 551.

(5) Sheldrick, G. M. *Acta. Crystallogr. Sect. A.* **1990**, 467.

(6) Sheldrick, G. M. *SHELX-97, A Computer Program for Crystal Structure Refinement*; University of Gottingen, 1997.

(7) Kuhn, N.; Kratz, T. *Synthesis* **1993**, 561.

(8) Arduengo, A. J.; Krafczyk, R.; Schmutzler, R.; Craig, H. A.; Goerlich, J. R.; Marshall, W. J.; Unverzagt, M. *Tetrahedron* **1999**, *55*, 14523.

(9) Jazzar, R. F. R. PhD thesis, University of Bath, 2003.

(10) Harris, A. D.; Robinson, S. D. *Inorg. Chim. Acta* **1980**, *42*, 25.

(11) Ahmad, N.; Robinson, S. D.; Levinson, J. J.; Uttley, M. F. *Inorg. Synth.* **1974**, *15*, 48.

(12) Jazzar, R. F. R.; Macgregor, S. A.; Mahon, M. F.; Richards, S. P.; Whittlesey, M. K. *J. Am. Chem. Soc.* **2002**, *124*, 4944.

(13) Burling, S.; Mahon, M. F.; Paine, B. M.; Whittlesey, M. K.; Williams, J. M. J. *Organometallics* **2004**, *23*, 4537.

(14) Burling, S.; Kociok-Kohn, G.; Mahon, M. F.; Whittlesey, M. K.; Williams, J. M. J. *Organometallics* **2005**, *24*, 5868

(15) Ahmad, N.; Levison, J. J.; Robinson, S. D.; Uttley, M. F. *Inorg. Synth.* **1990**, *28*, 81.

(16) Billig, E.; Jamerson, J. D.; Pruett, R. L. *J. Organomet. Chem.* **1980**, *192*, C49.

(17) *Ortho* and *para* phenyl peaks under solvent peak, bridging CO groups not visible due to excessive coupling effects.

# Chapter 5

# Appendices

# 5. Appendices

**5.1.** ***Appendix 1:*** crystallographic data, bond lengths and angles for $[RhH(I^iPr_2Me_2)(PPh_3)_2]$ (**72**).[1]

| **$[RhH(I^iPr_2Me_2)(PPh_3)_2]$** | |
|---|---|
| Empirical formula | $C_{47}H_{51}N_2P_2Rh$ |
| Formula weight | 808.75 |
| Temperature | 150(2) K |
| Wavelength | 0.71073 Å |
| Crystal system | Monoclinic |
| Space group | C2/c |
| Unit cell dimensions | a = 24.0740(3)Å α = 90° |
| | b = 10.48500(10)Å β = 116.866(1)° |
| | c = 18.6690(2)Å γ = 90° |
| Volume | 4203.73(8) $Å^3$ |
| Z | 4 |
| Density (calculated) | 1.278 $Mg/m^3$ |
| Absorption coefficient | 0.516 $mm^{-1}$ |
| F(000) | 1688 |
| Crystal size | 0.25 x 0.25 x 0.20 mm |
| Theta range for data collection | 3.80 to 27.48° |
| Index ranges | -31<=h<=31; -13<=k<=13; -24<=l<=24 |
| Reflections collected | 30096 |
| Independent reflections | 4803 [R(int) = 0.0342] |
| Absorption correction | Semi-empirical from equivalents |
| Reflections observed (>2σ) | 4346 |
| Max. and min. transmission | 0.91 and 0.88 |
| Refinement method | Full-matrix least-squares on $F^2$ |
| Data / restraints / parameters | 4803 / 1 / 270 |
| Goodness-of-fit on $F^2$ | 1.055 |
| R indices (all data) | $R^1 = 0.0346$ $wR_2 = 0.0758$ |
| Largest diff. peak and hole | 0.414 and -0.629 $eÅ^{-3}$ |

| Bond lengths (Å) for $RhH(I^iPr_2Me_2)(PPh_3)_2$ | | | |
|---|---|---|---|
| Rh(1)-H(1) | 1.5965 | Rh(1)-C(1) | 2.068(2) |
| Rh(1)-P(1) | 2.2368(4) | Rh(1)-P(1)#1 | 2.2368(4) |
| P(1)-C(13) | 1.828(2) | P(1)-C(7) | 1.8425(18) |
| P(1)-C(19A) | 1.846(4) | P(1)-C(19) | 1.852(2) |
| N(1)-C(1) | 1.361(2) | N(1)-C(2) | 1.402(2) |
| N(1)-C(3) | 1.476(2) | C(1)-N(1)#1 | 1.361(2) |
| C(2)-C(2)#1 | 1.353(4) | C(2)-C(6) | 1.490(3) |
| C(3)-C(4) | 1.515(3) | C(3)-C(5) | 1.518(3) |
| C(7)-C(8) | 1.397(3) | C(7)-C(12) | 1.398(3) |
| C(8)-C(9) | 1.385(3) | C(9)-C(10) | 1.389(3) |
| C(10)-C(11) | 1.375(3) | C(11)-C(12) | 1.395(3) |
| C(13)-C(18) | 1.389(3) | C(13)-C(14) | 1.395(3) |
| C(14)-C(15) | 1.369(4) | C(15)-C(16) | 1.361(5) |
| C(16)-C(17) | 1.396(5) | C(17)-C(18) | 1.391(4) |
| C(19)-C(20) | 1.3900 | C(19)-C(24) | 1.3900 |
| C(20)-C(21) | 1.3900 | C(21)-C(22) | 1.3900 |
| C(22)-C(23) | 1.3900 | C(23)-C(24) | 1.3900 |
| C(19A)-C(20A) | 1.3900 | C(19A)-C(24A) | 1.3900 |
| C(20A)-C(21A) | 1.3900 | C(21A)-C(22A) | 1.3900 |
| C(22A)-C(23A) | 1.3900 | C(23A)-C(24A) | 1.3900 |
| H(1)-Rh(1)-C(1) | 180.0 | H(1)-Rh(1)-P(1) | 80.2 |

| Bond angles (°) for $RhH(I^iPr_2Me_2)(PPh_3)_2$ | | | |
|---|---|---|---|
| C(1)-Rh(1)-P(1) | 99.804(13) | H(1)-Rh(1)-P(1)#1 | 80.2 |
| C(1)-Rh(1)-P(1)#1 | 99.804(13) | P(1)-Rh(1)-P(1)#1 | 160.39(3) |
| C(13)-P(1)-C(7) | 99.86(8) | C(13)-P(1)-C(19A) | 106.67(19) |
| C(7)-P(1)-C(19A) | 98.14(15) | C(13)-P(1)-C(19) | 98.68(16) |
| C(7)-P(1)-C(19) | 104.33(12) | C(19A)-P(1)-C(19) | 9.2(3) |
| C(13)-P(1)-Rh(1) | 115.30(6) | C(7)-P(1)-Rh(1) | 120.65(6) |
| C(19A)-P(1)-Rh(1) | 113.83(17) | C(19)-P(1)-Rh(1) | 114.83(12) |
| C(1)-N(1)-C(2) | 111.60(15) | C(1)-N(1)-C(3) | 120.92(16) |
| C(2)-N(1)-C(3) | 127.49(16) | N(1)#1-C(1)-N(1) | 104.0(2) |
| N(1)#1-C(1)-Rh(1) | 128.02(10) | N(1)-C(1)-Rh(1) | 128.02(10) |
| C(2)#1-C(2)-N(1) | 106.42(10) | C(2)#1-C(2)-C(6) | 127.58(13) |
| N(1)-C(2)-C(6) | 125.99(18) | N(1)-C(3)-C(4) | 111.82(18) |
| N(1)-C(3)-C(5) | 112.78(17) | C(4)-C(3)-C(5) | 112.56(19) |
| C(8)-C(7)-C(12) | 118.20(17) | C(8)-C(7)-P(1) | 117.81(14) |
| C(12)-C(7)-P(1) | 123.87(14) | C(9)-C(8)-C(7) | 121.07(19) |
| C(8)-C(9)-C(10) | 119.9(2) | C(11)-C(10)-C(9) | 119.89(19) |
| C(10)-C(11)-C(12) | 120.4(2) | C(11)-C(12)-C(7) | 120.47(19) |
| C(18)-C(13)-C(14) | 119.0(2) | C(18)-C(13)-P(1) | 117.29(16) |
| C(14)-C(13)-P(1) | 123.60(18) | C(15)-C(14)-C(13) | 121.0(3) |
| C(16)-C(15)-C(14) | 120.1(3) | C(15)-C(16)-C(17) | 120.6(3) |
| C(18)-C(17)-C(16) | 119.5(3) | C(13)-C(18)-C(17) | 119.8(3) |
| C(20)-C(19)-C(24) | 120.0 | C(20)-C(19)-P(1) | 117.3(2) |
| C(24)-C(19)-P(1) | 122.7(2) | C(19)-C(20)-C(21) | 120.0 |
| C(22)-C(21)-C(20) | 120.0 | C(21)-C(22)-C(23) | 120.0 |
| C(22)-C(23)-C(24) | 120.0 | C(23)-C(24)-C(19) | 120.0 |
| C(20A)-C(19A)-C(24A) | 120.0 | C(20A)-C(19A)-P(1) | 117.9(3) |
| C(24A)-C(19A)-P(1) | 122.1(3) | C(19A)-C(20A)-C(21A) | 120.0 |
| C(22A)-C(21A)-C(20A) | 120.0 | C(21A)-C(22A)-C(23A) | 120.0 |
| C(24A)-C(23A)-C(22A) | 120.0 | C(23A)-C(24A)-C(19A) | 120.0 |

**5.2.** ***Appendix 2:*** crystallographic data, bond lengths and angles for [RhH(IMes)($PPh_3$)$_2$] (**80**).[2]

| **[RhH(IMes)($PPh_3$)$_2$]** | |
|---|---|
| Empirical formula | $C_{61}H_{63}N_2OP_2Rh$ |
| Formula weight | 1004.98 |
| Temperature | 150(2) K |
| Wavelength | 0.71073 Å |
| Crystal system | Triclinic |
| Space group | P-1 |
| Unit cell dimensions | a = 12.1420(2)Å α = 102.252(1)° |
| | b = 13.1670(2)Å β = 90.491(1)° |
| | c = 16.2580(3)Å γ = 90.206(1)° |
| Volume | 2539.89(7) $Å^3$ |
| Z | 2 |
| Density (calculated) | 1.314 $Mg/m^3$ |
| Absorption coefficient | 0.443 $mm^{-1}$ |
| F(000) | 1052 |
| Crystal size | 0.20 x 0.20 x 0.03 mm |
| Theta range for data collection | 3.58 to 27.53° |
| Index ranges | -15<=h<=15; -16<=k<=17; -21<=l<=21 |
| Reflections collected | 40799 |
| Independent reflections | 11530 [R(int) = 0.0795] |
| Reflections observed (>2σ) | 7475 |
| Absorption correction | None |
| Refinement method | Full-matrix least-squares on $F^2$ |
| Data / restraints / parameters | 11530 / 11 / 609 |
| Goodness-of-fit on $F^2$ | 1.010 |
| Final R indices [I>2σ(I)] | $R^1$ = 0.0502 $wR_2$ = 0.0912 |
| R indices (all data) | $R^1$ = 0.1050 $wR_2$ = 0.1064 |
| Largest diff. peak and hole | 0.827 and -0.738 $eÅ^{-3}$ |

| Bond lengths (Å) for [RhH(IMes)($PPh_3$)$_2$] | | | |
|---|---|---|---|
| Rh(1)-C(1) | 2.024(3) | Rh(1)-P(2) | 2.2527(8) |
| Rh(1)-P(1) | 2.2894(8) | P(1)-C(34) | 1.836(3) |
| P(1)-C(22) | 1.838(3) | P(1)-C(28) | 1.856(3) |
| P(2)-C(46) | 1.847(3) | P(2)-C(52) | 1.849(3) |
| P(2)-C(40) | 1.855(3) | N(1)-C(1) | 1.370(4) |
| N(1)-C(2) | 1.390(4) | N(1)-C(13) | 1.438(4) |
| N(2)-C(1) | 1.378(4) | N(2)-C(3) | 1.385(4) |
| N(2)-C(4) | 1.447(4) | C(2)-C(3) | 1.335(4) |
| C(4)-C(5) | 1.390(4) | C(4)-C(9) | 1.394(4) |
| C(5)-C(6) | 1.394(5) | C(5)-C(10) | 1.496(5) |
| C(6)-C(7) | 1.373(5) | C(7)-C(8) | 1.380(5) |
| C(7)-C(11) | 1.517(5) | C(8)-C(9) | 1.395(5) |
| C(9)-C(12) | 1.501(5) | C(13)-C(18) | 1.398(4) |
| C(13)-C(14) | 1.397(4) | C(14)-C(15) | 1.388(4) |
| C(14)-C(19) | 1.509(4) | C(15)-C(16) | 1.387(5) |
| C(16)-C(17) | 1.386(5) | C(16)-C(20) | 1.514(5) |
| C(17)-C(18) | 1.384(4) | C(18)-C(21) | 1.517(4) |
| C(22)-C(27) | 1.389(4) | C(22)-C(23) | 1.398(4) |
| C(23)-C(24) | 1.376(4) | C(24)-C(25) | 1.381(5) |
| C(25)-C(26) | 1.371(5) | C(26)-C(27) | 1.395(4) |
| C(28)-C(33) | 1.388(4) | C(28)-C(29) | 1.392(4) |
| C(29)-C(30) | 1.385(5) | C(30)-C(31) | 1.369(5) |
| C(31)-C(32) | 1.373(5) | C(32)-C(33) | 1.387(5) |
| C(34)-C(35) | 1.394(4) | C(34)-C(39) | 1.403(4) |
| C(35)-C(36) | 1.382(4) | C(36)-C(37) | 1.384(4) |
| C(37)-C(38) | 1.385(4) | C(38)-C(39) | 1.377(4) |
| C(40)-C(45) | 1.389(4) | C(40)-C(41) | 1.394(4) |
| C(41)-C(42) | 1.382(4) | C(42)-C(43) | 1.374(5) |
| C(43)-C(44) | 1.372(4) | C(44)-C(45) | 1.390(4) |

| | | | |
|---|---|---|---|
| C(46)-C(51) | 1.386(4) | C(46)-C(47) | 1.397(4) |
| C(47)-C(48) | 1.386(4) | C(48)-C(49) | 1.381(5) |
| C(49)-C(50) | 1.372(5) | C(50)-C(51) | 1.396(4) |
| C(52)-C(57) | 1.389(4) | C(52)-C(53) | 1.393(4) |
| C(53)-C(54) | 1.392(4) | C(54)-C(55) | 1.379(4) |
| C(55)-C(56) | 1.371(5) | C(56)-C(57) | 1.388(4) |
| O(102)-C(103) | 1.402(7) | O(102)-C(101) | 1.404(7) |
| C(105)-C(104) | 1.481(8) | C(105)-C(101) | 1.509(8) |
| C(104)-C(103) | 1.529(9) | C(201)-C(202) | 1.376(13) |
| C(201)-C(205) | 1.565(14) | C(202)-O(203) | 1.425(13) |
| O(203)-C(204) | 1.559(15) | C(204)-C(205) | 1.484(15) |

| Bond angles (°) for [RhH(IMes)($PPh_3$)$_2$] | | | |
|---|---|---|---|
| C(1)-Rh(1)-P(2) | 155.43(8) | C(1)-Rh(1)-P(1) | 105.14(8) |
| P(2)-Rh(1)-P(1) | 99.38(3) | C(34)-P(1)-C(22) | 106.56(14) |
| C(34)-P(1)-C(28) | 96.61(13) | C(22)-P(1)-C(28) | 98.09(13) |
| C(34)-P(1)-Rh(1) | 112.01(10) | C(22)-P(1)-Rh(1) | 112.38(10) |
| C(28)-P(1)-Rh(1) | 128.45(10) | C(46)-P(2)-C(52) | 103.99(13) |
| C(46)-P(2)-C(40) | 98.86(13) | C(52)-P(2)-C(40) | 99.39(14) |
| C(46)-P(2)-Rh(1) | 110.94(11) | C(52)-P(2)-Rh(1) | 114.57(10) |
| C(40)-P(2)-Rh(1) | 126.10(10) | C(1)-N(1)-C(2) | 111.7(3) |
| C(1)-N(1)-C(13) | 125.1(2) | C(2)-N(1)-C(13) | 123.0(3) |
| C(1)-N(2)-C(3) | 111.5(3) | C(1)-N(2)-C(4) | 125.2(3) |
| C(3)-N(2)-C(4) | 122.2(3) | N(1)-C(1)-N(2) | 102.7(2) |
| N(1)-C(1)-Rh(1) | 128.3(2) | N(2)-C(1)-Rh(1) | 128.4(2) |
| C(3)-C(2)-N(1) | 106.8(3) | C(2)-C(3)-N(2) | 107.2(3) |
| C(5)-C(4)-C(9) | 121.5(3) | C(5)-C(4)-N(2) | 120.7(3) |
| C(9)-C(4)-N(2) | 117.7(3) | C(4)-C(5)-C(6) | 118.1(3) |
| C(4)-C(5)-C(10) | 122.1(3) | C(6)-C(5)-C(10) | 119.7(3) |
| C(7)-C(6)-C(5) | 122.2(3) | C(6)-C(7)-C(8) | 118.1(3) |
| C(6)-C(7)-C(11) | 120.9(4) | C(8)-C(7)-C(11) | 121.0(4) |
| C(7)-C(8)-C(9) | 122.6(3) | C(8)-C(9)-C(4) | 117.4(3) |
| C(8)-C(9)-C(12) | 120.8(3) | C(4)-C(9)-C(12) | 121.8(3) |
| C(18)-C(13)-C(14) | 121.3(3) | C(18)-C(13)-N(1) | 119.1(3) |
| C(14)-C(13)-N(1) | 119.4(3) | C(15)-C(14)-C(13) | 117.9(3) |
| C(15)-C(14)-C(19) | 121.1(3) | C(13)-C(14)-C(19) | 121.0(3) |
| C(16)-C(15)-C(14) | 122.4(3) | C(17)-C(16)-C(15) | 117.8(3) |
| C(17)-C(16)-C(20) | 120.9(3) | C(15)-C(16)-C(20) | 121.2(3) |
| C(18)-C(17)-C(16) | 122.3(3) | C(17)-C(18)-C(13) | 118.2(3) |
| C(17)-C(18)-C(21) | 120.8(3) | C(13)-C(18)-C(21) | 121.0(3) |
| C(27)-C(22)-C(23) | 118.3(3) | C(27)-C(22)-P(1) | 126.5(2) |
| C(23)-C(22)-P(1) | 115.1(2) | C(24)-C(23)-C(22) | 120.7(3) |

| | | | |
|---|---|---|---|
| C(23)-C(24)-C(25) | 120.6(3) | C(26)-C(25)-C(24) | 119.5(3) |
| C(25)-C(26)-C(27) | 120.5(3) | C(22)-C(27)-C(26) | 120.3(3) |
| C(33)-C(28)-C(29) | 116.9(3) | C(33)-C(28)-P(1) | 118.2(2) |
| C(29)-C(28)-P(1) | 124.8(2) | C(30)-C(29)-C(28) | 120.9(3) |
| C(31)-C(30)-C(29) | 120.8(3) | C(30)-C(31)-C(32) | 119.6(3) |
| C(31)-C(32)-C(33) | 119.4(3) | C(28)-C(33)-C(32) | 122.3(3) |
| C(35)-C(34)-C(39) | 118.0(3) | C(35)-C(34)-P(1) | 124.7(2) |
| C(39)-C(34)-P(1) | 117.3(2) | C(36)-C(35)-C(34) | 121.0(3) |
| C(37)-C(36)-C(35) | 120.2(3) | C(36)-C(37)-C(38) | 119.5(3) |
| C(39)-C(38)-C(37) | 120.5(3) | C(38)-C(39)-C(34) | 120.7(3) |
| C(45)-C(40)-C(41) | 117.2(3) | C(45)-C(40)-P(2) | 121.2(2) |
| C(41)-C(40)-P(2) | 121.4(2) | C(42)-C(41)-C(40) | 121.2(3) |
| C(43)-C(42)-C(41) | 120.6(3) | C(42)-C(43)-C(44) | 119.5(3) |
| C(43)-C(44)-C(45) | 120.1(3) | C(40)-C(45)-C(44) | 121.4(3) |
| C(51)-C(46)-C(47) | 117.8(3) | C(51)-C(46)-P(2) | 117.1(2) |
| C(47)-C(46)-P(2) | 124.9(2) | C(48)-C(47)-C(46) | 120.9(3) |
| C(49)-C(48)-C(47) | 120.4(3) | C(50)-C(49)-C(48) | 119.7(3) |
| C(49)-C(50)-C(51) | 120.0(3) | C(46)-C(51)-C(50) | 121.2(3) |
| C(57)-C(52)-C(53) | 117.5(3) | C(57)-C(52)-P(2) | 119.1(2) |
| C(53)-C(52)-P(2) | 123.4(2) | C(54)-C(53)-C(52) | 121.2(3) |
| C(55)-C(54)-C(53) | 119.8(3) | C(56)-C(55)-C(54) | 119.9(3) |
| C(55)-C(56)-C(57) | 120.3(3) | C(56)-C(57)-C(52) | 121.2(3) |
| C(103)-O(102)-C(101) | 111.6(5) | C(104)-C(105)-C(101) | 103.8(5) |
| C(105)-C(104)-C(103) | 107.1(5) | O(102)-C(103)-C(104) | 106.3(5) |
| O(102)-C(101)-C(105) | 109.1(5) | C(202)-C(201)-C(205) | 107.3(11) |
| C(201)-C(202)-O(203) | 102.2(12) | C(202)-O(203)-C(204) | 107.1(11) |
| C(205)-C(204)-O(203) | 101.0(11) | C(204)-C(205)-C(201) | 104.6(11) |

**5.3.** ***Appendix 3:*** crystallographic data, bond lengths and angles for $[\{Rh(PPh_3)_2\}_2(\mu\text{-}H)(\mu\text{-}PPh_2)]$ (**83**).[3]

| **$[\{Rh(PPh_3)_2\}_2(\mu\text{-}H)(\mu\text{-}PPh_2)]$** | |
|---|---|
| Empirical formula | $C_{84}H_{71}P_5Rh_2$ |
| Formula weight | 1441.08 |
| Temperature | 293(2) K |
| Wavelength | 0.67750 Å |
| Crystal system | Monoclinic |
| Space group | $P2_1/c$ |
| Unit cell dimensions | a = 24.3635(11)Å α = 90° |
| | b = 13.4417(6)Å β = 95.026(1)° |
| | c = 21.1106(10)Å γ = 90° |
| Volume | 6886.9(5) $Å^3$ |
| Z | 4 |
| Density (calculated) | 1.390 $Mg/m^3$ |
| Absorption coefficient | 0.641 $mm^{-1}$ |
| F(000) | 2960 |
| Crystal size | 0.18 x 0.10 x 0.10 mm |
| Theta range for data collection | 1.65 to 28.92° |
| Index ranges | -34<=h<=34; -19<=k<=19; -30<=l<=30 |
| Reflections collected | 80730 |
| Independent reflections | 20885 [R(int) = 0.0802] |
| Reflections observed (>2σ) | 13601 |
| Absorption correction | SADABS |
| Max. and min. transmission | 0.8843 and 0.9427 |
| Refinement method | Full-matrix least-squares on $F^2$ |
| Data / restraints / parameters | 20885 / 1 / 821 |
| Goodness-of-fit on $F^2$ | 0.795 |
| Final R indices [I>2σ(I)] | $R^1 = 0.0321$ $wR_2 = 0.0559$ |
| R indices (all data) | $R^1 = 0.0570$ $wR_2 = 0.0589$ |
| Largest diff. peak and hole | 0.560 and -0.412 $eÅ^{-3}$ |

| Bond lengths (Å) for [{Rh(PPh$_3$)$_2$}$_2$(μ-H)(μ-PPh$_2$)] | | | |
|---|---|---|---|
| Rh(1)-H(1) | 1.7888 | Rh(1)-P(1) | 2.2378(5) |
| Rh(1)-P(3) | 2.2599(5) | Rh(1)-P(2) | 2.3266(5) |
| Rh(1)-Rh(2) | 2.9226(2) | Rh(2)-H(1) | 1.8193 |
| Rh(2)-P(5) | 2.2454(5) | Rh(2)-P(1) | 2.2488(5) |
| Rh(2)-P(4) | 2.3320(5) | P(1)-C(1) | 1.826(2) |
| P(1)-C(7) | 1.841(2) | P(2)-C(13) | 1.833(2) |
| P(2)-C(19) | 1.842(2) | P(2)-C(25) | 1.845(2) |
| P(3)-C(31) | 1.8361(19) | P(3)-C(37) | 1.847(2) |
| P(3)-C(43) | 1.848(2) | P(4)-C(55) | 1.8399(19) |
| P(4)-C(49) | 1.8420(19) | P(4)-C(61) | 1.8541(19) |
| P(5)-C(73) | 1.840(2) | P(5)-C(79) | 1.8518(19) |
| P(5)-C(67) | 1.856(2) | C(1)-C(6) | 1.397(3) |
| C(1)-C(2) | 1.398(3) | C(2)-C(3) | 1.383(3) |
| C(3)-C(4) | 1.391(3) | C(4)-C(5) | 1.370(3) |
| C(5)-C(6) | 1.398(3) | C(7)-C(12) | 1.391(3) |
| C(7)-C(8) | 1.395(3) | C(8)-C(9) | 1.397(3) |
| C(9)-C(10) | 1.380(4) | C(10)-C(11) | 1.358(4) |
| C(11)-C(12) | 1.399(3) | C(13)-C(14) | 1.388(3) |
| C(13)-C(18) | 1.402(3) | C(14)-C(15) | 1.383(3) |
| C(15)-C(16) | 1.376(3) | C(16)-C(17) | 1.376(3) |
| C(17)-C(18) | 1.381(3) | C(19)-C(24) | 1.382(3) |
| C(19)-C(20) | 1.393(3) | C(20)-C(21) | 1.380(3) |
| C(21)-C(22) | 1.375(3) | C(22)-C(23) | 1.373(3) |
| C(23)-C(24) | 1.390(3) | C(25)-C(26) | 1.388(3) |
| C(25)-C(30) | 1.391(3) | C(26)-C(27) | 1.398(3) |
| C(27)-C(28) | 1.369(4) | C(28)-C(29) | 1.365(4) |
| C(29)-C(30) | 1.401(3) | C(31)-C(32) | 1.381(3) |
| C(31)-C(36) | 1.400(3) | C(32)-C(33) | 1.393(3) |
| C(33)-C(34) | 1.383(3) | C(34)-C(35) | 1.381(3) |

| | | | |
|---|---|---|---|
| C(35)-C(36) | 1.396(3) | C(37)-C(42) | 1.389(3) |
| C(37)-C(38) | 1.394(3) | C(38)-C(39) | 1.379(3) |
| C(39)-C(40) | 1.379(3) | C(40)-C(41) | 1.373(3) |
| C(41)-C(42) | 1.384(3) | C(43)-C(44) | 1.383(3) |
| C(43)-C(48) | 1.389(3) | C(44)-C(45) | 1.394(3) |
| C(45)-C(46) | 1.373(3) | C(46)-C(47) | 1.380(3) |
| C(47)-C(48) | 1.385(3) | C(49)-C(54) | 1.384(3) |
| C(49)-C(50) | 1.400(2) | C(50)-C(51) | 1.372(3) |
| C(51)-C(52) | 1.379(3) | C(52)-C(53) | 1.377(3) |
| C(53)-C(54) | 1.395(3) | C(55)-C(56) | 1.391(3) |
| C(55)-C(60) | 1.392(3) | C(56)-C(57) | 1.389(3) |
| C(57)-C(58) | 1.370(3) | C(58)-C(59) | 1.372(3) |
| C(59)-C(60) | 1.383(3) | C(61)-C(66) | 1.387(3) |
| C(61)-C(62) | 1.396(3) | C(62)-C(63) | 1.385(3) |
| C(63)-C(64) | 1.371(3) | C(64)-C(65) | 1.370(3) |
| C(65)-C(66) | 1.389(3) | C(67)-C(68) | 1.391(3) |
| C(67)-C(72) | 1.403(3) | C(68)-C(69) | 1.390(3) |
| C(69)-C(70) | 1.386(3) | C(70)-C(71) | 1.362(3) |
| C(71)-C(72) | 1.386(3) | C(73)-C(78) | 1.388(3) |
| C(73)-C(74) | 1.390(3) | C(74)-C(75) | 1.385(3) |
| C(75)-C(76) | 1.368(4) | C(76)-C(77) | 1.376(3) |
| C(77)-C(78) | 1.399(3) | C(79)-C(80) | 1.392(3) |
| C(79)-C(84) | 1.394(3) | C(80)-C(81) | 1.387(3) |
| C(81)-C(82) | 1.372(3) | C(82)-C(83) | 1.381(3) |
| C(83)-C(84) | 1.393(3) | | |

| Bond angles (°) for $[\{Rh(PPh_3)_2\}_2(\mu\text{-}H)(\mu\text{-}PPh_2)]$ | | | |
|---|---|---|---|
| H(1)-Rh(1)-P(1) | 85.7 | H(1)-Rh(1)-P(3) | 162.6 |
| P(1)-Rh(1)-P(3) | 101.097(19) | H(1)-Rh(1)-P(2) | 82.6 |
| P(1)-Rh(1)-P(2) | 148.80(2) | P(3)-Rh(1)-P(2) | 98.619(19) |
| H(1)-Rh(1)-Rh(2) | 36.3 | P(1)-Rh(1)-Rh(2) | 49.515(13) |
| P(3)-Rh(1)-Rh(2) | 146.050(15) | P(2)-Rh(1)-Rh(2) | 115.300(14) |
| H(1)-Rh(2)-P(5) | 164.4 | H(1)-Rh(2)-P(1) | 84.6 |
| P(5)-Rh(2)-P(1) | 99.809(18) | H(1)-Rh(2)-P(4) | 79.4 |
| P(5)-Rh(2)-P(4) | 102.269(18) | P(1)-Rh(2)-P(4) | 150.255(19) |
| H(1)-Rh(2)-Rh(1) | 35.6 | P(5)-Rh(2)-Rh(1) | 147.224(14) |
| P(1)-Rh(2)-Rh(1) | 49.188(13) | P(4)-Rh(2)-Rh(1) | 110.459(14) |
| C(1)-P(1)-C(7) | 105.52(9) | C(1)-P(1)-Rh(1) | 125.58(7) |
| C(7)-P(1)-Rh(1) | 108.60(6) | C(1)-P(1)-Rh(2) | 112.54(6) |
| C(7)-P(1)-Rh(2) | 123.44(7) | Rh(1)-P(1)-Rh(2) | 81.297(16) |
| C(13)-P(2)-C(19) | 100.96(9) | C(13)-P(2)-C(25) | 103.07(9) |
| C(19)-P(2)-C(25) | 99.17(9) | C(13)-P(2)-Rh(1) | 121.45(7) |
| C(19)-P(2)-Rh(1) | 111.80(7) | C(25)-P(2)-Rh(1) | 117.07(6) |
| C(31)-P(3)-C(37) | 109.12(9) | C(31)-P(3)-C(43) | 97.88(9) |
| C(37)-P(3)-C(43) | 99.29(9) | C(31)-P(3)-Rh(1) | 117.92(7) |
| C(37)-P(3)-Rh(1) | 109.11(7) | C(43)-P(3)-Rh(1) | 121.51(6) |
| C(55)-P(4)-C(49) | 101.68(8) | C(55)-P(4)-C(61) | 100.72(9) |
| C(49)-P(4)-C(61) | 98.10(8) | C(55)-P(4)-Rh(2) | 106.99(6) |
| C(49)-P(4)-Rh(2) | 122.68(6) | C(61)-P(4)-Rh(2) | 122.95(6) |
| C(73)-P(5)-C(79) | 97.00(9) | C(73)-P(5)-C(67) | 105.17(9) |
| C(79)-P(5)-C(67) | 100.95(9) | C(73)-P(5)-Rh(2) | 120.75(7) |
| C(79)-P(5)-Rh(2) | 121.79(6) | C(67)-P(5)-Rh(2) | 108.49(7) |
| C(6)-C(1)-C(2) | 117.92(19) | C(6)-C(1)-P(1) | 124.29(16) |
| C(2)-C(1)-P(1) | 117.59(14) | C(3)-C(2)-C(1) | 121.6(2) |
| C(2)-C(3)-C(4) | 119.6(2) | C(5)-C(4)-C(3) | 119.9(2) |
| C(4)-C(5)-C(6) | 120.6(2) | C(1)-C(6)-C(5) | 120.3(2) |

| | | | |
|---|---|---|---|
| C(12)-C(7)-C(8) | 117.3(2) | C(12)-C(7)-P(1) | 125.67(17) |
| C(8)-C(7)-P(1) | 116.86(16) | C(7)-C(8)-C(9) | 121.7(2) |
| C(10)-C(9)-C(8) | 119.1(3) | C(11)-C(10)-C(9) | 120.6(2) |
| C(10)-C(11)-C(12) | 120.4(2) | C(7)-C(12)-C(11) | 120.9(2) |
| C(14)-C(13)-C(18) | 118.27(19) | C(14)-C(13)-P(2) | 117.15(15) |
| C(18)-C(13)-P(2) | 124.52(16) | C(15)-C(14)-C(13) | 120.7(2) |
| C(16)-C(15)-C(14) | 120.2(2) | C(17)-C(16)-C(15) | 120.1(2) |
| C(16)-C(17)-C(18) | 120.1(2) | C(17)-C(18)-C(13) | 120.6(2) |
| C(24)-C(19)-C(20) | 117.9(2) | C(24)-C(19)-P(2) | 118.37(16) |
| C(20)-C(19)-P(2) | 123.67(16) | C(21)-C(20)-C(19) | 120.8(2) |
| C(22)-C(21)-C(20) | 120.4(2) | C(23)-C(22)-C(21) | 119.8(2) |
| C(22)-C(23)-C(24) | 119.7(2) | C(19)-C(24)-C(23) | 121.3(2) |
| C(26)-C(25)-C(30) | 118.2(2) | C(26)-C(25)-P(2) | 121.10(17) |
| C(30)-C(25)-P(2) | 120.37(18) | C(25)-C(26)-C(27) | 121.1(2) |
| C(28)-C(27)-C(26) | 120.0(3) | C(29)-C(28)-C(27) | 119.8(2) |
| C(28)-C(29)-C(30) | 120.9(3) | C(25)-C(30)-C(29) | 120.0(2) |
| C(32)-C(31)-C(36) | 118.64(18) | C(32)-C(31)-P(3) | 117.26(14) |
| C(36)-C(31)-P(3) | 123.69(16) | C(31)-C(32)-C(33) | 121.2(2) |
| C(34)-C(33)-C(32) | 120.0(2) | C(35)-C(34)-C(33) | 119.6(2) |
| C(34)-C(35)-C(36) | 120.6(2) | C(35)-C(36)-C(31) | 120.0(2) |
| C(42)-C(37)-C(38) | 117.9(2) | C(42)-C(37)-P(3) | 126.47(16) |
| C(38)-C(37)-P(3) | 115.58(15) | C(39)-C(38)-C(37) | 121.2(2) |
| C(40)-C(39)-C(38) | 120.0(2) | C(41)-C(40)-C(39) | 119.6(2) |
| C(40)-C(41)-C(42) | 120.7(2) | C(41)-C(42)-C(37) | 120.5(2) |
| C(44)-C(43)-C(48) | 117.60(19) | C(44)-C(43)-P(3) | 122.85(16) |
| C(48)-C(43)-P(3) | 119.55(16) | C(43)-C(44)-C(45) | 121.2(2) |
| C(46)-C(45)-C(44) | 120.3(2) | C(45)-C(46)-C(47) | 119.2(2) |
| C(46)-C(47)-C(48) | 120.3(2) | C(47)-C(48)-C(43) | 121.4(2) |
| C(54)-C(49)-C(50) | 117.89(17) | C(54)-C(49)-P(4) | 119.55(14) |
| C(50)-C(49)-P(4) | 122.50(15) | C(51)-C(50)-C(49) | 121.08(19) |
| C(50)-C(51)-C(52) | 120.74(19) | C(53)-C(52)-C(51) | 119.1(2) |

| | | | |
|---|---|---|---|
| C(52)-C(53)-C(54) | 120.5(2) | C(49)-C(54)-C(53) | 120.67(18) |
| C(56)-C(55)-C(60) | 118.46(18) | C(56)-C(55)-P(4) | 124.82(15) |
| C(60)-C(55)-P(4) | 116.71(15) | C(57)-C(56)-C(55) | 120.39(19) |
| C(58)-C(57)-C(56) | 120.3(2) | C(57)-C(58)-C(59) | 119.9(2) |
| C(58)-C(59)-C(60) | 120.5(2) | C(59)-C(60)-C(55) | 120.4(2) |
| C(66)-C(61)-C(62) | 117.83(18) | C(66)-C(61)-P(4) | 123.02(15) |
| C(62)-C(61)-P(4) | 119.11(15) | C(63)-C(62)-C(61) | 121.0(2) |
| C(64)-C(63)-C(62) | 120.1(2) | C(65)-C(64)-C(63) | 120.0(2) |
| C(64)-C(65)-C(66) | 120.3(2) | C(61)-C(66)-C(65) | 120.8(2) |
| C(68)-C(67)-C(72) | 117.38(19) | C(68)-C(67)-P(5) | 118.30(15) |
| C(72)-C(67)-P(5) | 124.26(16) | C(69)-C(68)-C(67) | 121.4(2) |
| C(70)-C(69)-C(68) | 119.9(2) | C(71)-C(70)-C(69) | 119.4(2) |
| C(70)-C(71)-C(72) | 121.2(2) | C(71)-C(72)-C(67) | 120.6(2) |
| C(78)-C(73)-C(74) | 118.29(19) | C(78)-C(73)-P(5) | 117.76(16) |
| C(74)-C(73)-P(5) | 123.59(17) | C(75)-C(74)-C(73) | 121.1(2) |
| C(76)-C(75)-C(74) | 120.1(2) | C(75)-C(76)-C(77) | 120.1(2) |
| C(76)-C(77)-C(78) | 120.1(2) | C(73)-C(78)-C(77) | 120.3(2) |
| C(80)-C(79)-C(84) | 117.57(18) | C(80)-C(79)-P(5) | 120.11(16) |
| C(84)-C(79)-P(5) | 122.26(16) | C(81)-C(80)-C(79) | 121.1(2) |
| C(82)-C(81)-C(80) | 120.4(2) | C(81)-C(82)-C(83) | 120.0(2) |
| C(82)-C(83)-C(84) | 119.5(2) | C(83)-C(84)-C(79) | 121.4(2) |

**5.4.** ***Appendix 4:*** crystallographic data, bond lengths and angles for $[RhH(IMes)_2(CO)]$ **(86)**.[4]

| **$[RhH(IMes)_2(CO)]$** | |
|---|---|
| Empirical formula | $C_{43}H_{47}N_4ORh$ |
| Formula weight | 738.76 |
| Temperature | 150(2) K |
| Wavelength | 0.71073 Å |
| Crystal system | Orthorhombic |
| Space group | Pbca |
| Unit cell dimensions | a = 17.2090(1)Å α = 90° |
| | b = 19.1070(1)Å β = 90° |
| | c = 23.1810(1)Å γ = 90° |
| Volume | 7622.20(7) $Å^3$ |
| Z | 8 |
| Density (calculated) | 1.288 $Mg/m^3$ |
| Absorption coefficient | 0.485 $mm^{-1}$ |
| F(000) | 3088 |
| Crystal size | 0.60 x 0.50 x 0.40 mm |
| Theta range for data collection | 3.52 to 30.04° |
| Index ranges | -24<=h<=24; -26<=k<=26; -32<=l<=32 |
| Reflections collected | 149425 |
| Independent reflections | 11139 [R(int) = 0.0496] |
| Reflections observed (>2σ) | 9193 |
| Absorption correction | Semi-empirical from equivalents |
| Max. and min. transmission | 0.79 and 0.76 |
| Refinement method | Full-matrix least-squares on $F^2$ |
| Data / restraints / parameters | 11139 / 0 / 453 |
| Goodness-of-fit on $F^2$ | 1.082 |
| Final R indices [I>2σ(I)] | $R^1 = 0.0338$ $wR_2 = 0.0876$ |
| R indices (all data) | $R^1 = 0.0455$ $wR_2 = 0.0977$ |
| Largest diff. peak and hole | 1.025 and -0.757 $eÅ^{-3}$ |

| Bond lengths (Å) for [RhH(IMes)$_2$(CO)] | | | |
|---|---|---|---|
| Rh(1)-H(1) | 1.76(3) | Rh(1)-C(1) | 1.843(2) |
| Rh(1)-C(23) | 2.0165(16) | Rh(1)-C(2) | 2.0191(17) |
| O(1)-C(1) | 1.144(3) | N(1)-C(2) | 1.356(2) |
| N(1)-C(3) | 1.392(2) | N(1)-C(5) | 1.434(2) |
| N(2)-C(2) | 1.368(2) | N(2)-C(4) | 1.394(2) |
| N(2)-C(14) | 1.437(3) | N(3)-C(23) | 1.361(2) |
| N(3)-C(24) | 1.398(2) | N(3)-C(26) | 1.439(2) |
| N(4)-C(23) | 1.372(2) | N(4)-C(25) | 1.393(2) |
| N(4)-C(35) | 1.434(2) | C(3)-C(4) | 1.331(3) |
| C(5)-C(6) | 1.393(2) | C(5)-C(10) | 1.393(3) |
| C(6)-C(7) | 1.384(3) | C(6)-C(11) | 1.500(3) |
| C(7)-C(8) | 1.380(4) | C(8)-C(9) | 1.396(4) |
| C(8)-C(12) | 1.508(4) | C(9)-C(10) | 1.387(4) |
| C(10)-C(13) | 1.508(3) | C(14)-C(15) | 1.393(3) |
| C(14)-C(19) | 1.402(3) | C(15)-C(16) | 1.395(3) |
| C(15)-C(20) | 1.511(3) | C(16)-C(17) | 1.387(3) |
| C(17)-C(18) | 1.387(3) | C(17)-C(21) | 1.514(3) |
| C(18)-C(19) | 1.390(3) | C(19)-C(22) | 1.501(3) |
| C(24)-C(25) | 1.345(3) | C(26)-C(31) | 1.396(2) |
| C(26)-C(27) | 1.401(3) | C(27)-C(28) | 1.391(3) |
| C(27)-C(32) | 1.509(3) | C(28)-C(29) | 1.394(3) |
| C(29)-C(30) | 1.386(3) | C(29)-C(33) | 1.511(3) |
| C(30)-C(31) | 1.394(3) | C(31)-C(34) | 1.503(3) |
| C(35)-C(36) | 1.392(3) | C(35)-C(40) | 1.401(3) |
| C(36)-C(37) | 1.394(3) | C(36)-C(41) | 1.505(3) |
| C(37)-C(38) | 1.394(3) | C(38)-C(39) | 1.388(3) |
| C(38)-C(42) | 1.517(3) | C(39)-C(40) | 1.390(3) |
| C(40)-C(43) | 1.509(3) | | |

| Bond angles (°) for [RhH(IMes)$_2$(CO)] | | | |
|---|---|---|---|
| H(1)-Rh(1)-C(1) | 178.6(9) | H(1)-Rh(1)-C(23) | 85.3(8) |
| C(1)-Rh(1)-C(23) | 94.61(8) | H(1)-Rh(1)-C(2) | 87.6(8) |
| C(1)-Rh(1)-C(2) | 92.41(8) | C(23)-Rh(1)-C(2) | 172.91(7) |
| C(2)-N(1)-C(3) | 111.70(16) | C(2)-N(1)-C(5) | 125.02(15) |
| C(3)-N(1)-C(5) | 123.24(16) | C(2)-N(2)-C(4) | 111.19(17) |
| C(2)-N(2)-C(14) | 123.76(15) | C(4)-N(2)-C(14) | 125.05(17) |
| C(23)-N(3)-C(24) | 112.09(15) | C(23)-N(3)-C(26) | 123.91(14) |
| C(24)-N(3)-C(26) | 123.96(15) | C(23)-N(4)-C(25) | 111.66(16) |
| C(23)-N(4)-C(35) | 123.79(14) | C(25)-N(4)-C(35) | 124.09(15) |
| O(1)-C(1)-Rh(1) | 178.5(2) | N(1)-C(2)-N(2) | 103.43(15) |
| N(1)-C(2)-Rh(1) | 128.42(13) | N(2)-C(2)-Rh(1) | 128.14(13) |
| C(4)-C(3)-N(1) | 106.84(18) | C(3)-C(4)-N(2) | 106.84(18) |
| C(6)-C(5)-C(10) | 121.99(19) | C(6)-C(5)-N(1) | 119.08(17) |
| C(10)-C(5)-N(1) | 118.91(17) | C(7)-C(6)-C(5) | 117.86(19) |
| C(7)-C(6)-C(11) | 120.69(19) | C(5)-C(6)-C(11) | 121.44(18) |
| C(8)-C(7)-C(6) | 122.2(2) | C(7)-C(8)-C(9) | 118.2(2) |
| C(7)-C(8)-C(12) | 121.1(3) | C(9)-C(8)-C(12) | 120.7(3) |
| C(10)-C(9)-C(8) | 121.8(2) | C(9)-C(10)-C(5) | 117.8(2) |
| C(9)-C(10)-C(13) | 122.2(2) | C(5)-C(10)-C(13) | 120.1(2) |
| C(15)-C(14)-C(19) | 122.05(19) | C(15)-C(14)-N(2) | 119.26(17) |
| C(19)-C(14)-N(2) | 118.69(19) | C(14)-C(15)-C(16) | 118.01(19) |
| C(14)-C(15)-C(20) | 121.6(2) | C(16)-C(15)-C(20) | 120.3(2) |
| C(17)-C(16)-C(15) | 121.8(2) | C(18)-C(17)-C(16) | 118.3(2) |
| C(18)-C(17)-C(21) | 120.38(19) | C(16)-C(17)-C(21) | 121.4(2) |
| C(17)-C(18)-C(19) | 122.54(18) | C(18)-C(19)-C(14) | 117.33(19) |
| C(18)-C(19)-C(22) | 121.68(18) | C(14)-C(19)-C(22) | 120.98(18) |
| N(3)-C(23)-N(4) | 103.10(14) | N(3)-C(23)-Rh(1) | 127.00(13) |
| N(4)-C(23)-Rh(1) | 129.90(13) | C(25)-C(24)-N(3) | 106.32(16) |
| C(24)-C(25)-N(4) | 106.82(17) | C(31)-C(26)-C(27) | 122.04(17) |

| | | | |
|---|---|---|---|
| C(31)-C(26)-N(3) | 119.04(16) | C(27)-C(26)-N(3) | 118.92(16) |
| C(28)-C(27)-C(26) | 118.09(18) | C(28)-C(27)-C(32) | 121.05(19) |
| C(26)-C(27)-C(32) | 120.86(18) | C(27)-C(28)-C(29) | 121.42(19) |
| C(30)-C(29)-C(28) | 118.75(19) | C(30)-C(29)-C(33) | 121.1(2) |
| C(28)-C(29)-C(33) | 120.2(2) | C(29)-C(30)-C(31) | 122.04(19) |
| C(30)-C(31)-C(26) | 117.64(18) | C(30)-C(31)-C(34) | 120.89(17) |
| C(26)-C(31)-C(34) | 121.47(17) | C(36)-C(35)-C(40) | 122.11(17) |
| C(36)-C(35)-N(4) | 120.17(16) | C(40)-C(35)-N(4) | 117.72(16) |
| C(35)-C(36)-C(37) | 117.83(18) | C(35)-C(36)-C(41) | 121.96(17) |
| C(37)-C(36)-C(41) | 120.19(17) | C(38)-C(37)-C(36) | 121.83(19) |
| C(39)-C(38)-C(37) | 118.41(19) | C(39)-C(38)-C(42) | 120.9(2) |
| C(37)-C(38)-C(42) | 120.7(2) | C(38)-C(39)-C(40) | 122.00(19) |
| C(39)-C(40)-C(35) | 117.82(18) | C(39)-C(40)-C(43) | 121.70(18) |
| C(35)-C(40)-C(43) | 120.47(18) | | |

**5.5.** ***Appendix 5:*** crystallographic data, bond lengths and angles for $[\{Rh(I^iPr_2Me_2)\}(\mu\text{-}CO)_2\{Rh(PPh_3)_2]$ (**87**).[5]

| **$[\{Rh(I^iPr_2Me_2)\}(\mu\text{-}CO)_2\{Rh(PPh_3)_2]$** | |
|---|---|
| Empirical formula | $C_{30}H_{35}N_2OPRh$ |
| Formula weight | 573.48 |
| Temperature | 150(2) K |
| Wavelength | 0.71073 Å |
| Crystal system | Monoclinic |
| Space group | C2 |
| Unit cell dimensions | a = 18.7420(2)Å α = 90° |
| | b = 13.3980(2)Å β = 118.4930(10)° |
| | c = 12.55700(10)Å γ = 90° |
| Volume | 2771.21(6) $Å^3$ |
| Z | 4 |
| Density (calculated) | 1.375 $Mg/m^3$ |
| Absorption coefficient | 0.698 $mm^{-1}$ |
| F(000) | 1188 |
| Crystal size | 0.50 x 0.25 x 0.10 mm |
| Theta range for data collection | 3.56 to 28.27° |
| Index ranges | -24<=h<=24; -17<=k<=17; -16<=l<=16 |
| Reflections collected | 23814 |
| Independent reflections | 6654 [R(int) = 0.0472] |
| Reflections observed (>2σ) | 6310 |
| Absorption correction | Semi-empirical from equivalents |
| Max. and min. transmission | 0.88 and 0.57 |
| Refinement method | Full-matrix least-squares on $F^2$ |
| Data / restraints / parameters | 6654 / 1 / 317 |
| Goodness-of-fit on $F^2$ | 1.057 |
| Final R indices [I>2σ(I)] | $R^1 = 0.0267$ $wR_2 = 0.0611$ |
| R indices (all data) | $R^1 = 0.0304$ $wR_2 = 0.0635$ |
| Absolute structure parameter | -0.040(19) |

| | |
|---|---|
| Largest diff. peak and hole | 1.022 and -0.916 eÅ$^{-3}$ |

| Bond lengths (Å) for [{Rh(I$^i$Pr$_2$Me$_2$)}(μ-CO)$_2${Rh(PPh$_3$)$_2$}] | | | |
|---|---|---|---|
| Rh(1)-C(1)#1 | 1.995(3) | Rh(1)-C(1) | 1.995(3) |
| Rh(1)-P(1)#1 | 2.3019(6) | Rh(1)-P(1) | 2.3019(6) |
| Rh(1)-Rh(2) | 2.6939(3) | Rh(2)-C(1) | 2.005(3) |
| Rh(2)-C(1)#1 | 2.005(3) | Rh(2)-C(2)#1 | 2.073(2) |
| Rh(2)-C(2) | 2.073(2) | P(1)-C(25) | 1.831(3) |
| P(1)-C(19) | 1.836(2) | P(1)-C(13) | 1.845(2) |
| O(1)-C(1) | 1.1570(18) | N(1)-C(2) | 1.355(3) |
| N(1)-C(3) | 1.403(3) | N(1)-C(5) | 1.479(3) |
| N(2)-C(2) | 1.365(3) | N(2)-C(4) | 1.402(3) |
| N(2)-C(10) | 1.481(3) | C(3)-C(4) | 1.354(3) |
| C(3)-C(8) | 1.495(3) | C(4)-C(9) | 1.488(4) |
| C(5)-C(6) | 1.516(4) | C(5)-C(7) | 1.527(4) |
| C(10)-C(11) | 1.518(4) | C(10)-C(12) | 1.528(4) |
| C(13)-C(18) | 1.394(4) | C(13)-C(14) | 1.401(4) |
| C(14)-C(15) | 1.390(4) | C(15)-C(16) | 1.360(6) |
| C(16)-C(17) | 1.394(5) | C(17)-C(18) | 1.383(4) |
| C(19)-C(20) | 1.392(4) | C(19)-C(24) | 1.391(4) |
| C(20)-C(21) | 1.383(4) | C(21)-C(22) | 1.383(4) |
| C(22)-C(23) | 1.377(4) | C(23)-C(24) | 1.394(4) |
| C(25)-C(30) | 1.394(4) | C(25)-C(26) | 1.395(4) |
| C(26)-C(27) | 1.396(5) | C(27)-C(28) | 1.363(5) |
| C(28)-C(29) | 1.379(5) | C(29)-C(30) | 1.389(4) |

| Bond angles (°) for [{Rh($^i$Pr$_2$Me$_2$)}(μ-CO)$_2${Rh(PPh$_3$)$_2$}] | | | |
|---|---|---|---|
| C(1)#1-Rh(1)-C(1) | 95.64(16) | C(1)#1-Rh(1)-P(1)#1 | 107.83(3) |
| C(1)-Rh(1)-P(1)#1 | 109.60(3) | C(1)#1-Rh(1)-P(1) | 109.60(3) |
| C(1)-Rh(1)-P(1) | 107.83(3) | P(1)#1-Rh(1)-P(1) | 122.91(3) |
| C(1)#1-Rh(1)-Rh(2) | 47.82(8) | C(1)-Rh(1)-Rh(2) | 47.82(8) |
| P(1)#1-Rh(1)-Rh(2) | 118.543(16) | P(1)-Rh(1)-Rh(2) | 118.543(16) |
| C(1)-Rh(2)-C(1)#1 | 95.03(16) | C(1)-Rh(2)-C(2)#1 | 168.07(7) |
| C(1)#1-Rh(2)-C(2)#1 | 86.29(9) | C(1)-Rh(2)-C(2) | 86.29(9) |
| C(1)#1-Rh(2)-C(2) | 168.07(7) | C(2)#1-Rh(2)-C(2) | 94.87(12) |
| C(1)-Rh(2)-Rh(1) | 47.52(8) | C(1)#1-Rh(2)-Rh(1) | 47.52(8) |
| C(2)#1-Rh(2)-Rh(1) | 132.57(6) | C(2)-Rh(2)-Rh(1) | 132.57(6) |
| C(25)-P(1)-C(19) | 102.14(11) | C(25)-P(1)-C(13) | 103.58(12) |
| C(19)-P(1)-C(13) | 97.99(12) | C(25)-P(1)-Rh(1) | 114.13(8) |
| C(19)-P(1)-Rh(1) | 117.78(8) | C(13)-P(1)-Rh(1) | 118.58(8) |
| C(2)-N(1)-C(3) | 111.5(2) | C(2)-N(1)-C(5) | 121.2(2) |
| C(3)-N(1)-C(5) | 127.2(2) | C(2)-N(2)-C(4) | 111.27(19) |
| C(2)-N(2)-C(10) | 121.76(19) | C(4)-N(2)-C(10) | 127.0(2) |
| O(1)-C(1)-Rh(1) | 125.7(3) | O(1)-C(1)-Rh(2) | 149.6(3) |
| Rh(1)-C(1)-Rh(2) | 84.663(6) | N(1)-C(2)-N(2) | 104.35(19) |
| N(1)-C(2)-Rh(2) | 130.01(17) | N(2)-C(2)-Rh(2) | 125.54(16) |
| C(4)-C(3)-N(1) | 106.5(2) | C(4)-C(3)-C(8) | 127.9(2) |
| N(1)-C(3)-C(8) | 125.5(2) | C(3)-C(4)-N(2) | 106.4(2) |
| C(3)-C(4)-C(9) | 127.8(2) | N(2)-C(4)-C(9) | 125.8(2) |
| N(1)-C(5)-C(6) | 113.5(2) | N(1)-C(5)-C(7) | 110.8(2) |
| C(6)-C(5)-C(7) | 113.6(2) | N(2)-C(10)-C(11) | 112.3(2) |
| N(2)-C(10)-C(12) | 112.3(2) | C(11)-C(10)-C(12) | 112.1(2) |
| C(18)-C(13)-C(14) | 118.2(2) | C(18)-C(13)-P(1) | 116.46(19) |
| C(14)-C(13)-P(1) | 125.3(2) | C(15)-C(14)-C(13) | 119.9(3) |
| C(16)-C(15)-C(14) | 121.2(3) | C(15)-C(16)-C(17) | 119.8(3) |
| C(18)-C(17)-C(16) | 119.6(3) | C(17)-C(18)-C(13) | 121.2(3) |

| | | | |
|---|---|---|---|
| C(20)-C(19)-C(24) | 119.4(2) | C(20)-C(19)-P(1) | 122.01(19) |
| C(24)-C(19)-P(1) | 118.6(2) | C(21)-C(20)-C(19) | 120.6(2) |
| C(20)-C(21)-C(22) | 120.1(3) | C(23)-C(22)-C(21) | 119.6(2) |
| C(22)-C(23)-C(24) | 121.1(3) | C(19)-C(24)-C(23) | 119.3(3) |
| C(30)-C(25)-C(26) | 117.7(3) | C(30)-C(25)-P(1) | 122.2(2) |
| C(26)-C(25)-P(1) | 119.7(2) | C(27)-C(26)-C(25) | 121.2(3) |
| C(28)-C(27)-C(26) | 119.8(3) | C(27)-C(28)-C(29) | 120.3(3) |
| C(28)-C(29)-C(30) | 120.2(3) | C(29)-C(30)-C(25) | 120.7(3) |

**5.6.** ***Appendix 6:*** crystallographic data, bond lengths and angles for $[Rh(I^iPr_2Me_2)_3(CO)][PF_6]$ **(89)**.

| **$[Rh(I^iPr_2Me_2)_3(CO)][PF_6]$** | |
|---|---|
| Empirical formula | $C_{34}\ H_{60}\ F_6\ N_6\ O\ P\ Rh$ |
| Formula weight | 816.76 |
| Temperature | 150(2) K |
| Wavelength | 0.71073 Å |
| Crystal system | Monoclinic |
| Space group | P-1 |
| Unit cell dimensions | a = 9.9830(1)Å α = 80.367(1)° |
| | b = 12.7140(1)Å β = 76.200(1)° |
| | c = 16.4590(1)Å γ = 80.032(1)° |
| Volume | 1980.69(3) $Å^3$ |
| Z | 2 |
| Density (calculated) | 1.369 $Mg/m^3$ |
| Absorption coefficient | 0.534 $mm^{-1}$ |
| F(000) | 856 |
| Crystal size | 0.45 x 0.40 x 0.40 mm |
| Theta range for data collection | 3.56 to 30.91 °. |
| Index ranges | -14<=h<=14; -18<=k<=18; -22<=l<=23 |
| Reflections collected | 40529 |
| Independent reflections | 12310 [R(int) = 0.0399] |
| Reflections observed (>2σ) | 11164 |
| Absorption correction | Semi-empirical from equivalents |
| Max. and min. transmission | 0.82 and 0.70 |
| Refinement method | Full-matrix least-squares on $F^2$ |
| Data / restraints / parameters | 12310 / 0 / 461 |
| Goodness-of-fit on $F^2$ | 1.046 |
| Final R indices [I>2σ(I)] | $R^1 = 0.0306$ $wR_2 = 0.0743$ |
| R indices (all data) | $R^1 = 0.0361$ $wR_2 = 0.0774$ |
| Largest diff. peak and hole | 0.864 and -0.846 $eÅ^{-3}$ |

| Bond lengths (Å) for $[Rh(I^iPr_2Me_2)_3(CO)][PF_6]$ | | | |
|---|---|---|---|
| Rh(1)-C(1) | 1.8367(15) | Rh(1)-C(13) | 2.0738(14) |
| Rh(1)-C(24) | 2.0775(13) | Rh(1)-C(2) | 2.1490(13) |
| P(1)-F(2) | 1.5839(17) | P(1)-F(4) | 1.5886(17) |
| P(1)-F(1) | 1.5897(12) | P(1)-F(6) | 1.5912(13) |
| P(1)-F(5) | 1.5920(12) | P(1)-F(3) | 1.5960(13) |
| O(1)-C(1) | 1.1415(19) | N(1)-C(2) | 1.3682(17) |
| N(1)-C(3) | 1.3974(18) | N(1)-C(5) | 1.4743(19) |
| N(2)-C(2) | 1.3649(18) | N(2)-C(4) | 1.3948(18) |
| N(2)-C(10) | 1.4764(19) | N(3)-C(13) | 1.3620(19) |
| N(3)-C(14) | 1.3999(19) | N(3)-C(16) | 1.481(2) |
| N(4)-C(13) | 1.3554(18) | N(4)-C(15) | 1.398(2) |
| N(4)-C(21) | 1.472(2) | N(5)-C(24) | 1.3658(17) |
| N(5)-C(25) | 1.395(2) | N(5)-C(27) | 1.4825(19) |
| N(6)-C(24) | 1.3546(17) | N(6)-C(26) | 1.3983(19) |
| N(6)-C(32) | 1.4725(18) | C(3)-C(4) | 1.352(2) |
| C(3)-C(8) | 1.497(2) | C(4)-C(9) | 1.497(2) |
| C(5)-C(6) | 1.520(2) | C(5)-C(7) | 1.530(2) |
| C(10)-C(12) | 1.524(2) | C(10)-C(11) | 1.528(2) |
| C(14)-C(15) | 1.348(3) | C(14)-C(19) | 1.498(2) |
| C(15)-C(20) | 1.497(2) | C(16)-C(18) | 1.527(2) |
| C(16)-C(17) | 1.528(2) | C(21)-C(23) | 1.517(3) |
| C(21)-C(22) | 1.521(2) | C(25)-C(26) | 1.353(2) |
| C(25)-C(30) | 1.493(2) | C(26)-C(31) | 1.496(2) |
| C(27)-C(29) | 1.524(2) | C(27)-C(28) | 1.527(2) |
| C(32)-C(34) | 1.512(2) | C(32)-C(33) | 1.523(2) |

| Bond angles (°) for $[Rh(I^iPr_2Me_2)_3(CO)][PF_6]$ | | | |
|---|---|---|---|
| C(1)-Rh(1)-C(13) | 87.95(6) | C(1)-Rh(1)-C(24) | 90.23(6) |
| C(13)-Rh(1)-C(24) | 177.56(5) | C(1)-Rh(1)-C(2) | 176.38(6) |
| C(13)-Rh(1)-C(2) | 90.01(5) | C(24)-Rh(1)-C(2) | 91.90(5) |
| F(2)-P(1)-F(4) | 178.80(11) | F(2)-P(1)-F(1) | 89.49(9) |
| F(4)-P(1)-F(1) | 89.65(9) | F(2)-P(1)-F(6) | 90.02(10) |
| F(4)-P(1)-F(6) | 90.81(11) | F(1)-P(1)-F(6) | 89.38(7) |
| F(2)-P(1)-F(5) | 88.24(9) | F(4)-P(1)-F(5) | 90.94(10) |
| F(1)-P(1)-F(5) | 91.37(7) | F(6)-P(1)-F(5) | 178.10(10) |
| F(2)-P(1)-F(3) | 91.60(10) | F(4)-P(1)-F(3) | 89.27(11) |
| F(1)-P(1)-F(3) | 178.84(9) | F(6)-P(1)-F(3) | 90.21(8) |
| F(5)-P(1)-F(3) | 89.08(8) | C(2)-N(1)-C(3) | 111.23(12) |
| C(2)-N(1)-C(5) | 122.24(12) | C(3)-N(1)-C(5) | 126.47(12) |
| C(2)-N(2)-C(4) | 111.59(12) | C(2)-N(2)-C(10) | 122.41(12) |
| C(4)-N(2)-C(10) | 125.99(12) | C(13)-N(3)-C(14) | 110.87(13) |
| C(13)-N(3)-C(16) | 122.04(12) | C(14)-N(3)-C(16) | 126.74(13) |
| C(13)-N(4)-C(15) | 110.87(13) | C(13)-N(4)-C(21) | 121.07(13) |
| C(15)-N(4)-C(21) | 127.93(14) | C(24)-N(5)-C(25) | 110.74(12) |
| C(24)-N(5)-C(27) | 122.36(12) | C(25)-N(5)-C(27) | 126.86(13) |
| C(24)-N(6)-C(26) | 111.10(12) | C(24)-N(6)-C(32) | 121.52(12) |
| C(26)-N(6)-C(32) | 127.29(12) | O(1)-C(1)-Rh(1) | 177.73(16) |
| N(2)-C(2)-N(1) | 103.87(11) | N(2)-C(2)-Rh(1) | 128.24(10) |
| N(1)-C(2)-Rh(1) | 127.85(10) | C(4)-C(3)-N(1) | 106.75(13) |
| C(4)-C(3)-C(8) | 127.55(15) | N(1)-C(3)-C(8) | 125.68(15) |
| C(3)-C(4)-N(2) | 106.56(13) | C(3)-C(4)-C(9) | 127.63(14) |
| N(2)-C(4)-C(9) | 125.79(15) | N(1)-C(5)-C(6) | 110.81(13) |
| N(1)-C(5)-C(7) | 112.80(14) | C(6)-C(5)-C(7) | 113.19(15) |
| N(2)-C(10)-C(12) | 111.24(13) | N(2)-C(10)-C(11) | 112.36(12) |
| C(12)-C(10)-C(11) | 113.15(13) | N(4)-C(13)-N(3) | 104.80(12) |
| N(4)-C(13)-Rh(1) | 126.29(11) | N(3)-C(13)-Rh(1) | 128.90(10) |

| | | | |
|---|---|---|---|
| C(15)-C(14)-N(3) | 106.49(14) | C(15)-C(14)-C(19) | 128.29(15) |
| N(3)-C(14)-C(19) | 125.16(16) | C(14)-C(15)-N(4) | 106.97(13) |
| C(14)-C(15)-C(20) | 127.70(17) | N(4)-C(15)-C(20) | 125.33(17) |
| N(3)-C(16)-C(18) | 110.73(13) | N(3)-C(16)-C(17) | 114.00(14) |
| C(18)-C(16)-C(17) | 111.57(14) | N(4)-C(21)-C(23) | 111.01(14) |
| N(4)-C(21)-C(22) | 112.65(16) | C(23)-C(21)-C(22) | 114.34(17) |
| N(6)-C(24)-N(5) | 104.78(11) | N(6)-C(24)-Rh(1) | 126.03(10) |
| N(5)-C(24)-Rh(1) | 129.12(10) | C(26)-C(25)-N(5) | 106.84(13) |
| C(26)-C(25)-C(30) | 127.51(16) | N(5)-C(25)-C(30) | 125.64(16) |
| C(25)-C(26)-N(6) | 106.54(13) | C(25)-C(26)-C(31) | 127.87(15) |
| N(6)-C(26)-C(31) | 125.60(15) | N(5)-C(27)-C(29) | 111.57(13) |
| N(5)-C(27)-C(28) | 113.41(14) | C(29)-C(27)-C(28) | 111.56(14) |
| N(6)-C(32)-C(34) | 111.81(13) | N(6)-C(32)-C(33) | 112.00(13) |
| C(34)-C(32)-C(33) | 112.81(16) | | |

**5.7.** ***Appendix 7:*** crystallographic data, bond lengths and angles for $[Rh(ICy)_3(CO)][PF_6]$ (**90**).

| **$[Rh(ICy)_3(CO)][PF_6]$** | |
|---|---|
| Empirical formula | $C_{46}\ H_{72}\ F_6\ N_6\ O\ P\ Rh$ |
| Formula weight | 972.98 |
| Temperature | 150(2) K |
| Wavelength | 0.71073 Å |
| Crystal system | Monoclinic |
| Space group | $P2_1/c$ |
| Unit cell dimensions | a = 15.0300(1)Å $\alpha = 90^o$ |
| | b = 15.0630(1)Å $\beta = 96.431(1)^o$ |
| | c = 21.6460(2)Å $\gamma = 90^o$ |
| Volume | 4869.75(6) $Å^3$ |
| Z | 4 |
| Density (calculated) | 1.327 $Mg/m^3$ |
| Absorption coefficient | 0.446 $mm^{-1}$ |
| F(000) | 2048 |
| Crystal size | 0.50 x 0.50 x 0.15 mm |
| Theta range for data collection | 3.65 to 30.06°. |
| Index ranges | -21<=h<=21; -21<=k<=21; -30<=l<=30 |
| Reflections collected | 86647 |
| Independent reflections | 14144 [R(int) = 0.0397] |
| Reflections observed (>2σ) | 12777 |
| Absorption correction | Semi-empirical from equivalents |
| Max. and min. transmission | 0.88 and 0.78 |
| Refinement method | Full-matrix least-squares on $F^2$ |
| Data / restraints / parameters | 14144 / 0 / 550 |
| Goodness-of-fit on $F^2$ | 1.030 |
| Final R indices [I>2σ(I)] | $R^1 = 0.0286$ $wR_2 = 0.0719$ |
| R indices (all data) | $R^1 = 0.0331$ $wR_2 = 0.0755$ |
| Largest diff. peak and hole | 0.478 and -0.819 $eÅ^{-3}$ |

| Bond lengths (Å) for $[Rh(ICy)_3(CO)][PF_6]$ | | | |
|---|---|---|---|
| Rh(1)-C(1) | 1.8322(15) | Rh(1)-C(17) | 2.0638(11) |
| Rh(1)-C(32) | 2.0642(11) | Rh(1)-C(2) | 2.1321(12) |
| P(1)-F(5) | 1.5818(13) | P(1)-F(1) | 1.5858(11) |
| P(1)-F(3) | 1.5904(11) | P(1)-F(6) | 1.5916(13) |
| P(1)-F(2) | 1.5946(11) | P(1)-F(4) | 1.5949(11) |
| O(1)-C(1) | 1.143(2) | N(1)-C(2) | 1.3665(16) |
| N(1)-C(3) | 1.3878(19) | N(1)-C(5) | 1.4719(17) |
| N(2)-C(2) | 1.3675(17) | N(2)-C(4) | 1.3851(19) |
| N(2)-C(11) | 1.4696(17) | N(3)-C(17) | 1.3628(15) |
| N(3)-C(18) | 1.3878(16) | N(3)-C(20) | 1.4734(16) |
| N(4)-C(17) | 1.3619(15) | N(4)-C(19) | 1.3905(16) |
| N(4)-C(26) | 1.4705(16) | N(5)-C(32) | 1.3607(15) |
| N(5)-C(33) | 1.3901(16) | N(5)-C(35) | 1.4728(16) |
| N(6)-C(32) | 1.3673(15) | N(6)-C(34) | 1.3888(15) |
| N(6)-C(41) | 1.4740(16) | C(3)-C(4) | 1.334(2) |
| C(5)-C(10) | 1.5261(19) | C(5)-C(6) | 1.5304(19) |
| C(6)-C(7) | 1.536(2) | C(7)-C(8) | 1.528(2) |
| C(8)-C(9) | 1.523(2) | C(9)-C(10) | 1.525(2) |
| C(11)-C(16) | 1.5325(19) | C(11)-C(12) | 1.535(2) |
| C(12)-C(13) | 1.520(2) | C(13)-C(14) | 1.517(2) |
| C(14)-C(15) | 1.520(3) | C(15)-C(16) | 1.523(2) |
| C(18)-C(19) | 1.3449(19) | C(20)-C(21) | 1.5233(18) |
| C(20)-C(25) | 1.5279(19) | C(21)-C(22) | 1.5316(19) |
| C(22)-C(23) | 1.525(2) | C(23)-C(24) | 1.522(2) |
| C(24)-C(25) | 1.527(2) | C(26)-C(27) | 1.5267(18) |
| C(26)-C(31) | 1.5296(19) | C(27)-C(28) | 1.530(2) |
| C(28)-C(29) | 1.527(2) | C(29)-C(30) | 1.520(2) |
| C(30)-C(31) | 1.527(2) | C(33)-C(34) | 1.3468(19) |
| C(35)-C(40) | 1.5204(18) | C(35)-C(36) | 1.522(2) |

| | | | |
|---|---|---|---|
| C(36)-C(37) | 1.536(2) | C(37)-C(38) | 1.527(3) |
| C(38)-C(39) | 1.518(3) | C(39)-C(40) | 1.533(2) |
| C(41)-C(42) | 1.5222(18) | C(41)-C(46) | 1.5323(19) |
| C(42)-C(43) | 1.535(2) | C(43)-C(44) | 1.527(2) |
| C(44)-C(45) | 1.526(2) | C(45)-C(46) | 1.5265(19) |

| Bond angles (°) for $[Rh(ICy)_3(CO)][PF_6]$ | | | |
|---|---|---|---|
| C(1)-Rh(1)-C(17) | 88.44(6) | C(1)-Rh(1)-C(32) | 89.05(6) |
| C(17)-Rh(1)-C(32) | 177.39(5) | C(1)-Rh(1)-C(2) | 177.86(7) |
| C(17)-Rh(1)-C(2) | 90.93(5) | C(32)-Rh(1)-C(2) | 91.60(5) |
| F(5)-P(1)-F(1) | 90.90(8) | F(5)-P(1)-F(3) | 89.22(9) |
| F(1)-P(1)-F(3) | 179.68(7) | F(5)-P(1)-F(6) | 179.80(10) |
| F(1)-P(1)-F(6) | 89.27(7) | F(3)-P(1)-F(6) | 90.61(8) |
| F(5)-P(1)-F(2) | 89.55(9) | F(1)-P(1)-F(2) | 90.31(7) |
| F(3)-P(1)-F(2) | 89.99(6) | F(6)-P(1)-F(2) | 90.57(8) |
| F(5)-P(1)-F(4) | 90.28(8) | F(1)-P(1)-F(4) | 90.13(7) |
| F(3)-P(1)-F(4) | 89.57(6) | F(6)-P(1)-F(4) | 89.60(8) |
| F(2)-P(1)-F(4) | 179.53(7) | C(2)-N(1)-C(3) | 111.50(12) |
| C(2)-N(1)-C(5) | 127.53(11) | C(3)-N(1)-C(5) | 120.93(12) |
| C(2)-N(2)-C(4) | 111.11(12) | C(2)-N(2)-C(11) | 128.24(11) |
| C(4)-N(2)-C(11) | 120.63(12) | C(17)-N(3)-C(18) | 111.29(10) |
| C(17)-N(3)-C(20) | 124.20(10) | C(18)-N(3)-C(20) | 124.05(11) |
| C(17)-N(4)-C(19) | 110.75(10) | C(17)-N(4)-C(26) | 122.66(10) |
| C(19)-N(4)-C(26) | 125.21(10) | C(32)-N(5)-C(33) | 111.18(10) |
| C(32)-N(5)-C(35) | 122.95(10) | C(33)-N(5)-C(35) | 125.08(10) |
| C(32)-N(6)-C(34) | 111.03(10) | C(32)-N(6)-C(41) | 123.54(10) |
| C(34)-N(6)-C(41) | 124.08(10) | O(1)-C(1)-Rh(1) | 178.8(2) |
| N(1)-C(2)-N(2) | 103.36(11) | N(1)-C(2)-Rh(1) | 128.13(9) |
| N(2)-C(2)-Rh(1) | 128.49(9) | C(4)-C(3)-N(1) | 106.62(14) |
| C(3)-C(4)-N(2) | 107.41(14) | N(1)-C(5)-C(10) | 109.82(11) |
| N(1)-C(5)-C(6) | 109.99(12) | C(10)-C(5)-C(6) | 111.12(11) |
| C(5)-C(6)-C(7) | 111.92(13) | C(8)-C(7)-C(6) | 111.86(13) |
| C(9)-C(8)-C(7) | 111.59(13) | C(8)-C(9)-C(10) | 110.30(14) |
| C(9)-C(10)-C(5) | 111.25(12) | N(2)-C(11)-C(16) | 109.46(12) |
| N(2)-C(11)-C(12) | 109.69(12) | C(16)-C(11)-C(12) | 111.58(12) |
| C(13)-C(12)-C(11) | 112.32(13) | C(14)-C(13)-C(12) | 110.70(14) |

| | | | |
|---|---|---|---|
| C(13)-C(14)-C(15) | 111.63(13) | C(14)-C(15)-C(16) | 111.68(14) |
| C(15)-C(16)-C(11) | 113.05(12) | N(4)-C(17)-N(3) | 104.24(10) |
| N(4)-C(17)-Rh(1) | 127.51(9) | N(3)-C(17)-Rh(1) | 128.20(8) |
| C(19)-C(18)-N(3) | 106.52(11) | C(18)-C(19)-N(4) | 107.20(11) |
| N(3)-C(20)-C(21) | 112.65(11) | N(3)-C(20)-C(25) | 110.68(10) |
| C(21)-C(20)-C(25) | 110.40(11) | C(20)-C(21)-C(22) | 110.14(12) |
| C(23)-C(22)-C(21) | 111.26(12) | C(24)-C(23)-C(22) | 110.47(12) |
| C(23)-C(24)-C(25) | 111.35(13) | C(24)-C(25)-C(20) | 109.37(11) |
| N(4)-C(26)-C(27) | 111.66(11) | N(4)-C(26)-C(31) | 109.34(10) |
| C(27)-C(26)-C(31) | 112.04(11) | C(26)-C(27)-C(28) | 111.29(12) |
| C(29)-C(28)-C(27) | 111.30(12) | C(30)-C(29)-C(28) | 110.57(12) |
| C(29)-C(30)-C(31) | 110.79(13) | C(30)-C(31)-C(26) | 111.52(12) |
| N(5)-C(32)-N(6) | 104.12(10) | N(5)-C(32)-Rh(1) | 127.65(9) |
| N(6)-C(32)-Rh(1) | 128.17(8) | C(34)-C(33)-N(5) | 106.83(11) |
| C(33)-C(34)-N(6) | 106.82(11) | N(5)-C(35)-C(40) | 111.97(11) |
| N(5)-C(35)-C(36) | 110.20(11) | C(40)-C(35)-C(36) | 111.15(12) |
| C(35)-C(36)-C(37) | 110.22(14) | C(38)-C(37)-C(36) | 110.47(19) |
| C(39)-C(38)-C(37) | 110.42(13) | C(38)-C(39)-C(40) | 111.34(13) |
| C(35)-C(40)-C(39) | 110.66(12) | N(6)-C(41)-C(42) | 113.40(11) |
| N(6)-C(41)-C(46) | 109.77(10) | C(42)-C(41)-C(46) | 110.21(11) |
| C(41)-C(42)-C(43) | 109.66(12) | C(44)-C(43)-C(42) | 111.66(13) |
| C(45)-C(44)-C(43) | 111.29(12) | C(44)-C(45)-C(46) | 110.37(12) |
| C(45)-C(46)-C(41) | 110.32(12) | | |

**5.8.** ***Appendix 8:*** crystallographic data, bond lengths and angles for $[Rh(I^iPr_2Me_2)_3(CO)][(PMe_2)_3(O)_4H]$ **(91)**.[6]

| **$[Rh(I^iPr_2Me_2)_3(CO)][(PMe_2)_3(O)_4H]$** | |
|---|---|
| Empirical formula | $C_{40}H_{79}N_6O_5P_3Rh$ |
| Formula weight | 919.91 |
| Temperature | 150(2) K |
| Wavelength | 0.71073 Å |
| Crystal system | Monoclinic |
| Space group | Pc |
| Unit cell dimensions | a = 10.2330(1)Å □ = 90° |
| | b = 12.8590(1)Å □ = 94.501(1)° |
| | c = 18.6340(2)Å □ = 90° |
| Volume | 2444.42(4) $Å^3$ |
| Z | 2 |
| Density (calculated) | 1.250 $Mg/m^3$ |
| Absorption coefficient | 0.492 $mm^{-1}$ |
| F(000) | 982 |
| Crystal size | 0.15 x 0.15 x 0.15 mm |
| Theta range for data collection | 3.65 to 30.05° |
| Index ranges | -14<=h<=14; -18<=k<=17; -26<=l<=26 |
| Reflections collected | 48250 |
| Independent reflections | 14250 [R(int) = 0.0384] |
| Reflections observed (>2□) | 13384 |
| Absorption correction | None |
| Refinement method | Full-matrix least-squares on $F^2$ |
| Data / restraints / parameters | 14250 / 2 / 525 |
| Goodness-of-fit on $F^2$ | 1.074 |
| Final R indices [I>2□(I)] | $R^1$ = 0.0305 $wR_2$ = 0.0682 |
| R indices (all data) | $R^1$ = 0.0356 $wR_2$ = 0.0705 |
| Absolute structure parameter | -0.042(11) |
| Largest diff. peak and hole | 1.129 and -0.537 $eÅ^{-3}$ |

| Bond lengths (Å) for $[Rh(I^iPr_2Me_2)_3(CO)][(PMe_2)_3(O)_4H]$ | | | |
|---|---|---|---|
| Rh(1)-C(1) | 1.833(2) | Rh(1)-C(24) | 2.0762(18) |
| Rh(1)-C(13) | 2.0770(18) | Rh(1)-C(2) | 2.1362(19) |
| P(1)-O(2) | 1.5975(17) | P(1)-O(3) | 1.6532(16) |
| P(1)-C(36) | 1.851(3) | P(1)-C(35) | 1.859(2) |
| P(2)-O(4) | 1.6221(16) | P(2)-O(3) | 1.6287(17) |
| P(2)-C(38) | 1.860(2) | P(2)-C(37) | 1.861(3) |
| P(3)-O(5) | 1.5909(16) | P(3)-O(4) | 1.6566(16) |
| P(3)-C(40) | 1.865(3) | P(3)-C(39) | 1.870(3) |
| O(1)-C(1) | 1.147(3) | N(1)-C(2) | 1.362(2) |
| N(1)-C(3) | 1.395(3) | N(1)-C(5) | 1.480(2) |
| N(2)-C(2) | 1.363(2) | N(2)-C(4) | 1.391(3) |
| N(2)-C(10) | 1.489(3) | N(3)-C(13) | 1.358(2) |
| N(3)-C(14) | 1.403(2) | N(3)-C(16) | 1.481(3) |
| N(4)-C(13) | 1.360(2) | N(4)-C(15) | 1.401(3) |
| N(4)-C(21) | 1.477(3) | N(5)-C(24) | 1.358(2) |
| N(5)-C(25) | 1.404(3) | N(5)-C(27) | 1.473(2) |
| N(6)-C(24) | 1.360(2) | N(6)-C(26) | 1.405(2) |
| N(6)-C(32) | 1.483(2) | C(3)-C(4) | 1.365(3) |
| C(3)-C(8) | 1.493(3) | C(4)-C(9) | 1.501(3) |
| C(5)-C(7) | 1.518(3) | C(5)-C(6) | 1.518(3) |
| C(10)-C(11) | 1.518(3) | C(10)-C(12) | 1.523(3) |
| C(14)-C(15) | 1.347(3) | C(14)-C(19) | 1.498(3) |
| C(15)-C(20) | 1.493(3) | C(16)-C(18) | 1.522(4) |
| C(16)-C(17) | 1.524(3) | C(21)-C(23) | 1.512(4) |
| C(21)-C(22) | 1.527(3) | C(25)-C(26) | 1.354(3) |
| C(25)-C(30) | 1.496(3) | C(26)-C(31) | 1.494(3) |
| C(27)-C(28) | 1.518(3) | C(27)-C(29) | 1.520(3) |
| C(32)-C(34) | 1.515(3) | C(32)-C(33) | 1.526(3) |

| Bond angles (°) for $[Rh(I^iPr_2Me_2)_3(CO)][(PMe_2)_3(O)_4H]$ | | | |
|---|---|---|---|
| C(1)-Rh(1)-C(24) | 88.44(8) | C(1)-Rh(1)-C(13) | 88.58(8) |
| C(24)-Rh(1)-C(13) | 175.89(7) | C(1)-Rh(1)-C(2) | 178.14(9) |
| C(24)-Rh(1)-C(2) | 90.39(7) | C(13)-Rh(1)-C(2) | 92.67(7) |
| O(2)-P(1)-O(3) | 111.26(9) | O(2)-P(1)-C(36) | 112.54(12) |
| O(3)-P(1)-C(36) | 107.15(12) | O(2)-P(1)-C(35) | 110.69(11) |
| O(3)-P(1)-C(35) | 106.47(10) | C(36)-P(1)-C(35) | 108.47(12) |
| O(4)-P(2)-O(3) | 112.68(8) | O(4)-P(2)-C(38) | 110.40(11) |
| O(3)-P(2)-C(38) | 106.50(10) | O(4)-P(2)-C(37) | 106.50(11) |
| O(3)-P(2)-C(37) | 109.54(12) | C(38)-P(2)-C(37) | 111.29(12) |
| O(5)-P(3)-O(4) | 112.04(9) | O(5)-P(3)-C(40) | 111.75(12) |
| O(4)-P(3)-C(40) | 106.25(12) | O(5)-P(3)-C(39) | 112.15(11) |
| O(4)-P(3)-C(39) | 105.09(11) | C(40)-P(3)-C(39) | 109.17(14) |
| P(2)-O(3)-P(1) | 137.98(11) | P(2)-O(4)-P(3) | 143.64(11) |
| C(2)-N(1)-C(3) | 111.84(16) | C(2)-N(1)-C(5) | 122.17(16) |
| C(3)-N(1)-C(5) | 125.79(16) | C(2)-N(2)-C(4) | 111.45(17) |
| C(2)-N(2)-C(10) | 122.28(17) | C(4)-N(2)-C(10) | 126.25(17) |
| C(13)-N(3)-C(14) | 110.89(16) | C(13)-N(3)-C(16) | 122.57(15) |
| C(14)-N(3)-C(16) | 126.50(16) | C(13)-N(4)-C(15) | 111.10(17) |
| C(13)-N(4)-C(21) | 121.47(16) | C(15)-N(4)-C(21) | 127.41(17) |
| C(24)-N(5)-C(25) | 111.13(15) | C(24)-N(5)-C(27) | 121.38(15) |
| C(25)-N(5)-C(27) | 127.46(16) | C(24)-N(6)-C(26) | 111.05(14) |
| C(24)-N(6)-C(32) | 122.30(15) | C(26)-N(6)-C(32) | 126.20(15) |
| O(1)-C(1)-Rh(1) | 178.8(2) | N(1)-C(2)-N(2) | 104.02(16) |
| N(1)-C(2)-Rh(1) | 127.66(13) | N(2)-C(2)-Rh(1) | 128.10(14) |
| C(4)-C(3)-N(1) | 105.92(18) | C(4)-C(3)-C(8) | 127.1(2) |
| N(1)-C(3)-C(8) | 126.91(19) | C(3)-C(4)-N(2) | 106.76(18) |
| C(3)-C(4)-C(9) | 126.3(2) | N(2)-C(4)-C(9) | 127.0(2) |
| N(1)-C(5)-C(7) | 111.43(18) | N(1)-C(5)-C(6) | 113.41(17) |
| C(7)-C(5)-C(6) | 113.08(18) | N(2)-C(10)-C(11) | 111.86(17) |

| | | | |
|---|---|---|---|
| N(2)-C(10)-C(12) | 111.97(18) | C(11)-C(10)-C(12) | 112.46(18) |
| N(3)-C(13)-N(4) | 104.66(15) | N(3)-C(13)-Rh(1) | 128.72(13) |
| N(4)-C(13)-Rh(1) | 126.09(13) | C(15)-C(14)-N(3) | 106.80(18) |
| C(15)-C(14)-C(19) | 127.0(2) | N(3)-C(14)-C(19) | 126.16(19) |
| C(14)-C(15)-N(4) | 106.53(19) | C(14)-C(15)-C(20) | 127.5(2) |
| N(4)-C(15)-C(20) | 126.0(2) | N(3)-C(16)-C(18) | 111.74(19) |
| N(3)-C(16)-C(17) | 112.66(18) | C(18)-C(16)-C(17) | 111.76(19) |
| N(4)-C(21)-C(23) | 111.70(18) | N(4)-C(21)-C(22) | 111.1(2) |
| C(23)-C(21)-C(22) | 113.9(2) | N(5)-C(24)-N(6) | 104.74(15) |
| N(5)-C(24)-Rh(1) | 127.30(13) | N(6)-C(24)-Rh(1) | 127.95(13) |
| C(26)-C(25)-N(5) | 106.56(17) | C(26)-C(25)-C(30) | 128.27(19) |
| N(5)-C(25)-C(30) | 125.16(19) | C(25)-C(26)-N(6) | 106.48(16) |
| C(25)-C(26)-C(31) | 128.30(18) | N(6)-C(26)-C(31) | 125.13(17) |
| N(5)-C(27)-C(28) | 112.11(17) | N(5)-C(27)-C(29) | 112.16(17) |
| C(28)-C(27)-C(29) | 113.28(18) | N(6)-C(32)-C(34) | 113.40(17) |
| N(6)-C(32)-C(33) | 110.24(16) | C(34)-C(32)-C(33) | 113.54(17) |

**5.9.** ***Appendix 9:*** crystallographic data, bond lengths and angles for $[Rh(I^iPr_2Me_2)_2(ICy)(CO)][PF_6]$ (**95**).[7]

| **$[Rh(I^iPr_2Me_2)_2(ICy)(CO)][PF_6]$** | |
|---|---|
| Empirical formula | $C_{39}\ H_{66}\ Cl_2\ F_6\ N_6\ O\ P\ Rh$ |
| Formula weight | 953.76 |
| Temperature | 150(2) K |
| Wavelength | 0.71073 Å |
| Crystal system | Triclinic |
| Space group | P-1 |
| Unit cell dimensions | a = 10.5110(1)Å α = 84.158(1)° |
| | b = 14.4190(1)Å β = 78.804(1)° |
| | c = 15.4100(1)Å γ = 86.557(1)° |
| Volume | 2277.22(3) $Å^3$ |
| Z | 2 |
| Density (calculated) | 1.391 $Mg/m^3$ |
| Absorption coefficient | 0.589 $mm^{-1}$ |
| F(000) | 996 |
| Crystal size | 0.25 x 0.25 x 0.20 mm |
| Theta range for data collection | 3.53 to 30.54° |
| Index ranges | -15<=h<=15; -20<=k<=20; -21<=l<=21 |
| Reflections collected | 47613 |
| Independent reflections | 13880 [R(int) = 0.0351] |
| Reflections observed (>2σ) | 12834 |
| Absorption correction | Semi-empirical from equivalents |
| Max. and min. transmission | 0.90 and 0.85 |
| Refinement method | Full-matrix least-squares on $F^2$ |
| Data / restraints / parameters | 13880 / 0 / 517 |
| Goodness-of-fit on $F^2$ | 1.040 |
| Final R indices [I>2σ(I)] | $R^1 = 0.0305$ $wR_2 = 0.0756$ |
| R indices (all data) | $R^1 = 0.0348$ $wR_2 = 0.0778$ |
| Largest diff. peak and hole | 0.883 and -0.687 $eÅ^{-3}$ |

| Bond lengths (Å) for $[Rh(I^iPr_2Me_2)_2(ICy)(CO)][PF_6]$ | | | |
|---|---|---|---|
| Rh(1)-C(1) | 1.8392(14) | Rh(1)-C(2) | 2.0677(13) |
| Rh(1)-C(28) | 2.0818(13) | Rh(1)-C(13) | 2.1341(13) |
| Cl(1)-C(39) | 1.746(2) | Cl(2)-C(39) | 1.729(2) |
| P(1)-F(2) | 1.5695(14) | P(1)-F(1) | 1.5841(13) |
| P(1)-F(4) | 1.5871(13) | P(1)-F(5) | 1.5871(15) |
| P(1)-F(6) | 1.5892(12) | P(1)-F(3) | 1.6036(12) |
| O(1)-C(1) | 1.1445(18) | N(1)-C(2) | 1.3668(16) |
| N(1)-C(3) | 1.4012(18) | N(1)-C(5) | 1.4798(19) |
| N(2)-C(2) | 1.3530(18) | N(2)-C(4) | 1.4007(18) |
| N(2)-C(10) | 1.4783(19) | N(3)-C(13) | 1.3671(17) |
| N(3)-C(14) | 1.3900(18) | N(3)-C(16) | 1.4744(17) |
| N(4)-C(13) | 1.3647(17) | N(4)-C(15) | 1.3899(18) |
| N(4)-C(22) | 1.4729(17) | N(5)-C(28) | 1.3598(17) |
| N(5)-C(29) | 1.4001(19) | N(5)-C(31) | 1.4846(18) |
| N(6)-C(28) | 1.3681(16) | N(6)-C(30) | 1.3997(18) |
| N(6)-C(36) | 1.4817(18) | C(3)-C(4) | 1.356(2) |
| C(3)-C(8) | 1.495(2) | C(4)-C(9) | 1.495(2) |
| C(5)-C(6) | 1.525(2) | C(5)-C(7) | 1.530(2) |
| C(10)-C(12) | 1.514(3) | C(10)-C(11) | 1.521(2) |
| C(14)-C(15) | 1.347(2) | C(16)-C(21) | 1.527(2) |
| C(16)-C(17) | 1.533(2) | C(17)-C(18) | 1.535(2) |
| C(18)-C(19) | 1.519(3) | C(19)-C(20) | 1.529(3) |
| C(20)-C(21) | 1.531(2) | C(22)-C(27) | 1.528(2) |
| C(22)-C(23) | 1.529(2) | C(23)-C(24) | 1.526(2) |
| C(24)-C(25) | 1.522(3) | C(25)-C(26) | 1.526(3) |
| C(26)-C(27) | 1.534(2) | C(29)-C(30) | 1.357(2) |
| C(29)-C(34) | 1.496(2) | C(30)-C(35) | 1.496(2) |
| C(31)-C(32) | 1.514(2) | C(31)-C(33) | 1.514(2) |
| C(36)-C(37) | 1.524(2) | C(36)-C(38) | 1.526(2) |

| Bond angles (°) for $[Rh(I^iPr_2Me_2)_2(ICy)(CO)][PF_6]$ | | | |
|---|---|---|---|
| C(1)-Rh(1)-C(2) | 87.26(6) | C(1)-Rh(1)-C(28) | 92.26(6) |
| C(2)-Rh(1)-C(28) | 178.34(5) | C(1)-Rh(1)-C(13) | 173.92(6) |
| C(2)-Rh(1)-C(13) | 89.93(5) | C(28)-Rh(1)-C(13) | 90.70(5) |
| F(2)-P(1)-F(1) | 91.14(11) | F(2)-P(1)-F(4) | 90.01(10) |
| F(1)-P(1)-F(4) | 178.65(10) | F(2)-P(1)-F(5) | 179.17(11) |
| F(1)-P(1)-F(5) | 89.51(11) | F(4)-P(1)-F(5) | 89.34(10) |
| F(2)-P(1)-F(6) | 90.59(8) | F(1)-P(1)-F(6) | 90.19(8) |
| F(4)-P(1)-F(6) | 89.10(8) | F(5)-P(1)-F(6) | 89.92(9) |
| F(2)-P(1)-F(3) | 89.17(8) | F(1)-P(1)-F(3) | 89.79(8) |
| F(4)-P(1)-F(3) | 90.92(7) | F(5)-P(1)-F(3) | 90.33(9) |
| F(6)-P(1)-F(3) | 179.76(9) | C(2)-N(1)-C(3) | 110.76(12) |
| C(2)-N(1)-C(5) | 121.32(12) | C(3)-N(1)-C(5) | 127.31(12) |
| C(2)-N(2)-C(4) | 111.38(12) | C(2)-N(2)-C(10) | 120.58(12) |
| C(4)-N(2)-C(10) | 127.69(13) | C(13)-N(3)-C(14) | 111.35(12) |
| C(13)-N(3)-C(16) | 126.69(11) | C(14)-N(3)-C(16) | 121.85(12) |
| C(13)-N(4)-C(15) | 111.47(12) | C(13)-N(4)-C(22) | 126.50(11) |
| C(15)-N(4)-C(22) | 122.00(12) | C(28)-N(5)-C(29) | 111.30(12) |
| C(28)-N(5)-C(31) | 120.92(12) | C(29)-N(5)-C(31) | 127.77(13) |
| C(28)-N(6)-C(30) | 110.94(12) | C(28)-N(6)-C(36) | 121.90(11) |
| C(30)-N(6)-C(36) | 126.43(12) | O(1)-C(1)-Rh(1) | 174.78(15) |
| N(2)-C(2)-N(1) | 104.75(11) | N(2)-C(2)-Rh(1) | 126.64(10) |
| N(1)-C(2)-Rh(1) | 128.62(10) | C(4)-C(3)-N(1) | 106.67(12) |
| C(4)-C(3)-C(8) | 127.69(15) | N(1)-C(3)-C(8) | 125.58(14) |
| C(3)-C(4)-N(2) | 106.44(13) | C(3)-C(4)-C(9) | 128.51(14) |
| N(2)-C(4)-C(9) | 125.03(15) | N(1)-C(5)-C(6) | 113.74(13) |
| N(1)-C(5)-C(7) | 111.30(13) | C(6)-C(5)-C(7) | 111.38(12) |
| N(2)-C(10)-C(12) | 110.36(15) | N(2)-C(10)-C(11) | 112.56(13) |
| C(12)-C(10)-C(11) | 115.58(16) | N(4)-C(13)-N(3) | 103.68(11) |
| N(4)-C(13)-Rh(1) | 127.14(9) | N(3)-C(13)-Rh(1) | 129.17(9) |

| | | | |
|---|---|---|---|
| C(15)-C(14)-N(3) | 106.77(13) | C(14)-C(15)-N(4) | 106.72(12) |
| N(3)-C(16)-C(21) | 109.32(13) | N(3)-C(16)-C(17) | 110.69(12) |
| C(21)-C(16)-C(17) | 111.86(13) | C(16)-C(17)-C(18) | 111.61(14) |
| C(19)-C(18)-C(17) | 111.66(17) | C(18)-C(19)-C(20) | 111.75(14) |
| C(19)-C(20)-C(21) | 110.91(16) | C(16)-C(21)-C(20) | 111.79(15) |
| N(4)-C(22)-C(27) | 110.91(12) | N(4)-C(22)-C(23) | 109.66(12) |
| C(27)-C(22)-C(23) | 111.59(12) | C(24)-C(23)-C(22) | 111.81(14) |
| C(25)-C(24)-C(23) | 111.72(15) | C(24)-C(25)-C(26) | 111.37(14) |
| C(25)-C(26)-C(27) | 110.86(15) | C(22)-C(27)-C(26) | 110.43(14) |
| N(5)-C(28)-N(6) | 104.54(11) | N(5)-C(28)-Rh(1) | 126.13(10) |
| N(6)-C(28)-Rh(1) | 129.33(10) | C(30)-C(29)-N(5) | 106.53(13) |
| C(30)-C(29)-C(34) | 128.23(15) | N(5)-C(29)-C(34) | 125.24(15) |
| C(29)-C(30)-N(6) | 106.70(12) | C(29)-C(30)-C(35) | 128.07(15) |
| N(6)-C(30)-C(35) | 125.15(15) | N(5)-C(31)-C(32) | 112.19(13) |
| N(5)-C(31)-C(33) | 111.98(13) | C(32)-C(31)-C(33) | 113.30(15) |
| N(6)-C(36)-C(37) | 114.15(12) | N(6)-C(36)-C(38) | 110.51(13) |
| C(37)-C(36)-C(38) | 111.97(13) | Cl(2)-C(39)-Cl(1) | 113.09(13) |

**5.10.** ***Appendix 10:*** crystallographic data, bond lengths and angles for $ICyHPF_6$ (**94**).[8]

| | **$ICyHPF_6$** |
|---|---|
| Empirical formula | $C_{15}\ H_{25}\ F_6\ N_2\ P$ |
| Formula weight | 378.34 |
| Temperature | 150(2) K |
| Wavelength | 0.71073 Å |
| Crystal system | Orthorhombic |
| Space group | Pbca |
| Unit cell dimensions | a = 14.61600(10)Å α = 90° |
| | b = 15.11600(10)Å β = 90° |
| | c = 16.1410(2)Å γ = 90° |
| Volume | 3566.12(6) $Å^3$ |
| Z | 8 |
| Density (calculated) | 1.409 $Mg/m^3$ |
| Absorption coefficient | 0.212 $mm^{-1}$ |
| F(000) | 1584 |
| Crystal size | 0.25 x 0.25 x 0.25 mm |
| Theta range for data collection | 3.76 to 27.48 °. |
| Index ranges | -18<=h<=18; -19<=k<=19; -20<=l<=20 |
| Reflections collected | 62341 |
| Independent reflections | 4064 [R(int) = 0.0427] |
| Reflections observed (>2σ) | 3235 |
| Absorption correction | Semi-empirical from equivalents |
| Max. and min. transmission | 0.95 and 0.90 |
| Refinement method | Full-matrix least-squares on $F^2$ |
| Data / restraints / parameters | 4064 / 0 / 222 |
| Goodness-of-fit on $F^2$ | 1.033 |
| Final R indices [I>2σ(I)] | R1 = 0.0353 wR2 = 0.0881 |
| R indices (all data) | R1 = 0.0490 wR2 = 0.0971 |
| Largest diff. peak and hole | 0.231 and -0.248 $eÅ^{-3}$ |

| Bond lengths (Å) for $ICyHPF_6$ | | | |
|---|---|---|---|
| P(1)-F(4) | 1.5893(9) | P(1)-F(2) | 1.5916(9) |
| P(1)-F(3) | 1.5934(9) | P(1)-F(6) | 1.5935(9) |
| P(1)-F(5) | 1.5995(9) | P(1)-F(1) | 1.6019(8) |
| F(1)-H(1) | 2.236(16) | N(1)-C(1) | 1.3263(17) |
| N(1)-C(2) | 1.3750(18) | N(1)-C(4) | 1.4821(16) |
| N(2)-C(1) | 1.3240(17) | N(2)-C(3) | 1.3727(18) |
| N(2)-C(10) | 1.4812(16) | C(2)-C(3) | 1.349(2) |
| C(4)-C(9) | 1.5171(19) | C(4)-C(5) | 1.5175(19) |
| C(5)-C(6) | 1.532(2) | C(6)-C(7) | 1.519(2) |
| C(7)-C(8) | 1.521(2) | C(8)-C(9) | 1.528(2) |
| C(10)-C(11) | 1.521(2) | C(10)-C(15) | 1.5234(18) |
| C(11)-C(12) | 1.532(2) | C(12)-C(13) | 1.521(2) |
| C(13)-C(14) | 1.514(2) | C(14)-C(15) | 1.5319(19) |

| Bond angles (°) for $ICyHPF_6$ | | | |
|---|---|---|---|
| F(4)-P(1)-F(2) | 179.12(5) | F(4)-P(1)-F(3) | 90.32(6) |
| F(2)-P(1)-F(3) | 89.78(5) | F(4)-P(1)-F(6) | 90.17(5) |
| F(2)-P(1)-F(6) | 90.71(5) | F(3)-P(1)-F(6) | 90.26(5) |
| F(4)-P(1)-F(5) | 89.99(6) | F(2)-P(1)-F(5) | 89.91(5) |
| F(3)-P(1)-F(5) | 179.54(6) | F(6)-P(1)-F(5) | 90.07(5) |
| F(4)-P(1)-F(1) | 89.59(5) | F(2)-P(1)-F(1) | 89.54(5) |
| F(3)-P(1)-F(1) | 90.14(5) | F(6)-P(1)-F(1) | 179.53(5) |
| F(5)-P(1)-F(1) | 89.53(5) | P(1)-F(1)-H(1) | 123.4(4) |
| C(1)-N(1)-C(2) | 108.02(11) | C(1)-N(1)-C(4) | 123.50(11) |
| C(2)-N(1)-C(4) | 128.37(11) | C(1)-N(2)-C(3) | 108.16(11) |
| C(1)-N(2)-C(10) | 126.28(11) | C(3)-N(2)-C(10) | 125.38(11) |
| N(2)-C(1)-N(1) | 109.38(11) | C(3)-C(2)-N(1) | 107.18(12) |
| C(2)-C(3)-N(2) | 107.26(13) | N(1)-C(4)-C(9) | 111.68(11) |
| N(1)-C(4)-C(5) | 109.20(11) | C(9)-C(4)-C(5) | 112.11(11) |
| C(4)-C(5)-C(6) | 110.02(12) | C(7)-C(6)-C(5) | 111.06(13) |
| C(6)-C(7)-C(8) | 111.05(13) | C(7)-C(8)-C(9) | 111.51(13) |
| C(4)-C(9)-C(8) | 109.08(12) | N(2)-C(10)-C(11) | 109.63(11) |
| N(2)-C(10)-C(15) | 111.20(11) | C(11)-C(10)-C(15) | 111.78(12) |
| C(10)-C(11)-C(12) | 109.98(12) | C(13)-C(12)-C(11) | 110.77(13) |
| C(14)-C(13)-C(12) | 111.43(13) | C(13)-C(14)-C(15) | 110.50(12) |
| C(10)-C(15)-C(14) | 109.06(12) | | |

**5.11.** ***Appendix 11:*** crystallographic data, bond lengths and angles for $[Rh(IEt_2Me_2)_4][PPh_2O_2H]$ (**96**).[9]

| **$[Rh(IEt_2Me_2)_4][PPh_2O_2H]$** | |
|---|---|
| Empirical formula | $C_{60}H_{86}N_8O_2PRh$ |
| Formula weight | 1085.25 |
| Temperature | 150(2) K |
| Wavelength | 0.71073 Å |
| Crystal system | Monoclinic |
| Space group | C2 |
| Unit cell dimensions | a = 23.6780(2)Å α = 90° |
| | b = 11.4130(1)Å β = 108.191(1)° |
| | c = 22.5860(3)Å γ = 90° |
| Volume | 5798.52(10) $Å^3$ |
| Z | 4 |
| Density (calculated) | 1.243 $Mg/m^3$ |
| Absorption coefficient | 0.370 $mm^{-1}$ |
| F(000) | 2312 |
| Crystal size | 0.30 x 0.25 x 0.05 mm |
| Theta range for data collection | 3.53 to 20.00° |
| Index ranges | -22<=h<=22; -10<=k<=10; -21<=l<=21 |
| Reflections collected | 29137 |
| Independent reflections | 5357 [R(int) = 0.0396] |
| Reflections observed (>2σ) | 5209 |
| Absorption correction | Semi-empirical from equivalents |
| Max. and min. transmission | 0.96 and 0.87 |
| Refinement method | Full-matrix least-squares on $F^2$ |
| Data / restraints / parameters | 5357 / 1 / 650 |
| Goodness-of-fit on $F^2$ | 1.043 |
| Final R indices [I>2σ(I)] | $R^1 = 0.0242$ $wR_2 = 0.0588$ |
| R indices (all data) | $R^1 = 0.0272$ $wR_2 = 0.0602$ |
| Largest diff. peak and hole | 0.478 and -0.429 $eÅ^{-3}$ |

| Bond lengths (Å) for $[Rh(IEt_2Me_2)_4][PPh_2O_2H]$ | | | |
|---|---|---|---|
| Rh(1)-C(1) | 2.042(4) | Rh(1)-C(1)#1 | 2.042(4) |
| Rh(1)-C(10)#1 | 2.047(4) | Rh(1)-C(10) | 2.047(4) |
| Rh(2)-C(28) | 2.041(4) | Rh(2)-C(28)#2 | 2.041(4) |
| Rh(2)-C(19) | 2.040(4) | Rh(2)-C(19)#2 | 2.040(4) |
| P(1)-O(1) | 1.484(3) | P(1)-O(2) | 1.492(3) |
| P(1)-C(37) | 1.824(4) | P(1)-C(43) | 1.830(4) |
| N(1)-C(1) | 1.379(5) | N(1)-C(2) | 1.388(5) |
| N(1)-C(4) | 1.446(5) | N(2)-C(1) | 1.375(5) |
| N(2)-C(3) | 1.395(5) | N(2)-C(8) | 1.457(5) |
| N(3)-C(10) | 1.381(5) | N(3)-C(11) | 1.401(5) |
| N(3)-C(13) | 1.450(5) | N(4)-C(10) | 1.355(5) |
| N(4)-C(12) | 1.405(5) | N(4)-C(17) | 1.459(5) |
| N(5)-C(19) | 1.374(5) | N(5)-C(20) | 1.394(5) |
| N(5)-C(22) | 1.458(5) | N(6)-C(19) | 1.368(5) |
| N(6)-C(21) | 1.407(5) | N(6)-C(26) | 1.469(5) |
| N(7)-C(28) | 1.377(5) | N(7)-C(29) | 1.394(5) |
| N(7)-C(31) | 1.461(5) | N(8)-C(28) | 1.368(5) |
| N(8)-C(30) | 1.395(5) | N(8)-C(35) | 1.463(5) |
| C(2)-C(3) | 1.342(6) | C(2)-C(6) | 1.497(6) |
| C(3)-C(7) | 1.503(6) | C(4)-C(5) | 1.507(6) |
| C(8)-C(9) | 1.504(6) | C(11)-C(12) | 1.341(5) |
| C(11)-C(15) | 1.496(6) | C(12)-C(16) | 1.484(5) |
| C(13)-C(14) | 1.515(6) | C(17)-C(18) | 1.520(6) |
| C(20)-C(21) | 1.332(5) | C(20)-C(24) | 1.500(6) |
| C(21)-C(25) | 1.491(6) | C(22)-C(23) | 1.509(6) |
| C(26)-C(27) | 1.506(6) | C(29)-C(30) | 1.338(6) |
| C(29)-C(33) | 1.497(6) | C(30)-C(34) | 1.497(6) |
| C(31)-C(32) | 1.527(5) | C(35)-C(36) | 1.512(6) |
| C(37)-C(38) | 1.395(6) | C(37)-C(42) | 1.396(6) |

| | | | |
|---|---|---|---|
| C(38)-C(39) | 1.386(6) | C(39)-C(40) | 1.363(6) |
| C(40)-C(41) | 1.378(6) | C(41)-C(42) | 1.384(6) |
| C(43)-C(48) | 1.278(8) | C(43)-C(44A) | 1.317(14) |
| C(43)-C(44) | 1.388(9) | C(43)-C(48A) | 1.672(7) |
| C(44)-C(45) | 1.364(11) | C(45)-C(46) | 1.378(13) |
| C(46)-C(47) | 1.379(12) | C(47)-C(48) | 1.405(11) |
| C(49)-C(54) | 1.362(7) | C(49)-C(50) | 1.381(7) |
| C(50)-C(51) | 1.361(7) | C(51)-C(52) | 1.375(8) |
| C(52)-C(53) | 1.327(7) | C(53)-C(54) | 1.357(7) |
| C(55)-C(56) | 1.380(7) | C(55)-C(60) | 1.421(6) |
| C(56)-C(57) | 1.373(7) | C(57)-C(58) | 1.382(6) |
| C(58)-C(59) | 1.365(6) | C(59)-C(60) | 1.361(6) |
| C(48A)-C(47A) | 1.3911 | C(47A)-C(46A) | 1.324(19) |
| C(44A)-C(45A) | 1.49(2) | C(45A)-C(46A) | 1.42(3) |

| Bond angles (°) for $[Rh(IEt_2Me_2)_4][PPh_2O_2H]$ | | | |
|---|---|---|---|
| C(1)-Rh(1)-C(1)#1 | 89.5(2) | C(1)-Rh(1)-C(10)#1 | 179.86(18) |
| C(1)#1-Rh(1)-C(10)#1 | 90.37(14) | C(1)-Rh(1)-C(10) | 90.37(14) |
| C(1)#1-Rh(1)-C(10) | 179.86(18) | C(10)#1-Rh(1)-C(10) | 89.7(2) |
| C(28)-Rh(2)-C(28)#2 | 89.6(2) | C(28)-Rh(2)-C(19) | 90.18(13) |
| C(28)#2-Rh(2)-C(19) | 178.97(17) | C(28)-Rh(2)-C(19)#2 | 178.97(17) |
| C(28)#2-Rh(2)-C(19)#2 | 90.18(13) | C(19)-Rh(2)-C(19)#2 | 90.1(2) |
| O(1)-P(1)-O(2) | 121.30(17) | O(1)-P(1)-C(37) | 108.11(19) |
| O(2)-P(1)-C(37) | 108.69(18) | O(1)-P(1)-C(43) | 108.0(2) |
| O(2)-P(1)-C(43) | 109.05(19) | C(37)-P(1)-C(43) | 99.53(19) |
| C(1)-N(1)-C(2) | 111.8(3) | C(1)-N(1)-C(4) | 122.1(3) |
| C(2)-N(1)-C(4) | 126.1(3) | C(1)-N(2)-C(3) | 111.7(3) |
| C(1)-N(2)-C(8) | 123.8(3) | C(3)-N(2)-C(8) | 124.4(3) |
| C(10)-N(3)-C(11) | 111.4(3) | C(10)-N(3)-C(13) | 123.5(3) |
| C(11)-N(3)-C(13) | 125.2(3) | C(10)-N(4)-C(12) | 112.4(3) |
| C(10)-N(4)-C(17) | 123.4(3) | C(12)-N(4)-C(17) | 124.2(3) |
| C(19)-N(5)-C(20) | 111.6(3) | C(19)-N(5)-C(22) | 123.0(3) |
| C(20)-N(5)-C(22) | 125.4(3) | C(19)-N(6)-C(21) | 111.8(3) |
| C(19)-N(6)-C(26) | 123.2(3) | C(21)-N(6)-C(26) | 124.9(3) |
| C(28)-N(7)-C(29) | 111.8(3) | C(28)-N(7)-C(31) | 122.8(3) |
| C(29)-N(7)-C(31) | 125.4(3) | C(28)-N(8)-C(30) | 112.5(3) |
| C(28)-N(8)-C(35) | 122.9(3) | C(30)-N(8)-C(35) | 124.5(3) |
| N(2)-C(1)-N(1) | 102.7(3) | N(2)-C(1)-Rh(1) | 128.6(3) |
| N(1)-C(1)-Rh(1) | 128.7(3) | C(3)-C(2)-N(1) | 107.1(3) |
| C(3)-C(2)-C(6) | 130.6(4) | N(1)-C(2)-C(6) | 122.3(4) |
| C(2)-C(3)-N(2) | 106.7(3) | C(2)-C(3)-C(7) | 130.6(4) |
| N(2)-C(3)-C(7) | 122.6(4) | N(1)-C(4)-C(5) | 113.4(3) |
| N(2)-C(8)-C(9) | 113.0(4) | N(4)-C(10)-N(3) | 103.1(3) |
| N(4)-C(10)-Rh(1) | 129.8(3) | N(3)-C(10)-Rh(1) | 127.1(3) |
| C(12)-C(11)-N(3) | 106.9(3) | C(12)-C(11)-C(15) | 128.9(4) |

| | | | |
|---|---|---|---|
| N(3)-C(11)-C(15) | 124.2(4) | C(11)-C(12)-N(4) | 106.3(3) |
| C(11)-C(12)-C(16) | 130.3(4) | N(4)-C(12)-C(16) | 123.4(3) |
| N(3)-C(13)-C(14) | 114.3(4) | N(4)-C(17)-C(18) | 113.4(3) |
| N(6)-C(19)-N(5) | 102.8(3) | N(6)-C(19)-Rh(2) | 128.5(3) |
| N(5)-C(19)-Rh(2) | 128.6(3) | C(21)-C(20)-N(5) | 107.4(3) |
| C(21)-C(20)-C(24) | 129.7(4) | N(5)-C(20)-C(24) | 122.9(4) |
| C(20)-C(21)-N(6) | 106.3(3) | C(20)-C(21)-C(25) | 130.3(4) |
| N(6)-C(21)-C(25) | 123.4(4) | N(5)-C(22)-C(23) | 113.7(3) |
| N(6)-C(26)-C(27) | 113.3(3) | N(8)-C(28)-N(7) | 102.3(3) |
| N(8)-C(28)-Rh(2) | 128.8(3) | N(7)-C(28)-Rh(2) | 128.9(3) |
| C(30)-C(29)-N(7) | 107.0(3) | C(30)-C(29)-C(33) | 129.9(4) |
| N(7)-C(29)-C(33) | 123.0(4) | C(29)-C(30)-N(8) | 106.3(4) |
| C(29)-C(30)-C(34) | 131.1(4) | N(8)-C(30)-C(34) | 122.6(4) |
| N(7)-C(31)-C(32) | 112.8(3) | N(8)-C(35)-C(36) | 113.6(4) |
| C(38)-C(37)-C(42) | 117.8(4) | C(38)-C(37)-P(1) | 121.2(3) |
| C(42)-C(37)-P(1) | 121.0(3) | C(39)-C(38)-C(37) | 120.3(4) |
| C(40)-C(39)-C(38) | 120.8(5) | C(39)-C(40)-C(41) | 120.1(4) |
| C(40)-C(41)-C(42) | 119.7(4) | C(41)-C(42)-C(37) | 121.2(4) |
| C(48)-C(43)-C(44A) | 101.3(8) | C(48)-C(43)-C(44) | 121.5(6) |
| C(44A)-C(43)-C(44) | 24.3(6) | C(48)-C(43)-C(48A) | 33.4(3) |
| C(44A)-C(43)-C(48A) | 110.5(7) | C(44)-C(43)-C(48A) | 118.7(5) |
| C(48)-C(43)-P(1) | 122.5(4) | C(44A)-C(43)-P(1) | 132.4(7) |
| C(44)-C(43)-P(1) | 115.8(5) | C(48A)-C(43)-P(1) | 116.2(3) |
| C(43)-C(44)-C(45) | 118.5(8) | C(46)-C(45)-C(44) | 121.6(8) |
| C(47)-C(46)-C(45) | 117.1(8) | C(46)-C(47)-C(48) | 120.1(9) |
| C(43)-C(48)-C(47) | 120.7(8) | C(54)-C(49)-C(50) | 120.1(5) |
| C(51)-C(50)-C(49) | 119.0(5) | C(50)-C(51)-C(52) | 119.0(5) |
| C(53)-C(52)-C(51) | 122.0(5) | C(52)-C(53)-C(54) | 119.5(5) |
| C(49)-C(54)-C(53) | 120.3(5) | C(56)-C(55)-C(60) | 120.0(5) |
| C(55)-C(56)-C(57) | 119.6(5) | C(58)-C(57)-C(56) | 120.1(5) |
| C(59)-C(58)-C(57) | 120.5(5) | C(58)-C(59)-C(60) | 121.0(4) |

| | | | |
|---|---|---|---|
| C(59)-C(60)-C(55) | 118.7(4) | C(47A)-C(48A)-C(43) | 122.23(19) |
| C(46A)-C(47A)-C(48A) | 118.0(8) | C(43)-C(44A)-C(45A) | 126.4(12) |
| C(46A)-C(45A)-C(44A) | 116.4(11) | C(47A)-C(46A)-C(45A) | 126.1(13) |

**5.12.** ***Appendix 12:*** crystallographic data, bond lengths and angles for $[Rh(ICy)_4]^+$ **(98).**[10]

| | $[Rh(ICy)_4]^+$ |
|---|---|
| Empirical formula | $C_{61}H_{98}N_8Rh$ |
| Formula weight | 1046.38 |
| Temperature | 150(2) K |
| Wavelength | 0.69340 Å |
| Crystal system | Tetragonal |
| Space group | $P42_12$ |
| Unit cell dimensions | a = 17.8829(10)Å α = 90° |
| | b = 17.8829(10)Å β = 90° |
| | c = 12.5784(15)Å γ = 90° |
| Volume | 4022.5(6) $Å^3$ |
| Z | 2 |
| Density (calculated) | 0.864 $Mg/m^3$ |
| Absorption coefficient | 0.244 $mm^{-1}$ |
| F(000) | 1130 |
| Crystal size | 0.05 x 0.05 x 0.02 mm |
| Theta range for data collection | 3.35 to 21.53° |
| Index ranges | -17<=h<=18; -18<=k<=8; -12<=l<=13 |
| Reflections collected | 12220 |
| Independent reflections | 2471 [R(int) = 0.0572] |
| Reflections observed (>2σ) | 2070 |
| Absorption correction | SADABS |
| Refinement method | Full-matrix least-squares on $F^2$ |
| Data / restraints / parameters | 2471 / 0 / 159 |
| Goodness-of-fit on $F^2$ | 1.106 |
| Final R indices [I>2σ(I)] | $R^1 = 0.0541$ $wR_2 = 0.1427$ |
| R indices (all data) | $R^1 = 0.0648$ $wR_2 = 0.1488$ |
| Largest diff. peak and hole | 0.996 and -0.621 $eÅ^{-3}$ |

| Bond lengths (Å) for $[Rh(ICy)_4]^+$ | | | |
|---|---|---|---|
| Rh(2)-C(1)#1 | 2.070(5) | Rh(2)-C(1) | 2.070(5) |
| Rh(2)-C(1)#2 | 2.070(5) | Rh(2)-C(1)#3 | 2.070(5) |
| N(1)-C(1) | 1.384(7) | N(1)-C(2) | 1.410(7) |
| N(1)-C(4) | 1.466(7) | N(2)-C(1) | 1.351(7) |
| N(2)-C(3) | 1.372(7) | N(2)-C(9) | 1.472(8) |
| C(2)-C(3) | 1.309(9) | C(4)-C(8) | 1.528(8) |
| C(4)-C(5) | 1.529(8) | C(5)-C(6) | 1.530(8) |
| C(6)-C(7) | 1.509(8) | C(7)-C(42) | 1.538(9) |
| C(8)-C(42) | 1.514(9) | C(9)-C(14) | 1.535(9) |
| C(9)-C(10) | 1.537(9) | C(10)-C(11) | 1.529(9) |
| C(11)-C(12) | 1.539(9) | C(12)-C(13) | 1.498(10) |
| C(13)-C(14) | 1.513(9) | | |

| Bond angles (°) for $[Rh(ICy)_4]^+$ | | | |
|---|---|---|---|
| C(1)#1-Rh(2)-C(1) | 179.8(3) | C(1)#1-Rh(2)-C(1)#2 | 90.000(1) |
| C(1)-Rh(2)-C(1)#2 | 90.000(1) | C(1)#1-Rh(2)-C(1)#3 | 90.000(1) |
| C(1)-Rh(2)-C(1)#3 | 90.000(1) | C(1)#2-Rh(2)-C(1)#3 | 179.8(3) |
| C(1)-N(1)-C(2) | 109.5(5) | C(1)-N(1)-C(4) | 127.5(5) |
| C(2)-N(1)-C(4) | 122.9(5) | C(1)-N(2)-C(3) | 112.7(5) |
| C(1)-N(2)-C(9) | 126.8(5) | C(3)-N(2)-C(9) | 120.3(5) |
| N(2)-C(1)-N(1) | 103.0(4) | N(2)-C(1)-Rh(2) | 129.7(4) |
| N(1)-C(1)-Rh(2) | 127.3(4) | C(3)-C(2)-N(1) | 107.6(5) |
| C(2)-C(3)-N(2) | 107.1(5) | N(1)-C(4)-C(8) | 110.2(5) |
| N(1)-C(4)-C(5) | 110.6(5) | C(8)-C(4)-C(5) | 110.5(5) |
| C(4)-C(5)-C(6) | 111.3(5) | C(7)-C(6)-C(5) | 112.7(5) |
| C(6)-C(7)-C(42) | 110.4(5) | C(42)-C(8)-C(4) | 111.7(5) |
| N(2)-C(9)-C(14) | 111.8(5) | N(2)-C(9)-C(10) | 111.1(5) |
| C(14)-C(9)-C(10) | 109.2(5) | C(11)-C(10)-C(9) | 113.6(6) |
| C(10)-C(11)-C(12) | 108.6(6) | C(13)-C(12)-C(11) | 111.5(5) |
| C(12)-C(13)-C(14) | 112.4(6) | C(13)-C(14)-C(9) | 113.4(5) |
| C(8)-C(42)-C(7) | 111.0(6) | | |

**5.13.** ***Appendix 13:*** crystallographic data, bond lengths and angles for ICy:$CO_2$ (**108**).

| | **ICy:$CO_2$** |
|---|---|
| Empirical formula | $C_{16}H_{24}N_2O_2$ |
| Formula weight | 276.37 |
| Temperature | 150(2) K |
| Wavelength | 0.71073 Å |
| Crystal system | Monoclinic |
| Space group | P21/a |
| Unit cell dimensions | a = 12.1770(2)Å α = 90° |
| | b = 9.4380(2)Å β = 111.608(1)° |
| | c = 13.9000(3)Å γ = 90° |
| Volume | 1485.22(5) $Å^3$ |
| Z | 4 |
| Density (calculated) | 1.236 $Mg/m^3$ |
| Absorption coefficient | 0.082 $mm^{-1}$ |
| F(000) | 600 |
| Crystal size | 0.17 x 0.15 x 0.10 mm |
| Theta range for data collection | 3.60 to 27.49° |
| Index ranges | -15<=h<=15; -12<=k<=12; -18<=l<=18 |
| Reflections collected | 26351 |
| Independent reflections | 3385 [R(int) = 0.0955] |
| Reflections observed (>2σ) | 2552 |
| Absorption correction | None |
| Refinement method | Full-matrix least-squares on $F^2$ |
| Data / restraints / parameters | 3385 / 0 / 182 |
| Goodness-of-fit on $F^2$ | 1.021 |
| Final R indices [I>2σ(I)] | $R^1$ = 0.0437 $wR_2$ = 0.0949 |
| R indices (all data) | $R^1$ = 0.0694 $wR_2$ = 0.1065 |
| Largest diff. peak and hole | 0.305 and -0.349 $eÅ^{-3}$ |

| Bond lengths (Å) for ICy:$CO_2$ | | | |
|---|---|---|---|
| O(1)-C(4) | 1.2432(16) | O(2)-C(4) | 1.2396(16) |
| N(1)-C(1) | 1.3511(16) | N(1)-C(2) | 1.3783(17) |
| N(1)-C(5) | 1.4877(16) | N(2)-C(1) | 1.3482(17) |
| N(2)-C(3) | 1.3844(17) | N(2)-C(9) | 1.4906(15) |
| C(1)-C(4) | 1.5342(18) | C(2)-C(3) | 1.3525(19) |
| C(5)-C(8) | 1.5221(19) | C(5)-C(19) | 1.5256(18) |
| C(6)-C(16) | 1.522(2) | C(6)-C(7) | 1.526(2) |
| C(7)-C(8) | 1.527(2) | C(9)-C(10) | 1.5257(18) |
| C(9)-C(14) | 1.5294(19) | C(10)-C(11) | 1.5248(18) |
| C(11)-C(12) | 1.522(2) | C(12)-C(13) | 1.525(2) |
| C(13)-C(14) | 1.5286(19) | C(16)-C(19) | 1.5312(19) |

| Bond angles (°) for ICy:$CO_2$ | | | |
|---|---|---|---|
| C(1)-N(1)-C(2) | 109.08(11) | C(1)-N(1)-C(5) | 126.83(11) |
| C(2)-N(1)-C(5) | 123.80(11) | C(1)-N(2)-C(3) | 109.14(11) |
| C(1)-N(2)-C(9) | 127.69(11) | C(3)-N(2)-C(9) | 122.90(11) |
| N(2)-C(1)-N(1) | 107.22(11) | N(2)-C(1)-C(4) | 126.96(11) |
| N(1)-C(1)-C(4) | 125.81(11) | C(3)-C(2)-N(1) | 107.50(12) |
| C(2)-C(3)-N(2) | 107.06(12) | O(2)-C(4)-O(1) | 130.00(13) |
| O(2)-C(4)-C(1) | 115.21(11) | O(1)-C(4)-C(1) | 114.79(11) |
| N(1)-C(5)-C(8) | 108.88(11) | N(1)-C(5)-C(19) | 111.66(11) |
| C(8)-C(5)-C(19) | 111.00(11) | C(16)-C(6)-C(7) | 111.35(12) |
| C(8)-C(7)-C(6) | 111.44(13) | C(5)-C(8)-C(7) | 110.08(12) |
| N(2)-C(9)-C(10) | 109.71(10) | N(2)-C(9)-C(14) | 109.11(10) |
| C(10)-C(9)-C(14) | 111.28(11) | C(11)-C(10)-C(9) | 110.56(11) |
| C(12)-C(11)-C(10) | 110.72(12) | C(11)-C(12)-C(13) | 109.90(12) |
| C(12)-C(13)-C(14) | 111.14(12) | C(13)-C(14)-C(9) | 110.90(11) |
| C(6)-C(16)-C(19) | 111.61(12) | C(5)-C(19)-C(16) | 109.26(11) |

## 5.14. References

(1) Asymmetric unit consists of ½ of a molecule, with the central ruthenium, carbene carbon and hydride located on a crystallographic 2-fold rotation axis that serves to generate the remainder of the molecule. Hydride hydrogen located and refined at 1.6 Å from the central metal. The phenyl ring based on C19 is disordered over 2 sites in a 60:40 ratio. Both partial occupancy fragments refined as rigid hexagons. Atoms in minor component are labelled with suffix 'A'.

(2) Asymmetric unit contains 1 molecule of THF solvent which exhibits substantial disorder. Optimal convergence achieved by treating solvent as 2 fragment of with 7:3 occupancy ratio. Hydride readily located and refined at distance of 1.6 Å from central metal.

(3) Bridging hydride located and refined to have similar bond distances to each rhodium centre.

(4) H1 located and refined without and restraints.

(5) Asymmetric unit is ½ of a dimmer molecule. The remainder is generated *via* a 2-fold rotation axis on which both Rh1 and Rh2 are sited.

(6) H2 located and refined without constraints. No absorption correction (on merit).

(7) Asymmetric unit contains 1 molecule of dichloromethane.

(8) Potential for lots of C-H...F interactions in lattice.

(9) The asymmetric unit in this structure consists of two crystallographically independent cation halves, with the central metal in each case located on a 2-fold rotation axis implicit in the space group symmetry, an addition to one $Ph_2PO_2^-$ anion, and 2 benzene molecules. 5 carbons in one of the phenyl rings in the anion exhibited 70:30 disorder, which was duly modelled.

(10) Early refinements of the structural model indicated that there was diffuse electron density in the lattice. Subsequent examination with PLATON showed that it contains large regions between molecules and that these are occupied by fractional amounts of solvent, but disorder was so extensive that a sensible atomic model could not be developed. The solvent was modelled using the SQUEEZE procedure in PLATON. This yielded an estimate of the solvent content (based on the approximate number of electrons contained in the voids) as being in the region of 2 whole carbons and 4 hydrogen atoms per unit cell. F(000) and related parameters, as presented, are derived on the basis of inclusion of this solvent in the unit cell. Data cut off at a resolution of 0.95 Å is a consequence of a decline in diffracting ability of the crystal at higher Bragg angles, which is probably a symptom of the presence of diffuse solvent.